BIODEVICES 2008

International Conference on
Biomedical Electronics and Devices

Proceedings

Volume 1

Funchal, Madeira - Portugal · 28 - 31 January, 2008

TECHNICAL CO-SPONSORSHIP BY

IEEE EMB

CO-ORGANIZED BY

INSTICC

UNIVERSIDADE da MADEIRA

IN COOPERATION WITH

aaai

INSTICC PRESS

BIODEVICES 2008

Proceedings of the
First International Conference on
Biomedical Electronics and Devices

Volume 1

Funchal, Madeira - Portugal

January 28 – 31, 2008

Co-organized by
INSTICC – Institute for Systems and Technologies of Information,
Control and Communication
and
UMA – University of Madeira

Technical Co-sponsorship by
IEEE EMB – Engineering in Medicine and Biology Society

In Cooperation with
AAAI – Association for the Advancement of Artificial Intelligence

Edited by Teodiano Bastos e Filho and Hugo Gamboa

Printed in Portugal

ISBN: 978-989-8111- 17-3

Depósito Legal: 268553/07

http://www.biodevices.org

secretariat@biodevices.org

BIODEVICES is part of BIOSTEC – International Joint Conference on Biomedical Engineering Systems and Technologies

BRIEF CONTENTS

INVITED SPEAKERS

Sérgio Cerutti

Polytechnic University of Milan

Italy

Kevin Warwick

University of Reading

U.K.

Fernando Henrique Lopes da Silva

University of Amsterdam

The Netherlands

Vipul Kashyap

Partners HealthCare System, Clinical Informatics R&D

U.S.A.

David Hall

Research Triangle Institute in North Carolina

U.S.A.

Albert Cook

University of Alberta, Faculty of Rehabilitation Medicine

Canada

ORGANIZING AND STEERING COMMITTEES

CONFERENCE CO-CHAIRS

Ana Fred, IST- Technical University of Lisbon, Portugal

Joaquim Filipe, INSTICC / Polytechnic Institute of Setúbal, Portugal

Hugo Gamboa, Telecommunications Institute / Portugal

Jorge Cardoso, University of Madeira - UMA / Madeira, Portugal

PROGRAM CO-CHAIRS

Teodiano Freire Bastos Filho, Federal University of Espírito Santo, Brazil

Hugo Gamboa, Telecommunications Institute, Portugal

LOCAL CHAIR

Paulo Sampaio, University of Madeira - UMA, Portugal

PROCEEDINGS PRODUCTION

Paulo Brito, INSTICC, Portugal

Marina Carvalho, INSTICC, Portugal

Helder Coelhas, INSTICC, Portugal

Vera Coelho, INSTICC, Portugal

Andreia Costa, INSTICC, Portugal

Bruno Encarnação, INSTICC, Portugal

Bárbara Lima, INSTICC, Portugal

Vitor Pedrosa, INSTICC, Portugal

Vera Rosário, INSTICC, Portugal

Mónica Saramago, INSTICC, Portugal

CD-ROM PRODUCTION

Paulo Brito, INSTICC, Portugal

GRAPHICS PRODUCTION AND WEB DESIGNER

Marina Carvalho, INSTICC, Portugal

SECRETARIAT AND WEBMASTER

Marina Carvalho, INSTICC, Portugal

PROGRAM COMMITTEE

Julio Abascal, University of the Basque Country-Euskal Herriko Unibertsitatea, Spain

Amiza Mat Amin, Universiti Malaysia Terengganu, Malaysia

Rodrigo Varejão Andreão, UFES, Brazil

Ramon Pallàs Areny, Technical University of Catalonia (UPC), Spain

Luis Azevedo, Instituto Superior Técnico - Technical University of Lisbon, Portugal

Rafael Barea, University of Alcalá, Spain

Antonio Barrientos, Universidad Politécnica de Madrid, Spain

Roberto Boeri, Universidad Nacional de Mar del Plata, Argentina

Luciano Boquete, Alcala University, Spain

Susana Borromeo, Universidad Rey Juan Carlos Spain, Spain

Eduardo Caicedo Bravo, Universidad del Valle, Colombia

Enrique A. Vargas Cabral, Facultad de Ciencias y Tecnología - Universidad. Católica de Asunción, Paraguay

Sira Palazuelos Cagigas, University of Alcalá, Spain

Leopoldo Calderón, Consejo Superior de Investigaciones Científicas - IAI, Spain

Alicia Casals, Technical university of Catalonia, Spain

Gert Cauwenberghs, University of California San Diego, U.S.A.

Ramón Ceres, Instituto de Automatica Industrial- CSIC, Spain

Luca Cernuzzi, Universidad Católica "Nuestra Señora de la Asunción", Paraguay

Alberto Cliquet Jr., USP, UNICAMP, Brazil

Fernando Cruz, School of Technology of Setúbal/Polytechnic Institute of Setúbal, Portugal

Pedro Pablo Escobar, Ingeniería Electromedica, Facultad de Ingeniería, Universidad Nacional del Centro, Argentina

Marcos Formica, Bioengineering Faculty, Entre Ríos National University, Argentina

Juan Carlos Garcia Garcia, University of Alcala, Spain

Gerd Hirzinger, German Aerospace Center (DLR), Germany

Jongin Hong, Imperial College London, U.K.

Giacomo Indiveri, UNI - ETH Zurich, Switzerland

Dinesh Kumar, RMIT University, Australia

Eric Laciar Leber, Universidad Nacional de San Juan, Argentina

José Luis Martinez, Universidad Politécnica de Madrid, Spain

Manuel Mazo, University of Alcala, Spain

Paulo Mendes, University of Minho, Portugal

José del R. Millán, IDIAP Research Institute, Switzerland

Joseph Mizrahi, Technion, Israel Institute of Technology, Israel

Raimes Moraes, Federal University of Santa Catarina, Brazil

Pedro Noritomi, Renato Archer's Research Center - CenPRA, Brazil

Maciej J. Ogorzalek, Jagiellonian University, Poland

Kazuhiro Oiwa, National Institute of Information and Communications Technology, Japan

José Raimundo de Oliveira, Universidade Estadual de Campinas, Brazil

Evangelos Papadopoulos, National Technical University of Athens, Greece

Laura Papaleo, University of Genova, Italy

Francisco Novillo Parales, Escuela Superior Politécnica del Litoral, ESPOL, Ecuador

Qibing Pei, University of California, Los Angeles, U.S.A.

José M. Quero, Universidad de Sevilla, Spain

Antonio Quevedo, University of Campinas, Brazil

Alejandro Ramirez-Serrano, University of Calgary, Canada

Adriana María Rios Rincón, Universidad del Rosario, Colombia

Joaquin Roca-Dorda, Universidad Politécnica de Cartagena (UPCT), Spain

PROGRAM COMMITTEE (CONT.)

Adson da Rocha, University of Brasilia, Brazil

Joel Rodrigues, Institue of Telecommunications / University of Beira Interior, Portugal

Carlos F. Rodriguez, Universidad de Los Andes, Colombia

Mario Sarcinelli-Filho, Federal University of Espirito Santo, Brazil

Fernando di Sciascio, Universidad Nacional de San Juan, Argentina

Jorge Vicente Lopes da Silva, "Renato Archer" Research Center, Brazil

Amir M. Sodagar, University of Michigan, U.S.A.

Juan Hernández Tamames, Rey Juan Carlos University, Spain

Mário Vaz, Faculty of Engineering University of Porto, Portugal

António Veloso, Faculty of Human Kinetics, Portugal

Peter Walker, University of Leeds, U.K.

Jonathan Wolpaw, Wadsworth Center, NY State Department of Health, U.S.A.

Miguel Yapur, Escuela Superior Politécnica del Litoral (ESPOL), Ecuador

AUXILIARY REVIEWERS

José M. R. Ascariz, Alcala University, Spain

Leandro Bueno, Politechnique University of Madrid, Spain

Natalia López Celan, Gabinete de Tecnología Médica, Instituto de Automática, Facultad Ingeniería, Universidad Nacional de San Juan, Argentina

Andre Ferreira, Federal University of Espirito Santo, Brazil

Vicente González, DEI - Univerisdad Católica "Nuestra Señora de la Asunción", Paraguay

Muhammad Suzuri Hitam, Universiti Malaysia Terengganu, Malaysia

Joaquin Roca-Gonzalez, Polytechnic University of Cartagena, Spain

Rober Marcone Rosi, Federal University of Espirito Santo, Brazil

Evandro Ottoni Teatini Salles, Federal University of Espirito Santo, Brazil

Hugo Humberto Plácido Silva, Instituto de Telecomunicações, Portugal

Andrés Valdéz, Gabinete de Tecnología Médica, Facultad Ingeniería, Universidad Nacional de San Juan, Argentina

SELECTED PAPERS BOOK

A number of selected papers presented at BIODEVICES 2008 will be published by Springer, in a book entitled Biomedical Engineering Systems and Technologies. This selection will be done by the conference co-chairs and program co-chairs, among the papers actually presented at the conference, based on a rigorous review by the BIOSTEC 2008 program committee members.

OFFICIAL CARRIER

FOREWORD

This volume contains the proceedings of the *First International Conference on Biomedical Electronics and Devices* (BIODEVICES 2008), organized by the Institute for Systems and Technologies of Information Control and Communication (INSTICC) and the University of Madeira, technically co-sponsored by the IEEE Engineering in Medicine and Biology Society (EMB) and in cooperation with AAAI.

The purpose of the *International Conference on Biomedical Electronics and Devices* is to bring together researchers and practitioners from electronics and mechanical engineering, interested in studying and using models, equipments and materials inspired from biological systems and/or addressing biological requirements. Monitoring devices, instrumentation sensors and systems, biorobotics, micro-nanotechnologies and biomaterials are some of the technologies addressed at this conference.

BIODEVICES is one of three integrated conferences that are co-located and constitute the International Joint Conference on Biomedical Engineering Systems and Technologies (BIOSTEC). The other two component conferences are HEALTHINF (International Conference on Health Informatics) and BIOSIGNALS (International Conference on Bio-inspired Systems and Signal Processing).

The joint conference, BIOSTEC, has received 494 paper submissions from more than 40 countries in all continents. 65 papers were published and presented as full papers, i.e. completed work (8 pages/30' oral presentation), 189 papers reflecting work-in-progress or position papers were accepted for short presentation, and another 86 contributions were accepted for poster presentation. These numbers, leading to a "full-paper" acceptance ratio below 14% and a total oral paper presentations acceptance ratio below 52%, show the intention of preserving a high quality forum for the next editions of this conference.

The conference included a panel and six invited talks delivered by internationally distinguished speakers, namely: Sergio Cerutti, Kevin Warwick, F. H. Lopes da Silva, Vipul Kashyap, David Hall and Albert Cook. Their participation has positively contributed to reinforce the overall quality of the Conference and to provide a deeper understanding of the field of Biomedical Engineering Systems and Technologies.

The proceedings of the conference will be indexed by several major indices including DBLP, INSPEC and ISI-Proceedings and it will also be submitted for indexing to EI. A book with the revised versions of a short list of selected papers from the conference will be published by Springer-Verlag in the new CS book series: Communications in Computer and Information Science (CCIS). Additionally, a special issue of the IEEE Transactions on Biomedical Circuits and Systems will be edited based on the very best papers of the conference.

The program for this conference required the dedicated effort of many people. Firstly, we must thank the authors, whose research and development efforts are recorded here. Secondly, we thank

FOREWORD (CONT.)

the members of the program committee and the additional reviewers for their diligence and expert reviewing. Thirdly, we thank the keynote speakers for their invaluable contribution and for taking the time to synthesise and prepare their talks. Fourthly, we thank the program chairs, Teodiano Freire Bastos Filho and Hugo Gamboa, whose collaboration was much appreciated. Finally, special thanks to all the members of the INSTICC team, especially Marina Carvalho at the conference secretariat, and the local organising committee from the University of Madeira, especially Jorge Cardoso and Paulo Sampaio, whose collaboration was fundamental for the success of this conference.

This year, the organization will distribute two paper awards at the conference closing session: the best paper award and the best student paper award. The decision was mainly based on the paper classifications provided by the Program Committee.

We wish you all an exciting conference and an unforgettable stay in the lovely island of Madeira. We hope to meet you again next year for the 2nd BIODEVICES, details of which are available at http://www.biodevices.org.

Joaquim Filipe

INSTICC/Polytechnic Institute of Setúbal

CONTENTS

POSTERS

INVITED SPEAKERS

KEYNOTE LECTURES

MULTIVARIATE, MULTIORGAN AND MULTISCALE INTEGRATION OF INFORMATION IN BIOMEDICAL SIGNAL PROCESSING

Sergio Cerutti
Department of Bioengineering, Polytechnic University, Milano, Italy
sergio.cerutti@polimi.it

Abstract: Biomedical signals carry important information about the behavior of the living systems under studying. A proper processing of these signals allows in many instances to obtain useful physiological and clinical information. Many advanced algorithms of signal and image processing have recently been introduced in such an advanced area of research and therefore important selective information is obtainable even in presence of strong sources of noise or low signal/noise ratio. Traditional stationary signal analysis together with innovative methods of investigation of dynamical properties of biological systems and signals in second-order or in higher-order approaches (i.e., in time-frequency, time-variant and time-scale analysis, as well as in non linear dynamics analysis) provide a wide variety of even complex processing tools for information enhancement procedures. Another important innovative aspect is also remarked: the integration between signal processing and modeling of the relevant biological systems is capable to directly attribute patho-physiological meaning to the parameters obtained from the processing and viceversa the modeling fitting could certainly be improved by taking into account the results from signal processing procedure. Such an integration process could comprehend parameters and observations detected at different scales, at different organs and with different modalities. This approach is reputed promising for obtaining an olistic view of the patient rather than an atomistic one which considers the whole as a simple sum of the single component parts.

BRIEF BIOGRAPHY

Sergio Cerutti is Professor in Biomedical Signal and Data Processing at the Department of Bioengineering of the Polytechnic University in Milano, Italy. In the period 2000-2006 he has been the Chairman of the same Department. His research interests are mainly in the following topics: biomedical signal processing (ECG, blood pressure signal and respiration, cardiovascular variability signals, EEG and evoked potentials), neurosciences and cardiovascular modelling. In his research activity he has put emphasis on the integration of information at different modalities, at different sources and at different scales in various physiological systems. Since 1983 he has taught a course at a graduate and a doc level on Biomedical Signal Processing and Modelling at Engineering Faculties (Milano and Roma) as well as at Specialisation Schools of Medical Faculties (Milano and Roma). He has been Elected Member of IEEE-EMBS AdCom (Region 8) in the period 1993-1996. He is actually Fellow Member of IEEE and of EAMBES and Associate Editor of IEEE Trans BME. He is a member of the Steering Committee of the IEEE-EMBS Summer School on Biomedical Signal Processing: he was the local organiser of four Summer Schools held in Siena. He has been Visiting Professor at Harvard-MIT Division Health Science and Technology, Boston, USA for an overall period of 1 year. He is the Author of more than 400 international scientific contributions (more than 180 on indexed scientific journals).

1 INTRODUCTION

Biomedical signals and imaging carry important information about the behavior of the living systems under studying. A proper processing of these signals and images allow in many instances to obtain useful physiological and clinical information. Actually, many advanced algorithms of digital signal and image processing are at disposal and therefore

important selective information is now obtainable even in presence of strong sources of noise or low signal/noise ratio. In most of the cases it is not sure whether such sources might derive even by complex and unknown interactions with other biological systems whose implications could be important from the physiological or clinical standpoints. Traditional stationary signal analysis together with innovative methods of investigation of dynamical properties of biological systems and signals in second-order or in higher-order approaches (i.e., in time-frequency, time-variant and time-scale analysis, as well as in non linear dynamics analysis) provide a wide variety of even complex processing tools for information enhancement procedures in the challenging studying of a better explanation of many physiological and clinical phenomena.

2 INTEGRATION BETWEEN SIGNAL PROCESSING AND PHYSIOLOGICAL MODELING

Another important innovative aspect to improve the information content from biomedical data is constituted by the integration between signal processing and modeling of the relevant biological systems, thus directly attributing patho-physiological meaning to the model parameters obtained from the processing; and, viceversa, the modeling fitting could certainly be improved by taking into account the results from signal/image processing procedures.

3 MONOVARIATE AND MULTIVARIATE SIGNAL PROCESSING

Other kinds of integration may be fulfilled, taking into account more signals from the same system in a multivariate way (i.e. from a single-lead vs multichannel EEG or ECG analysis) and combining also the action of different systems such as autonomic nervous system, cardiovascular and respiratory systems, etc. Sleep is a formidable example of multiorgan involvement in both physiological (sleep staging and correlation with cardiorespiratory system) and pathological conditions (sleep apnea, sleep deprivation, restless leg syndrome and so on).

4 MULTISCALE APPROACH

Further, modern rehabilition techniques (motor and /or cognitive) make use actually of objective indices obtained from the patient's biosignals and images to better "personalize" rehabilitation protocols (from EEG, EP's, ERP's, MRI, fMRI, NIRS, etc). In neurosciences such an integration process could comprehend parameters and observations detected also at different scales, from genome and proteome up to the single organ and to the entire body compartment. Examples will be described where an animal model (murine model) is developed by alterating a gene putative to a determined pathology (i.e.epilepsy) and changes in EEG signals are studied (spike/wave occurrences and modifications in signal power bands). In clinical applications, it is worth mentioning the important data fusion which could be fulfilled by the integration of simultaneous EEG recordings and fMRI in some epileptic patients during inter-critical or critical events.

Finally, another important integration can be obtained along different observation scales. Traditionally, biological signal analysis is carried out at the level of organ or system to be investigated (i.e., ECG or EEG signal, arterial blood pressure, respiration and so on). It is very clear the advantage of correlating this information with that one obtained about the same system, but at different scale level, i.e. at cellular level or even at subcellular level (for example, analyzing possible genetic correlates or typical patterns of proteins or even DNA/RNA sequences). Biomedical engineering as a dedicated discipline may strongly contribute to this multiscale information processing

Along this approach line, even the long-QT syndrome, can be efficiently studied at different scale level: a mutation in a portion of gene SCN5A which presents a phenotype compatible to long-QT3 type, is known to produce an altered function of Na+ channels. Through a proper model which describes the functioning of ventricular cells is possible to evidence that this alteration may induce a prolongation of QT duration, as detected on ECG tracing. This event is further correlated with an increased risk of ventricular tachyarrhythmias. Hence, the path is completed: from the genetic expression up to the disease manifestation (Clancy and Rudy, 1999), (Priori ey al., 2003). Many different signal processing and modeling are involved in this paradigmatic example: an integration along the various scales of observation may undoubtedly contribute to a better

understanding of the complex pathophysiological correlates.

A great effort is on course nowadays for creating very large databases and networking of models and technologies for integrating such information (Physiome project (Hunter et al., 2002), (Rudy, 2000) to be connected with Genome and Proteome projects and Virtual Physiological Human project – VPH – which is inserted into the activities of the 7th Framework Programme of EU).

Other examples are constituted by the studying of the profile of expressed proteins in 2D-gel supports, or after mass-spectrometry analysis, relative to a variety of pathologies (i.e. epilepsy, peripheral neuropathies or Amyotrophic Lateral Sclerosis (ALS), or in oncological studies) thus singling out the set of proteins which present a correlate with the pathology in respect to the control group.

This overall approach is reputed promising for obtaining an olistic view of the patient rather than an atomistic one which considers the whole as a simple sum of the single component parts.

REFERENCES

G. Baselli, S. Cerutti, S. Civardi, A. Malliani and M. Pagani, Cardiovascular variability signals: towards the identification of a closed-loop model of the neural control mechanisms, *IEEE Trans Biomed Eng*., vol.35(12):1033-46(1988).

E. N. Bruce, *Biomedical Signal Processing and Signal Modelling*, J. Wiley (2001).

C. E. Clancy and Y. Rudy, Linking a genetic defect to its cellular phenotype in a cardiac arrhythmia, *Nature*, vol. 400(6744):566-569 (1999).

A. Cohen, *Biomedical Signal Analysis*, Vol. I, II, CRC Press (1986).

P. Hunter, P. Robbins and D. Noble, The IUPS human physiome project, *Pflugers Arch-Eur. J. Physiol*., vol. 445:1-9 (2002).

R. I. Kitney, A nonlinear model for studing oscillations in the blood pressure control system*, J. Biomed. Eng*., vol I,n. 2: 88-89 (1979).

H. P. Koepchen, History of studies and concepts of blood pressure wave, in: *Mechanisms of blood pressure waves (*Miyakawa K., Koepchen, H.P., Polosa C. eds): 3-23, Springer-Verlag (1984).

M. C. Mackey and J.C. Milton, Dynamical diseases, *Ann N Y Acad.Sc.,* vol.504:16-32 (1987).

C.-K. Peng, S. Havlin, J.M. Hausdorff, J.E. Mietus, H.E. Stanley and A.L. Goldberger, Fractal mechanisms and heart rate dynamics long-range correlation and their breakdown with diseases, *Journal of Electrocardiology*, vol.28: 59-65 (1995).

S. G. Priori, P.J. Schwartz, C. Napolitano, R. Bloise, E. Ronchetti, M. Grillo, A. Vicentini, C. Spazzolini, J. Nastoli, G. Bottelli, R. Folli and D. Cappelletti, Risk stratification in the long-QT sindrome, *N Engl J Med*., May 8, vol.348(19):1866-74 (2003).

Y. Rudy, From Genome to Physiome: integrative models of cardiac excitation, *Ann. Biom. Engineer*, vol 28: 945-950 (2000).

Cerutti S, Esposti F, Ferrario M, Sassi R, Signorini MG, Long-term invariant parameters obtained from 24-h Holter recordings: a comparison between different analysis techniques, Chaos, vol.17(1):015108, (2007).

Foffani G, Ardolino G, Rampini P, Tamma F, Caputo E, Egidi M, Cerutti S, Barbieri S, Priori A., Physiological recordings from electrodes implanted in the basal ganglia for deep brain stimulation in Parkinson's disease: the relevance of fast subthalamic rhythms, Acta Neurochir Suppl, vol. 93:97-9, (2005).

OUTTHINKING AND ENHANCING BIOLOGICAL BRAINS

Kevin Warwick
University of Reading, UK

Keywords: Brain-Computer Interface, Biological systems, Implant technology, Feedback control.

Abstract: In this paper an attempt has been made to take a look at how the use of implant and electrode technology can now be employed to create biological brains for robots, to enable human enhancement and to diminish the effects of certain neural illnesses. In all cases the end result is to increase the range of abilities of the recipients. An indication is given of a number of areas in which such technology has already had a profound effect, a key element being the need for a clear interface linking the human brain directly with a computer. An overview of some of the latest developments in the field of Brain to Computer Interfacing is also given in order to assess advantages and disadvantages. The emphasis is clearly placed on practical studies that have been and are being undertaken and reported on, as opposed to those speculated, simulated or proposed as future projects. Related areas are discussed briefly only in the context of their contribution to the studies being undertaken. The area of focus is notably the use of invasive implant technology, where a connection is made directly with the cerebral cortex and/or nervous system.

Tests and experimentation which do not involve human subjects are invariably carried out *a priori* to indicate the eventual possibilities before human subjects are themselves involved. Some of the more pertinent animal studies from this area are discussed including our own involving neural growth. The paper goes on to describe human experimentation, in which neural implants have linked the human nervous system bi-directionally with technology and the internet. A view is taken as to the prospects for the future for this implantable computing in terms of both therapy and enhancement.

BRIEF BIOGRAPHY

Kevin Warwick is Professor of Cybernetics at the University of Reading, England, where he carries out research in artificial intelligence, control, robotics and cyborgs. He is also Director of the University KTP Centre, which links the University with Small to Medium Enterprises and raises £2.5 million each year in research income. As well as publishing 500 research papers, Kevin is perhaps best known for his experiments into implant technology. He has been awarded higher doctorates (DScs) both by Imperial College and the Czech Academy of Sciences, Prague. He was presented with The Future of Health Technology Award in MIT, was made an Honorary Member of the Academy of Sciences, St. Petersburg and in 2004 received The IEE Achievement Medal.

1 INTRODUCTION

Research is being carried out in which biological signals of some form are measured, are acted upon by some appropriate signal processing technique and are then employed either to control a device or as an input to some feedback mechanism (Penny et al., 2000), (Roitberg, 2005). In many cases neural signals are employed, for example Electroencephalogram (EEG) signals can be measured externally to the body, using externally adhered electrodes on the scalp (Wolpaw et al., 1990) and can then employed as a control input. Most likely this is because the procedure is relatively simple from a research point of view and is not particularly taxing on the researchers involved. However, reliable interpretation of EEG data is extremely complex – partly due to both the compound nature of the multi-neuronal signals being measured and the difficulties in recording such highly attenuated

In the last few years interest has also grown in the use of real-time functional Magnetic Resonance

Imaging (fMRI) for applications such as computer cursor control. This typically involves an individual activating their brain in different areas by reproducible thoughts (Warwick, 2007) or by recreating events (Pan et al., 2007). Alternatively fMRI and EEG technologies can be combined so that individuals can learn how to regulate Slow Cortical Potentials (SCPs) in order to activate external devices (Hinterberger et al., 2005). Once again the technology is external to the body. It is though relatively expensive and cumbersome.

It is worth noting that external monitoring of neural signals, by means of either EEG analysis or indeed fMRI, leaves much to be desired. Almost surely the measuring technique considerably restricts the user's mobility and, as is especially the case with fMRI, the situation far from presents a natural or comfortable setting. Such systems also tend to be relatively slow, partly because of the nature of recordings via the indirect connection, but also because it takes time for the individual themselves to actually initiate changes in the signal. As a result of this, distractions, both conscious and sub-conscious, can result in false indicators thus preventing the use of such techniques for safety critical, highly dynamic and, to be honest, most realistic practical applications. Despite this, the method can enable some individuals who otherwise have extremely limited communication abilities to operate some local technology in their environment, and, in any case, it can serve as a test bed for a more direct and useful connection.

The definition of what constitutes a Brain-Computer Interface (BCI) is extremely broad. A standard keyboard could be so regarded. It is clear however that various wearable computer techniques and virtual reality systems, e.g. glasses containing a miniature computer screen for a remote visual experience (Mann, 1997), are felt by some researchers to fit this category. Although it is acknowledged that certain body conditions, such as stress or alertness, can be monitored in this way, the focus of this paper is on bidirectional BCIs and is more concerned with a direct connection between a biological brain and technology, and ultimately a human and technology.

2 *IN VIVO* STUDIES

Non-human animal studies can be considered to be a pointer for what is potentially achievable with humans in the future. As an example, in one particular animal study the extracted brain of a lamprey, retained in a solution, was used to control the movement of a small wheeled robot to which it was attached (Reger et al., 2000). The lamprey innately exhibits a response to light reflections on the surface of water by trying to align its body with respect to the light source. When connected into the robot body, this response was utilised by surrounding the robot with a ring of lights. As different lights were switched on and off, so the robot moved around its corral, trying to position itself appropriately.

Meanwhile in studies involving rats, a group of rats were taught to pull a lever in order to receive a suitable reward. Electrodes were then chronically implanted into the rats' brains such that the reward was proffered when each rat thought (one supposes) about pulling the lever, but before any actual physical movement occurred. Over a period of days, four of the six rats involved in the experiment learned that they did not in fact need to initiate any action in order to obtain a reward; merely thinking about it was sufficient (Chapin, 2004).

In another series of experiments, implants consisting of microelectrode arrays have been positioned into the frontal and parietal lobes of the brains of two female rhesus macaque monkeys. Each monkey learned firstly how to control a remote robot arm through arm movements coupled with visual feedback, and it is reported that ultimately one of the monkeys was able to control the arm using only brain derived neural signals with no associated physical movement. Notably, control signals for the reaching and grasping movements of the robotic arm were derived from the same set of implanted electrodes (Carmena et al., 2003), (Nicolelis et al., 2000).

Such promising results from animal studies have given the drive towards human applications a new impetus.

3 ROBOT WITH A BIOLOGICAL BRAIN

Human concepts of a robot may involve a little wheeled device, perhaps a metallic head that looks roughly human-like or possibly a biped walking robot. Whatever the physical appearance our idea tends to be that the robot might be operated remotely by a human, or is being controlled by a simple programme, or even may be able to learn with a

microprocessor/computer as its brain. We regard a robot as a machine.
In a present project neurons are being cultured in a laboratory in Reading University to grow on and interact with a flat multi-electrode array. The neural culture, a biological brain, can be electronically stimulated via the electrodes and its trained response can be witnessed.

The project now involves networking the biological brain to be part of a robot device. In the first instance this will be a small wheeled robot. The input (sensory) signals in this case will be only the signals obtained from the wheeled robot's ultrasonic sensors. The output from the biological brain will be used to drive the robot around. The goal of the project initially will be to train the brain to drive the robot forwards without bumping into any object. Secondly, a separate biological brain will be grown to be the thinking process within a robot head (called Morgui) which houses 5 separate sensory inputs.

What this means is that the brain of these robots will shortly be a biological brain, not a computer. All the brain will know is what it perceives from the robot body and all it will do will be to drive the robot body around or control the robot head respectively. The biological brain will, to all intents and purposes, be the brain of the robot. It will have no life, no existence outside its robotic embodiment.

Clearly this research alters our concept of what a robot is, particularly in terms of ethical and responsibility issues. If a role of animal research is to open up possibilities for future human trials, then in this case the research could well be opening a window on the ultimate possibility of human neurons being employed in a robot body. All the 'human' brain would know would be its life as a robot.

4 HUMAN APPLICATION

At the present time the general class of Brain-Computer Interfaces (BCIs) for humans, of one form or another, have been specifically developed for a range of applications including military weapon and drive systems, personnel monitoring and for games consoles. However, by far the largest driving force for BCI research to date has been the requirement for new therapeutic devices such as neural prostheses.

The most ubiquitous sensory neural prosthesis in humans is by far the cochlea implant (Fin and LoPresti, 2003). Here the destruction of inner ear hair cells and the related degeneration of auditory nerve fibres results in sensorineural hearing loss. As such, the prosthesis is designed to elicit patterns of neural activity via an array of electrodes implanted into the patient's cochlea, the result being to mimic the workings of a normal ear over a range of frequencies. It is claimed that some current devices restore up to approximately 80% of normal hearing, although for most recipients it is sufficient that they can communicate to a respectable degree without the need for any form of lip reading. The typically modest success of cochlea implantation is related to the ratio of stimulation channels to active sensor channels in a fully functioning ear. Recent devices consist of up to 32 channels, whilst the human ear utilises upwards of 30,000 fibres on the auditory nerve. There are now reportedly well over 10,000 of these prostheses in regular operation.

Studies investigating the integration of technology with the human central nervous system have varied from merely diagnostic to the amelioration of symptoms (Warwick and Gasson, 2004). In the last few years some of the most widely reported research involving human subjects is that based on the development of an artificial retina (Rizzo, 2001). Here, small electrode arrays have been successfully implanted into a functioning optic nerve. With direct stimulation of the nerve it has been possible for the otherwise blind recipient to perceive simple shapes and letters. The difficulties with restoring sight are though several orders of magnitude greater than those of the cochlea implant simply because the retina contains millions of photodetectors that need to be artificially replicated. An alternative is to bypass the optic nerve altogether and use cortical surface or intracortical stimulation to generate phosphenes (Dobelle, 2000).

Most invasive BCIs monitor multi-neuronal intracortical action potentials, requiring an interface which includes sufficient processing in order to relate recorded neural signals with movement intent. Problems incurred are the need to position electrodes as close as possible to the source of signals, the need for long term reliability and stability of interface in both a mechanical and a chemical sense, and adaptivity in signal processing to deal with technological and neuronal time dependence. However, in recent years a number of different collective assemblies of microelectrodes have been successfully employed both for recording and stimulating neural activity. Although themselves of small scale, nevertheless high density

connectors/transmitters are required to shift the signals to/from significant signal processing and conditioning devices and also for onward/receptive signal transmission.

Some research has focussed on patients who have suffered a stroke resulting in paralysis. The most relevant to this paper is the use of a '3rd generation' brain implant which enables a physically incapable brainstem stroke victim to control the movement of a cursor on a computer screen (Kennedy, 2000), (Kennedy, 2004). Functional Magnetic Resonance Imaging (fMRI) of the subject's brain was initially carried out to localise where activity was most pronounced whilst the subject was thinking about various movements. A hollow glass electrode cone containing two gold wires and a neurotrophic compound (giving it the title 'Neurotrophic Electrode') was then implanted into the motor cortex, in the area of maximum activity. The neurotrophic compound encouraged nerve tissue to grow into the glass cone such that when the patient thought about moving his hand, the subsequent activity was detected by the electrode, then amplified and transmitted by a radio link to a computer where the signals were translated into control signals to bring about movement of the cursor. With two electrodes in place, the subject successfully learnt to move the cursor around by thinking about different movements. Eventually the patient reached a level of control where no abstraction was needed – to move the cursor he simply thought about moving the cursor. Notably, during the period that the implant was in place, no rejection of the implant was observed; indeed the neurons growing into the electrode allowed for stable long-term recordings.

Electronic neural stimulation has proved to be extremely successful in other areas, including applications such as the treatment of Parkinson's disease symptoms. With Parkinson's Disease diminished levels of the neurotransmitter dopamine cause over-activation in the ventral posterior nucleus and the subthalamic nucleus, resulting in slowness, stiffness, gait difficulties and hand tremors. By implanting electrodes into the subthalamic nucleus to provide a constant stimulation pulse, the over activity can be inhibited allowing the patient, to all external intents and purposes, to function normally (Pinter et al., 1999).

5 BRAIN WITHIN A BRAIN

Ongoing research, funded by the UK Medical Research Council, is investigating how the onset of tremors can be accurately predicted such that merely a stimulation current burst is required rather than a constant pulsing (Gasson et al., 2005: pp.16/1-16/4). This has implications for battery inter-recharge periods as well as limiting the extent of in-body intrusive signalling. The deep brain stimulator can be used to collect local field potential (LFP) signals generated by the neurons around the deep brain electrodes (Gasson et al., 2005: pp.16/1-16/4). Determining the onset of events can be investigated by using fourier transforms to transfer the time based signal to a frequency based spectrogram to determine the change in frequency at the critical time period. However, in addition to that, the frequency changes in the period of time immediately prior to the tremor occurrence can give important information.

Fig.1 shows the results of an initial attempt to train an artificial neural network to indicate not only that a Parkinsonian tremor is present but also that one is very likely to occur in the near future. The aim of this research is that, once a reliable predictor has been obtained, the stimulating pulsing will only be enacted when a tremor is predicted, in order to stop the actual physical tremor occurring before it even starts in the first place.

The bottom trace in Fig.1 shows emg (muscular) signals, measured externally, associated with movement due to the tremors. It can be seen that the tremors in this incident actually start at around the 45 to 50 second point. The trace just above this indicates the corresponding electrical data measured as deep brain Local Field Potentials in the Sub-Thalamic Nucleus of the patient involved. It can be witnessed how, in this case, the electrical data takes on a different form (in terms of variance at least) at around the 45 to 50 second point. The four top plots meanwhile indicate the outputs from 4 differently structured artificial neural networks, based on multi-layer perceptrons with different numbers of neurons in the hidden (middle) layer.

It can be seen how, for each network, the output of the network goes high (logic 1) at the 45 to 50 second point, to indicate the presence of a Parkinsonian tremor. This is all well and good, what is important however is that the output of the networks also briefly goes high around the 30

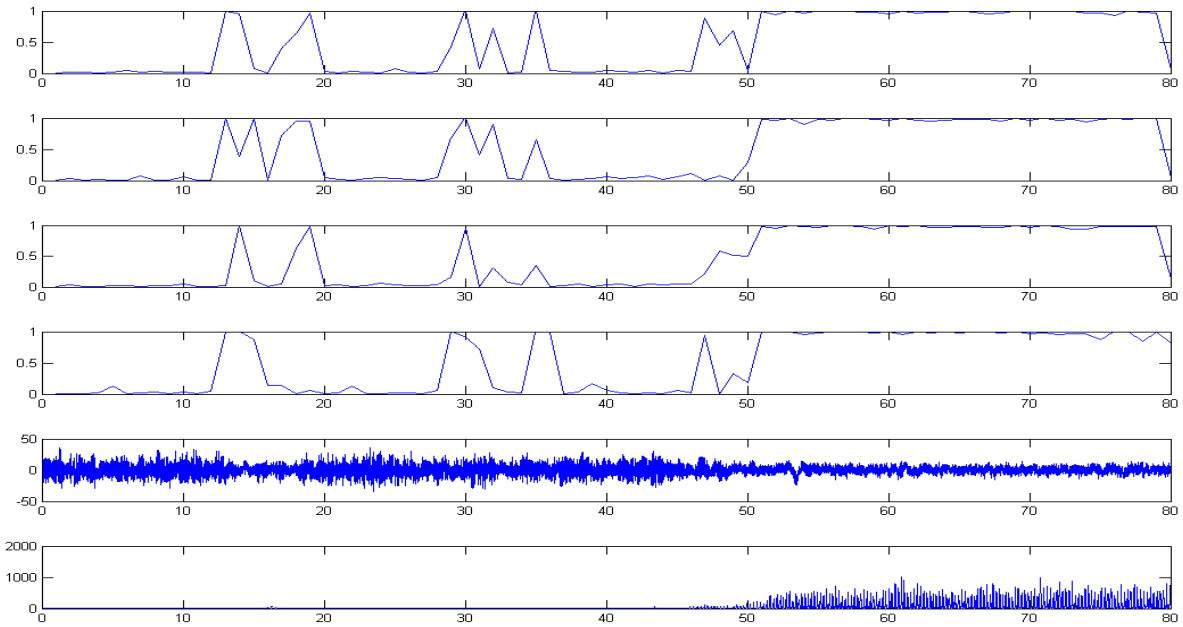

Figure 1: Time plot of the onset of a Parkisonian tremor incident with corresponding artificial neural network indicators.

second point and this can be seen as an indication of the fact that a tremor will shortly occur. Ongoing research is involved with selection of the type and number of inputs to the network, presently these being based on the energy spectrum in different frequency ranges. The networks are also being tested on considerable amounts of resting data, that is long periods of brain activity where no tremors at all actually occur in patients. Clearly the aim is that a network will not give false predictions of tremors.

In fact false positive predictions are not so much of a critical problem. The end result with a false positive is that a stimulation may occur when it is not strictly necessary. In any event no actual tremor would occur, which is indeed a good outcome, however unnecessary energy would have been used – in fact if numerous false predictions occurred the intelligent stimulator would tend toward the present 'blind' stimulator. Effectively the occasional false positive prediction is perhaps not a problem, unless it became a regular occurrence. The good news is that results show that the network can be readily tuned to avoid false positives anyway.

6 GENERAL IMPLANT STUDIES

Some of the most impressive human research to date has been carried out using the microelectrode array, shown in Figure 2. The individual electrodes are only 1.5mm long and taper to a tip diameter of less than 90 microns. Although a number of trials not using humans as a test subject have occurred (Branner and Normann, 2000), human tests are at present limited to two studies. In the second of these the array has been employed in a recording only role (Donoghue et al., 2002), (Donoghue et al., 2004), (Friehs et al., 2004), most notably recently as part of the 'Braingate' system. Essentially activity from a few neurons monitored by the array electrodes is decoded into a signal to direct cursor movement. This has enabled an individual to position a cursor on a computer screen, using neural signals for control combined with visual feedback. The first use of the microelectrode array (Figure 2) will be discussed in the following section as this has considerably broader implications which extend the capabilities of the human recipient.

A key selection point at the present time are what type of implant to employ, as several different possibilities exist, ranging from single electrode devices to multielectrode needles which contain electrode points at different depths to multielectrode arrays which either contain a number of electrodes which penetrate to the same depth (as in Figure 2) or are positioned in a banked/sloped arrangement. A further key area of consideration is the exact positioning of a BCI. In particular certain areas of the brain are, apparently, only really useful for monitoring purposes whilst others are more useful for stimulation.

Actually deriving a reliable command signal from a collection of captured neural signals is not necessarily a simple task, partly due to the complexity of signals recorded and partly due to time constraints in dealing with the data. In some cases however it can be relatively easy to look for and obtain a system response to certain anticipated neural signals – especially when an individual has trained extensively with the system. In fact neural signal shape, magnitude and waveform with respect to time are considerably different to the other signals that it is possible to measure in this situation.

If a greater understanding is required of neural signals recorded, before significant progress can be made, then this will almost surely present a major problem. This is especially true if a number of simultaneous channels are being employed, each requiring a rate of digitization of (most likely) greater than 20KHz in the presence of unwanted noise. For real time use this data will also need to be processed within a few milliseconds (100 milliseconds at most). Further, although many studies have looked into the extraction of command signals (indicating intent) from measured values, it is clear that the range of neural activity is considerable. Even in the motor area not only are motor signals present but so too are sensory, cognitive, perceptual along with other signals, the exact purpose of which is not clear – merely classifying them as noise is not really sufficient and indeed can be problematic when they are repeated and apparently linked in some way to activity.

It is worth stressing here that the human brain and spinal cord are linking structures, the functioning of which can be changed through electronic stimulation such as that provided via an electrode arrangement. This type of technology therefore offers a variety of therapeutic possibilities. In particular the use of implanted systems when applied to spinal cord injured patients, in whom nerve function is disordered, was described in (Warwick, 2004) as having the following potential benefits (among others):

1. Re-education of the brain and spinal cord through repeated stimulation patterns
2. Prevention of spinal deformity
3. Treatment of intractable neurogenic and other pain
4. Assisting bladder emptying
5. Improving bowel function
6. Treatment of spasticity
7. Improvement of respiratory function – assisting coughing and breathing
8. Reduction of cardiovascular maleffects
9. Prevention of pressure sores – possibly providing sensory feedback from denervated areas
10. Improvement and restoration of sexual function
11. Improved mobility
12. Improved capability in daily living, especially through improved hand, upper limb and truncal control

Sensate prosthetics is another growing application area of neural interface technology, whereby a measure of sensation is restored using signals from small tactile transducers distributed within an artificial limb (Fin and LoPresti, 2003). The transducer output can be employed to stimulate the sensory axons remaining in the residual limb which are naturally associated with a sensation. This more closely replicates stimuli in the original sensory modality, rather than forming a type of feedback using neural pathways not normally associated with the information being fed back. As a result it is supposed that the user can employ lower level reflexes that exist within the central nervous system, making control of the prosthesis more subconscious.

One final noteworthy therapeutic procedure is Functional Electrical Stimulation (FES), although it is debatable if it can be truly referred to as a BCI, however it aims to bring about muscular excitation, thereby enabling the controlled movement of limbs. FES has been shown to be successful for artificial hand grasping and release and for standing and walking in quadriplegic and paraplegic individuals as well as restoring some basic body functions such as bladder and bowel control (Grill and Kirsch, 2000). It must be noted though that controlling and coordinating concerted muscle movements for complex and generic tasks such as picking up an arbitrary object is proving to be a difficult, if not insurmountable, challenge.

In the cases described in which human subjects are involved, the aim on each occasion is to either restore functions since the individual has a physical problem of some kind or it is to give a new ability to an individual who has very limited motor abilities. In this latter case whilst the procedure can be regarded as having a therapeutic purpose, it is quite possible to provide an individual with an ability that they have in fact never experienced before. On the one hand it may be that whilst the individual in question has never previously experienced such an ability, some or most other humans have – in this

case it could be considered that the therapy is bringing the individual more in line with the "norm" of human abilities.

It is though also potentially possible to give extra capabilities to a human, to enable them to achieve a broader range of skills – to go beyond the "norm". Apart from the, potentially insurmountable, problem of universally deciding on what constitutes the "norm", extending the concept of therapy to include endowing an individual with abilities that allow them to do things that a perfectly able human cannot do raises enormous ethical issues. Indeed it could be considered that a cochlea implant with a wider frequency response range does just that for an individual or rather an individual who can control the curser on a computer screen directly from neural signals falls into this category. But the possibilities of enhancement are enormous. In the next section we consider how far things could be taken, by referring to relevant experimental results.

7 HUMAN ENHANCEMENT

The interface through which a user interacts with technology provides a distinct layer of separation between what the user wants the machine to do, and what it actually does. This separation imposes a considerable cognitive load upon the user that is directly proportional to the level of difficulty experienced. The main issue it appears is interfacing the human motor and sensory channels with the technology. One solution is to avoid this sensorimotor bottleneck altogether by interfacing directly with the human nervous system. It is certainly worthwhile considering what may potentially be gained from such an invasive undertaking.

Advantages of machine intelligence are for example rapid and highly accurate mathematical abilities in terms of 'number crunching', a high speed, almost infinite, internet knowledge base, and accurate long term memory. Additionally, it is widely acknowledged that humans have only five senses that we know of, whereas machines offer a view of the world which includes infra-red, ultraviolet and ultrasonic. Humans are also limited in that they can only visualise and understand the world around them in terms of a limited dimensional perception, whereas computers are quite capable of dealing with hundreds of dimensions. Also, the human means of communication, essentially transferring an electro-chemical signal from one brain to another via an intermediate, often mechanical medium, is extremely poor, particularly in terms of speed, power and precision. It is clear that connecting a human brain, by means of an implant, with a computer network could in the long term open up the distinct advantages of machine intelligence, communication and sensing abilities to the implanted individual.

As a step towards this more broader concept of human-machine symbiosis, in the first study of its kind, the microelectrode array (as shown in Figure 2) was implanted into the median nerve fibres of a healthy human individual (myself) in order to test *bidirectional* functionality in a series of experiments. A stimulation current direct onto the nervous system allowed information to be sent to the user, while control signals were decoded from neural activity in the region of the electrodes (Gasson et al., 2005:pp 365-375), (Warwick et al., 2003).

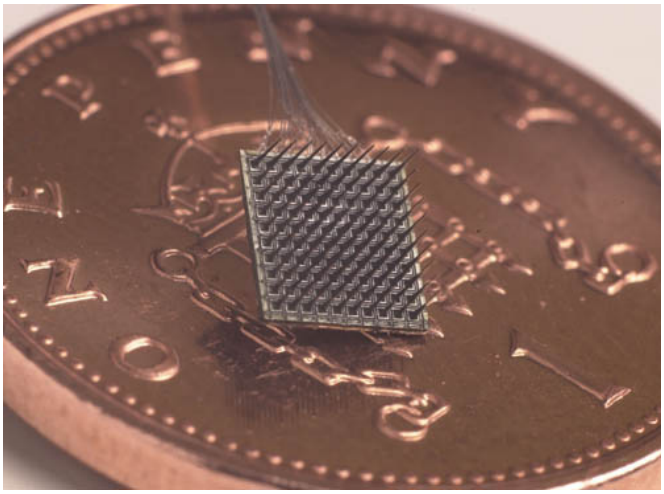

Figure 2: A 100 electrode, 4X4mm Microelectrode Array, shown on a UK 1 pence piece for scale.

In this way a number of experimental trials were successfully concluded (Warwick et al., 2004), (Warwick et al., 2005): In particular:

1. Extra sensory (ultrasonic) input was successfully implemented and made use of.
2. Extended control of a robotic hand across the internet was achieved, with feedback from the robotic fingertips being sent back as neural stimulation to give a sense of force being applied to an object (this was achieved between New York (USA) and Reading(UK))
3. A primitive form of telegraphic communication directly between the nervous systems of two humans was performed.
4. A wheelchair was successfully driven around by means of neural signals.
5. The colour of jewellery was changed as a result of neural signals – as indeed was the behaviour of a collection of small robots.

In each of the above cases it could be regarded that the trial proved useful for purely therapeutic reasons, e.g. the ultrasonic sense could be useful for an individual who is blind or the telegraphic communication could be very useful for those with certain forms of Motor Neurone Disease. However each trial can also be seen as a potential form of augmentation or enhancement for an individual. The question then arises as to how far should things be taken? Clearly enhancement by means of BCIs opens up all sorts of new technological and intellectual opportunities, however it also throws up a raft of different ethical considerations that need to be addressed directly.

8 ON STIMULATION

After extensive experimentation it was found that injecting currents below 80µA onto the median nerve fibers had little perceivable effect. Between 80µA and 100µA all the functional electrodes were able to produce a recognizable stimulation, with an applied voltage of 40 to 50 volts, dependant on the series electrode impedance. Increasing the current above 100µA had no apparent additional effect; the stimulation switching mechanisms in the median nerve fascicle exhibited a non-linear thresholding characteristic.

During this experimental phase, it was pseudo randomly decided whether a stimulation pulse was applied or not. The volunteer (myself), wearing a blindfold, was unaware of whether a pulse had been applied or not, other than by means of its effect in terms of neural stimulation. The user's accuracy in distinguishing between an actual pulse and no pulse at a range of amplitudes is shown in Figure 3.

In all subsequent successful trials, the current was applied as a bi-phasic signal with pulse duration of 200 µsec and an inter-phase delay of 100 µsec. A typical stimulation waveform of constant current being applied to one of the MEA's implanted electrodes is shown in Fig 4.

It was, in this way, possible to create alternative sensations via this new input route to the nervous system. Of the 5 enhancement features mentioned in the previous section, this one will be described, as an example, in further detail. Background information on the other enhancements can be found in a number of references, e.g. (Gasson et al., 2005:pp 365-375), (Warwick et al., 2003), (Warwick et al., 2004), (Warwick and Gasson, 2004).

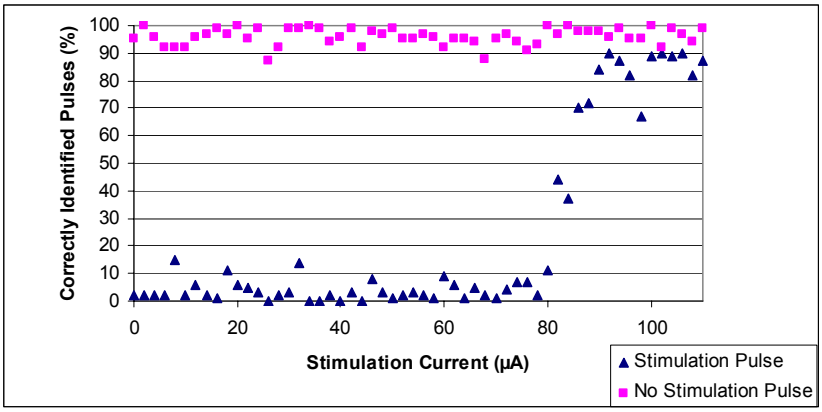

Figure 3: Effect of stimulation amplitude on the number of correctly identified pulses and absence of pulses (over 100 trials).

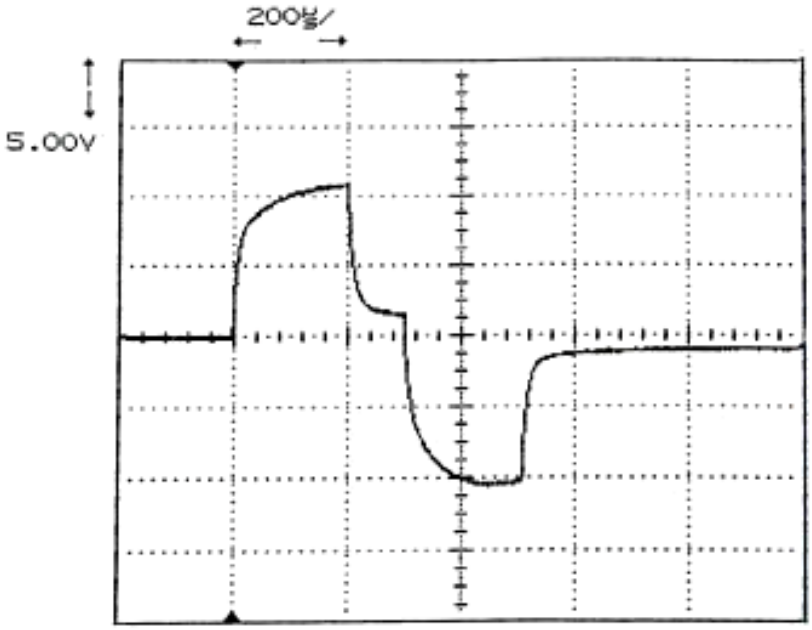

Figure 4: Voltage profile during one bi-phasic stimulation pulse cycle with a constant current of 80µA.

It must be reported that it took 6 weeks for my brain to repetitively recognize the stimulating signals accurately. This time period can be due to a number of contributing factors:

(a) The team had to learn which signals (what amplitude, frequency etc.) would be best in order to bring about a recognizable stimulation.

(b) The recipient's brain had to learn to recognize the new signals it was receiving.

(c) The bond between the recipient's nervous system and the implant was physically changing (becoming stronger).

9 EXTRA SENSORY EXPERIMENT

An experiment was set up to determine if the human brain is able to understand and successfully operate with sensory information to which it had not previously been exposed. Whilst it is quite possible to feed in such sensory information via a normal human sensory route, e.g. electromagnetic radar or infra-red signals are converted to visual, what we were interested in was feeding such signals directly onto the human nervous system, thereby bi-passing the normal human sensory input.

Ultrasonic sensors were fitted to the rim of a baseball cap (see Figure 5) and the output from these sensors, in the form of a proportional count, was employed to bring about a direct stimulation of the nervous system. Hence when no objects were in the vicinity of the sensors, no stimulation occurred, and as an object moved close by so the rate of stimulation pulses being applied increased in a linear fashion up to a pre-selected maximum rate. No increase in stimulation occurred when an object moved closer than 10cm to the sensors.

The ultrasonic sensors were open type piezoelectric ceramic transducers with conical metal resonators and operated at 40 KHz. These were used in a pair, one for transmit and one for receive, to give maximum sensitivity for small and distant objects. The most useful range for the experimentation was found to be 2 – 3m, this being also dependent on the size of object. A simple microcontroller was programmed to perform the echo ranging on the pair of transducers, and provide the range to the first detectable object only. This was translated into a stimulation pulse train, which operated on a single pin of the electrode array. Pins on the array had been tested for their suitability for stimulation by the earlier experimentation in which the recipient identified the presence or absence of stimulation pulse trains at various amplitudes and repetition frequencies.

Figure 5: Experimentation and testing of the ultrasonic baseball cap.

It was found that very little learning was required for the new ultrasonic sense to be used effectively and successfully – merely a matter of 5/6 minutes. This said it must be remembered that it had already taken several weeks for the recipient's brain to successfully, accurately recognize the current signals being injected.

As a result, in a witnessed experiment, the recipient, whilst wearing a blindfold, was able to move around successfully within a cluttered laboratory environment, albeit at a slower than normal walking pace. The sensory input was "felt" as a new form of sensory input (not as touch or movement) in the sense that the brain made a direct link between the signals being witnessed and the fact that these corresponded in a linear fashion to a nearby object.

10 CONCLUSIONS

External input-output interfaces with human and animal brains have been studied for many years. These are sometimes referred to as Brain-Computer Interfaces (BCIs) even though the interface may be external to the (human) body and its sensorimotor mechanism. In this paper an attempt has been made to put such systems in perspective. Emphasis has been placed on such interfaces that can be obtained by means of implanted devices through invasive surgery and actual direct neural connections. In particular a number of trials in this area have clearly shown the possibilities of monitoring, stimulating and enhancing brain functioning.

Although there is no distinct dividing line it is quite possible as far as humans are concerned to investigate BCIs in terms of those employed for direct therapeutic means and those which can have an enhanced role to play. It is clear that the interaction of electronic signals with the human brain can cause the brain to operate in a distinctly different manner. Such is the situation with the stimulator implants that are successfully used to counteract, purely electronically, the tremor effects associated with Parkinson's disease. Such technology can though potentially be employed to modify the normal functioning of the human brain and nervous system in a number of different ways.

The same stimulator, with slightly different positioning, has been shown to elicit feelings of sadness or happiness in the recipient. Given the nature of the intelligent stimulator described here it would appear to be possible to monitor, in real time, a human brain with a computer brain, and for the computer brain to predict when the human is going to feel sad – quite some time before they actually feel sad. In theory a signal could then be injected at

that time to make them feel happy, or at least to stop them actually ever feeling sad in the first place. Maybe this could be regarded as an electronic anti-depressant. There are of course questions about recreational use here – but this would need a deep brain implant which might well prove to be rather too onerous for most people.

Perhaps understandably, invasive BCIs are presently far less well investigated in University experiments than their external BCI counterparts. A number of animal trials have though been carried out and the more pertinent have been indicated here along with the relevant human trials and practice. In particular the focus of attention has been given to the embodiment of grown neural tissue within a technological body. Whilst only 1,000 or so neurons are involved this presents an interesting research area in a number of ways. But once the number of such neurons used increases 1,000 or 1,000,000-fold, it also raises enormous philosophical and ethical issues. For example is the robot 'thinking' and what rights should it have?

The potential for BCI applications for individuals who are paralysed is enormous, where cerebral functioning to generate command signals is functional despite the motor neural pathways being in some way impaired – such as in Lou Gehrig's disease. The major role is then either one of relaying a signal of intention to the appropriate actuator muscles or to reinterpret the neural signals to operate technology thereby acting as an enabler. In these situations no other medical 'cure' is available, something which presents a huge driver for an invasive implant solution for the millions of individuals who are so affected. Clearly though, bidirectional signalling is important, not only to monitor and enact an individual's intent but also to provide feedback on that individual's resultant interaction with the real world. For grasping, walking and even as a defensive safety stimulant, feedback is vital. This paper has therefore focussed on such studies.

Where invasive interfaces are employed in human trails, a purely therapeutic scenario often exists. In a small number of instances, such as use of the microelectrode array as an interface, an individual has been given different abilities, something which opens up the possibilities of human enhancement. These latter cases however raise more topical ethical questions with regard to the need and use of a BCI. What might be seen as a new means of communication for an individual with an extreme form of paralysis or a new sensory input for someone who is blind, opening up a new world for them, can also be seen as an unnecessary extra for another individual, even though it may provide novel commercial opportunities. What is therapy for one person may be regarded as an enhancement or upgrading for another.

Whilst there are still many technical problems to be overcome in the development of BCIs, significant recent experimental results have indicated that a sufficient technological infrastructure now exists for further major advances to be made. Although a more detailed understanding of the underlying neural processes will be needed in the years ahead, it is not felt that this will present a major hold up over the next few years, rather it will provide an avenue of research in which many new results will shortly appear through trials and experimentation, possibly initially through animal studies although it must be recognised that it is only through human studies that a full analysis can be made and all encompassing conclusions can be drawn. Nevertheless the topic opens up various ethical questions that need to be addressed and as such, research in this area should, I believe, only proceed in light of a pervasive ethical consensus.

ACKNOWLEDGEMENTS

The Author would like to acknowledge the considerable assistance and input of the Consultant Neurosurgeons Mr. Peter Teddy, Mr. Amjad Shad, Mr. Ali Jamous and Mr. Tipu Aziz and researchers Iain Goodhew, Mark Gasson, Ben Whalley and Ben Hutt. Ethical approval for the author's research was obtained from the Ethics and Research Committee at the University of Reading, UK and with regard to the neurosurgery aspect, the Oxfordshire National Health Trust Board overseeing the Radcliffe Infirmary, Oxford, UK.

REFERENCES

Branner, A. and Normann, R. (2000) A multielectrode array for intrafascicular recording and stimulation in the sciatic nerve of a cat, *Brain Research Bulletin*, Vol.51, pp.293-306.

Chapin, J.K. (2004) Using multi-neuron population recordings for neural prosthetics. *Nature Neuroscience*, 7, 452-454.

Carmena, J., Lebedev, M., Crist, R., O'Doherty, J., Santucci, D., Dimitrov, D. Patil, P., Henriquez, C. and Nicolelis, M. (2003) Learning to control a brain-

machine interface for reaching and grasping by primates, *Plos Biology*, Vol.1, Issue.2, article number e2.
Dobelle, W. (2000) Artificial vision for the blind by connecting a television camera to the visual cortex, ASAIO J, Vol.46, pp.3-9.
Donoghue, J. (2002) Connecting cortex to machines: recent advances in brain interfaces, *Nature Neuroscience Supplement*, Vol.5, pp.1085-1088.
Donoghue, J., Nurmikko, A., Friehs, G. And Black, M. (2004) Development of a neuromotor prosthesis for humans, Chapter 63 in *Advances in Clinical Neurophysiology, Supplements to Clinical Neurophysiology*, Vol.57, pp.588-602.
Finn, W. and LoPresti, P. (eds.) (2003) Handbook of Neuroprosthetic methods, CRC Press.
Friehs, G., Zerris, V., Ojakangas, C., Fellows, M. and Donoghue, J. (2004) Brain-machine and brain-computer interfaces, *Stroke*, Vol.35, Issue.11, pp.2702-2705.
Gasson, M., Hutt, B., Goodhew, I., Kyberd, P. and Warwick, K. (2005) Invasive neural prosthesis for neural signal detection and nerve stimulation, Proc. International Journal of Adaptive Control and Signal Processing, Vol.19, No.5, pp.365-375.
Gasson, M., Wang, S., Aziz, T., Stein, J. and Warwick, K. (2005) Towards a demand driven deep brain stimulator for the treatment of movement disorders, Proc. 3rd IEE International Seminar on Medical Applications of Signal Processing, pp.16/1-16/4.
Grill, W. and Kirsch, R. (2000) Neuroprosthetic applications of electrical stimulation, *Assistive Technology,* Vol.12, Issue.1, pp.6-16.
Hinterberger, T., Veit, R., Wilhelm, B., Weiscopf, N., Vatine, J. and Birbaumer, N. (2005) Neuronal mechanisms underlying control of a brain-computer interface, *European Journal of Neuroscience*, Vol.21, Issue.11, pp.3169-3181.
Kennedy, P., Bakay, R., Moore, M., Adams, K. and Goldwaith, J. (2000) Direct control of a computer from the human central nervous system, *IEEE Transactions on Rehabilitation Engineering*, Vol.8, pp.198-202.
Kennedy, P., Andreasen, D., Ehirim, P., King, B., Kirby, T., Mao, H. and Moore, M. (2004) Using human extra-cortical local field potentials to control a switch, *Journal of Neural Engineering*, Vol.1, Issue.2, pp.72-77.
Mann, S. (1997) Wearable Computing: A first step towards personal imaging, *Computer*, Vol. 30, Issue.2, pp. 25-32.
Nicolelis, M., Dimitrov, D., Carmena, J., Crist, R., Lehew, G., Kralik, J. and Wise, S. (2003) Chronic, multisite, multielectrode recordings in macaque monkeys, *Proc. National Academy of the USA*, Vol.100, Issue.19, pp.11041-11046.
Penny, W., Roberts, S., Curran, E., and Stokes, M. (2000) EEG-based communication: A pattern recognition approach, *IEEE Transactions on Rehabilitation Engineering*., Vol. 8, Issue.2, pp. 214-215.
Pinter, M., Murg, M., Alesch, F., Freundl, B., Helscher, R. And Binder, H. (1999) Does deep brain stimulation of the nucleus ventralis intermedius affect postural control and locomotion in Parkinson's disease?, *Movement Disorders*, Vol.14, Issue.6, pp.958-963.
Reger, B., Fleming, K., Sanguineti, V., Simon Alford, S., Mussa-Ivaldi, F. (2000) Connecting Brains to Robots: an artificial body for studying computational properties of neural tissues, *Artificial life*, Vol.6, Issue.4, pp.307-324.
Rizzo, J., Wyatt, J., Humayun, M., DeJuan, E., Liu, W., Chow, A., Eckmiller, R., Zrenner, E., Yagi, T. and Abrams, G. (2001) Retinal Prosthesis: An encouraging first decade with major challenges ahead, *Opthalmology,* Vol.108, No.1.
Roitberg, B. (2005) Noninvasive brain-computer interface, *Surgical Neurology*, Vol.63, Issue.3, p.195.
Warwick, K. (2004) I Cyborg, University of Illinois Press.
Warwick, K., Gasson, M., Hutt, B., Goodhew, I., Kyberd, P., Andrews, B., Teddy, P., Shad, A. (2003) The application of implant technology for cybernetic systems. *Archives of Neurology*, 60 (10), pp.1369-1373.
Warwick, K., Gasson, M., Hutt, B., Goodhew, I., Kyberd, P., Schulzrinne, H. and Wu, X. (2004) Thought Communication and Control: A First Step Using Radiotelegraphy, *IEE Proceedings on Communications,* Vol.151, No. 3, pp 185-189.
Warwick, K., Gasson, M., Hutt, B. and Goodhew, I. (2005) An Attempt to Extend Human Sensory Capabilities by means of Implant Technology. Proc. IEEE Int. Conference on Systems, Man and Cybernetics, Hawaii.
Wolpaw, J., McFarland, D., Neat, G. and Forheris, C. (1990) An EEG based brain-computer interface for cursor control, *Electroencephalogr. Clin. Neurophysiol*., Vol.78, pp.252-259.
Pan, S., Warwick, K., Gasson, M., Burgess, J., Wang, S., Aziz, T. and Stein, J. (2007) Prediction of parkinson's disease tremor onset with artificial neural networks", Proc. IASTED Conference BioMed 2007, Innsbruck, Austria, pp.341-345.
Warwick, K. (2007) The promise and threat of modern cybernetics, Southern Medical Journal, Vol.100, Issue.1, pp.112-115.
Warwick, K. and Gasson, M.N. (2004) Practical Interface Experiments with Implant Technology, in "Computer Vision in Human-Computer Interaction", Sebe, N., Lew, M.S and Huang, T.S. (eds.), Lecture Notes in Computer Science, Vol. 3058, pp.7-16.Xie, S., Yang, Z. and Yang, Y. (2004) Brain-computer interface based on event-related potentials during imitated natural reading, International Journal of Psychology, Vol.39, Issue.5-6, Supplement S., p.138.
Yoo, S., Fairneny, T., Chen, N., Choo, S., Panych, L., Park, H., Lee, S. and Jolesz, F. (2004) Brain-computer interface using fMRI: spatial navigation by thoughts, *Neuroreport*, Vol.15, Issue.10, pp.1591-1595.
Yu, N., Chen, J. and Ju, M. (2001) Closed-Loop Control of Quadriceps/Hamstring activation for FES-Induced Standing-Up Movement of Paraplegics, *Journal of Musculoskeletal Research*, Vol. 5, No.3, pp.173-184.

ANALYSIS AND MODELS OF BRAIN EPILEPTIC ACTIVITIES

Fernando Henrique Lopes da Silva
University of Amsterdam, The Netherlands

Abstract: The essence of epilepsy is the sudden occurrence of a qualitative change in the behaviour of neuronal networks of some specific areas of the brain. In general we may assume that neuronal networks possess multistable dynamics. We may simplify this concept considering the case that a neuronal network may display, at least, two dynamical states: an interictal state characterised by a normal on-going neural activity, as revealed in the Eletcroencephalogram of Magnetoencephalogram (EEG, MEG), that may be apparently random, and another one – the ictal state - that is characterised by the sudden occurrence of synchronous oscillations, most commonly with large amplitude. The latter becomes manifest as a paroxysmal change of behaviour and /of the state of consciousness of a patient, i.e. an epileptic seizure. In the terminology of the mathematics of non-linear systems, we may state that a neuronal network behaves as a bistable system with two attractors, to which the system converges depending on initial conditions and on the system's parameters.

We propose schematically that the transition between the normal on-going to the seizure activity can take place according to three basic models: Model I – a transition may occur due to random fluctuations of some system's parameters. These transitions are thus unpredictable. Models II and III – a transition may result from a gradual change of some unstable parameters, either due to endogenous (model II) or exogenous (model III). In these cases the change of parameter values causes a deformation of the attractor resulting in a transition from the basin of the attractor corresponding to the normal state, to the attractor corresponding to the seizure dynamical state. Some experimental findings obtained in different cases of epilepsy, both in human and in animals, are compatible with each of these 3 models. Some examples of these cases are illustrated.

BRIEF BIOGRAPHY

Fernando Henrique Lopes da Silva received his Medical Degree from the University of Lisbon in 1959, got his Ph.D. from the University of Utrecht in 1970, and in 1980 was appointed Full Professor of General Physiology at the Faculty of Science at the University of Amsterdam (since 2002 part of the Swammerdam Institute for Life Sciences). From 1993 to 2000 he was Director of the newly created Institute of Neurobiology of the University of Amsterdam, and member of the Scientific Directorate of the Graduate School Neurosciences Amsterdam. In 2000, when he reached the retirement age of 65, he became Emeritus Professor of the same University, and has at present a free-lance contract with the Swammerdam Institute for Life Sciences.

Since 1970, he supervised a large number of student trainees from different Universities and Faculties: Medical, Biology, Sciences, (Bio-medical) Engineering. Supervised 65 Ph.D. students (up to December 2006).

His research interests are centred on the biophysical aspects of electrical activity of the brain and the functional organization of neuronal networks, namely of the cerebral cortex and the limbic system, with a special interest in the generation and functional significance of brain rhythmic activities. He published more than 220 papers in peer-reviewed journals and contributed Chapters to 10 multi-authored books (of 6 he is co-editor), among which the Handbook "Electroencephalography: Basic principles, clinical applications and related fields", Niedermeyer, E. and Lopes da Silva, F.H. (Eds), published by Lippincott, Williams and Wilkins, Baltimore; 5 Editions: 1982, 1987, 1993, 1998, 2004. In addition he contributed chapters to to the Encyclopedia of Neuroscience (George Adelman, Barry H. Smith. Eds), Elsevier Science, 2003 (3rd edition), to the Encyclopedia of the Human Brain (Ed. V. S. Ramachandran), Academic Press, 2002, and to The Handbook of Brain Theory and Neural Networks (Ed. Michael A. Arbib), The MIT Press, 2003 (2nd edition).

Selection of Scientific Awards

- 1975 He received the Winkler Medal from the Netherlands Association for Neurology for scientific contributions in the field of neurosciences.
- 1985 Elected member of the Royal Netherlands Academy of Arts and Sciences.
- 1990 "Lord Adrian" Lecturer at the 12th World Congress of Electroencephalography and Clinical Neurophysiology in Rio de Janeiro, Brazil.
- 1992 Honorary President of the VIIth European Congress of Clinical Neurophysiology, Budapest, Hungary.
- 1995 Honorary Life Member of The British Society for Clinical Neurophysiology (Formerly The EEG Society), London, United Kingdom.
- 1997 Doctor Honoris Causa of the University of Lisbon (Portugal).
- 1997 Special "Berger" Lecturer at the 14th International Congress of EEG and Clinical Neurophysiology in Florence, Italy.
- 1999 Recipient of the Herbert H. Jasper Award, selected by the American Clinical Neurophysiology Society for his "lifetime of outstanding contributions to the field of clinical neurophysiology.''
- 2000 Recipient of the 'Storm van Leeuwen/ Magnus Prize' of the Dutch Society of Clinical Neurophysiology.
- 2000 Honorary member of the Portuguese Society of Electroencephalography and Clinical Neurophysiology.
- 2002 Recipient of the Ragnar Granit Prize for his work on the field of Bioelectromagnetism.
- 2002 Doctor Honoris Causa of the University of Porto (Portugal).
- 2004 Recipient of the first Prize "Universidade de Coimbra" for a (sic) "person of Portuguese nationality who has made a particular relevant and innovative contribution in the fields of culture or science."

General Honors

- 2000 High Officer of the Order of Santiago da Espada, for outstanding achievements in the field of Science/Art/Literature, awarded by the President of the Republic of Portugal.
- 2001 Knight of the Order of the 'Nederlandse Leeuw' awarded by the Queen of the Netherlands in appreciation for his achievements in science.

FROM THE BENCH TO THE BEDSIDE

The Role of Semantics in Enabling the Vision of Translational Medicine

Vipul Kashyap
Partners HealthCare System, Clinical Informatics R&D, USA

Abstract: Biomedical research and healthcare clinical transactions are generating huge volumes of data and information. At the same time, the results of biomedical research in the form of new molecular diagnostic tests and therapies are being increasingly used in the context of clinical practice. There is a critical need to speed "translation" of genomic research insights into clinical research and practice. In this talk, we will discuss challenges faced by a healthcare enterprise in realizing the vision of Translational Medicine, such as:

- The need to create structured and semantic representations of genotypic and phenotypic data such as clinical observations and molecular diagnostic tests.
- The need for cost-effective and incremental data integration for combining genotypic and phenotypic information at the point of care.
- The need for actionable decision support for suggesting molecular diagnostic tests and therapies in the context of clinical care.
- The need for knowledge update, propagation and consistency to keep abreast of the rapid pace of knowledge discovery being witnessed in the life sciences, a crucial pre-requisite to reduce the cost of knowledge acquisition and maintenance.

Semantics-based approaches to address the above-mentioned challenges, including the applicability of semantic web standard (RDF, OWL, Rules); and issues related to the value proposition of these technologies will be presented.

BRIEF BIOGRAPHY

Vipul Kashyap, PhD is a Senior Medical Informatician in the Clinical Informatics Research & Development group at Partners HealthCare System and is currently the chief architect of a Knowledge Management Platform that enables browsing, retrieval, aggregation, analysis and management of clinical knowledge across the Partners Healthcare System. Vipul received his PhD from the Department of Computer Science at Rutgers University in New Brunswick in the area of metadata and semantics-based knowledge and information management. He is also interested in characterization of the value proposition of semantic technologies in the enterprise context. Before coming to Partners, Vipul has held positions at MCC, Telcordia (Bellcore) and was a fellow at the National Library of Medicine. Vipul has published 2 books on the topic of Semantics, 40-50 articles in prestigious conferences and journals; and has participated in panels and presented tutorials on the topic of semantic technologies. Vipul sits on the technical advisory board of an early stage company developing semantics-based products, and represents Partners on the W3C advisory committee and the HealthCare Information Technology Standards Panel (HITSP).

THE CANCER INFORMATICS ECOSYSTEM

A Case Study in the Accretion of Federated Systems based on Service Oriented Architectures, Semantic Integration and Computing Grids

David Hall
Research Triangle Institute in North Carolina, USA

Abstract: Information technology is playing an increasingly critical role in health and life sciences research due to the profound expansion in the scope of research projects in the post-genomic age. Robust data management and analysis systems are becoming essential enablers of these studies. Driven by funding agency requirements, funding opportunities, and grass roots organizing, efforts are underway to develop standards and technologies to promote large-scale integration of publicly-funded systems and databases including infrastructure developed for individual studies. Predicted benefits include an enhanced ability to conduct meta-analyses, an increase in the usable lifespan of data, a funding agency-wide reduction in the total cost of IT infrastructure, and an increased opportunity for the development of third party software tools. This presentation will critically examine efforts towards developing publicly-accessible interoperable and distributed production systems in the health and life sciences via ontologies, formal metadata, service oriented architectures, and grid computing models with a focus on several projects under the direction of the author in the area of cancer informatics.

BRIEF BIOGRAPHY

David Hall is a Senior Software Project Leader at RTI International based in North Carolina, USA. He leads teams of up to 30 developers implementing computer systems that support large biomedical and biotechnological research enterprises in cancer research, drug discovery, genetic epidemiology, and plant biotechnology. His area of interest is the practical application of bioinformatics and medical informatics methods, technologies, and standards in the development of production software. Particular topics of interest include data visualization, semantic integration, systems integration, and high performance computing. Recent clients include the US National Institutes of Health, GlaxoSmithKline, Syngenta, and Duke University. Data systems developed by David's group manage clinical and research data for nearly one million patients. Applications include data warehouses, metadata registries, workflow systems, high resolution image databases, analytical applications, and web services. David is currently Principal Investigator of the Informatics Support Center for the National Cancer Institute's Breast and Colon Cancer Family Registries. He holds a Ph.D. in Genetics from the University of Georgia and a B.S. in Computer Science from Wake Forest University.

ICT AND PERSONS WITH DISABILITIES
The Solution or the Problem?

Albert M. Cook
Faculty of Rehabilitation Medicine, University of Alberta, Edmonton Alberta, Canada
al.cook@ualberta.ca

Keywords: Assistive technologies, information and computer technologies, persons with disabilities.

Abstract: In order to lead full and productive lives, persons with disabilities need to have the same access to information and communication systems as the rest of the population. Advances in information and communication technologies (ICT) are occurring quickly, and the capability of technologies to meet the needs of persons with disabilities is growing daily. Future developments in assistive technologies (AT) and the successful application of these technologies to meet the needs of people who have disabilities are dependent on exploitation of these ICT advances. AT also involves the development of specialized interfaces such as the brain computer interface (BCI), adaptive interfaces that accommodate for changes in the user's physical skills, cognitive interfaces that allow understanding of the human technology interface by individuals with intellectual disabilities and systems that accommodate for user needs based on environmental sensing (e.g., GPS interfaces) and downloading of profiles to meet specific user needs. Universal Design (or design for all) calls for the design of products and environments to be usable by all people, to the greatest extent possible, without the need for adaptation or specialized design. In the physical world this often means ramps, curb cuts and other adaptations to the built environment to accommodate individuals who have disabilities. In the ICT world the barriers to access are technological, and the goal for ICT universal design is to have an environment with enough embedded intelligence to be easily adaptable to the varying cognitive, physical and sensory skills of a wide range of individual's in order to meet their productivity, leisure and self care needs. If ICT advances are not adaptable enough to be accessible to persons with disabilities it will further increase the disparity between those individuals and the rest of the population leading to further isolation and economic disadvantage. On the other hand, availability of these technologies in a transparent way will contribute to full inclusion of individuals who have disabilities in the mainstream of society.

BRIEF BIOGRAPHY

Dr. Albert Cook is Professor of Speech Pathology and Audiology and currently Dean of the Faculty of Rehabilitation Medicine and Chair of the Health Sciences Council at the University of Alberta. Dr. Cook has worked with interdisciplinary teams to develop assistive devices and to assess the effectiveness of technology being used by persons with disabilities. Dr. Cook is also associated with the I CAN Centre the Glenrose Rehabilitation Hospital. He was formerly Professor of Biomedical Engineering at California State University, Sacramento where he established the graduate program in biomedical engineering and directed it for 12 years. He also served as Co-Director of the Assistive Device Center in Sacramento, California, helping over 500 persons with disabilities to identify and obtain assistive technologies.

He received his Bachelor of Science in Electrical Engineering at the University of Colorado, a Masters in Bioengineering and his doctorate from the University of Wyoming He is a member of Tau Beta Pi, Phi Kappa Phi and Gold Key honorary societies.

Dr. Cook co-authored with Janice Polgar, OTR, Cook and Hussey's Assistive Technologies: Principles and Practice 3nd edition, published in October 2007 by Elsevier. He has co-edited three other textbooks with John Webster and others and has written numerous chapters in rehabilitation and biomedical engineering texts and monographs.

Dr. Cook's research interests include augmentative and alternative communication, biomedical instrumentation and assistive technology design, development and evaluation. His most recent

research has focussed on the use of robotics with young children who have severe disabilities to develop and assess cognitive and linguistic skills. He has US and foreign patents and numerous publications and conference presentations in these areas. He has been principal investigator on research and training grants in augmentative communication, assistive technologies and biomedical engineering.
Dr. Cook is Past-President and Fellow of RESNA, a major professional society for assistive technology practitioners in North America. He has also served in national united States positions in the Institute of Electrical and Electronic Engineers Engineering in Medicine and Biology Society, the American Society for Engineering Education, the Biomedical Engineering Society, the International Society for Augmentative and Alternative Communication and the Association for the Advancement of Medical Instrumentation. Dr. Cook is a registered professional engineer (electrical) in California.

1 ICT AND PERSONS WITH DISABILITIES TECHNOLOGY AND PROGRESS

Societal Progress requires change much of which is accomplished through advances in technology. In his book, *A Short History of Progress*, Ronald Wright *(*2004) points out that this characteristic has been true for millions of years as societies have advanced through greater utilization of technology.

Wright goes on to describe the problems that technology typically creates such as over consumption, environmental ruin, and separation of classes. These problems are amplified for people who have disabilities, and they lead to a gap in the access to work, self care and community participation for persons with disabilities compared to the general population. Since people with disabilities often depend on technologies for societal participation, the lack of availability of accessible technology or the obsolescence of accessible technologies isolates them further. This is an extension of the concept of the "digital divide" that separates people along socioeconomic lines based on their access to ICT. I refer to it as the "disability gap".

2 ADVANCES IN INFORMATION AND COMMUNICATION TECHNOLOGIES (ICT)

The 21st Century is characterized by a continuous move from a machine-based to a knowledge based economy (Ungson & Trudel, 1999). In this shift, the basis of competence is changing to knowledge skills from machine skills. Information currently amounts to 75% of value added to products This will continually increase, and connectivity will be the key to business success. There is also a move from a regional or national scope of business influence to a global scope, in which virtual networks dictate organizational structures.

Key players in business development are becoming communication suppliers with the move from host-based to network based systems. Telephone, cable TV and internet service providers control commercial growth. Along with these changes networks will become more graphically-based moving increasingly from text-based systems. In order to lead full and productive lives, persons with disabilities need to have the same access to this new information and communication system as the rest of the population.

2.1 What Can we Expect from Technology in the Next 20 Years?

The cost of information technology is continually dropping for comparable or increased computing power and speed. There is also a greater understanding of the biological/physical interface for the control of computers. The human computer interface (HCI) is being developed to be more human-like, more user oriented and more intelligent-providing additional capabilities for searching, processing and evaluating information.

There are a number of changes that are likely to occur over the next few years (Applewhite, 2004). There will be an increase in automated transactions between individuals and organizations enabling people to complete all transactions without face-toface interactions. It is expected that we will achieve equalized access to the web and information between the developed and developing world. Embedded systems will dramatically increase with application such as "intelligence in the doorknob" that recognizes the owner and doesn't require key manipulation. We are likely to see much greater

understanding of the biological to physical interface for the control of computers.

2.2 Changes in Mainstream Tech with AT Implications

There are many examples of emerging mainstream technologies with potential for assisting people with disabilities to access ICT systems. A few of these are described in this section.

Display-based assistive technologies present an array of choices for a user to select from (Cook & Polgar, 2007). This often referred to as scanning since the choices are highlighted sequentially and then chosen using some sort of gross movement. One of the problems associated with this approach is that there must be a physical display for making selections. This often requires the overall system to be larger and more bulky or places a display between a user and a communication partner. A new development is a direct retinal display that creates image that overlays view of real object (Lewis, 2004). The retinal display is low powered because it is shined on retina directly. Scanning light into the eye allows the image to overlay an object such as a communication partner's face-enabling eye contact and small size. The scanning array could be the retinal image, since display scans across the retina power levels can be kept low kept low for safety.

Another development is 3-D displays that create a more intuitive view of objects, events and activities (Lewis, 2004). This type of display may be helpful to individuals who have cognitive disabilities. It might also create new challenges for individuals with visual limitations.

Embedded automatic speech recognition is being developed for PDAs because of the need for keyboards with more and more functions and the limitations of very small keyboards (Kumagai, 2004). This feature could be very useful to reduce individuals who have limited hand function or for those who cannot see the keyboard to make entries.

3 MEETING THE ICT NEEDS OF PERSONS WITH DISABILITIES

Over the centuries, our ability to make tools is what distinguishes us as human, but our tools ultimately control us by making us dependent on them (Wright, 2004). This dependence is less optional for people who have disabilities

3.1 Impact of Technology Advances on People who have Disabilities

Technology advances increase the gap between people who have disabilities and those who don't (Wright, 2004). All societies become hierarchical with an upward concentration of wealth (including aggregations of technology tools) that ensures that "there can never be enough to go around", and this disparity contributes to the "digital divide" and the "disability gap". As advances occur more quickly, the gap widens faster and the people who are poor and/or disabled loose out even more completely and faster. This is a characteristic of cultural and societal "progress" over centuries-technology drives change, and creates both positive and negative outcomes in the process

The prognosis is not good for people with disabilities unless there is considerable effort to keep them connected to ICT and thereby to commerce, employment and personal achievement. There two fundamental approaches to this problem (1) make mainstream technologies accessible to people who have disabilities, or (2) design special purpose technologies specifically for people with disabilities. The former approach is referred to as *universal design* or *design for all*. The second approach utilizes *assistive technologies*.

3.2 Implications for Assistive Technologies

Access to ICT for people with disabilities is a significant global problem, and it has major implications for assistive technologies. There is a constant challenge to keep ICT systems accessible to persons who have disabilities as mainstream advances occur and adaptations become potentially incompatible with the new systems. Communication technologies change rapidly, and each change may result in the need to re-design accessible interfaces. We are closer to goal of having assistive technology adaptations available when the mainstream consumer product ships, but there are still many problems with "workarounds" necessary to make mainstream operating system, productivity software and internet access accessible to people with disabilities.

Development and maintenance of access to ICT must be driven by the needs of people with disabilities. Developments which broaden the scope, applicability and usability of the human technology

interface will be driven, at least in part by the needs of people who have disabilities.

The Internet (e-mail and chat rooms) have the advantage of anonymity, and this can be a major benefit to individuals who have disabilities. Because the person's disability is not immediately visible, people who have disabilities report that they enjoy establishing relationships with people who experience them first as a person and then learn of their disability. For example, Blackstone, (1996) describes some of the advantages of e-mail for individuals who have disabilities. Since the receiver of the message reads it at a later time composition can be at a slower speed. The person with a disability can communicate with another person without someone else being present, establishing a greater sense of privacy than situations in which an attendant is required. It is also possible to work form any location-avoiding some transportation problems

3.3 Universal Design

Increasingly, commercial products are being designed to be usable by all people, to the greatest extent possible, without the need for adaptation or specialized design (NC State University, The Center for Universal Design, 1997).

3.3.1 General Principles of Universal Design

Features are built into products to make them more useful to persons who have disabilities (e.g., larger knobs; a variety of display options--visual, tactile, auditory; alternatives to reading text--icons, pictures) are built into the product. This is much less expensive than modifying a product after production to meet the needs of a person with a disability. The North Carolina State University Center for Universal Design, in conjunction with advocates of universal design, have compiled a set of principles of universal design, shown in Box 1. This center also maintains a Web site on universal design (www.design.ncsu.edu/cud).

3.3.2 Universal Design for ICT

In universal design for ICT the barriers are technological rather than political and economic barriers that characterize architectural and commercial product design (Emiliani, 2006). The goal of universal design for ICT is to have an environment with enough embedded intelligence to be easily adaptable. The features of future information services are that there will be no clearly predefined service and little distinction between interpersonal communication and access to information. Services will need to be highly interactive, inherently multimedia, sensory multimodal (i.e., access via auditory or visual means is equally possible). To achieve this cooperation between users or representatives of users is critical in a variety of contexts of use. The overall goal is to have access to information involving communities of users with a wide range of motor, sensory and cognitive skills.

ONE: EQUITABLE USE
The design is useful and marketable to people with diverse abilities.
TWO: FLEXIBILITY IN USE
The design accommodates a wide range of individual preferences and abilities.
THREE: SIMPLE AND INTUITIVE USE
Use of the design is easy to understand, regardless of the user's experience, knowledge, language skills, or current concentration level.
FOUR: PERCEPTIBLE INFORMATION
The design communicates necessary information effectively to the user, regardless of ambient conditions or the user's sensory abilities.
FIVE: TOLERANCE FOR ERROR
The design minimizes hazards and the adverse consequences of accidental or unintended actions.
SIX: LOW PHYSICAL EFFORT
The design can be used efficiently and comfortably and with a minimum of fatigue.
SEVEN: SIZE AND SPACE FOR APPROACH AND USE
Appropriate size and space is provided for approach, reach, manipulation, and use regardless of user's body size, posture, or mobility.

Box 1: Principles of Universal Design From North Carolina State University, The Center for. Universal Design, 1997.

In addition to Universal Design for ICT, access to capabilities of mainstream technologies includes individualized assistive technologies that are easily – customized. This in return requires an increased understanding of the biological/physical interface for the control of assistive technologies and expanded availability of embedded systems networks.

3.4 A Working Definition of Assistive Technologies

The *International Classification of Functioning, Disability and* Health (ICF) is a system developed by the World Health Organization (WHO) that is designed to describe and classify health and health related states. These two domains are described by

body factors (body structures and functions) and individual and societal elements (activities and participation) (WHO, 2001). The ICF recognizes two contextual factors that modify health and health related states: the environment and personal factors (WHO, 2001). Environmental elements include assistive technologies in relation to activities of daily living, mobility, communication, religion and spirituality as well as in specific contexts such as education, employment and culture, recreation and sport (WHO, 2001). Other environmental elements such as access to public and private buildings, and the natural and built outdoor environments, also have implications for assistive technologies.

A commonly used definition of assistive technology is from the Technical Assistance to the States Act in the United States (Public Law (PL) 100-407): ***Any item, piece of equipment or product system whether acquired commercially off the shelf, modified, or customized that is used to increase, maintain or improve functional capabilities of individuals with disabilities.***

3.4.1 Hard and Soft Technologies

Odor (1984) has distinguished between hard technologies and soft technologies. Hard technologies are readily available components that can be purchased and assembled into assistive technology systems. The main distinguishing feature of hard technologies is that they are tangible. On the other hand, soft technologies are the human areas of decision making, strategies, training, concept formation, and service delivery as described earlier in this chapter. Soft technologies are generally captured in one of three forms: (1) people, (2) written, and (3) computer (Bailey, 1997). These aspects of technology, without which the hard technology cannot be successful, are much harder to obtain. Soft technologies are difficult to acquire because they are highly dependent on human knowledge rather than tangible objects. This knowledge is obtained slowly through formal training, experience, and textbooks such as this one. The development of effective strategies of use also has a major effect on assistive technology system success. Initially the formulation of these strategies may rely heavily on the knowledge, experience, and ingenuity of the assistive technology practitioner. With growing experience, the assistive technology user originates strategies that facilitate successful device use. There is a false belief that progress is solely driven by "hard" technological change The gap between the general public and persons with disabilities can only be closed by gains in both soft and hard technologies

3.4.2 Mainstream Technologies to Specially Designed Technologies: A Range of Options

As illustrated in Figure 1, the needs of people with disabilities can be met in a number of ways. Off the shelf "standard" (i.e., mainstream technologies) commercially available devices (especially those designed using the principles of universal design) can often be used by people with a variety of disabilities. For example, standard personal computers designed for the general population are often used by persons with disabilities. Sometimes these need to be modified however, to make them useable. Another type of commercially available device is one that is mass-produced but specifically designed for individuals with disabilities *(special commercially available devices)*. These devices often need to be modified to meet the needs of a specific individual. Our goal is to reduce the amount of modification necessary and to make mainstream technologies as accessible as possible. However, there will always be a portion of the disabled population that will require specifically designed assistive technologies.

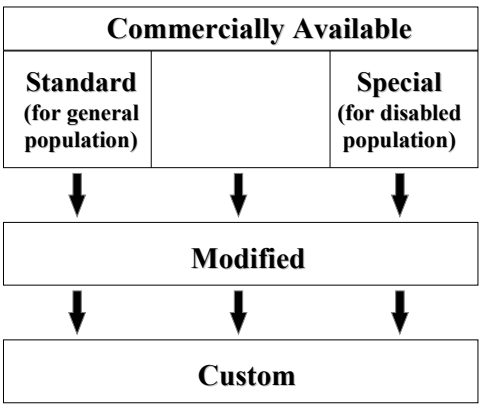

Figure 1: This diagram shows the progression from commercially available devices for the general population and commercially available devices for special populations to modified devices and custom devices. From Cook and Polgar, (2007).

3.5 The Human Technology Interface for ICT

3.5.1 General Concepts

It is estimated that as many as 40 million persons in the United States alone have physical, cognitive, or sensory disabilities (Lazzaro, 1999). The world-wide impact is significantly larger. If these people are to compete on an equal basis with non-disabled individuals, then it is extremely important that the internet be accessible to all. As the internet becomes more and more dependent on multimedia representations involving complex graphics, animation, and audible sources of information, the challenges for people who have disabilities increase. In order for access to the Internet to be useful to people with disabilities, the accessibility approach must be independent of individual devices. This means that users must be able to interact with a *user agent* (and the document it renders) using the input and output devices of their choice based on their specific needs. A **user agent** is defined as software to access Web content (www.w3.org/wai). This includes desktop graphical browsers, text and voice browsers, mobile phones, multimedia players, and software assistive technologies (e.g., screen readers, magnifiers) that are used with browsers. The person with a disability interacts with technology through the Human Technology Interface (HTI) (Cook and Polgar, 2007).

The graphical user interface (GUI) has both positive and negative implications for persons with disabilities. The positive features are those that apply to non-disabled users (e.g., use of icons, recognition rather than recall memory, screen icons for the same task look the same, operations such as opening and closing files are always the same). The GUI is the standard user interface because of its ease of operation for novices and its consistency of operation for experts. The latter ensures that every application behaves in basically the same way. People with motor disabilities may not have the necessary physical (eye-hand coordination) and visual skills to navigate the GUI. Modification of the GUI to allow specialized access (see Figure 1) can also be more challenging for GUI-based operating systems.

As networks are expanded and more devices (e.g., cell phones, PDAs) have open architectures, it will be possible to download profiles, adaptations and special instructions that enable adaptable systems to be developed to meet the needs of people who have disabilities. Some examples are (1) trainable hearing aids that adjust automatically to the environments in which they are used; (2) a "Smart House" that assesses occupants current state and the state of various home utilities to aid with common activities of daily living, provides feedback should residents become disoriented or confused and report medical emergencies automatically; an orientation and direction finding device that senses the current location (via GPS) and gives directions to a desired location for individuals who cannot read maps because of visual or cognitive disabilities.

3.5.2 Access for Motor Impairment

There are a significant number of people who cannot effectively use standard keyboards, mouse controls or switches. It is likely that we will see a much greater understanding of the biological/physical interface for the control of computers in the future (Applewhite, 2004).

One approach that may offer promise is the brain computer interface (BCI). BCI systems may be grouped into a set of functional components including the input device, amplification, feature extraction, feature translation and user feedback (Mason and Birch, 2003). Signals are mathematically analyzed to extract features useful for control (Fabiani, Mcfarland, Walla, and Pfurtscheller 2004). Features or signals that have been used include slow cortical potentials, P300 evoked potential, sensorimotor rhythms recorded from the cortex and neuronal action potentials recorded within the cortex). A typical task for a user is to visualize different movements or sensations or images.

Another approach to cursor control is the use of a digital camera and image recognition software to track a particular body feature to control an on-screen mouse cursor (Betke, Gips and Fleming, 2002). The most easily tracked feature is the tip of the nose, but the eye (gross eye position not point of gaze), lip, chin and thumb have also been used. Non-disabled subjects used this approach and fund that the camera mouse was accurate but slower than a typical hand-controlled mouse. Using an on-screen keyboard the camera mouse was half as fast as a regular mouse in a typing task, but the accuracy obtained was equivalent on each system. More and more computers have built-in cameras, so the camera mouse requires only software to capture the body feature image and interpret its movement as mouse commands. This may lead to wider application of this technique.

There are many other approaches that are used to provide access to and control over technologies for people with severe motor disabilities (Cook and Polgar, 2007) \. These range form keyboards of various type, to automatic speech recognition to mouse and mouse emulators systems to single and multiple switches.

3.5.3 Access for Cognitive Impairment

Cognitive disabilities include a wide range of skills and deficiencies. Learning disabilities typically involve significant difficulties in understanding or in using either spoken or written language, and these difficulties may be evident in problems with reading, writing, mathematical manipulation, listening, spelling or speaking (Edyburn, 2005). These limitations make it increasingly difficult to access complicated Web sites that may include flashing pictures, complicated charts, and large amounts of audio and video data. While there are assistive technologies that are specifically designed to address these areas (discussed later in this chapter), many of the technological tools are useful for all students, and are part of instructional technology (Ashton, 2005). Even the so-called assistive technologies have features (e.g., multimedia, synthetic speech output, voice recognition input) that are useful to all learners.

For individuals with acquired cognitive disabilities due to injury (e.g., traumatic brain injury) or disease (e.g., stroke (CVA) or dementia) changing features such as font size, background/ foreground color combinations, contrast, spacing between words, letters and paragraphs and using graphics can all improve access to screen-based information. Another technological concept for these individuals is a cognitive prosthesis, which is a custom-designed computer-based compensatory strategy that directly assists in performing daily activities[1]. It may also include additional technologies such as a cell phone, pager, digital camera or low tech approaches

Persons with intellectual disabilities have difficulties with memory, language use and communication, abstract conceptualization, generalization and problem identification/problem solving. Characteristics of the HTI that are important for these individuals include simplicity of operation, capacity of the technology to support repetition, consistency in presentation, and inclusion of multiple modalities (e.g., speech, sounds and graphical representations) (Wehmeyer, Smith and Davies, 2005).

An example of technology designed for cognitive needs is the Planning and Execution Assistant and Trainer (PEAT). It is a PDA-based personal planning assistant designed to assist individuals with cognitive disorders due to brain injury, stroke, Alzheimer's disease, and similar conditions (Levinson, 1997). PEAT employs artificial intelligence to automatically generate plans and also to revise those plans when unexpected events occur. PEAT uses a combination of manually entered schedules and a library of stored scripts describing activities of daily living (e.g., morning routine or shopping). Scripts can be used for both planning and for execution. Planning involves a simulation of the activity with key decision points presented and prompts (auditory and visual) supplied necessary to aid the individual through the planning process. The plan to be executed can be either the stored script or a modified script based on the simulation. The PEAT artificial intelligence software generates the best strategy to execute the required steps in the plan (LoPresti, Mihailidis, and Kirsch, 2004). PEAT also automatically monitors performance, and corrects schedule problems when necessary.

3.5.4 Access for Auditory Impairment

Since web pages are a mixture of text, graphics, and sound, people who are deaf may be prevented from accessing some information unless alternative methods are available. The primary approach for thee individual is the use of the Microsoft Synchronized Accessible Media Interchange (SAMI), which allows authors of Web pages and multimedia software to add closed captioning for users who are deaf or hard of hearing. This approach is similar to the use of closed captioning for television viewers. The W3C WAI SMIL (www.w3.org/WAI) is designed to facilitate multimedia presentations in which an author can describe the behavior of a multimedia presentation, associate hyperlinks with media objects, and describe the layout of the presentation on a screen

Trainable hearing aids adjust automatically to the environments in which they are used through access to embedded information networks. This allows automatic adaptation to changing noise levels and environments.

[1] Institute for Cognitive Prosthetics, http://www.brain-rehab.com/ definecp.htm

3.5.5 Access for Visual Impairment

The W3C WAI user agent guidelines are based on several principles that are intended to improve the design of both types of user agents. The first is to ensure that the user interface is accessible. This means that the consumer using an adapted input system must have access to the functionality offered by the user agent through its user interface. Second, the user must have access to document content through the provision of control of the style (e.g., colors, fonts, speech rate, and speech volume) and format of a document. A third principle is that the user agent help orient the user to where he is in the document or series of documents. In addition to providing alternative representations of location in a document (e.g., how many links the document contains or the number of the current link), a well-designed navigation system that uses numerical position information allows the user to jump to a specific link. Finally, the guidelines call for the user agent to be designed following system standards and conventions. These are changing rapidly as development tools are improved.

Communication through standard interfaces is particularly important for graphical desktop user agents, which must make information available to assistive technologies. Technologies such as those produced by the W3C include built-in accessibility features that facilitate interoperability. The standards being developed by the W3C WAI provide guidance for the design of user agents that are consistent with these principles. The guidelines are available on the W3C WAI Web page (www.w3.org/wai).

3.5.6 Other ICT Access

Cellular telephones are becoming more powerful with capabilities approaching that of personal computers. This expanded capability will provide significant advantages for people with disabilities, especially those with low vision or blindness. describes Three changes will be particularly valuable to people who have disabilities:: (1) standard cell phones will have sufficient processing power for almost all the requirement of persons with visual impairments, (2) software will be able to be downloaded into these phones easily, (3) wireless connection to a worldwide network will provide a wide range of information and services in a highly mobile way (Fruchterman, 2003). Because many of these features will be built into standard cell phones the cost will be low and reachable by persons with disabilities. A major advance will occur if the cell phone industry moves away from proprietary software to an open source format providing the basis for a greater diversity of software for tasks such as text-to-speech output, voice recognition and optical character recognition in a variety of languages. Many applications for people with disabilities will be able to be downloaded from the internet. With expanded availability of embedded systems, it will be possible for a user to store their customized programs on the network and download them as needed form any remote location.

Downloading a talking book program into a cell phone can provide access to digital libraries for persons who are blind. Outputs in speech or enlarged visual displays can be added as needed by the user. With a built-in camera and network access a blind person could obtain a verbal description of a scene by linking to on-line volunteers who provide descriptions of images. These applications will depend on the increasing application of universal design in information technology products (Tobias, 2003). These applications include ATMs, cell phones, vending machines and other systems that are encountered on a daily basis (Tobias, 2003).

4 INFRASTRUCTURE FOR FUTURE ACCESSIBILITY

The infrastructure for future accessibility consists of: (1) an expanded, smarter and more available "real" and "virtual" internet, (2) Home automation systems that are smarter and have greater interconnectivity, (3) universal design principles that are applied more widely, (4) alternative approaches for accessing information technologies, and (5) special-purpose assistive technologies.

The Infrastructure for future accessibility will depend on several factors. These include: Web-based virtual systems, home automation, universal design for ICT, alternatives for accessing information technologies and special-purpose assistive technologies. In addition there is n on going need for the development of soft technology tools.

If ICT advances are not adaptable enough to be accessible to persons with disabilities it will further increase the disparity between those individuals and the rest of the population leading to further isolation and economic disadvantage. On the other hand, availability of these technologies in a transparent way will contribute to full inclusion of individuals who have disabilities in the mainstream of society.

5 CONCLUSIONS

The move to the information age offers great promise for persons with disabilities. It also holds great threats for persons with disabilities. Constant vigilance is required to insure that information technologies remain accessible and responsive to the needs of persons with disabilities. The future for persons with disabilities will not be driven by advances in technology, but rather by how well we can take advantage of those advances for the accomplishment of the many tasks of living that require technological assistance

6 SUMMARY

Anticipated changes in technologies coupled with the focus on the social aspects of disability, provide a significant opportunity for major advances in the degree to which individuals with disabilities can participate in all aspects of life, including work, school, leisure and self care.

Technological advances will be particularly important as the percentage of the population that is elderly rises. Concepts from universal design will be important in ensuring that this segment of the population remains active and is able to participate in society. This new group of elderly individuals will also be more experienced with computers and other technologies than their predecessors and they may well demand greater performance and adaptability from both assistive technologies and mainstream ICT (e.g., telephones, internet communication).

The percentage of individuals with long-term disabilities who join the over 65 age group will also increase. These individuals will have been long-term users of assistive technologies, and their experience will have major implications for developments to meet future needs.

While much of what I have described is conjecture, it is based on modest extrapolation from the current state of the art. There are some things that we know with a high degree of certainty. We know that computer systems will be faster, have more memory be smaller and be less expensive for the same or greater functionality. We also know that the communication channel bandwidth will continue to increase allowing much more information and much more sophisticated information processing. Finally, it is clear that people with disabilities will continue to assert their right to fully participate in society.

Technological advances also raise questions for people who have disabilities. The most important of these is whether accessibility will keep pace with technological developments. For example, will assistive technologies for input and output be compatible with the user agents and operating systems of tomorrow. A second major question is whether the needs of persons with disabilities will be a driving force in future technological developments. Will people who have disabilities have to adapt to the existing technologies based on characteristics for non-disabled people or will universal design become a greater reality? In the latter case, adaptations will become less important and accessibility will become the rule rather than the exception.

For people who have disabilities, there are significant implications of emerging information processing technologies. If not closely monitored, these could result in less rather than more access to the new information economy for persons with disabilities. Despite the wider use of universal design principles, there will still be a need for effective assistive technology design and application if individuals with disabilities are to realize the full potential of the new information age.

REFERENCES

Applewhite A: (2004). 40 years: the luminaries. *IEEE Spectrum,* 41(11), 37-58.

Ashton T.M. (2005). Students with learning disabilities using assistive technology in the inclusive classroom, pp. 229-238, in Edyburn D., Higgins K.. & Boone R. (eds.): *Handbook of Special Education Technology Research and Practice,* Whitefish Bay, Wisconsin: Knowledge by Design, Inc.

Bailey, R.W: (1996). *Human performance engineerin.,* ed 2, Upper Saddle River, NJ, , Prentice Hall.

Betke M., Gips J. & Fleming P: (2002). The camera mouse: Visual tracking of body features to provide computer access for people with severe disabilities. *IEEE Trans. Neural Systems and Rehabilitation Engineering,* 10(1): 1-10.

Blackstone S. (1996). The Internet: what's the big deal *Augment Commun News* 9(4):1-5.

Cook A.M. & Polgar J.M. (2007). *Cook and Husey's Assistive Technologies: Principles and Practice*, 3rd ed St. Louis: Elsevier.

Edyburn D.L. (2005). Assistive technology and students with mild disabilities: from consideration to outcome measurement, pp 239-270, in Edyburn D, Higgins K. & Boone R. (eds.): *Handbook of Special Education Technology Research and Practice,* Whitefish Bay, Wisconsin: Knowledge by Design, Inc.,

Emiliani, P.L. (2006). Assistive technology (AT) versus Mainstream Technology (MST): The research perspective. *Tech Disab*, 18, 19-29,

Fabiani G.E., Mcfarland D.J., Wolpaw J.R., & Pfurtscheller G (2004). Conversion of EEG activity into cursor movement by a brain-computer interface (BCI). *IEEE Trans. Neural Systems and Rehab Engr*, 12: 331-338.

Fruchterman J.R: (2003) In the palm of your hand: A vision of the future of technology for people with visual impairments. *J Vis Impair Blindness, 97*(10), 585-591.

Kumagai, J. (2004).Talk to the machine. *IEEE Spectrum,* 39(9): 60- 64.

Lazzaro J.L. (1999). Helping the web help the disabled, *IEEE Spectrum* 36(3): 54-59

Levinson R.L. (1997): The planning and execution assistant and trainer. *J. head trauma rehabilitation*, 12(2): 769-775.

Lewis, J.R. (2004). .In the eye of the beholder*, IEEE Spectrum,* 41(5)24- 28.

LoPresti E.F., Mihailidis A. & Kirsch N. (2004): Assistive technology for cognitive rehabilitation: State of the art. *Neuropsychological Rehabilitation,* 14(1): 5-39.

Mason S.G. & Birch G.E: (2003).A general framework for brain-computer interface design. *IEEE Trans. Neural Systems and Rehab Engr*, 11, 70-85.

Odor P. (1984): Hard and soft technology for education and communication for disabled people, *Proc Int Comp Conf*, Perth, Western Australia,

Tobias J: (2003). Information technology and universal design: An agenda for accessible technology. *J Vis Impair Blindness, 97*(10), 592-601.

Ungson G.R. and Trudel J.D. (1999). The emerging knowledge-based economy. *IEEE Spectrum*, 36(5):60-65.

Wehmeyer M.L., Smith S.J., Palmer SB, Davies D.K. & Stock S.E: (2004). Technology use and people with mental retardation. *International Review of Research in Mental Retardation,* 29: 291-337.

World Health Organization (2001): *International classification of functioning disability and health*-ICF, Geneva, World Health Organization

Wright, RA. (2004). *A Short History of Progress*, Toronto: Anansi Publications.

FULL PAPERS

BRAIN COMPUTER INTERFACE
Comparison of Neural Networks Classifiers

José Luis Martínez Pérez and Antonio Barrientos Cruz
Grupo de Robótica y Cibernética, Universidad Politécnica de Madrid, C/José Gutierrez Abascal 2, Madrid, España
jlmartinez@etsii.upm.es, antonio.barrientos@upm.es

Keywords: Electroencephalography, Brain Computer Interface, Spectral Analysis, Biomedical Signal Detection, Pattern recognition.

Abstract: Brain Computer Interface is an emerging technology that allows new output paths to communicate the user's intentions without use of normal output ways, such as muscles or nerves(Wolpaw, J. R.; et al., 2002).
In order to obtain its objective BCI devices shall make use of classifier which translate the inputs provided by user's brain signal to commands for external devices.
The primary uses of this technology will benefit persons with some kind blocking disease as for example: ALS, brainstem stroke, severe cerebral palsy (Donchin et al., 2000).
This report describes three different classifiers based on three different types of neural networks: Radial Basis Functions *RBF*, Probabilistic Neural Networks *PNN*, and Multi-Layer Perceptrons *MLP*. The report compares the results produced by them in order to obtain conclusions to apply to an on-line BCI device, it also describes the experimental procedure followed in the experiments.
As result of the tests carried out on five healthy volunteers an estimation of the success rate for each type of classifier, the type and architecture of the classifier, and filtering windows are established.

1 INTRODUCTION

Brain Computer Interface technology(Wolpaw, J.R.; et al., 2000), BCI, is aimed to communicate human beings with external computerised devices using the electroencephalographic signal as primary source of commands (Birbaumer, N; et al., 2000); in the first international meeting for BCI technology in 1999 it was established that BCI *"must not depend on the brain's normal output pathways of peripheral nerves and muscles"*

In order to control an external device using thoughts it is necessary to associate some mental patterns to device commands, so an algorithm that detects, acquires, filters and classifies the human electroencephalographic signal is required (Kostov, A.; Polak, M., 2000) (Pfurtscheller et al., 2000).

This article compares results coming from three different classifiers based on neural networks: Radial Basis Function, Probabilistic Neural Networks, and Multi Layer Perceptron.

In the experiments considered for this article a low number of electrodes has been used to capture the endogenous electroencephalographic subject's signal. In order to facilitate the use of this technology it is important to make it easy to use, the number of electrodes employed in these devices is a global key feature, as the fewer of electrodes used, the higher the comfort (Wolpaw, 2007).

Because the main changes in brain activity are associated to changes in the power amplitude of band frequencies, spectrograms based on FFT are used to obtain initial feature vectors (Obermaier et al., 2001) (Proakis and Manolakis, 1997). Principal Component Analysis (PCA) is used to combine these initial features in order to reduce the dimensionality of the input space. To minimise the leakage effect seven different types of preprocess windows has been considered: rectangular, triangular, Blackman's, Hamming's, Hanning's, Kaiser's and Tukey's (Harris, 1978). The existence of statistical evidence in the feature population associated to different brain activities

has been previously shown (Peña Sánchez de Rivera, 1986) (Martinez, J.L.; et al., 2006).

The results provided by each classifier are compared using the confusion matrix (Duda et al., 2001).

This article is composed of the following sections:

Section 2 briefly describes the methodology.

Section 3 describes the algorithmics used in the experiments.

Section 4 and 5 present and analyse the results.

Section 6 is devoted to conclusions.

2 EXPERIMENTAL PROCEDURE

The tests described below were carry out on five male healthy subjects, one of them has been trained before, but the other four were novice in the use of the system.

In order to facilitate the mental concentration on the proposed activities, the experiments were carried on in a room with low level of noise and under controlled environmental conditions, all electronic equipments external to the experiment around subject were switched off to avoid electromagnetic artifacts. The experiments were carry out between 10:00 a.m. and 14:00 p.m. The subjects were sat-down in front of the acquisition system monitor, at 50 cm from the screen, their hands were in a visible position, the supervisor of the experiment controlled the correct development of it.

2.1 Methodology

The experimental process is shown on figure 1.

Test of system devices. Checks the correct level of battery, and the correct state of the electrodes.

System assembly. Device connections: superficial electrodes (Grass Au-Cu), battery, bio-amplifier (g.BSamp by g.tec), acquisition signal card (PCI-MIO-16/E-4 by National Instrument), computer.

System test. Verifies the correct operation of the whole system. To minimise noise from the electrical network the Notch filter (50Hz) of the bio-amplifier is switched on.

Subject preparation for the experiment. Application of electrodes on subject's head. It is verified that electrode impedance was lower than 4 KOhms.

System initialisation and setup. Verification of data register. The temporal signal evolution is monitored, in the spectrogram should appear a very low 50 Hz component.

Experiment setup. The supervisor of the experiment sets-up the number of replications, $N_{rep} = 10$, and the quantity of different mental activities. The

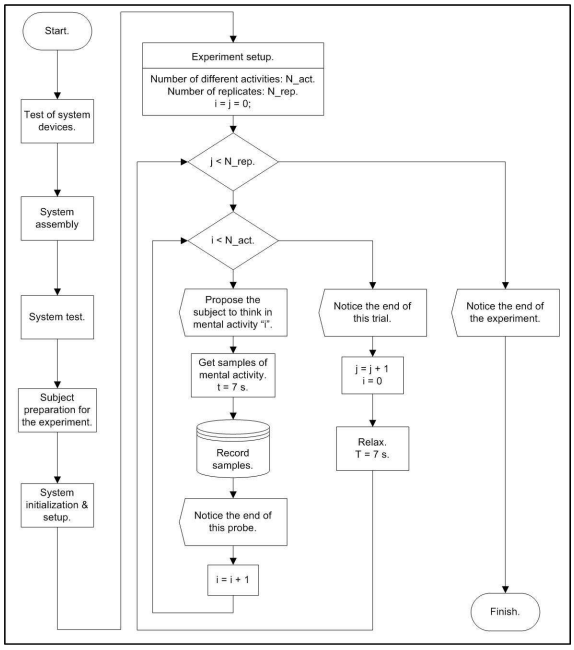

Figure 1: Diagram of the experiment realization.

duration of each trial is $t = 7s$, the acquisition frequency is $f_s = 384Hz$. The system suggests to the subject to think about the proposed mental activity. A short relax is allowed at the end of each trial; between replications the relax time is $t = 7s$.

2.2 Position of Electrodes

Electrodes were placed in the central zone of the skull, next to C3 and C4 (Penny, W. D.; et al., 2000), two pair of electrodes were placed in front of and behind of Rolandic sulcus, this zone is one with the highest discriminant power, it takes signal from motor and sensory areas of the brain (Birbaumer, N; et al., 2000). Reference electrode was placed on the right mastoid, two more electrode are placed near to the corner of the eyes to register blinking.

Figure 2: Electrode placement.

2.3 Description of Cerebral Activities

The supervisor of the experiment asks the subject to figure out the following mental activities, these activities will be the cerebral patterns to differentiate among them(Neuper, C.; et al., 2001).

Activity A. Mathematical task. Recursive subtraction of a prime number, i.e. 7, from a big quantity, i.e. 3.000.000.

Activity B. Movement task. This task is subdivided in:

B-1 Movement imagination. The subject imagines moving their limbs or hands, but without the materialisation of the movement.

B-2 Movement realization.. The subject is able to move their hands.

Activity C. Relax. The subject is relaxed.

3 ALGORITHM

This section describes the procedure applied to recorded signal just before its classification.

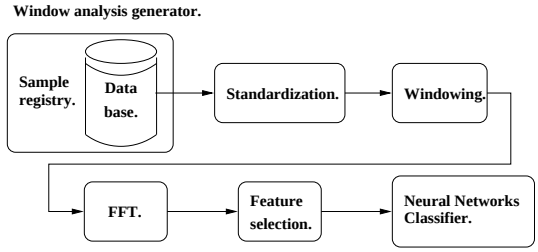

Figure 3: Algorithm.

3.1 Window Analysis Generator

In this block the registered signal is chopped in packages of samples, similar to the bundles of samples obtained from an acquisition card in an on-line BCI application. The number of samples in each package is a compromise between the goodness of the classification and the amount of time taken by this classification. An algorithm with very good classification and low number of mistakes will take a very big package, so the time between classifications will be also very big, it will do the algorithm useless for a real on-line BCI system, neither a very fast algorithm with small packages of samples but with a high number of mistakes will be useful.

In this work we have considered packages of 128 samples, the sample frequency is $F_s = 384Hz.$, and the classification latency is $t = 1/3s$.

The duration of each activity is 7s, so there will be 21 classifications obtained from each register, no overlap between windows have been considered.

3.2 Standardisation

To compare the signal of different sessions is necessary to standardise the samples, avoiding for example that variations in the impedance of the electrodes changes the classification result.

The standardisation of each analysis window consists in the subtraction of the average value and the division by the standard deviation.

$$\mu = \frac{\Sigma_{i=1}^{i=N} x_i}{N}; \quad \sigma^2 = \frac{(x-\mu)^2}{N}$$

$$x' = \frac{x-\mu}{\sigma}$$

3.3 Windowing

In this block different kind of windows are convoluted with the standardise signal.

The frequency leakage effect occurs when signals with low frequency components are chopped or convoluted with windows with sharp edges, in this cases in the spectrogram appears high frequency components (Harris, F.J., 1978).

The following types of windows have been considered:

- Rectangular.
- Triangular.
- Blackman's.
- Hamming's.
- Hanning's.
- Kaiser's.
- Tukey's.

3.4 FFT

The cerebral activity becomes apparent mainly through the frequency components of the electroencephalographic signal. Different kind of mental activities have different frequency components(Harris, F.J., 1978). For this reason it is necessary to transform the sampled time domain signal to frequency domain, so a Fast Fourier Transform is applied to each block of 2^7 sampled data.

Having in mind that the sample frequency is 384Hz, the frequency resolution is:

$$\Delta f = \frac{384Hz}{128} = 3Hz.$$

In this application the useful information is in the amplitude of the frequency components, so the phases are discarded, we focus our attention on the spectrograms of each of the analysis windows.

Considering the properties of the Fourier Transform and having in mind that the signal in the time domain only have real components, in the Nyquist

frequency is produced the reflection effect, so the signal information is in the first halve of the components (Harris, F.J., 1978).

3.5 Feature Selection

A vector of features is extracted from each signal analysis window. This vector is made up as the mean of the amplitudes of the frequency bands. Because the frequency of normal human brain is under 40-50Hz, only frequencies between 6 and 38Hz have been considered.

Table 1: Feature vector.

FFT index.	Frequency.	Denomination.
1	0 - 2	Not considered
2	3 - 5	Not considered
3	6 - 8	θ.
4	9 - 11	α_1.
5	12 - 14	$\alpha 2$.
6 - 7	15 - 20	β_1.
8 - 10	21 - 29	β_2.
11 - 13	30 - 38	β_3.
14 - 64	39 - 192	Not considered

3.6 Classifiers

Three different types of classifiers have been considered, each one of them based on different types of neural networks (Ripley, 2000) (Bishop, 1995):

- Multi-Layer Perceptrons (MLP).
- Radial Basis Functions (RBF).
- Probabilistic Neural Networks (PNN).

Each classifier applies the following procedure to the vector of features extracted previously:

1. Determination of the learning (50%), test (25%) and validation (25%) sets of data.
2. Attainment of the normalisation matrix for the learning data set.
3. Application of Principal Component Analysis to the learning data set in order to reduce the dimensionality of the data input space.
4. Learning of the input data set by the neural network.
5. Application of the neural network to the test data set, if the error test is bellow the goal error the learning process is stopped, in other case the network is trained again.
6. Application of the neural network to the validation data set in order to estimate the performance error.
7. Application of the neural net to the whole data set and result registration.
8. Attainment of the confusion matrices for each experiment.

3.6.1 Multi-Layer Perceptron Classifier

The setup parameters used in this classifier are:

- Learning algorithm: Levenberg-Marquardt (Backpropagation).
- Number of hidden unit neurons: 60.
- Number of output neurons: 3.
- Goal error = $1e^{-5}$.
- Epochs = 400.
- Max. fail = 5.
- Mem. reduc. = 1.
- Min. grad. = $1e^{-10}$.
- $\mu = 1e^{-3}$.
- $\mu_{dec} = 0.1$.
- $\mu_{inc} = 10$.
- $\mu_{max} = 1e^{-5}$.

3.6.2 Radial Basis Function Classifier

The setup parameters used in this classifier are:

- Number of hidden neurons: The learning algorithm used by this type of neural networks determine the number of neurons in the hidden layer through an iterative process, it starts with a reduced number of hidden neurons and it is increased meanwhile the goal error is not achieved or a maximum number of neurons is reached.
- Spread constant : 0.25 (Determine the zone of influence of each neuron).
- Number of output neurons : 3.

3.6.3 Probabilistic Neural Network Classifier

The setup parameters used in this classifier are:

- Number of hidden neurons: The learning algorithm used as much hidden neurons as pairs of input vector - target vector were in the learning data set.
- Spread constant : 0.25 (Determine the zone of influence of each neuron).
- Number of output neurons : 3.

4 RESULTS

The figures in the appendix summarised on vertical axis the percentage of correct classifications obtained from the confusion matrices applied to each one of the three classifiers. It shall be noted that the scale has been broken in order to appreciate the scattering results. On the horizontal axis appears the different types of filtering windows taken into account.

For each filtering window appears a bar with the results of each classifier: maximum, minimum and median percentage values.

It is also shown the results obtained when the classifier use two different types of architectures, one with only one neural network that gathers all vectors of features for each electroencephalographic channel, and other that employs two neural networks, one for each electroencephalograpic channel.

5 DISCUSSION

From the analysis of the results the following considerations are extracted:

- Classifiers based on Probabilistic Neural Networks or Radial Basis Functions perform better than ones based on Multi Layer Perceptrons.
- Result stability. For all test the procedure was replicated three times, both PNN and RBF classifiers produced the same confusion matrices, instead of MLP classifiers which produced different confusion matrices for each replica.
- Comparison between PNN and RBF classifiers showed higher maximum percentages of correct classifications for PNN but also a higher variability.
- Classifiers based on only one neural network that considers at the same time features obtained from both electroencephalographic channels not always perform better than classifiers based on two neural networks, one for each channel.
- Considering the different types of filtering windows, the best results are obtained for Kaiser's, rectangular and Tukey's windows.

6 CONCLUSIONS

This report demonstrates that it is possible to discriminate mental activity from the electroencephalographic signal, it also compares three different types of neural networks classifiers applied to an off-line prototype of BCI device that use FFT in order to estimate the power spectrum of the recorded signal when volunteers carried out specific mental tasks.

Both classifiers based on Probabilistic Neural Networks and Radial Basis Functions produced better and more stable results than the classifier based on Multi Layer Perceptrons. It is possible due to the vector feature distributions associate to each mental activity and to the interpolation capability of PNN and RBF, this capability is higher in PNN and RBF than in MLP neural networks.

It is hoped that On-line BCI devices based on classifiers that make use of neural networks like RBF or PNN will perform better than other based on MLP or equivalents.

In order to improve the success rate of classifications the use of filtering windows has been proved to be a good technique. In the same manner a classifier with a multiple network architecture followed by a block that weighs the network outputs could produce better results than classifiers based on only one neural network.

REFERENCES

Birbaumer, N; et al. (2000). The thought translation device (TTD) for completely paralyzed patients. *IEEE Transactions on Rehabilitation Engineering.*, 8(2):190–193.

Bishop, C. (1995). *Neural Networks for Pattern Recognition Analysis*. Oxford University Press, London, 1st edition.

Donchin, E., Spencer, K. M., and Wijesinghe, R. (2000). The mental prosthesis: assessing the speed of a p300-based brain-computer interface. *Rehabilitation Engineering, IEEE Transactions on [see also IEEE Trans.on Neural Systems and Rehabilitation]*, 8(2):174–179.

Duda, R. O., Hart, P. E., and Strok, D. G. (2001). *Pattern classification*. John Wiley & sons, New York etc. Richard O. Duda, Peter E. Hart, David G. Strok.

Harris, F. J. (1978). On the use of windows for harmonic analysis with the discrete fourier transform.

Harris, F.J. (1978). On the Use of Windows for Harmonic Analysis with the Discrete Fourier Transform. *Proceedings of the IEEE*, 66(1):51–83.

Kostov, A.; Polak, M. (2000). Parallel man-machine training in development of EEG-based cursor control. *IEEE Transactions on Rehabilitation Engineering.*, 8(2):203–205.

Martinez, J.L.; et al. (2006). The windowing Effect in Cerebral Pattern Classification. An Application to BCI Technology. *IASTED Biomedical Engineering BioMED 2006*, pages 1186–1191.

Neuper, C.; et al. (2001). Motor Imagery and Direct Brain-Computer Communication. *Proceedings of the IEEE*, 89(7):1123–1134.

Obermaier, B., Neuper, C., Guger, C., and Pfurtscheller, G. (2001). Information transfer rate in a five-classes brain-computer interface. *IEEE Transactions on Neural Systems and Rehabilitation Engineering.*, 9(3):283–288. Importante.

Peña Sánchez de Rivera, D. (1986). *Estadística : modelos y métodos*, volume 109-110. Alianza, Madrid. Daniel Pea Sanchez de Rivera; 2 v. 23 cm; 1. Fundamentos – 2. Modelos lineales y series temporales.

Penny, W. D.; et al. (2000). EEG-based communication: A pattern recognition approach. *IEEE Transactions on Rehabilitation Engineering.*, 8(2):214–215.

Pfurtscheller et al. (2000). Current trends in Graz brain-computer interface (BCI) research. *IEEE Transactions on Rehabilitation Engineering.*, 8(2):216–219.

Proakis, J. G. and Manolakis, D. G. (1997). *Tratamiento digital de seales : [principios, algoritmos y aplicaciones]*. Prentice-Hall, Madrid.

Ripley, B. (2000). *Pattern Recognition and Neural Networks*. Cambridge University Press, London, 2nd edition.

Wolpaw, J. R. (2007). Brain-computer interfaces as new brain output pathways. *The Journal of Physiology*.

Wolpaw, J. R.; et al. (2002). Brain-Computer interface for communication and control. *Clinical Neurophysiology*, 113:767–791.

Wolpaw, J.R.; et al. (2000). Brain-Computer Interface Technology: A Review of the First International Meeting. *IEEE Transactions on Rehabilitation Engineering.*, 8(2):164–171.

APPENDIX

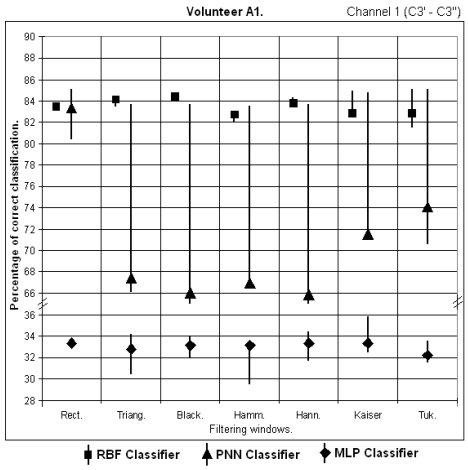

Figure 4: Channel 1. Correct classification.

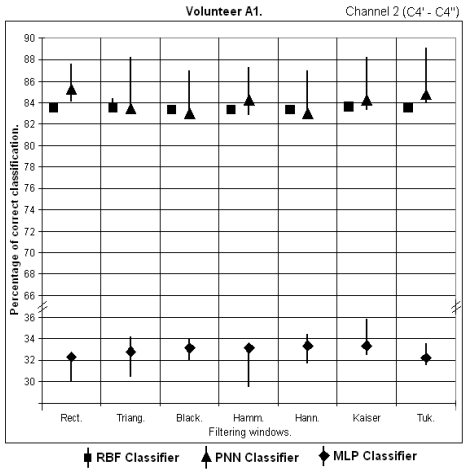

Figure 5: Channel 2. Correct classification.

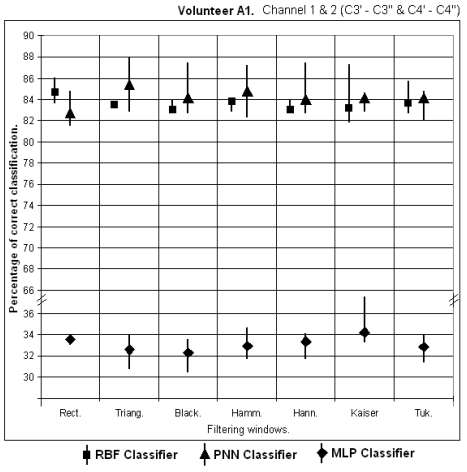

Figure 6: Channel 1 and 2. Correct classification.

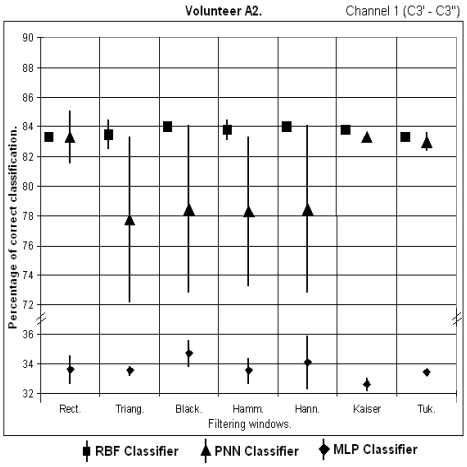

Figure 7: Channel 1. Correct classification.

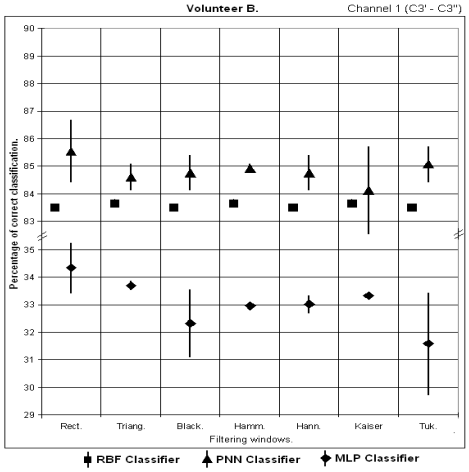

Figure 10: Channel 1. Correct classification.

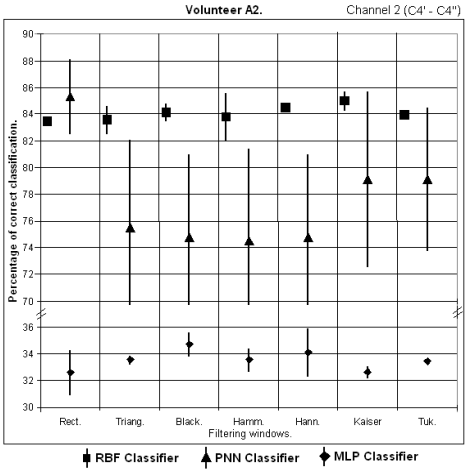

Figure 8: Channel 2. Correct classification.

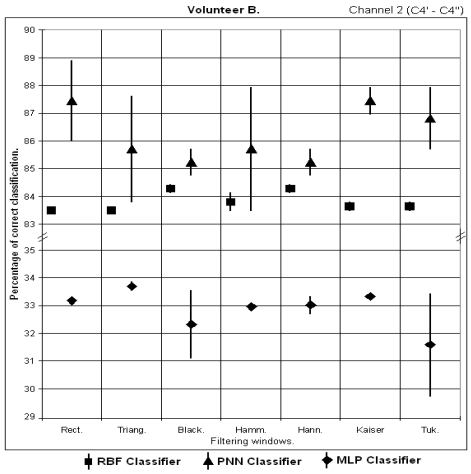

Figure 11: Channel 2. Correct classification.

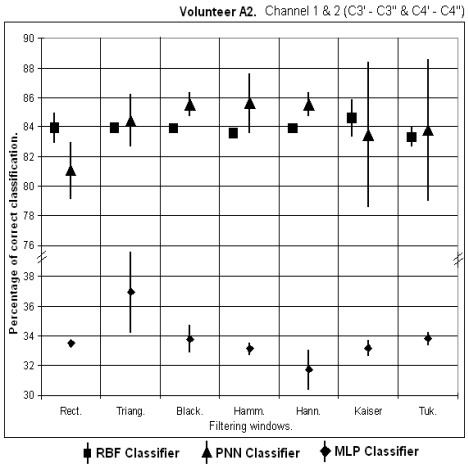

Figure 9: Channel 1 and 2. Correct classification.

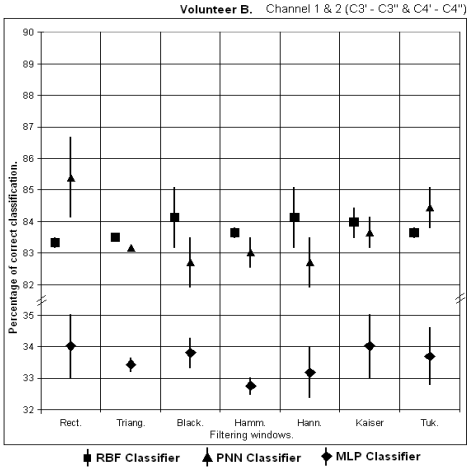

Figure 12: Channel 1 and 2. Correct classification.

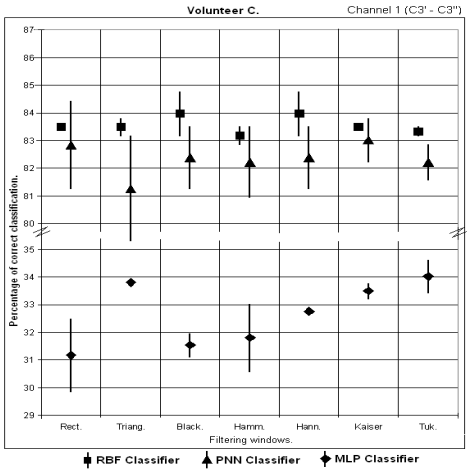

Figure 13: Channel 1. Correct classification.

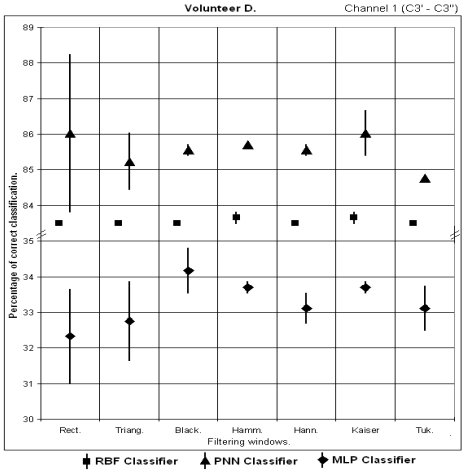

Figure 16: Channel 1. Correct classification.

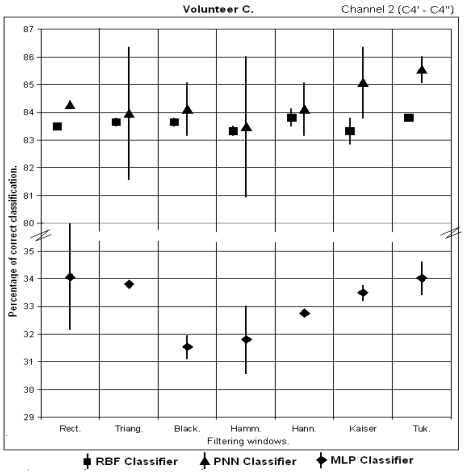

Figure 14: Channel 2. Correct classification.

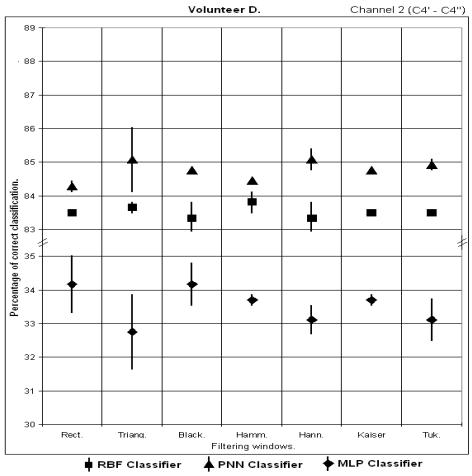

Figure 17: Channel 2. Correct classification.

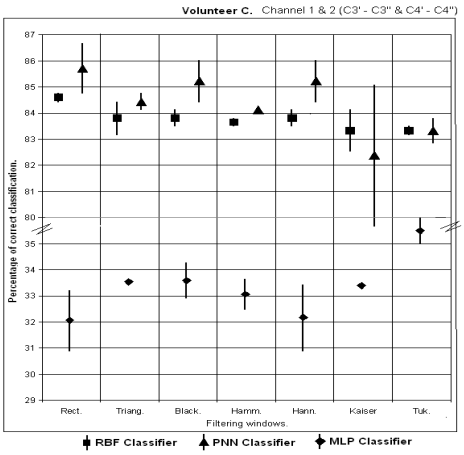

Figure 15: Channel 1 and 2. Correct classification.

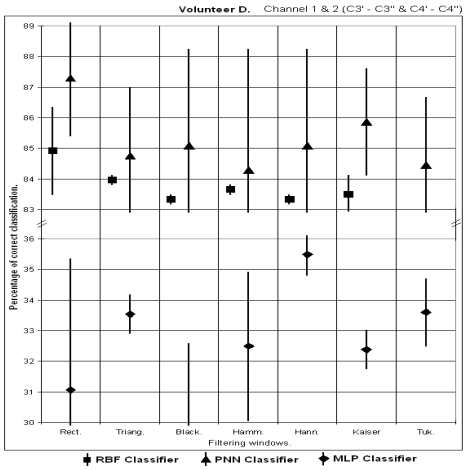

Figure 18: Channel 1 and 2. Correct classification.

AUTOREGRESSIVE FEATURES FOR A THOUGHT-TO-SPEECH CONVERTER

N. Nicolaou, J. Georgiou and M. Polycarpou
Department of Electrical and Computer Engineering, University of Cyprus, 75 Kallipoleos Street, Cyprus
nicoletta.n@ucy.ac.cy, julio@ucy.ac.cy, mpolycar@ucy.ac.cy

Keywords: Brain-Computer Interface, electroencephalogram, Morse Code, thought communication, speech impairment.

Abstract: This paper presents our investigations towards a non-invasive custom-built thought-to-speech converter that decodes mental tasks into morse code, text and then speech. The proposed system is aimed primarily at people who have lost their ability to communicate via conventional means. The investigations presented here are part of our greater search for an appropriate set of features, classifiers and mental tasks that would maximise classification accuracy in such a system. Here Autoregressive (AR) coefficients and Power Spectral Density (PSD) features have been classified using a Support Vector Machine (SVM). The classification accuracy was higher with AR features compared to PSD. In addition, the use of an SVM to classify the AR coefficients increased the classification rate by up to 16.3% compared to that reported in different work, where other classifiers were used. It was also observed that the combination of mental tasks for which highest classification was obtained varied from subject to subject; hence the mental tasks to be used should be carefully chosen to match each subject.

1 INTRODUCTION

The development of techniques that offer alternative ways of communication by bypassing conventional means is an important and welcome advancement for improving quality of life. This is especially desirable in cases where the conventional means of communication, such as speech, is impaired. We envisage the development of a simple and wearable system that communicates by converting thoughts into speech via morse code and a text-to-speech converter.

In this paper we present preliminary investigations towards the development of such a system. The investigations form part of our search for features, classifiers and mental tasks that are appropriate for utilisation in our system. In particular, we compare the classification accuracy obtained between combinations of mental task pairs when (i) autoregressive (AR) coefficients and Power Spectral Density (PSD) values are utilised as features; and (ii) Support Vector Machine (SVM), Linear Discriminant Analysis (LDA) and Neural Network (NN) are utilised as classifiers. Our investigations suggest that the combination of AR coefficients and SVM is more appropriate for our application, as an increase in classification accuracy ranging from 8.2-16.3% has been observed compared to classification of the same features using LDA and NN.

The paper is organised as follows. Section 2 provides a background into communication via thoughts and how morse code has been utilised for this purpose so far. This is followed by section 3 where a description of the system envisaged, the objectives that motivated these preliminary investigations and a description of the methods utilised are provided. The findings are presented in section 4 followed by a discussion towards how these could be interpreted and understood as part of the proposed system. The main conclusions and plans for future work emerging from these investigations are outlined in section 5.

2 BACKGROUND

A number of conditions, such as amyotrophic lateral sclerosis, strokes and speech impairment, affect the ability to communicate with the environment through speech. The problem becomes more severe when limb or muscle control is also affected, since other means of communication e.g. typing, are eliminated. An alternative method of communication

is achieved by utilising brain activity as an input signal to a device for spelling purposes (brain-computer interface, BCI). A BCI is "a communication system that does not depend on the brain's normal output pathways of peripheral nerves and muscles" (Wolpaw et al., 2000). This technology is primarily aimed at people who have lost conventional means of communication, but whose brain function remains intact.

Current BCI applications are limited by the trade-off between speed and accuracy. Thus, the most common application still remains 1-dimensional cursor movement on a computer screen, which offers the ability to communicate with the environment when teamed with a "virtual keyboard". Communication can be achieved by mentally controlling cursor movement on the screen for choosing letters on a "virtual keyboard" (Wolpaw et al, 2002) or to highlight the desired character from a scrolling list (Scherer et al., 2004). Different mental tasks are associated with left/right and/or up/down cursor movement, thus allowing the subject to pick characters and spell words. Despite the simplicity of these applications, current BCI systems are faced with som: (i) 25 bits/min is the maximum speed of communication reported (Vaughan et al., 2003). If we consider a character with 8 bit resolution this is equivalent to 3.13 chars/min, which is not acceptable for normal speech; and (ii) current systems are bulky and non portable. It is envisaged that the development of custom-built hardware as part of the proposed system will provide a solution to both these issues. In addition, these can be aided if the "virtual keyboard" is substituted by a simplified set of characters whose choice is directly associated with particular mental tasks, thus eliminating the intermediate step of cursor movement.

Such a potential simplification could be achieved via the use of Morse Code (MC), which has already been utilised for communication for disabled people. In MC transmission of information is based on short and long elements of sound (dots and dashes) and was originally created for telegraph communication. The elegance of MC lays in its simplicity and the high speech reception and transmission rates. A skilled MC operator can receive MC in excess of 40 words per minute (Coe, 2003). The world record for understanding MC was set in 1939 and still stands at 75 words per minute (French, 1993). Utilisation of MC for the disabled is commonly based on some form of muscle movement, such as operating a switch (Park et al, 1999) or a sip-puff straw (Levine et al., 1986). However, certain disabilities affect muscle movement, but even if not, then such systems are difficult to operate on a daily basis as they cause fatigue.

The use of MC for directly translating thoughts into words has been considered in very few BCI systems, mainly as an extension to traditional BCI communication methods. In (Palaniappan, 2005) the "virtual keyboard" was substituted with the two MC elements, "." and "-", and the user chose through mentally controlling cursor movement. Another MC-BCI system is described in (Altschuler and Dowla, 1998) based on the attenuation of power in the μ band (8-13Hz) during motor imagery, whose duration corresponds either to a "."or a "-" (shorter or longer motor imagery duration respectively). Spelling is achieved by interchanging motor imagery with baseline task (representing a "pause"). In addition, (Huan and Palaniappan, 2004) showed how communication in a BCI system could conceptually be achieved via a tri-state MC scheme and utilising a fuzzy ARTMAP as classifier. In such a system a ".", a "-" or a "space" would be represented by 3 mental tasks and the continuous EEG would be sampled every, e.g., 0.5s, for decision making. In (Huan and Palaniappan, 2002) it is stated that the conversion of a mental task into one of the 3 MC elements would take 6ms of computation time; however this heavily depends on a number of operating system factors.

The concept behind the latter two systems is closer to the concept of the proposed system, as the intermediate step of cursor movement is eliminated. The use of MC is advantageous as it simplifies the dictionary to 3 symbols, the choice of which will be achieved through 2 mental tasks. This reduces the system complexity and improves communication speed. Hence, we envisage the development of a portable, embedded, custom and wearable MC-based BCI system that could be used either as an assistive or as an enhancing communication aid.

3 PERFORMANCE OPTIMISATION

The proposed system is shown in figure 1 and consists of 4 parts: (1) EEG signals are recorded from a patient performing two mental tasks, each corresponding to either a "." and "-" (depending on the task duration) or a "pause". The patient is

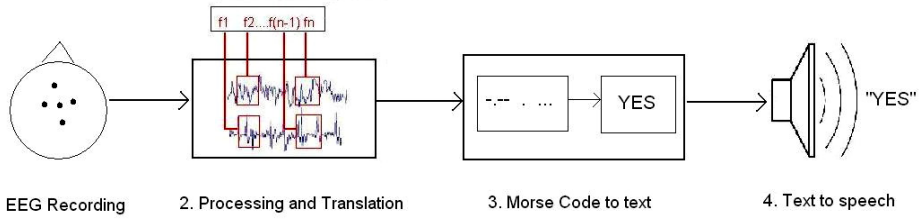

Figure 1: The proposed MC-BCI system.

mentally spelling letters and words in MC; (2) windows of specified duration of the recordings are processed and classified as ".", "-" or "pause"; (3) MC is then converted into text, which is in turn converted to speech via a text-to-speech converter (4). At this stage our priority is to maximise correct interpretation of EEG data. Computational efficiency is not a key consideration as we will be designing custom hardware tailored to the chosen processing methods. Therefore, it is imperative to firstly converge on a particular combination of signal processing methods that could be used reliably in the proposed system. The preliminary investigations presented in this paper are associated with part 2 of the proposed system and are part of our greater search for the optimal combination of features and classifiers.

3.1 Methods

3.1.1 Feature extraction

AR models are commonly utilised in EEG analysis (Wright et al., 1990). More specifically, the estimated AR coefficients have been shown to capture well the differences between various mental tasks, and as a result are frequently used as features in mental task classification and BCIs (Guger et al., 2000). Eq. 1,

$$x_t = \sum_{\tau=1}^{p} a_\tau x_{t-\tau} + \varepsilon_t \qquad (1)$$

represents an AR(p) model where p is the model order, x_t is the time series to be modelled, a_τ, τ=1,…,p are the estimated coefficients of the p^{th}-order AR model and ε_t is zero-mean random noise (commonly Gaussian with unit variance). In EEG analysis an AR(p) is fitted to the data and the p^{th} dimensional vector of estimated coefficients represents the different mental tasks, as a variation of the coefficients depending on the mental task is observed. The AR model order used in EEG analysis ranges from 5 up to 13 (Lopes daSilva, 1998). For the specific dataset used here an order of 6 was chosen as suggested in (Keirn and Aunon, 1990). Estimation of the coefficients is possile via a number of ways – here we used the method of Least Squares.

The second set of features utilised is PSD values obtained via parametric spectral analysis. In particular an AR(p) model (here p=6) is first fitted on the data and the power spectrum is subsequently obtained from the estimated coefficients via

$$S(f) = \frac{\hat{\sigma}_p^2}{N \sum_{k=0}^{p} a_k e^{-j2\pi fk/N}} \qquad (2)$$

where a_k, k=1,…,p are the estimated coefficients, f is a vector of chosen frequencies, $\hat{\sigma}_p^2$ is the estimated noise variance and N is the number of samples. The advantage of parametric methods for spectrum estimation is the ability to specify a set of frequencies of interest over which the spectrum is estimated.

3.1.2 Classification

The choice of the classifier should have little effect on the classification rate if the chosen features are good representations of the data to be classified. Given that the features capture the data characteristics well, then classification becomes an easier problem. However, the properties of the classifier must be well-matched to the feature dimensionality or separability (linear or non-linear). The problem of choosing a classifier is enhanced if the feature dimensionality is high, as this does not allow the visualisation of the features and, consequently, whether they are linearly separable or not.

SVMs offer a solution to this issue, as both linear and non-linear classification can be obtained simply by changing the "kernel" function utilised

(Burges, 1998). Due to the fairly new development of SVMs they are not commonly utilised in BCI systems (see (Gysels and Celka, 2004) for an example). Thus, their performance for mental task classification has not been widely assessed and their application in such systems can be considered novel.

SVMs belong to the family of kernel based classifiers. The main concept of SVMs is to implicitly map the data into the feature space where a hyperplane (decision boundary) separating the classes may exist. This implicit mapping is achieved via the use of Kernels, which are functions that return the scalar product in the feature space by performing calculations in the data space. The simplest case is a linear SVM trained to classify linearly separable data. After re-normalisation, the training data, $\{x_i, y_i\}$ for i=1, …, m and $y_i \in \{-1,1\}$, must satisfy the constraints

$$\mathbf{x}_i \mathbf{w} + b \geq +1 \quad \text{for } y_i = +1 \tag{3}$$

$$\mathbf{x}_i \mathbf{w} + b \leq -1 \quad \text{for } y_i = -1 \tag{4}$$

where $\boldsymbol{w}$ is a vector containing the hyperplane parameters and b is an offset. The points for which the equalities in the above equations hold have the smallest distance to the decision boundary and they are called the support vectors. The distance between the two parallel hyperplanes on which the support vectors for the respective classes lie is called the *margin*. Thus, the SVM finds a decision boundary that maximises the margin. Finding the decision boundary then becomes a constrained optimization problem amounting to minimisation of $\|w\|^2$ subject to the constraints in (3) and (4) and is solved using Lagrange optimisation framework. The general solution is given by

$$f(x) = \sum_i \alpha_i y_i \langle x_i, x \rangle \tag{5}$$

In the case of non-linear classification, Kernels (functions of varying shapes, e.g. polynomial or Radial Basis Function) are used to map the data into a higher dimensional feature space in which a linear separating hyperplane could be found. The general solution is then of the form:

$$f(x) = \sum_i \alpha_i y_i K\langle x_i, x \rangle \tag{6}$$

Depending on the choice of the Kernel function SVMs can provide both linear and non-linear classification, hence a direct comparison between the two can be made without having to resort to utilisation of different classifiers.

3.1.3 Data

At this stage we utilise EEG data that is available online. The dataset chosen is well-known and has been used in various BCI applications. It contains EEG signals recorded by Keirn and Aunon during 5 mental tasks and is available from (http://www.cs .colostate.edu/~anderson). Each mental task lasted 10s and subjects participated in recordings over 5 trials and a number of sessions (subjects 2 and 7 participated in 1 session, subject 5 in 3 and subjects 1, 3, 4 and 6 in 2). The data was recorded with a sampling rate of 250Hz from 6 EEG electrodes placed at locations C3, C4, P3, P4 and O1 (more details on the recording protocol can be found in (Keirn and Aunon, 1990)). The 5 mental tasks are: (1) Baseline: subjects are relaxed and should be thinking of nothing particular; (2) Multiplication: subjects are asked to perform non-trivial mental multiplication problems; it is highly likely that a solution was not arrived at by the end of the allocated recording time; (3) Rotation: a 3-dimensional geometric figure is shown on the screen for 30s, after which the subjects are asked to mentally rotate the figure about an axis; (4) Letter composition: subjects are asked to mentally compose a letter, continuing its composition from where it was left off at the end of each trial; and (5) Counting: subjects are asked to count sequentially by imagining the numbers being written on a blackboard and rubbed off before the next number is written. In each trial counting resumes from where it was left off in the previous trial.

This dataset has been chosen for two reasons. Firstly, it contains recordings from mental tasks that are traditionally associated with BCI systems. Secondly, it allows the investigation of a large combination of mental task pairs as it contains recordings from 5 different tasks – this will allow us to identify whether the choice of tasks depends on the subject and whether other non-traditional tasks should also be investigated. In addition, a third good reason is that it allows direct comparison with results from the literature.

4 RESULTS

To allow a direct comparison of the results with those presented in (Huan and Palaniappan, 2004), we used data from 2 sessions and 4 subjects

(subjects 1, 3, 5 and 6). The data was split in non-overlapping segments of 0.5s duration, resulting in 200 segments per task per subject, over 2 sessions. The SVM classification rate was averaged over 10 trials, where in each trial a randomly chosen set of 100 segments was used for training, with the remaining segments used for testing. All 10 pair combinations of the 5 mental tasks were classified and the pair of tasks with the maximum average classification rate for each subject was identified. The average classification rate was estimated as $(TP_1+TP_2)/2$, where TP_i (true positive) is the number of segments classified correctly for mental task *i*. The feature vectors describing each 0.5s segment are 36-dimensional in the AR(6) case and 300-dimensional in the PSD values case (6 AR coefficients and 50 PSD values per electrode; the final feature vectors consisted of the concatenated AR coefficients and PSD values for all electrodes respectively).

The classification results for the AR(6) features are presented in table 1. It can be seen that the choice of classifier had a positive effect on the classification accuracy. The use of an SVM increased the accuracy by up to nearly 13% compared to that obtained for the same features using LDA and by up to 16.3% using an NN (see table 2 for details), as presented in (Huan and Palaniappan, 2004). In theory, the choice of classifier has a smaller effect on the classification rate if the features utilised represent the data well. Nonetheless, the use of an SVM with RBF Kernel increases the classification rate by a large margin and, hence these results indicate that the use of an SVM is more appropriate for these features. In addition, the pair of tasks which provided the highest average classification was different than the equivalent pair from (Huan and Palaniappan, 2004). However, it was also observed that the task pair which gave highest average classification varied with each subject, in agreement with (Huan and Palaniappan, 2004). Hence a particular task pair for which optimal operation can be obtained should be identified for each subject. In addition, performance could be improved if the tasks utilised had a more intuitive connection with the way of thinking associated with MC.

The classification rates for the PSD features are presented in table 3. The rates obtained are much lower than the ones reported in (Palaniappan et al., 2002). This could be attributed to three reasons. Firstly, in this work classification between pairs of tasks was obtained as opposed to between 3 tasks as in (Palaniappan et al., 2002) hence a direct comparison is not appropriate. Secondly, the PSD features are already of high dimension (300-dimensional) and an SVM may not be appropriate for classification when the feature space is already of high dimension. Thirdly, the classification rates presented in (Palaniappan et al., 2002) were averaged for a single training set whose ordering of the training patterns was randomly varied 10 times, hence the high classification rate reported may have been a side-effect of the particular choice of training set. In addition, another issue with utilisation of PSD values as features is the partial spectrum overlarp of certain artefacts (such as eye movements) with EEG activity, which can potentially adversely affect the classification rate.

Table 1: Maximum average classification rate (%) for AR(6) features with SVM. Results presented are averaged over 10 trials.

Subj.	Class. Rate	Tasks	Kernel
1	88.4	Letter vs multiplication	RBF
3	87.9	Letter vs counting	RBF
5	83.9	Roration vs counting	RBF
6	92.4	Counting vs multiplication	Linear

Table 2: Maximum average classification rate (%) for AR(6) features. Column 2 presents our results, while columns 3 and 4 give the best rates presented in (Huan and Palaniappan, 2004) for LDA and NN.

Subj.	SVM	LDA	NN
1	88.4	80.2	78.9
3	87.9	73.6	73.9
5	83.9	71.4	67.6
6	92.4	84.3	77.6

Table 3: Maximum average classification rate (%) for power spectrum values with SVM. Results presented are averaged over 10 trials.

Subj.	Class. Rate	Tasks	Kernel
1	58.0	Letter vs multiplication	RBF
3	56.6	Letter vs counting	RBF
5	68.0	Roration vs counting	RBF
6	60.2	Counting vs multiplication	Polyno-mial

The feature vectors were created by concatenating the estimated AR coefficients from all 6 electrodes. However, the wearability and portability of an MC-based BCI is facilitated by

employing a small number of electrodes –ideally two, or even a single, electrode(s). It may be possible to obtain higher classification rates by utilising a single electrode that is more relevant to the specific mental task rather than using a combination of electrodes, all of which are not as relevant to the task. This is also advantageous as it decreases the feature dimensionality.

5 CONCLUSIONS

This paper presents the results of initial investigations in the search for appropriate features and classifier towards the development of a thought-to-speech converter. The results indicate that the use of an SVM for the classification of AR coefficients is more appropriate than LDA and NN and will be utilised in the development of the proposed system.

The proposed system is promising as it offers the ability to communicate more efficiently via direct conversion of thoughts into speech. In order to ensure optimal operation other aspects of the system must also be investigated. Firstly, a more extensive set of features and classifiers will be examined such that the optimal combination in terms of maximising accuracy is determined – computational efficiency is not a consideration as the system will be customised and capable of parallel processing. Secondly, these investigations suggest that different combinations of mental tasks seem to be more appropriate for different subjects. We are going to look into finding a combination of tasks that are more intuitive and more closely related to the concept of MC, as this could improve classification accuracy and facilitate easier operation.

REFERENCES

Altschuler, E.L., and Dowla, F.U., 1998. Encephalolexianalyzer. United States Patent Number: 5,840,040. November 24.

Burges, C. J. C., 1998. A tutorial on Support Vector Machines for Pattern Recognition. In *Data Mining and Knowledge Discovery*, U. Fayyad, Ed. Boston: Kluwer Academic Publishers, pp. 121-167.

Coe, L., 2003. Telegraph: A History of Morse's invention and its predecessors in the United States. McFarland & Company.

French, T., 1993. McElroy, World's Champion Radio Telegrapher. Artifax Books.

Guger, C., Schlogl, A., Neuper, C., Walterspacher, D., Strein, T., and Pfurtscheller, G., 2000. Rapid Prototyping of an EEG-based Brain-Computer Interface (BCI). In *IEEE Trans. on Neural Systems and Rehab. Eng.,* Vol. 9, issue 1, pp.49-58, March.

Gysels, E., and Celka, P., 2004. Phase synchronisation for the recognition of mental tasks in a brain-computer interface. In *IEEE Trans. on Neural Systems and Rehab. Eng.*, Vol. 12, issue 4, pp. 406-415.

Huan, N.-J., and Palaniappan, R., 2004. Neural network classification of autoregressive features from electroencephalogram signals for brain-computer interface design. In *Journal of Neural Eng.*, Vol. 1, pp.142-150.

Keirn, Z.A., and Aunon, J.I., 1990. A new mode of communication between man and his surroundings. In *IEEE Trans. Biomed. Eng.,*, Vol. 37, pp.1209-1214.

Levine, S.P., Gauger, J.R.D., Bowers. L.D., and Khan, K.J., 1986. A comparison of Mouthstick and Morse code text inputs. In *Augmentative and Alternative Communication*, Vol. 2, issue 2, pp.51-55.

Lopes da Silva, F., 1998. EEG analysis: Theory and Practice. In *Electroencephalography: Basic Principles, Clinical Applications and Related Fields*, Ch. 6, pp.1135-1163.

Palaniappan, R., Paramesan, R., Nishida, S., and Saiwaki, N., 2002. A new brain-computer interface design using Fuzzy ARTMAP. In *IEEE Trans. On Neural Systems and Rehab. Eng.*, Vol. 10, issue 3, pp.140-148.

Palaniappan, R., 2005. Brain computer interface design using band powers extracted during mental tasks. In *Procs. of the 2nd International IEEE EMBS Conf. on Neural Eng.,* Arlington, Virginia. March 16-19.

Park, H.-J., Kwon, S.-H., Kim, H.-C., and Park, K.-S., 1999. Adaptive EMG-driven communication for the disability. In *Procs. of 1st Joint BMES/EMBS Conf. Serving Humanity, Advancing Technology.* Atlanta, USA, October 13-19. p.656.

Scherer, R., Muller, G. R., Neuper, C., Graimann, B., and Pfurtscheller, G., 2004. An Asynchronously controlled EEG-based virtual keyboard: improvement of the spelling rate. In *IEEE Trans. on Biomed. Eng.*, Vol. 51, issue 6, pp.979-984.

Vaughan, T.M., et al., 2003. Brain-computer Interface Technology: a review of the second international meeting (Guest Editorial). In *IEEE Trans. on Neural Systems and Rehab. Eng.*, Vol. 11, issue 2, pp.94-109.

Wolpaw, J.R., et al., 2000. Brain-Computer Interface Technology: a review of the First International meeting. In *IEEE Trans. on Rehab. Eng.*, Vol. 8. issue 2, pp.164-173.

Wolpaw, J.R., Birbaumer, N., McFarland, D.J., Pfurtscheller, G., and Vaughan, T.M., 2002. Brain-Computer Interfaces for communication and control. In *Clinical Neurophysiology*, Vol. 113, pp.767-791.

Wright, J.J., Kydd, R.R., and Sergejew, A.A., 1990. Autoregression Models of EEG. In *Biological Cybernetics*, Vol. 62, pp.201-210.

TREATMENT OF MITRAL VALVE INSUFFICIENCY BY SHAPE MEMORY POLYMER BASED ACTIVE ANNULOPLASTY

Pilar Lafont Morgado, Andrés Díaz Lantada, Héctor Lorenzo-Yustos, Julio Muñoz-García
División de Ingeniería de Máquinas – E.T.S.I. Industriales – Universidad Politécnica de Madrid
C/ José Gutiérrez Abascal, nº 2. 28006 – Madrid, Spain (+34) 913364217
andresdiazlantada@gmail.com

Ignacio Rada Martínez, Antonio Jiménez Ramos, José Luis Hernández Riesco
Hospital Gómez Ulla
Glorieta del Ejército s.n. 28047 – Madrid, Spain

Keywords: Shape Memory Polymers (SMP), Mitral valve Insufficiency, Annuloplasty ring, Laser Stereolithography, Silicone mould vacuum casting, Biomaterials.

Abstract: Active materials are capable of responding in a controlled way to different external physical or chemical stimuli by changing some of their properties. These materials can be used to design and develop sensors, actuators and multifunctional systems with a large number of applications for developing medical devices. (for both surgery and implants).
Shape memory polymers are active materials with thermo-mechanical coupling (changes in temperature induce shape changes) and a capacity to recover from high levels of distortion, (much greater than that shown by shape memory alloys), which combined with a lower density and cost has favoured the appearance of numerous applications. In many cases, these materials are of medical grade, which increases the chances of obtaining biocompatible devices.
This paper presents the design, manufacture, "shape memory" programming process and in vitro trials of an active annuloplasty ring for the treatment of mitral valve insufficiency, developed by using shape memory polymers. This has been done with the collaboration betweeen researchers from Universidad Politécnica de Madrid and doctors from the Hospital General Central de la Defensa.

1 MITRAL INSUFFICIENCY AND POSSIBLE IMPROVEMENTS IN ANNULOPLASTY TREATMENT

1.1 Mitral Valve Insufficiency

The mitral valve is made up of two components whose mission is to channel the blood from the left auricle to the left ventricle. Firstly, there is the so-called "mitral valve complex" comprising the mitral annulus, the valve leaflets, and the commissures joining both valves. Apart from the mitral valve complex itself, this valve has the so-called "tensor complex", which in turn comprises the chordae tendineae which continue with the papillary muscles attached to the left ventricle.

A failure of any of these elements leads to functional changes in the mitral apparatus, such as mitral insufficiency, explained below, and hemodynamic repercussions.

Mitral insufficiency (or regurgitation) is defined as the systolic regurgitation of blood from the left ventricle to the left auricle, due to incompetence in mitral valve closing. This can arise for three main reasons: a) primary disease of the mitral valve; b) an anatomic or functional alteration in the chordae tendineae or in the papillary muscles, and c) a disorder in the correct function of the left auricle and the left ventricle (Díaz Rubio, 1994).

Valve reconstruction is currently the preferred treatment for mitral insufficiency provided this is possible. With the aid of preoperative transesophagic echocardiography lesions can be located and their extent seen, so a surgeon can evaluate if valve repair is possible and thus design an exact plan for any

operation required. Nowadays, the object of this surgery is not simply limited to eliminating mitral insufficiency but in many cases to reconstructing the geometry of the entire mitral valve apparatus to ensure a durable repair.

Surgically restoring the geometry to normal conditions consists in: a) augmenting or reducing the abnormal leaflets; b) replacing broken or short chordae tendineae using "Goretex" type sutures, and c) annuloplasty.

1.2 Treating Mitral Insufficiency with Annuloplasty

Carpentier's description of a rigid prosthetic ring to allow a selective reduction of the entire mitral annulus opened the way to modern mitral repair. Annuloplasty consists in inserting the said ring-shaped device into the coronary sinus and after applying traction, retraction or heat, it reduces its perimeter, thereby reducing the mitral annulus and improving the contact between the valve leaflets, which leads to a reduction in the patient's degree of mitral insufficiency (Hernández, 2005).

Since then, a series of implants have been developed that can be basically classified as rigid or flexible and total or partial. Rigid monoplane implants have been displaced due to the large number of experimental and clinical works showing that the perimeter of the mitral annulus constantly changes in size and shape during the heart cycle. The recent findings showing that these changes are produced in a three-dimensional way with a hyperbolic paraboloid shaped ring has given rise to new rigid three-dimensional prosthesis. Duran proposes replacing the most conventional devices for other flexible or semi-rigid designs that reproduce the three-dimensional shape, such as the one marketed by Medtronic Inc..

1.3 Desirable Improvements Employing Progressive Procedures

However, inserting a device to close the mitral valve means making additional demands on the heart that may lead to postoperatory problems. It would be ideal to insert a ring with the same shape as the patient's mitral annulus and, when they have recovered from the operation, progressively act on this ring (in several stages) and remotely. This seeks to maintain a balanced situation and not excessively overload the patient's heart during the operation.

In this way, the progressive closing of the patient's mitral annulus can be controlled and, by using non-invasive inspection technologies, the improvement in the patient's mitral insufficiency can be evaluated after each stage of the ring actuation.

2 SOLVING MECHANICAL OPERATION USING SHAPE MEMORY POLYMER BASED DEVICES

2.1 Shape Memory Polymers in Medical Devices

Shape memory polymers (SMPs) are materials that give a mechanical response to temperature changes. When these materials are heated above their "activation" temperature, there is a radical change from rigid polymer to an elastic state that will allow deformations of up to 300%. If the material is cooled after manipulation it retains the imposed shape; it "freezes", the said structure returning to a rigid but "non-equilibrium" state. When the material is heated above its activation temperature, it recovers its initial undeformed state.

The cycle can be repeated numerous times without degrading the polymer and most suppliers can formulate different materials with activation temperatures ranging between –30 ºC and 260 ºC, depending on the application required.

They are therefore active materials that present thermomechanical coupling and a capacity to recover from high levels of distortion, (much greater than shown by shape memory alloys), which combined with a lower density and cost has favoured the appearance of numerous applications. Their properties allow applications for manufacturing sensors and actuators, especially for the aeronautic, automobile and medical industry (Lendlein, Kelch, 2002).

The main problem associated with the use of shape memory polymers is the lack of structured processes for developing devices based on these materials. The design process for these devices and the transformation processes for these materials need to be more thoroughly investigated.

The main advantages of shape memory polymers are:

- They are new materials with the ability to change their geometry from an initial deformed shape to a second shape predetermined during the manufacturing process.

- They are more economical than shape memory alloys.
- Different additives can be used to change their properties "a la carte", to better adapt them to the end application.
- The levels of deformation are much greater than those obtainable using shape memory alloys.
- They can also be more easily processed and allow the use of "Rapid Prototyping Technologies", which speeds up the production of devices.
- More complex geometries and actuators can be obtained than with developments based on shape memory alloy.

However, due to their recent appearance, in many cases their mechanical and thermomechanical properties are still not completely typified, which gives rise to doubts concerning how devices based on these materials will react. One of the basic aims of current research is to increase knowledge of the properties of these polymers by improving characterization processes.

Regarding the development of medical devices, both surgical and implantable ones, they have additional advantages to those mentioned above:

- They are frequently medical grade materials which increases the chances of obtaining biocompatible devices.
- The combined use of preoperative inspection technologies and CAD-CAE-CAM technologies means that prostheses and customised devices can be tailored for patients.
- Their activation temperature and properties can be adapted to the application, thanks to the amount of copolymers employed and the use of additives.

Among the medical devices developed that take benefit from the advantages of these polymers, the most notable are self-expanding stents, drug release devices, thrombectomy devices, intelligent sutures and active catheters (Lendlein, 2002, 2005, Wilson, 2006).

2.2 Shape Memory Polymers for Active Annuloplasty

Commercial annuloplasty rings based on shape memory polymers have been patented but not yet developed.

The Sorin Group's Memo 3D manages to reduce its shape by using a shape memory alloy (Nitinol type, similar to those used in the manufacture of self-expanding stents). However, the change of shape is produced during the operation itself on making contact with human body temperature, which means that no postoperative measures are possible.

Besides, the capacity of shape memory polymers to recover their shape against efforts of up to around 7 MPa means that a 3 mm thick annuloplasty ring, similar to devices currently in use, manufactured with these materials will be able to overcome a circumferential force of between 4 N to 12 N that is imposed by the patient's mitral annulus.

In accordance with the above, what is proposed is a ring made of shape memory polymer and electrical resistances or heaters distributed inside to activate the "shape memory effect" and therefore the required shape change.

Firstly, the ring adapts to the end size required (that needed to eliminate the mitral insufficiency) and with the resistances already in place. The ring is then uniformly heated to a temperature higher than the transition temperature (situated for the end product between 41 ºC and 43 ºC) and is forced to take on the expanded transitory shape (to do this cone-shaped tools can be used with a cross section similar to that of the mitral annulus), letting it cool down to room temperature. The device also consists of a battery to power the resistances and heat them. The rise in temperature of the resistances causes a local rise in temperature, which, if suitably controlled leads to a change in phase of the SMP and the associated size reduction.

Using an associated electronic control enables the resistances to be operated in pairs and at different times, in order to carryout the progressive or "step by step" operation required on the ring. Figure 1 shows a preliminary design.

Figure 1: Preliminary active annuloplasty ring design. SMP with internal resistances for heating.

A patent for this device was applied for by the authors under the title of "Active annuloplasty system for the progressive treatment of valve insufficiencies and other cardiovascular pathologies"

on 13 December 2006 with Application Number P200603149 and is currently being evaluated by the Spanish Patents and Trade Marks Office.

The following sections present the design alternatives and the prototypes obtained, as well as the first "in vitro" trials performed, the results, and future recommendations for optimising the results. The development has been carried out in collaboration between researchers from from Universidad Politécnica de Madrid and doctors from the Hospital General Central de la Defensa.

3 DESIGN AND MANUFACTURE OF PROTOTYPES

Computer aided design and calculation technologies, (CAD – Computer Aided Design and CAE – Computer Aided Engineering), have become an essential tool for developing medical devices. They enable alternative shapes and designs to be obtained quickly, as well as making it easier to evaluate their advantages by being able to analyse stress, deformations, ergonomics or dynamic response. They are also highly valuable for comparing and selecting the different materials that can be used. In addition, when combined with preoperative inspection techniques, they serve to design implantable devices tailored for the patient measurements and simulate their implantation.

Figure 2 shows alternative designs for annuloplasty rings made by using the "Solid Edge v.18" computer design package. With the help of these programmes it is very simple to change the parameters of a design, which enables a shape to be adapted to the size of a particular patient's mitral annulus or change the thickness of rings depending on how long the device is required to last.

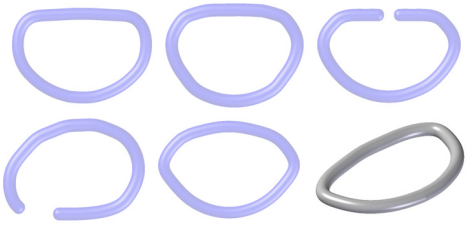

Figure 2: Alternative designs for annuloplasty rings produced with CAD technologies.

Bellow is explained how prototypes are manufactured from the designs shown and the advantages of using rapid prototyping and rapid tooling technologies.

Figure 3 shows the physical models obtained in epoxy resin by laser stereolithography using an SLA-350 machine available at the Product Development Laboratory of Universidad Politécnica de Madrid, from the designs shown in Figure 2. Together with the annuloplasty designs, also shown is a 3 mm thick, 30 mm outer diameter toroidal ring to give the image an idea of scale.

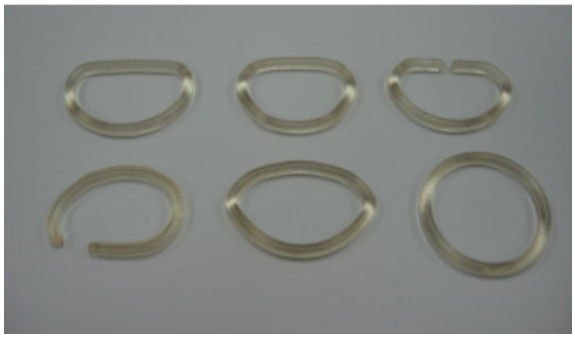

Figure 3: Models obtained by laser stereolithography from files containing the 3D part geometry.

The parts obtained by stereolithography are particularly suitable for checking sizes, shapes and appearance. They can also be used as models for obtaining silicone moulds, which are subsequently used to obtain polyurethane resin replicas, more resistant and suited to working trials, and which also possess shape memory properties. With the vacuum casting process different types of bicomponent resins can be used, with a wide range of properties, and the prototypes obtained reproduce the mould cavities with great precision (roughnesses of up to 50 μm) (Lafont, 2000).

The chosen material is a polyurethane resin from MCP Iberia company with reference 3174 which is supplied in bicomponent form, which means it can be cast (after mixing the two components) in silicone moulds to obtain the prototype shape required.

It must be pointed out that shape change temperature of the polyurethane resin used is not suited to the "in vivo" end trials, nor fits the initial specifications which required a range of 41 to 43 ºC to activate the shape memory effect.

However, this polyurethane resin has been used because it is easies to manipulate and cast in silicone moulds, which enables prototypes to be made in less than 5 days from computer file to end material.

Other mould manufacture technologies are currently being used for casting alternative shape memory polymers which do not attack the silicone moulds and whose transition temperature can be set from 4 to 6 ºC above that of the human body, suited to the "in vivo".

Figure 4 shows silicone moulds obtained from the physical epoxy resin models displayed in Figure 3. These moulds enable prototypes to be obtained from the material with shape memory properties.

Figure 4: Silicone moulds obtained from laser stereolithographic models.

Enhanced design models have led to the construction of new silicone moulds and the obtaining of improved prototype annuloplasty rings, both solid ones and with circumferential grooves for housing the heating resistances. These are shown in Figure 5.

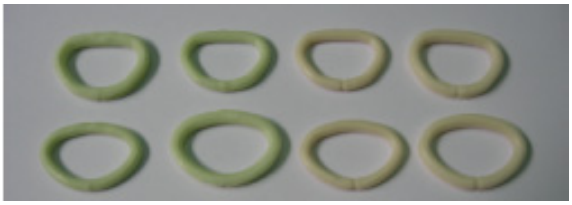

Figure 5: Different polyurethane resin prototypes obtained under vacuum casting in silicone moulds. Both open and closed rings were made to analyse alternative performances.

4 PROGRAMMING PROCESS OF THE SHAPE MEMORY

When the annuloplasty rings have been shaped to ensure the mitral valve closes properly, they need to undergo heat deformation at 80 ºC in the case of polyurethane resin, (higher temperature than that needed to activate the shape memory effect), to increase their cross section until it coincides with the patient's mitral valve annulus in the initial state of insufficiency.

By doing this, a temporary shape is obtained and the ring can be implanted without submitting the patient's heart to an additional overload due to a sudden reduction in the section of the mitral valve.

After the surgical operation the recovery effect of the original shape is activated, which produces a gradual, controllable closure of the valve and a controlled recovery of mitral regurgitation.

To perform this "shape memory programming process", tools were used that were obtained by laser stereolithography in the form of a cone base with a similar cross section to that of the patient´s mitral annulus.

Figures 6 shows the tool and deformations caused to ring prototypes thanks to the use of a counter-shape that acts as a press on the tool and the prototype.

Figure 6: Design and prototype of a tool for programming shape memory effect. Deformation caused at 80 ºC to obtain a temporary shape.

Figure 7 shows an annuloplasty ring with the temporary shape already applied and prepared for implant and the first "in vitro" trials. With the aid of a cone base a 15% increase in cross section was produced (maximum inner diameter ring size pass from 26 to 28 mm), which will be used to evaluate the subsequent shape memory recovery in "in vitro" trials.

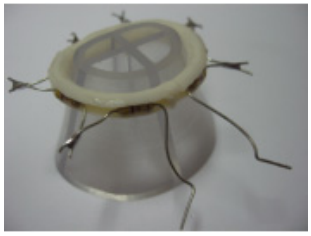

Figure 7: Active ring with heating resistances with the temporary shape already applied. It is ready to be implanted and subsequently activated.

5 RESULTS OF "IN VITRO" TRIALS

For performing the first "in vitro trials" two pig hearts were used because of their similarity to human ones, as is demonstrated by their being used for biological valve replacement operations.

Figure 8 shows the process for activating the shape memory process in the ring and reducing the associated mitral ring cross section.

The 4,7 Ω resistances (a total of 7 resistances with serial connection) were supplied with power by a 12 V transformer. Thus an intensity of 364 mA was obtained, similar to what can be supplied by

implantable commercial devices. The images (left to right) show a 10.7% reduction in cross section during an operating period of 150 seconds. This means a 71%, recovery compared to effort since the increase in cross section induced was 15%.

By interrupting heating the temperature decreases and the recovery process is halted, which means the required effect can be obtained step by step. By recommencing the heating process the recovery will continue, although in these first "in vitro" trials heating was done continuously in order to evaluate the maximum recovery that could be obtained and the duration of the entire process. Temperature was continuoustly measured using a thermocouple.

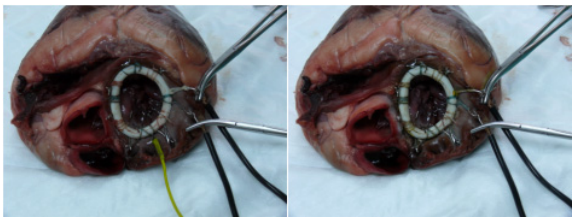

Figure 8: Activating the shape memory effect using heating resistances.

Despite it being desirable a cross section reduction of 15% to 20%, it is very important to point out the material's capacity for recovery while overcoming the forces imposed by the mitral annulus of the hearts used.

6 FUTURE IMPROVEMENTS AND CONCLUSIONS

For the postoperative and progressive treatment of mitral insufficiency the use of an annuloplasty device made of shape memory polymer has been proposed. It has electrical resistances distributed inside it to activate the "shape memory" effect, so that the required change in shape to reduce mitral regurgitation can be progressively induced. This provides an alternative to current devices, that do not permit any change of shape after implantation, and therefore any errors committed during the operation cannot be corrected.

The design, manufacturing, "shape memory" effect programming and "in vitro" trials of such an annuloplasty ring for treating mitral insufficiency, developed by using shape memory polymers, have been presented.

This has been done in collaboration between researchers from from Universidad Politécnica de Madrid and doctors from the Hospital General Central de la Defensa.

Using computer aided manufacture and design technologies has enabled different designs and prototypes to be produced in parallel, as well as rapid improvements to obtain the devices that were used in the in vitro trials.

Future actions regarding improvements in the shape memory programming process should lead to optimising the reduction in mitral ring cross section up to the required 15% to 20%. Using alternative shape memory polymers with a lower activation temperature will also result in more suitable devices, since they will require a smaller size heating system and will be easier to manufacture.

However, it is very important to point out the material's capacity for recovery against the forces imposed by the mitral annulus of the hearts used, which shows the feasibility of developing an active annuloplasty system based on the use of shape memory polymers.

REFERENCES

Díaz Rubio, M., Espinós, D., 1994. Tratado de Medicina Interna. *Editorial Médica Panamericana*.

Carpentier, A., 1983. Cardiac Valve Surgery – The French Correction. *Journal of Thoracic and Cardiovascular Surgery*.

Duran, C., 1992. Duran Flexible Annuloplasty Repair of the Mitral and Tricuspid Valves: Indications, Patient Selection, and Surgical Techniques Using the Duran Flexible Annuloplasty Ring. *Medtronic Inc.*.

Hernández, J.M., 2005. Manual de Cardiología Intervencionista. *Sociedad Española de Cardiología. Sección de Hemodinámica y Cardiología Intervencionista.*

Lendlein, A., S. Kelch, 2002. Shape-Memory Polymers. *Angewandte Chemie International*.

Lendlein, A., Langer, R., 2002. Biodegradable, elastic shape-memory polymers for potential biomedical applications. *Science*.

Lendlein, et al., 2005. Light-induced shape-memory polymers. *Nature*.

Wilson,T., et al., 2006. Shape Memory Polymer Therapeutic Devices for Stroke. *Lawrence Livermore National Laboratory*.

Lafont, P., Lorenzo, H. et al., 2000. Rapid Tooling: moldes rápidos a partir de estereolitografía. *Revista de plásticos modernos*.

BIOMATERIAL FOR SOFT TISSUE REPLACEMENTS

David N. Ku and Jin Wu Fan
Georgia Institute of Technology, Atlanta, GA 30332-0405, USA
david.ku@me.gatech.edu

Keywords: Biomaterial, mechanics, elasticity, strength, wear, biocompatibility, medical devices.

Abstract: Typical biomaterials are stiff, difficult to manufacture, and not initially developed for medical implants. A new biomaterial is proposed that is similar to human soft tissue. The biomaterial provides mechanical properties similar to soft tissue in its mechanical and physical properties. Characterization is performed for modulus of elasticity, ultimate strength and wear resistance. The material further exhibits excellent biocompatibility with little toxicity and low inflammation. The material can be molded into a variety of anatomic shapes for use as a cartilage replacement, heart valve, and reconstructive implant for trauma victims. The biomaterial may be suitable for several biodevices of the future aimed at soft-tissue replacements.

1 BACKGROUND

Most of the existing biomaterial technology is limited to materials such as silicones, Teflon®, polyethylene, metal and polyurethanes that do not exhibit the mechanical and physical properties of natural tissue. These materials are stiff, difficult to manufacture, and not initially developed for medical implants. Artificial tissue substitutes have not been found to withstand the rigors of repetitive motion and associated forces of normal life. Cadaver tissue is limited in supply and due to the risk of infection is coming under increased scrutiny by FDA and is not accepted in Europe.

As an example, one of the most successful medical implants is the artificial knee replacement for the treatment of arthritis. Arthritis and joint pain as a result of injury are major medical problems facing the US and patients worldwide. Worldwide, approximately 190 million people suffer from osteoarthritis. This condition affects both men and women, primarily over 40 years of age. The spread of arthritis is also fueled by the rise of sports injuries. Activities enjoyed by many can translate into injury or joint damage that may set up a process of deterioration that can have devastating effects decades later. The number of patients that have arthritis is staggering and growth is expected with baby boomers entering the prime "arthritis years" with prolonged life expectancies. Growth of the world's elderly is expected to increase three times faster than that of the overall population.

Current standard treatment is to surgically implant a total knee replacement (TKR) that is made of metals such as cobalt chromium or titanium. These devices are highly rigid, providing no shock absorption. Further, the metal integrates poorly with bone and the HMWPE caps often create micro-particulate debris with strong inflammation. The invasive surgery not indicated for those under age 60 and usually reserved for end-stage patients. A revision procedure is technically demanding, and amputation may be required.

An alternative biodevice may be a soft tissue replacement. Arthritis stems from damage to cartilage, the soft tissue between the bones. Damaged cartilage leads to grinding of bone on bone and eventual pain and limited joint function. Biodevices that replace the soft tissue would restore diarthroidal joint function much better and protect further damage by a more natural stress distribution.

A similar problem exists for heart valves. Prosthetic heart valves are made from metal and pyrolitic carbon which do not function like native heart valves. The use of hard materials creates high shear zones for hemolysis and platelet activation. Tissue valves are subject to calcification, again a problem of hard tissues not acting like natural soft tissue. An alternative would be to design a biodevice with soft tissue flexibility and endothelial cell

covering to provide a wide-open central flow and low-thrombogenic surface.

Yet another example for the need for soft tissue replacements is a replacement part for reconstructive surgery after traumatic accidents or cancer resection. For many parts of the body, a replacement shape needs to have smooth contours as well as soft tissue compliance to yield a natural shape. The base biomaterial should not have chemical composition that is non-organic, such as silicone, which can induce a hyper-immunogenic response.

Soft tissue replacements should start with a biomaterial that has compliance ranges similar to human soft tissue, be strong and wear resistant, manufactured to personal shapes, and have long-term biocompatibility. Cellular in-growth or preloading of cells can then be performed on this established scaffold. These features are demonstrated in a new biomaterial described in this paper.

2 METHODS

2.1 Biomaterials

Soft tissue-like devices can be made from polymers such as poly vinyl alcohol as thermoset materials. As an example, a PVA cryogel can be made according to the full descriptions in US Patent U.S. Patent Numbers 5,981,826 and 6,231,605. The cryogels are made in a two stage process. In the first stage a mixture of poly (vinyl alcohol) and water is placed in a mold, and repeatedly frozen and thawed, in cycles, until a suitable cryogel is obtained.

Poly(vinyl alcohol) having an average molecular weight of from about 85,000 to 186,000, degree of polymerization from 2700 to 3500, and saponified in excess of 99% is preferred for creating soft tissue-like mechanical properties. High molecular weight poly (vinyl alcohol) in crystal form is available from the Aldrich Chemical Company. The PVA is then solubilized in aqueous solvent. Isotonic saline (0.9% by weight NaCl, 99.1% water) or an isotonic buffered saline may be substituted for water to prevent osmotic imbalances between the material and surrounding tissues if the cryogel is to be used as a soft tissue replacement.

Once prepared, the mixture can be poured into pre-sterilized molds. The shape and size of the mold may be selected to obtain a cryogel of any desired size and shape. Vascular grafts, for example, can be produced by pouring the poly (vinyl alcohol)/water mixture into an annular mold. The size and dimensions of the mold can be selected based upon the location for the graft in the body, which can be matched to physiological conditions using normal tables incorporating limb girth, activity level, and history of ischemia.

The new biomaterial, commercially available as Salubria® from SaluMedica, LLC, Atlanta, GA is similar to human tissue in its mechanical and physical properties. The base organic polymer is known to be highly biocompatible and hydrophilic (water loving). The hydrogel composition contains water in similar proportions to human tissue. Unlike previous hydrogels, Salubria is wear resistant and strong, withstanding millions of loading cycles; yet it is compliant enough to match normal biological tissue. The material can be molded into exact anatomic configurations and sterilized without significant deterioration.

2.2 Mechanical Characterization

2.2.1 Tensile Testing

Tensile test specimens were cut from sheets of Salubria. They were tested in accordance with ASTM 412 (die size D) in tension to failure using an Instron Model 5543 electro-mechanical load frame pulling at a rate of 20 inches per minute.

2.2.2 Stress-Strain Constitutive Relationship

The stress is a function of the load and the cross-sectional area. However, the cross-sectional area was difficult to measure. But the stretch ratio relates the final and initial area due to the assumption of incompressibility. That means the final area equals the initial area divided by the stretch ratio. Therefore, the ultimate stress calculation is a function of the load at the breaking point of the sample, the stretch ratio and the initial cross-sectional area. The initial cross-sectional area is the product of the initial width of the sample, w_o, and the initial thickness, t_o.

Stretch Ratio: $\lambda = C / C_o$ (1)

Initial Cross-Section Area: $A_o = w_o * t_0$ (2)

Final Stress: $$\sigma_{ult} = \frac{F_{ult} * \lambda}{A_o}$$ (3)

In order to get an estimation of the pressure in an intact tube the following simplified assumptions were used. It was assumed that a tubular specimen will burst when the circumferential wall stress is

equal to the ultimate stress σ_{ult}. However, when an artery is under physiologic load conditions it is in a state of plane strain and undergoes finite two dimensional stretches.

The stretch ratios are:

$$\lambda_\theta = \frac{r}{R} \tag{4}$$

$$\lambda_z = \frac{l}{L} \tag{5}$$

Rewritten to solve for the pressure, P:

$$P = \frac{T\sigma_\theta}{\lambda_\theta^2 \lambda_z R} \tag{6}$$

This equation can calculate the pressure if we know that data of the initial dimensions, the stress and the stretch ratios. From the equation (6) we can estimate the corresponding pressures.

2.2.3 Unconfined Compression

Cylindrical unconfined compression samples were cast in a custom mold. Samples were tested in unconfined compression on an Instron Model 5543 electro-mechanical load frame and on a DMTA IV dynamic mechanical analyzer. Rates of 1% strain per second and 20 inches per minute were tested.

2.2.4 Ultimate Strength

Ring specimens were pulled in tension until they failed. Ring specimens of Salubria were preconditioned twenty five cycles. Then the specimens were distracted at 0.1mm/s, 1m/s, 10mm/s, and 100mm/s using a MTS 858Mini Bionix Test System. Comparisons are made to normal coronary arteries using identical protocols. The load at failure was recorded as the ultimate load, and the ultimate stress was calculated. Failure of the ring specimen was defined as a complete tear of the ring through the entire wall. The stress was derived based on the assumption of incompressibility and was defined as the ratio of load and cross-sectional area. The stretch ratio was defined as the ratio of the final and initial circumference. The final stress at failure represented the ultimate strength for the tension tests. To determine the final stress, an equation was derived based on the assumption of incompressibility [3] which means that the initial volume V_o and final volume V are equal. In the present experiments the stretch ratio is defined as the ratio of the final and initial circumference, Equation (1). The ultimate stress, σ_{ult} defined by the load at the breaking point of the sample divided by the final cross-sectional area, was calculated using Equation (3).

2.2.5 Fatigue Resistance

Ring specimens were cycled at different cycles, and then pulled in tension until failure. The frequency of the cyclic tests was set at 2 Hz because this value is close to physiologic frequency of heart beats (~1.2 Hz) and strain rates effects testing showed that there are no significant difference to do cyclic test under 1HZ to 5HZ. The purpose of the cyclic tests was to experimentally determine how the fatigue affects the ultimate strengths of porcine common carotid arteries.

2.2.6 Cyclic Compression

A cyclic compression study was performed to assess the response of Salubria biomaterial cylinders to repetitive compressive loading at physiologic stress of approximately 1.3 MPa. The specimen is loaded for 1 million loading cycles at a rate of approximately 1.5 Hz. Dimensional integrity was measured using an optical comparator and mechanical modulus of elasticity was determined at 20% strain.

2.2.7 Wear Testing

An accelerated wear tester was built to test the wear rate of Salubria biomaterial. Polished stainless steel rollers with a diameter of 1 5/8 inches (chosen to approximate the average radius of the femoral condyles) are rotated so that they slide and roll across the test sample, creating a peak shear load of approximately 90N (0.2 MPa). Separate testing has shown the coefficient of friction for polished stainless steel against Salubria biomaterial to be equivalent to that of porcine femoral condyle with the cartilage surface abraded away to subchondral bone or roughly 4 times that of porcine femoral condyle with intact cartilage surface. The rotating cylinders exert a normal load of approximately 200N on the sample. The wear tester is operated at a rate that subjects the sample to 1000 wear cycles per hour where one cycle is defined as one roller to sample contact. Data has been collected with the sample lubricated and hydrated with water (a worst case scenario since synovial fluid should provide some surface lubrication). Wear rate is measured by

weight loss of the sample over a number of cycles. Salubria biomaterial is tested for >10,000,000 cycles against polished stainless steel rollers.

2.3 Biocompatibility

Biomaterials for use in humans must pass a full complement of biocompatibility tests as specified by ISO and the USFDA. The material was tested for ability to produce cytotoxicity, intracutaneous irritation, sensitization by Kligman maximization, Ames mutagenicity, chromosomal aberration, and chronic toxicity.

2.3.1 Rabbit Osteochondral Defect Model

In addition to the standard biocompatibility testing, the ability of Salubria biomaterial to withstand load or cause local inflammatory responses in a widely used rabbit osteochondral defect model was assessed (e.g., Hanff et al., 1990). A cylindrical plug (3.3 mm diameter, 3 mm depth) was implanted in the right knee of each of sixteen New Zealand white rabbits. An unfilled drill hole was made in the left knee of each animal to serve as an operative control.

After three months of implantation in the patellofemoral groove, eight rabbits were sacrificed for histologic analysis of the implant site and surrounding synovium. The remaining eight animals were sacrificed and the implant assessed for any change in physical properties. In addition, the distant organ sites that are known targets for PVA injected intravenously were assessed histologically for any sign of toxicity due to implantation. Tissues assessed included liver, spleen, kidney, and lymph node.

2.3.2 Particulate Inflammation

Salubria biomaterial was tested for particulate toxicity or inflammatory reaction in the joint. The study design was based on a study conducted by Oka et al. (2000) on a similar PVA-based biomaterial in comparison to UHMWPE. Particulate sizes for the study varied from approximately 1 micron to 1000 microns. The total volume of particulate injected over the 2 divided doses was designed to represent full-thickness wear of 10 x 10 mm diameter cartilage implants.

2.3.3 Ovine Knee Inflammation Model

In vivo testing was performed using a meniscus shaped device made of Salubria and implanted into the sheep knee joint. Devices were removed at 2 week, 3 week, 2 month, 4 month and 1 yr. intervals. Animals were fully load-bearing on the day of operation and after. Full range of motion with no disability was observed. Gross examination of surrounding tissues and histology of target end organs (liver, kidney, spleen, and lymph nodes) were evaluated for acute or chronic toxicity.

3 RESULTS

3.1 Tensile Testing

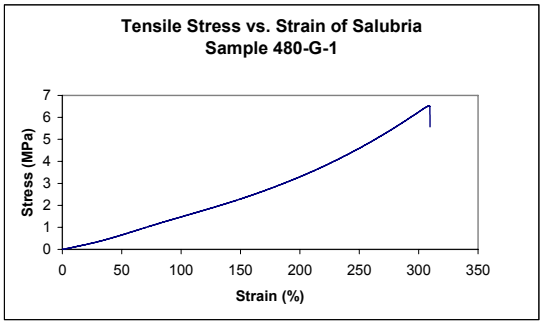

Figure 1: Representative Tension Curve.

Plots of stress versus strain in tension (figure 1) show a non-linear response. Due to the non-linearity of the loading curve, tangent modulus values at a defined percent strain are used to characterize the material stiffness. Tangent modulus ranges from 1.2-1.6 MPa. Ultimate tensile strength is 8-10 MPa. The stress-strain curve exhibits a non-linear elastic behavior similar to natural soft tissue.

3.2 Unconfined Compression

Figure 2 is a representative curve of stress versus strain in compression. Compression loading curves show a non-linearity suggesting that Salubria is a viscoelastic material similar to cartilage. Tangent modulus values in compression range from 0.1 to 7 MPa. Plastic compressive failure occurs at or above 65% strain.

3.3 Creep and Creep Recovery

Creep and creep recovery experiments were performed to assess the performance of Salubria biomaterial under long-term static loading at physiologic loads of up to 480 N-force. High loads were applied for 24 hours creating deformation of

50% of the initial height. Initial loading demonstrates a biphasic visco-elastic behavior. After 24 hours of recovery in saline, sample height had returned to within 5% of the original height. The compressive modulus of the material before the test and after creep recovery was unchanged.

3.4 Wear Testing

Results for one formulation of Salubria biomaterial tested for >2,000,000 cycles against polished stainless steel rollers demonstrate minimal wear.

3.5 Cyclic Compression

Repetitive compressive loading at physiologic stress of approximately 1.3 MPa was imposed. After 1 million loading cycles at a rate of approximately 1.5 Hz, there was minimal change (<5%) in sample dimensions and no change in modulus of elasticity at 20% strain.

3.6 Ultimate Strength

Sixty-four specimens were pulled at four different stain rates. Ultimate stress increased as a weak function of increasing strain rates. The ultimate stress at 100 mm/s was 4.54 MPa, greater than the 3.26 MPa at 0.1 mm/s. The differences between 0.1mm/s and 100 mm/s was highly significant with $p<0.001$. The differences between 0.1 mm/s and 10 mm/s gave $p=0.013$; and 1 mm/s to 100 mm/s was $p=0.018$. The difference between 1 mm/s and 10 mm/s was not statistical significance. Strain rates between 1 and 100 mm/s correspond to a cyclic frequency of 0.5 Hz to 5 Hz for fatigue testing.

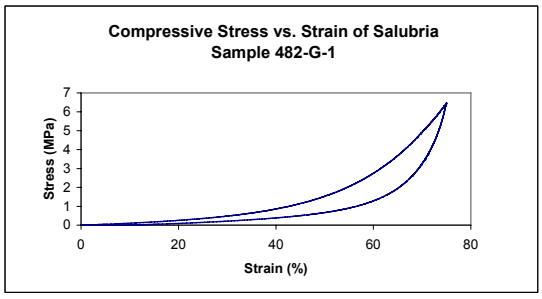

Figure 2: Representative Compression Curve.

3.7 Biocompatibility

The following table outlines the results of standard biocompatibility testing performed on Salubria biomaterial, in accordance with ISO 10993-1 and FDA Blue Book Memorandum #G95-1.

3.8 Animal Testing

After three months of implantation in the patellofemoral groove, eight rabbits were sacrificed for histologic analysis of the implant site and surrounding synovium. Tissues assessed included liver, spleen, kidney, and lymph node. The Salubria biomaterial was well-tolerated with subchondral bone formation surrounding the implant, no fibrous tissue layer or inflammatory response, no implant failures or evidence of wear debris formation, no osteolysis, and no toxic effects on the implant site or distant organ tissues.

At time of explantation, the samples were essentially unchanged (see Fig. 3). Based on histologic examination in comparison to the operative control, there was no evidence of inflammatory reaction in either the surrounding cartilage/bone (see Fig. 4) or in the synovium. In fact, a layer of normal hyaline cartilage partially covered the implant surface. The cartilage surface of the patella also showed no changes in the area articulating against the Salubria implant. There was no sign of toxicity on histologic examination of the distant organ sites.

Figure 3: The left-hand knee shows a Salubria implant in the patellofemoral joint of a rabbit knee after 3 months implantation. The right-hand knee is an operative control.

On excision for mechanical testing, the sample edges firmly adhere to the surrounding bone. The indentation force (i.e., the force required to cause a certain amount of sample deformation) of the implant is unchanged from a non-implanted control. Comparison material characterization testing showed that the implanted samples were not different from non-implanted controls.

Table 1: Biocompatibility Testing.

ISO 10993-1 Recommended Testing Requirement	Test Performed	Test Results
Cytotoxicity, ISO 10993-5	ISO MEM Elution L929 cells, GLP.	**Pass**
	Direct Contact Neurotoxicity	**Pass**
Sensitization and Irritation, ISO 10993-10	Kligman Maximization Method	**Pass**
	Primary Vaginal Test: Repeat Exposure	**Pass**
Sub-acute and Sub-Chronic Toxicity, ISO 10993-6	Sub-acute and sub-chronic toxicity	**Pass**
Genotoxicity, ISO 10993-3	Ames Mutagenicity: Dimethyl Sulfoxide Extract, 0.9% Sodium Chloride Extract	**Pass**
	Chromosomal Abberation	**Pass**
Implantation, ISO 10993-6 and 10993-11	Subacute or site Specific Implantation with chronic Toxicity	**Pass**
	Biocompatibility study in Rabbits following Intra-articular injections.	**Pass**
	Rabbit Trochlear Osteochondral Defect	**Pass**

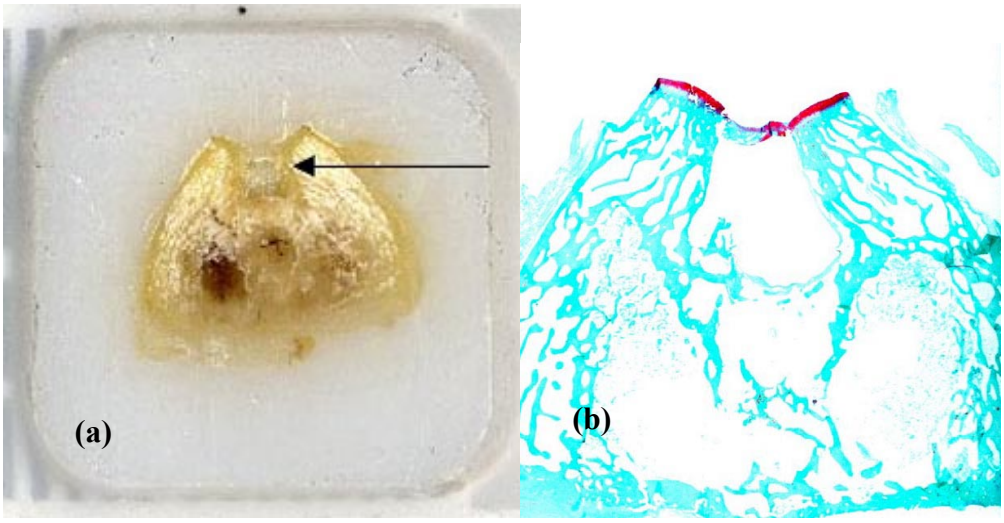

Figure 4: (a) This digital scan of a paraffin tissue block containing a Salubria implant demonstrates that the implant remains in place over 3 months of implantation in the rabbit patellofemoral groove. (b) Hematoxylin and eosin stain of a section from the tissue block in (a) showing the implant site – the implant has been removed during the staining process. There is no evidence of inflammatory reaction; the surrounding cartilage and bone are normal in histologic appearance.

Salubria biomaterial was tested for particulate toxicity or inflammatory reaction in the joint. Salubria particulates were biologically well-tolerated. The biomaterial particulate was deposited on the superficial synovium with minimal inflammatory reaction. There was no evidence of migration from the joint space or toxicity in the knee or at distant organ sites. There was no evidence of third body wear or osteolysis.

For the goat study, the native articular cartilage surfaces were protected in the test group compared to extensive damage from the control meniscectomy group. No local inflammation was noted on MRI or histology. No distant organ inflammation was seen

in these large animals, confirming the observations in the rabbits.

4 DISCUSSION

The biomaterial described here exhibits the requisite characteristics for soft tissue replacements. For knee cartilage, the material has non-linear viscoelastic properties similar to native tissue. The strength and fatigue properties exceed the requirements for a fully loaded knee articular joint (Stammen, 2001). For heart valves, the material must be moldable to complex anatomies and exhibit low thrombogenicity. For reconstructive anatomic parts, the biomaterial should be easily molded to custom shapes and have low inflammation potential. The biomaterial presented here exhibits these properties and opens the potential for soft tissue replacements that more closely match the anatomic and physiologic requirements.

Although ring specimens and dumbbell shape specimens are both one-dimensional tests, ring specimens were used because they provide a good gripping connection. Ring samples can relieve the experimental error comes from the inappropriate clamping dumbbell specimens which can cause the specimens to slide or break in the neighborhood of the clamp. There may be damage from preparing uniaxial dumbbell shaped strips. Dumbbell strips would also be difficult to obtain because of the small diameter of the tubular samples.

The biocompatibility testing for Salubria reflects previous carcinogenicity testing on other PVA-based biomaterials. PVA hydrogels in the literature are non-carcinogenic with rates of tumorigenicity similar to the well-accepted medical-grade materials, silicone and polyethylene. Nakamura (2000) reports on a 2-year carcinogenicity study conducted on a PVA-based biomaterial subcutaneously implanted in rats. Pre-clinical investigation of other PVA-based hydrogels and Salubria biomaterial demonstrates that these materials are biocompatible in the joint space (Oka et al., 1990). The rabbit is the most commonly published cartilage repair model with study lengths varying from 3 months to 1 year, with little difference in results at 3 months from those at 1 year. These studies indicate that 3 months is sufficient to assess biocompatibility and early treatment failure in the rabbit model. These results are further confirmed by clinical results on SaluCartilage^{TM}.

Based on this study, Salubria soft tissue biomaterial has been shown to be biocompatible with long-term implantation. There is no evidence of inflammatory response or local or distant toxicity. Furthermore, the biomaterial has stable, durable physical properties over the period of implantation in joints and would be suitable for use as structure deceives such as a cartilage replacement. The biomaterial presented here opens the potential for soft tissue replacements that more closely match the anatomic and physiologic requirements for human biodevices.

REFERENCES

Hanff, G., Sollerman, C., Abrahamsson, S. O., and G. Lundborg. 1990. Repair of osteochondral defects in the rabbit knee with Gore-TEXTM (expanded polytetrafluoroethylene). Scandinavian Journal of Plastic and Reconstructive Hand Surgery. 24: 217-223.

Oka, M., et al., Development of an artificial articular cartilage. Clin Mater, 1990. **6**(4): p. 361-81.

Stammen, J.A., Williams, S., Ku, D. N., and R. E. Guldberg. 2001. Mechanical properties of a novel PVA hydrogel in shear and unconfined compression. Biomaterials 22(8): 799-806.

PRECLINICAL TESTING OF A NEW VENOUS VALVE

Laura-Lee Farrell and David N. Ku
Georgia Institute of Technology, Atlanta, GA 30332-0405, USA
david.ku@me.gatech.edu

Keywords: Vein, venous valves, thrombosis, patency.

Abstract: Venous valvular incompetency is a debilitating disease affecting millions of patients. Unfortunately, the current physiologic and surgical treatments are prone to the extreme risk of post-operative thrombosis. A new design for venous valves has been proposed using biomimicry. The medical device has the shape of a natural valve with sufficient elasticity to maintain patency and competency in the leg veins. The venous valve was tested for patency, competency, cyclic fatigue, compressibility, and thrombogenicity. Patency is maintained with a low opening pressure of less than 3 mmHg. Competency is maintained with backpressures exceeding 300 mmHg. The valve is fatigue resistant to over ¼ million cycles. The valve can maintain its integrity when compressed in a stent and deployed without tilting or mal-alignment. Little thrombus forms on the valve with perfusion of whole blood under pulsatile flow conditions. The pre-clinical tests demonstrate efficacy as a new venous valve for treatment of chronic venous insufficiency.

1 BACKGROUND

Venous disease will affect 1-3% of the western world at some point in their lives, yet there are few effective treatments for the venous system. One such disease is chronic venous insufficiency (CVI), a painful and debilitating illness that affects the superficial and deep vein valves of the legs. When the valves become incompetent they allow reflux and subsequent pooling of blood. Symptoms include swelling, edema, pain, itching, varicose veins, skin discoloration, ulceration and limb loss. Post-thrombotic damage within the deep veins is the most significant cause of CVI, reported as high as 95%. Current clinical therapies are only moderately effective; and therefore, the need for a better solution remains.

Surgical treatment for CVI is avoided due to lack of accurate surgical technology and the extreme risk of post-operative thrombosis. Valvuloplasty is extensively time consuming and reserved for patients with a congenital absence of functional valves and severe cases of CVI. This surgical procedure involves a venotomy, where the valve cusps are plicated 20-25%. A singular valvuloplasty is usually sufficient to correct CVI except in systems that include occlusion of the femoral or popliteal vein, or absence/incompetence of the communicating leg veins.

Previous prosthetic vein valves have experienced complications due to either *in vivo* thrombosis, in-growth, foreign body reaction, or prosthetic disorientation (tilting). The umbilical vein valves and pellethane valves by Hill *et al.* failed due to thrombotic occlusion (Hill et al, 1985). Two-thirds of the autogenous venous valves by Rosenbloom *et al.* failed from complications arising to thrombosis (Rosenbloom et al, 1988). The mechanical valves by Taheri *et al.* failed after three months due to severe thrombotic occlusion (Taheri and Schultz, 1995). Partial thrombosis appeared in the valve cusps of the polyetherurethane valves by Uflacker (Uflacker, 1993). Thrombosis occurred immediately after deployment of the gluteraldehyde-fixed bovine external jugular by Gomez-Jorge *et al.* (Gomez-Jorge et al, 2000). Glutaraldehyde-preserved bovine jugular valve-bearing venous xenograft show thrombosis by histology (de Borst et al, 2003).

A second cause of failure is hyperplasia. Biocompatibility was the primary concern for Taheri *et al.* and Gomez-Jorge *et al.* The two-year non-patent mechanical valves by Taheri *et al.* failed due to dense in-growth of intimal hyperplasia, which rendered the valves functionless. The gluteraldehyde-fixed bovine external jugular by Gomez-Jorge *et al.* produced a granulomatous response and foreign body reaction (Gomez-Jorge et

al, 2000). Between 2000 and 2005 Pavcnik *et al* reported on a stent-based porcine small intestine submucosa prosthesis (Pavcnik et al, 2005); all failed valves were the result of prosthesis tilting. Overall, eight out of ten of the reported valve designs experienced complications due to thrombosis.

A new design for venous valves has been proposed using biomimicry. The medical device has the shape of a natural valve with sufficient elasticity to maintain patency and competency in the leg veins. This paper describes the pre-clinical verification and validation testing of this new venous valve.

2 METHODS

The venous devices were subjected to a battery of tests to demonstrate sufficient function as a one-way valve, propensity for thrombosis, and suitability for minimally invasive delivery. The new "GT" vein valve prosthetic is presented in Figure 1.

2.1 Pulsatile Flow System

This pulsatile system was designed to mimic the physiologic flow conditions present in the lower extremity venous system. During normal walking, compression occurs about 40 times a minute (0.67 Hz). Fresh, whole, porcine blood with heparin (6.0 ± 0.2 U/mL) was transferred into a blood donor collection bag. The collection bag was raised 30 cm above the test section, rotated on an orbital mixer, and attached to 90 cm of vinyl tubing, followed by a 3-way valve, a pressure tap and the test section. Downstream of the test section, a 50 cm segment of tubing (3.5 mm inner diameter) was passed through a pulsatile pump rotating at a frequency of 0.75 Hz. Pressure upstream of the vein valve was recorded with a pressure transducer (Harvard Apparatus, South Natick, MA) and the flow rate was calculated from measurements with a graduated cylinder and a stopwatch. The experiment proceeded until flow cessation by occlusion or the contents of the fluid reservoir were emptied.

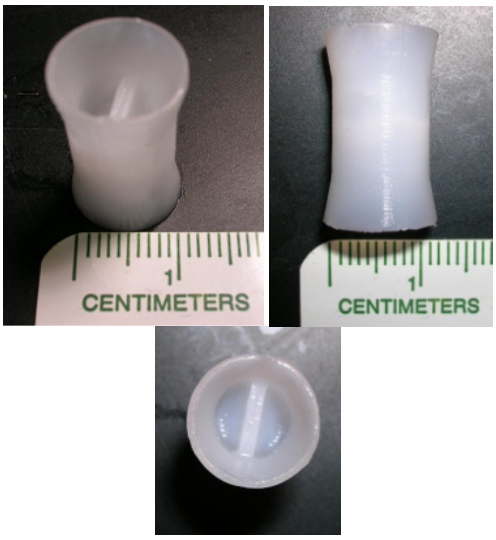

Figure 1: GT vein valve. Upper left, isometric view. Upper right, cross sectional view. Lower, downstream view.

2.2 Test Section

The test section included a vein valve, a flexible venous-like tube, and suture material. The valves were manufactured according to the procedure outlined in reference (Sathe, 2007). The valve material was made from a PVA hydrogel biomaterial. The valve was inserted into the flexible tube and tightly tied in place to prevent blood from passing between the valve and the vessel wall. The flexible tube was further attached to the vinyl tubing by securing it with suture.

2.3 Dacron Lined Valve

A Dacron-lined valve acted as the positive control. The lining was constructed from a commercially available cardiovascular Dacron patch often used clinically of approximately 14 mm ± 1 mm by 9 mm ± 0.5 mm, which was then sutured to the GT valve. One stitch was placed on each Dacron piece on the upstream side, these sutures held the Dacron against the GT valve.

2.4 Pressure Tests

A syringe was attached to a three-way valve with the test section and the pressure transducer (Harvard Apparatus, South Natick, MA); downstream the test section was open to atmosphere. Pressure was applied with the syringe and read upstream of the test section. For opening pressure, the prosthetic vein valve was orientated with the distal end closest

to the syringe, and the proximal end facing ambient atmosphere. For backpressure, the prosthetic valve was reversed in orientation.

2.5 Thrombosis of Whole Blood

Whole blood samples were harvested from pigs and quickly anti-coagulated with porcine heparin to a final concentration of 6.0 ± 0.2 U/mL. The samples were mixed with a nutating rocker at approximately 42 rpm for 15 minutes prior to the experiment. Experiments were completed within eight hours of harvesting the blood and conducted at room temperature.

2.6 Histology

Samples were fixed in 10% formalin (VWR International, West Chester, PA) for at least 72 hours. Samples were processed and embedded in paraffin. Deformation of the samples during processing was expected to be between 30 to 50%. Samples were cut into 5-micron thin circular cross-sections, oriented perpendicular to flow. Eight sections from orifice areas were collected from each sample. Alternating samples were stained with Haematoxylin and Eosin stain (H&E), and Carstair's stain (specific for platelets). Sections were analyzed microscopically using a Nikon E600 microscope, a digital camera and Q-capture software.

2.7 Flat Compression

The valves were evaluated for plastic deformation with respect to compression time. Initially, they were evaluated for opening pressure and backpressure conditions. At periodic time points the valves were allowed to expand and were re-evaluated for opening pressure and backpressure conditions.

2.8 Radial Compression

The GT valves were inserted into balloon expandable Palmaz stents, 10mm diameter and 20-25mm in length, (Cordis Endovascular, Miami, FL; and IntraTherapeutics, St. Paul, MN), and sutured into place. The valves were evaluated for opening pressure and backpressure.

2.9 *In Vivo* Placement

Placement inside an actual vein has been problematic for some previous designs. The valves might tilt or dislodge in the vein. Thus, our valves were surgically placed in the correct anatomic position in animals. The external jugular veins (EJV) were exposed on four previously deceased, 2.5 year old, 50-60 Kg Dorset ewe sheep. A vertical incision was performed on the EJV and the prosthetic was placed inside the vein. The vessel diameter was measured and the prosthetic valve was manipulated to evaluate potential misplacement. This procedure was repeated on the iliac veins.

3 RESULTS

The GT vein valve was evaluated for patency, competency and cyclic life (Sathe, 2006). The valve withstood 300 mm Hg of backpressure with less than 0.3 mL leakage per minute, demonstrated a burst pressure of 530 ± 10 mm Hg , opened with a pressure gradient as low as 2.0 ± 0.5 mm Hg. The patency and competency endpoints were statistically unchanged after 500,000 cycles of cyclic testing.

3.1 Thrombosis from Pulsatile Blood Flow

Blood was perfused through five GT vein valves; a graphical representation is shown in Figure 2. All five valves remained patent after 20 minutes of blood flow without significant flow rate deterioration. The average blood flow rate was 11.8 ± 0.4 mL/min. The upstream pressure fluctuated between 15 – 21 mmHg. Once the system was exhausted of blood, the pressure dropped off to just above 10 mmHg. When the flow system depleted the blood reservoir the roller pump tried to pull blood through the valve, the upstream and downstream sections of the valve would collapse due to the negative pressure. There was no gross thrombus visible on any of the valve leaflets. The leaflets remained functional and the valves remained competent against backpressure.

The Dacron-lined valves initially produced the same velocity profiles as the GT valves; though, they did not remain patent for the experiment, but rather occluded completely. The flow rate reduced after two to eight minutes into the perfusion. On average, the Dacron lined valves occluded after 6 ± 3.6 min of perfusion. The upstream pressure fluctuation prior to occlusion was between 15 – 21 mmHg, and after occlusion, the pressure was constant at 24 ± 1mmHg. The frequency of occlusion for the Dacron lined valves in this assay was significant to $p<0.02$. With occlusion, the

flexible tube collapsed violently instead of the valve reopening. Thus, the system was a severe demonstration of the adherent nature of the occluding thrombus. The Dacron valves were visually inspected at the end of the experiment. The polyester fibers were covered with red blood and were visibly matted down. After occlusion, some red clot remained in the lumen of the tubes. The GT valves and Dacron lined valves were preserved for histological analysis.

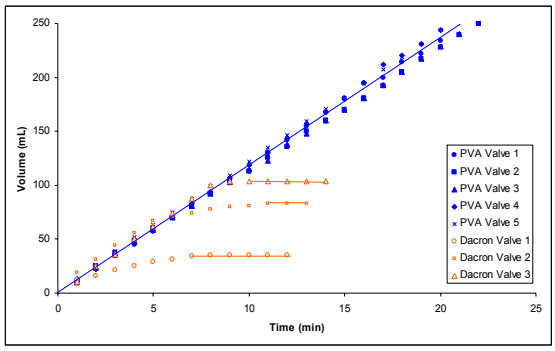

Figure 2: Perfused blood volume over time in the GT and Dacron-lined valves. The GT valves produced a constant flow rate; whereas, the Dacron lined valves produced a gradual cessation of flow.

Histology was performed on both the GT and Dacron lined valves to identify cell accumulation and the cause for cessation of flow. The histology stains used were Haematoxylin and Eosin stain (H&E), and Carstair's stain (specific for platelets). The PVA material is represented as pink in the H&E stain and a faint blue-grey in the Carstair's stain. With regard to the Dacron lined valve slides, the gray circular structures represented the Dacron fibers. The red debris located between the Dacron leaflets represented the cellular material that was preventing blood from passing through the leaflets in the *in vitro* model. Further analysis with Carstair's stain revealed that platelet aggregation with fibrin strands was a key component in the red debris. The presence of platelets on the Dacron leaflets, and the complete absence of platelets on the GT valves confirmed that the in vitro blood flow assay had the potential to thrombose, yet the GT valves do not exhibit any thrombosis or clot in this system.

3.2 Plastic Deformation – Flat Compression.

Valves were subjected to flat compression. Prior to compression the valves demonstrated an opening pressure of 3 mm Hg ± 1 mm Hg, and a backpressure of at least 100 mm Hg. Subsequently at 2 hrs, 4 hrs and 6 hrs after compression the valves exhibited an opening pressure of 3 mm Hg and maintained competency with a backpressure of 100 mm Hg.

3.3 Radial Compression

The average initial outside diameter of the valve-stent system was 8.8 mm ± 0.1 mm. Prior to compression exposure the valves demonstrated an opening pressure of 3 mm Hg ± 1 mm Hg, and a minimum backpressure of 100 mm Hg. The average compressed outside diameter of the valve-stent system was 6.5 mm ± 0.1 mm. They were compressed for 1hr and subsequently expanded, shown in Figure 3. Visually the expanded valves retained their original configuration. The valves exhibited an opening pressure of 4 mm Hg ± 1 mm Hg and withstood a backpressure of 100 mm Hg. The average expanded outside diameter of the valve-stent system was 9.5 mm ± 0.5 mm. All valves met the original design criteria of opening pressure below 5 mm Hg and a backpressure up to 100 mm Hg.

3.4 *In Vivo* Placement

The prosthetic was positioned inside the external jugular veins and iliac veins of four sheep as depicted in Figure 4. The 10 mm prosthetic vein valve was of appropriate size for the EJV of sheep.

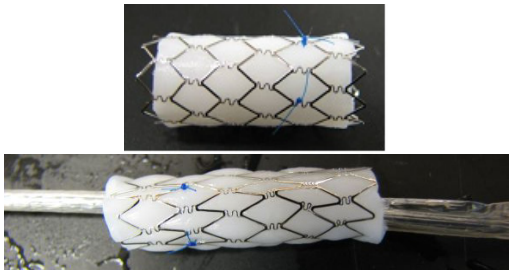

Figure 3: Above, Genesis Palmaz Stent (Cordis) with GT vein valve. Below, radially compressed valve and stent on a balloon catheter.

The 10 mm prosthetic vein valve was too small for the iliac vein. Vigorous manipulation of the prosthetic *in situ* did not cause any misplacement, tilting, or orientation problems. Tilting was of no concern due to the long profile of the prosthetic. A suite of valve sizes ranging from 10mm to 4 mm in 2 mm increments were created to account for varying vessel sizes, as seen in the iliac of sheep.

4 DISCUSSION

Evaluating the thrombotic potential of a prosthetic vein valve in an *in vitro* set-up is a novel process, as the thrombotic potential is typically evaluated in an animal model. Animal studies require the long process of approval from animal care and use committees, the trials are costly, the study itself is time consuming, and animal lives are sacrificed. *In vivo* models are necessary to determine the biocompatibility of the prosthetic device, and an important step towards clinical trials; yet using an *in vitro* thrombosis model provides an appropriate intermediate step between valve development and expensive *in vivo* studies.

The GT venous valve demonstrates low thrombus formation in the whole blood perfusion system, as it remained patent after 20 minutes of perfusion with no adherent platelets. In contrast, the Dacron valves occluded after 6 ± 3.6 min of perfusion. Histology revealed adherent fibrin, RBCs and platelet thrombus under histological analysis. The time of occlusion for the Dacron lined valves in this assay was significantly shorter than the GT valves ($p<0.02$).

When designing an *in vitro* model it is most relevant for the model to be as close to physiologic conditions as possible. The *in vitro* model perfuses whole porcine blood through a prosthetic vein valve. The pulsatile frequency of the system, 0.75Hz, approximates the normal walking cadence of an adult. A potential limitation to this *in vitro* set-up is that the flow through the prosthetic valves was 11.8 ± 0.4 mL/min, yet the blood flow through the femoral vein is around 70 mL/min. The flow was lower than physiologically observed valves because the frequency and collection time were selected, but the tubing diameter was restricted. The tubing diameter could not be increased to reduce flow as it was limited to the pulsatile pump tubing specifications. Even though platelet adhesion in a stenosis happens at high velocities, vein thrombosis typically is thought to occur at low velocities. Therefore modeling a low flow rate may be more appropriate, since it is a worse-case scenario.

For instance, when one sits for a long period of time on a transatlantic flight and the calf pump is not actively engaged, the blood is traveling at a lower velocity back to the heart.

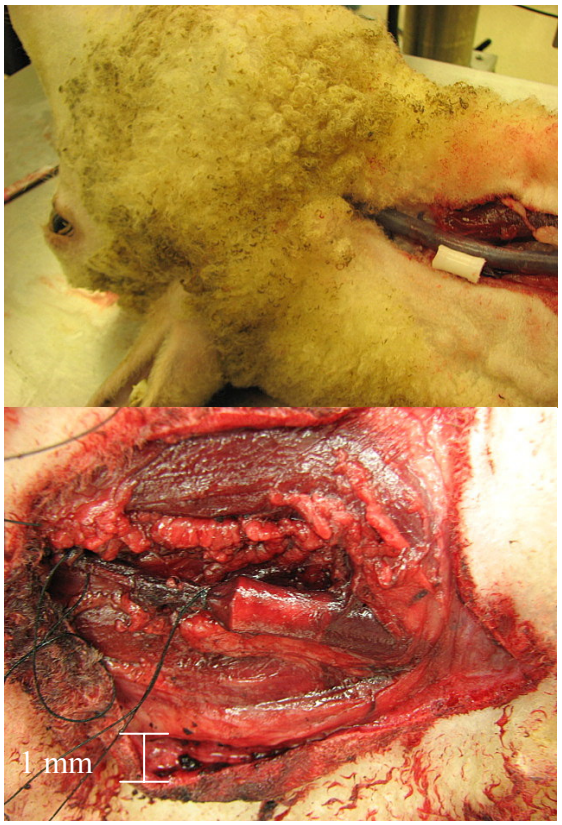

Figure 4: Above, GT valve positioned beside right external jugular vein. Below, GT valve implanted into right external jugular vein.

The future of medical implants lies in percutaneous devices; therefore, to create a marketable and less invasive implant, a percutaneous delivery system has been designed for the GT vein valve. An appropriate delivery route may be from the external jugular vein down through the heart to the femoral or iliac vein. Reduction of the crimped valve profile may be achieved by decreasing the thickness of the cylindrical supporting material. Future improvements could include incorporation of antithrombotics or other eluting drugs into the valve to limit thrombosis, inflammation or foreign body response mechanisms. Due to the low *in vitro* thrombotic potential and the successful previous clinical use of the material as a medical implant material, clinical trials may be considered.

Given the successful implementation of pre-procedure crimping of percutaneous heart valves (Edwards Life Sciences), a similar technique was pursued for the GT vein valve to allow it to be compressed within 6 hours of implantation. The portable stent crimper makes this possible. Evaluating the thrombotic potential of a prosthetic

vein valve in an *in vitro* blood set-up is a novel process. The most common practice to test the thrombotic potential is in an animal model, where eight out of ten studies reviewed failed due to *in vivo* thrombosis. The two most successful vein valve studies use acellular tissues: the SG-BVV was constructed from porcine small intestine submucosa (SIS), and the PVVB used gluteraldehyde-preserved bovine jugular valves (Moll, 2003), (Gale et al, 2004). The GT vein valve provides several advantages over SIS and gluteraldehyde-preserved bovine jugular valves. Zoonosis from animal tissue prosthetics is possible and the use of animal derived prosthetics may be culturally or religiously controversial, therefore a synthetic material would alleviate these concerns. The PVVBs are fixed with gluteraldehyde, which is a toxic substance that will prevent cells from integrating into the material *in vivo*. This gluteraldehyde preservation process will cause a limited cyclic life due to the cross-linking of the collagen fibers, and ongoing biocompatibility issues due to the gluteraldehyde toxicity. The SIS tissue appears to be an appropriate material for vein valve prosthetics with regards to its biocompatibility. However, despite revisions to the SIS vein valve, the SG-BVV continues to experience *in vivo* tilting. Tilting is not an issue with the GT vein valve because of the long axial dimension. In addition, GT vein valve can be mass-produced and the design is easily modified. This is unlike acellular tissues which require extensive tissue preparation and processing times and modification of the tissue valve design could create concerns regarding suturing locations and tissue-to-stent attachment sites.

Another feature of the new GT Valves is that they may be processed to include embedded drugs, which could promote cell growth and/or reduce thrombus formation. It has superior biocompatibility and structural integrity, may be mass-produced, and has the potential to utilize new drug delivery technologies.

Providing relief to chronic venous insufficiency is a worthwhile pursuit as patients experience swelling, edema, pain, itching, varicose veins, skin discoloration, ulceration and limb loss. Current clinical therapies are only modestly effective; and therefore, a prosthetic vein valve may provide a cure for this debilitating disease. With successful animal and human trials this valve could provide a useful therapy the 7 million people suffering from chronic venous insufficiency. The GT valve exhibits excellent flow, full competency, fatigue-resistance, low-thrombogenicity, material flexibility, and *in situ* placement consistency.

REFERENCES

de Borst, G.J., et al., *A percutaneous approach to deep venous valve insufficiency with a new self-expanding venous frame valve.* Journal Of Endovascular Therapy, 2003. 10(2): p. 341-349.

Gale, S.S., et al., *Percutaneous venous valve bioprosthesis: initial observations.* Vascular And Endovascular Surgery, 2004. 38(3): p. 221-224.

Gomez-Jorge, J., A.C. Venbrux, and C. Magee, *Percutaneous deployment of a valved bovine jugular vein in the swine venous system: a potential treatment for venous insufficiency.* Journal Of Vascular And Interventional Radiology: JVIR, 2000. 11(7): p. 931-936.

Hill, R., et al., *Development of a prosthetic venous valve.* Journal of biomedical materials research., 1985. 19(7): p. 827.

Moll, F. *Venous Valves for Chronic Venous Insufficiency*. in *Vascular and Endovascular Controversies*. 2003. London, UK.

Pavcnik, D., et al., *Significance of spatial orientation of percutaneously placed bioprosthetic venous valves in an ovine model.* Journal Of Vascular And Interventional Radiology, 2005. 16(11): p. 1511-1516.

Rosenbloom, M.S., et al., *Early experimental experience with a surgically created, totally autogenous venous valve: a preliminary report.* Journal of vascular surgery, 1988. 7(5): p. 642.

Sathe, R.D. and D.N. Ku, *Design and Development of a Novel Implantable Prosthetic Vein Valve.* J Med Devices, 2007. 1: p. 105-112.

Taheri, S.A. and R.O. Schultz, *Experimental prosthetic vein valve. Long-term results.* Angiology., 1995. 46(4): p. 299.

Uflacker, R. *Percutaneously introduced artificial venous valve: Experimental use in pigs*. in *The 1993 Annual Meeting of the Western Angiographic & Interventional Society*. 1993. Portland, OR.

MULTIPARAMETER SINGLE LOCUS INTEGRATED MULTILAYER POLYMER MICROSENSOR SYSTEM

Yindar Chuo and Bozena Kaminska
School of Engineering, Faculty of Applied Science, Simon Fraser University, 8888 University Drive, Burnaby, Canada
yychuo@sfu.ca, kaminska@sfu.ca

Keywords: Biosensor, multiparameter, microintegration, flexible polymer system-in-package, MEMS, health monitoring, wireless senor, cardio health monitoring.

Abstract: Miniaturization and microintegration is well known for their potentials in providing microsystems and sensors with unmatched performance, reliability, and lower costs. Current technologies in implementation of microsensors, however, span a large variety of platforms. It is thus common for microsensors measuring differing parameters to exist on different combinations of substrates, not to even mention the associated signal conditioning, processing, and data communication electronics. It remains a challenge to integrate multiple sensors with complex electronics into a single high-density microsystem, particularly for certain applications in medical diagnostics and healthcare, where mechanical flexibility of the substrate and biocompatibility also becomes crucial considerations. Traditional microintegration technologies such as system-in-package, system-on-chip, and advanced assembly and packaging, may often be inadequate. A mutliparameter single locus integrated multilayer polymer microsensor system is proposed to address the fundamental issues of high-density integration, flexibility, biocompatibility, easy application, high sensitivity, and reliability for medical grade diagnostics and other physiological applications. The architecture of the multilayer system is discussed, as well, implementation and fabrication of the multisensor layer is demonstrated, and the results on performance discussed.

1 INTRODUCTION

Miniaturization and microintegration of sensors through novel microelectronics and microelectromechanical systems (MEMS) technologies have demonstrated large potentials in providing unmatched performance, reliability, and cost effectiveness (Wang, 2002) over the recent years in many applications. Particularly, in applications involving physiological monitoring and healthcare, microintegrated sensors have been able to provide the combination of high analyte sensitivity, electrical responsiveness, precise temporal control, small feature sizes, and low power consumption, that otherwise is often very difficult to achieve through traditional technologies (Richards Grayson, 2004).

Current technologies in miniaturization of sensors span a large domain. Much research has focused on microfabrication of sensors through microelectronics and MEMS (Richards Grayson, 2004). Methods in fabrication include various lithographic techniques, stereolithography, lithographie galvanoformung abformung (LIGA), and micro injection molding, to just name a few. Processes are often different and specific to each type of microsensor. As a result, integration of various microsensors and microelectronics is difficult.

Thus far, technologies for microintegration include system-on-chip (SoC) (Kundert, 2000), system-in-package (SiP) (Matthews, 2003), and advanced assembly and packaging (Fraunhofer Institut Zuverlassigkeit und Mikrointegration). SoC concepts allow designers to combine sensors and system electronics on the same substrate, on a single chip. An example is the popular lab-on-chip technologies (Pai, 2001); however, often in biological and environmental applications, it is inherently difficult to design sensors on the same substrate as the remaining electronic system (Zhang, 2007). SiP technology provides integration of multiple sensors and system electronics from differing substrates at the board level. Commonly, unpackaged chips are placed and connected on one single substrate or printed circuit board (PCB). This

allows for a high-density integrated system, but is often limited by its rigid integration substrate, and board 'real-estate'.

In this paper, a multiparameter single locus microintegrated sensor system is proposed for, but not limited to, cardiac physiological signal acquisition in diagnostics and health monitoring. This novel integration technology platform proposes higher density integration through multilayering of mechanically flexible polymer substrates, while providing a thin flexible profile for skin tissue conformity. A complete system including multiple microsensors, filtering, digitization, processing, and communication electronics is proposed. In this manner, the microintegration platform provides advantages of high sensitivity, high actuation-to-sensor coupling, and noise reduction through local filtering and immediate digitization, for a system that can provide medical diagnostic grade precision, yet is flexible, compact and robust.

One particular implementation includes a surface biopotential electrode integrated along with a MEMS 3-axis accelerometer and signal filtering electronics all together forming the multiparameter sensor layer of the multilayer system. In this implementation, parameters of interest include electric potential and motion of the heart, recorded simultaneously, in what is known as ballistoelectrocardiography (BECG).

2 MULTIPARAMETER SENSOR SYSTEM ARCHITECTURE

The multiparameter single locus integrated multilayer sensor system consists of five functional groups (Figure 1); the multisensors, signal conditioning, microprocessor, communication terminals, and powering. Multiple sensors acquire signals of different parameters, and convert the signals to electrical outputs. The signals are conditioned through appropriate filters and amplifiers, as close to the sensing elements as possible, to minimize noise. Signals are then routed to the mixed signal microprocessor (MSP) where it is digitized, processes, and transmitted through radio or wired communication portals. The system is powered through either permanent or disposable micro-batteries.

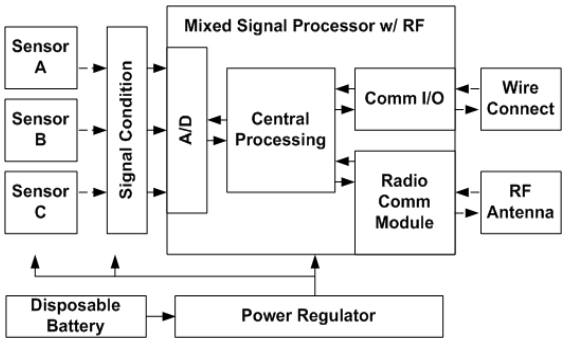

Figure 1: Modules of the integrated sensors system.

The conceptual assembly of the system is shown in Figure 2. The system consists of two layers, with option to be detachable from each other, and is connected through columnar interconnects. Each layer is composed of a flexible substrate (e.g. polyimide), on top of which the electronic system is placed and routed. Intermediate and encapsulating each layer is a flexible material (e.g. silicone) acting as insulation, structural support, and mechanical protection. The intermediate layer can be shaped and is electrically patternable such that electrical interconnects, inter-layer attachment anchors, and sensing element windows can be designed.

Here, with reference to both Figure 1 and Figure 2, the multiple sensors and signal conditioning electronics are shown on the lower layer, which allows the sensing elements to be closer to their corresponding physiological actuations. Also situated on the lower layer is a mini-connector for applications requiring wired connections. The MSP with build-in radio-frequency (RF) communication module and the RF antenna are both placed on the upper layer. Signals from the conditioning module on the bottom layer are routed to the processor on the top layer through the interconnects. Signals between the processor to and from the wired connection are also routed through the interconnects.

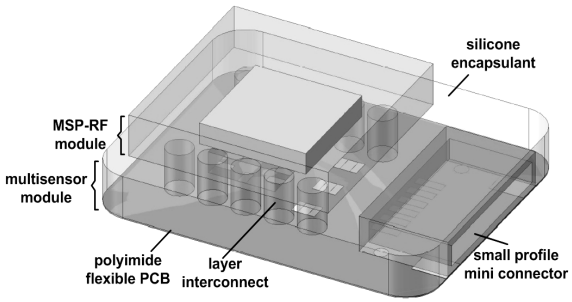

Figure 2: The multiparameter single locus integrated multilayer polymer microsensor system.

Another important part of the integrated multilayer sensor system is the attachment mechanism to a subject surface. Since the integrated multilayer sensor system is designed to be flexible, with a low profile, to conform well to the contours of human skin surface, the attachment mechanisms must not alter this feature. Figure 3 shows how the integrated multilayer sensor device is conceptually applied to a subject tissue surface by attachment of a novel disposable adhesive. This disposable adhesive must be very thin, attachable on both sides and conductive at portions where it is required.

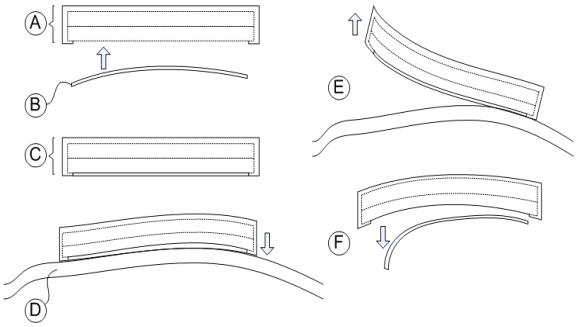

Figure 3: Application of integrated sensor device with novel disposable adhesive: The integrated sensor device (A) is attached on the bottom side with the disposable adhesive (B) forming a ready-to-apply device (C), where then it can be attached to subject skin surface (D) with high conformity. Device is removed from subject by simply pealing (E) off from attached surface, while disposable adhesive can then be removed from device (F) for hygienics.

3 IMPLEMENTATION OF MULTISENSOR LAYER

A model of the multisensor layer of the multiparameter single locus integrated multilayer sensor system has been implemented and fabricated, while the reminder of the system is underway. This paper will only discuss the implementation and fabrication of the multisensor layer.

Figure 4 shows the system blocks for the multisensor layer. Two sensor modules were included; one, a three-axis accelerometer, and the other, a single-channel surface biopotential electrode. Signal output from the accelerometer was passed through passive low-pass filtering prior to the terminal connections. There was no local filtering implemented for the electrode signal to maintain relative simplicity of the system such that focus at this stage of development can be placed on overall system integration. Power input stabilization was included to maintain optimal performance of the powered components. Input and output terminals of the multisensor layer were connected via thin wires to macro-scale connectors for testing purposes.

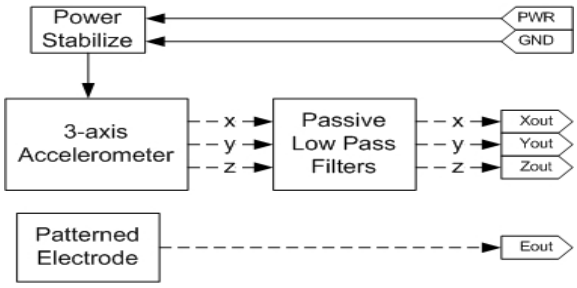

Figure 4: System blocks of the multisensor layer.

Figure 5 shows the model assembly of the multisensor layer. Base substrate of this layer was chosen to be 50-micron polyimide flexible PCB. Polyimide is a strong thermalset with excellent tear-resistance, thermal and chemical resistance (Callister, 2003). The three-axis accelerometer, filtering, and power stabilizing electronics were placed and routed on the top-side of the polyimide cell. The biopotential electrode was designed and patterned on the reverse-side of the polyimide cell, and connected to the top-side through micro-jumper wire. Alternatively, metal-plated vias through the polyimide substrate would be ideal, but to reduce model fabrication complexity and costs, jumpers were chosen. A small profile mini-connector was placed at one end of the polyimide cell for signal acquisition and testing. As will be further discussed in the next section, during model fabrication and assembly, the mini-connector was replaced with thin wires and then joined to a larger connector, again, to simplify fabrication and assembly complexity and reduce costs.

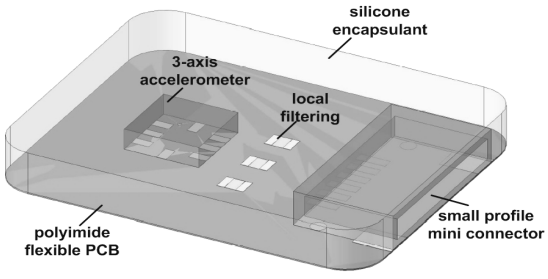

Figure 5: Multisensor layer of multilayer integrated system.

Lastly, encapsulation of the polyimide cell was chosen to be with electronic grade silicone encapsulant. Typical electronic grade silicone encapsulant provides good insulation and mechanical protection for the underlying devices while allowing for shapability. Transition to fabrication with medical grade silicone encapsulants would be straightforward because of the silicone's relatively similar compositions. Rapid prototyping moulding techniques were applied to provide the desired resulting shape. The total thickness of the entire cell was targeted at 3mm to maintain the feature of skin contour compliance.

4 FABRICATION METHOD

Fabrication and assembly of the multisensor layer could be categorized into four sections; one, fabrication of the polyimide circuit; two, device component population; three, encapsulation; and four, preparation of double-sided conducting adhesive. This paper will focus on discussions for the first two aspects of device fabrication. Since fabrication was for a set of model devices, techniques employed were mostly rapid prototyping methods with simplified steps rather than larger scale manufacturing processes.

4.1 Polyimide Circuit

Fabrication of the polyimide circuit is a standard process in the industry (Egloff, n.d.). It is also commonly known as flexible PCB circuit printing. Printing of flexible PCB circuits is provided by many fabrication houses around the world; however, due to its specialty, most orders are still costly and require large quantities not suitable for prototyping or model trials.

Fabrication was thus contracted through the Institute for Micromachining and Microfabrication Research at Simon Fraser University. Layout of the single-layer double-sided polyimide circuit was submitted electronically, for the fabrication process to be done with proprietary metal-on-polyimide rapid prototyping process.

4.2 Components and Population

Components for the model multisensor layer were carefully selected to ensure ease of assembly without elaborate processes or tools, while maintaining relatively small device profile. As a result, all electronic components used were surface mount devices with package size no greater than 5mmx5mm^2 and bonding pad pitch larger than 0.65mm. Bonding of the device was through cold soldering (silver epoxy, conductive ink) by hand. Heat soldering with temperatures greater than 200°C was too hot for the thin metal film deposited on the polyimide under the particular polyimide metallization process carried out. Alternatively, a thicker film metallization on polyimide circuit would allow heat soldering, but such was not the objective of this research.

5 RESULTS AND EVALUATION

5.1 Flexibility

A total of four devices were populated, assembled and encapsulated using the fabrication method described in the previous section. Figure 6 shows one of two devices encapsulated in 5mm thick silicone encapsulant. Although it was 2mm thicker than the 3mm that was planned, the device was flexible enough to bend up to 30° without any visible cracking or detachment between the substrate and encapsulant.

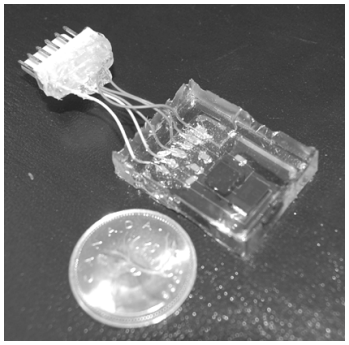

Figure 6: Encapsulated multisensor layer with macro-scale connector for testing attached, comparison with a Canadian quarter.

The remaining two of the four devices were encapsulated in 0.5mm thick silicone. Figure 7 shows one of the two devices wrapped around a finger demonstrating its flexibility. With the 0.5mm encapsulation thickness, although no quite enough to form a levelled-surface over the larger components, it was sufficient to provide electric insulation on most parts and some degree of mechanical protection. The device was able to bend up to 90° without any visible cracking or detachment between the substrate and encapsulant.

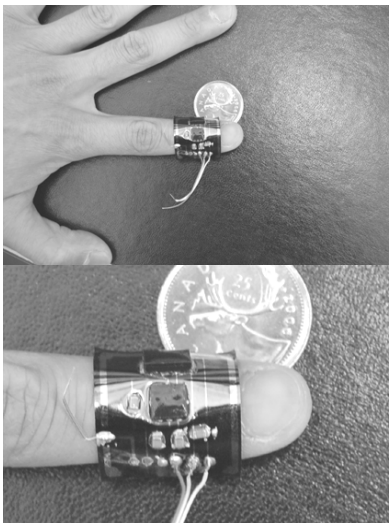

Figure 7: Thin encapsulation of multisensor layer allowing for extra flexibility; Top, sensor device wrapped around the first digit of a finger; Bottom, close-up of sensor wrapped around finger.

5.2 Size and Dimensions

The model multisensor layer devices were approximately 2.0cmx2.5cm. As can be seen in Figure 6 and Figure 7, the metal traces were relatively thick, components were relatively large, and spacing between components was maintained such that assembly by hand without any precision tools can be managed. Should the devices be populated on the substrate without the manufacturer packaging, and/or smaller footprints and traces applied, the device dimensions should be easily reduced to half the model size, say 1.0cmx1.5cm.

5.3 Comparative Functional Assessment

Initial comparative function assessment was conducted to provide quick insight into how the novel device's sensing capabilities compared to traditional devices in the particular application. The comparative assessment gave an overview of the device functional performance prior to engaging into more detailed studies of its performance characteristics, which will be topic of another discussion.

In the comparative assessment, the multisensor was applied in the same manner as traditional accelerometers on the chest of the subject in obtaining BCGs (McKay, 1999). Figure 8 shows the sensor locations and reference electrode locations for comparative study. Locations 1, 2, 3, show the various positions the sensors can be placed along the subject's sternum in recording heart motion. Ideally, sensors should be situated simultaneously at the same location for most accurate comparison, but such placement is not possible. Differences in signal outputs due to location were thus considered during the analysis. Two electrodes, *E*, approximately 2" apart were placed beside the sternum along the sternal midline to form a reference modified-ECG-lead in studying a subject's BECG.

At this stage, only the motion sensing element of the multisensor was compared with other traditional sensors. It is important to assess first whether or not the signal pickup by the integrated sensors suffers any unwanted effects due to the flexible substrate. For testing purposes, attachment of the sensors to the subject skin surface was with common off-shelf non-conducting double-sided medical adhesives.

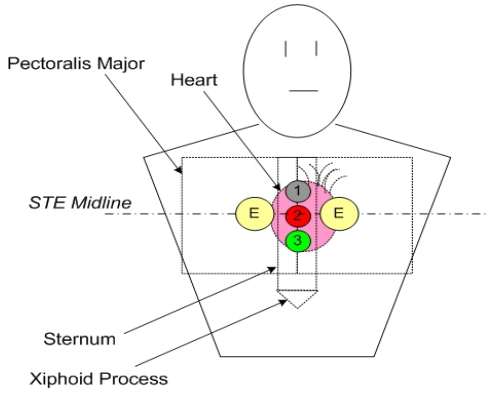

Figure 8: Sensor placement locations in comparative assessment; *E* denotes electrode locations, while *1*, *2*, *3*, denotes sensor locations.

The data acquisition system and sensor powering is shown below in Figure 9. The flexible multisensor was connected with power input, and signal output routed to filtering and amplification circuits. The conditioned signals were then passed into a data acquisition system (National Instruments DAQ) stored and analysed. Additional sensors included in the comparison were also digitized and stored through the same data acquisition system such that precise synchronization between channels recording incoming signals can be obtained. The reference electrodes were connected to a standard ECG machine (Burdick) with analog output connected to the acquisition system as the sensors were.

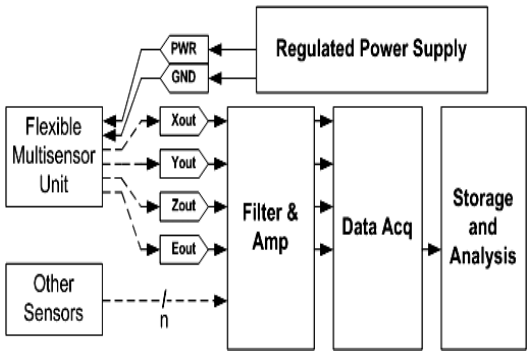

Figure 9: Data acquisition system and sensor connection setup.

Figure 10 shows the physiological signals of a single heart-cycle recorded through the acquisition system of the flexible multisensor with reference to synchronized ECG.

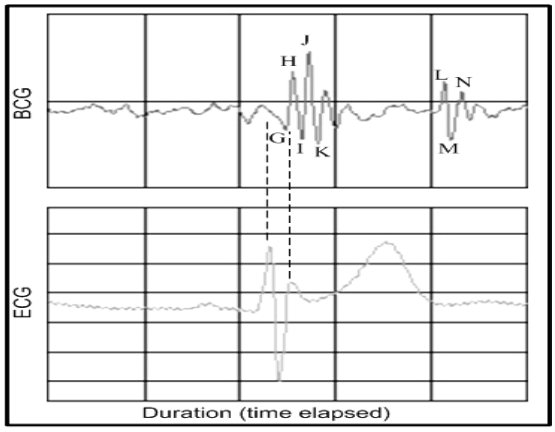

Figure 10: BCG signal of a single heart-cycle as recorded by the multisensor referenced to synchronized ECG.

As can be seen, all characteristic waveforms of a classical BCG signal, denoted by letters (H, I, J, etc.), similar to that measured through a high-precision accelerometer in McKay (1999), can be identified. Several feature extraction algorithms and physiological interpretation analysis were also developed; however, such topics were reserved for subject of a separate discussion.

A total of four comparative recordings were taken from a single subject. With a high-precision reference accelerometer (Bruel&Kjaer) fixed at location-3 (Figure 8), the flexible multisensor and a rigid sensor, housing the same MEMS 3-axis accelerometer on PCB, were rotated between location-1 and location-2. Samples were taken for duration of 30-seconds at 500Hz (each channel) over a total of four channels (3 sensors, 1 reference ECG-lead). Table 1 summarizes the recordings and the different sensor placements during each trial. From the combination of trials recorded and reference sensor comparison, the quality of signal related to sensor placement, and filtering differences can be qualitatively assessed.

Figure 11 shows a portion of the recorded signals from trial-I over a period of 2.6-seconds, or approximately three heart-beats. Channel-1 shows signal recorded from the rigid sensor, while channel-2 shows signal recorded from the flexible multisensor. Channel-3 and Channel-4 form the reference BCG and ECG signals respectively, in which the flexible sensor and rigid sensor were compared to. Although the sensitivities of the MEMS accelerometer is much lower than the high-precision reference accelerometer, it was qualitatively determined, that in general, the morphology of the BCG signals obtained from the flexible multisensor is very similar to that in the reference sensor.

Table 1: Summary of sensor recordings with location, filter, and overall sensitivity-gain indicated.

Trail	Sensor	Location	Filter	Overall Sensitivity/Gain (approx.)
I	Rigid	1	50Hz	3.0V/g
	Flex	2	100Hz	3.0V/g
	Reference	3	100Hz	9.8V/g
II	Rigid	2	50Hz	3.0V/g
	Flex	1	100Hz	3.0V/g
	Reference	3	100Hz	9.8V/g
III	Rigid	1	100Hz	3.0V/g
	Flex	2	50Hz	3.0V/g
	Reference	3	100Hz	9.8V/g
IV	Rigid	2	100Hz	3.0V/g
	Flex	1	50Hz	3.0V/g
	Reference	3	100Hz	9.8V/g

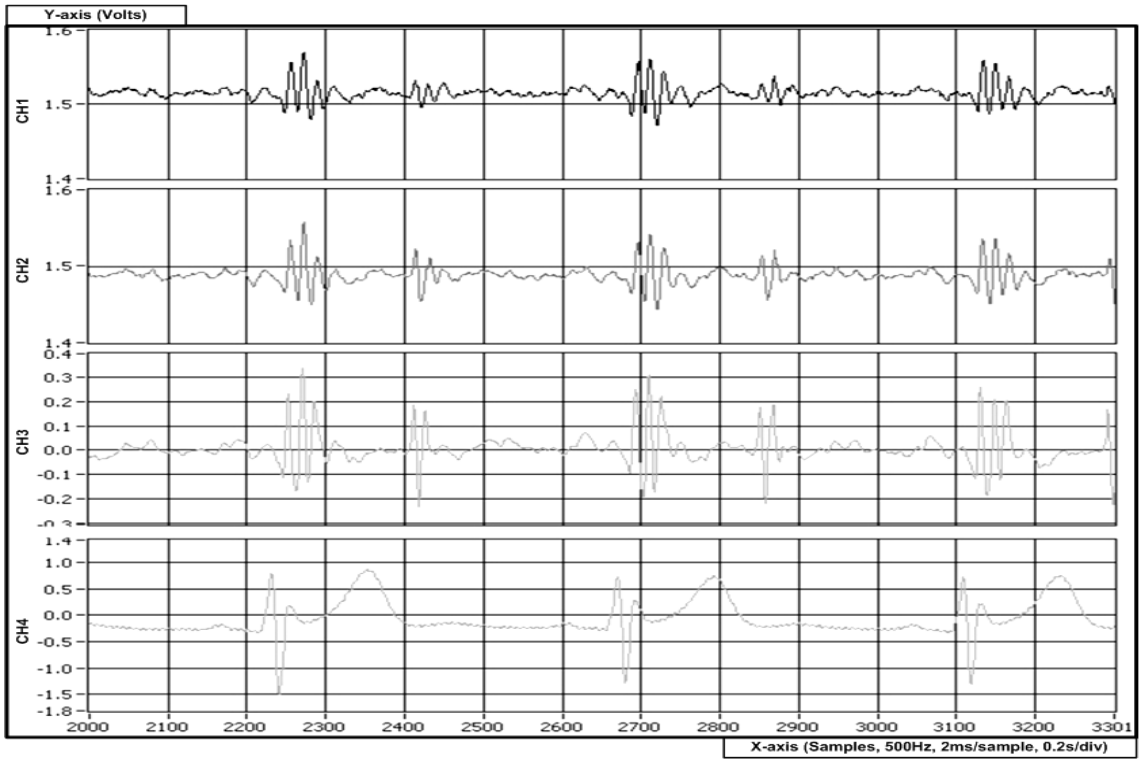

Figure 11: Portion of recording comparing novel flexible multisensor with rigid sensor and reference sensor and ECG; CH1 – rigid sensor; CH2 – flexible multisensor; CH3 – high-precision accelerometer reference; CH4 – ECG. All channels sampled at 500Hz.

Further, from trials-I and III, it was observed that altering the filtering cut-off frequencies in the signal conditioning stage did not have astonishing effects on the morphology of the signals as expected. On the other hand, situating sensors further away from the reference sensor did result in signals less similar in morphology and smaller amplitude compared to sensors closer to the reference sensor. That is to say, regardless of sensor type (rigid or flexible) and filtering cut-off frequency, a sensor placed at location-2 provided signals closer than a sensor placed at location-1 when compared to the reference at location-3. Nevertheless, the filtering and location effects observed should be subject for a more controlled study in the future.

From the qualitative comparative observations gathered, it can be concluded that first, the novel flexible multisensor provided similar functional sensitivity as the rigid PCB version housing the same 3-axis MEMS accelerometer. This was a preliminary indicator that suggested that the flexible substrate proposed in the multiparameter single locus multilayer integrated microsenor system does not inhibit the actuation-sensor coupling due to its flexibility. Next, the signals recorded from the flexible multisensor were essentially similar in morphology as the high-precision reference accelerometer. This is an indicator that the novel flexible multisensor has potential for applications in BECG with medical diagnostic grade precision, while providing a highly-integrated system in the near future.

6 CONCLUSIONS

State-of-the-art technologies in microintegrated multisensor systems were discussed. It was noted that the current systems lacked several important modules and features useful in certain specialized healthcare monitoring and medical diagnostic applications. A mutliparameter single locus integrated multilayer polymer microsensor system was proposed to incorporate high-density multisensor and microelectronics system integration on a flexible substrate platform that provides good skin conformity in physiological applications. Architecture of the proposed system was discussed, as well as the implementation and fabrication of the multisensor layer of the multilayer system. Model

devices of the multisensor layer were shown and their mechanical characteristics discussed, particularly, it demonstrated excellent flexibility for good skin conformity. It was also demonstrated that information on bodily motion due to cardiac contraction, or BCG signals, can be acquired through sensors integrated on the proposed platform. The system further shows potential for medical grade diagnostic performance. Further testing and characterization of more compact and highly-integrated models of the proposed system is under development, and will ultimately provide more insightful understanding of the effectiveness of the proposed microintegration platform.

ACKNOWLEDGEMENTS

The authors would like to thank Jasbir Patel from the Computational Integrative BioEngineering Research Lab and Microfluidics Lab at Simon Fraser University for his help on silicone microfabrication. The authors would also like to thank See-Ho Tsang from the Institute for Micromachining and Microfabrication Research at Simon Fraser University for his help on polyimide circuit fabrication. Further, the authors would like to acknowledge CMC Microsystems for their ongoing support in hybrid micro integration and device fabrication assistance.

REFERENCES

Wang, L., Tang, T.B., Johannessen, E., Astaras, A.,2002. An Integrated Sensor Microsystem for Industrial and Biomedical Applications. IEEE Instrument and Measurement, [online]. Available from: http://www.see.ed.ac.uk/~aa/WanTanJohAst02b.pdf [cited 18 June 2007].

Richards Grayson, A., Shawgo, R., Johnson, A., Flynn, N., Li, Y., Cima, M., Langer, R., 2004. A BioMEMS Review: MEMS Technology for Physiologically Integrated Devices. *Proceedings of the IEEE*, [online]. 92 (1), pp 6-20.

Kundert, K., Chang, H., Jefferies, D., Lamant, G., Malavasi, E., Sendig,F., 2000. Design of Mixed-Signal Systems-on-a-chip. *IEEE Transaction on Computer Aided Design of Integrated Circuits and Systems*. 19 (12), pp 1561-1571.

Matthews, D. J., Gaynor, M. P., 2003. RF System in Package: Considerations, Technologies and Solutions. Amkor Technologies. [online]. Available from: www.amkor.com/products/notes_papers/RF_SiP_Paper041403.pdf, [cited 18 June 2007]

Advanced Assembly and Packaging for Biomedical Devices. Fraunhofer Institut Zuverlassigkeit und Mikrointegration. [online].Available from: http://www.pb.izm.fhg.de/izm/040_Publi_News/index.html, [cited 18 June 2007]

Pai, R., Roussel, T., Crain, M., Jackson, D., Conklin, J., Baldwin, R., Keynton, R., Naber, J., Walsh, K., 2001. Integrated Electrochemical Detection for Lab on a Chip Analytical Microsystems. *Proceedings of the Fourteenth Biennial University/Government/Industry Micro electronics Symposium*. pp 167-170.

Zhang, J., Manson, A., 2007. Highly Adaptive Transducer Interface Circuit for Multiparameter Microsystems. *IEEE Transactions on Circuits and Systems.* 54 (1), pp 167-177.

Callister, 2003. Materials Science and Engineering and Introduction 6th ed., Wiley & Sons, USA.

Egloff, E. R., The Art of Design and Manufacture of Polymer Thick Film Circuits. *Screen Printing and Graphic Imaging Association International Technical Guidebook*. [online]. Available from: www.sgia.org/pdf_server.cfm?pdf=/members/tgbArchive/2028.pdf, [cited 19 June 2007].

McKay, W., Gregson, P., McKay, B., Militzer, J., 1999. Sternal Acceleration Ballistocardiography and Arterial Pressure Wave Analysis to Determine Stroke Volume. *Clin Invest Med.* 2 (1), pp 4-14.

NOVEL CONTROLLER FOR REBREATHER DIVING SYSTEMS

True Sensor Signal Validation and Safe Oxygen Injection

A. Sieber[1,2], B. Koss[2], R. Bedini[3], K. Houston[2], A. L'Abbate[2] and P. Dario[2]
[1]*Profactor Research and Solutions GmbH, Seibersdorf, Austria*
arne.sieber@profactor.at
[2]*Scuola Superiore Sant'Anna, Pisa, Italy*
[3]*CNR, Istituto di Fisiologia Clinica, Pisa, Italy*

Keywords: Rebreather, eCCR, mCCR, oxygen injection, pO_2 sensors, Oxygen, diving.

Abstract: In electronically controlled closed rebreather diving systems the partial pressure of oxygen (p O_2) inside the loop is controlled with 3 pO_2 sensors, a microcontroller and a solenoid valve, critical components that are prone to fail. State of the art failure detection integrated in rebreather diving systems for recreational purposes does not offer the necessary reliability required for life sustaining systems. The present paper describes a novel controller that combines true sensor signal validation with safe oxygen injection.

1 INTRODUCTION

In the past 30 years, underwater activities have registered a steep increase across Europe, going from few thousands of people in the 1980s, when diving was prevalently an elite activity, to 1.000.000 in 1990s, with scuba and apnoea EU divers engaged in diving activities worldwide (Divers Alert Network, 1992). Today about five million EU people are practicing diving activities. With an increasing number of divers also the diving industry is growing, presenting a continuous need for research and development in the field of recreational diving.

1.1 Open Circuit Diving

The breathing gas providing part of typical open circuit diving equipment for recreational purposes consists of a gas storage tank (typically 10 – 18l, 200 bar) and a two stage pressure regulator (SCUBA) (U.S. Navy Diving Manual, 2005), (NOAA Diving Manual). The first stage reduces the tank's pressure to a intermediate pressure around 8-10 bar higher than ambient pressure. The second stage, also known as the regulator, reduces the intermediate pressure to ambient pressure thus allowing the diver to breath underwater. Exhaled air is then vented through an exhaust valve into the water.

The maximum time a diver can stay under water is mainly determined by the amount of gas he is carrying with him, the depth, and the breathing volume per minute. So what is the gas efficiency of open circuit diving?

A normal relaxed diver metabolizes approximately 0,8 to 1 bar l /min O_2 (Noaa, Navy). This O_2 consumption may increase up to 2,5 to 3,5 bar l / min in the case of hard physical activities. As an example: A diver has a typical surface breathing minute volume of 25 bar l / min. This volume contains approximately 5,25 bar l O_2. But only 0,8 bar l are metabolized – means only 0,8 l of the 25 l are really needed. This results in a gas efficiency of approximately 3%. As the pressure increases with depth, this ratio decreases. At 40 m our example diver breathes now at 40 m again 25 l /min, but due to the increased ambient pressure (5 bar now instead of 1 bar at the surface), the consumed gas is 125 bar/l min. The O_2 metabolism is still the same 0,8 l/min, so the gas efficiency at 40 m drops to approximately 0,6 %. A tank with 10l volume, 200 bar pressure contains in this case enough gas for a period of 16 minutes. Besides the low efficiency, open circuit diving has additional drawbacks like very cold (due to expansion the gas is cooled) and dry (compressed air contains only a negligible amount of humidity) breathing gas and relatively high weight (~20kg for a 10l tank including the regulator and the buoyancy compensating jacket).

1.2 Rebreathers

A solution to increase the gas efficiency is using a rebreather, where the diver breathes in a loop instead of venting the exhaled gas into ambient. In a rebreather (figure 1 shows the schematics of an oxygen rebreather) (U.S. Navy Diving Manual, 2005) the diver exhales in a bag – the so called counter lung. A scrubber removed carbon dioxide and fresh gas is added to substitute metabolized O_2. This recycled gas is then inhaled by the diver again. In the case of a pure O_2 rebreather, the loop contains mainly O_2. The partial pressure of O_2 (pO_2) inside the loop is dependent on the depth, for example 1 bar at the surface and 2 bar in 10 m depth (each 10 m of depth the ambient pressure is increased by 1 bar). Such a rebreather has the advantages of maximized gas efficiency, bubble free and silent diving and warm and humid breathing gas.

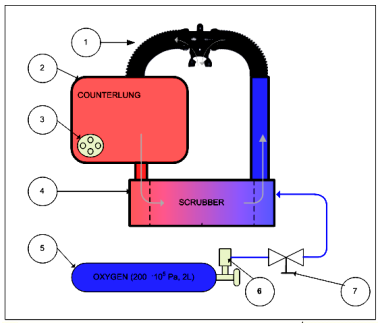

Figure 1: Schematics O_2 rebreather (1: mouthpiece, 2: counterlung, 3: overpressure valve, 4: scrubber, 5:oxygen tank, 7: manual valve).

The absolute pO_2 limits for a live sustaining breathing gas is 0,1 bar as the lower limit and 1,6 bar as maximum. A pO2 above this limit may lead to a oxygen intoxication, which can result in an epileptic fit like convulsion. In such a case the diver will loose his mouthpiece, drown and die. A pO_2 lower than 0,1 bar will lead to unconsciousness (Mount, T., Gilliam, B., Bohrer R., Taylor, L., Sommers, L.H., Crea, J., Nordsteam, R., 1992), (Ehm, O.F., Hahn, M., Hoffmann, U., Wenzel, J., 1996).

The maximum pO_2 limit of 1,6 bar sets the depth limit for pure O_2 rebreathers to 1,6 m and are normally used for military applications. Rebreathers used for recreational purposes are mostly either semi closed rebreathers (SCR) or manually or electronically controlled completely closed rebreathers (mCCR or eCCR).

In an SCR O_2 enriched air is being brought in the loop via a constant flow injector (commonly a orifice, typically 6 – 12 bar l / min) from tank to substitute the metabolized O_2. Every 4th or 5th gasp excessive gas is then vented through an overpressure valve. The maximum depth for SCR's is mainly limited by the percentage of O_2 in the supply gas.

In a mCCR or an eCCR the pO_2 is usually kept at constant level (Dederichs, H., Floren, G., Waldbrenner, M., Wilhelm, R., 2004), only the metabolized O_2 is substituted. To avoid the depth limit of 1,6 m of pure O_2 rebreathers, the breathing gas in a closed rebreather contains also N2 or He (He or He N_2 mixtures for deeper dives, normally known as technical dives).

To be able to keep the pO_2 at a constant level, a kind of regulation loop is needed (Straw, P.E., 2005). Therefore electrochemical oxygen sensors, whose output signal is proportional to the partial pressure of O_2, are used as sensing elements. In a mCCR the diver reads the pO_2 from a display (Baran, U., Frost, A.J., 2004) and if needed adds O_2 manually. In an eCCR this regulation task is usually performed with a microcontroller and a solenoid valve.

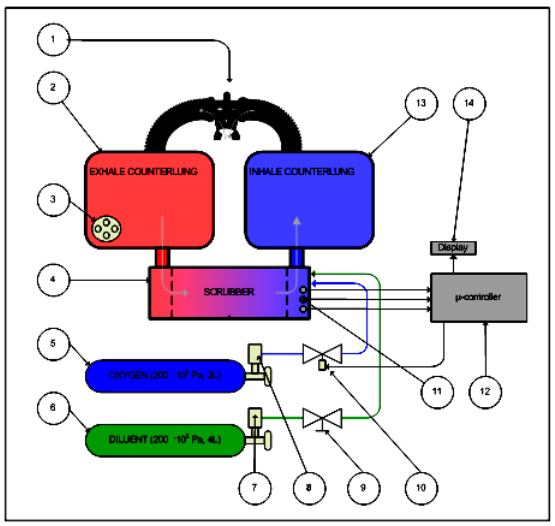

Figure 2: Schematics eCCR (1: mouthpiece, 2: exhale counterlung, 3: overpressure valve, 4: scrubber, 5: oxygen tank, 6: diluent tank, 7,8: pressure regulators, 9: manual diluent vlave, 10: solenoid, 11: pO_2 sensors, 12 µ-processor, 13: inhale counterlung, 14: display).

The regulation of the pO_2 inside the loop depends on the pO2 sensor signal. Unfortunately these electrochemical sensors are not reliable components and have a short life time of approximately 1 year in use. Typical problems that may occur are:

- non linearity
- current limitation (the output signal of the sensor is limited above a certain pO2)
- sensor failure

The consequence of a sensor failure may be a deviation of the pO_2 inside the loop, wich can be life threatening.

State of the art method to solve this problem is to use three pO_2 sensors instead of one (Deas, R.A., Evtukhov, M.V., 2003). If one sensor signal differs from the others, the sensor signal is "voted out" (voting algorithm) (Parker, M., 2005). Sensors of the same production lot and the same age often show the same failures at the same time. **Problems that occur because of wrong but similar sensor signals of at least two sensors can still not be detected because the voting algorithm will not work in this case as "voting" does not offer a real sensor signal validation.**

Another weak point in commercial available eCCR systems is the oxygen injection. Usually a solenoid valve is deployed for this task. Failures that may appear are that either the valve does not open anymore (defect in the solenoid or the electronics) or that it is stuck open (for example because of dirt). A valve that is stuck open will allow a free flow of O_2 that will lead in a short period of time to a life threatening pO_2 inside the loop. A solution, that can be found in eCCR for military applications is to use multiple solenoids for redundancy. In fact in recreational rebreathers this is still not state of the art.

The present paper describes a eCCR controller, that allows on the one hand a true sensor signal validation and on the other hand is equipped with a novel sensorized oxygen injection mechanism, that, in case of a failure, does not allow an O_2 free flow and enables reliable failure detection.

This eCCR controller enabled the development of a small and lightweight eCCR prototype for recreational proposes. It will be detailed in the section results.

2 METHODS

2.1 pO_2 Sensor Signal Validation

As described above, the state of the art voting algorithm does not provide a real sensor signal validation as it is based just on a comparison of the output signals of the sensors. A novel sensor signal validation procedure was developed to confront this problem.

The principle is based on injection of a gas with a known pO_2 in front of the pO_2 sensor membrane. With the help of another solenoid, gas from the diluent tank can be injected directly in front of the membrane of the oxygen sensors. With an orifice of 140 µm diameter the maximum flow is restricted to 2 bar l / min. Within an injection time of 5 s the pO_2 sensor signals should drop to the value corresponding to the pO_2 of the injected gas, which is given by the O_2 percentage of the diluent gas and the ambient pressure. A comparison of the sensor signal and the calculated reference signal allows then a reliable sensor signal validation and failure detection.

Figure 3a shows an enhanced version of the sensor signal validation apparatus, where it is not only possible to inject diluent gas in front of the sensor membrane but also pure O_2, to test the sensor for current limitation and linearity at preferable a depth between 6 and 10m. It has to be remarked that due to the small flow of just 2 bar l / min, the functionality of the rebreather is not negatively affected.

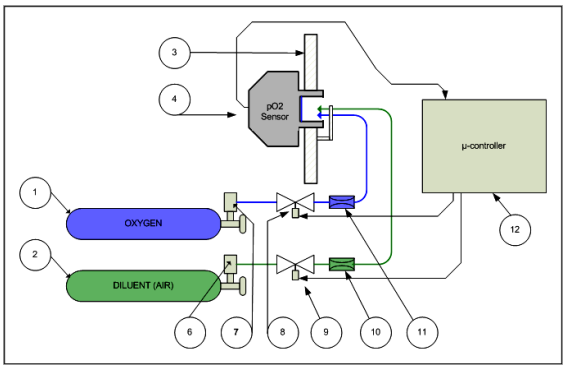

Figure 3a: The principle schematics of our true pO_2 sensor signal validation (1: oxygen tank, 2: diluent tank, 3: sensor support, 4: pO_2 sensor, 6,7: pressure regulators, 8,9: solenoids, 10,11: flow restriction orifices, 12 microcontroller).

2.2 Safe O_2 Injection

The metabolized O_2 has to be replaced by fresh O_2 from the tank. Therefore usually in eCCR a solenoid is controlled by a microcontroller as schematically displayed in figure 2. To confront the problems like a stuck solenoid valve, we invented a novel pO2 injection mechanism, displayed schematically in figure 3b.

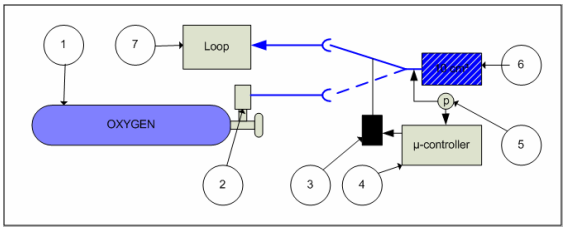

Figure 3b: Safe O_2 Injection.

O_2 is supplied from an oxygen tank (figure 3b). The pressure is then reduced with a oxygen compatible standard SCUBA fist stage (2) to a intermediate pressure of 10 bar over ambient. Instead of the state of the art 2/2 solenoid used for oxygen injection, a 2/3 version (3) is deployed. When powered though the microcontroller (4), the reservoir (6) is filled with 0,1 bar l O_2. When the solenoid is switched off, the gas in the reservoir is injected into the loop (7). To monitor the injection and detect reliably a failure, a pressure sensor is integrated (5) (the pressure of the successfully filled reservoir should be like the intermediate pressure 10 bar over ambient).

A failure of the solenoid (stuck open or closed) will not result in a free flow of O_2. A second benefit is that due to the design with a reservoir every O_2 injection will provide exactly 0,1 bar l of O_2. This allows an easy calculation of the O_2 metabolism of the diver.

2.3 Electronics - Hardware

As core component of the electronics the 8 Bit RISC microcontroller ATMEGA 32 from ATMEL () was chosen (32kByte flash ROM, 2 kByte RAM). A 4x20 characters display is connected via SPI bus (EA DIP 204-4, www.lcd-module.de). To enable a detailed post dive analysis a slot for SD memory cards was integrated in the set up. Three N-FET NDS355 serve as solenoid drivers.

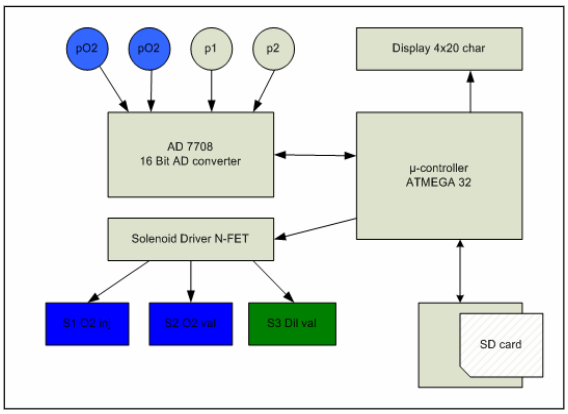

Figure 4: Electronics.

For the sensor signal processing the 16 Bit AD7708 (figure 5) analog to digital converter from Analog Devices is connected via SPI bus to the microcontroller. Its high resolution and the programmable input stage allows directly connecting the pO2 sensors (electrochemical pO2 sensors used in rebreathers have a typical output signal of approximately 8-13 mV @ 0,21 bar pO2). Two Motorola MPX5999 pressure sensors are used to measure on the one hand the ambient pressure (there the negative pressure port is closed) and on the other hand the differential pressure of the reservoir to ambient.

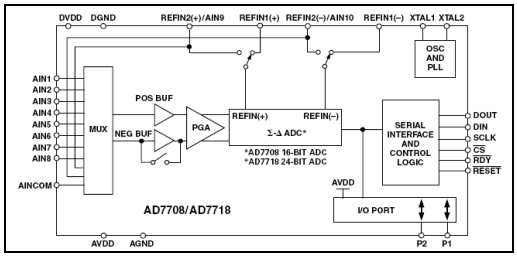

Figure 5: Analog Devices AD 7708.

Two low drop voltage regulators from Texas Instruments are used to provide 5V for the microprocessor, the display, the AD converter and the pressure sensors and 3,3V for the operation of the SD memory card.

Figure 6: Scrubber and scrubber head with solenoids, pressure sensors and two pO2 sensors (Analytical Industries, PSR 11-39-MD2).

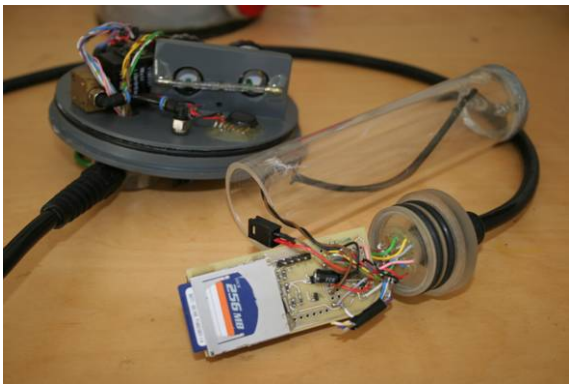

Figure 7: Electronics with the SD card slot and the lexan housing depth rated to 120 m.

2.4 Software

As programming platform the ATMEL AVR Studio 4 together with the free of charge GNU C compiler WinAVR (http://winavr.sourceforge.net/) was used under Windows XP.

The pO_2 control loop is designed in a way to keep the pO_2 inside the loop constant at 1,3 bar at a depth greater than 16 m. In the range between the surface and 16 m the pO_2 is increasing linear from 0,5 bar on the surface to 1,3 bar in 16m (compare figure 9 A and 9 B).

Error messages are created if a pO_2 sensor signal is outside the limits, the sensor signals differs more than 0,01 bar from each other, the battery voltage is below 6,5V and if the calculated O_2 metabolism of the diver is less than 0,3 or more than 3 bar l / min.

Every 120 seconds the sensor signal validation procedure with diluent as validation gas is carried out which results in the spikes in the readings of the pO_2 sensors (figure 9B, 10C). During the validation cycle the calculated O_2 in % has to drop to a value less than 25% (figure 9C and 9D). If not, an alarm signal is generated.

Optionally at a depth between 6 and 10 m once a dive the pO_2 sensors are checked for linearity and current limitation by injection of pure O_2 in front of the sensor membrane.

For the pre dive preparations the system can perform automatically a negative pressure test, a positive pressure test and the pO_2 sensor calibration.

All sensor data are stored on SD card in spreadsheet format. FAT 16 or FAT 32 formatted SD memory cards can be used. For each dive a new file is created. Additionally data like battery voltage, oxygen injection, oxygen consumption and error messages are stored.

3 RESULTS

This novel device with its true sensor signal validation and the safe oxygen injection is the key component of our eCCR prototype with the following specifications:

- Outer dimension: 45x25x18 cm³
- Scrubber: 1,5 kg
- Max depth: 50m
- 1 oxygen tank: 1,5 l, 200 bar
- 1 diluent tank: 1,5 l, 200 bar
- total weight: 12 kg
- maximum dive time: 180 min

After the dive the SD card can be read out with every PC equipped with a memory card reader and visualized with suitable programs like Microsoft EXCEL Figure 9 shows data of a test dive with 45 min duration to a maximum depth of 22m.

Figure 8: One of our eCCR test divers is preparing for a dive with our first prototype.

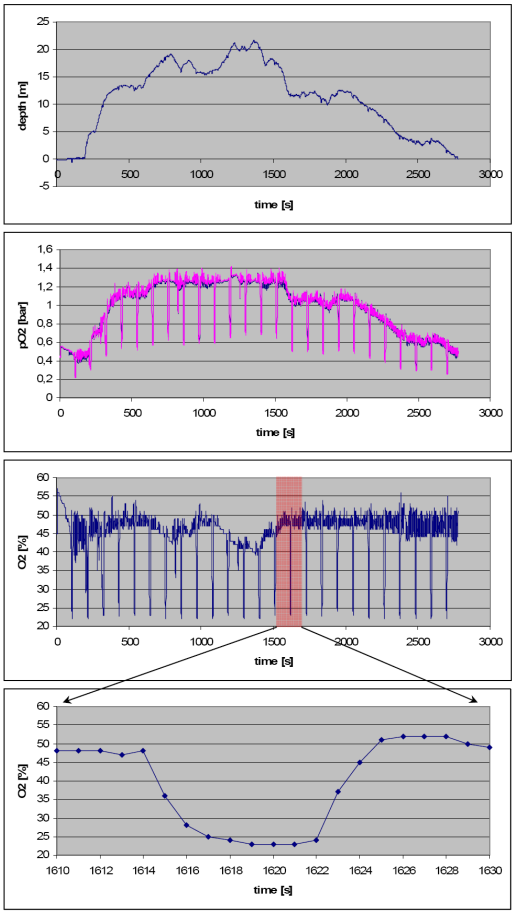

Figure 9: Data of a 45 min test dive in the mediterranian sea to a maximum depth of 22m; A: depth profile; B: pO_2 sensor signals of 2 sensors; C: calculated $\%O_2$; D: one validation cycle.

4 CONCLUSIONS

ECCR have a variety of advantages like:

- silent diving
- no bubbles
- maximized gas efficiency
- warm breathing gas
- humid breathing gas

Disadvantages are that the control of the pO_2 to keep it within life sustaining limits at a constant level depends on sensors which, with a low mean time between failure (MTBF) of less than a year, are prone to fail. State of the art solution is to deploy 3 pO_2 sensors for redundancy. This allows a reliable detection of one sensor failure, but cases, where more than one sensor show the same wrong values cannot be detected, which may lead to a non life sustaining pO_2 inside the loop followed by the death of the diver. A stuck open solenoid is another failure that may occur in a eCCR, resulting in a free flow of O_2, where the pO_2 inside the loop is increasing rapidly, or the case where the solenoid is stuck closed allowing no injection of fresh O_2 inside the loop anymore.

The present paper describes a novel apparatus that combines true sensor signal validation and a reliable sensor failure detection with a safe injection of O_2, where cases like a free flow of O_2 are not possible anymore.

In principle the apparatus can work with just one pO_2 sensor, where in the case of a sensor failure a alarm is given telling the diver to use his separate emergency gas supply in open circuit mode and to abort the dive.

As this system needs just one (or for redundancy two pO_2 sensors, in the case of the failure of one pO_2 sensor, the dive can be continued with the other working one). The costs for the yearly maintenance are dramatically decreased (pO_2 sensors should be changed once a year).

The authors are convinced that the further development of this novel device will lead to a novel kind of diving device for recreational purposes with a dramatically increased safety, low weight of the overall system and independency (180 min maximum dive duration).

5 FUTURE WORK

Near future work will include a further development of the presented electronics, an integration of a second controller for redundancy, a head up display mounted on the mouthpiece with LEDs for status information and a breathing frequency sensor. As the breathing frequency increases with increasing work load (and O_2 metabolism), this parameter allows another cross check giving more safety to the final product.

Typical for electrochemical pO_2 sensors for diving is that at the end of the dive the signal is slightly deviating from the reference signal (during a dive the sensors are very warm and humid gas under high pO_2, factors which present a quite extreme environment – so even if most pO_2 Sensors are temperature compensated changes in the slope of the sensors are not unusual during a dive) Another function that will be implemented in the next firmware release is an advanced sensor signal processing that, in the case of relatively small signal deviations allows a sensor recalibration during the dive (but only if the sensor is still linear, which can be checked with 2 reference gases (O_2 and diluent).

REFERENCES

Divers Alert Network, 1992, *Report on Diving Accidents & Fatalities*, Divers Alert Network, Box 3823, Duke University Medical Center, Durham, NC 27710, 1994.

U.S. Navy Diving Manual, 2005, Volume 2 and Volume 4, SS521-AG-PRO-010, Direction of Commander, Naval Sea Systems Command, USA

NOAA Diving Manual, *Diving for Science and Technology*, 4th edition, US Department of Commerce, National Technical Information Service, Springfield

Ehm, O.F., Hahn, M., Hoffmann, U., Wenzel, J., 1996, *Der neue Ehm, Tauchen noch sicherer*, 9th edition, ISBN 3-275-01484-6, Mueller Rueschlikon Verlags AG, CH-6330 Cham.

Dederichs, H., Floren, G., Waldbrenner, M., Wilhelm, R., 2004, *Handbuch Technisches Tauchen*, ISBN 3-275-01492-7, Mueller Rueschlikon Verlags AG, CH-6330 Cham.

Mount, T., Gilliam, B., Bohrer R., Taylor, L., Sommers, L. H., Crea, J., Nordsteam, R., 1992, *Mixed Gas Diving*, ISBN 0-922769-30-3, Watersports Publishing, San Diego, USA.

Deas, R.A., Evtukhov, M.V., 2003, *Control electronics system for rebreather*, UK Patent Application, GB 2404539 A.

Deas, R.A., Evtukhov, M.V., 2003, *Automatic Control System for Rebreather*, United States Patent Application Publication, US 2003/0188744 A1

Baran, U., Frost, A.J., 2004, *Diving Equipment Monitor, PCT*, WO 2004/112905 A1

Straw, P.E., 2005, *Rebreather Setpoint Controller and Display*, PCT, WO 2005/107390 A2

Parker, M., 2005, *Evolution Closed Circuit Rebreather* and *Inspiration Closed Circuit Rebreather*, Ambient Pressure Diving Ltd., Helston, Cornwall, UK

ANIMAL STUDIES USING AN OXYGEN-TENSION SENSOR FOR TISSUE VIABILITY MONITORING

Dafina Tanase
Electronic Instrumentation Laboratory, Delft University of Technology, Mekelweg 4, Delft, The Netherlands
d.tanase@tudelft.nl

Niels Komen
Erasmus Medical Centre, Rotterdam, The Netherlands
n.komen@erasmusmc.nl

Arie Draaijer
TNO Quality of Life, Zeist, The Netherlands
arie.draaijer@tno.nl

Johan F. Lange, Gert-Jan Kleinrensink, Johannes Jeekel
Erasmus Medical Centre, Rotterdam, The Netherlands
j.lange@erasmusmc.nl, g.kleinrensink@erasmusmc.nl, j.jeekel@erasmusmc.nl

Paddy J. French
Delft University of Technology, Delft, The Netherlands
p.j.french@tudelft.nl

Keywords: Oxygen-tension sensor, tissue viability, colon, optical method.

Abstract: Leakage at the site of an anastomosis is the main, yet unsolved reason for mortality in abdominal surgery. Every year, a large number of patients die due to anastomotic leakage after surgery. An objective aid to monitor the anastomotic site pre- and postoperatively and detect leakage at an early stage, is needed. Therefore, a miniature, wireless measurement system to detect tissue viability during and after colon surgery (continuously for 7 days) is being developed. The complete sensor chip should include an oxygen-saturation sensor (sO_2), an oxygen-tension sensor (pO_2), a carbon-dioxide tension sensor (pCO_2) and a temperature sensor. The present work focuses on the use of the oxygen-tension and temperature sensors for animal studies. Initial in-vivo measurements were carried out on the small and large intestines of male wistar rats. The main goal was to measure the distribution of pO_2 on the colon around the anastomosis and to determine the changes in pO_2 during repetitive ischemia-and-reperfusion experiments on the small intestine. The paper presents the obtained measurement results.

1 INTRODUCTION

An anastomosis is the surgical connection of two tubular segments to restore continuity (Figure 1). Leakage of a colorectal anastomosis is a complication in which intestinal content leaks into the abdominal cavity due to a "defect" in the anastomosis. This defect can be caused by a reduced oxygen supply and it can lead to cell death and necrosis of the anastomosis. As a result, leakage can occur and as a consequence, peritonitis may develop and can lead further to sepsis, multiple-organ failure

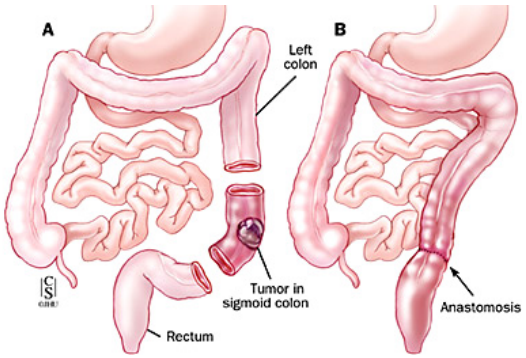

Figure 1: A colon anastomosis.

and ultimately death. Therefore, anastomotic leakage of a colorectal anastomosis is considered a potentially lethal complication.

The reported incidence varies between 10 % and 13 % (Kanellos, 2004; Guenaga, 2003; Peeters, 2005), with a mortality rate that can be as high as 32 % (Choi, 2006). To date, no peroperative methods to avoid or predict anastomotic leakage, or any validated, objective parameters for detection of anastomotic leakage in an early postoperative phase, exist. Current diagnostic methods include observation of clinical signs and symptoms (fever and pain), while confirmation is obtained by imaging. These methods are faced with several disadvantages. When anastomotic leakage has progressed to a state of clinical manifestation, the patient is already ill and treatment needs to be initiated. Imaging modalities, more specifically abdominal CT-scans and/with contrast enemas, are normally used to confirm a clinical diagnosis of anastomotic leakage, meaning the patient is already ill (Eckmann, 2004).

At present, clinically relevant anastomotic leakage is usually diagnosed approximately 6 to 8 days after surgery (Kanellos, 2004; Alves 1999). Some studies report an even longer interval (12 days) between operation and diagnosis of anastomotic leakage (Hymann, 2007). The long intervals between the construction of the anastomosis and the diagnosis of anastomotic leakage are detrimental for the prognosis, increasing mortality rates (Macarthur, 1998).

Therefore, a biomarker reflecting the viability of the anastomosis, could be a fast and objective diagnostic tool in addition to current methods, allowing diagnosis of anastomotic leakage before its clinical presentation.

In this respect, the main goal of this research is to develop a miniature, wireless sensor system to monitor tissue viability pre- and postoperative, continuously for 7 days. The complete sensor chip should include an oxygen-saturation sensor (sO_2), an oxygen-tension sensor (pO_2), a carbon-dioxide tension sensor (pCO_2) and a temperature sensor (Figure 2).

The present work focuses on the use of the oxygen-tension and temperature sensors for animal studies.

2 MEASUREMENT SETUP

The measurement setup for the animal studies is shown in Figure 3. It consists of the pO_2 and temperature sensor block and a notebook for reading and processing the data from the sensors. The investigations were performed in the Erasmus Medical Centre in Rotterdam, using male wistar rats, 12 weeks old. They were prepared for surgery by shaving their abdomen and disinfecting it with 70% alcohol.

.

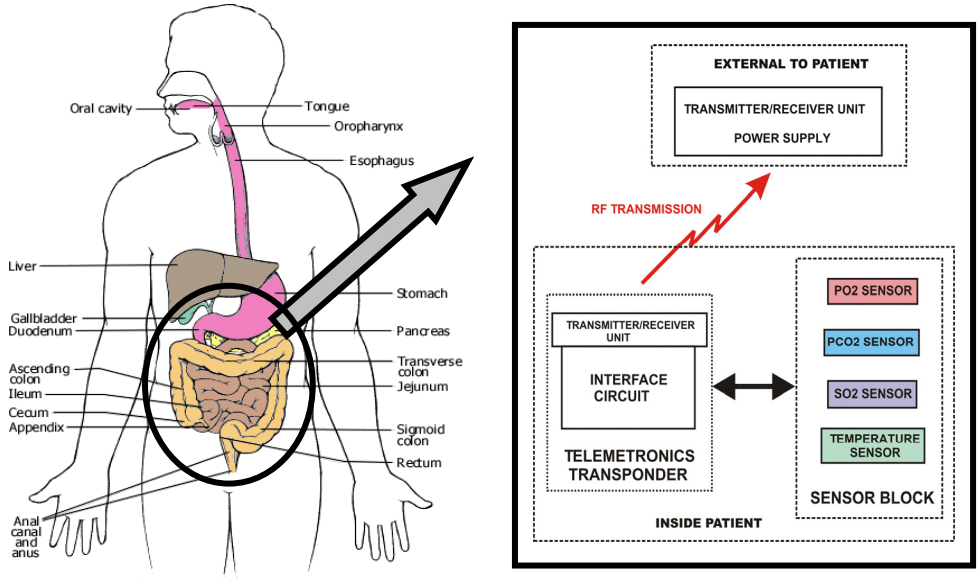

Figure 2: Schematic of the complete sensor system for tissue viability monitoring.

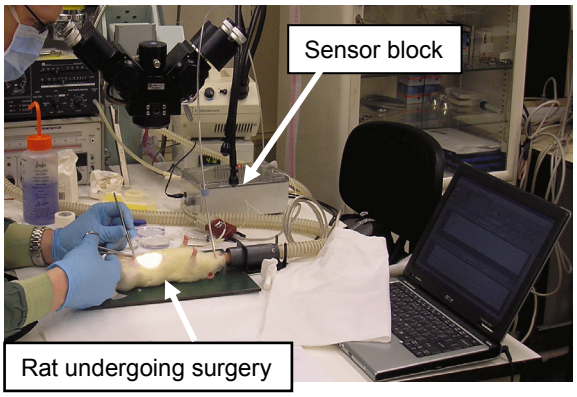

Figure 3: Measurement setup at Erasmus Medical Centre in Rotterdam comprising the sensor block and the notebook for data processing.

Afterwards, the animal undergoing surgery was placed on a hot plate and anesthetised throughout the intervention by administering a mixture of isoflurane, oxygen and air (the fraction of inspired oxygen, FiO_2=66 %). Access to the internal anatomical structures of the animals was gained by laparotomy (surgical incision into the abdominal wall) with an incision length of 4 cm. After opening the abdomen and exposing the ascending colon, the oxygen-tension and temperature sensors were fixed together and placed at pre-defined locations along the ascending colon, laterally (with respect to the peritoneal membrane) and antimesenterial (opposed to the peritoneal membrane).

The sensors were fabricated at TNO Quality of Life, The Netherlands (Draaijer, 1999) and they have been tested in a previous study (Tanase, 2007). The block diagram of the sensors is shown in Figure 4. The pO_2 sensor consists of a coating at the tip of an optical fibre (3 mm diameter) and works on the principle of dynamic quenching by oxygen of fluorescent particles immobilized in a gas permeable polymer. In our case, the fluorescent particle is ruthenium, which enters an excited state caused by the LED excitation with a wavelength of 470 nm. The excited state of ruthenium is deactivated by the collision process with oxygen, the particles emitting light with a wavelength of 600 nm. The emitted signals are detected by a photodiode (PD) and converted to a digital signal using an on-board analogue-to-digital (ADC) converter. The oxygen concentration is determined by measuring the fluorescence lifetime. In addition to the pO_2 sensor, the sensor block contains the temperature sensor (NTC type, *Farnell*), whose output is also converted via an ADC. The total sequence of data sent to the computer (via a serial connection RS 232) is BG, I1, I2 and T (the background, the two intensities at successive times and the temperature). From these data, the software (LabView, *National Instruments*) computes the oxygen tension and indicates the temperature.

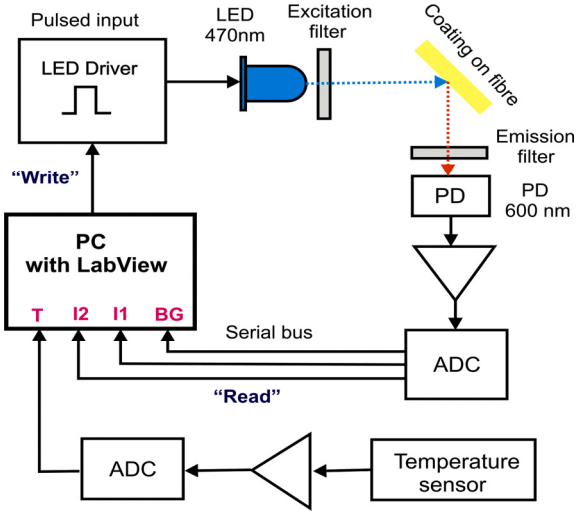

Figure 4: Schematic of the sensors with the LED driver circuit, the read-out of the photodiode and of the temperature sensor.

Figure 5 presents a photograph of the sensor block with the two sensors and a magnified view of the fibre tip with the oxygen-sensitive coating.

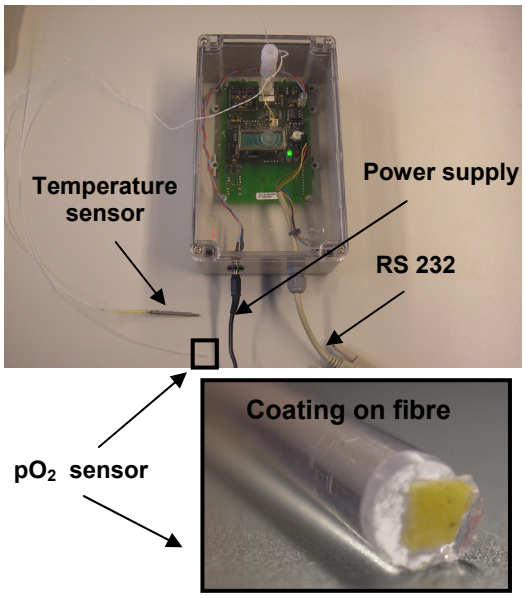

Figure 5: Photograph of the sensor block with the two sensors and a magnified view of the fibre tip showing the oxygen sensitive coating.

3 MEASUREMENT RESULTS

Initial tests were performed by placing the sensors on the colon after the construction of the anastomosis. Figure 6 shows the sensors at a distance of 1 cm away from the anastomosis, while Figure 7 presents the table and graph with the measurement results, for different sensor locations around the anastomosis. The sensors were placed radial (lateral and antimesenterial) and longitudinal, at ten different locations on both sides of the anastomosis, as indicated in Figure 7.

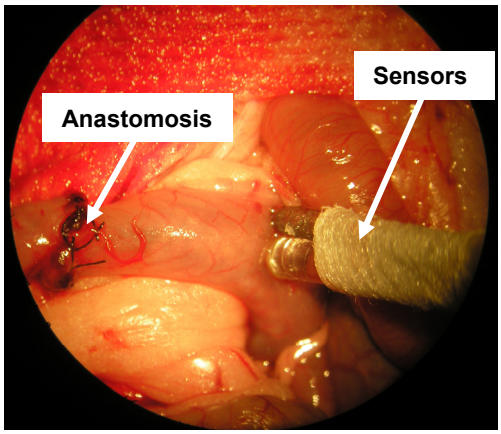

Figure 6: Photograph showing the sensors on the colon, 1 cm away from the anastomosis.

The lowest oxygen-tension values are obtained on the anastomosis (part 3 and part 8 in Figure 7). This is an expected effect - due to local cell death, tissue oxygenation at the site of the anastomosis is reduced. The farther from the anastomosis we measure, the better the oxygenation, and the higher the oxygen-tension values. The spikes on the graph are artefacts visible only at the moments when the sensors are moved from one tissue location to another, because then, for a short period of time, the fibre is in air. The temperature changes corresponding to tissue and air are visible on the temperature graph.

Another series of measurements were performed with the sensors on the small intestine (Figure 8). In this case, the blood supply to the central part of the small intestine was obstructed by two strings that were fastened for ischemia and released for reperfusion. The measurement results during the ischemia-reperfusion experiment are shown in Figure 9.

At the beginning of the test, the sensors were placed on the small intestine and by fastening the strings, the intestine was made ischemic (part 1). The values readily decreased to 4 mmHg, indicating total ischemia. Once the strings were released, an overshoot was noted, showing a maximum at 202 mmHg. Two other cycles were repeated to test the correctness of the measurement. Also in this case, the results of the tests met our expectations.

In addition to these measurements, other tests were performed by changing the levels of inspired oxygen (33.4 %, 42.8 %, 66.7 % and 91 %). We noted that the local pO_2 changed accordingly to the inspired oxygen. For an even better characterisation, a new series of tests is currently performed, during which the animals are intubated. In this way, the inspired oxygen can be accurately controlled, while the rats are being continuously monitored.

4 CONCLUSIONS

The paper has presented the initial measurements and results with an optical oxygen-tension sensor and a temperature sensor. The performed tests have shown that the principle of optical sensing is suitable for tissue measurements.

The first series of measurements has shown a significant decrease (approximately 40 mmHg) in pO_2 on the anastomosis as compared to the other measurement sites on the colon. It was also shown that on two points (lateral and antimesentery) of the anastomosis, the values for the pO_2 were approximately the same.

The ischemia and reperfusion experiments have shown that the sensor system reacted as expected to the local changes on the small intestine. When the intestine was made ischemic, the pO_2 decreased and when the obstruction was removed, the pO_2 increased significantly, with an overshoot.

This cycle was repeated three times to test the correctness and repeatability of the measurement.

LATERAL				ANTIMESENTERY			
#	Location [cm]	Start time [sec]	pO_2 [mmHg]	#	Location [cm]	Start time [sec]	pO_2 [mmHg]
1	1	100	152->126	**6**	1	4900	122->209
2	0.5	1600	126->112	**7**	0.5	5600	209->125
3	**On anastomosis**	**2050**	**112->43**	**8**	**On anastomosis**	**6400**	**125->38**
4	0.5	2900	43->85	**9**	0.5	7500	38->100
5	1	4000	85->122	**10**	1	8200	100->100

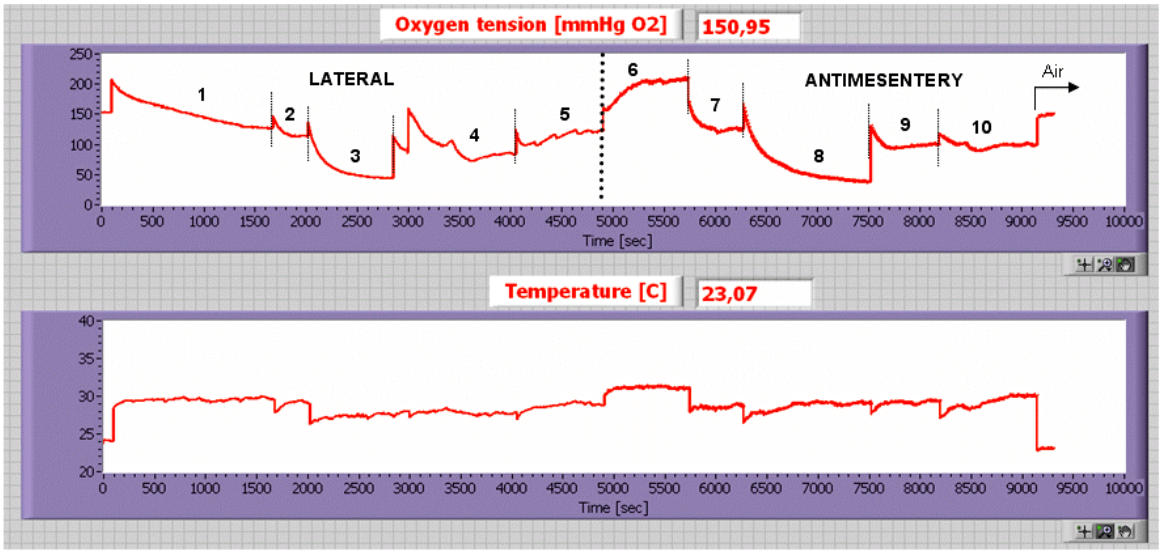

Figure 7: The numeric results and the graphical representation of the tests performed on the colon, to determine the distribution of the oxygen radially and longitudinally with respect to the anastomosis, at different locations.

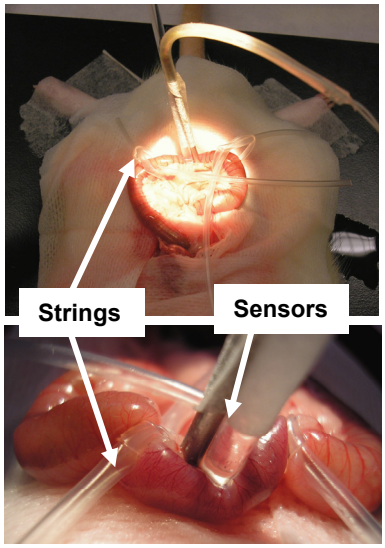

Figure 8: An overall view and a close-up of the small intestine showing the strings (used to obstruct the blood flow) and the sensors.

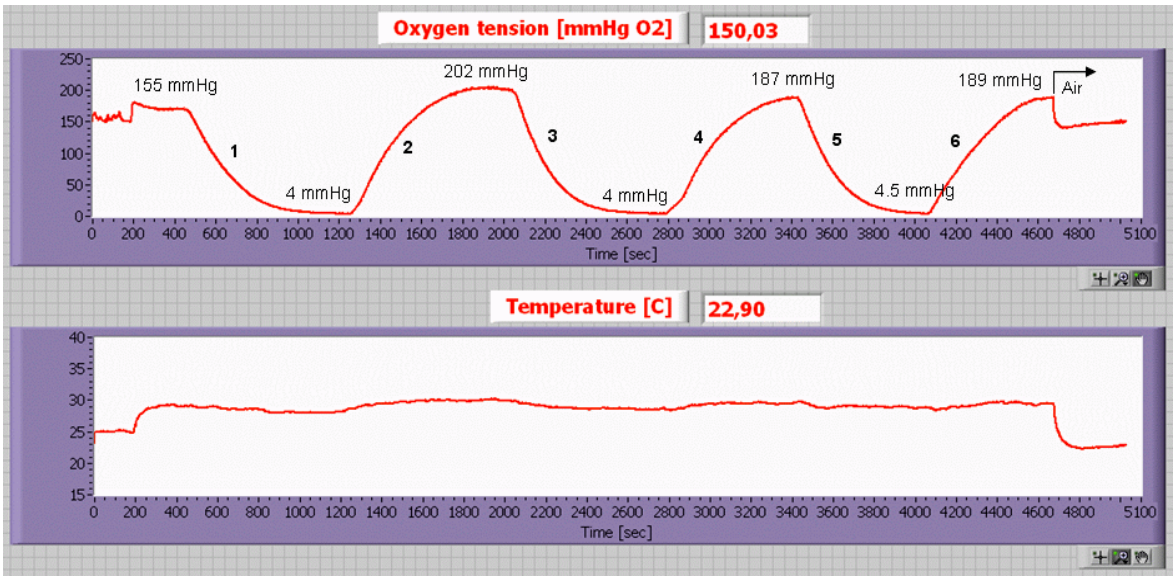

Figure 9: The graphical representation of the ischemia-reperfusion experiment on the small intestine.

Although not presented in this paper, the first steps towards an integrated sensor system have been taken. The sensor-system design is currently underway and issues regarding device sterilisation and packaging are already taken into account.

A new study is currently planned for more detailed investigations, considering also the aspects of biocompatibility.

REFERENCES

Alves A., Panis Y., Pocard M., Regimbeau J.M., Valleur P. (1999). Management of anastomotic leakage after nondiverted large bowel resection. *J Am Coll Surg*, 189(6):554-559

Choi H-K., Lau W-L., Ho J.W.C., (2006). Leakage after resection and intraperitoneal anastomosis for colorectal malignancy: analysis of risk factors, *Dis. Colon Rectum*, 49:1719-1725

Draaijer A., Konig J.W., Gans O., Jetten J., Douwma A.C. (1999). A novel optical method to determine oxygen in beer bottles. *EMC Congress, France*

Eckmann C., Kujath P., Schiedeck T.H., Shekarriz H., Bruch H.P. (2004). Anastomotic leakage following low anterior resection: results of a standardized diagnostic and therapeutic approach. *Int J Colorectal Dis*, 19(2):128-133

Guenaga K.F., Matos D., Castro A.A., Atallah A.N., Wille-Jorgensen P. (2003). Mechanical bowel preparation for elective colorectal surgery. *Cochrane Database Syst Rev* 2:CD001544

Hyman N., Manchester T.L., Osler T., Burns B., Cataldo P.A. (2007). Anastomotic leaks after intestinal anastomosis: it's later than you think. *Ann Surg*, 245(2):254-258

Kanellos I., Vasiliadis K., Angelopoulos S. et al. (2004). Anastomotic leakage following anterior resection for rectal cancer. *Tech Coloproctol*, 8 Suppl 1:s79-81

Macarthur D.C., Nixon S.J., Aitken R.J.(1998). Avoidable deaths still occur after large bowel surgery. *British J Surg*, 85(1):80-83

Peeters K.C., Tollenaar R.A., Marijnen C.A. et al. (2005). Risk factors for anastomotic failure after total mesorectal excision of rectal cancer. *British Journal of Surgery*, 92(2):211-216

Tanase D., Komen N., Draaijer A., Kleinrensink G.J., Jeekel J., Lange J.F., French P.J. (2007), Oxygen-tension measurements – the first step towards prevention and early detection of anastomotic leakage, *To be published in Proceedings of the IEEE Sensors 2007 Conference, Atlanta, USA*

A MECHATRONIC DEVICE FOR THE REHABILITATION OF ANKLE MOTION

Giuseppe Bucca, Alberto Bezzolato, Stefano Bruni
Department of Mechanical Engineering, Politecnico di Milano, Via La Masa 34, Milano, Italy
giuseppe.bucca@polimi.it,stefano.bruni@polimi.it

Franco Molteni
Valduce Villa Beretta Rehabilitation Centre, Italy
francomolteni@libero.it

Keywords: Mechatronics, gait analysis, biomechanic models.

Abstract: The paper presents the main results from a research aiming at the design of an electro-mechanical actuator to assist walking movements of the ankle articulation, for use in the rehabilitation of lower limb motion in patients suffering neurological disease. Motivations for the research project are discussed within the framework of the application of mechatronic concepts within rehabilitation practice. The entire design process is then described, from the definition of project target through the mechanical concept and control design steps until design validation by means of numerical simulations and tests on a prototype.

1 INTRODUCTION

In recent years, mechatronics has emerged as a powerful approach to provide innovative solutions in many technical fields related with mechanical and electronic engineering, and also in the field of bioengineering. This paper presents an application of mechatronic concepts to improve the effectiveness of therapies addressing the rehabilitation of lower limb motion in patients suffering neurological disease.

The project is being developed as a joint cooperation of the Politecnico di Milano (Technical University of Milan) and the Villa Beretta rehabilitation centre, part of Valduce Hospital, and is part of HINT@Lecco, a large research program aiming at the promotion of research fostering new applications in the fields of medical diagnostics and therapy.

Aim of the project is to design an electro-mechanical actuator to assist walking movements of the ankle articulation, referred to as "ankle actuator". The system has been designed for use either as integrated with the Lokomat rehabilitation device (Colombo et Al, 2000) presently in use at Villa Beretta, or as a standalone device to assist physiotherapy.

In the paper, the need and possible applications of the ankle actuator are described under the point of view of rehabilitation practice (Section 2), then the results of measurements and numerical simulations based on biomechanic multi-body models are reported, with the aim of setting the targets for the project (Section 3). The mechatronic design of the system and the identification of appropriate control strategies to meet the targets of the project are described in Sections 4 and 5. Finally, Section 6 reports about the final assessment of system performances, that was pursued by a combination of testing on a prototype demonstrator and multi-physics simulation of the actuator fitted on a person, involving the modelling of the lower limb and of the actuator together with the control unit.

2 USE OF THE DEVICE FOR REHABILITATION PURPOSES

The equinovarus foot is the most common pathological lower limb posture after lesions that result in an upper motor neuron syndrome (UMNS).

The lack of normal motor control and/or the presence of static foot deformity alters the cyclical kinematic pattern of lower limb and trunk during gait. There may be impairment of advancement of the body weight over the supporting limb and to

swing the unloaded limb forward in preparation for the next step. Foot pain, skin breakdown (lateral border, fifth metatarsal) and knee hyperextension (and/or varus) are frequently associated to this gait deviation and the compensation needed for the lack of adequate base of support, limitation of ankle dorsiflexion, dysrhytmic and restrained forward translation of body mass, asymmetrical weight transfer and interference with weight bearing on the involved limb. Gait deviations and compensations in the involved limb induce compensations for the non-involved limb, pain and fatigue.

The equinovarus foot impairment is the result of different combinations of the following dysfunctions:

a) decrease of dorsiflexor muscles motor control during swing phase;
b) increase activity of plantarflexor muscles;
c) reduction of the elastic properties of the calf muscles.

The main goal of rehabilitation procedures is to maintain ankle passive range of motion , to reduce "learning non use" due to weakness of dorsiflexor muscles, to maintain the elastic properties of dorsiflexor/plantarflexor muscles.

3 TARGETS FOR THE PROJECT

A first step of the research consisted in defining quantitative targets for the mechatronic ankle actuator, in view of allowing the correct choice of the actuation system and the proper mechanical design of the system. This was done through a combination of experiments to measure relevant gait parameters and of gait mechanics modelling and simulation by a biomechanical multi-body model.

3.1 Measure of Gait Parameters

An experimental campaign was performed on healthy subjects, with the aim of obtaining the references corresponding to correct motion, to be reproduced under the assistance of the mechatronic ankle actuator. Lower limb movements were measured by means of an ELITE opto-electronic system for motion analysis, whereas contact forces under the footprint were measured by means of dynamometric platforms.

These measurements allowed to quantify the required maximum speed, maximum force and power targets for the ankle actuator. Furthermore, a rather large set of measured data was made available, allowing the validation of the bio-mechanical multi-body model in view of its use in a later stage of the project (see Section 6.1). Some of the experimental results are shown in the next paragraph, where they are compared with the results of a simulation model. Despite it is known that in case of patients with neurological diseases, muscle configurations may present a different situation compared to the healthy population, the aim of this device is to reproduce a healthy subject gait on patients with moderate neurological diseases. Applications on subjects with more serious diseases have to be verified by means experimental tests.

3.2 Numerical Simulations

A multi-body human model was defined in ADAMS/LifeMOD environment, with the aim of complementing measurements to define the targets of the project. Moreover, the same model was used in a later stage of the project, being interfaced with a model of the ankle actuator, for performance assessment purposes (see Section 6.1).

The model includes the pelvis and the two legs, and was used to perform inverse and forward dynamic simulations. In the target definition phase, numerical simulations were used to evaluate gait parameters that could not be directly measured, as the ankle torque, and to derive gait parameters under conditions that could not be tested.

The multi-body model was validated based on comparison with the measurements described in Section 3.1. As an example, Figure 1 shows the time history of the measured and simulated vertical contact force component for a healthy male person weighting of 68kg and being 1,72m tall. Figure 2 shows the experimental vs. numerical comparison of right foot marker position during gait on a treadmill, for the same subject as in Fig. 1.

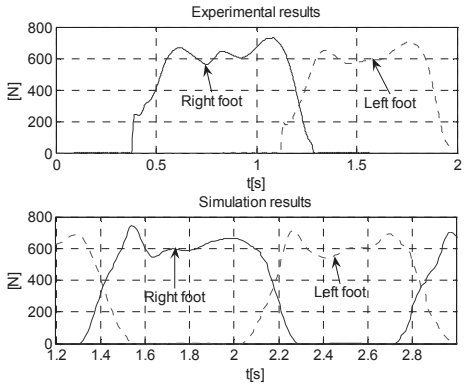

Figure 1: Contact forces for a male person. Up: experimental results; down: results of numerical simulation.

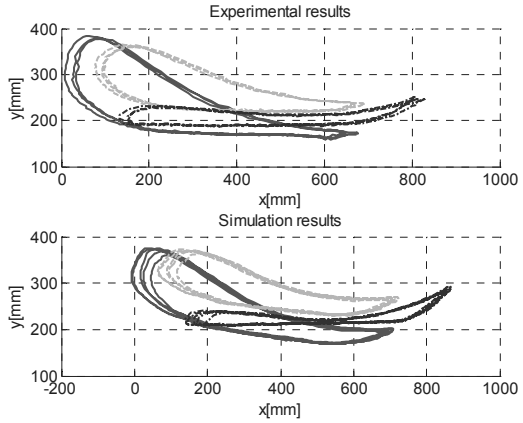

Figure 2: Right foot marker position for a male person: a) experimental results; b) results of numerical simulation.

The comparison of measured vs. simulated results allows to conclude that the mathematical model is able to capture correctly the main issues of gait mechanics and can be hence used to evaluate gait parameters under conditions that cannot be physically tested.

After validation, the model was used to derive quantitative targets for the ankle actuator, taking into consideration the effect of the Lokomat body weight support (b.w.s) system. The kinematic targets, not dependent upon the b.w.s. level, are listed in Table 1, while torque and power requirements for different levels of b.w.s. are compared in Table 2.

Table 1: Kinematic targets for the ankle actuator.

	MIN	MAX
Ankle rotation	-10°	20°
Ankle velocity	-200°/s	150°/s

Table 2: Torque and power targets corresponding to different body weight support (b.w.s) levels.

		MAX	RMS
b.w.s 0%.	Torque	112 Nm	54.4 Nm
	Power	152.6 W	48.6 W
b.w.s 25%	Torque	81.6 Nm	43.6 Nm
	Power	125.9 W	41.5 W
b.w.s 50%	Torque	65.1 Nm	31.2 Nm
	Power	90 W	29.3 W
b.w.s 75%	Torque	31.8 Nm	15.6 Nm
	Power	53.8 W	14.5 W
b.w.s 90%	Torque	24 Nm	8.37 Nm
	Power	34 W	7.36 W

Measurements described in a companion paper (Bocciolone et Al., 2008) showed that the Lokomat body weight support system provides a relief of at least 85% of patient's weight. Accordingly, torque and power targets for the project were assumed in a precautionary way to correspond to 75% body weight support.

The target motion of the ankle articulation was derived based on ELITE measurements (averaged to remove the intrinsic variability of each step) and on multi-body simulations. This was made considering a healthy subject, since the target of the system is to have the ankle performing a physiologically correct motion. As an example, the reference time history of ankle rotation for the same male subject considered above and for a walking speed of 2km/h is presented in Figure 3.

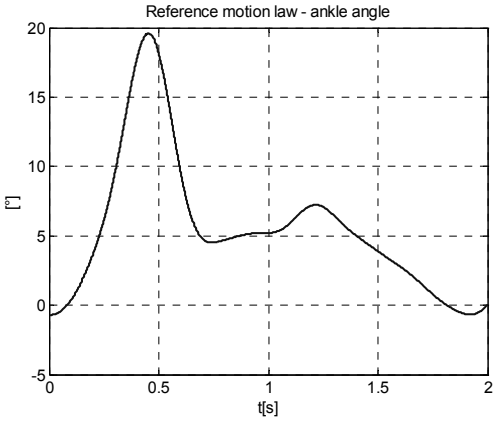

Figure 3: Reference motion law (talo-crural joint) for a male person.

4 THE CONCEPT

Besides the quantitative performance requirements resumed in Section 3, a number of qualitative requirements were defined for the ankle actuator, as detailed below:

- high intrinsic safety;
- fast and simple installation on the patient's leg (wearability);
- low weight, small size and low visual impact;
- low emission of noise and heat;

Furthermore, in case the device is used on a Lokomat machine, the mounting/dismounting of the ankle actuator over the Lokomat exoskeleton should not require any modification of the original structure.

The concept phase was then divided in two stages: selection of the type of actuator and design of the interface with the patient.

As far as the choice of the actuator is concerned, four alternatives were initially identified:

a) controlled electrical drive with rotating motor;
b) controlled electrical drive with linear motor;
c) controlled pneumatic actuator;
d) controlled Shape Memory Alloy (SMA) actuator.

These solutions were thoroughly analysed and compared evidencing for each advantages and weak points in view of the specific application. The main results of this comparison are summarized in Table 3.

Table 3: Comparison among main possible solution for the actuators of device.

Requirement	Solution			
	Rotating motor	Linear motor	Pneumatic actuator	SMA actuator
Max. Torque	Good	Very good	Very good	Poor
Dynamical response	Very good	Very good	Good	Poor
Wearability	Good	Good	Short	Fair
Cost	Good	Fair	Fair	Fair
Weight and dimensions	Very good	Very good	Poor	Good

The electrical drive with a rotating motor (DC or AC brushless) satisfies all main requirements: it has low weight and appropriate dimensions, affordable cost and simple structure which allows to build a device with a good wearability. Finally, a quite wide variety of solutions (in terms of size and specific features) is available on the market, allowing to tailor the choice in view of the requirements of the specific application. The drawback of this solution is the need of using an epicycloidal gear reducer, because rotating motors present high speed and low torque, while for ankle actuation, mechanical power is needed in the form of a relatively high torque acting at relatively low speed. The use of a gear reducer implies an increase in the weight of the device, which can be however kept within reasonable limits.

The linear motor mainly has the same advantages of the rotating motor and does not bear the drawback of using a gear reducer, because linear motors provide relatively high force at low speed, but is much more expensive than rotating motors, requires a more complicate mechanical design of the system and less alternatives are offered on the market.

Pneumatic actuation was considered also referring to previous applications to ankle actuation: (Sawicki, 2005) and (Ferris, 2005) showed that this kind of actuation is able to reproduce with good accuracy the features of actual ankle motion. In view of the aims of this project however, this solution compared to electromechanical solution provides lower actuation speed, lower maximum control force and requires auxiliary systems of relatively large size and potentially disturbing, like the air compressor.

The SMA actuator solution was also considered based on some tentative applications in the bio-medical field, including a parallel project within the HINT research project. However, besides some practical disadvantages like the need for a rather complicated cooling system, present SMA actuation technology appears to suffer from an insufficient dynamical response which is not able to ensure the required actuation speed to implement ankle motion control.

Based on the analysis summarized above, the solution based on rotating electric motor was identified as the most appropriate in terms of technical requirement and related costs and was chosen for development. In particular, a 150 W DC motor (MAXON RE40 150W), driven by a 4-Q-DC servoamplifier (MAXON ADS 50/10) and coupled with an epicycloidal gear reducer with a gear ratio of 1:113 (MAXON GP 52C) was chosen.

The second stage of the concept development consisted in the design of the interface between the actuator and the leg. The basic idea underlying this activity was to implement a configuration similar to the one used in the Lokomat machine. On that device, the feet are restrained by a sling held by an arm rigidly connected to the exoskeleton (Figure 4). The concept for interfacing active ankle actuation with the patient's leg was then based on the idea of replacing the passive arm with an articulated mechanical system, properly connected with the motor, so that ankle actuation may be obtained by an appropriate movement of the final link in the articulated system. The functional scheme of the solution identified is reported in Figure 5a: a support is fixed over the Lokomat exoskeleton, and connected by a hinge with a link which is actuated by a crank fitted on the gear output shaft. The rotation of the link produces a vertical motion of the sling holding patient's foot, which can be suitably controlled by the electric motor. Figure 5b shows a 3D rendering of the ankle actuator, including motor+gear, crank, link and connection to the Lokomat exoskeleton.

As shown in Figure 6, the mechanism has a gear ratio between the rotation of the gear output shaft and the rotation of the link which is almost constant and equal to 1:2.5. Figure 7 shows a picture of the developed device.

Figure 4: Passive sling of LOKOMAT.

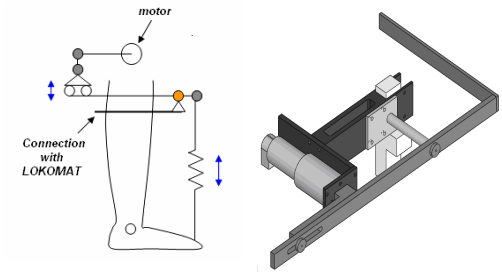

(a) (b)

Figure 5: a) Concept of active ankle actuation; b) Mechanical design of the ankle actuator.

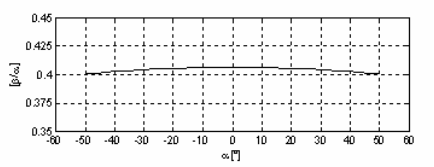

Figure 6: Gear ratio of kinematic mechanism versus angle of crank α.

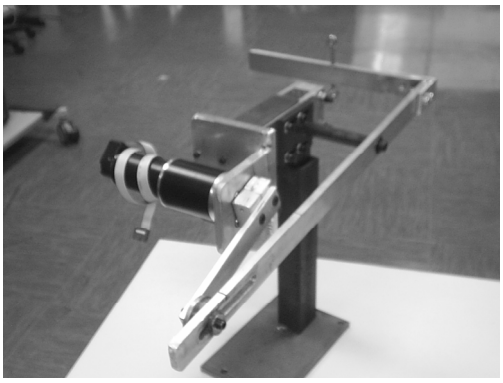

Figure 7: The developed device.

5 CONTROL DESIGN

A relevant part of the research consisted in the design of the control system for the electro-mechanical ankle actuator. A typical control architecture for electrical motors is composed of an internal feedback loop (called current loop) and an external feedback loop which in this case was defined to control the angular position of the motor (position loop), as shown in Figure 8. This configuration enables to increase the performances of the control system and to control at any time the electrical motor current in order to avoid working condition potentially dangerous for the electrical actuator.

The current feedback loop is implemented by the servoamplifier, which has a very high dynamic response. Control parameters for the current loop are optimised by the manufacturer, so it was decided to use it without any modifications. On the other hand, the regulator for the position loop was implemented using a programmable control board (DSP board). The inputs for the DSP board are the reference position signal and rotor position measured by an encoder, whereas the output of the position regulator is the reference current signal, which is fed into the current regulator.

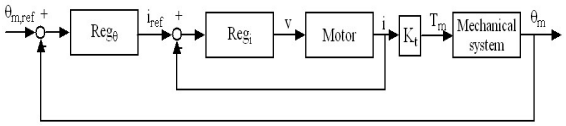

Figure 8: Block diagram of control system.

In order to define the reference signal for the position regulator, first of all a typical wave shape for ankle angular motion was derived taking into account the patient's anthropometry, by means of numerical simulations supported by measurements, as described in section 3. Figure 3 shows an example of reference motion law for ankle rotation.

Then, under the simplifying assumption of having a constant gear ratio between the output shaft of the gear and the ankle, the reference for ankle rotation was converted into a reference for the angular position of the motor.

In this first stage of study, a proportional-derivative (PD) regulator has been used for the design of the position loop. The gains of regulator were chosen to provide a good performance of control system and to assure a good dynamic

response. For the optimal design of the regulator, a simple linear model of the ankle actuator was defined. The model equations are:

$$\begin{aligned} v &= R \cdot i + L\frac{di}{dt} + e \\ e &= K_e \cdot \dot{\theta}_m \\ T_m &= K_t \cdot i \end{aligned} \tag{1}$$

$$J^* \cdot \ddot{\theta}_m = \eta_{tot} T_m - \frac{T_c(t)}{n} \tag{2}$$

where v and i are respectively the voltage and the current of electrical motor characterized by a resistance R and an inductance L, e is the electromotive force, K_e and K_t are respectively the speed and torque constants, T_m is the torque of motor, J^* is the equivalent moment of inertia of all parts of device, θ_m is the angular rotation of motor, η_{tot} is the coefficient of efficiency of the reducer, T_c the resistant torque and n the total gear ratio.

For the control design, the resistant torque T_c is considered as a known noise input signal and for this reason it's not considered during the design of regulator.

Finally, numerical tests were performed to verify the correct tuning of the gain parameter for the position regulator, using the more detailed non-linear model described in section 6.1.

6 SIMULATIONS AND TESTS FOR FINAL ASSESSMENT

6.1 Multi-physics Simulations

A multi-physics model of the ankle actuator was established, to verify the correct design of the system (including the regulator) and to assess its overall performances. The model is composed of:

- an electro-mechanical component, representing the electrical motor and the gear (see Fig. 9a);
- an electronic component, reproducing the control loops implemented in the motor drive (Fig. 9a);
- a multi-body biomechanical component, representing the lower limb and the mechanical linkages connecting the motor with the foot (Fig. 9b).

Contrarily to the simplified model used to perform the control design stage of the project, the multi-physics model used for verification and assessment is fully non-linear and accounts for the interaction effects between the different components of the system.

In particular, the linear equation (2), representing in a simplified way the mechanical component of the system, is replaced by a non-linear equation for the gear and by a fully non-linear model of the leg and of the mechanical linkages.

As far as the gear is concerned, a non-linear formulation is used, accounting for the different expression of power dissipation in the gear depending on the power flow being directed from the motor to the output shaft or vice-versa (Hannah, Hiller, 1995), so that having defined the mechanical power flowing in the gear from the motor to the output shaft W_g according to the following expression:

$$W_g = \left(T_m - J_m\ddot{\theta}_m\right)\dot{\theta}_m \tag{3}$$

the mechanical equation of the motor takes the following non-linear expression:

$$\begin{aligned} \eta_d T_m + \frac{T_c}{n} &= \left(\eta_d J_m + \frac{J_c}{n^2}\right)\ddot{\theta}_m \quad \text{for } W_g > 0 \\ T_m + \frac{\eta_r T_c}{n} &= \left(J_m + \frac{\eta_r J_c}{n^2}\right)\ddot{\theta}_m \quad \text{for } W_g < 0 \end{aligned} \tag{4}$$

where J_m is the moment of inertia of the rotor and gear input shaft, J_c is the moment of inertia of the gear output shaft, η_d and η_r are the efficiency coefficients of the gear (for other symbols, see Section 5).

The leg and the linkages in the ankle actuator are represented by a multi-body model with an excess of 30 states defined in ADAMS/LifeMOD environment. The model takes as input the rotation of the gear output shaft θ_c defined as:

$$\theta_c = n\theta_m \tag{5}$$

and by solving the direct dynamic problem for the linkages and leg returns the motion of the modelled bodies and the value of the resistant torque T_c, which is fed back into equation (4). The use of the non-linear multi-body model allows to represent in full detail the actual non-constant gear ratio of the linkage (see Figure 6), and to take into account the effect of actual loads (e.g. contact forces exchanged in the footprint) in the calculation of the resisting torque T_c, avoiding the simplifying assumptions that were introduced for control design purposes.

The model was implemented in Matlab/Simulink environment, using co-simulation with ADAMS to account for the coupling between the electro-

mechanical and electronic components of the model (implemented in Simulink) and the bio-mechanical model component (implemented in ADAMS). Figure 9a shows a high-level representation of the complete Simulink model, where co-simulation with the ADAMS subsystem is represented.

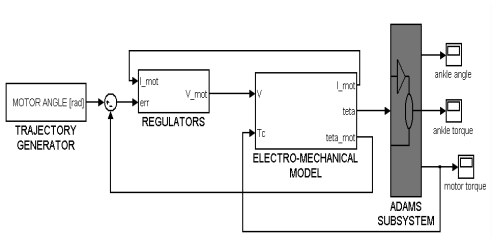

(a)

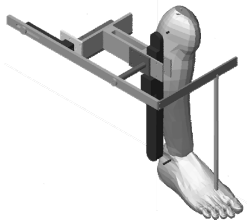

(b)

Figure 9: a) Co-simulation model; b) detail of ADAMS subsystem.

Figure 10 shows the results of a simulation reproducing the behaviour of the ankle actuator under the reference motion law shown in Figure 3 and considering 75% of body weight support. In the upper subfigure, the deviation of motor rotation with respect to the reference value is plotted: it is observed that the maximum deviation is in the range of 0.3%, indicating that the design of the regulators was performed correctly, so that the actuator is able to track position reference within accuracy levels that are fully satisfactory for the considered application.

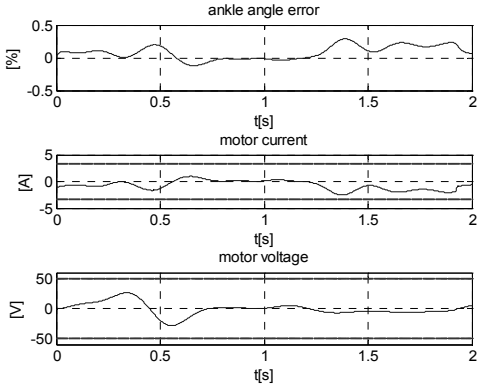

Figure 10: Co-simulation results.

In the central and lower subfigures of Figure 10, motor voltage and current are plotted, together with their respective limit values that cannot be exceeded to prevent damage and ensure durability of the motor. It is observed that for both voltage and current the maximum values achieved during the simulation are well below the limit values, demonstrating the correct dimensioning of the motor and actuator for the considered application.

In order to quantify the further ability of the device to withstand higher working loads (produced e.g. by unforeseen additional disturbances or by uncertainties in some design parameters), safety factors can be defined for voltage and current as the ratio between the limit value and the actual maximum absolute value of each quantity. For motor voltage, the safety factor is 1.70 whereas for motor current the safety factor is 1.32. These values are high enough to ensure the robustness of the system, but not so high to suggest the over-dimensioning of the motor.

6.2 Tests on a Demonstrator

Preliminary tests were performed on the physical demonstrator shown in Figure 7, to assess experimentally the performances of the device. At the present stage of the research, the demonstrator is not yet connected to the patient's leg, so passive masses are used to produce a resisting torque and inertial effect reproducing in first approximation the connection with the ankle.

In this section, three working conditions are considered:

a) An unloaded condition, which means that no external or inertial load is applied on the ankle actuator;
b) A loaded condition obtained by connecting a 5kg mass to the extremity of the sling, thus introducing a resisting force of about 50N and an additional inertial effect;
c) A loaded condition realised through a 10kg mass, producing a resisting force of about 100N and an inertial effect higher than in case b).

Tests were performed on the ankle actuator by using the reference ankle rotation represented in Figure 3 and measuring the actual motor position and the motor current.

Figure 11 shows the results obtained for working condition c) in the list above, corresponding to the most loaded condition. It is observed that the positioning error is always below 2%, which is a quite low value but still higher that the one obtained from the numerical simulation. This result could however be affected by some electrical noise disturbance in the measure of the motor angular

position, so that the actual positioning error could be in the same range of values as the one obtained by numerical simulation. More accurate tests are planned in order to clarify this point.

The motor current is quite low, with maximum value below 1A, to be compared with a limit value of 3.33A. This means that there is a large margin for further loading of the actuator.

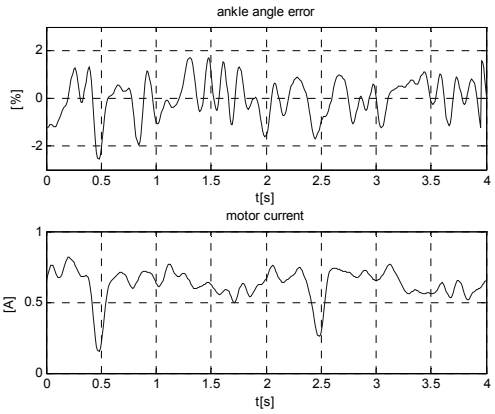

Figure 11: Experimental result in 100N load condition. Up: position error; down: motor current.

Table 4 compares the results of tests performed in working conditions a) to c), in terms of maximum angular position error of the motor and of maximum and r.m.s. value of the motor current required by the actuator. The maximum position error in the unloaded condition is much higher than in the two loading conditions. This is produced by the effect of plays that are present in the mechanical parts connecting the final link with the gear output shaft. The effect of plays is otherwise eliminated by the presence of the gravitational load applied by the masses in working conditions b) and c).

Table 4: Values of maximum ankle angle error, maximum motor current and RMS motor current in different loading condtions.

	$Error_{max}$	I_{max}	I_{RMS}
No load	5.12%	0.42A	0.1A
50N load	1.95%	0.71A	0.59A
100N load	2.55%	0.82A	0.64A

Considering a different working condition where the ankle actuator is connected with the patient's leg, the effect of plays can seriously affect the performances of the system, and therefore a new stage of the research was started to find an alternative design for the connection between the gear output shaft and the final link moving the patient's foot. A solution based on the use of toothbelt was developed and is presently under realisation. This new solution is expected to improve substantially the performances of the device in actual working conditions.

7 CONCLUSIONS

The paper has reported some results from an ongoing research having as objective the development of an electro-mechanical ankle actuator for use in the rehabilitation of lower limb motion in patients suffering neurological disease.

Preliminary results obtained by numerical simulation and tests show the ability of the developed system to actuate ankle motion within accuracy levels that are appropriate for rehabilitation purposes. Research is on going on introducing this device in physiotherapy. Preliminary test on healthy and diseased subjects are foreseen in a short time.

ACKNOWLEDGEMENTS

The work presented here was made possible through the financial support of CARIPLO foundation within the HINT@Lecco (Health Innovation Network Technology@Lecco) research project.

REFERENCES

Colombo G, Joerg M, Schreier R, Dietz V., 2000. Treadmill training of paraplegic patients using a robotic orthosis. *Journal of Rehabilitation Research and Development* 37(6):693-700.

M. Bocciolone, M. Lurati, M. Vanali, F. Molteni. Force measurement during gait therapy assisted by a robotic treadmill – The case of Lokomat, proposed as poster presentation for the *BIODEVICES 2008 Conference*, Funchal, Madeira, 28-31 January 2008.

G.S. Sawicki, K.E. Gordon e D.P. Ferris, 2005. Powered lower limb orthoses: applications in motor adaptation and rehabilitation. *9th International Conference on Rehabilitation Robotics*, June 28 - July 1, 2005, Chicago, IL, USA.

D. P. Ferris, J. M. Czerniecki, B Hannaford, 2005. An anckle-foot orthosis powered by artificial pneumatic muscles. *Journal of Applied Biomechanics*, 21, pp 189-197.

A.M. Sabatini, C. Martelloni, S. Scapellato, F. Cavallo, 2005. Assessment of walking feature from foot inertial sensing. *IEEE transactions on biomedical engineering* 52(3):486-489.

J. Hannah, M.J. Hillier, 1995. Applied Mechanics, Longman scientific &technical Editions.

NOVEL HAPTIC TOOL AND INPUT DEVICE FOR BILATERAL BIOMANIPULATION ADDRESSING ENDOSCOPIC SURGERY

K. Houston, O. Tonet, C. Eder, A. Menciassi, P. Dario
CRIM Laboratory, Scuola Superiore Sant'Anna, Pisa, Italy
keith.houston@sssup.it, oliver.tonet@sssup.it, ced@neurodan.dk, arianna@sssup.it, dario@sssup.it

A. Sieber
Profactor Research & Solutions GmbH, Austria
sieber@gmx.at

Keywords: Microhandling, sensorised, microgripper, teleoperation, haptic, force feedback.

Abstract: In this paper a teleoperation system is presented which consists of a sensorised polymer microgripper as a suitable end effector on an endoscopic microinstrument which is controlled by a novel tweezer-like haptic input device. This tweezer device gives the operator the ability to remotely feel these forces generated by grasping operations with the microgripper. This feedback is used to control the amount of force applied in manipulation of tissues during the procedure. The mechanical and electronic design of the microgripper, microinstrument and haptic tweezers is also presented and preliminary results detailed.

1 INTRODUCTION

Thanks to technological advances, an increasing number of precision operations are nowadays possible through key hole surgery interventions. However, during key hole surgery sensory feedback information is reduced, distorted or even absent, which is the case of visual, force and tactile information, respectively. These sensorimotor limitations also reduce dexterity in manipulation tasks. In this context, microengineering and microrobotics can help providing the surgeons with a new generation of smart instruments. Research efforts have been devoted to restoration of haptic (force and tactile) feedback (Kazi, A. et al, 2001). Forces exerted during surgery and the role of haptic perception have been investigated in many papers (Sheridan, T.B. et al, 1992, Kitagawa, M et al).. In traditional key hole surgery procedures, the attenuated haptic sensation still plays an important role (Bholat, O. S. et al, 1999), but it cannot be further restored or enhanced. In the case of mechatronic or robotic instruments, however, the interaction forces and torques between instrument and tissue can be measured and fed back to the surgeons hand by means of actuators and dedicated interfaces. Recent surgical instruments (Rosen, J. et al, 1999, Tavakoli, M. et al, 2005) and telerobotic systems used for research (Cavusoglu, M. C. et al, 2001, Mayer, H. et al, 2005) incorporating haptic interfaces have been developed (Menciassi, A. et al, 2001, Menciassi, A., 2003). The telesurgery concept has been enhanced and brought to a commercial stage, e.g. da Vinci Surgical System by Intuitive Surgical, Inc. (Guthart, G. S. et al, 2000), which however does not yet incorporate force feedback.

There are also several authors which have produced working prototype manipulation system with force feedback tools (Howe, R.D. et al, 2006, Pillarisetti, A. et al, 2006, Mitsuishi, M. et al, 2005) Howe, R.D. et al, 2006, Pillarisetti, A. et al, 2006, Mitsuishi, M. et al, 2005). This paper aims to present an entire teleoperation system which consists of an endoscopic tool with a microgripper end-effector and a novel haptic force sensing tweezers which can together give a remote force sensing ability during key hole surgery procedures, for example in laparoscopy or endoscopy . All of these new tools are connected to a user interface with micro-controller communication to dynamically display microscopic video, gripper force values and also modes to change the haptic behaviour of the tools in real-time.

2 METHODS

2.1 Microgripper

The sensorised microgripper used as end-effector for the endoscopic microinstrument is an SMA (shape memory alloy) wire actuated polymer type and has been detailed in previous work (Houston, K. et al, 2007). The SMA actuation principle is based on a simple SMA wire applying a tensile force through the centre of the symmetrical microgripper structure, thus causing the tips of the device to move inward (Figure 1). The advantages of this microgripper are that it is robust, has a large gripper tip span, is made primarily of polymer, and is low cost, as it can be mass-fabricated by SDM (shaped deposition manufacturing. The first polyurethane microgripper prototype measures 22 mm length in total, with a width of 6 mm. Figure 2 showing a FEMLAB 3.0 structural strain displacement simulation to verify the design.

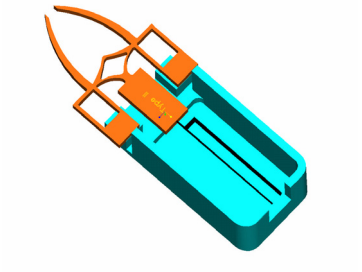

Figure1: SMA actuated microgripper.

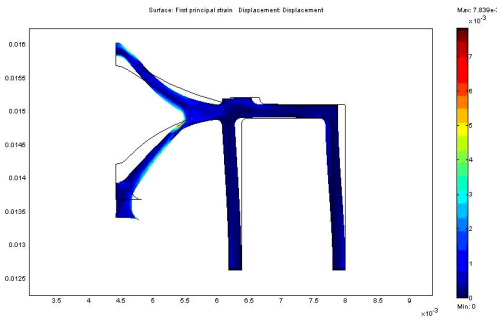

Figure 2: FEMLAB strain due to SMA wire force.

As an added part of this work, a further miniaturised SMA actuated microgripper shown in Figure 3 (right) was designed and fabricated using the same techniques, Figure 3 (left) shows the first sensorised prototype.

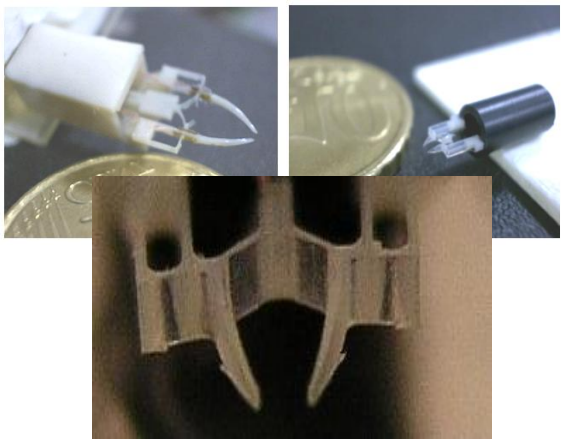

Figure 3: First gripper prototype (top left) and miniaturized version (top right, bottom).

To name a few advantages of the smaller microgripper, this device is less than half the total length of the first prototype (11 mm), half the width (3 mm), has a gripper tip maximum span of 500 µm and requires a lower operating power. Figure 8 shows a design of the device attached to the endoscopic tool. The microgripper itself is fabricated by the SDM process which has been implemented and detailed in many previous works with success (Eisinberg, A. et al, 2005). The four micro strain gauges are embedded in the microgripper at the points of maximum structural strain. In one version, all eight micro strain gauge wires and two SMA power supply wires are embedded in the polymer microgripper housing for robustness and a silicone membrane covers the opening of the actuator housing where the SMA wire connects with the moving microgripper structure. This allows the device to be used in fluid environments. Figure 4 shows another version where the moulded gripper structure is mounted on a glass substrate with a copper/polyamide flexible electrical connector. This allows all 8 strain gauge connections to be accessible inside the housing- in practical terms this means that there are no fragile wires coming from the microgripper, and makes the gripper assembly more modular and robust. There is then also the possibility of integrating electronics onto the substrate.

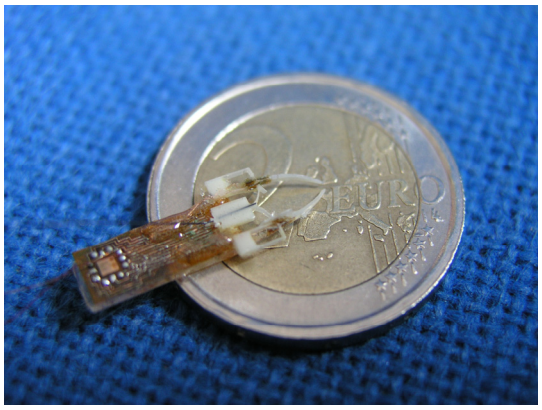

Figure 4: Modular design of the gripper structure on glass substrate with flexible circuit.

The microgripper requires a current of 70 mA for total tip closure. A step current input applied to the SMA actuator demonstrates the dynamic behaviour of the device (step response plotted for six current steps from 40 to 90 mA) in Figure 5. The calculated time constant is 8 seconds, while although quite high is normal for SMA mechanisms. In order to decrease the time constant and thus the speed of grasping, a preheating control strategy was used which maintained the SMA wire heated with a current of 40 mA; this was below the actuation current of the wire. In order to actuate the gripper, the current was then increased above 40 mA, and this makes the actuator more responsive. Using this strategy, the time constant was reduces to 2 s, a substantial improvement in the dynamic response of the microgripper. Figure 6 shows the improvement in tip displacement of the microgripper against time.

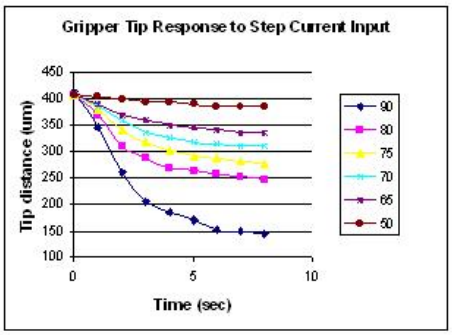

Figure 5: Response of SMA microgripper to step current input.

The signal of the strain gages in the microgripper is sampled with an Analog Devices AD 7730 analog to digital converter as shown in Figure 7. Offering a programmable input stage (±80 mV to ± 10 mV) and 24 bit resolution this device is suitable for bridge/transducer applications.

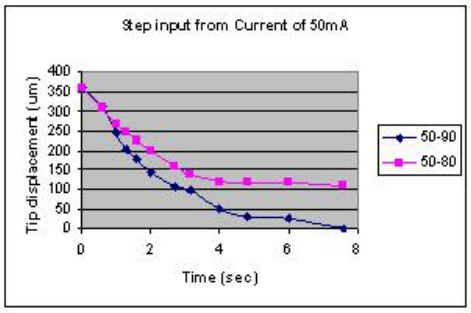

Figure 6: Improved response of SMA microgripper due to preheating.

Further signal processing is then done by a separate Atmel microcontroller (ATMEGA8) connected via USB to PC. The software for the microcontroller is programmed in C++, while the visualisation of the data is performed under National Instruments LabView.

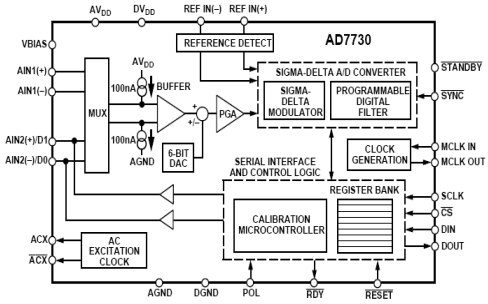

Figure 7: AD7730 strain gauge signal processing circuit.

2.2 Endoscopic Device

The microgripper is mounted on the tip of the endoscopic device (Figure 8), which can be bent in two degrees of freedom up to ±90˚. Bending of the tip is performed by pulling on steering wires. The principle of the mechanism is described in detail in (Harada, K. et al, 2005). For precise actuation of the 4 steering wires two high precision servo drives with a theoretical resolution of 13 bit are used. The tube is made of hard *Delrin* plastic, machined using traditional turning techniques, while the rolling spheres are of polyurethane, procured from off-the-shelf stock. The smaller micro parts for passage of wires and location of the spheres were machining using a precision CNC milling machine. The all-plastic assembly is finished with the controlling wires which can be any type of strong wire-for the prototype, a fishing line wire was used .

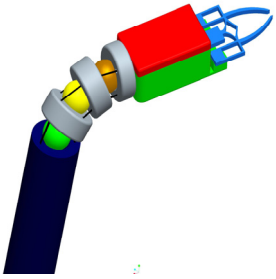

Figure 8: CAD drawing of the endoscopic instrument with the gripper as end-effector.

2.3 Interfacing the Heptic Input Device

In the lower arm of the tweezers like input device two strain gauges are integrated to allow a force measurement, as shown in Figure 9. The signal of these two strain gauges is processed in a half Wheatstone bridge configuration and then amplified by a factor of 100. To digitize the signal the first channel AD0 of the Atmel ATMEGA8 microcontroller is used. Analogue channel 1 is used to acquire the signal of the potentiometer integrated in the Servo (Graupner 381) giving real feedback of the position of the servo. One digital output is used to drive the Servo with pulses in the length of 1 to 2 ms with a resolution of 0,5 µs. Figure 12 shows the haptic tweezers being used in a micromanipulation task with force feedback. Figure 10 shows the actual haptic tweezers prototype in the users hand.

Figure 11 show the flow diagram for the haptic tweezers in active mode. The AD7730 ADC is continuously updating the microgripper tip force. As this is happening, the ATMEL ADC is updating the strain gauge voltage which relates to the actual haptic tweezer force that the user perceives. The microcontroller then compares the perceived and actual forces and updates the new haptic tweezer servo value to reflect the force changes, if any.

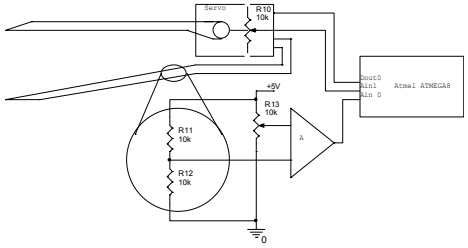

Figure 9: Haptic tweezers circuit.

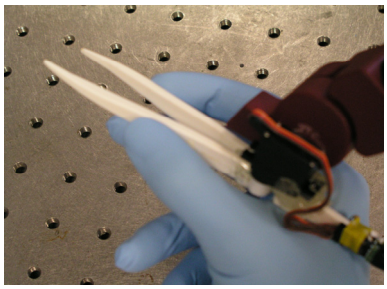

Figure 10: Hepatic tweezers in users hand.

Thus in real life, when one grasps a pair of tweezers, as the tips close, the force perceives on the finger tips increases linearly. This is exactly how the haptic tweezers behaves, in that when the user picks up the tweezers, there is initially no movement.

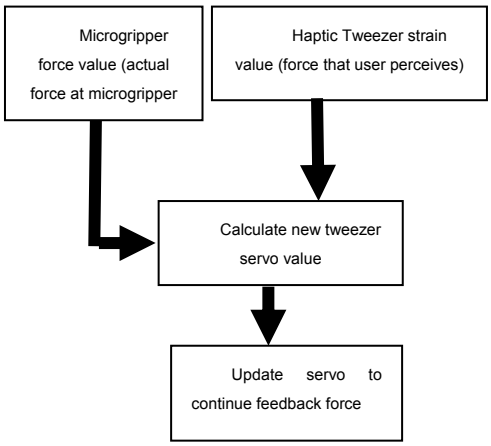

Figure 11: Force feedback flow diagram.

When the user then applies a force with the finger tips to close the tweezer tips, the strain gauge on the device detects this force and activates the servo motor-the position of the servo is always such as to follow the finger tips of the user, while all the time giving the sensation of a natural spring.

In the active mode (when there is an actual force on the tips of the microgripper tool), the scheme in Figure 11 is followed: the difference between the force on the microgripper tips and the force perceived by the user is used to update the haptic tweezer servo value-this is done continuously.

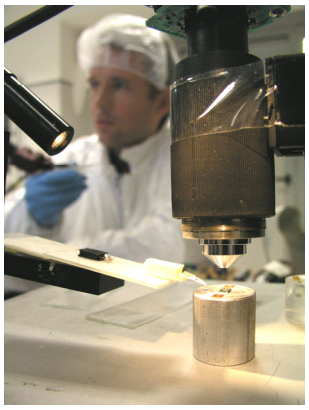

Figure 12: Haptic tweezers being used for micromanipulation task with force feedback under microscope.

2.4 Software

The current, and thus the actual position of the microgripper, is set according to the actual position of the control device. The feedback parameter is the force sensed by the microgripper. This parameter together with the position of the actuator and the signal of the strain gauges integrated in the lower arm of the device are used to drive the input devices actuator (PID control). Figure 13 shows the software flow scheme for the system.

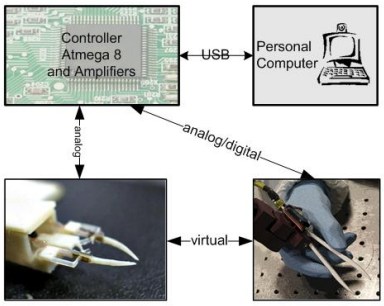

Figure 13: Software scheme.

be used for surgical or biomanipulation task in a haptic environment. At 3 mm in diameter, the tool is suitable for keyhole surgery and can achieve ±90 degrees rotations around both axes.

The prototype sensorised microgripper has a tip distance of 500-800 µm, and can be set to any distance in the assembly process. The maximum tip force is approximately 1 mN. The tip of the sensorised microgripper is a flat edge of 100 µm, however this geometry can be tailored in the design of the mould according to the task. The tool length is 22 mm and is 6 mm wide.

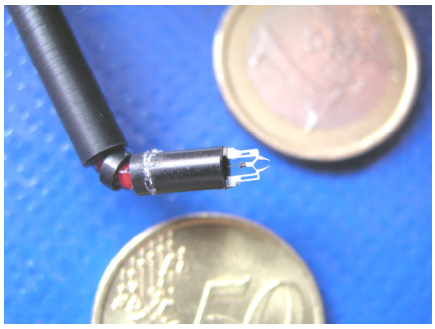

Figure 14: Prototype haptic biomanipulation tool.

The smaller microgripper has a smaller tip distance of 400 µm and again can be set during assembly. The diameter is 3 mm, the tip has a right angled point edge which is useful for precision grasping of small particle without minimisation of adhesive forces.

The prototype haptic tweezers has the dimensions of a normal off-the-shelf pair of plastic tweezers used in a medical lab (length of approx. 150 mm, width can be set by software, but as with a normal pair of tweezers, a maximum tip distance of approx. 40 mm is optimum). This prototype has a working tweezer angle of 90 degrees, however only about 20 degrees of movement is necessary to simulate a pair of tweezers-a larger angle is not very comfortable for the fingers when used for long periods. Because the servo is a 13 bit model of high resolution, the 20 degree angle sweep of opening and closing the tweezers has a resolution of over 40 increments per degree, giving a very smooth movement with no vibrations. The position of the tweezer tips is updated at a frequency of 50 Hz. The maximum torque of the input device is approx. 190 g/cm and the device is designed so that one arm of the tweezers will snap off easily before the maximum torque is reached.

3 CONCLUSIONS

Nowadays robot aided key hole surgery and teleoperated surgical techniques lack devices able to provide haptic feedback to the surgeon, particularly in the small scale. This paper presented a new teleoperation system with a novel endoscopic tool, force sensing microgripper and haptic tweezers which allows the surgeon to feel the gripping force at the tip of a microgripper instrument, even if as in the case of teleoperated surgery, they are miles away.

The authors are convinced that these first promising results are one step closer to a new era of surgical instruments giving "reality-like feelings" in endoscopic and teleoperated surgery.

ACKNOWLEDGEMENTS

The work described in this paper was supported by the ASSEMIC project, a Marie Curie Research & Training Network (MRTN-CT- 2003-504826) and PROFACTOR Research and Solutions GmbH – Austria. A special mention to Mr. C. Filippeschi for his continuous and invaluable help.

REFERENCES

Bholat, O. S. , Haluck, R. S., Murray, W. B., Gorman, P. J. and Krummel, T. M., 1999, *"Tactile feedback is present during minimally invasive surgery",* J Am Coll Surg,, 189(4):349–55.

Cavusoglu, M. C., Williams, W., Tendick, F. and Sastry, S.S., 2001 "*Robotics for telesurgery: second generation Berkeley/UCSF laparoscopic telesurgical workstation and looking towards the future applications*" In Proceedings of .the 39th Allerton Conference of Communication, Control and Computing.

Guthart, G. S. and Salisbury, J. K., 2000 *"The Intuitive$_{TM}$ telesurgery system: overview and application",* in Proceedings of ICRA 2000, pages 618–621, DaVinci.

Wagner,C.R., Perrin,D.P., Howe,R.D., "*Force Feedback in a Three-Dimensional Ultrasound-Guided Surgical Task*", Symposium on Haptic Interfaces for Virtual Environment and Teleoperator Systems 2006, March 25 - 26, Alexandria, Virginia, USA

Pillarisetti,A.,Pekarev,M., Brooks,A.D., Desai, J.P., *"Evaluating the Role of Force Feedback for Biomanipulation Tasks"* Symposium on Haptic Interfaces for Virtual Environment and Teleoperator Systems 2006 March 25 - 26, Alexandria, Virginia, USA

Pitakwatchara,P., Warisawa,S.,Mitsuishi, M., "*Force Feedback Augmentation Modes in the Laparoscopic Minimal Invasive Telesurgical System"* Aug. 2007, IEEE /ASME Transactions on Mechatronics Volume: 12, Issue: 4, pages: 447-454

Kazi, A., 2001, "*Operator performance in surgical telemanipulation. Presence*", 10:495– 510.

Kitagawa, M., Okamura, A.M., Bethea, B.T., Gott, V.L., and Baumgartner, A.A., "*Analysis of suture manipulation forces for teleoperation with force feedback"*, /Lect. Not. Comp. Sci./, vol. 2488, pp. 155–162.

Mayer, H., N´agy, I., Knoll, A., Schirmbeck E. U., and Bauernschmitt, R., 2005 "*An experimental system for robotic heart surgery"* in IEEE 18th International Symposium on Computer-Based Medical Systems (CBMS), Dublin, Ireland.

Menciassi, A., Eisinberg, A., Carrozza, M.C. and Dario. P., 2003, "*Force sensing microinstrument for measuring tissue properties and pulse in microsurgery*", IEEE/ASME Transactions on Mechatronics, 8(1):10–17.

Menciassi, A., Eisinberg, A., Scalari, G., Anticoli, C., Carrozza,M.C. and Dario, P., 2001 *,"Force feedback-based microinstrument for measuring tissue properties and pulse in microsurgery",* in Proc. IEEE International Conference on Robotics and Automation (ICRA).

Rosen, J., Hannaford, B., MacFarlane, M., and Sinanan, M., 1999 *"Force controlled and teleoperated endoscopic grasper for minimally invasive surgery – experimental performance evaluation",* IEEE Transactions on Biomedical Engineering, 46(10):1212–1221.

Sheridan, T.B., 1992, *"Telerobotics, automation and human supervisory control*", MIT Press, Cambridge, MA, USA.

Tavakoli, M., Patel, R.V. and Moallem, M. , 2005 , "*Haptic interaction in robot-assisted endoscopic surgery: a sensorized end-effector*", International Journal of Medical Robotics and Computer Assisted Surgery, 1(2):53–63.

Houston, K., Eder, C., Sieber, A., Menciassi, A. Carrozza, M. C., Dario, P., 2007 "Polymer sensorised microgrippers using SMA actuation", ICRA 2007.

Eisinberg, A., Izzo, I., Menciassi, A. Houston, K. , Valdastri, P., Dario, P., Gustafsson., R., Simu, U., Johansson S., 2005 , ***"****Design and shape deposition manufacturing (SDM) fabrication of a PZT-actuated tool for micromanipulation",* Computational Intelligence in Robotics and Automation, CIRA 2005.

Harada, K., Tsubouchi, K., Fujie, M. G., Chiba, T., 2005, "*Micro Manipulators for Intrauterine Fetal Surgery in an Open MRI",* Proceedings of the 2005 IEEE International Conference on Robotics and Automation Barcelona, Spain.

MEMS ANTENNA FOR WIRELESS BIOMEDICAL MICROSYSTEMS

Extremely Small Antenna for RF Receivers in Implantable Devices

P. M. Mendes
DEI, University of Minho, Campus de Azurém, 4800-058 Guimarães, Portugal
paulo.mendes@dei.uminho.pt

L. A. Rocha
DECE, FEUP, University of Porto, Rua Dr. Roberto Frias 4200-465 Porto, Portugal
larocha@fe.up.pt

Keywords: MEMS, Wireless Communications, Antenna, Bio-Telemetry, Implantable.

Abstract: This paper presents an extremely small antenna, together with its model, for wireless biomedical devices. Most of the implantable devices require very small dimensions. On way to achieve it is to use microtechnologies to obtain the required size reduction. One of the most challenging devices to integrate is the antenna, required if we want to communicate with the device trough a wireless link. The proposed antenna uses a MEMS structure to convert the incoming electromagnetic field into a voltage. This antenna allows the reception of signals using a carrier in the kHz range and uses only a chip area of 2x2 mm^2.

1 INTRODUCTION

Invasive and implantable biomedical devices used for diagnostic and therapy, ranging from neural prosthesis to video-capsule endoscopy (VCE) systems, are emerging innovative technologies and they are expected to originate significant business activity in the near future. The success of such systems is in part due to the advent of microtechnologies, which made possible the miniaturization of several sensors and actuators, as well their integration with readout and communication electronics.

Several people from all ages suffer from incontinence or other urinary pathologies. The bladder and the intestines perform their function in an autonomous way, independently from the individual will. However, any disorder in the healthy behavior leads to the problem of urinary incontinence, bladder infections, low bladder capability and fecal incontinency.

The healthy working of the urinary tract is essential for health and well being in general, and even more critical for patients with lesions in the spinal cord. In this situation, catheters are commonly used to control the daily volume of urine inside the bladder. However, the complications related to the use of catheters, together with the fact that, most of the times, the spinal segments which controls the bladder are intact, are driving the development of several devices to improve the control the inferior urinary system (Gaunt and Prochazka, 2005).

The new biomedical devices offer the possibility of improved quality of life, as well cost savings associated with health care services. However, one open challenge is to communicate to and from a biomedical device placed inside the human body with devices outside the human body. The lack of antennas, small enough to be integrated with the sensing microsystem, is a difficult task to overcome because such communications must be made at relatively low frequencies, due to live tissue signal attenuation (Kitchen, 1993). The straightforward solution is to increase the devices size to dimensions where it becomes possible to integrate an antenna. Up to now solutions, use conventional antennas together with miniaturization techniques to achieve the smallest antennas possible. However, the size of such devices is usually limited by the antenna and, is some cases, also by the batteries size.

In this paper, it is first discussed the need for small wireless biomedical devices, paying special attention to patients suffering from urinary

pathologies. Afterwards, MEMS structures, previously used for non-conventional front-ends, will be introduced and investigated, having in mind the new application. The MEMS structure will be modeled when operating as an antenna.

2 IMPLANTABLE DEVICE

In patients with spinal cord injury at a level that leaves the sacral segments intact, detrusor hyperreflexia and detrusor sphincter dyssynergia (DSD) develops after an initial phase of spinal shock. This type of bladder is responsible for important morbidity. The hyperreflexia impairs the reservoir function of the bladder and the DSD causes a high resistance against micturition. This results in reflex incontinence, recurrent urinary tract infection, and autonomic dysreflexia in high lesions and threatens these patients with renal failure.

All of these severe disturbances may be well managed by sacral deafferentation (SDAF) and implantation of an anterior root stimulator (SARS).

2.1 Electrical Stimulation

Fig. 1 shows the commonly adopted system architecture to control the inferior urinary system.

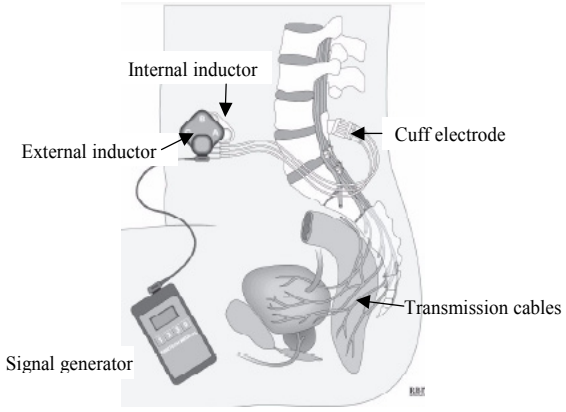

Figure 1: Schematic view of the overall system used for bladder control.

The system has a signal generator that generates the appropriate stimulus to activate, e.g., the bladder. That stimulus is transmitted to the external coil, which induces the signal in the internal coil. Reaching the biologic environment, a receiver module delivers the stimulus trough the transmission cables that carry the signal to the cuff electrode.

Since the internal coil is placed in the frontal region and the electrodes are in the back, the transmission cables must go through the body and are one main cause of system failure. Moreover, the existence of these cables requires a small opening in the duramater, not good for the spinal cord integrity. One main benefit of the microsystem approach is the possibility to avoid cables trespassing the duramater.

2.2 Anatomy of spinal cord

Fig. 2 shows the anatomy of the spinal cord. This is the place where the microsystem must be designed to operate.

Figure 2: Spinal cord cut, showing the region where the microdevice must be placed (1– intervertebral disk, 2- vertebral body, 3- duramater, 4– epidural space, 5- spinal medulla, 6- subarachnoid space).

From the figure we see that the microdevice must fit in a very small region, inside the duramater. It can be placed in two places, or in region 4 or in region 6. The best place is 6, the subarachnoid space, since the duramater can be totally closed after surgical intervention. The available space in region 6 varies between 3 mm and 9 mm [4]. This is room enough to accommodate a small microdevice.

The conventional surgical procedure requires the duramater opening to place the electrodes in contact with the sacral roots (Fig. 3).

The electrodes are connected to the leads coming from the stimulator, leaving a small opening in the duramater. As we can see from Fig. 3, there is plenty of room to place the microsystem in the implant region.

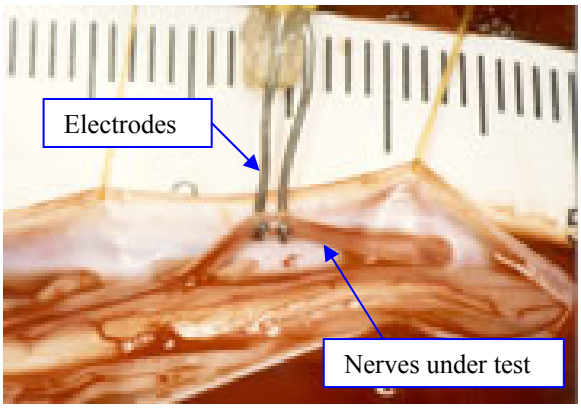

Figure 3: Placement of electrodes (testing the nerves to be used).

3 MICROSYSTEM

The need to reduce the failure associated with long wires that are used, to reduce the risk of infection or shifts in the wires is driving researchers to find a solution using microthecnologies. Also, and very important, is the internment period associated with the surgical intervention. Due to the highly invasive intervention that is required using the traditional technique, the patients, even when there are no complications, are required to stay a few days in the hospital. The availability of a device to allow a less invasive method would be more comfortable for the patient, reducing also the hospital costs associated to the surgery.

To make it possible to use, the device must be small enough to fit inside the spinal cord, it must be able to deliver the required stimulus (power and timing) and it must be possible to communicate with the device using a radio-frequency signal. This requires the use of a microsystem completely integrated, from sensors to communications, thus requiring the use of integrated antennas. Moreover, the antenna integration requires the availability of an electrically small antenna fabricated on materials compatible with the fabrication of integrated circuits. This integration requires the use MEMS techniques, like micromachining and wafer level packaging.

The microsystem must be designed taking into account the place where it will be required to operate because we cannot change the human body electrical system. As we saw, the human body anatomy will place constrains on available room for the microdevice, on power required for system powering and/or telemetry, and on required power for stimulation.

The final device to implant must not fail during its lifetime, must be stable and must be biocompatible (citotoxity, sensibilization, genotoxity, chronic toxity, carciginosity, and intracutaneous irritation).

3.1 CMOS Microsystem

The most suitable technology to implement the microsystem is the CMOS technology. It is the cheapest technology, with low power consumption, and adequate for this device since there are no high power delivery requirements.

In face of constrains, we have three solutions to design the microsystem. One is to design a chip, which acts only as a stimulus converter. The second option is to implement a full microsystem, with the ability to be remotely powered and controlled (Piella, 2001). The third is to use a microsystem with local power and a wireless receiver (Carmo *et al*., 2006). The first solution is the simplest, however the second and third are more flexible and, despite its higher complexity, fit in the available room for implant. The main drawback of third solution is the need of a local source of energy, battery or energy harvesting.

3.2 Wireless link

Antenna integration is a hard task to accomplish since it requires joining the knowledge from antennas, microwaves, circuit design, and materials. Moreover, the on-chip antenna integration requires an electrically small antenna, due to wafer cost and devices size constrains, and operating on a substrate that was not initially intended for that purpose (Mendes and Correia, 2007).

Despite it is used to transmit data or to power the device, it is necessary to have a wireless link operating at one frequency. As is well known, the human body shows higher attenuation to higher frequencies. This means that, the lower the frequency, the higher the power we receive in the implant. Moreover, the attenuation is highly dependent on water content in tissues. The water content depends on the type of tissue and part of the body.

Micro-Electro-Mechanical Systems (MEMS) are becoming an available option for RF communication systems since they can offer, simultaneously, devices with improved performance and they use IC-compatible materials, allowing their integration in a silicon chip, side by side with semiconductor

circuits. Up to now, MEMS have been used for antenna applications to obtain non-conventional front-ends with improved, or new characteristics. However, some preliminary tests have shown that some MEMS structures could have the ability to operate as an antenna itself and this solution would have the potential to be smaller than the conventional antennas.

The basic principle of micromachined cantilevers offers an interesting possibility to measure a variety of physical parameters (Lange *et al.*, 2002). When used as a sensor, a MEMS structure requires the use of a sensing mechanism and the most widely used is the capacitive method. The moving structure, and a fixed plate, forms a parallel plate capacitor, where the structure movement is translated into a capacity change.

4 MEMS ANTENNA

4.1 Cantilever Antenna

The U-shaped cantilever, proposed to detect a time-varying magnetic field, is presented in Fig. 4.

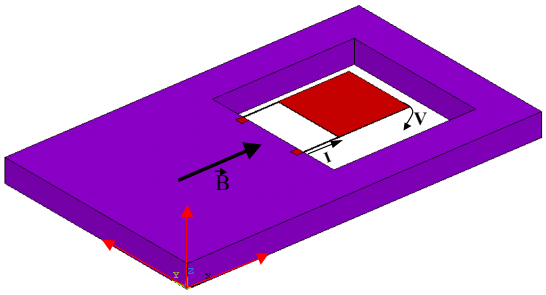

Figure 4: Cantilever used to detect a time-varying magnetic field.

To measure magnetic fields with cantilever structures, the Lorentz-force is used on a current carrying lead (Keplinger, 2004). A cantilever of this type measures only the magnetic flux density in the direction parallel to the arms of the cantilever, i. e., x-axis of Fig. 4. The Lorentz-force acting on a lead is used to bend a micromachined cantilever. Deflections, which are small compared to the length of the cantilever, are a directly proportional measure of the applied force. To reach the highest possible sensitivity it is advisable to use a resonant mechanism, where the cantilever is excited by an AC current with a frequency equal to an eigen-frequency of the elastic structure. Due to the high quality factors of Si structures, which are at least several hundred, this is an efficient way to enhance the sensitivity.

Electromagnetic field can be sensed using an optical, capacitive, or piezoelectric sensing solution. The most attractive options are capacitive and piezoelectric. These solutions can be easily integrated with the MEMS structure and have the potential for low power consumption (except the optical solution). Since the desirable displacement depends on structure dimensions and material properties, electrostatic actuation can be used as the actuation mechanism for MEMS micro-antennas. However, if large displacements are required or if the MEMS structure area becomes too small for capacitive detection, the use of a piezoelectric material can be the solution since it can act both as sensor and actuator. Moreover, the operation is only voltage based, leading to low power driving operation. Furthermore, it produces a voltage in response to a deflection leading to simple readout electronics.

4.2 Antenna Packaging

Fig. 5 shows a solution to integrate the proposed antenna structure. It consists of three stacked wafers, where the bottom wafer is used to place the reading and controlling electronics, the middle wafer is used to implement the U-shaped cantilever, and the bottom wafer encapsulates the device, enabling a very small microsystem with integrated antenna.

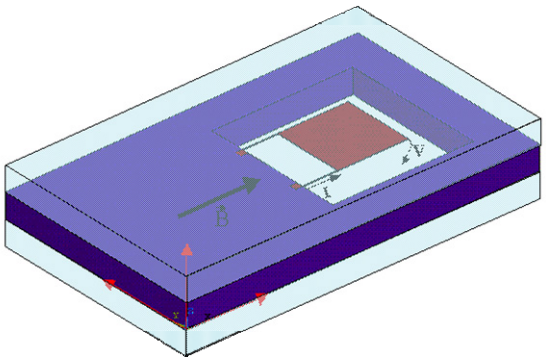

Figure 5: Use of WLCSP to integrate the proposed MEMS antenna.

4.3 Antenna Modelling

The proposed MEMS structures were engineered to have the desired electrical and geometrical properties, as well the requirements to be used in a post-process module compatible with integrated circuit (IC) fabrication.

Fig. 6 shows the 3D FEM (finite element modelling) model being used to analyse the receiving properties for a cantilever operating as an antenna. FEM modelling is a very powerful technique to predict the interaction between different domains (electrical, mechanical, and electromagnetic).

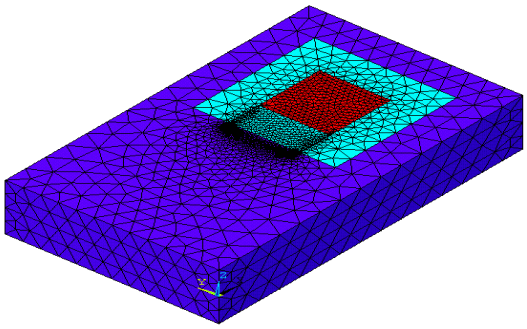

Figure 6: Model of structure used to sense the electromagnetic field.

However, it is also very time consuming and, in this case, very complex to set up a simulation and get data we can rely on it. In this way, a simple model was derived to understand the requirements and potentials of a structure like this one, if operated as an antenna.

4.4 Modulation Modelling

Considering the structure proposed in Fig. 4, we can represent it using the simplified model of Fig. 7. The electrical behaviour is modelled by the beam of length L and the current I, whereas the mechanical behaviour can be described using the spring k.

Considering that the magnetic field, B, is applied perpendicularly to the current I, trough the length L, the resulting Lorentz force, F_L, will be given by:

$$F_L = (B \times I)L \tag{1}$$

The MEMS structure will move when the Lorentz force becomes higher then the elastic force (Rocha *et al.*, 2004).

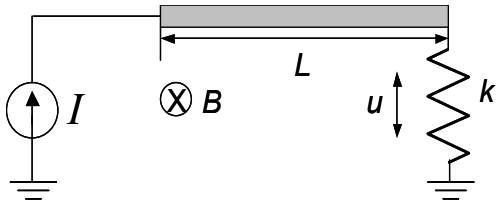

Figure 7: Simplified model of a cantilever operating as an antenna.

Due to the applied force F_L, the structure will move, and the following equation can be written:

$$F_L = (B \times I)L = ku = F_e \tag{2}$$

where F_e stands for elastic force, u for displacement and k is the spring constant of the structure. From the previous equation, we can find the displacement:

$$u = \frac{(B \times I)L}{k} \tag{3}$$

Independent of the detection method, optical or capacitive, the displacement will give origin to a received voltage, V_R, which will be proportional to the applied magnetic field, B.

$$V_R \propto u \propto B \tag{4}$$

If the magnetic field was originated by a modulated signal:

$$B(t) = A(t)\cos(2\pi f(t) + \phi(t)) \tag{5}$$

the received voltage will be:

$$V_R(t) = G\frac{LI}{k}A(t)\cos(2\pi f(t) + \phi(t)) \tag{6}$$

where G represent the system gain.

4.5 Antenna Analysis

From equation 6 it is possible to conclude that the proposed device will actuate as a signal receiver if the spectral properties of the modulated signal are chosen to fall inside the device operating frequency limit.

The first parameter requiring analysis is the force such a structure can produce when in presence of a magnetic field. From equation 2, if we consider I = 100 mA, L = 1,1 mm and B = 10 mT, then the resulting force will be 1.1 μN. This is enough force to produce movement in this kind of structure.

A key advantage of this solution is that it can deliver gain trough the increase of the current I. If the resistivity of the beam material is kept low, then we can have a low power device, since the voltage drop will be small.

The other requirement is that the modulation type must be selected carefully. Even if the modulating signal bandwidth is inside the MEMS device bandwidth, if we chose, e.g., FSK, the

resulting bandwidth may be outside the structure bandwidth due to the instantaneous required frequency shifts. In this way, a continuous modulating method must be used instead.

To check the ability to operate as a radiating element, some preliminary tests were also conducted, where it was used a scaled model of the proposed structure. A commercially available magnetic sensor was connected to a signal acquisition board that was connected to a personal computer. A current was injected into a scaled structure of Fig. 4, and the signal was recorded with the magnetic sensor. When the transmitting structure was oscillating at 100 KHz, it was possible to easily detect that signal with the magnetic sensor.

5 CONCLUSIONS

This paper described the design, and modelling of chip-size MEMS antennas for short-range wireless microsystems. These antennas allow the fabrication of an implantable microsystem with integrated wireless communications. The antenna integration is based on wafer-level packaging techniques, which enables the integration of new materials with the standard silicon processing steps, as well the fabrication of complex three-dimensional structures, in an economically acceptable way.

MEMS were explored as a new solution to obtain structures that can sense electromagnetic fields. Thus, instead of having the need to design very advanced antenna structures to achieve antenna size reduction, the standard MEMS devices, e.g. cantilevers, will be used to save system space and improve system integration. A novel electrically very small antenna using MEMS structures, and a model to describe the operation of that structure; is presented.

The present solution envisions power saving, smaller volume, lower cost, and increased system lifetime, which are very important features in biomedical microsystems for diagnosis and therapy.

ACKNOWLEDGEMENTS

We would like to acknowledge Medical Doctor Paulo Vale for his support in this research work.

REFERENCES

Carmo, J. P., Mendes, P..M., Couto, C., Correia, J.H., 2006, “5.7 GHz on-chip antenna/RF CMOS transceiver for wireless sensors network,” Journal Sensors and Actuators A, Elsevier Science, Vol. 132, pp. 47-51,

Gaunt, R. A, and Prochazka, A., 2005, “Control of urinary bladder function with devices: successes and failures,” Progress in Brain Research, Elsevier, Vol. 152, pp. 163-194.

Keplinger, F., Kvasnica, S., Jachimowicz, A., Kohl, F., Steurer, J., and Hauser, H., 2004, “Lorentz force based magnetic field sensor with optical readout,” *Sens. Actuators A,* 110, (1–3):112–118.

Kitchen, R, 1993, *RF Radiation Safety Handbook*, Butterworth-Heinemann.

Lange, D., Brand, O., and Baltes, H., 2002, *CMOS Cantilever Sensor Systems: Atomic Force Microscopy and Gas Sensing Applications*., Springer.

Mendes, P. .M., and Coreeia, J. H., 2007, "MEMS Micro-Antennas for Wireless Biomedical Systems," in "Wireless Communications Research Trends", ISBN: 1-60021-674-9, 2007, edited by Tong S. Lee, Nova Publishers.

Piella, J. P., 2001, Energy management, wireless and system solutions solutions for highly intregated implantable devices. PhD Thesis, Universitat Autónoma de Barcelona, Barcelona.

Rocha, L. A., Cretu, E., Wolffenbuttel, R. F. 2004, “Analysis and Analytical Modeling of Static Pull-In With Application to MEMS-Based Voltage Reference and Process Monitoring,” Journal Of Microelectromechanical Systems, Vol. 13, No. 2, pp. 342-354.

MACHINE BIOLOGICAL CLOCK
The Time Dimension in a Organic-Based Operating System

Mauro Marcelo Mattos
Computing Systems Department, FURB- University of Blumenau, R.Braz Wanka 238, Brazil
Blumenau, Santa Catarina, Brazil mattos@furb.br

Keywords: Organic Computing, Machine Biological Clock, Knowledge-based Operating System.

Abstract: A Knowledge-Based Operating System is an embodied, situated, adaptive and autonomic system based on knowledge abstraction which has identity and intelligent behavior when executed. We have identified three dimensions over which such a new operating system paradigm has to be based: (i) physical dimension, (ii) logical dimension, and (iii) temporal dimension. The physical dimension describes the physical components and their structural relationship. The logical dimension describes the functional characteristics of each physical component and the time dimension is provided in order to enable the entire system to perceive the time flow – as a biological clock in human beings. This work presents the Machine Biological Clock concept.

1 INTRODUCTION

"*Twenty years ago, on November 12, 1986, Fred Turek, Dave Hudson, Joe Takahashi, and Gene Block founded the Society for Research on Biological Rhythms. Who would have imagined that today we are analyzing the structural biology of bacterial clock proteins? Or that we are performing real-time measurements of rhythmic gene expression within individual cells in a dish? Or that we are delineating the neurobiology of a neurotransmitter that underlies narcolepsy? And that's just for starters. Every other year, we have been gathering at this meeting to announce, debate, and celebrate these advances, in presentations that cut across*." (Schwartz, 2006).

In his effort to describe time as a subjective experience in terms of his philosophy of Phenomenology, Husserl grapples with the succession of perceived moments of conscious existence by using the example of the melody to illustrate his point. In a melody, each successive note exists in time for a moment, and each moment represents a new 'now' point. Each part of the melody is related to its antecedent and to the notes yet to come. Our apprehension of the melody cannot be obtained outside the context of successive notes. "Therefore, the perceiving of a melody is in fact a temporally extended, gradually and continuously unfolding act, which is constantly an act of perceiving." (Husserl, 1893-1917). This temporality is a subjective construct. (Craft, 2000).

According to Stulp and Beetz (2002), agent-based systems are solving more and more complex tasks in increasingly challenging domains, the systems themselves are becoming more complex too, often compromising their adaptivity and robustness.

In robotics projects, system designers cannot foresee each situation, or all the possible outcomes of an action. Therefore, hand-coding the controllers is considered intractable and failure-prone task.

This situation is a reality in general purpose computational systems. According to Hayes-Roth (2006), "the best systems of our times have been hand-crafted by great engineers. These system makers have analyzed the task environments, knowledge requirements, and reasoning skills necessary for successful applications. This approach can work for any well-defined and sufficiently narrow task. But, if the system fails, the engineers would diagnose and debug the errors. They would determine what knowledge to add or modify, how to program it, and how to modify and rebalance the pre-existing programs to accommodate the new performance without harming the parts that already worked well. Automation in adaptation, learning, and knowledge acquisition was very limited – a tiny fraction of the overall knowledge required, which the engineers mostly prepared manually. We have

not yet figured out how to make the systems responsible for their own debugging and improvement".

A promising approach to solve this problem is to provide agents with reflective capabilities. Agents that can reflect on the effects and expected performance of their actions are more aware and knowledgeable of their capabilities and shortcomings. This is called "action awareness" (Stulp and Beetz, 2002).

Another approach is based on an "efficient thought" concept (Hayes-Roth, 2006). This concept lists eight steps that the most complex organizations, in general, perform in parallel. This approach states that the intelligent being (a) observes what's happening in the environment, (b) assesses the situation for significant threats and opportunities, (c) determines what changes would be desirable, (d) generates possible plans to operate those changes, (e) projects the likely outcomes of those plans, (f) selects the best plan, and (f) communicates that plan to key parties before implementing it. Throughout the process, the intelligent being (g) validates and improves its model.

The new research area that intends to solve some of the problems pointed out is called Organic Computing (OC). The main goal of OC is the technical usage of principles observed in natural systems. (Muller-Schloer, 2004).

In this paper, we introduce a computational model for what we call "machine biological clock" in order to make possible to build a really reflexive environment where the system can perceive the time flow. This concept, that has been ignored in previous works is, in our point of view, the most important concept that has to be considered if we plan to build intelligent systems. Or, as said in Brachman (2002) 0, if "we want to transform them from systems that simply react to inputs into systems that are truly, in a word, cognitive. Most formal and intuitive definitions tell us that cognition is about knowing. Our image of a cognitive system, then, is one that can indeed know things and act on that knowledge. It can take explicit knowledge gleaned in a host of ways and go beyond it to important implicit knowledge, ranging from pure and simple logical deduction to what we might call 'plausible reasoning' ".

The paper is organized as follows: a problem's contextualization in operating system area is presented in section 2; a knowledge-based operating system concept in section 3; an overview of the biological clock concept in section 4; section 5 describes the time dimension in a KBOS system; section 6 presents some related works and in the conclusion section the final comments are presented.

2 WHY A NEW CONCEPT?

In our point of view, three concepts contribute to reduce our possibilities in building really intelligent systems: (i) the multitasking concept, (ii) the operator concept and, (iii) the program concept.

Traditional operating systems support the notion of a hardware abstraction level in which each application is supposed to possess its own processor (and other resources). This situation and the fact that, in general, all commercial operating systems are based on a multitasking concept (introduced in 1964), contribute to the permanence of problems identified 30 years ago (Linde, 1975). The problems range from security to usability, including lack of adequate behavior in fluctuating execution conditions and user's privacy (Brachman, 2002).

Today we are also faced by new demands like pervasive computing and organic computing, where self-adaptation and self-reconfiguring are the main goals.

Besides that, there are two other concepts that contribute to make things worse: (i) the operator concept, and (ii) the program concept.

The operator function was necessary during the first years of computing since computers were big and difficult to use. Operators, at that time, were responsible for turning the machine on/off, starting programs, collecting reports, restarting programs and so on. This scenario has changed as the computers become smaller, cheaper and faster as they are today. However, what was a real need in the past is employed today as if there was no other way to interact with computers. In fact, we are nowadays operators – all of us using some kind of computer (desktops, palmtops, and mobile phones). We are trained today to learn how to pull virtual buttons the same way the former operators were trained to pull real buttons in real panels on those old mainframes.

This aspect has consequences and the program concept is the main one. A program could be thought as the programmer's hands virtually extended inside our machines. The programmer has the knowledge about some specific domain and knows how to establish the correct sequence of steps in order to solve the problem. In this scenario, we are users of such routines – in other words: operators. Programs, within this context, are the way through which programmers can implement their procedural knowledge about the problem's domain.

This model does not enable the actual operating system to acquire knowledge about what is happening inside the machine. We believe that this is one of those several sources of problems that we experience today. So, we have proposed a new model.

3 A KNOWLEDGE-BASED OS

The novel concept introduced in Mattos (2003) says that a knowledge-based operating system is: "an embodied, situated, adaptive and autonomic system based on knowledge abstraction which has identity and intelligent behavior when executed".

The whole system is built inside a shell which gives the endogenous characteristic. A hyper dimensional world model (Mattos, 2005) enables the entire system to perceive evolving and/or fluctuating execution conditions (fig. 1).

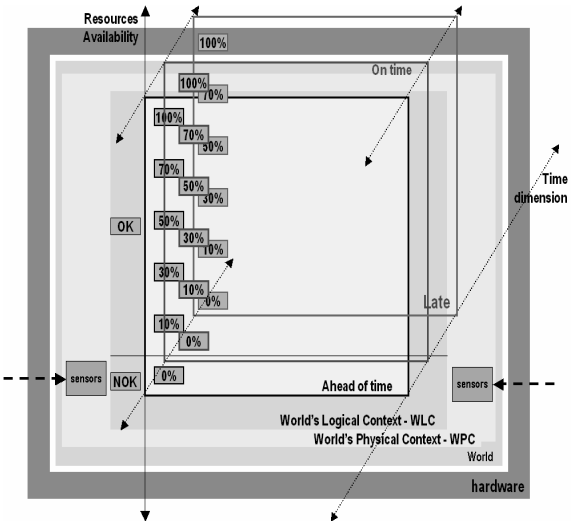

Figure 1: Hyper-dimensional World Model.

3.1 The Dimensions

We have identified 3 dimensions over which such a new operating system paradigm has to be based: (i) Physical dimension, (ii) Logical dimension, and (iii) Temporal dimension.

The physical dimension describes the physical components and their structural relationship.

The logical dimension describes the functional characteristics of each physical component. It is called: physical context of a device. A state machine describes the dynamic aspects of the component's behavior. Merging the entire physical context of all physical devices described at the physical dimension, we obtain the world's physical context (WPC). The logical dimension is provided by a DEVS run-time environment (Mattos, 2005b).

The Time Dimension is provided in order to enable the entire system to perceive the time flow – as a biological clock in human beings.

3.2 Knowledge based OS and Knowledge Acquisition

Some works (Samsonnet et al, 1982; Vilensky, Arens and Chin, 1984; Chikayama, 1988; Genera 2003; Larner, 1990; Yokote, 1992; Li et al, 1995; Patki, Raghunathan and Khurshid, 1997) have been described as aiming to develop a complete knowledge-based operating system. Other approaches consists of applying IA techniques through making kernel implants (Seltzer, Small and Smith, 1995) in order to get better user interfaces in traditional operating systems (Pasquale 1988; Cockcroft,1995; Hernández, Vivancos and Botti 1998; Zomaya, Clements and Olariu, 1998; Kandel, Zhang and Henne, 1998; Siraj, Bridges e Vaughn, 2001). However, all of them have failed into achieving their objectives because the main concept over which they should base their work has not been clearly specified – "what" is the knowledge. This aspect has transformed those supposed new operating systems projects into traditional operating systems architectures with many specialized libraries over some multitasking platform.

Knowledge in this context is conceived as being a set of logical-algebraic operational structures that makes possible to organize the system functioning according to interconnection laws and behavior laws. It is well known that a significant obstacle to the construction of knowledge-based systems is the process of knowledge acquisition.

The key to this process is how we may effectively acquire the knowledge that will be implemented in the knowledge base. In an operating system environment, this is not an easy task. It is usually done by hooking the OS API calls and recording logs for further analysis. This is a time and resources consuming process. The main drawbacks to this approach are: (i) the information gathering process impacts the overall performance, influencing other applications that aren't involved in the application context being considered; (ii) this impact on performance also interferes with the application being considered; and (iii) this scenario is probably different from that of where the application was developed.

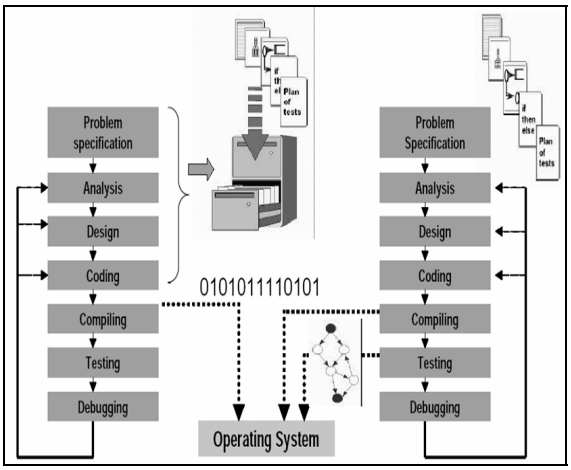

Figure 2: (a) General framework (b) Proposed framework.

3.2.1 Learning Phase

Figure 2a shows the traditional application life-cycle characterizing that the documentation produced during the analysis and design, in general, is stored in folders after the implementation phase is concluded. The traditionals operating systems usually receives only binary code to manage.

In our approach, the development process must be oriented by the application dynamics. As a prerequisite, a KBOS environment establishes that each application developed must have (i) a state-machine that describes all dynamic behaviour and (ii) the source-code associated (Figure 2b).

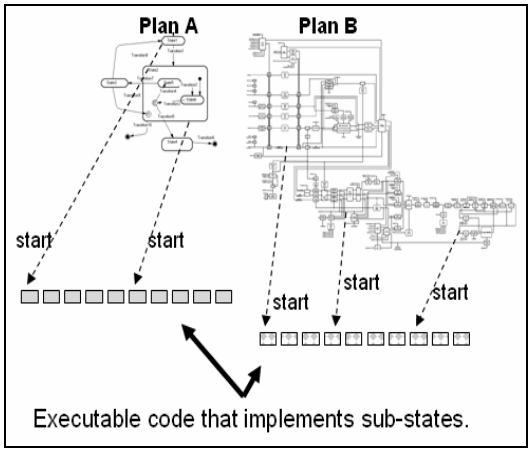

Figure 3: Plans registering relative starting time for each sub-plans or sub-states.

This is the input for our system to learn about the application's intentions and to generate the executable code. When the KBOS runtime environment receives a new application state-machine, it starts a procedure to convert sub-states and portions of source-code into execution plans. Those execution plans are built in a parallel functional decision trees format and constitutes the executable code that KBOS recognizes.

The knowledge at OS level emerges from a library of execution plans and from the system's experience in running those plans.

Figure 3 shows an example with two plans A and B. Each plan has its own sub-state architecture (according to their particular purpose). Each sub-plan is implemented by a set of machine instructions (executable code). The time needed to execute each sub-state is determined during the software test phases by the development team and delivered with the software (including the state machines – dynamic model of the software).

4 BIOLOGICAL CLOCK

According to Siegel (2006), living organisms evolved an internal biological clock, called the circadian rhythm, to help their bodies adapt themselves to the daily cycle of day and night (light and dark) as the Earth rotates every 24 hours. The term 'circadian' comes from the Latin words for about (circa) a day (diem). Circadian rhythms are controlled by "clock genes" that carry the genetic instructions to produce proteins. The levels of these proteins rise and fall in rhythmic patterns. These oscillating biochemical signals control various functions, including when we sleep and rest, and when we are awake and active. Circadian rhythms also control body temperature, heart activity, hormone secretion, blood pressure, oxygen consumption, metabolism and many other functions.

A biological clock has three parts: a way to receive light, temperature or other input from the environment to set the clock; the clock itself, which is a chemical timekeeping mechanism; and genes that help the clock control the activity of other genes. (Siegel, 2006)

In the last few decades, scientists have discovered the genes responsible for running the internal clocks: period (per), clock (clk), cycle (cyc), timeless (tim), frequency (frq), double-time (dbt) and others. Genes that control circadian rhythms have been found in organisms ranging from people to mice, fish, fruit flies, plants, molds and even single-celled, blue-green algae known as cyanobacteria. (Siegel, 2006)

The master circadian clock that regulates 24-hour cycles throughout our bodies is found in a region

called the suprachiasmatic nuclei (SCN) in the hypothalamus of the brain. The SCN is made up of two tiny clusters of several thousand nerve cells that "tell the time" based on external cues, such as light and darkness. The SCN regulates sleep, metabolism, and hormone production (Siegel, 2006).

The SCN is believed to synchronize "local" clocks in organs and tissues throughout the body, either through hormones or changes in body temperature. Gene-operated clocks independent from the brain's master pacemaker have been found in the liver, lung, testis, connective tissue and muscle (Siegel, 2006).

4.1 Perception of Time

People and other animals are able to perceive the duration of intervals between events, and the accuracy of their perceptions can be assessed. In situations in which there are many different time intervals, these can be combined for the assessment of the typical interval. Associative learning is dependent upon time perception, and the mechanisms of time perception involve an internal clock (Church, 2006).

According to Craft (2000), “we take it for granted that each experience takes place in a continuum of time. In the course of the daily routine one rarely, if ever, stops to notice as such the passing of physical and psychological events while they happen. But each passing moment, noticed or unnoticed, is a successive instance of the ‘now’ that marches on into a presumably infinite past that we construct in memory. By extension, we anticipate a succession of future ‘now’ moments that have yet to come. In this process we meld our “experience of heterogeneous events into a coherent sense of persistence” (Flaherty, 1999 apud Craft, 2000).

It has been physically hypothesized that biological processes and environmental factors provide cues through which we construct our perception of temporality. It has been suggested that there is some sort of “biological clock” that regulates our perception of time. This is not to be confused with the more commonly known “circadian” rhythms which have been usually observed in most living things. Flowering plants, bees and other animals demonstrate the existence of internal or innate timing mechanisms in their blossoming and movement patterns. Although much attention has been given to these patterns in human subjects, more notably in the isolation studies of Aschoff and Weaver, such circadian clocks are not likely to be involved in human time perception on the fine scale of minutes and seconds (Campbell, 1990 apud Craft 2000).

The concept of ordered time, the fixed intervals of minutes and seconds, and the synchronicity between 10 minutes on the clock and the same amount of time in lived duration is, at least partially, a socialized phenomenon (Flaherty, 1991 apud Craft, 2000).

5 THE TIME DIMENSION

In the current paradigm of computing systems, the time is a variable that has to be explicitly read in order to enable software entities to perceive the time flow. It implies that if the program does not read that variable, it will not be able to perceive the time flow.

In a KBOS system, the time flow is part of the system and it is implemented in two phases: (i) by establishing units of time flow perception and (ii) by time-stamping the state machine that drives the executable code (in KBOS run-time environment executable code is implemented as parallel functional decision trees) with that information.

The first phase makes possible the creation of a kind of “machine biological clock” (MBC) concept – a time unit that the whole system can perceive as flowing and that is different from the time-slice concept as adopted in multitasking based operating systems today. The second phase enables parts of code to perceive time without the need of explicitly reading clock variables.

Figure 4 shows the situation in which one of the sub-states of plan A at the second MBC unit perceives that its sub-state is delayed in comparison with the original situation presented by the figure 3. Figure 4 also shows that hardware events (time ticks from real-time clock and other hardware events from mouse, hard disk and network card) demand specific plans to be executed (fig. 5).

The MBC makes possible to introduce another concept: the work capacity (WC) of a machine. This concept is related to the amount of work a machine can do in some BMC and introduces the capacity of a system to perceive if it is becoming overloaded or not.

Figure 6a shows an example of a program that is time dependent. In general, the program needs to call the getTime API in order to discover the current time and make some calculation to discover if it is delayed, on time or ahead of time. Also, in general, only some portions of the code running in a system have to deal with such constraints so we have a mix of code dealing with time and code that was not

conceived to deal with time running together on the same environment.

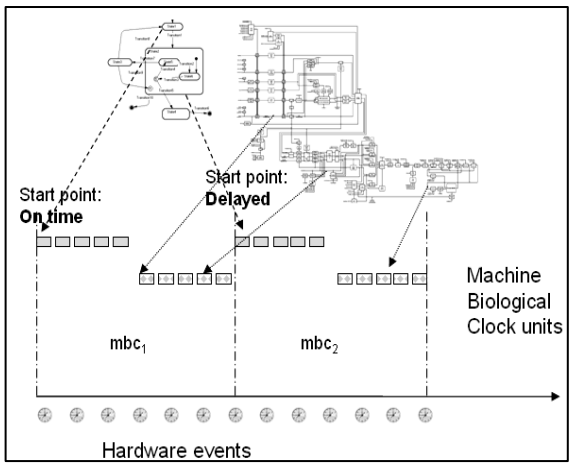

Figure 4: Plans A and B perceiving delays.

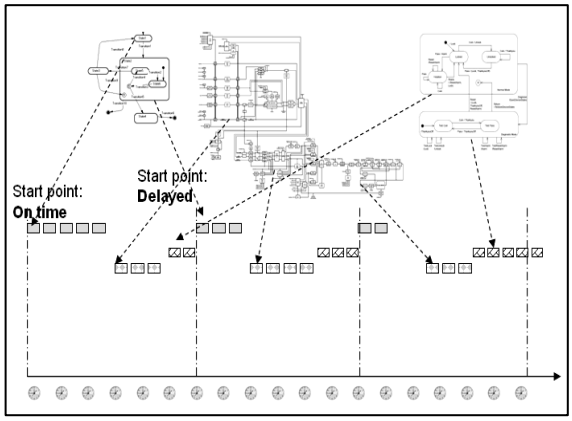

Figure 5: Plans A, B and C perceiving delays.

Figure 6b shows how a plan (in KBOS context) should be developed: each procedure/function has to explicitly declare sections where the time dimension has to be considered as a functional requisite. During the execution time of that plan, the system activates the appropriated section (delayed, onTime or aheadOfTime) according to the situation of that plan. If the developer do not know what to do in some situation, he can explicitly use an IDoNotKnowWhatToDo clause and the KBOS run-time will take appropriate actions.

The time dimension also makes possible to introduce the notion of space concept. In other words, if two different plans perceive that both are delayed it is equivalent to say to each one that there is someone else sharing resources within the same MBC unit. It leads the logical path of some plan to be changed to another path that implements the same functionality but demands less resources. The self-adaptive and self-reconfigurable characteristic of the system is based on this facility.

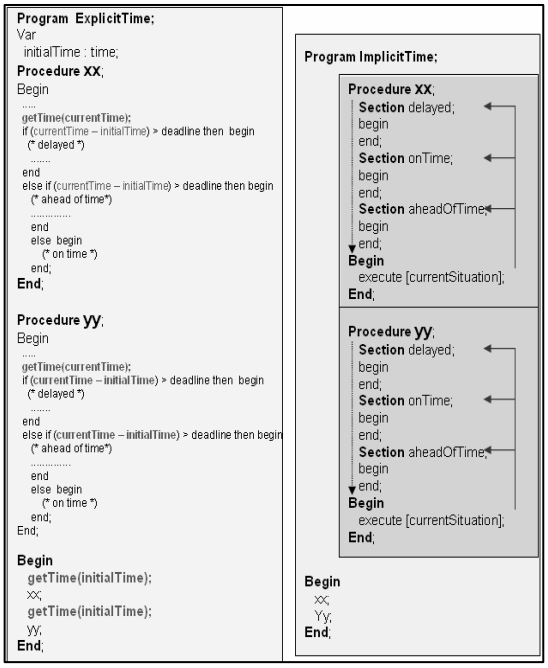

Figure 6: (a) Explicit time (b) implicit time.

5.1 Identity and Intelligent Behaviour

A KBOS framework enables to introduce the identity concept, which is resultant from the embodiment, situatedness, adaptiveness and autonomy characteristics. This leads to an emergence concept. According to Muller-Schloer (2004), emergence is defined as a property of a total system which cannot be derived from the simple summation of properties of its constituent subsystems. Emergent phenomena are characterized by (i) the interaction of mostly large numbers of individuals (ii) without central control with the result of (iii) a system behavior, which has not been explicitly "programmed" into the individuals.

In this sense, the set of characteristics enables the system to perceive, in an individualized manner, a set of events occurring in some instant of time. Thus, the intelligent behavior emerges from the previous characteristics plus the relationship between the system and the surrounding environment.

6 RELATED WORK

Stulp and Beetz (2006), proposed a novel computational model for the acquisition and application of action awareness, showing that it can be obtained by learning predictive action models from observed experience and also demonstrating how action awareness can be used to optimize, transform and coordinate underspecified plans with highly parametrizable actions in the context of robotic soccer. The system works in two moments: (a) idle time when the agent learns prediction models from the actions in the action library and, (b) during operation time, when action chains are generated.

Tannenbaum (2007) argues that self-awareness means learned behaviors that emerge in organisms whose brains have a sufficiently integrated, complex ability for associative learning and memory. Continual sensory input of information related to the organism causes its brain to learn its (the organism's) physical characteristics, and produce neural pathways, which come to be reinforced,, so that the organism starts recognizing, several features associated to each reinforced pathway. The self-image characteristic provides a mechanistic basis for the rise of the concept of emergency of behavior that, on its turn, is connected to the concepts of self-awareness and self-recognition. On the basis of all that process there is the notion of time perception.

7 CONCLUSIONS AND FURTHER WORK

We have briefly given an overview of an endogenous self-adaptive and self-reconfigurable approach to operating system design and introduced the MBC concept. The main aspect to be pointed out is that there is no separation between what is known as operating system and what is known as application programs in today's paradigm.

In a KBOS environment all the executable code takes part into the system and all the code has the ability to perceive the time flow. This perception enables the whole code to execute self-adaptation without explicitly demanding routines.

REFERENCES

R.J.Brachman. *Systems That Know What They're Doing*. IEEE- Intelligent Systems. Nov/Dec 2002. pp.67-71.

T.Chikayama. *Overview of the Parallel Inference Machine Operating system (PIMOS)*. Proc. Of the Intl. Conference of Fifth Generation Computer Systems. Pp. 230-235. 1988.

R.M.Church. *Time Perception*. Encyclopedia of Cognitive Science. John Wiley & Sons, Ltd. 2006.

A.Cockcroft. *New release of the SE Performance Toolkit*. March 1995. Available in www.sun.com/960301/columns/adrian/ column7.html, March 1995.

B.Craft. *Twitch of the Snooze Button: Time Perception and Cognition in Humans*. Submitted in partial fulfillment of the requirements for HCI 450, DePaul University. January 31, 2000.

Genera Concepts: *The Best Software Environment Available*. March 2003. Available in http://kogs-www.informatik.uni-hamburg.de/~MOELLER/ symbolics-info/GENERA/genera.html.

R.Hayes-Roth. P*uppetry vs. Creationism: Why AI Must Cross the Chasm*. IEEE Intelligent Systems. September/October 2006; 21(5):7-9.

L.Hernández,E.Vivancos,V.Botti. *Intelligent Scheduling of Production Systems in a Real-Time Architecture*. IBERAMIA'98,1998,p429-438.

A.Kandel,Y.Zhang, M.Henne. *On use of fuzzy logic technology in operating systems*. Fuzzy Sets and Systems 99, Elsevier Science, pp 241-251, 1998.

Larner,D.L. A *Distributed, Operating System Based, Blackboard Architecture for Real-Time Control*. CACM. 1990.

R.Linde. *Operating Systems Penetration*. AFIPS Conf. Proceedings, Vol 44, 1975.

M.M.Mattos. *Main Concepts to Build Knowledge-Based Operating Systems*. Doctoral thesis. UFSC-Universidade Federal de Santa Catarina, Brasil, Novembro, 2003. (In Portuguese)

M.M.Mattos. *Next Generation of Operating Systems Design Based on Knowledge Abstraction*. In: Proceedings of the IADIS International Conference on Applied Computing. Algarve, Portugal. 2005.

M.M.Mattos. *KBOS Run-Time Environment Based on DEVS Formalism*. In: Proceedings of the IADIS - International Conference on Applied Computing. Algarve, Portugal. 2005.

C.Müller-Schloer. *Organic computing: on the feasibility of controlled emergence*. In Proceedings of the 2nd IEEE/ACM/IFIP international Conference on Hardware/Software Codesign and System Synthesis (Stockholm, Sweden, September 08 - 10, 2004). CODES+ISSS '04. ACM Press, New York, NY, 2-5. DOI= http://doi.acm.org/10.1145/1016720.1016724.

A.B.Patki , G.V.Raghunathan ,A.Khurshid. *FUZOS—Fuzzy Operating System support for Information Technology*. Proceedings of Second On-line World Conference On Soft Computing In Engineering, Design And Manufacturing. Cranfield University, UK, June 1997.

J.Pasquale. *Using Expert Systems to Manage Distributed Computer Systems*. IEEE Network. Set.1988.

J.P.Sansonnet,M.Castan,C.Percebois,D.Botella,J.Perez. *Direct Execution of LISP on a List Directed Architecture.* Proceedings of ASPLOS. Palo Alto, Califórnia, March 1982, pp. 132-139.

M.Seltzer,C.Small,K.Smith. *The Case for Extensible Operating Systems.* Harward Computer Center for Research in computing Technology -Technical Report TR-16-95 Depto. Of Computer Science, Harward University. 1995.

L.J. Siegel. *The Time of Our Lives*. Learn.Genetics – Genetic Science Learning Center. The University of Utah. In: learn.genetics.utah.edu/features/clockgenes. 2006.

A.Siraj.,S.Bridges,R.Vaughn. *Fuzzy Cognitive Maps for Decision Support in Intrusion Detection Systems*.2001. Available in http://www.sc.msstate.edu/~security/iids/publications/nafips_ifsa_2001.htm.

F. Stulp and M. Beetz. *Action awareness – enabling agents to optimize, transform, and coordinate plans*. In Proceedings of the Fifth International Joint Conference Autonomous Agents and Multiagent Systems (AAMAS), 2006.

W. J. Schwartz. *President's Welcome*. In Proceedings of the Tenth Meeting of Society for Research on Biological Rhythms, Sandestin, FL. May 21–25, 2006.

E.Tannenbaum. *Speculations on the emergence of self-awareness in big-brained organisms*. Jun 2007. Available in http://eprintweb.org/S/article/q-bio/0701017.

R.Vilensky,Y.Arens,D.Chin. *Talking to Unix in English: An Overview of UC*. CACM 17,6,pp.574-593, Junho 1984.

Y.Yokote. *The Apertos Reflective Operating System: The Concept and Its Implementation*. Proceedings of OOPSLA'92, ACM Sigplan Notices, v. 27, pages 414–434, 1992.

A.Zomaya,M.Clements, S.Olariu. *A Framework for Reinforcement-Based Scheduling in Parallel Processor Systems.* IEEE Transactions on Parallel and Distributed Systems. V9, N3,p249-260,Mar 1998.

COMPUTER-CONTROLLED NEUROSTIMULATION FOR A VISUAL IMPLANT

S. Romero
Department of Computer Science, University of Jaén, Campus Las Lagunillas s/n, Jaén, Spain
sromero@ujaen.es

C. Morillas, F. Pelayo
Department of Computer Architecture and Technology, University of Granada, Granada, Spain
cmorillas@atc.ugr.es, fpelayo@ugr.es

E. Fernández
Institute of Bioengineering, University Miguel Hernandez, Elx, Spain
e.fernandez@umh.es

Keywords: Artificial vision, electrical neurostimulation, microelectrodes, active implants, phosphene, neuroprosthesis.

Abstract: Current research in therapies for restoring a functional form of sight to the blind includes interfacing electronic neurostimulators with some point of the visual pathway. This approach requires controlling a number of waveform parameters which might vary for every implanted patient and for every channel in an interface that may have hundred or thousands of electrodes. Therefore, the clinical, acute research stage of the implant should be controlled in a flexible and easy way, in order to obtain the information that will lead to a chronic implantable device. We describe such a system, based on a PC connected to an electronic neurostimulator, which delivers bi-phasic pulses to a set of implanted microelectrodes. This platform performs an automated patient-driven procedure to find stimulation thresholds. The system implements a set of physchophysical tests in order to determine the properties of the elicited visual perceptions, and applies an automatic re-mapping of the electrodes to obtain better recognizable patterns of percepts. Our platform can interface some other tools oriented to obtain, in a next research stage, a portable and chronic version of the visual implant.

1 INTRODUCTION

World Health Organization estimates that about 37 million persons are completely blind, while those affected by low vision sum up to 124 million (WHO, 2005). These numbers are increasing due to the ageing of population in developed countries, and to a variety of pathologies and accidents affecting one or more of the components of the complex visual system.

Major causes of blindness are age-related macular degeneration (AMD), diabetic retinopathy, glaucoma or traumatic damage.

Therapeutic choices for blindness might be as varied as its causes. Clinical treatments are available for some kinds of visual impairments, as the ones caused by cataracts. However, a strong research is undergoing for other types of visual pathologies, for which no clinical solutions are available yet.

These research lines include retinal cell transplantation, the use of growth factors, or gene therapy, mainly applied to retinitis pigmentosa (RP).

Apart from biological approaches, a number of research groups are working towards the development of visual prostheses, which would replace one or more of the damaged stages of the visual pathway, providing a rudimentary, but functional, form of visual perceptions.

Depending on the point of the visual pathway on which the neurostimulation interface is placed, we can classify visual neuroprostheses as retinal (Humayun, 2003), optic nerve (Veraart, 1998), or cortical implants (Dobelle, 2000; Troyk, 2003; Fernández, 2005).

In retinal prostheses, the set of electrodes are implanted below or onto the retina, in order to replace the role of photoreceptors, or ganglion cells, respectively. In the case of optic nerve implants, a cuff electrode is placed around the bunch of axons of the ganglion cells connecting the output of the retina to the next stage of the visual pathway. In cortical implants, electrical pulses are directly delivered to the visual area of the brain cortex, by using surface planar electrodes, or penetrating tips.

Whatever is the selected interface for visual neurostimulation, the employment of this kind of devices implies a high degree of complexity.

The amount of channels in the different prototypes used in research range from 16 to 100 electrodes (Normann, 1999), although some studies have shown that a number between 600 and 1000 electrodes would be required to obtain an adequate performance in basic tasks, such as object discrimination, recognition of big characters or pedestrian navigation (Cha, 1992).

The signal delivered to every electrode is a bi-phasic charge-balanced pulse, and includes a set of parameters such as phase width, pulse duration, pulse current amplitude, number of pulses in a train, inter-pulse interval, inter-train interval, etc. The set of values for these parameters might vary from channel to channel, and are expected to be different for every implanted individual (see Fig. 1).

This way, the process of tuning all the parameters for the prosthesis after safe implantation is a complex and lengthy task, which is unavoidable in the research to determine the feasibility of a neurostimulation-based visual prosthesis.

In this paper, we describe a computer-based set of software and hardware conceived for research with visual neuroprostheses. Our platform is mainly oriented to test cortical implants, but it is easily extendable for other types of implants.

The purpose of the research platform is to provide automated and patient-driven procedures for prosthesis parameter tuning and psychophysical testing. The computer-controlled neurostimulator serves as an abstraction layer to hide the complexity of handling such an intricate implant.

The platform is part of a set of tools designed to cover different needs in the development of a full visual prosthesis, such an artificial retina model, or an automated synthesizer for embedded circuits to obtain a portable, low power consumption controller for the stimulator.

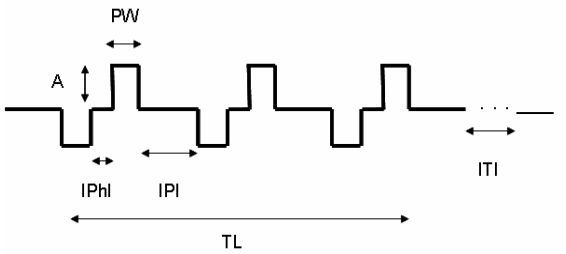

Figure1: Biphasic pulse train for cortical neurostimulation. Pulse trains contain a number of parameters that can be selected, as amplitude (A), pulse width (PW), inter-phase interval (IPhI), interpulse interval (IPI), train length (TL), and inter-train interval (ITI).

2 A VISUAL PROSTHESIS MODEL

The platform described in this paper has been developed to assist in the post-implantational stage of research of a visual neuroprosthesis project. The whole project, known as CORTIVIS (Cortical Visual Neuroprosthesis for the Blind) (CORTIVIS, 2002), has been carried out by a consortium of seven research labs and a small company under European funding (see Fig. 2).

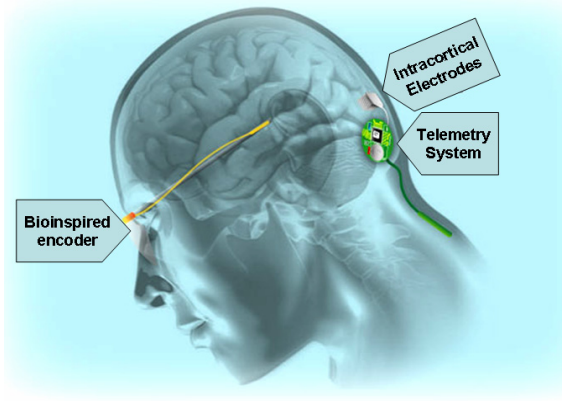

Figure 2: Scheme of the visual prosthesis proposed by CORTIVIS. A camera grabs images, which are processed by a bioinspired encoder. The encoder sends stimulation commands wirelessly to the intracranial telemetry system. Finally, the array of microelectrodes stimulates the visual cortex of the subject.

The model selected for the CORTIVIS prosthesis includes one or two cameras, as input, which feed a bio-inspired retinal encoder, which partially replaces the role of the visual processing taking place at the retina, and determines the moment in which specific implanted electrodes should be activated. The output

of this stage is an address-event representation (AER) indicating the number of electrode which will be stimulated. This stream of addresses is sent through a wireless link to the implanted section of the prosthesis. The RF link also provides energy for the implanted stimulator. This neurostimulator is finally connected to an array of microfabricated electrodes, which are inserted into the visual area of the brain cortex. In our case, the Utah Electrode Array (Normann, 1999), bearing 100 electrodes, has been selected as the neuroelectrical interface.

3 RESEARCH PLATFORM

In this section, we describe the organization, operation modes and capabilities of the research platform we have developed for the testing and tuning of cortical visual neuroprostheses.

3.1 System Architecture

Fig. 3 shows the building blocks that integrate the experimenting station. A PC which runs the software required to control the platform is connected to an electronic neurostimulator. The connection is made through one of the computer ports. Initially, we employed the LPT port. However, the second version of the neurostimulator is using a USB port to exchange information with the PC. An opto-coupling stage protects the patient against electrical risks, as required for biomedical instruments.

The second stage of the platform is an electronic equipment which receives and decodes commands from the PC, according to a pre-established protocol. This neurostimulator can receive configuration, stimulation and test commands. Whenever a configuration word is received, it stores the waveform parameters for the corresponding channel in a configuration memory. If a stimulation command is sent from the PC, the equipment selects the corresponding output channel through a demultiplexor, and drives a Digital-to-Analog converter so that a biphasic waveform is sent to the output, according to the stored parameters for the corresponding channel. Test commands just check the state of the electronics, in order to detect malfunctioning electrodes (due to encapsulation, breakage during insertion, etc.).

The last block in the platform is the intra-cranial implant, which is connected to the output of the neurostimulator. In our case, we have selected the Utah Electrode Array, which is a microfabricated array of 10x10 microelectrodes (Fig. 4). This array is pneumatically inserted into the brain cortex, so that the tips of the electrodes are expected to reach layer IV of the visual cortex. Previous experiences have shown that electrical stimulation of cells in this layer evoke visual percepts, similar to stars in the night, which are called “phosphenes” (Schmidt, 1996).

In this acute clinical version of the CORTIVIS prosthesis, a set of wires is used to connect the stimulation equipment to the implant, discarding for later use the radio-frequency link.

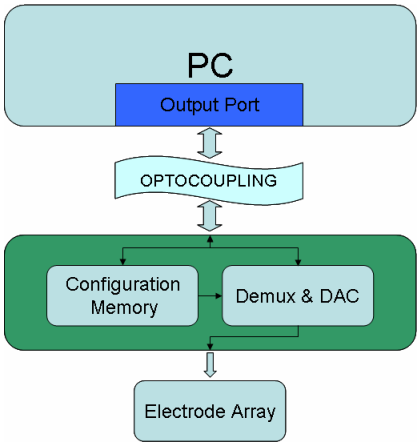

Figure 3: Structure of the research platform. A PC runs a control software, and sends configuration and stimulation commands through a PC port. An optocoupling stage protects the patient against electrical risks. The next block is the neurostimulation electronics. A configuration memory stores the waveform parameters for every channel, and a demultiplexing and digital-to-analog convertion block issues the corresponding waveform, and sends it to the proper electrode in the array.

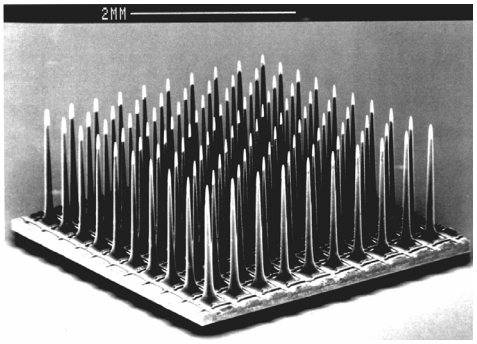

Figure 4: the Utah Electrode Array (UEA). It is a 10x10 electrode matrix, bearing 1.5 mm tips, separated by 400 microns. It is microfabricated in silicon and platinum (Normann, 1999).

3.2 Operation Modes

The experimental set-up can present two different configurations, called "stimulation" and "simulation/training" modes.

The neurostimulation configuration corresponds to the set described in section 3.1, that is, a PC controlling a neurostimulator, which delivers pulses to an implanted array of electrodes. The purpose of this set is to allow researcher tuning the set of parameters required to elicit phosphenes in the visual field of the patient, and then, run a series of psychophysical tests, in order to characterize the evoked perceptions.

However, an alternative configuration is available for debugging and training purposes (with sighted volunteers). In this second choice, the electronic neurostimulator and the implanted array of electrodes are replaced by a second PC with head-mounted displays. The first PC plays the same role as in the previous configuration. The commands sent through the communication port are received by the second PC, which implements simulation rules including random values for current threshold, and phosphene location in the visual field. The simulator in the second PC leads to a representation of a set of phosphenes in a head mounted display, according to the information obtained in similar experiences with human visual intra-cortical microstimulation.

4 SOFTWARE CONTROL

The platform described in the former section runs a program written in C++, under Microsoft Windows, which controls all the automated procedures to be carried out for stimulation parameter tuning and psychophysical testing.

The control application, named "V1 Cortistim" has a graphical user interface that allows the experimenter to select every stimulation parameter for the waveform, and run or stop every test. However, in order to accelerate the lengthy process of tuning the stimulation parameters for each implanted electrode, and executing an extensive set of psychophysical essays, every of these procedures have been automated. This way, the patient becomes the operator of the system, setting the pace of the experimenting steps, and avoiding verbal interaction, so the feedback given by the implanted individual by means of the computer input mechanisms, is automatically recorded, launching the next action of the process. In the following sections, we detail the procedures that are implemented in the research platform.

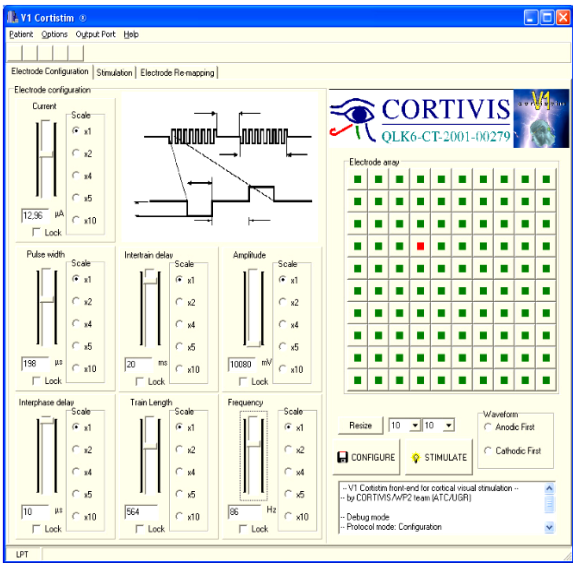

Figure 5: V1 Cortistim Graphical User Interface, allowing to control every waveform parameter for every channel in the microelectrode array.

4.1 Current Threshold Finding

The first task after the patient has been safely implanted is finding the lowest current amplitude required to evoke a phosphene. This procedure has to be done for every channel of the implant. This way, the objective is to have as many phosphenes as possible forming patterns of percepts, but injecting a minimum amount of charge into the cortical tissue.

As mentioned before, this procedure is patient-driven, so the response of the patient triggers the next step of the process. The basic algorithm selects every channel, and issues pairs of configuration and stimulation commands to the stimulator with increasing current amplitude, until the patient signals the occurrence of a phosphene in his/her visual field, by clicking a mouse button. Then, the process is repeated for the next electrode.

We have included two modifications to this basic search algorithm to reduce the number of total steps required to complete the process. We have to take into account that in a near future, next generations of implants might include an amount of electrodes over the thousand, and for each electrode a set of current values should be tested, leading to a very tedious and lengthy process. The first modification is employing a binary search scheme, instead of a linear model, reducing the complexity of the problem. The second enhancement takes into

account that current thresholds are expected to gather around a mean value. Having this, we set the starting point for the binary search for a channel to the threshold found for the previous channel.

Applying this procedure, a set of 100 electrodes can be configured in less than 5 minutes (for a step of 1 second between consecutive stimulations).

A similar scheme can be applied to the rest of parameters of the stimulation waveforms, although most experimental implants take amplitude as the main parameter. In any case, all the parameters are interrelated, as they influence the amount of charge injected, which is the main responsible for phosphene evocation.

Experimental results of using the platform to generate biphasic stimulation pulses are exposed in Fig. 6 and in Fig. 7.

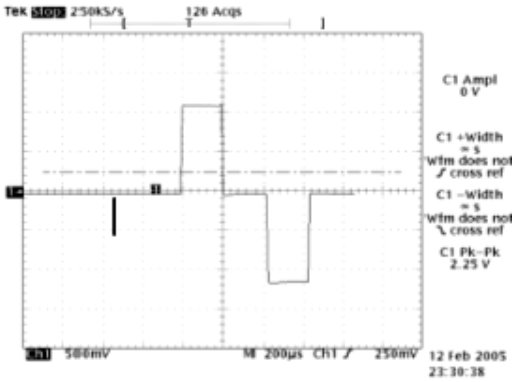

Figure 6: Example of biphasic pulse obtained with the experimental neurostimulation platform (vertical scale: 500 mV/div; horizontal scale: 200 microsec/div).

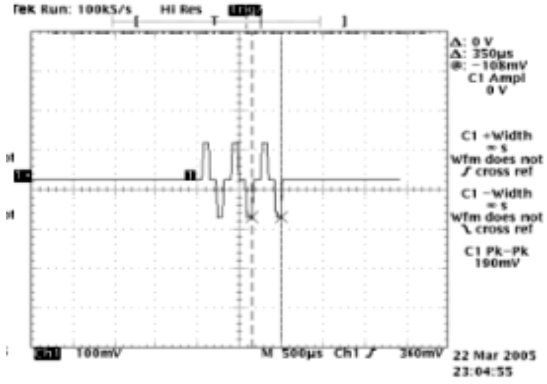

Figure 7: Example of pulse train obtained with the experimental neurostimulation platform (vertical scale: 100 mV/div; horizontal scale: 500 microsec/div).

4.2 Psychophysical Tests

After the threshold current has been determined for every channel, a set of tests is required to be carried out in order to characterize the psychophysical properties of the evoked percepts.

This way, an extensive set of perceptual tests has to be run, which again requires making this process as easy and agile as possible. Following the same philosophy as for the threshold finding procedure, a patient-driven automated scheme is again employed.

The V1 Cortistim platform provides the following set of psychophysical essays:

- Brightness sensitivity: a change in certain parameters of the waveform (mainly amplitude) will modify the perceived brightness of the evoked phosphene. A pair of phosphenes is elicited, and the brightness of one of them changes until the patient finds no change.
- Spatial resolution: a pair of phosphenes produced by distant electrodes is evoked consecutively with closer and closer electrodes until the patient cannot differentiate them.
- Phosphene cluster count: a set of 1, 2 or 3 phosphenes from adjacent electrodes is elicited. The patient gives feedback on the number of phosphenes perceived.
- Motion mapping and orientation selectivity: a straight line of electrodes (row, column or diagonal) in the matrix consecutively get activated. The patient indicates the general direction of apparent motion of the phosphene.
- Simple pattern discrimination: a simple pattern (similar to Snellen symbols) and its "mirrored" pattern are consecutively activated in the electrode array. The subject tells if they seem to be different or similar.

5 PHOSPHENE MAPPING AND RE-MAPPING

A key aspect in the design of a phosohene-based visual neuroprosthesis is the ability to evoke patterns of percepts that can be matched to known models from the visual world.

Experiments both with human and non-human subjects have shown that the correspondence between the spatial location of the stimulation point in the cortex and the position of the evoked

phosphene in the visual field can present strong deformations (Normann, 2001).This is especially remarkable for high density arrays of electrodes, in which the correspondence between the stimulation and the perceptual spaces is highly non-linear and non conformal. This fact might be caused by the complex interconnections among the neural cells that respond to stimulation in the area of influence of an electrode. Anyway, a mapping between the location of the activated electrode and the position of its corresponding phosphene in the visual field should be built for every channel of the implant. Correspondingly, an inverse transformation or re-mapping, indicating which electrodes should be activated to get a specific pattern of phosphenes is required in order to evoke recognizable percepts. We describe the solutions implemented for our experimentation platform both for the mapping and re-mapping objectives.

5.1 Phosphene Mapping

Several mapping methods have been used for building a table to determine the spatial coordinates of a phosphene corresponding to the activation of every electrode, as joysticks, dartboards or digital tablets. Our objective in this procedure is not only, as before, to obtain an agile system by avoiding verbal interaction, and by having an automated patient-driven process, but also achieving precision in a process that is very prone to inaccuracy.

Our platform includes a mapping process based on a tactile screen placed just in front of the patient, as exposed in Fig. 8. A consecutive pair of phosphenes is elicited, and the patient touches the tactile screen in the points in where the percepts appear on the visual field. The platform, in training mode, is able to find out the mapping error, as the real location of the evoked phosphenes in the head mounted displays is computer-generated, and can be compared to the position pointed out by the subject.

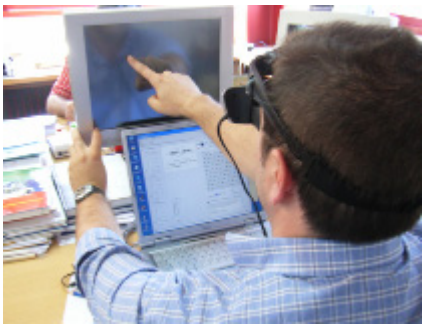

Figure 8: Example of usage of the automated phosphene mapping system. The platform is being used in training mode. A sighted volunteer wearing Head Mounted Displays perceives computer-generated phosphenes, and indicates their location on his visual field by touching a tactile screen in front of him.

5.2 Re-mapping Procedure

Once an electrode-to-phosphene map is available, a pattern of phosphenes can be elicited by stimulating the corresponding electrodes. So, whenever a specific distribution of phosphenes is required in the visual field of the patient, a list of electrodes has to be determined. This process is called re-mapping.

The map of phosphenes elicited with intra-cortical microstimulation appears to be stable for a given patient (Schmidt, 1996). However, there are a limited number of phosphenes available in specific locations of the visual field, which have to be used to evoke any desired pattern.

Our first approach is to project the desired pattern on the center of the visual field, and then, select, for every desired point, the closest phosphene to it. With a reverse look up at the mapping table, its corresponding electrode is found.

Instead of selecting the absolutely closest phosphene in the map to the desired point, we choose the closest phosphene which hasn't already been selected. That way, we can obtain patterns including a maximum number of phosphenes, rather than having more precise locations with less percepts. Although the patterns can present some more deformation, its completeness, along with the training of the patient, is expected to lead to a better recognition, as illustrated in Figs. 9 and 10.

Additionally, this selection procedure enhances the response whenever the distribution of the map is highly uneven. So, in the case we have a region of the visual field covered by a small group of phosphenes, and another region with a high density of percepts, a moving object in the visual field should be composed of the same number of phosphenes. Direct selection of the closest phosphene would lead to a different number of points in a pattern, depending on the location of the object in the visual field (which makes difficult, for example, recognize a moving object as a unit). With our algorithm, an object is always composed of the same number of phosphenes, regardless of its location in the visual field. The shape of the pattern can vary, in an effect similar to looking a moving objective through a frosted glass.

Figure 9: Phosphene pattern that would be elicited after direct selection of the top row and central column of an electrode array. Although the distribution of electrodes forms a "T" shape, the evoked pattern is unrecognizable, so a remapping is required. This set of phosphenes corresponds to a randomly generated mapping (25x25).

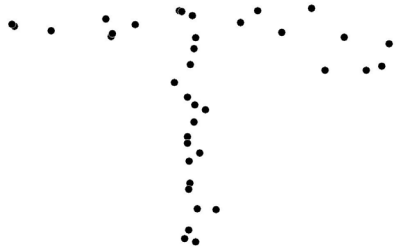

Figure 10: after our remapping algorithm is applied to the previous figure, a different set of electrodes are activated, yielding a better recognizable pattern of phosphenes, closer to the desired "T" shape.

6 ADDITIONAL TOOLS FOR VISUAL NEUROPROSTHETICS

The platform described in this paper is a specific design for the clinical testing stage of a complete visual neuroprosthetic system.

However, corresponding to the whole system architecture depicted in Fig. 2, some other relevant blocks are required for achieving a complete, portable visual prosthesis.

Regarding this point, we give a brief reference of additional platforms and hardware/software tools developed to contribute to the complete prosthetic system. Details of every one of them can be found elsewhere.

Direct stimulation of the visual cortex requires, somehow, replacing the image processing carried out by earlier stages of the visual pathway, such as the spatio-temporal filtering performed by the retina.

For this purpose, a retina-like processing software platform has been developed in Matlab, which allows experimentation with an extensive set of parameters, so that a video or live camera capture can be processed, and the electrode firings (corresponding to the activity of retinal ganglion cells) are obtained. This way, the response of our artificial retina can be compared to the one given by biological retinae when exposed to the same stimuli.

Further information can be found at (Pelayo, 2004).

A second objective of the CORTIVIS project is to achieve a portable, low power consumption version of the previous retinal pre-processor, so that the patient can wear a camera mounted on eyeglasses frame, and the processor will transmit activation commands to the corresponding channels of the intra-cranial segment of the implant via a wireless link.

A plug-in module for the Retiner program has been built, which is able, to translate the retinal model designed with our software into a configuration file for a programmable logic chip, so that all the retinal processing is carried out by a single, portable integrated circuit. References can be found at (Martínez, 2005).

7 CONCLUSIONS

We present a computer-controlled platform conceived to control a neural interface. The main objective is to provide a friendly and automated way of performing experiments after implantation of an array of microelectrodes into the visual cortex of a patient. The platform serves as interface to handle the complexity inherent to a multi-channel brain-computer link that requires tuning biphasic stimulation pulse trains for every electrode.

Every experimental procedure is automated, and patient-driven, in order to make the tuning and testing process as fast as possible. The platform includes a set of psychophysical tests to determine key features of the electrically evoked percepts.

As previous micro-stimulation experiences confirm, the elicited patterns of phosphenes suffer strong deformations with respect to the distribution of the corresponding electrodes in the array. As the objective is to evoke recognizable patterns, a re-organization (re-mapping) between the stimulation and perceptual spaces is required. Our platform includes a re-mapping algorithm for such a purpose.
We also make a brief reference to some additional tools developed by our research group, also

contributing to the development of a complete independent prosthetic system. These tools include a flexible retinal processing model, an automatic synthesizer to program integrated circuits for retinal processing, and a system to include binocular and spatial information in the set of stimuli sent to the brain.

Unfortunately, it is difficult to provide a detailed and standardized comparison against other systems under development. On one hand, these kinds of systems are specifically designed and fitted to control a particular implant, so no compatibility criteria are considered. On the other hand, as neuroengineering is a young field of research, no standards for measuring and comparing the performance of a prosthetic system are available.

Nevertheless, some relevant organizations involved in blindness and low vision research, as the ARVO (ARVO, 2007), or the Smith-Kettlewell Eye Research Institute (SKERI, 2007), are organizing and conducting specific meetings aiming to arrive to a standardized set of tests that will be useful to provide a measurement of the performance of these implants.

ACKNOWLEDGEMENTS

This work has been carried out with the support of the European project CORTIVIS (ref. QLK6-CT-2001-00279), the National Spanish Grants DEPROVI (ref. DPI 2004-07032), IMSERSO-150/06, and by the Junta de Andalucía Project: P06-TIC-02007.

REFERENCES

ARVO (Association for Research in Vision and Ophthalmology) *website*. Available online at: http://www.arvo.org.

Cha, K., Horch, K. W., & Normann, R. A. 1992 Mobility performance with a pixelized vision system. *Vision Research* (32): 1367–1372.

CORTIVIS, 2002. *CORTIVIS project website*. Available online at: http://cortivis.umh.es.

Dobelle, W. H., 2000. Artificial Vision for the Blind by Connecting a Television Camera to the Visual Cortex. *American Society of Artificial Internal Organs (ASAIO) Journal* (46):3-9.

Fernández, E., Pelayo, F., Romero, S., Bongard, M., Marin, C., Alfaro, A., Merabet, L. 2005. Development of a cortical visual neuroprosthesis for the blind: The relevance of neuroplasticity. *Journal of Neural Engineering* (4): R1-R12.

Humayun, M. S., 2003. Visual perception in a blind subject with a chronic microelectronic retinal prosthesis. *Vision Research* 43 (24): 2573-2581.

Martínez A., Reyneri L. M., Pelayo F. J., Romero S., Morillas C. A., and Pino B. 2005. Automatic generation of bio-inspired retina-like processing hardware. *Lecture Notes in Computer Science* (3512): 527–533.

Moore, R., Lopes, J., 1999. Paper templates. In *TEMPLATE'06, 1st International Conference on Template Production*. INSTICC Press.

Normann, R. 1999. A neural interface for a cortical vision prosthesis. *Vision Research.*(39): 2577-2587.

Normann, R.A., Warren, D.J., Ammermuller, J., Fernandez, E., Guillory, S. 2001. High-resolution spatio-temporal mapping of visual pathways using multi-electrode arrays. *Vision Research* (41): 1261-1275.

Pelayo F. J., Romero S., Morillas C., Martínez A., Ros E., Fernández E., 2004. Translating image sequences into spikes patterns for cortical neuro-stimulation. *Neurocomputing* (58-60): 885–892.

Schmidt, E.M., Bak, M, Hambrecht, F.T., Kufta, C.V., O'Rourke, D.K., and Vallabhanath, P. 1996. Feasibility of a visual prosthesis for the blind based on intracortical microstimulation of the visual cortex. *Brain* (119): 507-522.

SKERI (Smith-Kettlewell Eye Research Institute) *website*. Available online at: http://www.ski.org.

Troyk, P. et al., 2003. A Model for Intracortical Visual Prosthesis Research. *Artificial Organs* (11):1005–1015.

Veraart, C., 1998. Visual sensations produced by optic nerve stimulation using an implanted self-sizing spiral cuff electrode. *Brain Research* (813):181-186.

WHO (World Health Organization), 2005. *Prevention of avoidable blindness and visual impairment*, Available on-line: http://www.who.int/gb/ebwha/pdf_files/EB117/B117_35-en.pdf.

POSTERS

BIOMETRIC AUTHENTICATION DEVICES AND SEMANTIC WEB SERVICES

An Approach for Multi Modal Fusion Framework

L. Puente Rodríguez
Universidad Carlos III de Madrid, Avda de la Universidad, 30, Leganés, Madrid, Spain
lpuente@it.uc3m.es

M. J. Poza
Universidad Francisco de Vitoria. Ctra. Pozuelo-Majadahonda Km. 1.800. Pozuelo de Alarcón, Madrid, Spain
mj.poza.prof@ufv.es

J. M. Gómez, B. Ruiz
Universidad Carlos III de Madrid, Avda de la Universidad, 30, Leganés, Madrid, Spain
juanmiguel.gomez@uc3m.es, bruiz@inf.uc3m.es

Keywords: Biometrics, Authentication Devices, Emerging Technologies, Data Integration, Semantic Web Services, Ontologies.

Abstract: Identity verification is now a days a crucial task for security applications. In the near future organizations dedicated to store individual biometric information will emerge in order to determine individual identity. Biometric authentication is currently information intensive. The volume and diversity of new data sources challenge current database technologies. Biometric identity heterogeneity arises when different data sources interoperate. New promising application fields such as the Semantic Web and Semantic Web Services can leverage the potential of biometric identity, even though heterogeneity continues rising. Semantic Web Services provide a platform to integrate the lattice of biometric identity data widely distributed both across the Internet and within individual organizations. In this paper, we present a framework for solving biometric identity heterogeneity based on Semantic Web Services. We use a multimodal fusion recognition scenario as a test-bed for evaluation.

1 INTRODUCTION

Identity recognition is performed now a days by the use of traditional techniques such as PINs, passwords, digital signatures, etc. Biometrics promise to offer a new alternative, portable, easy to use, free of memory, loss or theft problems. A global solution will be based on the creation of specialized organizations offering authentication services. This Biometric Accreditation Entities (BAE) will base their services on previously acquired biometric data.

Biometrics authentication usually refers to the identification of an individual based on his or her distinguishing traits. In principle, a biometric identity is based on the premise that a measurable physical or behavioural trait is a more reliable indicator of identity than the traditional systems such as pairs composed by password and username, Personal identification numbers (PIN) and the akin. Particularly, since biometric identity technologies deal with security and privacy issues, the challenge for the research community is to attain integrated solutions that address the entire problems from sensors and data acquisition to biometric data analysis and system design.

Presently, the lack of performance of biometric systems is being alleviated by the use of multiple biometric indicators for identifying an individual in order to increase its accuracy when using a technique called Multimodal Fusion (Kittler, J. Hatef, R. Matas, J. G., 1998) (Jain R. and J. Quian, 2001). As a result of this, biometric information has grown exponentially and algorithms for feature extraction, matching score or decision levels handle a tremendous amount of data. Furthermore, the

recent years have provided with a lattice of duplicated efforts in building test databases such as face recognition databases (e.g. FERET, PIE or BANCA) (Bailly-Baillière E., S. Bengio et al., 2003) and a lack of uniform standards and granted open access to these databases, as discussed in (Ming, A. Ma, H., 2007).

Hence, arguably the most critical need in biometric identity recognition is to overcome semantic heterogeneity i.e. to identify elements in the different databases that represent the same or related biometric identities and to resolve the differences in database structures or schemas, among the related elements. Such data integration is technically difficult for several reasons. First, the technologies on which different databases are based may differ and do not interoperate smoothly. Standards for cross-database communication allow the databases (and their users) to exchange information. Secondly, the precise naming conventions for many scientific concepts in fast developing fields such as biometrics are often inconsistent, and so mappings are required between different vocabularies.

Hence, we present in this paper a framework for solving multimodal fusion oriented biometric identity data heterogeneity problems, keeping the structure of databases created with the aim of being used for identity accreditation and distributed over the Web. Our approach is based on the breakthrough of adding semantics to Web Services which perform a role of entry points for such databases. Fundamentally, this implies that our framework enables different biometric identity data to be discovered, located and accessed since they provide formal means of leveraging different vocabularies and terminologies and foster mediation.

The remainder of this paper is organized as follows. In Section 2, a brief state-of-the-art on the technologies employed in our research is given. Section 3 defines some terms we use along this paper. Section 4 identifies the heterogeneity of data involved in the biometric identification process. Section 5 describes the framework for solving problems using Semantic Web Services. Finally, conclusions and related work are discussed in Section 6.

2 STATE-OF-THE-ART

Semantic Web Services and Ontologies are the cornerstone technologies applied in our research. On the one hand, data interoperability between different information sources is achieved by means of ontologies and their mapping. On the other hand, Web Services semantically annotated are the software entities responsible for providing a normalized interface to disparate functionality and data sources. In this section, a brief description of each of these technologies is put forward.

2.1 Ontologies

Although a number of different ontology definitions can be found currently in literature, in this work we use Borst's one (Borst, W.N., 1997): "an ontology is a formal specification of a shared conceptualization", where 'formal' refers to the need of machine-understandable ontologies. This definition emphasizes the need of agreement in carrying out a conceptualization. On the other hand, 'shared' refers to the type of knowledge contained in the ontologies, that is, consensual, non-private knowledge. In this work, this definition of ontology has been adopted.

Ontologies have become the de-facto standard knowledge representation technology after the emergence of the Semantic Web along with Semantic Web Services and the Semantic Grid. For all these new research branches, ontologies are the cornerstone technology. Knowledge in ontologies is mainly formalized using five kinds of components: classes, relations, functions, axioms and instances (Gruber, T. R., 1993). There are several formal languages used to construct ontologies, that is, ontology languages, including KIF, OCML and F-Logic. Along with the Semantic Web, new markup ontology languages have come out such as SHOE, DAML+OIL, and the current *de facto* standard, OWL (Web Ontology Working Group, 2004).

2.2 Semantic Web Services

Semantic Web Services are a new technology resulting from the combination of other two technologies, namely, the Semantic Web and Web Services. On the one hand, the Semantic Web (SW) aims at adding semantics to the data published on the Web (i.e., establish the meaning of the data), so that machines are able to process these data in a similar way a human can do (Berners-Lee, T., Hendler, J., Lassila, O., 2001). Ontologies are the backbone technology of the SW as they provide structured vocabularies that describe the relationships between different terms, allowing computers (and humans) to interpret their meaning flexibly yet unambiguously.

On the other hand, Web Services (WS) technology extends the Web from a distributed source of information to a distributed source of functionality. It is based on a set of standard protocols, namely, UDDI (Universal Description, Discovery and Integration), SOAP (Simple Object Access Protocol), and WSDL (Web Services Description Language). Therefore, WS provide the means to develop globally accessible loosely-coupled applications. However, as the Web grows in size and diversity, there is, composition and invocation can be carried out by autonomous software entitiesan increased need to automate traits of WS such as discovery, selection, composition and execution. The problem is that current technology around UDDI, WSDL, and SOAP provide limited support for all that (Fensel, D. & Bussler, C., 2002). As a consequence, the principles behind SW technology were applied to WS leading to what we know as Semantic Web Services (SWS) technology. It consists of annotating WS with semantic content so that service discovery.

The W3C is currently examining various approaches with the purpose of reaching a standard for the SWS technology: OWL-S (OWL Web Ontology Language for Services) (OWL-S W3C Submission, 2004), WSMO (Web Service Modeling Ontology) (WSMO W3C Submission, 2005), SWSF (Semantic Web Services Framework) (SWSF W3C Submission, 2005), and WSDL-S (Web Service Semantics) (WSDL-S W3C Submission, 2005). The two most widespread approaches are OWL-S and WSMO. OWL-S is an ontology for services that makes it possible for agents to discover, compose, invoke, and monitor services with a high degree of automation. Similarly, WSMO provides a conceptual framework for semantically describing all relevant traits of WS in order to facilitate the automation of discovering, combining and invoking electronic services over the Web.

3 SOME DEFINITIONS

A trait is defined as any physical, motor or psychomotor human characteristic capable of being used in biometric identification.

A user is any person for the system to recognize, and whose traits are stored somehow in the database.

A donor is every person (user or not) whose trait is captured, voluntary or involuntary, by a sensor of the system.

A sample is defined in (Mansfield, J. Wayman, J.L., 2002) as a biometric measure presented by the donor which eventually results in an image or signal.

4 IDENTITY HETEROGENEITY PROBLEMS

A typical biometric system presents a well defined structure (Mansfield, J. Wayman, J.L., 2002) that includes two phases: enrolment and testing. Enrolment faces the creation of a type of model representing the user in a univocal way, while testing tries to determine if the donor matches or not the model.

This two phases share the steps related to sample acquisition, pre–processing signal and feature extraction. Enrolment completes its chain with a model creation, while testing do it with a matching step.

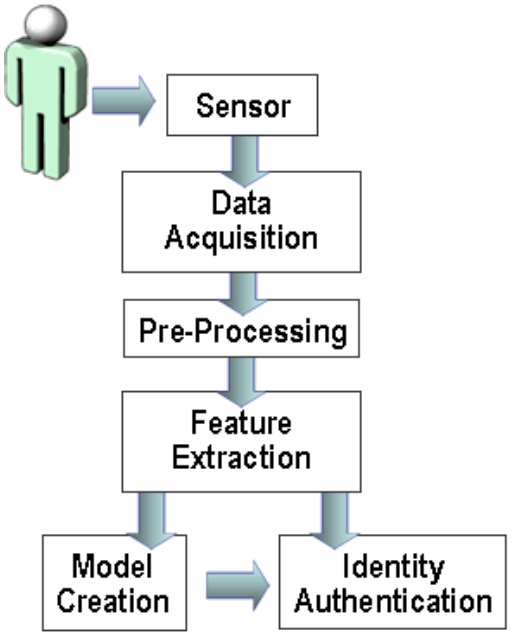

Figure 1: The process.

Acquisition implies that one or more sensors acquire one or more samples of certain donor biometric traits presented to the biometric systems (e.g. fingerprint, face, iris image). Different kind of sensors capturing different biometric donor traits generate different kind of samples.

After capture, samples are pre–processed by cleaning and normalizing in order to adapt the signal to further data extraction, which means signal

filtering, enhancement, energy detection, image centring...

The feature extraction module obtains certain information values supposedly related to the donor in a univocal way. These values are collected in sets called “feature vectors”. Different feature extraction algorithms generate different vectors types.

During enrolment a set of homogeneous vectors are used to create a new model of the related trait of the user. While testing the identity claim user model is compared with another set of vectors obtained from the current donor.

For mono–modal biometric systems only one trait is scanned, and of course only one model is generated for each user.

In our multi–modal biometric fusion approach, multiple user models are generated: one for each modality. Every kind of sensor, scanning different traits, generates different signals. Every one of them flows through different acquisition–preprocessing–extraction chains. The testing phase matches the resulting vectors of every chain with the correspondent model, obtaining as a result a confidence level which informs of the probability that the sample belongs to the user identity claim. Finally, these results are collected by a decision module which will decide to validate or reject the donor.

Different capture, pre-processors or feature extractor algorithms generate different kind of models. Then, other kind capture–process–extractor chain generate feature vectors that should not match properly the model. That’s why semantic information should be added to raw data in order to identify such a variety.

5 THE FRAMEWORK

All over the world we can find heterogeneous databases as a set of biometric recorded data. In this section, we present an integrated approach that address the entire problem of enabling entities (organizations) to confirm individual authentication, based on biometric models (traits) stored in different databases all over the Web. The main requirements of our framework are as follows:

• Provide a platform that allows data matching of acquired biometric samples against individual biometric models (traits) stored in certain databases

• Provide catalogues of data that allows to determine a given model location and make these catalogues available via the Web.

• Use of the Web Service technology to make this access a reality and provide the plumbing communication technology over the wire.

• Use of Semantics to find the most accurate model source for the biometric testing that is taking place.

• And finally use available Web Services in order to ask for autentication for acquired samples.

In our framework, we have addressed this process, taking into account the growing complexity of having a multimodal biometrics test. For that, we notice that our work is mostly oriented to multiple biometric fusion strategies, where multiple biometric measures are utilized (Kittler, J. Hatef, R. Matas, J. G., 1998).

A graphical representation of our framework is depicted in the figure 2.

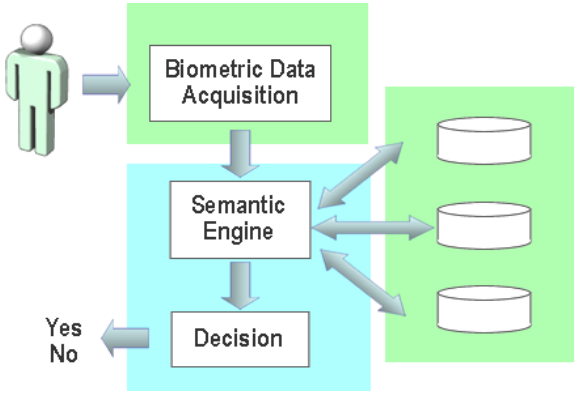

Figure 2: The framework.

The first part of the aforementioned steps i.e. the capture of the biometric samples and certain steps of the signal-process is addressed by the Biometric Data Acquisition System. The goal of this system is to encapsulate the biometric measure with a “data cover” that includes the type of the measure (voice, image, fingerprint, etc.) and a number of significant attributes that can describe the measure and the identity claim.

The second one, the Semantic Service Engine, takes the measure and its “data cover” and accesses the different data storages looking for the best fitting for the cover along the Web. A Semantic Service is an execution environment for the Semantic Web Services initiatives described in section 2. Along with some of the W3C submissions, different tools have been implemented that bring together the major Semantic Web Services functionalities in an integrated framework. One example is WSMX (Web Services Execution Environment), an execution

environment to perform dynamic discovery, selection, mediation, invocation and inter-operation of Semantic Web Services. Another example is IRS (the Internet Reasoning Service), a Semantic Web Services framework which allows applications to semantically describe and execute Web Services. The IRS system supports the provision of semantic reasoning services within the context of the Semantic Web.

In both cases, a Semantic Service Engine would take the measure and its "data cover" to hook it up with the Web Service that fits the most and behaves as an entry point of the aforementioned databases, as it is show in Figure 1.

Finally, the Decision Module component produces a typical index called matching score. A match or no-match decision can be made according to whether this score exceeds a decision threshold or not. This implies an attempt to validate or not the claim of identity, which outcomes a final decision about the biometric identity.

6 CONCLUSIONS AND RELATED WORK

Since Biometric technologies are intended to tackle security and privacy issues, the integration of access control mechanisms and information security are also areas of growing interest.

The creation of Biometric Accreditation Entities will be an alternative in the near future to the current digital certification organisms.

In this environment the heterogeneity of sample capture and data process should not become a barrier for the use of this identification technology.

As the use of Semantic Web Services grows, the problem for searching, interacting and integrating relevant services is becoming increasingly a hurdle for the leverage of existing Semantic Web technologies which have reached a certain level of maturity.

In this paper, we have proposed a conceptual approach for a effective solution in this heterogeneous environment. It is based on the application of the Semantic Web Services properties. It requires to add semantic to the data stored in the biometric accreditation entities databases, and provide the adequate services to the SWS servers.

It has already been proposed the idea of using agents. They can take advantage of the machine-processable metadata provided by the Semantic Web Services. In (Hendler, J., 2001), the author points out how the ontology languages of the Semantic Web can lead to more powerful agent-based approaches for using services offered on the Web. A more practical approach is shown in (Gandon, F. and Sadeh, N., 2004), where the authors describe an application where intelligent agents, aided by context information provided by Semantic Web Services, assist their users with different sets of tasks.

Finally, our future work will focus on creating a complete adapted ontology and to define a standard for required services on SWS, identifying real–world scenarios and validating the efficiency of our approach and to determine its feasibility. This work is related to existing efforts about ontology merging and alignment. A future version of our framework will be orientated towards that direction.

ACKNOWLEDGEMENTS

This work is founded by the Ministry of Science and Technology of Spain under the PIBES project of the Spanish Committee of Education & Science (TEC2006-12365-C02-01).

REFERENCES

Bailly-Baillière E., S. Bengio et al., 2003. "The BANCA Database and Evaluation Protocol," in Springer LNCS-2688, 4th Int. Conf. Audio- and Video-Based Biometric Person Authentication, AVBPA'03. 2003, Springer-Verlag.

Berners-Lee, T., Hendler, J., Lassila, O., 2001. The Semantic Web. Scientific American, May 2001, pp. 34-43.

Borst, W.N., 1997. Construction of Engineering Ontologies for Knowledge Sharing and Reuse. PhD Thesis. University of Twente. Enschede, The Netherlands.

Fensel, D. & Bussler, C., 2002. The Web Service Modeling Framework WSMF. Electronic Commerce Research and Applications, 1(2).

Gruber, T. R., 1993. A translation approach to portable ontology specifications. Knowledge Acquisition Vol. 5:199-220.

Web Ontology Working Group, 2004. OWL Web Ontology Language Guide.

OWL-S W3C Submission, 2004. OWL Web Ontology Language for Services. Available at: http://www.w3.org/Submission/2004/07/

WSMO W3C Submission, 2005. Web Service Modeling Ontology. Available at: http://www.w3.org/ Submission/2005/06/

SWSF W3C Submission, 2005. Semantic Web Service Framework. Available at: http://www.w3.org/Submission/2005/07/

WSDL-S W3C Submission, 2005. Web Service Semantics. Available at: http://www.w3.org/Submission/2005/10/

Hendler, J., 2001. Agents and the Semantic Web. IEEE Intelligent Systems, 16(2): 30-37, March/April 2001.

Gómez, J. M., Rico-Almodóvar, M., García-Sánchez, F., Martínez-Bejar, R. & Bussler, C., 2004. GODO: Goal-driven Orchestration for Semantic Web Services. WSMO Implementation Workshop, September 2004.

Jain, K. Bolle, R. et al. Biometrics, 1999: Personal Identification in Networked Society. Kulwer Academic. 1999.

Jain R. and J. Quian, 2001: Information Fusion in Biometrics. Proc. 3rd International Conference on Audio and Video Based Person Authentication (AVBPA) pp. 354-391,Sweden, 2001.

Gibbins, N., Harris, S., Shadbolt, N., 2003. Agent-based Semantic Web Services. In Proc. of the 12th Int. World Wide Web Conference, May 2003.

Gandon, F. and Sadeh, N., 2004. Semantic Web Technologies to Reconcile Privacy and Context Awareness. Web Semantics Journal, 1(3), 2004.

Ming, A. Ma, H., 2007. An Algorithm Tested for the Biometrics Grid. Proceedings of the Second International Conference in Grid and Pervasive Computing (GPC07). Paris, France. 2007.

Mansfield, J. Wayman, J.L., 2002. Best Practices in Testing and Reporting Performance of Biometric Devices. National Physics Lab for Mathematics and Scientific Computing. 2002.

Kittler, J. Hatef, R. Matas, J. G., 1998. On Combining Classifiers. IEEE Transactions on PAMI, vol. 12 (1998). Pp. 226-339.

RESURE
Wireless Sensor Network for Health–Care Monitoring

Enrique A. Vargas Cabral, Vicente A. Gonzalez and Jean A. Guevara
Departamento de Electrónica e Informática, Facultad de Ciencias y Tecnología
Univ. Católica, Campus Univ.–Tte. Cantalupi y Villalon, Asunción, -Paraguay
evargas@uca.edu.py, vgonzale@uca.edu.py, jean_guevara@uca.edu.py

Keywords: Wireless Personal Area Network (WPAN), IEEE 802.15.4, Zigbee, Medical Care, Physiological signals.

Abstract: This work presents a sensor system to monitoring a patient vital signs remotely. The proposed sensor network architecture is based on IEEE 802.15.4 PAN technology with start topology. An experimental set-up was implemented including the development of some biological sensors. In the implementation stage we use Xbee modules, the remote sensors was configured as RFD devices and the network coordinator as FFD device. As central device a smart phone was used. From the results, we conclude that the IEEE 802.15.4 technology is appropriate for medical WPAN sensor network implementation.

1 INTRODUCTION

The World Health Organization (WHO) estimates that by the year 2025, more than 1,000 million people will be older than 60 years (WHO, 2004), in other words, the average age of the world-wide population is increasing. Normally, the aging comes accompanied by non-transmissible chronic diseases, such as cardiovascular disease and others that need a continuous monitoring. This scenario presents many challenges to modern societies; one of them is the design of sensor systems that can continuously record physiological variables, from these variables the health of the people can be inferred (Woodward and Rasid, 2003).

Nowadays, the technological advances in microelectronics and instrumentation ease the development of sophisticated, small size, low power consumption and relative low cost monitoring systems. In addition, the WPAN technology allows easy and fast interconnection of different kind of elements, i.e. earpieces for mobile phones, video, camera, audio reproducer, computers, etc. Therefore, the new technologies offer the possibility of transmitting physiological signs for processing or visualization devices (PCs, PDAs, screen, etc.) or to processing center without limiting the patient mobility (Rodríguez, J. et al., 2005). Due to medical and economical reasons, shorter periods of inpatient stay are desirable. Patients' monitoring at home environments is one of the most attractive areas for WPAN applications (Karl and Willig, 2005), because this technology can enable seamless connectivity in hospital and home environment. A WPAN central device can be implemented as a wristwatch or a small belt-worn box.The device could be able to communicate with the hospital monitoring system using the home network access points via wireless indoor communication systems like WLAN, DECT or Bluetooth. WPAN monitoring is also adequate for patients with chronic diseases such as diabetes, asthma and cardiovascular diseases. The employing of WPAN in the patient' home is useful for rehabilitation and post operational care. A central WPAN device with modules for accessing global wireless networks like GSM or UMTS can provide potentially worldwide mobility for WPAN users (Istepanian, R. et al., 2001). Summarizing, we can say that quality of life can be significantly improved.

2 REQUERIMENTS OF A MEDICAL SENSOR NETWORKS

A medical sensor network design greatly depends on the application and deployment environment. A sensor network designed for ad hoc deployment in an emergency site has very different requirements than one deployed permanently in a hospital. For example, the latter can make use of fixed, wall powered gateway nodes, which provide access to a wired network infrastructure. In general, we can identify seve-

ral characteristics that nearly all medical sensor networks should have (Shnayder, V. et al., 2005).

- **Scalability**: is the capability of a system to increase performance when new nodes are added.
- **Wearable Sensor Networks (WSN)**:Medical applications require very small, lightweight, and wearable sensors. Power consumption in a WSN is important since most or all devices must be battery powered. Replacing or recharging in short intervals will be impractical, so power consumption is of significant concern.
- **Reliable communications**:In medical settings, a great emphasis is placed on data availability, although intermittent packet loss due to interference may be acceptable. However, persistent packet loss would be a problem. Depending on the used sensors, sampling rates may vary between 1 to 1000 Hz or more, placing heavy demands on the wireless channel.
- **Device mobility**:Both patients and caregivers are mobile, requiring that the communication layer adapt rapidly to changes in link quality. For example, if a multihop routing protocol is in use, it should quickly find new routes when a doctor moves from room to room during his rounds.
- **Security**:The security in wireless networks is always of great importance. In sensor networks, it is especially important to have integrity and authentication. Integrity means that data should not be altered or destroyed in its way from the sender to the receiver and the authentication should ensure the identity of the sender and the receiver.
- **Association**:The service used to establish a device's membership in a WPAN. How a WPAN adds a new node is of interest in this kind of networks. As well as how one sensor is associated with the correct output at the central monitor side.
- **Cost**:To be able to compete in the international market it is essential that the components be at the lowest possible price. This is most important when the product shall be mass-produced.

3 SHORT RANGE WIRELESS TECHNOLOGIES

Based on the above mentioned requirements of medical WPAN systems, following the technical characteristics of some wireless technologies are presented, which according to the bibliographical review and our criteria, can be used to design a medical WPAN.

3.1 IEEE 802.15.1 / Bluetooth

The IEEE 802.15.1 standard is derived from the Bluetooth specification (version 1.1). In fact, the IEEE standard has added two clauses to the existing specification; WPAN architecture overview and Service Access Points (SAPs). In other words, the 802.15.1 standard presents a wireless personal area network that utilizes the Bluetooth wireless technology. A PAN is defined as a computer network used for communication among computer devices close to one person. The Bluetooth WPAN operates in the unlicensed 2.4 GHz industrial, scientific and medical (ISM) band. The Bluetooth 1.0 data rates include an asymmetric data rate of 721 kbit/s while permitting 57.6 kbit/s in the return direction; and a symmetric data rate of 432.6 kbit/s (IEEE Standard, 2002).

3.2 IEEE 802.15.4 /Low-Rate WPAN

IEEE 802.15.4 is a standard defined for low-rate (LR) WPANs. A LRWPAN is a simple, low cost communication network that allows wireless connectivity in applications with limited power and relaxed throughput requirements. The main objectives of a LR-WPAN are ease of installation, reliable data transfer, short-range operation, extremely low cost, and a reasonable battery life (IEEE Standard, 2003). Like all IEEE 802 standards, the IEEE 802.15.4 standard encompasses only those layers up to and including portions of the data link layer (DLL). I.e. the standard 802.15.4 defines only the PHY and the medium access layers (MAC). In particular, it defines two PHYs representing three license-free frequency bands that include sixteen channels at 2.4 GHz, ten channels at 902 to 928 MHz, and one channel at 868 to 870 MHz. The maximum data rates for each band are 250 kbps, 40 kbps and 20 kbps, respectively. A WPAN consists of several components; the most basic is the device. There are two different device types, which can participate in an LR-WPAN; a full-function device (FFD) and a reduced-function device (RFD). A FFD can talk to RFDs or other FFDs, while an RFD can talk only to an FFD. An RFD is intended for applications that are extremely simple, such as light switches or passive infrared sensors; they do not have the need to send large amounts of data and may only be associated with a single FFD at a time. Because of that, the RFD can be implemented using minimal hardware resources (Thraning, 2005).

Table 1: Comparison of short–range low power wireless technologies.

	Bluetooth	802.15.4	ZigBee
Data rate(Mbit/s)	1	0.250	0.250
Range(m)	10-100	10-100	10-100
Power supply	Medium	Very low	Low
Security	High	Medium	High
Scalability	7	255	255
Cost	Medium	Very low	Low

3.3 Zigbee

ZigBee was created to address a specific market need for an industrial standard to support automation and remote control applications. The ZigBee Alliance decided to use the IEEE 802.15.4 standard as the Physical layer and Media Access Control sub-layer, while the ZigBee Alliance defines the upper layers. The ZigBee network layer supports multiple network topologies including star, cluster tree, and mesh. The application layer consists of the application support layer (APS), the ZigBee device object (ZDO) and the manufacturer-defined application objects. The APS is responsible for maintaining tables for binding and forwarding messages between bound devices. A binding is the ability to match two devices together based on their services and their needs. The binding include the device discovery, which is the procedure to discover other devices that are operating in the same area (ZigBee Alliance, 2005).

The different IEEE 802.15 standards were designed with different purposes. Bluetooth was designed to replace cabling connections between devices, while 802.15.4 and ZigBee for network sensor targeted to home automation. Therefore, none of them was specifically designed to be used in medical sensor network.

4 PROPOSED ARCHITECTURE FOR THE SENSOR SYSTEM

In the absent of a specific standard, in this work we propose the use of the IEEE 802.15.4 and Zigbee standard as the more adequate solution for medical WPAN sensor networks. Most Bluetooth modules are not appropriate because its power requirement is high for battery-operated devices that cannot be charged or changed regularly. It is also restricted by its scalability capacity; it can only have seven active nodes in one network. 802.15.4 and ZigBee looks like a perfect fit, except for its low data rate. This technology presents low power requirement because the nodes are in sleep mode most of the time.

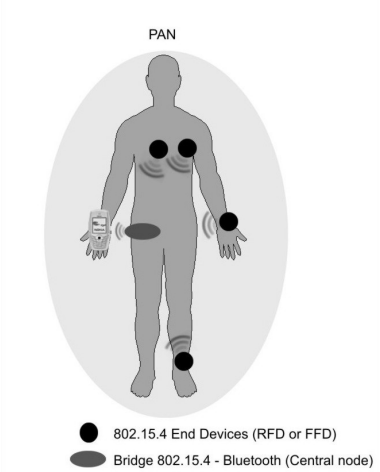

Figure 1: Proposed network architecture for biological signs monitoring.

By using ZigBee mesh topology supports (Thraning, 2005) there is no need of a master node in the WPAN, in this configuration every node/sensor can communicate directly and each node acts as a router. This way a data flow from one node can take multiple routes to its destination, making it very resilient; if a node drops out the flow, it is redirected through other nodes. A routing algorithm is used to ensure that the data takes the fastest possible route.

A drawback of mesh networking is synchronization. Two or more data flows that need to be time synchronized at the receiver may take different routes, resulting in different time delays. If this delay is greater than what is possible to buffer, data lost occur. To overcome the above mentioned problem, in this work we propose the use of IEEE 802.15.4 technology with a star network topology. With respect to power consumption, this technology has suitable characteristics for medical WPAN application since it was originally developed to have low power consumption; i.e. ideally a node should work for months or years without batteries changes. In addition, the standard was developed for the communication between sensors, which reduces its complexity, allowing lower implementation costs than Bluetooth technologies.

5 EXPERIMENTAL SET-UP

In order to validate the proposed network an experimental set-up was implemented, including the development of some biological sensors. Figure 1 presents the proposed network architecture. In the proposed topology the sensors are RFD devices which communicate to a central node, configured as FFD.

5.1 Hardware Components

There are many chips or modules manufacturers' following this standard, including Texas Instruments, Maxstream, FreeScale, among others. In this work, we select an OEM module from Maxstream Company, the XBee. This module has a 100 meters range for outdoor and 30 meters indoor, with a 1 mW of power in antenna, consuming 45 mA in transmission and 50 mA in reception modes. The XBee module uses the MC13193 transceiver chip working in the 2,4GHz frequency band and a MC9S08GB60 microcontroller, both from Freescale. In addition, the microcontroller has 8-channel analog to digital converter with 10 bits resolution and an UART interface (Digi International, 2006).

The WPAN central device is a mobile phone (Nokia 6620), which collects and processes the sensors signals, transmitting them to a central monitoring system through the mobile phone network using SMS and MMS protocols. Due to the novelty of IEEE 802.15.4 technology, the mobile phone does not support this standard, reason why we implemented an IEEE 802.15.4-to-Bluetooth bridge for integrate the phone to the sensor network. The Nokia 6620 was selected because it has Bluetooth interface and runs Symbian operating system, which allows the development of applications in C++ or Java programming languages.

In addition, a cardiac pulse sensor was implemented. Actually, we are developing others biological sensors such as ECG and pulse oximeter.The cardiac pulse sensor is implemented using a piezoelectric transducer that obtains the blood pressure pulse waveform across an artery. The SDT1-028KD PVDF piezoelectric transducer from MSI (Measurement Specialties, 2006) was selected.

The analog circuit for transducer signal conditioning consists basically of a differential charge amplifier which uses three op-amps in the classic instrumentation amplifiers configuration. The differential topology reduces line-noise pickup, which is a problem with high-gain circuits. Besides, an active guard has been used to compensate unbalances in the transducer terminals and a shield around the transducer behaves like a Faraday cage, connected to the active guard. The next amplifiers and filters stages are implemented as single ended devices. In the Figure 2 a simplified schematic of the charge amplifier is shown. The small pulses of charges are integrated and converted to differential voltages pulses at the output of the first stage. The second stage is a differential–to–single–ended amplifier. The gain of the differential stage is given by the ratio between C1 and C2, where C2 corresponds to the equivalent capacitance of piezofilm (Maxim Inc., 2002). The circuit has a good performance, with an S/N ratio of approximately 40 dB.

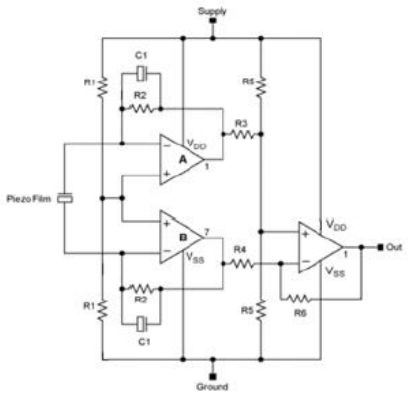

Figure 2: Charge amplifier schematic for the PVDF transducer.

Figure 3: Photo of the sensor node and the smart phone used as the central device.

Figure 3 is a photo of the designed sensor node. It can be seen the Xbee OEM module, the analog signal conditioning circuit for the PVDF transducer and the smart phone used as the central device.

5.2 Software Modules

On the Nokia 6620, both Java and C language can be used for applications development. While both languages are capable of connecting to the Bluetooth stack and communicate via GPRS, SMS or MMS; Java applications are halted if the user receives an incoming call or loads another Java application. Writing code in C language allows our program to continue capturing data from the sensor network in the background regardless of the task the mobile phone is doing on the foreground. The used development environment was the Carbide V1.0 with the Nokia Series 60 SDK 2nd Edition. This platform integrates a phone simulator for debugging purpose. Compiled

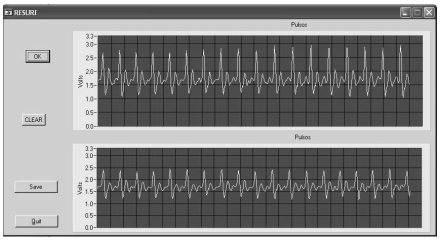

Figure 4: Measurements taken by two cardiac pulse sensors located on two different positions of the neck.

code was packaged into a Symbian .SIS installation file and downloaded to the phone via Bluetooth.

The Figure 4 shows some measurements taken by two cardiac pulse sensors located on two different positions in the neck. The signals are displayed on the screen of a test program developed using LabWindows environment. It can be observed that the shapes of the cardiac pulses are well defined and the signals have good signal–to–noise ratio. If analyzed by a physician, these waveforms could give information about the arteries' state.

6 NETWORK PERFORMANCE ANALYSIS

In order to validate the proposed network architecture performance, we implement two cardiac pulse sensors. From this test bench, we obtain some network parameters and acquired two pressure signals simultaneously from two different positions of the body.

Following, some results are presented:

- **Security**: The 802.15.4 Default Security protocol offers AES encryption with a 128-bit key. However, the use of this feature causes a packet overhead reducing the available bandwidth. That's why, the AES encryption is disable in the carried out experiments.
- **Battery lifetime**: With a 2400 mAh battery and a transmitter consumption of 45 mA with duty cycle of 100% we have a lifetime of 2400 mAh/45mA, approximately 53 hours. The calculation assumption of 100 % duty cycle is not realistic; it could be a lot less in this kind of networks. The question is how often do the sensors need to transmit? To achieve best possible effective data rate it is important to use the largest packet size possible. The Maxstream module can send up to 106 bytes per packet with a maximum 92 bytes payload. Each sample has 10 bit resolution, this means that 46 samples fit in each packet. The sensor, with 500 Hz sampling rate, takes a sample every 2 ms (1/500 Hz). If the sensor does not transmit until the packet is full (46 samples), the sensor transmits every 46*2 ms = 92 ms. Transmitting 106 bytes at 250 kbit/s takes 3.36 ms, to wake up the transmitter from sleep mode takes 2 ms and to access the channel 10 ms. An ACK frame of 11 bytes which takes 0.35 ms to be transmitted. Summarizing, the radio activity time is 2 ms + 10 ms + 3.36 ms + 0.35 ms =15.71ms. Considering that the radio can sleep when it is not in use and if no error occurs, the transmitter is in use during 15.71ms per each 92 ms which gives a 17% duty cycle. Beacon frames from the coordinator, for time synchronization, is not take into account. With the above considerations, the battery lifetime is approximately 2400mAh / (45mAh*0.17) = 313.72 hours. This is an optimistic result; actual battery lifetime will likely be somewhat below this. Also, note that sleep mode current is not taken into account; it is approximately 50 uA and his impact on the battery life will be minimal.
- **Scalability**: With a 500 sampling per second rate and a 10 bit resolution, 5000 bits needs to be transferred each second. Each packet in the network has 14 bytes overhead and 92 bytes payload. The required data rate to transmit 5000 bits per second is ((500/46)*106)*8 9.2 kbits/s; a very low data rate considering the 250 kbits/s bandwidth available between each sensor and the PAN coordinator. Theoretically, up to 25 nodes can be added to the network, but this is not a true number because of the IEEE 802.15.4 medium access control mechanism.

From the above analysis we can conclude that the IEEE 802.15.4 standard is appropriate for medical WPAN sensor network.

7 CONCLUSIONS

In this work a wireless sensor network for medical applications is proposed based on IEEE 802.15.4 standard. To validate the proposal a prototype, composed by two wireless blood pressure sensors, was build.

From the theoretical analysis and experimental tests, we can conclude that the IEEE 802.15.4 standard is appropriate for medical WPAN sensor network with respect to the following performance parameters: battery lifetime, scalability and security.

Actually, we are working on the development of other sensors, specifically an ECG and a oximeter sensors, which will be added as nodes in the WPAN sensors network. Also, we are working on a program

for the mobile device that will analyze the different signals in order to obtain useful information to be presented to the user.

REFERENCES

Digi International (2006). *802.15.4 Protocol-Maxstream (version 1.xAx)*. Digi International, www.maxstream.net.

IEEE Standard (2002). *IEEE Standard for Information technology - Telecommunications and information exchange between systems - Local and metropolitan area networks - Specific requirements Part 15.1: Wireless Medium Access Control (MAC) and Physical Layer (PHY) Specifications for Wireless Personal Area Networks (WPANs)*. IEEE, http://standards.ieee.org/.

IEEE Standard (2003). *IEEE Standard for Information technology - Telecommunications and information exchange between systems - Local and metropolitan area networks - Specific requirements Part 15.1: Wireless Medium Access Control (MAC) and Physical Layer (PHY) Specifications for Wireless Personal Area Networks (WPANs)*. IEEE, http://standards.ieee.org/.

Istepanian, R. et al. (2001). Advances in telemedicine using mobile communications. *Proceedings of the 23rd Annual EMBS International Conference,Istanbul,Turkey*.

Karl, H. and Willig, A. (2005). *Protocols and Architectures for Wireless Sensor Networks*. Wiley.

Maxim Inc. (2002). *Amplifier provides signal conditioning for piezofilm sensor*. Maxim Inc., http://www.maxim.com/.

Measurement Specialties (2006). Sdt shielded piezo sensors element with shielded cable. Technical report, MEASUREMENT SPECIALTIES, www.meas-spec.com.

Rodríguez, J. et al. (2005). Real-time classification of ECGs on a PDA. *IEEE Transactions on information technology in Biomedicine*, 9(1):23–34.

Shnayder, V. et al. (2005). Sensor networks for medical care. Division of Engineering and Applied Sciences TR-08-05, Harvard University. Available at http://www.eecs.harvard.edu/mdw/proj/codeblue.

Thraning, B. M. (2005). *The Impact of ZigBee in a BioMedical Environment*. Agder University College.

WHO (2004). http://www.who.int/mediacentre/news/releases/2004/pr60/es/.

Woodward, B. and Rasid, M. (2003). Wireless telemedicine: The next step? *Proc. of the 4th Annual IEEE Conf. on Information Technology Applications in Biomedicine*.

ZigBee Alliance (2005). *ZigBee Specification (Version 1.0)*. ZigBee Alliance, www.zigbee.org.

A PORTABLE ECG DEVICE IN A HOME CARE ENVIRONMENT USING BURST TRANSMISSION

Emilio M. Bumachar, Rodrigo V. Andreão
Department of Electrical Engineering, Federal University of Espírito Santo (UFES)
Av. Fernando Ferrari, s/nº - Goiabeiras CEP 29060-900 – Vitória – ES – Brazil
emiliobumachar@yahoo.com, rodrigo@ele.ufes.br

José G. Pereira-Filho
Department of Informatics, Federal University of Espírito Santo (UFES)
Av. Fernando Ferrari, s/nº - Goiabeiras CEP 29060-900 – Vitória – ES – Brazil
zegonc@inf.ufes.br

Keywords: ECG, electrocardiogram, home care, home monitoring, microcontroller, telemedicine, wireless.

Abstract: This article presents a wireless microcontrolled system for ECG home monitoring. The main particularity of the system is related to the data transmission strategy, which is intermittent to save battery power. In order to evaluate the potential of the strategy proposed to diminish power consumption, a comparison of the transmission time spent is made between a theoretical estimation and the experiments.

1 INTRODUCTION

Chronic heart patients need continuous monitoring due to the probability of a new event occurring that is harmful to their health. These patients could have better chances of recovery, mainly for psychological reasons, if they were able to be monitored at home instead of in a hospital. Also, the number of patients hospitalized could be reduced without affecting the quality of the medical care.

In that context, it is important to create conditions to allow for safe, efficient and reliable home monitoring, reducing costs and restrictions to the patient's activity and comfort.

Home monitoring is viable in the current technological environment. Even though transmission failure must still be addressed, current wireless technology allows for increasingly reliable links. Moreover, size, cost and power consumption of electronic components are lower than ever.

There are several applications for monitoring systems with wearable medical sensors. (Reisner, Shaltis and McCombie, 2004). Home patient monitoring is one of them. Different approaches have been proposed, such as: sending the data through the phone network using mobile phones (Istepanian, Woodward and Richards, 2001), (Boquete, Bravo, Barea, Ascariz and Martín, 2005); providing a terminal for the patient themselves to view data and register events (Segura-Juaréz, Cuesta-Frau, Samblas-Pena and Aboy, 2004); transmitting data through the Web (Fensli, Gunnarson and Gundersen, 2005); allowing direct use by nearby medical staff (Paim, Correa and Marques, 2004).

Existing works using wireless transmission keep the transceiver on all the time. This practice does not take advantage of the fact that the data being transmitted is usually much less than the data transmission rate.

This work presents a portable device able to acquire and transmit electrocardiogram (ECG) signal using a wireless link through a remote computer. It has been conceived in the context of a project called Telecardio, whose aim is to monitor cardiac patients at home (Andreão, Pereira-Filho and Calvi, 2006).

Our main contribution is related to the data transmission strategy. The data is stored in a memory, and only then the transceiver is activated to send all the data in a burst. This reduces battery consumption, improving the critical features of battery size, weight, and duration. These features are critical because the patients will need to carry the equipment (and the batteries) at all times, and interrupt their routine to change batteries.

2 MONITORING SYSTEM

The proposed device for home ECG monitoring (Bumachar, Andreão and Segatto, 2006) extends battery life by transmitting in bursts. It consists in:

- A battery-powered, microcontrolled acquisition device to be carried by the patient at all times, which pre-amplifies then samples their ECG, stores it and transmits periodically;
- A receiving station that receives the data and does some processing (such as filtering, segmentation and automatic analysis), then retransmits it through the internet;
- A telemonitoring server that can receive the data of several patients, sort it, store it and make it available to authorized parties.

The system is illustrated in Figure 1.

In order to control all these tasks, an algorithm has been developed to be run in the microcontroller, as follows.

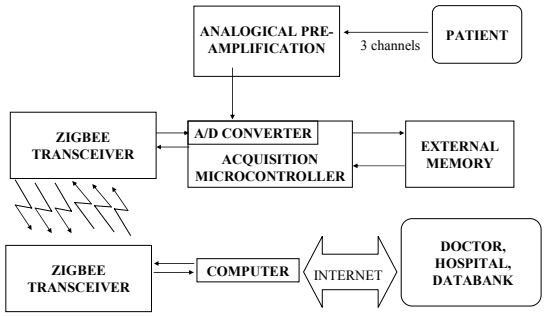

Figure 1: Monitoring system.

2.1 Microcontroller Algorithm

The embedded microcontroller spends most of the time idle, to save power. Every sample period, it is interrupted by an internal timer and samples the three A/D (analog-to-digital conversion) channels, obtaining three 12-bit samples. This data is organized in bytes and stored in internal memory, and then there is a return to inactivity.

This cycle repeats until there are 42 samples, or 63 bytes. Then a 1-byte counter is added as a header, completing a 64-bytes data vector, which is stored in the external memory using the I2C serial interface, freeing the internal memory for further samples.

The microcontroller counts these writing operations to keep track of the amount of data and, therefore, the amount of time stored. When 30 seconds of ECG are completed, the microcontroller wakes the transceiver from its sleep mode, which can take a few milliseconds. If a new data vector is completed in that time, it is properly stored in the external memory.

When the transceiver becomes active, the microcontroller repeatedly attempts to contact the receiving station until receiving an answer. The station can send to the microcontroller a transmit request or a repeat request.

After receiving a transmit request, the microcontroller will read from the external memory the oldest data packet and transmit it; after a repeat request, it will retransmit the last packet. A data packet is defined as 16 data vectors, or 1024 bytes.

While the microcontroller handles the transmission, sampling continues through interruptions, but the microcontroller no longer becomes idle. The internal memory is monitored and its content is transferred to the external memory, unless the later is being read for transmission. To avoid data loss in this situation, the internal memory buffer size is defined with a margin. Similarly, the external memory has a large margin to stand eventual wireless transmission failures.

Finally, after several transmissions, there will be no packets left in the external memory. Then, the microcontroller will answer the next transmission request with an ending request, and the receiving station will send an ending confirmation. The microcontroller will return the transceiver to sleep mode and begin data accumulation again, reinitiating the cycle.

2.2 Prototype

A prototype of the monitoring device was able to sample, packet, store and transmit three channels of pre-amplified signals.

The microcontroller, memory and transceiver used were Analog Devices' ADuC841, Microchip's 24AA515 and MaxStream's XBee respectively.

Despite the non-volatility of the memory being unnecessary, a serial EEPROM memory was selected instead of faster RAM memory because it requires less power – only the EEPROM page being written requires power, whereas RAM consumes power all the time just to maintain data.

Figures 2, 3 and 4 show the prototype.

This prototype works with a single-channel pre-amplifier to raise the very low biometric ECG signal to voltage levels that could be accurately sampled by the microcontroller's A/D converter. Since two other amplifiers are not yet available, the same amplified signal is sampled by all three channels. The amplifier contains lowpass filters and a Right-Drive-Leg terminal (which prevents amplifier saturation).

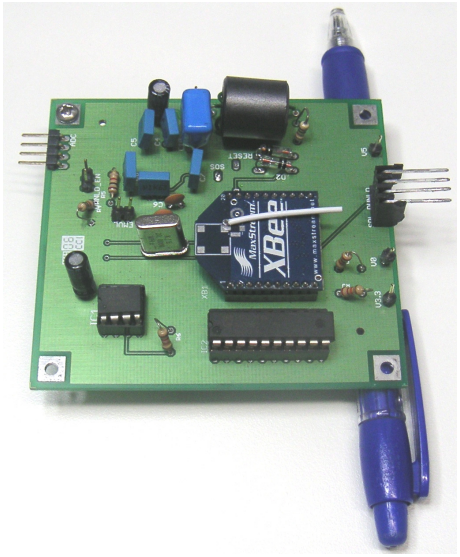

Figure 2: View of side one of the prototype.

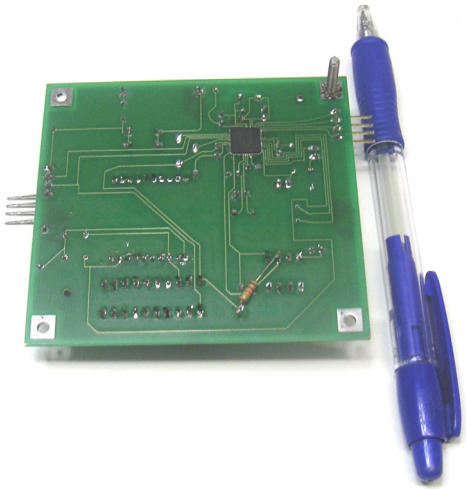

Figure 3: View of side two of the prototype.

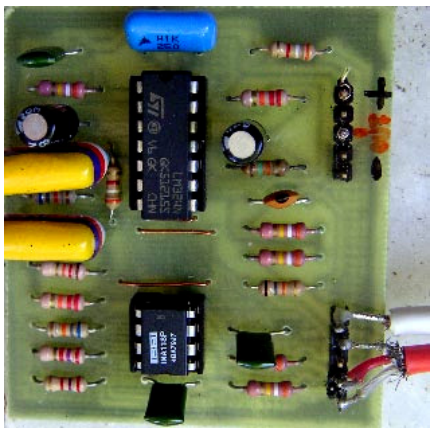

Figure 4: Single-channel amplifier.

3 TRANSMISSION TIME

The data storage time is the duration of each data storage phase, in which the acquisition device does not transmit. It has been fixed at 30 seconds.

The transmission phase lasts the time necessary to transmit all the samples taken during the transmission and storage phases.

There are three interfaces to be considered that can influence the transmission time: the I2C serial interface between the microcontroller and the memory, the UART serial interface between the microcontroller and the transceiver, and the ZigBee rf link between the transceiver and another transceiver at the receiving station.

3.1 Theoretical Minimum

The bottleneck of the transmission, theoretically, is the UART serial interface, with a rate of 115,2 kbps. Disregarding transmission overhead, acknowledgements, and processing delays (such as servicing interrupts), the transmission time will be given by the following equation:

$$T = \frac{30 \times 256 \times 3 \times 12}{115200 - 256 \times 3 \times 12} = 2{,}61 \qquad (1)$$

where 30 is the data storage time in seconds, T is the desired transmission time, 256 is the sampling frequency in Hertz, 3 is the number of A/D channels being sampled, 12 is the number of bits per channel, and 115200 is the bottleneck rate in bits per second. As a result, the desired transmission time T is 2,61 seconds, which corresponds to the transmission phase occurring 8% of the time, as shown in the following equation:

$$TP(\%) = \frac{2{,}61}{30 + 2{,}61} = 8\% \qquad (2)$$

3.2 Experimental Value

The I2C interface was implemented in software on the microcontroller's (master's) side. At first, was assumed that it was not the bottleneck, but it was so inefficient that it became the actual bottleneck, determining the transmission time of 19 seconds. Consequently, I2C interface implementation was improved, by having a timer do some counting previously done by executing useless processor instructions. However, after the I2C improvement, the device stopped functioning properly. Most data

would get through to the receiving station, but not all, at a distance too short for link failure.

The device worked properly when an arbitrary delay was inserted between transfers of each byte from memory to transceiver. This delay was then calibrated to its approximate minimum value that would still allow for proper functioning.

The resulting transmission time was 5,5 seconds. It is more than double the theoretical, ideal value. It corresponds to the transmission occurring 15,5% of the time.

3.3 Discussion

The acquisition device was not able to function with transmission time lower that 5,5 seconds, that is, it did not function properly without deliberate delays that increased the transmission time to 5,5 seconds.

The microcontroller code keeps the I2C interface from getting ahead of the UART interface, that is, the next byte is read from the memory only after the last byte is forwarded to the transceiver.

The UART interface is very much slower than the rf link, and the former shouldn't overwhelm the latter. However, the transceiver was configured not to wait for any number of bytes to form an rf packet, that is, as soon as a byte is received by the UART, it is put in an rf packet with significant overhead. (This configuration is necessary to transmit one-byte control messages used for reliability.) Therefore, if assembling the packet takes too long, perhaps the transceiver's transmission buffer overflows.

At the receiving station's side, the rf link, being faster then the UART interface, could overwhelm it This shouldn't happen since all the data coming through the rf link has passed by the UART interface at the acquisition device. However, non-uniform delays due to rf packet assembling and disassembling could cause the receiving buffer to overflow.

4 CONCLUSIONS

This work presented a wireless microcontrolled solution for an ECG home monitoring system application. It was based in the concept of battery power saving through intermittent data transmission.

It was observed that in practice the transmission time is much higher than the ideal theoretical minimum. Further experimentation is necessary to discover whether it can be reduced.

The use of intermittent data transmission has opened another strategy to reduce battery consumption by setting the power-down modes of the microcontroller and transceiver, but that wasn't achieved with this prototype. For example, if the storage phase power consumption can be ten percent of the transmission phase power consumption, then the total consumption as a percentage of the transmit-all-the-time consumption will be 24%.

Therefore, it is useful to use intermittent transmission instead of transmitting all the time.

ACKNOWLEDGEMENTS

This work is supported by FAPES – Fundação de Apoio à Ciência e Tecnologia do Espírito Santo (30899583/2005), and partially by CNPq.

REFERENCES

Reisner, A., Shaltis, P., McCombie, D., Asada, H., 2004. A Critical Appraisal of Opportunities for Wearable Medical Sensors. In *26th Annual International Conference of the IEEE EMBS*. San Francisco, USA. 2149-2152.

Istepanian, R. S. H., Woodward, B., Richards, C. I., 2001. Advances in Telemedicine Using Mobile Communications. In *23rd Annual EMBS International Conference*. Istambul, Turkey. 3556-3558.

Boquete, L., Bravo, I., Barea, R., Ascariz, J. M. R., Martín, J. L., 2005. Practical Laboratory Project in Telemedicine: Supervision of Electrocardiograms by Mobile Telephony. *IEEE Transactions on Education, vol. 48, no. 2*. 329-336.

Segura-Juárez, J. J., Cuesta-Frau, D., Samblas-Pena, L., Aboy, M., 2004. A Microcontroller-Based Portable Electrocardiograph Recorder. *IEEE Transactions on Biomedical Engineering, vol. 51, no. 9.* 1686-1690.

Fensli, R., Gunnarson, E., Gundersen, T., 2005. A Wearable ECG-recording System for Continuous Arrhythmia Monitoring in a Wireless Tele-Home-Care Situation. In *18th IEEE Symposium on Computer-Based Medical Systems*. 407-412.

Paim, F. C. A., Correa, R. S., Marques, J. L. B., 2004. Proposta de um Sistema de Monitoração de Pacientes em Programas de Reabilitação Cardíaca. In *III CLAEB*. João Pessoa, Brazil. 469-472.

Andreão, R.V., Pereira Filho, J., Calvi, C., 2006. TeleCardio - Telecardiology for Patient Support in Hospital and Domicile Environments (in Portuguese). In X Brazilian Conference in Health Informatics, Florianópolis, Brazil.

Bumachar E. M., Andreão R. V., Segatto M. V., 2006. Wireless ECG Monitoring with Partial Time Transceiver Use. In *SForum.* Ouro Preto, Brazil. 39-40.

SIMULATION TOOLS FOR WIRELESS SENSOR NETWORKS IN MEDICINE

A comparative Study

Paulo A. C. S. Neves
Superior School of Technology, Polytechnic Institute of Castelo Branco, Avenida do Empresário, Castelo Branco, Portugal
pneves@est.ipcb.pt

Joel F. P. Fonseca
Department of Informatics,University of Beira Interior, Rua Marquês D'Avila e Bolama,Covilhã, Portugal
joelfonseca@gmail.com

Joel J. P. C. Rodrigues
Institute of Telecommunications - Networks and Multimedia Group, Portugal
Department of Informatics, University of Beira Interior, Rua Marquês d'Ávila e Bolama, Covilhã, Portugal
joel@ubi.pt

Keywords: Wireless Sensor Networks, Simulation Tools, Medical applications of WSNs.

Abstract: This paper presents a study on three simulation tools for Wireless Sensor Nertworks (WSNs): Network Simulator 2 (ns-2), Java Simulator (J-Sim) and Sensor Network Emulator and Simulator (SENSE). We present the concept of WSNs, each simulator in terms of its features, a view on current applications of WSNs on medicine and a comparative study on the simulators studied. We conclude that SENSE presents the better approach for WSNs.

1 INTRODUCTION

Heart diseases are leading mortality in the United States, and aneurysm is the number one cause of death in Europe. The aging population of developed countries are posing significant weight in the budget of healthcare systems (Istepanian *et al*., 2004).

A Body Sensor Network (Aziz *et al*., 2006) can be used to monitor a patient in real world-life activities. Such network gathers data from several body parts for latter processing and detection of possible heart problems.

On-site patient monitoring leads to efforts in the concept of m-Health: "mobile computing, medical sensor, and communications technologies for health-care" (Istepanian *et al*., 2004).

Wireless Sensor Networks (WSNs) application began in military areas and are spanning into everyday life (Akyldiz *et al*., 2002). A WSN is composed of intelligent mobile sensors that comprise a processing part with memory, the sensing block, a wireless communication transceiver and a power module. The sensor nodes collaborate to gather data to another node, typically with more computational power and communication resources that receive the sensing data (Khemapech *et al.*, 2005). This node is commonly named sink, since it collects (sinks) data, or base station (since it can also send network parameters to the sensor network nodes).

Simulation has always been very popular among network-related research. However, WSNs presents additional challenges, since they are energy constrained, resource constrained and ideally, size constrained. Energy concerns bring communication challenges, since the majority of energy consumption in a node comes from wireless communication.

The rest of the paper is organized as follows. Section 2 shows the studied simulation tools and section 3 includes some applications of WSNs in medicine. Section 4 presents the comparative study and section 5 concludes the paper.

2 SIMULATION TOOLS

This paper studies three of the main simulation tools freely available: the Network Simulation 2 (ns-2, January 2007), the Java Simulator (J-Sim, January 2007, Sobeih *et al*., 2005) and SENSE (SENSE, March 2007).

2.1 Network Simulator 2 (ns-2)

The Network Simulator version 2 (ns-2) was developed in the University of Berkeley, CA, USA, and it is actually the the-facto standard on network simulation in general. The simulator is object-oriented and based in two languages: C++ as the development language and Object Tool Command Language (oTcl) as the simulation description language.

Ns-2 is in constant evolution and worldwide use. Current version is 2.31 released in March 2007 and version 2.32 is still a pending release. Some extensions provide Sensor Network simulation, like the one provided by the Naval research Laboratory.

The two languages approach may step up the learning curve. However, Tool Command Language (Tcl) is very appropriate for writing simulation code, presenting a good learning curve, and C++ provides execution performance.

2.2 Java Simulator (J-Sim)

The Java Simulator (J-Sim), developed by the Ohio State University, USA and is construction is based on the Autonomous Component Architecture.

This simulator also uses two languages, Java and OTcl. J-Sim is component-oriented, so the basic entities are components that communicate with each other via send/receive data through ports. Ports are also components whose behavior is defined by another component named contract.

J-Sim also provides a script interface that allows integration with different script languages such as Perl, Tcl or Python. Furthermore, a friendly and appropriate graphical interface for simulation results, although the graphical interface leaves something to desire. J-Sim provides a model to simulate WSNs, as depicted in Figure 1. We clearly define the nodes that will stimulate de WSN (target nodes), the nodes that will constitute the sensor network itself (sensor nodes), and the sink nodes (also known as base stations). As with any simulation, we clearly need to know simulation parameters.

Target nodes have only one communication channel, the sensor channel, since they only send stimulus to the sensor network, the sensor nodes communicate in two ways, sensor and wireless channel, and finally the sink nodes only communicate in the wireless channel.

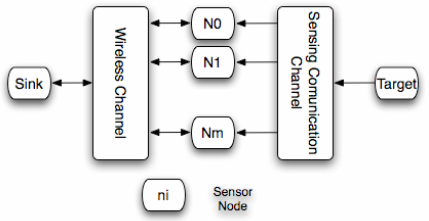

Figure 1: J-Sim simulation model for sensor networks.

2.3 Sensor Network Simulator and Emulator (SENSE)

Sensor Network Simulator and Emulator (SENSE) is the only simulator of the three that was specifically designed for sensor network simulation (SENSE, March 2007).

This simulator presents a component-based approach, created as a template class that allows the use of the component with different kinds of data. SENSE is still in an early stage of development. When trying to use the simulator we found some issues that were gladly solved by the developers. This simulator provides three user types: high level, network designers and component designers.

A component in SENSE communicates through ports: this model frees the simulator from interdependency. This also enables extensibility, reusability and scalability. Component extension in functionality is possible if the interface is compatible and no inheritance between components is used.

SENSE only uses C++ language and the interface only uses text, and the results are provided in a text file. This contributes to the efficient use of computational power, but greatly reduces the perceived user-friendliness.

SENSE requires that all nodes are identical. A common simulation engine stores the event queues of the system. SENSE compares the received signal strength with a threshold and decides if the packet has reached its destination.

3 MEDICAL APPLICATIONS OF WSNS

The use of intelligent medical monitoring can significantly decrease the number of hospitalizations and nursing visits (Heidenreich *et al*., 1999), by acting as an agent on human's behalf and launch of emergency alerts when appropriate. Human beings don't appreciate a visit to the hospital, even more when after a surgery (Naftalin and Habiba, 2000).

If a given health threat situation can be identified in advance, for instance the risk of an heart attack, measures can be taken to minimize or even suppress the risk. Some studies, namely on ECG (Zhou *et al.*, 2005) data retrieval, provide valuable insight on current health condition of a human being.

Body Sensor Networks usually consist of several implanted or wearable biosensors, such as ECG, EEG, glucose sensors, accelerometers, blood pressure and oxygen saturation sensors, temperature sensors, among others (Huaming and Jindong, 2006).

Medical applications span over different areas, such as heart-related, BSN applications, emergency response applications, asthma monitoring and even human error detection and correction. In (Lin *et al.*, 2006) authors present a solution for two important challenges: the first the discomfort of using a wired data-gathering system; and the achievement of the best path for data to flow in peer-to-peer wireless communication protocols.

A wearable ECG system, based on motes to create a WSN presented in (Taylor and Sharif, 2006), using the tMote Sky developed at Berkley University. In (Huaming and Jindong, 2006) authors used a WSN with BSN-MAC that they developed. A scheme collects context information through sensing and applies it to help detect QRS complex in an ECG. This information provides the means to build a personalized heart diary of a person. In (Lee *et al.*, 2007) authors present a WSN to collect ECG and body temperature. A server inside the hospital wirelessly receives data. Using this approach the patients are always being monitored and the server can process data in order to send alerts to medical staff. This presents great benefits when compared to the patient-initiated alarm.

(Lorincz *et al.*, 2004) present some challenges and opportunities for sensor networks in emergency response and a new architecture for wireless monitoring and tracking. In (Chu *et al.*, 2006), an experimental scenario is presented for patients with asthma or allergic situations, where a person is carrying a GPS-enabled system. A wireless system connects to a dedicated server in order to identify possible hazardous areas in the person's vicinity and issue an alert. In (Ohmura *et al.*, 2006), authors developed a sensor network in a real hospital environment that prevents medical accidents by monitoring nursing activities. The paper describes the design and implementation of the sensor network. Therefore, we can conclude that there is a broad range of applications for WSN in medicine, and that the development of novel sensors and novel ways to build sensors are of primordial importance, together with the wireless communication challenges and node deployment.

4 COMPARATIVE STUDY

Table 1 summarizes the main features of simulation tools ns-2, J-Sim and SENSE. J-Sim proves to be a good match for ns-2, no wonder that many researchers are using it instead of ns-2, mostly due to its ACA architecture. In (Sobeih *et al.*, 2005) a study is presented on the performance of ns-2 compared to J-Sim, so we target our efforts on J-Sim and SENSE.

Table 1: Summary of simulator tools features.

Event	***ns-2***	***J-Sim***	***SENSE***
Instalation	*Hard*	*Easy*	*Medium*
Version for Microsoft® Windows®	*No*	*Yes*	*No*
Popular in scientific and academic's	*Yes*	*Yes*	*No*
Object or component oriented	*Object*	*Comp*	*Comp*
Programming languages	*C++, oTcl*	*Java, oTcl*	*C++*
Learning curve	*Steep*	*Moderate*	*Moderate*
Easy to create only sample simulations	*No*	*No*	*Yes*
WSN simulation	*Extern*	*API*	*Dedicated*
Graphically-driven simulation build	*No*	*Yes*	*No*
Component diversity made to simulate	*Yes*	*Yes*	*No*
Supplies configuration network files	*Yes*	*Yes*	*Yes*
Easy to change a simulation model	*Yes*	*Yes*	*No*
Easy to define a simulation area	*No*	*Yes*	*No*
Easy to define number and position of nodes	*No*	*Yes*	*No*
Easy to create/change a protocol	*No*	*No*	*No*
Steps to run a simulation	*Few*	*Few*	*Some*
Display graphical mode to see simulation parameters	*Yes*	*Yes*	*No*

The first impression is that SENSE is more difficult to use than J-Sim: the "text-only" results, the C++ programming language for simulation creation and no graphical support.

We tried to simulate the sample WSN depicted in Figure 2 in J-Sim. On SENSE we managed to simulate a 11 nodes network, but not the same one.

It was not possible to simulate the same network in SENSE. In terms of battery the model Linear Battery was used, cpu base model for CPU, in the physical layer duplex transceiver was used, in the network layer a shr_ack and cbr in the application layer.

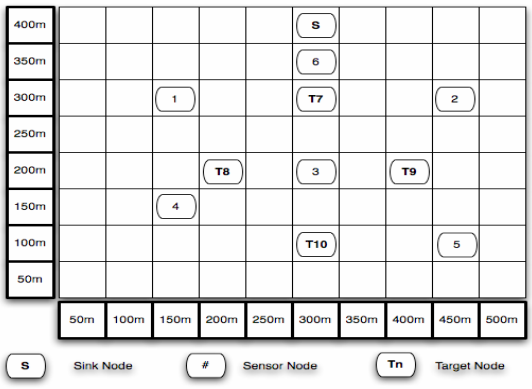

Figure 2: Simulated network node placement.

5 CONCLUSIONS

We provide some insight on three simulation tools used for simulating WSNs. The application on WSNs to medicine seems a very promising way to go, with clear benefits to users and medical staff.

Simulation rises as a good tool for early study of applications of WSNs in medicine, mainly if a given network is to be used and can be simulated.

In spite of a large user community and more experience on the J-Sim, we consider the SENSE simulator a better approach. Developed for WSN from scratch, the developing team answered very promptly to our requests and even released a new download to address the identified issues.

ACKNOWLEDGEMENTS

Part of this work has been supported by the Group of Networks and Multimedia of the Institute of Telecommunications – Covilhã Lab, Portugal.

REFERENCES

Akyldiz, I. F., Su, W., Sankarasubramaniam, Y. & Cayirci, E. (2002) Wireless Sensor Networks: a Survey. *Computer Networks (Elsevier),* 38**,** 393-422.

Aziz, O., Lo, B., King, R., Darzi, A. & Yang, G.-Z. (2006) Pervasive Body Sensor network: an Approach to Monitoring the Post-operative Surgical Patient. *International Workshop on Wearable and implantable Body Sensor Networks.*

Chu, H.-T., Huang, C.-C., Lian, Z.-H. & Tsai, T. J. P. (2006) A Ubiquitous Warning System for Asthma-Inducement. *IEEE Int. Conf. on Sensor Nets, Ubiquitous and Thrustworthy Computing.* Taiwan.

Heidenreich, P., Ruggerio, C. & Massie, B. (1999) Effect of a Home Monitoring System on Hospitalization and Resource Use for Patients with Heart Failure. *American Heart Journal,* 138**,** 633-640.

Huaming, L. & Jindong, T. (2006) Body Sensor Network Based Context Aware QRS Detection. IN IEEE (Ed.) *Pervasive Health Conference and Workshops.* Innsbruck, Austria, IEEE.

Istepanian, R. S. H., Jovanov, E. & Zhang, Y. T. (2004) Guest Editorial Introduction to the Special Section on M-Health: Beyond Seamless Mobility and Global Wireless Health-Care Connectivity. *IEEE Transactions on Information Technology in Biomedicine,* 8**,** 405-414.

The J-SIM Simulator, http://www.j-sim.org, (cited Jan' 2007).

Khemapech, I., Duncan, I. & Miller, A. (2005) A Survey of Wireless Sensor Networks Technology. IN PEREIRA, M. M. A. R. (Ed.) *6th Annual Postgraduate Symposium on the Convergence of Telecommunications, Networking and Broadcasting.* Liverpool, UK.

Lee, D.-S., Lee, Y.-D., Chung, W.-Y. & Myllyla, R. (2007) Vital Sign Monitoring System with Life Emergency Event Detection Using Wireless Sensor Network. *IEEE Conference on Sensors.* Daegu, Korea.

Lin, J.-L., *et al*. (2006) The Development of Wireless Sensor Network for ECG Monitoring. *28th Annual International Conference of the IEEE, Engineering in Medicine and Biology Society.* New York, NY, USA.

Lorincz, K., Malan, D. J., Fulford-Jones, T. R. F., Nawoj, A., Clavel, A., Shnayder, V., Mainland, G., Welsh, M. & Moulton, S. (2004) Sensor Networks for Emergency Response. *IEEE Pervasive Computing,* 3**,** 16-23.

Naftalin, N. J. & Habiba, M. A. (2000) Keeping Patients out of the Hospital - Patients Like it. *Bmj 2000,* 320**,** 262-263.

NS-2 Networking Simulator, http://www.isi.edu/nsnam/ns/, (cited Jan'2007=

Ohmura, R., Naya, F., Noma, H., Kuwahara, N., Toriyama, T. & Kogure, K. (2006) Practical Design of A Sensor Network for Understanding Nursing Activities. *31st IEEE Conference on Local Computer Networks.* Tampa, Florida, USA.

SENSE - Sensor Network Simulator and Emulator, http://www.ita.cs.rpi.edu/sense/index.html, [cited Mar'2007]

Sobeih, A., *et al*. (2005) J-Sim: A Simulation Environment for Wireless Sensor Networks. *38th Annual Simulation Symposium (ANSS '05).* San Diego, CA, USA.

Taylor, S. A. & Sharif, H. (2006) Wearable Patient Monitoring Application (ECG) using Wireless Sensor Networks. *28th Annual International Conference on the IEEE Engineering in Medicine and Biology Society.* New York, NY, USA.

Zhou, H., Hou, K. M., Ponsonnaille, J., Gineste, L. & Vaulx, C. D. (2005) A Real-Time Continuous Cardiac Arrhythmias Detection System: RECAD. IN IEEE (Ed.) *IEEE Engineering in Medicine and Biology Society.* Shanghai, China.

NONLINEAR MODELLING IN BIOMEDICAL APPLICATIONS USING ANNS

Vančo Litovski and Miona Andrejević Stošović
Faculty of Electronic Engineering, University of Niš, A. Medvedeva 14, 18000 Niš, Serbia
{vanco,miona}@elfak.ni.ac.yu

Keywords: Nonlinear modelling, hearing aid, transducer, artificial neural network.

Abstract: During the design of many biomedical prostheses based on electrical and electronic fundamental actions, simulation is indispensable. It comprises, however, necessity for adequate models to be used. Main difficulties related to the modelling of such devices is their nonlinearity and dynamic behavior. Here we report application of recurrent artificial neural network for modelling of a nonlinear two-terminal circuit equivalent to a specific implantable hearing device. The method is general in the sense that any nonlinear dynamic two-terminal device or circuit may be modelled in the same way. The model generated was successfully used for simulation and optimization of a driver (operational amplifier) - transducer ensemble. That confirms our claim that optimization in the electrical domain should take place in order to achieve best performance of the hearing aid. It is to be contrasted to the optical methods based on surgery frequently used.

1 INTRODUCTION

Most of the prostheses that are used nowadays are based on electrical and/or electronic transducers performing appropriate conversion of electrical signals into movement or vice-versa. Among these are the implantable hearing aids (IHA) that are mounted in the middle ear (Hakansson, 1994) so bypassing the tympanic membrane. As for example that will demonstrate the concepts we intend to implement, Fig. 1a represents a cross section of a part of the ear and the way how the IHA is mounted. This structure is known as floating mass transducer (FMT) (Dietz, T.G., 1997), (Ball G., 1996), (Dazert, S., 2000) as depicted in Fig. 1b. It consists of a solenoid (coil) that produces magnetic field forcing the iron core to move forth-and-back. The movement is limited by rubber balls that become compressed and produce repulsive force to limit the amplitude of the displacement. Note that the chamber is in vacuum to avoid acoustic effects due to air compression and decompression that would arise at the ends of the core. As an alternative to the FMT one may find TICA (totally integrated cochlear amplifier) as described in (Heinrich, B. M., 2005). The proceedings that follow are not restricted to any specific IHA.

The system may be characterized as two-terminal, electro-magneto-mechanical, dynamic, and nonlinear. The dynamic behaviour comes mainly from the coil while much of the nonlinearity comes from the balls (or springs) that are distorted under the pressure force. One can see from Fig. 1a that this device is excited by an electronic circuit - driver - that we here consider is an operational amplifier (OA) situated at the output of the complex electronic system that controls the intensity and the frequency characteristic of the signal coming from the microphone.

When designing such a system we may accept two approaches. One is to consider the electronic circuit as fixed and to optimize the FMT to get the desired performance. In the opposite approach, that will be considered here, we suppose that the FMT has fixed characteristics while the driver is subject to optimization.

To perform this we need electrical model, i.e. voltage-current dependence, of the FMT that will be used in conjunction with the transistor model existing in usual electronic simulator. That will allow for repetitive simulations with output-transistor's features optimized until optimum is reached.

In this paper we propose a new modelling procedure that results in a closed form model of nonlinear dynamic two port devices suitable for simulation application. It is based on implementation of so called recurrent artificial neural networks (ANN). We will also present the results obtained after one step

of driver optimization that represent a serious improvement in the system's high-frequency characteristic.

The paper is organized in the following way. We first discuss the problem of electronic modelling. After that we introduce the ANN for implementation of the black-box modelling concept. Follows the implementation and the results obtained.

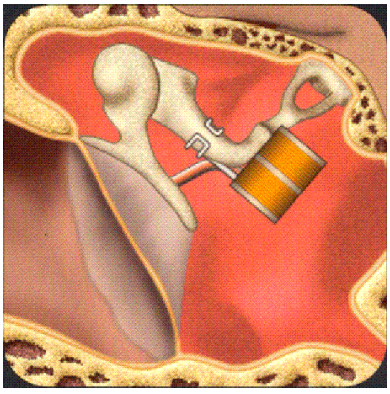
a)

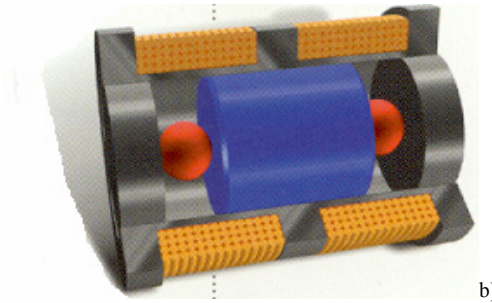
b)

Figure 1: a) Cross section of the ear showing the implant mounted on the incus, and b) the inner structure of the implant. (Photographs taken from Symphonix Devices marketing material).

2 ELECTRONIC DEVICE MODELLING

As mentioned above, we are looking for the current-voltage characteristic of the device under consideration expressed by a set of mathematical expressions. The following difficulties are encountered when generating a model of nonlinear dynamic devices:

- choice of approximation function
- choice of the excitation signal

To achieve this, two approaches are implemented (Chua, L., 1975).

a. Physical approach

To implement this approach one needs to understand physical processes in the component or system. Advantages of this approach are: the procedure is understandable, and there exists the correspondence between the physical and technological quantities and model parameters.

There are no disadvantages of the physical approach, but there is a problem when we do not understand the whole physics of the component, or when we are not aware of all the effects influencing the component including parasitics.

b. *Black box approach*

When using this concept, the characteristics of the modelling object have to be **measured** first, and then approximated using functions that fulfill the requirements imposed by the method for equation formulation implemented within the simulator.

Advantage of the black-box approach is getting a perfect model obtained with no need to fully know and understand the mechanisms behind the component's operation. This method is specially convenient for sensors and actuators modelling, because the price of modelling is very low.

Disadvantages related to this approach are:

- Difficult choice of approximation function (which function is the most convenient?)
- The model application is limited only to the conditions under which the measurement was done, referring to the signals (amplitudes, frequencies, wave forms) and ambient (temperature, brightness and so on).
- A special problem is the choice of the test signals needed for establishing the device properties by measurements.
- There is no correspondence between physical and technological process parameters and model parameters.

Having in mind that the ambient and signal conditions for operation of the transducer under consideration are well established, in order to apply this method, we will need to find appropriate approximants. That will be ANNs.

3 ANNS AND NETWORK MODELLING

Artificial neural network is (Hecht-Nielsen, R., 1989.):

- A set of mutually coupled computational operators with specific topology and computational potential, and
- algorithm for determining the operator coefficients (i.e. learning).

ANNs are considered to be universal approximators, meaning that ANN can interpolate any function

(Scarselli, F., 1998). It is the motive for using ANNs in modelling in black-box approach. They solve one of the basic problems: choice of approximation function. To shorten the explanations we refer to (Hecht-Nielsen, R., 1989) for detailed explanation of the ANN's structure and the properties of the processing elements.

Feed-forward ANNs were successfully used for many modelling applications the first being the modelling of the MOS transistor (Litovski, V., 1992). In (Litovski, V., 1997) a magnet with moving armature was modelled for the first time by ANNs. That, however, having no memory properties, is not convenient for modelling of dynamic circuits and systems. In order to introduce the memory property a structure depicted in Fig. 2 has to be used. It is time a delayed recurrent ANN.

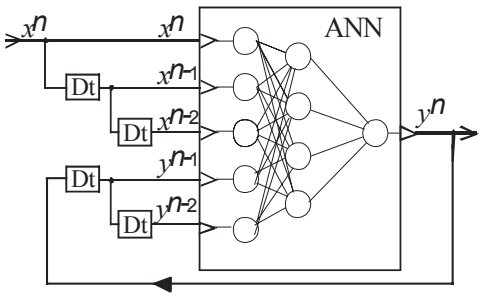

Figure 2: A time delayed recurrent ANN.

The learning procedures for such a network including choice of its complexity may be found in (Bernieri, A., 1994.).

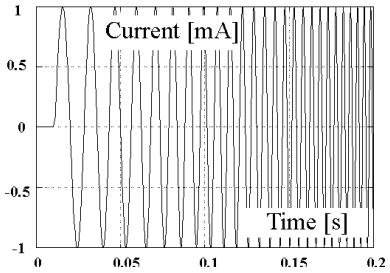

Figure 3: The exciting signal used for modelling.

To capture the dynamic properties of the system to be modelled and its nonlinearities by measurement, we propose the chirp signal depicted in Fig. 3. It is a constant amplitude linearly frequency modulated signal. The frequency interval is to be chosen so that to cover the complete frequency characteristic of the device while the amplitude is supposed to be large enough to capture all relevant nonlinearities.

To create the neural model of the device under consideration, after measurement, samples from the time domain response of the devices are used to train the ANN, as described in (Andrejević, M., 2002) and (Andrejević, M., 2003). After training the ANN is supposed to capture all electrical properties of the device seen from its terminals.

4 IMPLEMENTATION EXAMPLE

In order to demonstrate the method, instead of using a specific device, we propose a nonlinear dynamic electronic circuit (NDEC) as depicted in Fig. 4.

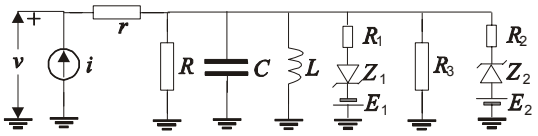

Figure 4: Nonlinear dynamic two terminal circuit.

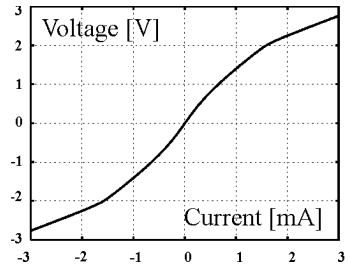

Figure 5: The static characteristic of the NDEC.

Its static characteristic is depicted in Fig. 5, while Fig. 6 represents its response to a chirp signal. After extracting the envelope one obtains the frequency response of the circuit as depicted in Fig. 7.

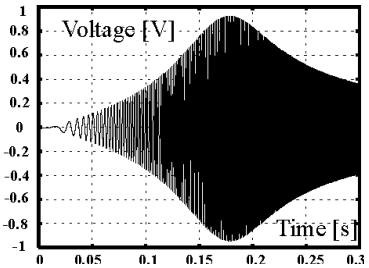

Figure 6: Time domain response of the test circuit.

Samples of the response from Fig. 6 were used to train the ANN in the time domain. Its response after training is exactly the same as the response of the original NDEC and is drawn in Fig. 7 overlapped with the frequency response of the original circuit.

That was used to load an OA supposed to drive the NDEC. The overall response of the driver-transducer ensemble is depicted in Fig. 8. This result is by itself an important one because it shows the ability of simulation of the NDEC in every environment.

To go further we redesigned (only one iteration) the output part of the OA in order to improve the frequency response of the ensemble. The result of the new design is depicted in Fig. 9. representing a full success.

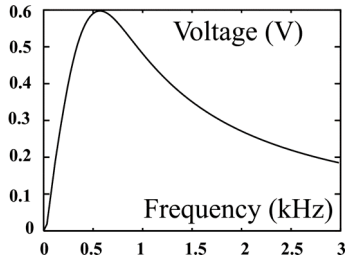

Figure 7: Frequency characteristic of the element being modelled (envelope of the time response), and Frequency characteristic of the model.

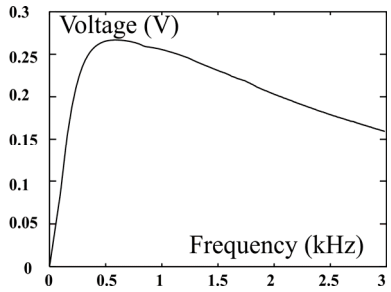

Figure 8: Frequency characteristic of the response of the OA loaded by the NDEC.

5 CONCLUSIONS

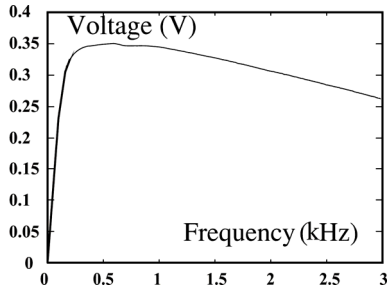

Figure 9: Frequency characteristic of the improved OA loaded by the NDEC.

A procedure for modelling nonlinear dynamic two-terminal circuits equivalent to IHAs is described. It enables complete characterization of the device and, in the same time, simulation and optimization of the driving circuitry. That, we consider, is more effective way for characterization of the device in comparison with optical methods, not to mention the optimization possibilities.

REFERENCES

Andrejević, M., Litovski, V., 2002. Non-Linear Dynamic Network Modelling Using Neural Networks, *Int. Congress on Comp. and Appl. Math.*, Leuven, pp. 16.

Andrejević, M., Litovski, V., 2003. Electronic Modelling using ANNs For Analogue and Mixed-Mode Behavioral Simulation, *Journal of Automatic Control*, University of Belgrade, Vol. 13, No. 1, pp. 31-37.

Ball G, Maxfield B., 1996. Floating mass transducer for middle ear applications. *Sec. Int. Symp Electr Impl*, Goeteborg, pp. 8.

Bernieri, A., et all., 1994. A Neural Network Approach for Identification and Fault Diagnosis on Dynamic Systems, *IEEE Trans. on Instrumentation and Measurement*, Vol. 43, No. 6.

Chua, L.O., and Lin, P.M., 1975. *Computer-Aided Analysis of Electronic circuits*, Prentice-Hall, New Jersey.

Dazert, S., et all., 2000. Das Mittelohrimplantat „Vibrant Soundbridge" zur Hörrehabilitation bei sensorischer Schwerhörigkeit**,** *Otologie, Laryngorhinootologie,* Vol. 79, pp. 459-464.

Dietz, T.G. Ball, G.R. Katz, B.H., 1997. **"**Partially implantable vibrating ossicular prosthesis", *Int. Conf. on Solid State Sensors and Actuators, Transducers '97,* Chicago*,* Vol. 1, pp. 433-436.

Hakansson, B. E., et all., 1994. "The bone-anchored hearing aid: principal design and audiometric results", *Ear-Nose-Throat J.*, Vol. 73, No. 9, pp. 670-675

Hecht-Nielsen, R., 1989. *Neurocomputing,* Addison-Wesley Publishing Company, Reading, MA.

Heinrich, B. M., 2005. *Evaluation eines VR (Virtuelle Realität)-Systems zur Ctbasierten Operationsplanung an der lateralen Schädelbasis*, Inaugural-Diss. zur Erlangung des Doktorgrades, Medizinischen Fakultät der Eberhard-Karls-Universität zu Tübingen.

Litovski, V.B. et all., 1992. MOS transistor modelling using neural network", *Electronics Letters*, Vol. 28, No.18, pp. 1766-1768

Litovski, V.B. , Mrčarica, Ž., and Ilić, T. , 1997. Simulation of non-linear magnetic circuits modelled using artificial neural network", *Simulation practice and Theory*, Vol. 5, pp. 553-570.

Scarselli, F., Tsoi, A.C., 1998. Universal Approximation Using Feedforward Neural Networks: A Survey of Some Existing Methods, and Some New Results, *Neural Networks*, Elsevier Science, Vol. 11, No. 1, pp 15-37.

A SIMPLE DEVICE TO MEASURE GAZE ANGLES IN VISUAL TASK ANALYSES

A. Page, B. Mateo, J. Garrido-Jaén, R. Marzo
Instituto de Biomecánica de Valencia, Universidad Politécnica de Valencia, Camino de Vera s/n, 46022 Valencia, Spain
alvaro.page@ibv.upv.es, begona.mateo@ibv.upv.es, david.garrido@ibv.upv.es, raquel.marzo@ibv.upv.es

J. C. Dürsteler, A. Giménez, C. Prieto
Indústrias de Óptica, S.A. (INDO). Alcalde Barnils, 72. 08174 Sant Cugat del Vallès, Barcelona, Spain
dus@indo.es, antonia@indo.es, c.prieto@indo.es

Keywords: Optometry, Visual strategy, Head Movements, Eye tracking, Progressive Addition Lenses.

Abstract: This paper presents a simple device to measure visual maps and head motion to analyze the visual strategy in optometric applications. Instead of using the common approach of conventional eye trackers based on continuous pupil–corneal reflection detection, a simple method based on photogrammetry is proposed. This method only measures the head movements, the gaze direction and the visual map can be calculated on the hypothesis that subjects' gaze follows a known visual stimulus accurately.
In order to validate this hypothesis, an experiment has been carried out to calculate the subject's accuracy when tracking the stimulus. The gaze direction was measured both with conventional eye tracking and with the proposed technique and the measured gaze angles were compared. The results show that the subjects effectively follow the stimulus during the task and thus the main hypothesis of the proposed system is confirmed. Therefore, the analysis of head movement can supply an indirect estimation of the visual angles that is as accurate as the measures obtained with more complex devices.

1 INTRODUCTION

Visual strategy can be defined as the coordination of eyes and head movements in order to perform a visual task. The study of visual strategy has received some interest from fields as diverse as neuroscience and psychophysics, customer behaviour analysis and advertising, ergonomics, sports or lenses design and optometry.

Techniques of eye-tracking have been used for a long time in the fields of psychophysics and neuroscience. Richardson and Spivey have published a complete survey about the main research areas in these fields (Richardson and Spivey, 2004[a]; Richardson and Spivey, 2004[b]). The analysis of visual strategies can also provide information about the consumer behaviour and thus help to identify factors that determine the attention allocated to different advertisements (Treistman and Gregg, 1979; Lohse, 1997).

In the ergonomics scope, research on visual strategy is mainly focused on the study of the visual demands of different tasks in order to improve the workplace design and task performance (Engström et al. 2005). Other applications are related to the design of technical aids for disabled people, such as control systems based on eye-gaze tracking (Sesin et al. 2003). The visual strategy is particularly important in the study of some complex tasks in sports such as ball sports or boxing, in which a player needs to determine the future trajectory of the ball (or hand). Thus, several studies have been carried out to analyze the influence of visual strategy on the subject skills (Ripoll et al. 1995; Land and McLeod, 2000).

The use of eye movement analysis in the field of optometry is more recent and its applications seem promising. Monitoring visual performance can help to quantify the state of the ocular motor system and provide valuable diagnosis and management support (Abadi, 2006). Besides, visual strategies analyses are the basis of some aspects of corrective lenses design, especially to assess the comfort of progressive addition lenses (PALs) wearers. Some studies in this field have been performed to understand the differences of users' behaviour when using different

PAL designs or single vision lenses (Selenow et al. 2002; Han et al. 2003; Hutchings et al. 2007).

Several techniques have been used for measuring eye movement as well as for characterizing visual strategies. Morimoto and Mimica (Morimoto and Mimica, 2005) present a good survey of techniques for eyes gaze tracking. The most widely used are based on the automatic detection of the pupil-corneal reflection. The eye is illuminated by a distant, low-power, infra-red light source, and this creates an image that is seen as a highlight spot on the surface of the cornea. The image is analysed by a computer, which calculates the centre of the corneal reflection as well as the centre of the pupil. The distance from the pupil centre to the corneal reflection is proportional to eye rotation, and thereby provides an estimation of the gaze direction. Since the eye position varies as the head moves, the head should remain still during the measurement; otherwise the movement of the head must be measured in order to transform the relative direction of gaze into absolute directions to the visual targets.

Then, a complete description of visual strategy needs both gaze direction and head position analysis. Head motion can be accurately measured in real-time by means of a magnetic location system (Hutchings et al. 2007), although these systems are intrusive because a device must be placed on the subject head. There have been some recent attempts to avoid such kind of devices by measuring head movements by means of a 3D face tracking analysis, as proposed in (Beymer and Flickner, 2003).

The systems based on pupil-corneal reflection need some type of calibration to transform the input data (reflections' locations) into absolute gaze directions. A typical calibration procedure presents the user a set of visual targets that the user has to look at while the corresponding measurement is taken. From these measurements a map of correspondences or calibration function can be obtained. Although several models to calibrate the eye tracker systems have been developed, the calibration process is one of the worst problems in current commercial systems. On the one hand, the calibration functions are very sensitive to head motion, which is the cause of the main source of inaccuracy. On the other hand, calibration is a troublesome process that demands controlled environmental conditions. For these reasons some tracking systems are difficult to use and inadequate for applications outside a research laboratory (Schnipke and Todd, 2000).

A strategy to improve the accuracy and simplicity of the systems is to adapt them to specific functions, so that only the precise information is measured in the simplest way. For example, some clinical and optometric applications are focused on the ocular motor performance when the subject performs a specific task with well-known stimuli (Abadi, 2006). This way, the measurement of the absolute gaze direction is unnecessary and the measurement of head movements and relative eyes motion is enough.

The objective of this paper is to describe and validate a new device to measure the relative motion of eyes with the aim of obtaining visual maps. This information could be useful to analyze differences of visual strategies in the design of progressive addition lenses. The device uses video-photogrammetry techniques and it is based on the assumption that only head motion measurement is necessary to estimate eye gaze direction when the target position is known.

In order to validate this proposed technique, an experimental study has been performed in which the subject accuracy when tracking a visual stimulus is calculated. The measures obtained with our device were compared with those a conventional eye tracker. The results show that the measurement of head movement can supply an indirect estimation of the visual angles when the tracked target locations are known and the results are as accurate as the measures obtained with more complex devices.

2 MATERIALS AND METHODS

2.1 General Description of the Equipment

The principle of operation of the proposed technique assumes that a subject can effectively gaze at a mobile target, so that eye gaze direction in relation to the head is determined by knowing both target and head positions, as well as the relative location of eyes with respect to head.

The measurement system consists of a 650 x 500 mm dark screen, which shows a 1 cm illuminated spot that moves along a continuous trajectory. At both sides of the screen, two synchronised video cameras record the subject's head motion. Cameras have a 640 X 480-pixel resolution with a 25 fps recording speed. The cameras are equipped with infrared filtersCameras have been previously calibrated using the DLT algorithm (Abdel-Aziz and Karara, 1971) and lenses distortion corrected by means of the procedure described in (Ahmed and

Farag, 2005). Therefore, it is possible to accurately measure head position and motion. This analysis can be made from the coordinates of some face distinctive points, using well-known image analysis protocols as the Harris corner detector (Hartley, 2004). However, in order to simplify the computations and to allow a real-time analysis, no computational expensive image processing has been used. Thus, the position and motion of head are measured by means of a set of active makers. The markers cluster consists of four infrared leds placed on a diadem that adjusts at the head.

Besides, the system has an infrared light source placed in the middle of the screen to create a corneal reflection that allows detecting eyes' position during the calibration step.

2.2 Measurement Process

The measurement process is performed in two steps: first the measurement of an initial reference position, and then the measurement phase, where visual angle is recorded during the performance of a tracking visual task. In the first step, the subject sits 50 cm in front of the screen. He is asked to adopt a neutral head posture with the gaze direction approximately horizontal. This position is considered as the reference posture. Then measurement system detects the markers' positions and places the target in the middle of the screen at approximately the eyes height. Eyes positions are detected by the corneal reflection produced by infrared light source. The corneal reflection 3D position is automatically measured. Thus, eyes centre position is calculated assuming a spherical shape of the cornea with known radius.

Simultaneously, markers' positions are determined and a local reference system linked to the subject's face is defined. The X axis is traced from left to right eyes. The local coordinate's origin O is placed in the middle point between the eyes. The Z axis is the most vertical axis belonging to the plane perpendicular to X axis which pass throughout O. Finally, the Y axis is defined to make the reference system right-handed.

Therefore, right eye coordinates in the local system are [d/2, 0, 0], where *d* is the subject's interpupilar distance.

Detection of corneal reflection is necessary only at the first step. Once eyes relative positions with respect to the diadem are identified, their position in space can be determined from the head motion, and no more check up is necessary. This fact avoids having to perform high computational cost image processing tasks and allows free head movements.

Figure 1 shows the equipment operating scheme during a tracking test of a moving target. At each instant, the target is located on the screen at a known position, **P**. The subject has moved his head from the reference position to a different one. This movement is defined by translation **t** of the local reference system and by the rotation matrix **R** in relation to the initial reference position. Using **t** and **R**, the eyes' current positions are determined. Specifically, right eye will be placed at point **D**.

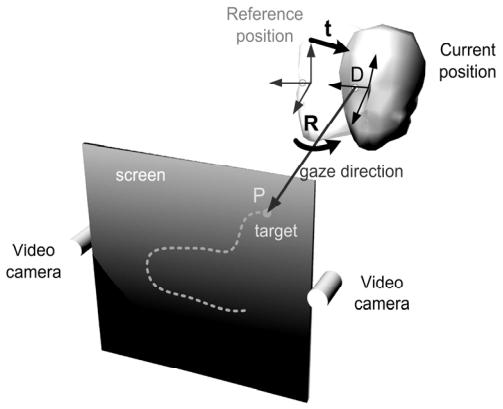

Figure 1: Equipment operating scheme.The subject looks at a mobile target P on the screen. Head position and motion are measured by means of two synchronized videocameras. Gaze direction is estimated from head position, location of P and the relative position of eyes in the head.

Calculation of head position and movement is performed in real time from the diadem's markers' coordinates by using the algorithm described in (Woltring et al., 1994). This algorithm allows obtaining rotation matrix **R** and translation vector **t**Assuming that a person tracks the target, actual gaze direction is given by vector **DP** (Figure 1) which can be calculated in the absolute reference system. If this vector is expressed in the local reference system, then the horizontal angle is calculated as the angle that forms the **DP** projection on the Z=0 plane with the local axis Y, whereas the vertical angle is the one formed by **DP** line with the Z=0 plane.

2.3 Equipment Accuracy Random Instrumental Errors

The measurement of vision angles has two main sources of error. First, the instrumental errors

associated to 3D reconstruction process and head movement measurement. Second, the error due to the subject's gaze deviation when tracking the target. The latter error is studied in the experiment described below, so this section focuses on instrumental accuracy only.

Measurement errors of the markers' coordinates depend on camera resolution, accuracy of the marker centroid determination, and separation between the cameras (Hartley, 2004). In our system, focal distance is close to 1000 pixels, measurement centroids accuracy is estimated to be 0.3 pixel and photogrammetric system baseline is b = 650 mm. This configuration provides instrumental coordinates' error of around 0.1 mm in X and Z coordinates and close to 0.2 mm in Y direction.

Angular and position errors associated to this coordinates' error estimation can be calculated by means of the procedure described in (Page et al., 2006). For the diadem geometry (four markers in a 15 x 15 cm squared), these errors are about 0.1º. Linear displacement error is less than 0.1 mm. The worst accuracy appears in the location of the eyes centres, where a well-known corneal radius is assumed. Then, an error of around 1 mm can be expected. Nevertheless, this error has little effect on the gaze angle estimation, because of the great distance between subject and screen. So, if this distance is 500 mm, the systematic angle error is less than 0.1º for a gaze angle of 20º. Note that a correct estimation of corneal radius is critical in conventional tracking systems, because angle direction computation depends upon this measure.

In summary, random instrumental errors associated to photogrammetic techniques are really small and they are negligible in relation with subject performance errors due to the subject's gaze deviation when tracking the target. This source of error is studied at the following section.

3 VALIDATION

The device operates on the hypothesis that subjects' gaze follows the target accurately. Consequently, it is possible to calculate the relative gaze direction from the target location and the head movements. Therefore, the validation consisted on evaluating the subject's gaze deviation from the target in a tracking visual task. In order to do it, the measures obtained with the proposed devices were compared with the ones provided by a commercial eye tracker.

Two visual tasks were performed. The first had to aim to estimate the accuracy of the conventional eye tracker. The second consisted on a dynamic task, tracking a moving target, with the aim to quantify the deviation of gaze direction with respect to the actual target location.

Five subjects participated in these experiments.

3.1 Equipment

Eye and head movements were recorded during the tasks using a head mounted eye-tracker (Model 501, ASL Applied Science Laboratories) integrated with a head-tracker, **3SPACE FASTRAK** (Polhemus, Colchester, VT 05446, USA).

The eye-tracker measures the angle of gaze with respect to a calibrated scene in the horizontal and vertical directions. The accuracy reported in the equipment specifications is less than 1 degree and may increase to 2 degrees in the periphery of the visual field.

3.2 Experimental Procedure

The visual tasks were displayed on a 19 inches computer screen. Subjects sat in front of the screen. The distance between monitor and subjects was 50 cm. The monitor height varied depending on the subject to obtain a zero vertical gaze angle when looking at the centre of the screen, point 5 in the calibration scene (Figure 2).

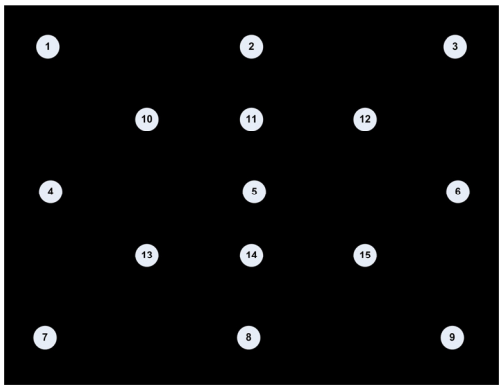

Figure 2: Calibration Scene.

Previous to performing the tasks a calibration process was completed for each user. This calibration consisted on looking at 17 target points located at known positions. During this process the eye tracker records the corneal reflection of the left eye as well as the pupil and head movements.

Once the calibration was carried out, the subjects performed two visual tasks. In the first task (static task) the subjects looked consecutively at each one to 17 target points of the calibration scene during

three seconds while the eye and head position were registered.In the second task (tracking task) subjects were asked to follow with their eyes a moving target onto the 19'' black screen. The target was a red spot moving with a pseudo-random trajectory on the screen during two minutes. The trajectory consisted on a set of concentric circles and radial lines from the centre of the screen with a randomized sequence (see figure 3). The velocity of the point motion was 7 cm/sec (8º/sec gaze angle, approximately). This velocity is similar to the one used to measure the visual maps.

4 RESULTS

The data registered in the static task was used to estimate the accuracy of the eye tracker system as the deviation between the gaze lines and the measured ones by means the eye-tracker.

For each subject, the accuracy of the eye tracker system was quantified as the standard deviation in degrees of the horizontal and vertical eye angle differences between actual and measures lines while performing this static task (Table 1)

Results show that the standard deviations of errors are smaller than 1º in all subjects for horizontal angles, and a bit greater in vertical angle measurements. Mean values of these errors are smaller than 1º. Thus, the calibrated eye tracker fulfils the accuracy specified by the manufacturer.

The eye angular deviation when executing the tracking task was obtained in a similar way. At each time, the theoretical eye line of gaze corresponding to the moving target was calculated and it was compared with actual gaze line measured by the eye-tracker. Vertical and horizontal angle deviations were analyzed.

Table 1: Errors in the static task. These errors quantify the accuracy of the reference conventional eye-tracker.

System Error (standard deviation)		
Subject	Horizontal (º)	Vertical (º)
s1	0.42	0.58
s2	0.51	0.53
s3	0.95	1.52
s4	0.67	0.47
s5	0.57	0.84
Mean	0.65	0.88

Table 2: Errors of the horizontal and vertical angles for the dynamic tracking task.

Tracking error (standard deviation)		
Subject	Horizontal (º)	Vertical (º)
s1	0.53	0.48
s2	0.49	0.61
s3	0.49	0.59
s4	0.56	0.77
s5	0.61	0.70
Mean	0.54	0.64

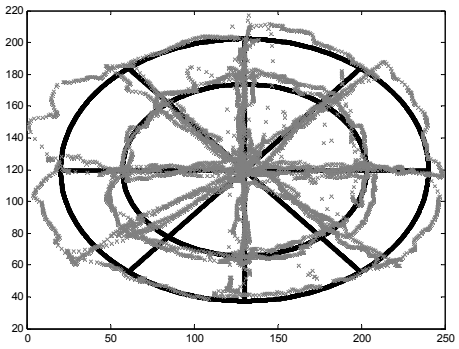

Figure 3: Deviations in tracking task. Black solid line is the trajectory of the target on the screen. Grey markers represent the actual gaze direction.

Figure 3 shows an example of the results in an individual dynamic task. The black solid line represents the actual trajectory of the moving target on the screen. The grey markers represent the intersection of measured gaze line with the screen. This way, the distances between the actual target location and the one obtained from the measured gaze line quantifies the gaze error when executing the task. These distances were normalized as angles (by means of the distance to the screen). The "accuracy" of the tracking task was quantified by the standard deviation of the measured angular deviations for both vertical and horizontal angles.

Table 2 shows the errors for each user as well as the mean of the sample. The errors are smaller than 1º in all cases, both for vertical and horizontal angles. In fact the order of magnitude is the same as the accuracy of the conventional eye-tracker in static calibrated tasks.

Note that the errors measured in the dynamic task have two sources of variance. First, we can expect some instrumental error associated to the accuracy of the eye-tracker device. This error can be estimated by the results obtained in the static task and is quantified in Table 1. Second, the dynamic errors depend on the subjects' ability to effectively follow the moving target. The errors described in table 2 are the associated to both sources.

By comparing the magnitude of static errors (Table 1) and total errors (Table 2), we can see that these errors are similar. Thus, the mean errors in the static tasks are around 0.65º for horizontal angles and around 0.88º for the vertical ones. The errors estimated in the tracking tasks were similar (0.54º and 0.64º, respectively). We can conclude that the subjects effectively follow the moving target during the experiments, in any case within the margin of accuracy of a conventional eye-tracker.

Therefore, the main hypothesis of operation of the proposed system is confirmed: it is possible to measure the relative gaze angles from the movements of the head if the location and motion of the target is known.

5 CONCLUSIONS AND DISCUSSION

Despite the extensive development of the eye tracking techniques, the available commercial devices present some problems, mainly related with a robust recognition of eye characteristics, their sensitivity to head movements and the necessity of previous calibrations. All these factors have influence on the devices' accuracy as well as on the reliability and feasibility of their use in poorly controlled environments.

However, some specific applications in the filed of optometry use only specific information about gaze lines that do not need complex equipment. This is the case of the visual maps measurement, an application of eye-tracking techniques to analyze the user response to progressive addition lenses. In these applications, the use of specifics technologies could avoid the drawbacks of conventional equipments.

In this paper we propose an effective and simple technique for the accurate measurement of the relative gaze angles while executing visual tasks. The system operates on a simple principle: the use of a visual target with controlled location and the measurement of head movements. Determining once the location of the subject's eyes in a reference posture, the estimation of gaze direction is feasible just with head movement measurement.

The use photogrammetric techniques allows a very accurate measurement of these movements, with an instrumental error lower than 0.5º. However, the system reliability depends on the subjects' effectiveness on tracking the target.

The experimental validation with subjects demonstrated accurate target tracking, with an error below the accuracy of the conventional eye-tracker used in the experimentation.

Therefore, the proposed technique permits a simple and robust measurement of the visual maps, with the same accuracy as the measure performed with a complex and expensive equipment.

ACKNOWLEDGEMENTS

This research has been partially supported by the Spanish Ministry of Science and Education Grant DPI2006-14722-C02-01 (A. Page).

REFERENCES

Abadi, R.V. 2006. Vision and eye movements. Clinical and Experimental-Optometry, 89, 2, pp 55-56

Abdel-Aziz, Y. I. and Karara, H. M., 1971. Direct linear transformation from comparator coordinates into object-space coordinates, in Proceedings ASP/UI Symposium on Close-Range Photogrammetry (American Society of Photogrammetry, Falls Church, VA) pp 1-18

Ahmed, M. and Farag, A., 2005. Nonmetric Calibration of Camera Lens Distortion: Differential Method and Robust Estimation. IEEE Transactions on Image Processing, 14, 8, pp 1215-1230

Beymer, D. and Flickner, M., 2003. Eye gaze tracking using an active stereo head, in: Proc. of the IEEE Conference on Computer Vision and Pattern Recognition, II, Madison, WI, pp. 451–458

Engström, J., Johansson, E. and Östlund, J., 2005. Effects of visual and cognitive load in real and simulated motorway driving. Transportation Research: Part F, 8, pp 97-12

Han, Y., Ciuffreda, K. J., Selenow, A. and Ali, S. R., 2003. Dynamic interactions of eye and head movements when reading with single-vision and progressive lenses in a simulated computer-based environment. Invest. Ophthalmol. Vis. Sci. 44, pp 1534–1545

Hartley, R. and Zisserman, A., 2004. "Multiple View Geometry in Computer Vision". Cambridge University Press.

Hutchings, N., Irving, E., Jung, N., Dowling, L. and Wells, K., 2007. Eye and head movement alterations in naïve progressive addition lens wearers. Ophthal. Physiol. Opt., 27, pp 142–153

Land, M.F. and McLeod,,P., 2000. From the eye to actions: how batsmen hit the ball. Nature Neuroscience, 3, pp 1340-1345

Lohse, G.L., 1997. Consumer eye movement patterns on Yellow Pages advertising, Journal of Advertising. 26, 1, pp 61-73

Morimoto, C.H. and Mimica, M.R.M., 2005. Eye gaze tracking techniques for interactive applications. Computer Vision and Image Understanding 98, pp 4–24

Page, A., De Rosario, H., Mata, V., Hoyos, J. and Porcar, R., 2006. Effect of marker cluster design on the accuracy of human movement analysis using stereophotogrammetry. Med Biol Eng Comput. 44, pp 1113-1120

Richardson, D.C. and Spivey, M., 2004a. Eye tracking: Characteristics and methods. In G. Wnek & G. Bowlin (Eds.) Encyclopedia of Biomaterials and Biomedical Engineering, pp.568-572. New York: Marcel Dekker, Inc.

Richardson, D.C. and Spivey, M., 2004b. Eye tracking: Research areas and applications. In G. Wnek & G. Bowlin (Eds.) Encyclopedia of Biomaterials and Biomedical Engineering, pp. 573-582. New York: Marcel Dekker, Inc.

Ripoll, H., Kerlirzin, Y., Stein, J. and Reine, B., 1995. Analysis of information processing, decision making, and visual strategies in complex problem solving sport situations. Human Movement Science, 14, pp 325-349

Selenow, A., Bauer, E. A., Ali, S. R., Spencer, L. W. and Ciuffreda, K. J., 2002. Assessing visual performance with progressive addition lenses. Optom. Vis. Sci. 79, pp 502–505

Sesin, A., Adjouadi, M. and Ayala, M., 2003. A calibrated, real-time eye gaze tracking system as an assistive system for persons with motor disability. 7th world multiconference on systemics, cybernetics and informatics, VI, proceedings, pp 399-404

Schnipke, S.K. and Todd, M.W., 2000. Trials and tribulations of using an eye-tracking system, in: Proc. ACM SIGCHI—Human Factors in Computing Systems Conference, pp. 273–274

Treistman, J. and Gregg, J. P., 1979. Visual, verbal, and sales responses to print ads. Journal of Advertising Research, 19, 4, pp 41-44

Woltring, H.J., Long, K., Osterbauer, P.J. and Fuhr, A.W., 1994. Instantaneous helical axis estimation from 3-D video data in neck kinematics for whiplash diagnostics. Journal of Biomechanics, 27, 12, pp 1415-1432

DEVELOPMENT OF A MULTI-CAMERA CORNEAL TOPOGRAPHER

Using an Embedded Computing Approach

A. Soumelidis, Z. Fazekas
Computer and Automation Research Institute, Budapest, Hungary
{*soumelidis, zfazekas*}*@sztaki.hu*

F. Schipp
Department of Numerical Analysis, Eötvös Loránd University, Budapest, Hungary
schipp@ludens.elte.hu

A. Edelmayer
CONTWARE Research and Development Ltd., Budapest, Hungary
edelmayer@contware.hu

J. Németh, B. Csákány
Department of Ophthalmology, Semmelweis University, Budapest, Hungary
{*nj, cb*}*@szem1.sote.hu*

Keywords: Corneal topography, stereo vision, specular surface reconstruction, partial differential equations, embedded computers.

Abstract: A multi-camera corneal topographer is presented in the paper. Using this topographer, the corneal surface under examination is reconstructed from corneal images taken synchronously by a number of calibrated cameras. The surface reconstruction is achieved by the joint solution of several partial differential equations (PDE's), one PDE for each camera. These PDE's describe the phenomenon of light-reflection for different overlapping regions of the corneal surface. Both algorithmic and implementation issues are covered in the paper.

1 INTRODUCTION

Due to the high refractive power of the human cornea, the knowledge of its detailed topography is of great diagnostic importance. Examination devices, such as keratometers, corneal topographers, and examination methods used in ophthalmology for exploring and measuring these topographies have a relatively long history (Jongsma et al., 1999). Nowadays, the corneal topographers are used in a wide range of ophthalmic examinations. They are used in the diagnostics of corneal diseases, in contact lens selection and fitting, in planning sight-correcting refractive surgical operations, and in their post-operative check-ups just to mention a few (Corbett et al., 1999). Also, dynamic properties – e.g., the average build-up time – of the pre-corneal tear-film can be examined and measured using fast-operation corneal topographers (Németh et al., 2002).

The majority of the measurement methods applied in the presently used corneal topographers rely on the specularity of the pre-corneal tear film that is coating the otherwise non-specular corneal surface. In these topographers, some bright measurement pattern of known and well-defined geometry, e.g., a concentric system of bright and dark rings (Placido rings), is generated and displayed in front of the eye. The reflection of this pattern on the pre-corneal tear film is photographed by one or – in recent topographer arrangements – several cameras. The distorted virtual image, or images taken by the camera are then analysed, and the corneal surface is mathematically reconstructed. Based on this reconstruction, maps showing the topography of corneal surface and its local optical properties (e.g., refractive power map) are computed and displayed.

In case of healthy and regular corneal surfaces, the presently available corneal topographers generally produce good quality corneal snapshots, and based on these, precise and reliable optical power maps are generated.

However, even for healthy and regular surfaces,

a small impurity, or a tiny discontinuity in the pre-corneal tear film can produce a significant and extensive measurement error, if too simplistic measurement patterns, e.g., a Placido ring-system, is used by the topographer device.

1.1 Reconstruction of Specular Surfaces

The mathematical reconstruction of specular surfaces has been an active area of research. Savarese and his co-authors, for example, concentrated on the local reconstruction of specular surfaces. For a given pair of object-point and image point, there are – in general – infinite number of specular surface-patches the could cause a light-ray emitted from the object-point to reach the image-point. In order to find out which of these patches is the real one, it is necessary to gain further information. This information could concern the global shape of the specular surface (e.g, planar, spherical, or a general second-order surface). Sufficient conditions for the uniqueness of the local reconstructions are provided in (Savarese et al., 2004).

Others – such as (Bonfort and Sturm, 2003), (Fleming et al., 2004), (Kickingereder and Donner, 2004) – published methods for global reconstruction of specular surfaces. Each of these methods relies on the smoothness of the surface to be reconstructed and uses several views – i.e., several cameras – to make the unique reconstruction possible.

The unit normal vector of a given specular surface-patch is the same no matter which camera of a multi-camera arrangement looks at it. Although, a normal vector itself cannot be seen, it can be calculated from the reflection of a light-ray at the given surface-patch. For an unknown smooth, convex specular surface – viewed by several cameras – those points are located on, or near to the surface for which the corresponding unit normal vectors – calculated from two or more views – are approximately the same. This observation is the basis of the voxel-carving method suggested by (Bonfort and Sturm, 2003). This method can be used only for those surface-patches that reflect the measurement pattern into more than one camera.

A mathematically more elegant approach was proposed by (Kickingereder and Donner, 2004) for global specular surface recognition. In their approach, the description of light-reflection by a smooth specular surface takes the form of a total differential equation. The partial differential equation-based method proposed in Sect. 2 is to some extent similar to their approach.

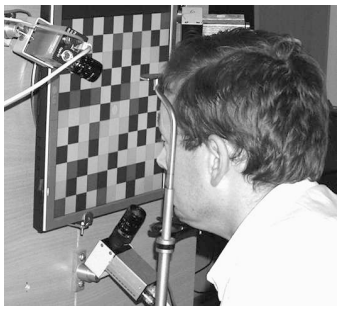

Figure 1: Taking corneal reflection images with the proposed multi-camera corneal topographer arrangement. A special colour-coded measurement pattern is used.

2 THE PROPOSED TOPOGRAPHER ARRANGEMENT AND RECONSTRUCTION METHOD

2.1 The Multi-camera Topographer Arrangement

The proposed corneal topographer arrangement consists of an embedded computer for handling user interactions and multiple camera inputs, generating various measurement patterns and computation; a TFT display that is used for displaying the measurement-pattern; and up to four colour cameras – mounted rigidly on the display – aimed at the patient's eye. A 3-camera arrangement is shown in Fig. 1.

It has been pointed out in the Introduction that a measurement pattern that is more complex and more informative than the frequently used Placido ring-system is required for robust corneal measurements, and particularly for the proper identification of corresponding object and image locations. To this end, the use of various colour-coded measurement patterns were suggested by (Griffin et al., 1992) and (Sicam et al., 2007).

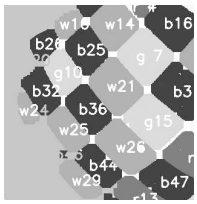

Figure 2: A part of the reflected colour-coded measurement pattern after colour segmentation and labeling.

In Fig. 1, a novel colour-coded measurement pattern – displayed in front of the patient's eye – is shown. It uses four colours, namely, red, green, blue,

and yellow, and ensures the unique identification of a 3-by-3 field-neighbourhood, even if it is rotated and its squares are distorted. In Fig. 2, a part of such a reflected image is shown after colour segmentation, morphological filtering and connected component labelling.

The measurement pattern itself was generated by a backtracking algorithm. Presently, this colour-coded measurement pattern is used in conjunction with a simple black-and-white one that is shown in Fig. 3.

Each of the white circular spots of the latter is placed in the centre of a red, green, blue, or yellow square. The black and white measurement pattern is used for determining the image grid-points with a sub-pixel accuracy, while the colour-coded one is used to ensure robust point-to-point correspondence.

2.2 The Mathematical Reconstruction of the Corneal Surface

Mathematically, the tear-film coated corneal surface is modelled with a smooth, convex surface F. This surface is described and sought in preferably chosen spatial polar-coordinate systems. Each of these polar-coordinate systems corresponds to one of the cameras of the topographer arrangement.

In Fig. 4, one of the mentioned polar coordinate systems is shown. Its origin B is placed in the camera's optical centre and its axis is the optical axis BB' of the camera.

The surface F – that is the corneal surface – is described in the following form:

$$F(x_1,x_2) = S(x_1,x_2)\hat{x} \qquad (\hat{x} = (x_1,x_2,1)^T)$$

Here, $S(x)$ $(x = (x_1,x_2))$ is the distance – measured from B – of the intersection point P defined by the light ray starting from B in direction $\hat{x} = P_xB$ on one hand, and the specular surface F on the other.

The propagation of light from the points of the measurement pattern to the distorted image, i.e., P_yPP_x, is described in the mentioned polar coordinate system. By doing so, a mapping is identified between the points P_y of the measurement pattern and

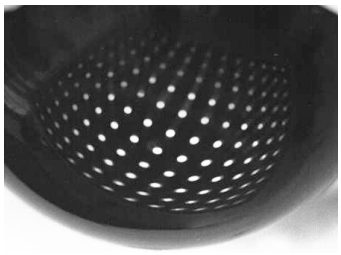

Figure 3: A simple measurement pattern being reflected by an artificial cornea.

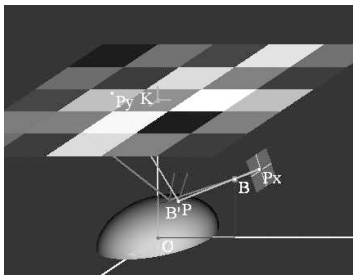

Figure 4: The spatial polar-coordinate system fixed to one of the cameras of the arrangement.

the points P_x of the camera-image. It follows from the conditions prescribed for the mathematical surface – that models the specular corneal surface – that this mapping is one-to-one.

It follows from the physical law of light-reflection, the two-variable function $S(x)$ describing surface F satisfies the following first-order partial differential equation (PDE):

$$\frac{1}{S(x)}\frac{\partial S(x)}{\partial x_j} = \frac{v_j(x) - x_j}{\langle \hat{x}, \hat{x} - v(x)\rangle} \qquad (j = 1,2),$$

where

$$v(x) = |\hat{x}|\frac{k + f(x) - S(x)\hat{x}}{|k + f(x) - S(x)\hat{x}|} \quad ,$$

and function $f(x)$ can be expressed with the inverse of the mentioned $P_y \to P_x$ mapping, that is, with mapping $P_x \to P_y$.

Referring to Fig. 4, $f(x) = KP_y$, where K is the origin of the coordinate system chosen in the plane of the measurement pattern, while $k = OK$ denotes a vector pointing to point K.

In the above PDE $\langle .,. \rangle$ denotes the scalar product of the 3D space.

It follows from the mathematical model described above that surface F can be determined uniquely under the starting condition of $S(0,0) = s_0$, if the $P_y \to P_x$ mapping is known.

A numerical procedure taking discrete values of the mapping $f(x)$ as input has been devised, firstly, to calculate the $P_x \to P_y$ mapping, and secondly, to solve the mentioned partial differential equation for a given

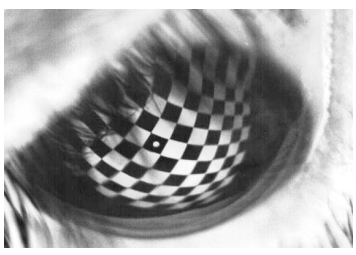

Figure 5: The virtual image of a simple chess board pattern as reflected by a living cornea.

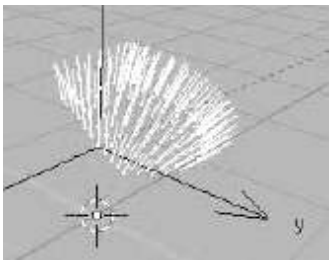

Figure 6: Normals of a surface region reconstructed from one camera view.

camera. In Fig. 6, the reconstructed surface and its normals are shown from a single camera-view.

In simulations carried out for known surfaces, good approximations of the original surfaces and their various curvatures were produced via the mentioned numerical surface reconstruction procedure. From these simulations it has turned out that the surface reconstruction procedure is clearly sensitive to the starting condition s_0, while it is much less sensitive to errors present in the $P_y \rightarrow P_x$ mapping.

In case of a multi-camera arrangement, the solution of the aforementioned PDE must start from a surface-point reflecting the measurement pattern, or more precisely, certain parts of it, to two, or more cameras. Let C_i denote the image of the reflected measurement pattern taken by i-th camera, and F_i the part of the corneal surface actually reflecting the measurement pattern into the i-th camera. The F_i and F_j surface-regions corresponding to the i-th and the j-th cameras of the proposed arrangement usually have overlapping regions. Nevertheless, in few cases, the patient's eye-lids and eye-lashes cover normally overlapping areas that would be important for the accurate surface reconstruction. It can be seen from Fig. 5 that eye-lashes might cause problems as early as the image segmentation stage of the measurement.

An algorithm has been devised that determines the distances of an arbitrarily chosen point of the overlapping surface-region from the i-th and the j-th cameras based on C_i and C_j images. This point and these distances will serve as the starting condition for the i-th and the j-th PDE (corresponding to the i-th and j-th cameras, respectively). After appropriate fitting, the union of the surface-regions will provide the reconstructed surface. Unit normal vectors, and the various curvatures used by the ophthalmologists can be calculated for any surface points.

3 CONCLUSIONS

The majority of the topographers in use, rely on one view only, which is theoretically insufficient for the unique reconstruction of the corneal surface. To overcome this essential measurement deficiency, a multi-camera arrangement is proposed. Several algorithmic and technical means were used to improve detection and surface reconstruction precision. Presently, test measurements are being carried out on artificial and living corneas.

ACKNOWLEDGEMENTS

This research has been partially supported by the National Office for Research and Technology (NORT), Hungary, under NKFP-2/020/04 research contract.

Certain parts of the work presented here were carried out for the Advanced Vehicles and Vehicle Control Knowledge Centre. This Centre is supported by NORT under OMFB-01418/2004 research contract. Both supports are gratefully acknowledged.

REFERENCES

Bonfort, T. and Sturm, P. (2003). Voxel carving for specular surfaces. In *9th IEEE Conference on Computer Vision, Vol. 2*. IEEE.

Corbett, M. C., Rosen, E. S., and O'Brart, D. P. S. (1999). *Corneal topography: principles and practice*. Bmj Publ. Group, London, UK, 1st edition.

Fleming, R. W., Torralba, A., and Adelson, E. H. (2004). Specular reflections and the perception of shape. *Journal of Vision*, (4):798–820.

Griffin, P. M., Narasimhan, S., and Yee, S. R. (1992). Generation of uniquely encoded light patterns for range data acquisition. *Pattern Recognition*, (6):609–616.

Jongsma, F., de Brabander, J., and Hendrikse, F. (1999). Review and classification of corneal topographers. *Lasers in Medical Science*, 14:2–19.

Kickingereder, R. and Donner, K. (2004). Stereo vision on specular surfaces. In *Proceedings of the Fourth IASTED International Conference on Visualization, Imaging, and Image Processing*. IASTED.

Németh, J., Erdélyi, B., Csákány, B., Gáspár, P., Soumelidis, A., Kahlesz, F., and Lang, Z. (2002). High-speed videotopographic measurement of tear film build-up time. *Investigative Ophthalmology and Vision Science*, 43(6):1783–1790.

Savarese, S., Chen, M., and Perona, P. (2004). What do reflections tell us about the shape of a mirror? In *Applied Perception in Graphics and Visualization, ACM SIGGRAPH*. ACM.

Sicam, V. A. D. P., Snellenburg, J. J., van der Heijde, R. G. L., and van Stokkum, I. H. M. (2007). New on-screen surface validation method in corneal topgraphy. In *ARVO Annual Meeting*, page P#3529. ARVO.

CAPILLARY ELECTROPHORESIS ELECTROCHEMICAL DETECTOR WITH NOBLE MICROCHANNEL STRUCTURE FOR MINIATURIZATION

Development of a Capillary Electrophoresis Microchip Format Electrochemical Detector for Endocrine Disruptors Sensing

Kon Ha[1*], Gi-sung Joo[2], Grace Nisola[3], Wook-Jin Chung[3], C. J. Kang[1] and Yong-Sang Kim[1,2]
[1] *Dept. of Nano Science and Engineering, Myongji University, Gyeonggi 449-728, Korea*
[2]*Dept. of Electrical Engineering, Myongji University, Gyeonggi 449-728, Korea*
[3]*Dept. of Environmental Engineering and Biotechnology, Myongji University, Gyeonggi 449-728, Korea*
hakon0919@mju.ac.kr, kys@mju.ac.kr

Keywords: Capillary electrophoresis, Electrochemical detector, Lab-On-a-Chip, Miniaturization, Endocrine disruptors, PDMS, ITO, bisphenol A (BPA).

Abstract: Numerous researches have been focused on capillary electrophoresis (CE) and amperometric detection (AD) using a double-T micro-channel configuration. The combination of these two techniques becomes a powerful analytical tool due to enhanced features in terms of sensitivity and selectivity. The developed CE-AD chip is low cost and requires less power consumption. Its high compatibility with micro-fabrication technology has made it popular for analysis of different compounds. However, due to the need to further miniaturize the CE-AD device, a twisted CE micro-channel configuration is fabricated and tested in this study. Furthermore, enhanced analyte separation due to delayed response time can be achieved using a serpentine CE separation micro-channel. Phenolic compounds were used as testing analytes to confirm the results using different types of running buffers. Also, the data gathered from the new micro-channel configuration is compared with the previously gathered results obtained from double-T separation micro-channels.

1 INTRODUCTION

Established analytical methods require sophisticated equipment in order to obtain accurate and reliable results. However, available apparatuses are bulky, expensive and require sample pre-treatment steps in order to minimize interferences. In lieu of these conventional techniques, the micro-scale lab-on-a-chip (LOC) devices could provide better performances and other benefits. One in particular is analytical cost reduction due to LOC cheaper production, lower reagent volume requirement and shorter analytical time. Though micro-fabrication has become successful to miniaturize capillary electrophoresis amperometric detector (CE-AD) LOC devices, numerous problems are yet to be solved. One of the common predicaments is the poor selectivity of the detector which is related to the unsatisfactory separation at the CE component. Double T configuration has been commonly used in CE microchannels. However, the effective length of a CE microchannel may not be sufficient to complete the separation process or may require longer channel in order to attain an effective separation, which defies the goal of miniaturization. Other ways include proper tuning of separation fields in order to provide an appropriate migration time for different analytes in the sample but this technique could not aid in further miniaturization of the device. Changing the microchannel configuration is another way to resolve separation problem. In this study, a twisted or serpentine CE microchannel configuration is investigated. An LOC device is fabricated with twisted microchannels with equivalent length of the previously reported double T configuration. In a twisted configuration, the size of the device can be further reduced. The influence of the separation field is much less at curved channel regions hence it is expected to have a more effective separation as it slightly increases migration time of different analytes. Interest in the use of polymeric materials such as poly-dimethylsilioxane (PDMS)

and poly-methylmethacrylate (PMMA) has increased over the past few years. PDMS has been widely discussed due to good optical transparency for detection, to cure at low temperatures, easily replicates molding and good adhesion. Many PDMS applications in CE microchip and microfluidic channel design have been reported. This study utilized PDMS as a substrate for formulating the twisted CE microchannel for CE-AD microchip device. As previously reported, a 3-microelectrode system was fabricated on a glass substrate using bare indium tin oxide (ITO) and Prussian blue (PB) as catalyst on the working electrode.

2 EXPERIMENTAL

2.1 Materials and Chemicals

The chemicals used for PB electroplating solution were composed of ferric chloride hexahydrate (97%), potassium ferricyanide (99%), potassium chloride, and hydrochloride acid (32%). The testing analyte bisphenol A (BPA) was supplied by Wako. All of which were diluted to get the desired concentrations. Reagents used for microchannels include Sylgard 184 PDMS from Dow Corning Corp. (Midland, MI, USA). In order to mold PDMS microchannels, negative photoresist SU-8 and XP SU-8 developer from MicroChem Company were used. Throughout the study, deionized water (DIW) was used.

2.2 Microchip Fabrication

Figure 1 shows the simple process flow diagram for the fabrication of the CE/ECD microchip. For the electrodes in CE/ECD system, the ITO layer was deposited on a glass substrate by R.F. magnetron sputtering system. The thickness of the ITO film is 3400 Å. The 1.8 μm thick photoresist (AZ1512) was spin-coated on the ITO-coated glass and patterned for ITO electrodes. The sputter deposited ITO layer was etched with $FeCl_3$/HCl solution. In order to avoid the interference of a high electric field with EC detection, one decoupling-ground electrode as the cathode of CE electric field was positioned in front of the three-electrode electrochemical system.
The PB film was electrodeposited on the working electrode. Electroplating solution is consisted of 20 mM FeCl3, 20 mM $K_3[Fe(CN)_6]$, 0.2 M KCl and 0.1 M HCl. All the PB electrode surfaces were cleaned with acetone and dried with N_2 gas. In order to fabricate microchannels, 40 μm thick photoresist (SU-8) was spin-coated and patterned on the silicon wafer. The height of the positive patterns on the moulding masters, which is equal to the channels depth created on the PDMS layer, was 40 μm when measured with a surface profiler. The PDMS layers were fabricated by pouring a degassed mixture of Sylgard 184 silicone elastomer and curing agent (10:1) onto a molding master, followed by curing for at least 1 hour at 72 °C. The cured PDMS was separated from the mold, and reservoirs were made at the end of each channel using a 3 mm circular punch. The channel width is 80 μm. The double-T injector channel had an offset of 170 μm with 5 cm long separation channels and 1 cm long injection channel. Also, the channel width is 80 μm. The twisted injector channel had an offset of 170 μm with 7 cm long separation channels and 1 cm long injection channel. Before bonding the PDMS layer to ITO-coated glass substrate containing the electrodes, the two components were UV-Ozone exposed to improve their bonding strengths.

2.3 Microchip Configuration

The microchip consists of four reservoirs and micro-channels from PDMS (Fig. 2(a)), three electrodes and electrodes for applying injection / separation electric field on the glass substrate (Fig. 2(b)). The width of the working electrode (W) is 100 μm, 50 μm for reference electrode (R) and 200 μm counter electrode (C). In order to lower noise level, the working electrode is surrounded by the reference electrode.

2.4 CE/ECD Procedure

Each microchannel was preconditioned prior to use. Acetone solution was flushed through the microchannel for about 40 min to clean the microchannels. Next, DIW and buffer solution were flushed through the capillary for an hour respectively. The running buffer solution was 10 mM 2-(N- morpholino) ethanesulfonic acid (MES) fixed to pH 6.5 using 10 N NaOH. After preconditioned, the entire microchannels would be full of buffer solution. For CE process, no bubbles in the capillary were permitted. The testing analytes were injected by applying electric field of + 50 V/cm from sample reservoir to sample waste reservoir. With this process, the testing analytes are placed at the head of the separation channel after about 7 sec and buffer solution is still inside the microchannels. Separation of the analytes was performed by applying electric field of + 60 V/cm between buffer

and detection reservoir. Amperometric detection was performed in a three-electrode configuration. The potential between working and reference electrode was +700 mV DC in case of ECD for PB/ITO electrode and +600 mV DC for bare ITO and Au electrodes. When redox reaction between electrodes and testing analytes happened, peak currents were detected, recorded and stored directly on a computer.

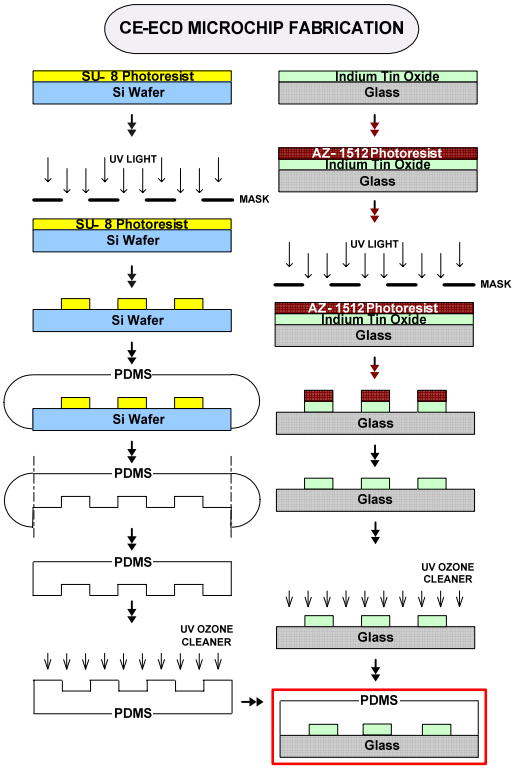

Figure 1: Process flow for the fabrication of the CE/ECD microchip.

3 RESULTS AND DISCUSSION

BPA was used to demonstrate the performance of CE-AD microchip. Measurements were repeated for several times. Figure 3 shows electropherogram of 1 mM BPA and butylphenol mixture by PB/ITO electrode using double-T channel. Figure 4 shows electropherogram of 1 mM BPA by PB/ITO electrode using twisted channel. Especially figure 4 shows reproducibility of BPA detection. At the same flow rates, the transport of ionic species to the working electrode by double-T channel is slightly faster than the twisted channel. Due to the curved corners in twisted channels, the ionic transport rate is slightly decreased. These zones are generally not

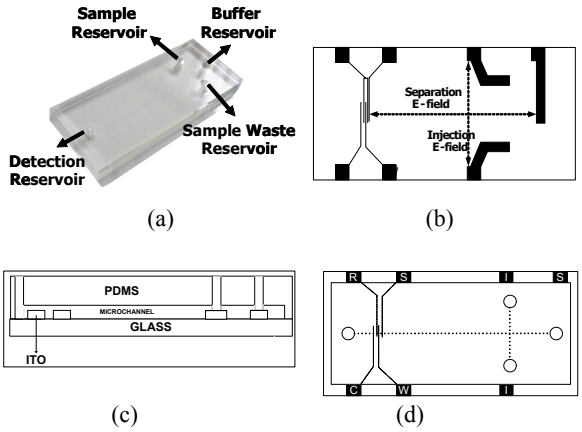

Figure 2: Configuration of (a) PDMS molding containing microchannels and reservoirs and (b) electrodes on the glass substrate. (c) Microchip side view and (d) Microchip top view.

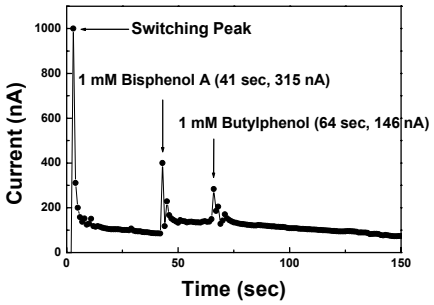

Figure 3: Electropherogram of ECD using double-T channel. Analytes are 1 mM BPA and 1 mM butylphenol mixture. (PB/ITO electrode); Condition: Separation voltage, 300 V; injection time, 7 sec; injection voltage, 60 V; detection voltage, 0.7 V

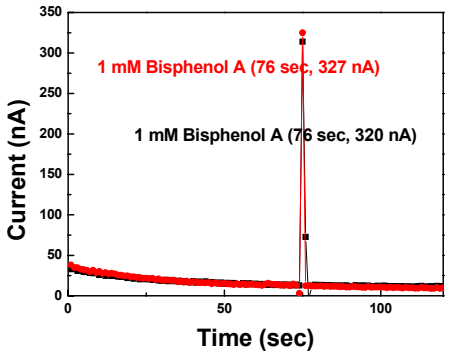

Figure 4: Electropherogram of ECD using twisted channel. Analytes are 1 mM BPA. (PB/ITO electrode); Condition: Separation voltage, 300 V; injection time, 7 sec; injection voltage, 60 V; detection voltage, 0.7 V.

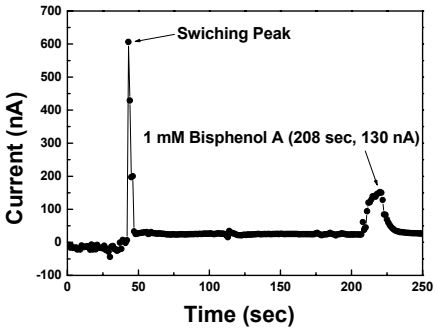

Figure 5: Electropherogram of ECD using sodium-borate buffer (pH 8.5). Analytes are 1 mM BPA. (bare ITO electrode); Condition: Separation voltage, 300 V; injection time, 40 sec; injection voltage, 60 V; detection voltage, 0.6 V.

affected by the separation electric field. The new CE-AD chip is a fused PDMS-glass substrate. With the CE-AD chip using twisted channel, 1 mM BPA was detected. Results revealed that twisted channels are effective to further miniaturize the exiting double-T channel CE-AD chip; it also has a more distinguished selectivity or analyte separation. After a sample injection, the EC detector current rapidly reached its steady-state background level with the pH 6.5 buffer solutions and the BPA was easily separated. The flat baseline and low noise level indicate an effective isolation from the driving voltage. Figure 5 show electropherogram of 1 mM BPA by bare ITO electrode using sodium-borate buffer. CE-AD using basic buffer is slower to flow than CE-AD using acid buffer. Even if working electrode is different, amperometric detector has same channel structure.

4 CONCLUSIONS

The performance of our CE-AD microchip using twisted channel was compared with those of conventional CE-AD microchip using double-T channel. Moreover, our device has several benefits such as fast separation, high sensitivity, and simple fabrication, which makes our CE-AD microchip a good candidate to substitute the conventional CE-AD devices. Our results demonstrate that twisted channel is an effective technique to further reduce the size of the current CE-AD LOC devices.

ACKNOWLEDGEMENTS

This work was supported by grant No. ROA-2006-000-10274-0 from the National Research Laboratory Program of the Korea Science & Engineering Foundation.

REFERENCES

Y. Watabe, K. Hosoya, N. Tanaka, T. Kondo, H. Imai, M. Morita, 2003. “ng/l Level of BPA Determination Existing in Natural Water with HPLC-Electrochemical Detection”, Japan analyst, Vol. 52, pp. 1167-1172

A. D'Antuono, V. C. Dall'Orto, A. L. Balbo, S. Sobral, I. Rezzano, 2001. “Determination of Bisphenol A in Food-Simulating Liquids Using LCED with a Chemically Modified Electrode”, Journal of agricultural and food chemistry, Vol. 49, pp. 1098-1101

J. H. Kim, C. J. Kang and Y. S. Kim, 2004. “A disposable polydimethylsiloxane-based diffuser micropump actuated by piezoelectric-disc”, Microelectronic Engineering, Vol. 71, pp. 119-124

J. H. Kim, C. J. Kang and Y. S. Kim, 2004. “A disposable thermopneumatic-actuated microvalve stacked with PDMS layers and ITO-coated glass”, Microelectronic engineering, Vol. 73/74, pp. 864-869

R. S. Martin, A. J. Gawron, S. M. Lunte, C. S. Henry, 2000. “Dual-Electrode Electrochemical Detection for Poly(dimethylsiloxane)-Fabricated Capillary Electrophoresis Microchips”, Anal.Chem. Vol. 72, pp. 3196–3202

A. J. Gawron, R. S. Martin, S. M. Lunte, 2001. “Fabrication and evaluation of a carbon-based dual-electrode detector for poly(dimethylsiloxane) electrophoresis chips”, Electrophoresis, Vol. 22 , pp. 242-248

J. Wang, M. P. Chatrathi, B. Tian, 2001. “Microseparation Chips for Performing ultienzymatic Dehydrogenase/Oxidase Assays: Simultaneous lectrochemical Measurement of Ethanol and Glucose”, Anal. Chem., Vol. 73, pp. 1296-1300

STUDY OF OXYGEN PLASMA FOR APPLICATION IN STERILIZATION PROCESSES

A. Moreira , T. Pinto
College of Pharmaceutical Sciences, Sao Paulo University, São Paulo, Brazil
adir@lsi.usp.br, tjapinto@usp.br

R. Mansano, N. Ordonez; L. Vilhegas
University of São Paulo Laboratory of Integrated Systems Polytechnic School, University of São Paulo, Brazil
mansano@lsi.usp.br, nordonez@lsi.usp.br

Keywords: Sterilization, Plasma, Microorganisms, contamination.

Abstract: The main objective of this work was to propose a technique of sterilization for medical devices with less exposition time than current plasma techniques, and also determine if this technique can be applied to temperature sensitive materials. Therefore, it was used as biological sensor Bacillus subtilis spores var. niger ATCC 9372 and Bacillus stearothermophilus. For Bacillus subtilis indicators were used two substrates: glass with 2,0 x 107 CFU/substrate of microbial load initial, and paper strips with 3,8 x 10^6 CFU/ substrate of microbial load initial. The efficacy of process was evaluated with the count of survivors and it respective value of decimal reduction (D value). In this work it was used RIE (Reactive Ion Etching). For all processes were used Petri dishes with the sample in triplicates for both microorganisms types. The process parameters was varied as follow: gas flow - 100, 200 and 500 sccm, pressure – 100 and 330 mTorr, RF power – 50, 100 and 150 Watts and the time were of 2 minutes up to 60 minutes. After these processes, we made the count of survivors, in order to evaluate the plasma efficiency as sterilizer agent. Espectrophotometric analysis was made to evaluate the oxygen consumption during all process, and was used a scanning electronic microscope to visualize the plasma effect over microorganisms. With these results it was possible to adapt the process parameters for each type of substrate.

1 INTRODUCTION

Sterilization processes aim at full elimination or destruction of microorganisms (viruses, bacteria, fungi in sporulated or vegetative state) in a certain material to attain an acceptable security level for both patients and operators. Sterilizing methods can be divided into physical, chemical or physical-chemical. Physical processes are e.g. saturated steam/autoclaves, dry heat/ovens, and radiation/gamma rays.

These methods' main problem is the high temperature that can degrade polymeric materials used in catheters and other devices. This limitation affects materials used in endoscopy and a wide variety of plastic and elastomeric materials used in a wide range of clinical, therapeutic and surgical techniques (Holy, 2001).

Plasma sterilization techniques provide a wide range of advantages compared with other methods used, because they can be effective in microbial load, besides working at room temperature and not using toxic gases. They expose materials with microorganisms to reactive species generated by a gas ionization (generally oxygen), using electromagnetic fields (Lerouge, 2000; Oshma, 1997; Hermelin, 1998; Rutala, 1999).

Ideal characteristics for a low temperature sterilization process include the following: high efficiency, fast action, great penetration power, compatibility with the largest number of materials possible, non use or generation of toxic products, efficiency even with organic material, easy adaptation in each environment (hospital and industry), possibility to be monitored and easy operation (Hoefel, 2002).

Considering those items, the best method approaching the ideal is the plasma process; however an effective method using plasma as the main sterilizing element has not been developed.

Current equipment use the plasma step to eliminate toxic residues generated by hydrogen peroxide or peracetic acid sterilization methods, as this plasma step is only performed at the end of the sterilization cycle (Hayakawa, 1998). Hence, there does not exist a specific method to use plasma for an effective sterilization, neither does there exist commercial equipment that allows using this sterilization method (Moisan, 2001).

Furthermore, possible limits regarding aspects of validation are known, be it on the dimensional limits of the sterilization chamber, be it on the configuration of the product. The reasons for these concerns are the homogeneous distribution of the formed plasma and the average lifetime of its constituents, which are known to be unstable.

2 EXPERIMENTAL

Reactive Ion Etching (RIE) system consists of a stainless steel chamber with 330 mm of diameter and 114 mm high. Inside is a 6-inch diameter electrode, which creates the plasma. The electrode is cooled at 20 °C, maintaining a constant temperature during the processes. The Radio Frequency for the generation of the plasma is 13.56 MHz; at this frequency, strong ion bombardment and high electric fields are the typical plasma characteristics.

In order to compare the process results, other sterilization tests were performed in an autoclave, Lutz Ironing, Model 39.211, with 6 kg/h of vapour production, 5 KW of power, and an X-ray Diffraction equipment, model URD6, with a molybdenum tube and a power capacity of up to 1000 W.

The indicators of *B. stearothermophilus*, inoculated on paper, with an initial load of 1 million UFC/ml, were submitted to plasma exposures at the following process conditions: 500 sccm of oxygen flow, 330 mTorr pressure, 100 W power and process times of 5 up to 60 minutes. For the indicators of *B. subtilis*, inoculated on glass plates, the gas flow was 200 sccm, for a pressure of 100 mTorr, and process times of 2 up to 120 minutes. Power levels of 100 W and 150 W were applied for each flow and pressure parameter. For all the processes, oxygen was injected into the chamber for 10 minutes before igniting the plasma, to guarantee that the chamber was full filled with this gas.

The sterilization process in the autoclave was performed for 15 minutes at a temperature of 121 °C.

The sterilization processes using X rays were done during 30 minutes, with power levels of 200, 400, 600, 800 and 1000 W. Finally, the UV processes were performed during 1, 5, 10, 30, 45 and 60 minutes, with an effective lamp power density of 14 mW/cm^2; hence the effective dose, being the effective power multiplied by the exposure time, was varied between 0,84 J/cm² and 50.4 J/cm²

The indicators of *B. stearothermophilus* used in the plasma sterilization processes, were produced on cellulosic strips of 50 mm by 5 mm with loads of 1.0 x 10^6 UFC/strips, and fabricated by the Steris Corporation. The celulosic strips, which support the *B. subtilis*, have dimensions of 40 mm by 3 mm and an initial load of 3.8 x 10^6 UFC/ml, fabricated by 3M. The indicators deposited on the glass plates, with dimensions of 18 mm by 18 mm, have an initial load of 2.0 x 10^7 UFC/glass and were fabricated by the college of Pharmaceutical Sciences of the University of São Paulo.

The procedure of counting the surviving spores was made like follows: first the spores had to be removed through mechanical agitation in test tubes with sterile water; then they were stirred in a bath of water at 70 °C for *B. Suitilis* and 82 °C for *B. Stearothermophilus* during 15 minutes. These samples were then diluted and 1 ml of these dilutions were placed on Petri dishes together with a culture of agar casein soy and placed in an oven. Incubation for the *B. Stearothermophilus* indicators was done at 45 °C during 72 hours and for the *B. Subtilis* indicators at 37 °C during 24 hours.

3 RESULTS AND DISCUSSIONS

Figure 1 shows the results of the RIE sterilization processes, using *B. stearothermophilus* indicators, inoculated on paper. It's possible to observe that after only 7 minutes, there already occurred significant reduction of microbial load. The process was performed in the following way: Petri glass dishes with strips containing *B. stearothermophilus* were placed, without a cover, inside the reactor. The pressure was lowered down to 10^{-3} Torr and the process gas was injected. The process duration varied from 2 to 60 minutes, with power level of 100 W, oxygen pressure of 330mTorr and oxygen flow of 500 sccm.

Figure 2 shows the relation of *B. stearothermophilus* samples before and after suffering an RIE type plasma sterilization process and a comparison with the autoclave sterilization

process. It can be observed that the plasma process is much more aggressive than the autoclave process. Each sample was analysed by scanning electron microscopy. After two minutes of plasma processing, only a few microorganisms could still be found on the paper, and many of those had their morphology modified. After 5 minutes of processing, the concentration of modified spores was higher. After 7 minutes, a lot of spores had been destroyed and the few that remained had a completely changed morphology. After 10 minutes of sterilization, it was very difficult to find any spore; many spores were split into several fragments. These results show that the process is efficient to sterilize these biological indicators. However, it is necessary to be careful with the time of exposure to the plasma, because for times higher than 15 minutes, the cellulose material starts to suffer degradation and it disintegrates completely after 30 minutes of plasma (Moreira, 2003).

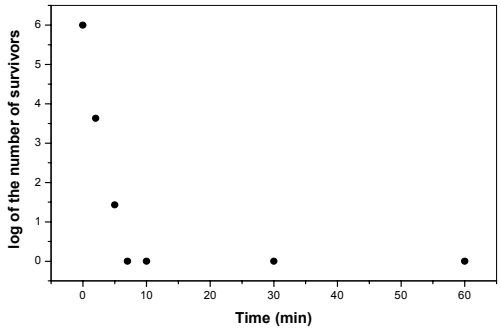

Figure 1: *B. stearothermophilus* exposed to RIE plasma at 330 mTorr pressure, 100 W power and 500 sccm O_2 flow.

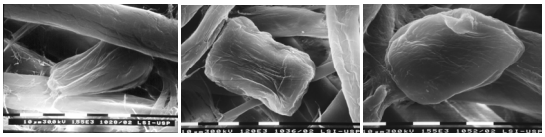

Figure 2: (a)- Spore before exposure to a plasma process; (b)- Spore after a 10-minute exposure to the plasma process; (c)- Spore after exposure to autoclave sterilization.

Figure 3 shows the number of survivors of *B. subtilis* microorganisms (inoculated on glass plates) when exposed to the oxygen plasma process. It can be observed that, after 20 minutes of processing, there is a reasonable decrease in the number of survivors at a power of 100 W, with this number being reduced to zero after around 60 minutes. When 150 W is applied, the microbial load is rapidly reduced, being zeroed out after 20 minutes of processing.

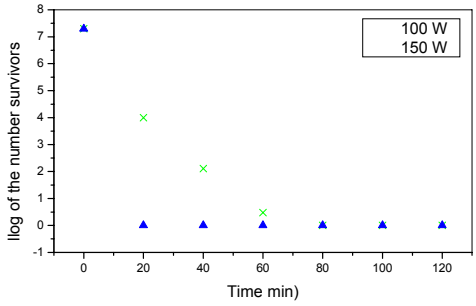

Figure 3.: Graphic of the number of survivors of the indicators *B. subtilis*, inoculated on glass plates and exposed to the plasma process for 2 to 120 minutes, under O_2 flow of 200 sccm and pressure of 100 mTorr.

Figure 4 shows a comparison of *B. subtilis* indicators before and after exposure to the plasma, X-ray and UV processes. When exposed to the X-ray and UV processes, the form of the microbes does not change when compared to it before the application of the processes. These micrographs corroborate the results of the survivor counts in which it was possible to verify the non-reduction of the microbial load. When it is used the oxygen plasma processes, deformation of the microorganisms is observed as well as spaces between them, something that does not happen in the other processes.

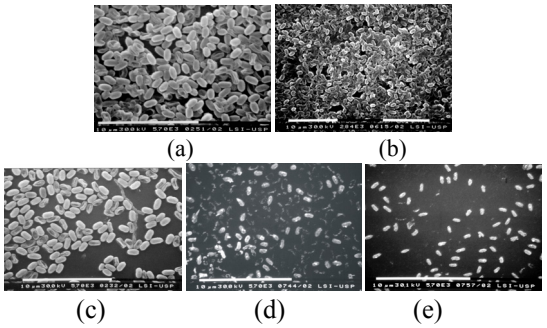

Figure 4.: (a) Sample before the processes; (b) Sample after the UV process; (c) Sample after the X-ray process; (d) Samples after the plasma process with 100 W of power; (e) Sample after the plasma process with 150 W.

4 CONCLUSIONS

The system proves to be efficient for sterilization; the process is fast and does not attack the materials being sterilized. As the sterilization time is quite short, the oxygen plasma can be applied to test its

potential to sterilize cellulose materials inoculated with *B. subtilis* and *B. stearothermophillus*. The tests with materials on small glass plates suggest the utilization of this technique for the sterilization of several medical products, because of the fact that with shorter exposure times, the microbial load is reduced to zero and the sterilized material is not attacked during the process. Besides, this process is safe for the operator and the environment. Once the process is fast and conducted at room temperature, it can also be used for sterilization of polymeric materials since tests are performed before to adjust the parameters of the process to the characteristics of the material to be sterilized.

The microbial load is reduced to zero in few minutes when 150 W of power, 100 mTorr of pressure and 200 sccm of oxygen flow is applied, requiring at the most a 20 minute process for *B. subtilis*. This duration must be increased to 60 minutes when 100 W of power is applied.

For the samples of *B. stearothermophillus*, the processing time to zero out the microbial load is around 15 minutes, using in this case 100 Watts of power, 330 mTorr of pressure and 500 sccm of flow.

For the X-ray sterilization tests, 200 to 1000 W were utilized in 30 minute processes, despite the high power levels applied (when compared with the plasma processes), the logarithmic reduction of the viability of the biological indicators remains very low to indicate a sterilization effect, what discourages the application of this technique for sterilization purposes. The UV sterilization tests at 14 W/cm² and 2 to 60 minute periods did not present satisfactory results, because the microbial load was only slightly reduced, showing that the UV radiation does not contribute to the sterilization effect.

ACKNOWLEDGEMENTS

The authors thank CNPQ for financial support, and Alexandre Marques Camponucci, José Antônio Rodrigues Porto, Rubens Pereira de Alcântara, Elisio José de Lima and Msc. Peter L. Polak for technical support.

REFERENCES

Holy, C.E., Cheng, C., Daves, J.E., Shoichet, M.S. Optimizing the sterilization of PLGA scaffolds for use in tissue engineering, *Biomaterials*, Amsterdam, v.22, p.25-31, 2001.

Lerouge, S., Wertheimer, M.R., Marchand, R., Tabriziani, M., Yahia, L'H. Effect of gas composition on spore mortality and etching during low-pressure plasma sterilization. *J. Biomed. Mater. Res.*, New York, v.51, n.1, p.129-135, 2000.

Rutala, W.A., Gergen, M.F., Weber, D.J. Sporicidal activity of a new low-temperature sterilization technology: the sterred 50 sterilizer. *Infect. Control Hosp. Epidemiol.*, New Jersey, v.20, n.7, p.514-516, 1999.

Hoefel, H.H.K. Esterilização. To be found at: http://www.cih.com.br. Acessed on: April 15th 2002.

Hayakawa, I. et al. Mechanism of inactivation of heat-tolerant spores of *Bacillus stearothermophilus* IFO 12250 by rapid decompression. *J. Food Sci.*, Chicago, v.63, n.3, p.371–374, 1998.

Moisan, M., Barbeau, J., Morteau, S., Pelletier, J., Tabriziani, M., Yahia, L.H. Low-temperature sterilization using gas plasmas: a review of the experiments and an analysis of the inactivation mechanisms. *Int. J. Pharm.*, Amsterdam, v.226, p.1-21, 2001.

Moreira,A. J; Mansano, R, D; Pinto,T. J.A; Ruas, R; Zambom, L.S; Silva,M.V; Verdonck, P. B. Sterilization by oxygen plasma, *Applied Surface Science*., Berlin, v.235, p.151-155. 2003.

Ohsima, T., Sata, K., Terauchi, H., Sato, M. Physical and chemical modifications of high-voltage pulse sterilization. *J. Electrost.*, Amsterdam, v.42, p.159-166, 1997.

Hermelin, I.J., Burtin, C., Leverge, R., Prugnaud, J.-L. Côut de fonctionemment de deux systèmes de stérilisation à basse température, centralisé et decentralisé. *J. Pharm. Clin.*, Paris, v.17, n.3, p.138-144, 1998.

THE DESIGN OF BIAXIAL JOINT FOR MOBILE ELECTRONICS WITH THE ANALYSIS ON ARTHROSIS

Zhao Danpu, Yi Qiang, Nie Chenghui, Chen Ken, Liu Li
Dept. of Precision Instruments and Mechanology, Tsinghua University, Beijing 100084, China
zhaodp03@mails.tsinghua.edu.cn, yiq04@mails.tsinghua.edu.cn, nch05@mails.tsinghua.edu.cn
kenchen@tsinghua.edu.cn, liuli@tsinghua.edu.cn

Xu Leon, Salo Antti
Nokia Research Center, Beijing 100013, China
leon.xu@nokia.com, antti.o.salo@nokia.com

Keywords: Bionic, joint, arthrosis.

Abstract: To bring forward the new form factors is one of the key drivers for future mobile electronic devices. On the other hand, some form factors in nature with evolution process have been the excellent and adaptive. In this paper, we pay attention to the characteristics of arthrosis, researched on the difference between the arthrosis and machine joint. Then the essentials and parameters of the biaxial joint design were introduced. After that a biaxial joint concept for portable electronics based on the bionic principle was proposed. Finally, we provided the statics analysis of the biaxial joint.

1 INTRODUCTION

In recent years, more and more mobile electronic devices have become an improtant part of people's life. One of the key drivers for future electronic mobile devices is to enable drastic change of the physical appearance of mobile terminals with totally new product category possibilities.

The clamshell type electronic mobile device is the most popular type. The joint divided into two parts and the opening angle is general at 160 degree. Obviously, the structure of the joint limits the opening angle. Another problem of this type of communication between two parts is secular fold. So many researches pay attention to the design of rotary joint.

Most of rotary joints only have one axial and two parts of joint turned encircling the axial. Because of the motion intervention, the friction cannot be avoided.

In our research, the design of a biaxial joint based on the bionic principle is introduced. The biaxial joint has two perpendicular axes. Two pairs of apposing movements take place along these axes respectively and circumduction is permitted.

2 THE CHARACTERISTICS OF ARTHROSIS

Locomotor system includes bones, joints and muscles. Each bone is linked with joints. Every arthrosis has some common structures. The typical one is as Figure 1. Compare with the machine joint, the arthrosis have some characteristics:

Figure 1: The structures of a typical synovial joint.

The articular surfaces are the smooth surfaces composed by non-standard curve or surfaces.

The articular surfaces indirectly connect with cartilages. The articular discs make joint surfaces fit further with one another, increase stability of joints and absorb large forces of compression and shear.

The ligaments are the driver of body structures. Usually, one arthrosis connects with one more ligaments. When the arthrosis move, the ligaments around it will cooperated drive the arthrosis to move with a non-repeated track.

3 DESIGN OF THE BIAXIAL JOINT

3.1 The Essentials of the Joint Design

In this project, a bionic joint would be designed for the joint of electronic devices. Therefore some essentials of the main joint design as follow:

While design joints the rolling friction should be selected for decreasing the affect of friction.

Usually the wire is easily failed when folded repeatedly. So the wire should cling on the joint surface to acquire the support. Also the curvature radius of joint should be enlarged at full steam.

As articular discs, some filling would be accepted and it can make joint surfaces fit further with each other, increase stability of joints and absorb the large forces of compression and shear.

Imitate the body drivers, some special drivers should be selected with the small structure and for parallel movement.

3.2 The Surfaces Design of Joint

In body, the hinge joint has two parts, concave and convex, and movement takes place on sagittal plane, e.g., the elbow and ankle. With the analysis on the structures of hinge joint, it is described as Figure 2.

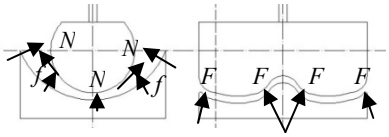

Figure 2: The sketch of hinge joint. The *N* means the support forces, *f* is the frictions, *F* is the transverse forces.

For avoiding the friction, the concave part will be replaced by convex, and the two parts are tangent. See Figure 3 (a). Transverse displacement should also be considered. Simulate the cooperation of the neck and convexity, some keys and slots should be designed. So the joint is showed as Figure 3 (b).

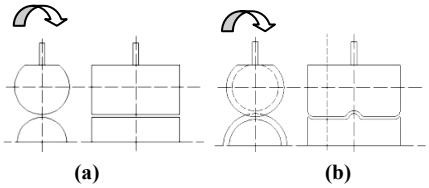

Figure 3: The sketch of joint.(a) joint with double convex, (b) joint with key and slot.

As the analysis before, the curvature radius should be enlarged. So the section of the joint part can be designed as demisemi circularity. So the biaxial joint structure is described as Figure 4.

Figure 4: The sketch of final biaxial joint structure.

3.3 The Design of Medium in Joint

For the fit and stable of the structure of synovial joints, there are other structures inside the joint, such as articular cartilages.

See the sagittal section of temporomandibular joint in Figure 5 (a), the articular disc suit on the surfaces of two joint parts.

Figure 5: (a) The sagittal section of temporomandibular joint. (b) The sketch of connective band.

Simulate the structure and function of the articular disc, a connective band is design as Figure 5 (b). It is suited on the surfaces of two joint parts.

For keeping balance, three bands from different directions interlude the joint cavity. See Figure 6.

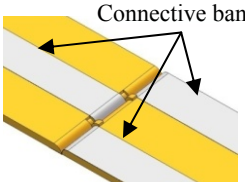

Figure 6: The biaxial joint with connective band.

3.4 The Design of the Joint Driver

In the movement of articular, muscles drive the joint. They compress and elongate to change the direction between two attachments on the different

bones. The greatest excellence of using muscle drivers in joint is the minimal volume. In this research, artificial muscles would be selected as joint drivers.

In the biaxial joint, one part would turn around the other back and forth. Therefore two couples of drivers should be emplaced on the double side of the joint.

For balance, they should be distributed symmetrically. In this design, the turn range of the joint can be from 0 to 360 degree. See Figure 7.

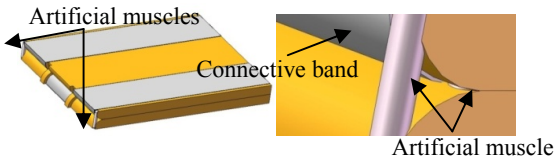

Figure 7: The biaxial joint with artificial muscles.

4 STATICS ANALYSIS OF THE BIO-JOINT

In this paper, because of the tangent motion between two joint surfaces, the slip resistance can be ignored.

Predigesting the joint structure, the joint surfaces with connective band can be modelled as Figure 8.

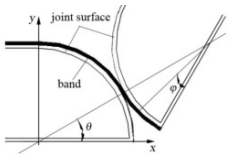

Figure 8: The model of the system.

4.1 The Motion Track

If we establish the coordinate at one of the circles, the other one rotated on its surfaces. So the motion track equation of discretionary point on the moving circle can be founded as

$$X=2R\cos\theta-R\sin(\pi/2-2\theta+\varphi) \quad (1)$$

$$Y=2R\sin\theta-R\cos(\pi/2-2\theta+\varphi) \quad (2)$$

Here φ is the angle between the point on the joint surface and underside of the joint.

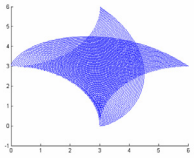

Figure 9: The motion track of the joint.

When the φ changed from 0 to $\pi/2$, we draw one track with every 0.25π degree. And the tracks are described as Figure 9 in area *XY*.

4.2 The Forces of the System

For ensuring the reliability of connection of two joint surfaces, beforehand force F would be added on the bands. The forces are showed in Figure 10.

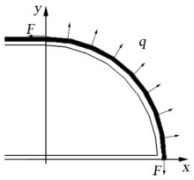

Figure 10: The sketch of the forces on system.

Here, F is the beforehand force, q is the forces density. So the force on arc with the length as $Rd\theta$ is $f=qRd\theta$.

The component of forces on the axial X and Y is

$$f_x=qRd\theta\cdot\sin\theta, f_y=qRd\theta\cdot\cos\theta \quad (3)$$

According to the principle of forces balance, it can be described as

$$F=\int_0^{\pi/2} qR\sin\theta d\theta \quad (4)$$

Then

$$q=F/R \quad (5)$$

4.3 The Stress

4.3.1 Stress on the Band

As it described before, in this design the fix up of joint is realized by some connective bands. So the bands are the primary force suffering object. With the repeatedly folding, it should be laid-back and wearing. Thereby the integrality and reliability of structure would be destroyed. So in this part, the stress of connective band would be analyzed.

Firstly, the normal stress for the beforehand forces can be

$$\sigma_{bF}=F/A_b \quad (6)$$

Here, A_b is the section area of connective band.

Then, the normal stress for bending moment is

$$\sigma_{bM}=My/I_{bz} \quad (7)$$

Here, y is the direction between the point and central on section. And $M=F(R-R\cos\theta)$ is the bending moment on the section, $I_{bz}=\int_{A_b} y^2 dA_b$ is the moment of inertia for axial z.

So the whole normal stress on connective band can be described as

$$\sigma_b=\sigma_{bF}+\sigma_{bM}=F/A_b+My/I_{bz} \quad (8)$$

The maximal normal stress on connective band is at the point when $y=y_{max}$. It changed with θ can be described as Figure 11 (a).

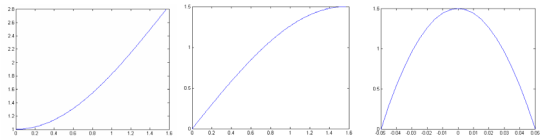

(a) (b) (c)

Figure 11: The maximal stress on connective band. (a) Normal stress changed with θ, (b) Shear stress changed with θ, (c) The τ_b change with y.

At the same time, the shear stress at y on section can be showed as

$$\tau_b=3F_{bs}(1-4y^2/h_b^2)/2bh_b \quad (9)$$

Here, h_b is the thickness of band, b is the breadth of it, and $F_{bs}=F\sin\theta$ is the shearing force on the section.

In Figure 11 (b) the curve of maximal shear stress changed with θ is described.

A maximum of F_{bs} when $\theta=\pi/2$ can be get. So the τ_b with such F_{bs} can be described as Figure 11 (c). The maximum of τ_b can be found when $y=0$.

4.3.2 Stress on the Joint Surface

Because of the no direct touch between two joint surfaces, the joint surface gets the press form connective bands only when it turned. See Figure 12. Due to the radial press with the forces density q, the axial loads is F, so the normal stress from the press on the joint surface is

$$\sigma_{jF}=qR/A_j=F/A_j \quad (10)$$

Here, A_j is the section area of joint surface.

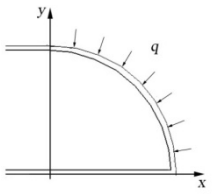

Figure 12: The sketch of the forces on joint surface.

Then, the normal stress for bending moment on the joint surface is

$$\sigma_{jM}=My/I_{jz} \quad (11)$$

Here, y is the direction between the point and central on section. And $M=\int_0^\theta qR^2\sin(\theta-\varphi)d\varphi$ is the bending moment on the section, $I_{jz}=\int_{A_j} y^2 dA_j$ is the moment of inertia for axial z.

So the whole normal stress on joint surface is

$$\sigma_j=-\sigma_{jF}+\sigma_{jM}=-F/A_j+My/I_{jz} \quad (12)$$

The maximal normal stress on joint surface is at the point when $y=y_{max}$. It changed with θ can be described as Figure 13.

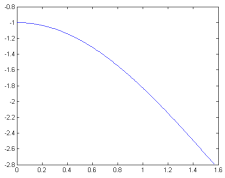

Figure 13: The maximal normal stress changed with θ.

Also, the shear stress is existed on the joint surface. The shear stress at y on section can be showed as

$$\tau_j=3F_{js}(1-4y^2/h_j^2)/2bh_j \quad (13)$$

Here, h_j is the thickness of joint, and $F_{js}=\int_0^\theta qR\cos(\theta-\varphi)d\varphi$ is the shearing force.

So we can get a similar curve as Figure 12, the maximal shear stress changed with y is described.

4.4 The results

In this design, when one surface round on another, although the point on one changed his track direction after it pass the tangency part, but due to the tangent point track is arc, the move is smooth.

Based on the forces analysis, there's no slip resistance between two surfaces. It's the virtue of such design, because it defence the energy wasting and surfaces wearing; and at the same time, it is a

shortcoming, because it can not stop at any part with friction. But here we bring out the driver of artificial muscle, the orientation is ensured.

When selecting the material of connective band, only if the allowed stress is larger than maximal one gained before, reliable structure can be accepted.

5 CONCLUSIONS

As one of the most important part of electronic mobile devices, the design of joint catches the great attention of researchs. One of the key drivers for the devices is to enable drastic change of the physical appearance of mobile terminals with totally new product category possibilities. In this paper, some characteristics of the arthrosis are analyzed. And we bring out a biaxial joint for electronic mobile devices based on the bionic principle. At last, the statics of such biaxial joint is analyzed.

REFERENCES

Stephanie, R., Michelle, M., Stephen, E., 2004. *Anatomy for Diagnostic Imaging*, SAUNDERS. Spain, 2nd edition.

Liu, Z. Y., 2007. *Chinese-English Textbook of Systemic Anatomy*, Science Publishing Company, China, 1nd edition.

William, C. M., 2005. *Smart Technology for Aging, Disability, and Independence: the state of the science*, WILEY-INTERSCIENCE. New Jersey, 1nd edition.

Ben P., 1975. *Dynamic Anatomy and Physiology*, Macmillan publishing Co. American, 1nd edition.

Zhou X., Zhao Zh., 2000. *Establishment of TMJ model including mandible by mean s of three-dimensional finite element method*. J Pract Stomatol, Vol. 16 (1), P17-19.

LI X., ZHANG R., 2004. *Artificial Muscles Based on Conducting Polymers*. Journal of Materials Science & Engineering, Vol. 22 (1), P128-131.

CAO X., WANG B., 2004. *The Decision of Fatigue Stress Table of Belt*. Journal Of Wuhan University Of Technology, Vol. 26 (9), P67-70.

A SIMULATION STUDY OF THE NEW CONCEPT OF A STAIR-CLIMBING WHEELCHAIR

Concept of Construction

Grzegorz Dobrzynski, Wlodzimierz Choromanski and Jerzy Kowara
Warsaw University of Technology, Faculty of Transport, Koszykowa 75, 00-662 Warsaw, Poland
gd@it.pw.edu.pl, wch@it.pw.edu.pl, jkowara@it.pw.edu.pl

Keywords: CAD, simulation study, stair-climbing wheelchair.

Abstract: The authors present an idea of construction, modelling and simulation studies of a new generation, mechatronical wheelchair. The wheelchair is meant to drive on various surfaces. Its important feature is the possibility to overcome obstacles, such as a doorstep of max. 220 mm. The construction model and simulation studies were carried out in the environment of MBS ADAMS package. An algorithm of controlling the process of overcoming the doorstep was proposed and an analysis of parametrical sensitivity of the construction was performed.

1 INTRODUCTION

Modern transport systems should be created with appropriate observance of the needs of the disabled. At the design stage, special attention should be paid to the needs of people with mobility problems. For these people, important elements of the transport system include: architectural features, specially adapted public means of communication, and individual means of transport (Axelson, 1995), (Blachowski, 1993). A wheelchair with special transport features is an important element in the whole system. The development of the motor industry led to a dramatic increase of accidents, which in turn increased the number of people suffering from permanent disability or impairment of their movement capabilities. The feedback received from the disabled clearly suggests that there are still many barriers that make it difficult for these people to function individually in society. Irrespective of the laws in force, the number of buildings that are not adapted for the disabled is large. And the adaptation process is long and expensive. What could help the disabled to overcome architectural obstacles is a new wheelchair with special functions, such as moving up and down the stairs or lifting the disabled person to such a height that is achievable by a healthy individual.

This paper presents assumptions and preliminary simulation tests of a new concept of a wheelchair for people with motion disabilities. The goal of the simulation model is first of all to optimize the wheelchair's parameters in order to achieve the most desirable safety and ergonomic conditions. The main advantage of the wheelchair will be its ability to overcome terrain obstacles, such as thresholds, stairs or curbs, or lifting the user to heights that are achievable by healthy people. The wheelchair will be able to drive into a low-deck bus or tram on its own. Furthermore, its construction will be simple and spatially limited.

2 THE CONCEPT OF A STAIR-CLIMBING WHEELCHAIR

The concept is presented in the form of a 3D picture (Fig. 1). The wheelchair can move over flat surfaces, as well as thresholds, stairs and curbs. The drive system of the wheelchair consists of two electric motors (4). The vehicle changes its direction by means of differentiating the speed between the two motors. The wheelchair systems are powered by two service-free gel batteries, 12 V, 2 x 40 Ah. The batteries are located relatively low to achieve the most advantageous location of the centre of gravity. Beneath the seat, there is a seat lifting mechanism (1). The seat lifting mechanism is connected with the system to correct the inclination of the seat while driving through an obstacle. The rear part of the wheelchair features an arm that can lift the

wheelchair over an obstacle (8). It is driven by a motor module with a gear (6). Distance measuring systems play an important role when the wheelchair is moving over an obstacle. There are two such systems: a front one (5) and a rear one (7). The slide skid (2) also proves useful in negotiating obstacles.

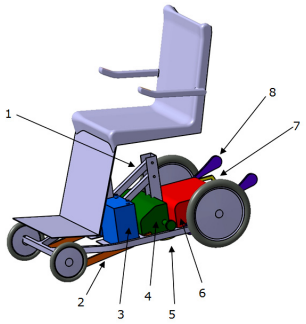

Figure 1: Wheelchair contraction model – own concept.

The wheelchair features two drive modes: "normal" and "obstacle". The normal mode is used to drive on flat or slightly uneven surfaces. The user has two gears to choose from: I and II. The first gear (I) allows the wheelchair to drive with the maximum speed of 3 km/h. It is meant to be used in small compartments or rooms. One of the benefits of using the first gear is that it makes steering the wheelchair much easier. Gear II is to be used for greater distances. It also requires a greater precision in handing the steering lever.

The wheelchair also features a lift function. It lifts the seat to a higher level, which is important for disabled people.When the lift function is activated, the wheels of the wheelchair are blocked and driving is not possible. An audible signal will be introduced to remind the user that the lift function has been activated.

3 OPERATIONAL PARAMETERS AND ALGORITHM FOR OVERCOMING OBSTACLES

The following operational parameters were assumed for the initial phase of the project:

- Threshold height (max) 0.22 m
- Threshold depth (min) 0.25 m
- Battery 12V, 2 x 40 Ah,
- Battery weight 24 kg
- Autonomy (working time) 5 hours
- Load bearing capacity 100 kg
- Weight 80 kg
- Min. space required for manoeuvring 1.1x1.1m
- Gear I speed 1 m/s
- Gear II speed 2 m/s
- Mean speed while overcoming stairs 0.1 m/s
- Minimum width of staircase 0.8 m
- Maximum surface inclination 35°
- Seat lift height 0.45 m

The above-mentioned values result from an analysis of specific features of the wheelchairs currently available on the market. These values are subject to minor modifications (Kowara, 2005), (Milanowska, 1997).

The algorithm used to overcome obstacles that is presented here explains the principles of operation of the construction described in the above paragraph. The ascending phases (Fig. 2.) will be carried out in the same manner if the wheelchair has several stairs to overcome: when Phase e) is completed, the system will carry on to Phase a) again. It will operate through all the phases in a closed loop until all stairs have been overcome. Descending the stairs (Fig. 2) will look exactly the same as descending a singular threshold. It will be carried out in a closed loop: when Phase g) is completed, the system will start from Phase c) again.

Ascending an Obstacle. To overcome an obstacle higher than 5 cm, the obstacle should be approached backwards, i.e. with the back of the wheelchair. When the user approaches an obstacle, such as a curb or stairs, he or she switches the driving mode to "obstacle". The speed of the main motors is reduced and the systems detecting distances are activated (Fig. 2, Phase a). The steering system brings the wheelchair to the appropriate distance from the edge of the obstacle and positions the wheelchair perpendicularly to it. Then, Phase b) starts. Main drive motors are de-activated and the drive wheels are blocked. The lift arm starts operating. Moving to subsequent Phases c) and d), the steering system controls the seat and keeps it horizontally. Phase e) starts when the lift arm makes a 180°- turn. The main drive motors are activated again and, at a reduced speed, bring the wheelchair onto the obstacle. The distance measuring systems keep checking if there is another obstacle for the wheelchair to overcome (such as another stair). In case there is another stair, the whole cycle starts form Phase a). When the last stair has been overcome, the wheelchair moves backwards at a reduced speed. During Phase f), the edge of the obstacle moves over the slide skid and the front wheels are mounted onto the obstacle. At the end of Phase g), the user switches the driving mode back to "normal".

Descending an Obstacle. Preparing to descend an obstacle, the wheelchair should be driven up to the

obstacle with the wheelchair front positioned perpendicularly to the edge of the obstacle. The "obstacle" mode should be used when the height of the obstacle (stair or threshold) is higher than 5 cm. It is the user who decides to switch to this mode of driving.

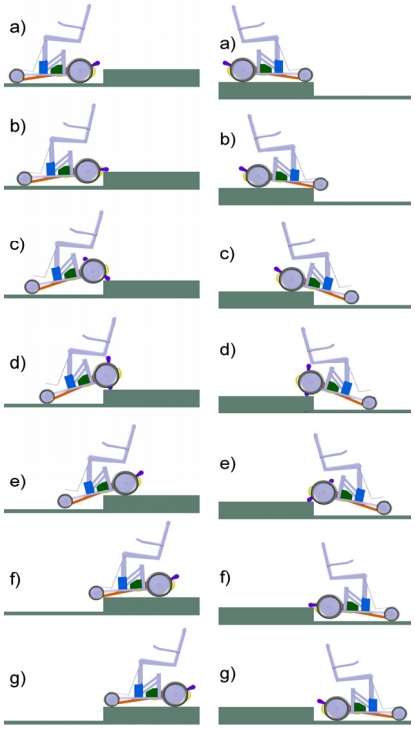

Figure 2: Ascending and descending an obstacle– algorithms of operation.

When the "obstacle" mode is activated (Phase a), the speed of the main drive motors are reduced and the distance measuring systems, located between the front and the rear axes of the wheelchair, start to operate. Watching the position of the wheelchair skids, the steering system corrects the direction of the wheelchair movement (Phase b). Continuing the descending movement, the distance measuring system stops the main drive motors at an appropriate moment (Phase c). Then, Phase d) begins. The drive wheels are blocked. The lift arm starts to operate. Moving to subsequent Phases e) and f), the steering system controls the seat and keeps it horizontally. Phase g) starts when the lift arm makes a 180°- turn. The main drive motors are activated again and, at a reduced speed, bring the wheelchair down the obstacle. The distance measuring systems keep checking if there is another obstacle for the wheelchair to overcome (another stair). In case there is another stair, the whole cycle starts form Phase d). When the last stair has been overcome, the wheelchair moves on at a reduced speed. At the end of Phase g), the user switches the driving mode back to "normal".

4 ASSUMPTIONS FOR BUILDING A SIMULATION MODEL

There is a huge variety of wheelchairs available on the market. Designers strive to achieve the most functional prototype, maintaining the most crucial features, such as low weight, simple and comfortable operation, and first of all: low price. The last aspect is very important in making the wheelchair available to a wide spectrum of the disabled who, very frequently, do not belong to the wealthiest groups of the society. To meet all these requirements, one must look for new methods of wheelchair designing and modelling. The literature available suggests that most research carried out in this field concentrates on determination the strength and resistance of the wheelchair construction, so that relevant safety standards and technical requirements are complied with. The majority of solutions focus on improving the form of additional equipment to be installed in the wheelchairs to overcome surface obstacles. They are developed without the use of computer simulation or dynamic tests.

The overview of the literature on wheelchairs able to overcome such obstacles as stairs or thresholds (Zabłocki, 2002), as well as simulation studies of simple constructions carried out in 2D-Working Model environment, shows the capabilities and limitations of this kind of vehicles. Due to the fact that one of the priorities of the model this study refers to is a simple and compact construction with due observance of the other requirements, an analysis of various systems used for overcoming obstacles of the threshold type led to the development of the structural concept presented in Chapter 3. An initial analysis of the systems lets the authors believe that the construction secures safe overcoming of obstacles and at the same time is simple and compact. For the purpose of the simulation tests, certain simplifications were made:

- The human model is represented by a number of permanently fixed solids with certain weight parameters.
- The human model is fixed to the seat.
- The surface on which the wheelchair moves is flat and horizontal.
- There is no friction between the front wheels and the front frame on the one hand, and the ground surface and the obstacle edges on the other hand.

- Ascending an obstacle, the wheelchair is positioned backwards to it.

The position of a human body's centre of gravity in the sitting position is an important variable in a simulation model of the construction. A real human body, as well as its individual elements, is a complex system with a continuous distribution of mechanical properties. Therefore, human body modelling as such is a vast area of science and the subject of a number of research projects. In this project, the approximate mass parameters of a human body model were chosen on the basis of data used in the research on car seats, and the model developed with the use of statistical data (Seireg & Arvikar, 1989), applied to analyze and simulate human walking. Using the above mentioned data, together with the recommendations made in PN ISO 7176-11 Standard, "Test dummies", the authors developed a body model of an average man of 78.5 kg in the sitting position. Catia system was used for this purpose.

Geometrical parameters of the wheelchair under this project were based on the measurements of an Explorer wheelchair carried out by the authors, as well as data found in the literature available.

When the wheelchair is in operation, certain parameters may change. It can be assumed that this has an impact on the performance of the wheelchair-user configuration while the wheelchair is in motion. To verify such a hypothesis, these variables need to be identified and their impact on the configuration performance needs to be assessed. Due to a vast number of various factors having an impact on the performance of the wheelchair-user configuration, only certain parameters were selected for further tests (i.e. those parameters that can significantly influence the performance of the vehicle while overcoming an obstacle):

- Friction between the wheels and the surface
- Obstacle height
- Distance of the user's centre of mass from the back support
- Obstacle approach angle.

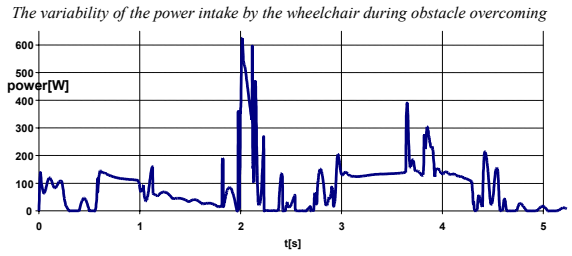

Figure 3: The variability of the power intake by the wheelchair during obstacle overcoming.

The scope of variability of individual parameters will be determined during simulation tests.

Examples of simulation results are presented below. The variability of power consumption while overcoming a 220 mm obstacle was determined.

5 CONCLUSIONS

The paper presented a constructional concept and simulative studies of a new generation wheelchair for motional disabled persons. Taking in consideration the wide range of studies and analyses the new construction is submitted to before it can be introduced into production, it should be acknowledged that this paper could be very helpful when creating the real wheelchair construction.

The most important elements of that study include:

- A study of the advanced schema of wheelchair construction,
- a study of the nominal model of the construction above,
- a proposal of the control algorithm when coming across a barrier,
- a construction of the simulative model in the Adams program.

ACKNOWLEDGEMENTS

The work was covered by a grant of *The National Foundation for the Rehabilitation of the Disabled* for the study on the construction and implementation series of stabilisers.

REFERENCES

Axelson P. March/April (1995), Chair and chair alike?, Sports'n Spokes, p. 26-61.

Blachowski W. (1993), Analiza porównawcza wózków inwalidzkich dostępnych w kraju, Artykuł z konferencji *Problemy techniki medycznej*, XXIV, nr1-2.

Kowara J. (2005), *Koncepcja konstrukcji i badania symulacyjne wózka inwalidzkiego nowej generacji*, praca dyplomowa, promotor W.Choromański, Politechnika Warszawska, SiMR.

Milanowska K.(1997), Znaczenie zwiększonej aktywności ruchowej osób niepełnosprawnych jako czynnika kompensującego ich sprawność psychofizyczną, *Sport szansą życia niepełnosprawnych*, PSON, p. 28-30.

Zabłocki M. (2002), Metodyka projektowania urządzeń technicznych dla osób niepełnosprawnych, WMRiT, (rozprawa doktorska), Politechnika Poznańska.

ELBOW FLEXION AND EXTENSION MOVEMENTS CHARACTERIZATION BY MEANS OF EMG

L. M. Bittar and M. C. F. Castro
Centro Universitário da FEI, Electrical Engineering Department, Av. Humberto A. C. Branco, 3972
São Bernardo do Campo, CEP 09850-901, Brazil.
unielbittar@fei.edu.br, mclaudia@fei.edu.br

Keywords: Electromyography, Biceps, Triceps, Elbow, Flexion, Extension.

Abstract: Electromyographic (EMG) signal is the electrical manifestation of neuromuscular activation associated with muscle contraction. The present work intends to characterize the behavior of the muscles biceps and triceps during elbow flexion and extension movements, without load. These movements were performed at horizontal and vertical planes. Three types of test were performed, for each plane, relating EMG signal with joint position. Five men volunteers, ages ranged between 18 and 21 years old, were selected to participate to the tests. The first test consisted to move 10 degrees for each three seconds until the allowed maximum flexion and then, to return at the same way to the initial position. For the second test, the same movement was made but continuously, without stopping at intermediate positions. And for the third test, continuously flexion and extension movements were repeated sequentially but for different amplitudes, increasing by 10 degrees each. The tests were repeated, three times each. Initially, graphical analysis of the data was made for standard behavior detection and, for a quantitative analysis, after EMG preprocessing, averages and variation coefficients were calculated from specific intervals at the beginning, middle and at the end of movement. Although an EMG signals inherent variability, results showed inter and intra subject's repeatability, but only for movements performed at the horizontal plane.

1 INTRODUCTION

The general mechanism of muscle contraction, under voluntary control, involves the following processes:

- stimulation of motor nerve by a neuronal action potential;
- secretion of neurotransmitter (acetylcholine) at the neuromuscular junction;
- propagation of a muscular action potential through the muscular fiber;
- ionic flow across the muscle membrane;
- contractile process itself (Guyton, 2002; Capucho, 2005).

The basic unit of the muscle is named motor unit and it is constituted by a motor neuron and all muscular fibers innervated by this neuron. The electrical signal that is detectable by each unit is named Motor Unit Action Potential (MUAP), and this constitutes the fundamental unit of Electromyographic (EMG) signal. The EMG signal is the electrical manifestation of neuromuscular activation associated with a muscle contraction, it is accessible at the body surface and it can be used for different purposes, as neuromuscular disease diagnoses, rehabilitation process evaluation and also to analyze muscle behavior performing specific movements.

The surface EMG signal amplitude ranged from 0 to 10 mV peak-to peak or from 0 to 1,5 mV rms, and frequency ranged from 0 to 500 Hz, with dominant energy between 50 and 150 Hz (DeLuca, 2002), but deterministic characteristics were during the initial 200 ms of the muscle contraction (DeLuca, 1979).

EMG signal detection and acquisition process need some caution due to several factors that can affect the results. The electronic apparatus used, the environment, the electrodes and the movement of the electrodes during the tests can introduce noise. This interference can be avoided or eliminated by using:

- differential electrode configuration and differential amplification;
- position of the electrodes on the midline of the muscle belly;
- rms value of the signal, for measuring the amplitude of the voluntarily elicited EMG signal

(consists to rectify and integrate the signal in data time interval) (DeLuca, 2002).

2 MATERIAL AND METHODS

Five men volunteers, ages between 18 and 21 years agreed to the test procedures, aiming to evaluate the contribution of biceps and triceps muscles during voluntary flexion and extension elbow movements, without load. For the accomplishment of the tests, a device for arm support and joint angle monitoring was used. The right arm were accommodated and fixed, allowing free elbow movement in only one plane and hindering other movements. For EMG signal acquisition, surface electrodes and the Powerlab PTB300 kit from ADInstrumets were used.

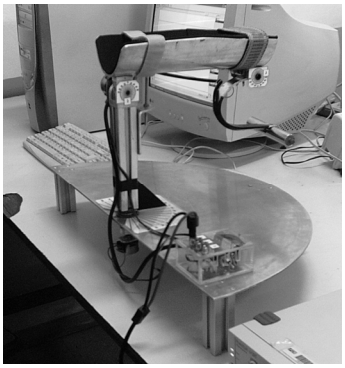

Figure 1: Device for arm support and joint angle monitoring.

The procedure consisted of three types of tests that would have to be repeated three times each for both horizontal and vertical planes.

Test 1: The volunteer had to move 10 degrees every 3 seconds, initiating in total extension and finishing with maximum flexion of 90 degrees, for the horizontal plane and 70 degrees for the vertical plane, and then had to return, to the initial position, by the same way.

Test 2: The volunteer had to repeat the amplitude of previous movement, but varying the joint position continuously, with controlled speed of 10 degrees for second, without stopping in the intermediate positions.

Test 3: The volunteer had to repeat several times elbow flexion/extension, but each time, amplitude movement was increased by 10 degrees. The initial amplitude was 10 degrees and the final amplitude was 90 degrees, for the horizontal plane and 70 degrees for the vertical plane.

The archives with the signal waveforms, obtained during the tests, were used for the result analysis, making possible the detection of standard behaviors. For the quantitative analysis, specific data intervals were fixed, considering beginning, middle and the end of movement, covering joint angles for extension and flexion positions. For these data sets, the mean and the variation coefficient were calculated for each one of the repetitions and among the three repetitions made by the same volunteer.

3 RESULTS

3.1 Movements at Horizontal Plane

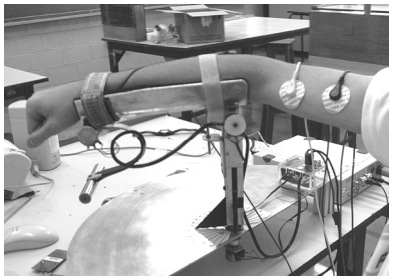

Figure 2: Arm position during movement at horizontal plane.

Figure 3 shows the signals acquired with one volunteer. From the top to the bottom, the first is the trigger signal for movement synchronism and speed control, joint angle position, biceps EMG signal, triceps EMG signal, rms of biceps EMG signal, rms of triceps EMG signal. And the columns represent each one of the repetitions of each of the three tests.

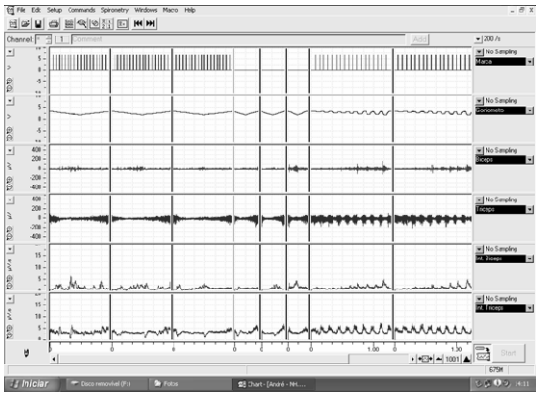

Figure 3: Waveforms obtained from the movements at horizontal plane with one volunteer.

Tests 1 and 2 showed that triceps acted more at the beginning and at the end of the movement, with

the arm around extension position (joint angle varying from 0º to 10º and from 10º to 0º), while biceps acted more at the central part of the movement, between the peaks of triceps performance (around 90º of flexion). Test 3 showed a quite constant intensity on triceps recruitment during movements, independently of the joint angle and movement amplitude. On the other hand, biceps signal showed an intensity increase as the amplitude of the movement increased.

In all the movements performed at the horizontal plane, for both muscles, were found a standard pattern at the values obtained from different volunteers, making possible the determination of representative means values as shown in table 1. The values were in accordance with the qualitative results presented before.

Table 1: Mean values obtained during muscle contraction from movements performed at horizontal plane (μV). (B.- Biceps; T. -Triceps).

Position	Test 1		Test 2		Amplitude	Test 3	
	B.	T.	B.	T.		B.	T.
Beginning 0º–10º Extension	1,5	3,7	1,3	3,72	Small 0º – 10º	1,29	3,75
Intermediate 40º–50º Flexion	1,71	3,26	1,72	3,21	Intermediate 0º – 40º	1,43	3,54
Middle 80º–90º Flexion	3,5	3,16	3,1	3,12	Intermediate 0º – 50º	1,5	3,6
End 10º–0º Extension	1,8	4,47	1,75	4,83	Maximum 0º – 90º	1,88	3,58

3.2 Movements at Vertical Plane

Tests 1 and 2 showed that the biceps had a large contribution during all the movement, but it was more requested at the beginning and at the end of the movement. Triceps acted a little more at the beginning of the movement, but its EMG signal was practically constant. In test 3, EMG signal was practically constant for both muscles, but the biceps EMG signal showed a greater intensity.

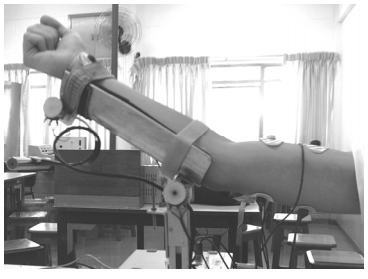

Figure 4: Arm position during movement at vertical plane.

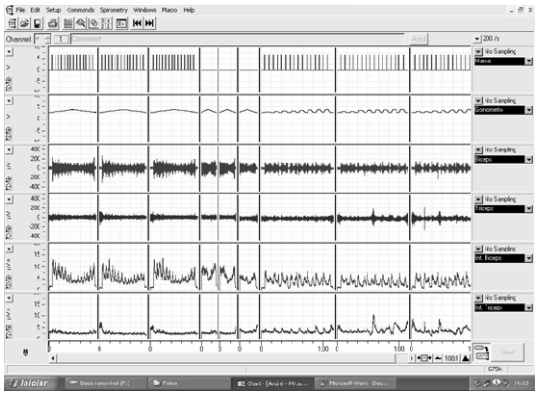

Figure 5: Waveforms obtained from the movements at vertical plane with one volunteer.

In the movements performed at the vertical plane there were no intensity pattern among volunteers for biceps recruitment as verified at horizontal plane. This indicates that each volunteer requested the muscle of different manner for the accomplishment of the same movement. By the other side, EMG signal from the triceps showed a standard pattern, making possible the determination of representative mean values as shown in table 2.

Table 2: Mean values obtained during muscle contraction from movements performed at vertical plane (μV). (B.- Biceps; T.- Triceps).

Position	Test 1		Test 2		Amplitude	Test 3	
	B.	T.	B.	T.		B.	T.
Beginning 0º–10º Extension	---	4,17	---	3,81	Small 0º – 10º	---	4,11
Intermediate 30º–40º Flexion	---	3,25	---	3,31	Intermediate 0º – 30º	---	3,88
Middle 60º–70º Flexion	---	2,98	---	3,04	Intermediate 0º – 40º	---	4,14
End 10º–0º Extension	---	3,32	---	3,68	Maximum 0º – 70º	---	4,18

4 DISCUSSION

Since the biceps acts for the flexion movement while the function of triceps is related with the elbow extension, the data obtained are consistent with the expected.

At the horizontal plane, EMG signal from the triceps had greater intensity at the beginning and at the end of the movement (intervals from 0º to 10º and from 10º to 0º). During these phases, the arm was at an extended position or near of it, needing to surpass the inertia of the movement. At the intermediate flexion position the contribution of the

triceps decreased while the contribution of the biceps increased, but even so the biceps EMG signal remained smaller than the triceps EMG signal. This situation changed at half of the movement, where the elbow was in a full flexed position, requesting more of the biceps.

On the other side, for the movements performed at the vertical plane, EMG signal from the biceps showed greater intensity at the beginning and at the end of the movement (intervals from 0º to 10º and from 10º to 0º). The gravity influence is greater over the biceps at this plane. To surpass inertia the requested muscle was not triceps, as verified at the horizontal plane, but it was the biceps. Quantitative analysis showed that the intensity of EMG signal of the triceps was quite constant at this plane.

Aiming to quantify the variability of data sets during the movement and among each repetition made by the same volunteer, coefficients of variation were calculated. According to Araújo (2000), the coefficient of variation from the EMG signal is very high, being around 21.61% the average of variation of that parameter. It means that values around 20% do not indicate, necessarily, different muscular activities. This high variation can be caused by factors as position and quality of the electrodes, change of temperature and changes in the metabolism.

The coefficients of variation values obtained from the tests performed at the horizontal plane were around 25%. Therefore, it can be considered that there was repeatability of the movements performed.

Moreover the repeatability inter the several movements executions made by the same volunteer, the existence of a standard pattern of EMG intensities for both muscles, certify that there is a repeatability intra volunteers and also the existence of a recruitment pattern.

Analyzing the coefficients of variation obtained from the movements performed at vertical plane, the values related with the triceps were around 25%, indicating the same pattern analyzed previously. By the other side, although the coefficients related with the biceps, for each repetition was small, indicating little variation during the test, the values between repetitions were around 35%, indicating that there was no repeatability among recruitment for each movement performed by the same volunteer. There were cases with coefficients above 50% that probably were related with some isolated stronger muscular contraction made during the test. At vertical plane it was not possible to identify a recruitment pattern due to the variability of the data.

Besides that, it was observed small displacements of electrode positions during movements, and it must be also considered interference due the signals of adjacent muscles. These comments are in accordance with verified by DeLuca (1997), in other experiments.

5 CONCLUSIONS

During the tests, the muscle triceps showed a quite constant behavior, with repeatability of movements at both planes. The muscle biceps demonstrated this behavior only for movements performed at the horizontal plane, in which it had a little recruitment. For movements performed at the vertical plane, the biceps was more requested, resulting in a greater intensity EMG signal, but without repeatability.

There are several factors that can disturb EMG signal, but despite of the interference, it is possible to characterize movements by means of EMG, showing the intensity of muscle recruitment.

The results showed the existence of a recruitment pattern for biceps and triceps among different subjects but only for movements performed at the horizontal plane.

ACKNOWLEDGEMENTS

The authors would like to thank FAPESP and FEI support.

REFERENCES

Araujo, R. C., Duarte, M., & Amadio, A. C. (2000). On the inter- and intra-variability of the electromyographic signal in isometric contractions. *Eletromyogr. Clin. Neurophysiol*., 40: 225-229.

Capucho, A. C. (2005). *Desenvolvimento de um Protótipo de um Aquisitor Portátil de Sinal Mioelétrico*. Dissertação de Mestrado em Bioengenharia, Universidade se São Paulo, São Carlos.

DeLuca, C. J. (1979). Physiology and Mathematics of Myoelectric Signals. *IEEE Trans. Biom. Eng.*, 26: 313-325.

DeLuca, C. J. (1997). The use of surface electromyography in biomechanics. *J. Appl. Biomech.*, 13(2): 135-163.

DeLuca, C. J. (2002). *Surface Electromyography: Detection and Recording*. DelSys Inc.

Guyton, A. C., & Hall, J. E. (2002). *Fundamentos de Guyton, Tratado de Fisiologia Médica*. Guanabara, Rio de Janeiro.

FPGA-BASED COMPUTATION OF THE INDUCTANCE OF COILS USED FOR THE MAGNETIC STIMULATION OF THE NERVOUS SYSTEM

Ionuţ Trestian, Octavian Creţ, Laura Creţ, Lucia Văcariu, Radu Tudoran
Computer Science and Electrotechnics Department, Technical University of Cluj-Napoca, Cluj-Napoca, Romania
Ionut.Trestian@com.utcluj.ro, {Octavian.Cret, Lucia.Vacariu, Radu.Tudoran}@cs.utcluj.ro, Laura.Cret@et.utcluj.ro

Florent de Dinechin
LIP, Ecole Normale Supérieure de Lyon, UMR CNRS / INRIA / ENS-Lyon / Université Claude Bernard Lyon 1
Florent.de.Dinechin@ens-lyon.org

Keywords: Magnetic stimulation, slinky coils, inductance computation, FPGA, floating point, VHDL

Abstract: In the last years the interest for magnetic stimulation of the human nervous tissue has increased considerably, because this technique has proved its utility and applicability both as a diagnostic and as a treatment instrument. Research in this domain is aimed at removing some of the disadvantages of the technique: the lack of focalization of the stimulated region and the reduced efficiency of the energetic transfer from the stimulating coil to the tissue. Better stimulation coils can solve these problems. Designing coils is so far a trial-and error process, relying on very compute-intensive simulations. In software, such a simulation has a very high running time. This paper proposes and demonstrates an FPGA-based hardware implementation of this simulation, which reduces the computation time by 4 orders of magnitude. Thanks to this powerful tool, some significant improvements in the design of the coils have already been obtained.

1 INTRODUCTION

The preoccupation for improving the quality of life, for persons with different handicaps, led to extended research in the area of functional stimulation. Due to its advantages compared to electrical stimulation, magnetic stimulation of the human nervous system is now a common technique in modern medicine (Mozek and Flak, 1999).

A difficulty of this technique is the need for accurate focal stimulation. Another one is the low efficiency of power transfer from the coil to the tissue. To address these difficulties, coils with special geometries must be designed.

This process requires testing a huge number of geometries to find an adequate solution for the desired application (Griškoval and Höppner, 2006).

One of the major problems that appear in the design phase is the computation of the inductivity of the stimulating coil. For simple shapes of the coils (circular), one can determine analytical computation formulas. When, however, the shape and the spatial distribution of the coil's turns do not belong to one of the known structures, a numerical method needs to be used for determining the inductivity.

The idea is to divide the coils in small portions. Starting from this method, two computation systems are presented in the paper:

- The first one is classical and it just consists of a software implementation (Matlab);
- The second one consists of realizing a hardware architecture that exploits the intrinsic parallelism of the problem. The physical support of this architecture is an FPGA device.

The problem with the software implementation is its running time. Coils are designed by trial-and-error, and this approach is impractical if each trial requires half a day of computation. Besides, as this time grows with the complexity of the coil, it prevents designing complex coils. This paper shows that FPGA-based hardware acceleration is able to solve this bottleneck.

The simulation of magnetic stimulators with complex forms requires dividing their coils in several parts. The self-inductance of the circuit, divided in n parts, can be computed with formula

(1). This mainly adds up the self-inductivities of the separate segments with the mutual inductivities of all the involved segments. The method is well described in (Creţ et. al., 2007); the operations involved in computing the inductivity of a coil are: logarithm, division, addition and multiplication.

$$L = \sum_{k=1}^{n} L_k + \sum_{k=1}^{n} \sum_{i=1}^{n} M_{ki}, \quad for \ (i \neq k) \qquad (1)$$

2 SOFTWARE IMPLEMENTATION

A coil is made up of a certain number of turns rolled around a central rod. Each turn can be considered as a perfect circle. The coil is structured on several vertical stages. On each stage there are more turns (horizontal turns). The coils parameters are: the radius, the diameter of the metallic turn and the distance (insulation) between consecutive turns.

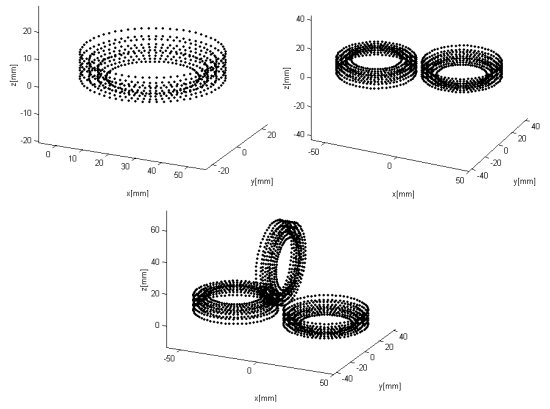

Figure 1: Coil approximation using a finite number of points.

It is possible to have a different number of turns on every vertical stage. It is also possible to have a variable number of vertical stages, as shown in Figure 1. A complete magnetic stimulation device contains a Slinky coil. Considering a coil with N turns, the "Slinky-k" coil is generated by spatially locating these turns at successive angles of $i \times 180/(k-1)$ degrees, were i = 0, 1, …, k-1. If the current passing through this coil is I, then the central leg carries the total current N x I. These coils are shown in Figure 2, where each rectangle represents a leaf of the coil, viewed in perspective.

The turns are approximated by a finite number of points. We considered, after a series of tests, that a suitable amount of points on a turn is 64.

We have to take each of the 64 points and combine them into segments made up of one point and the consecutive one. After this, each segment is held as a reference. Then, formula (1) is applied using this reference segment and all the other segments on the coil. For each pair of segments a value is obtained. These values must be added in order to obtain the coil's total inductance.

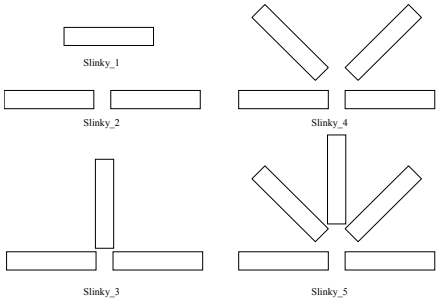

Figure 2: Magnetic coil structures of the stimulation device.

There are two phases in the functioning of the software implementation:

- In *Phase 1*, the coordinates of the points are generated. These are computed using trigonometric functions. The results produced in this phase are also used in the hardware implementation.
- In *Phase 2*, the actual computation of the values is performed. Finally, we accumulate the values corresponding to the mutual and self inductivities.

The accumulation value includes some intermediate values (var1 to 5) according to (Creţ et. al., 2007):

$$\text{Accumulator} = \text{Accumulator} + \frac{\text{var}_1}{\text{var}_2} \cdot \log \frac{\text{var}_3 + \text{var}_2 - \frac{\text{var}_5}{\text{var}_2}}{\text{var}_4 - \frac{\text{var}_5}{\text{var}_2}} \qquad (2)$$

The software implementation's main drawback is the extremely high running time, which can be in the order of tens of minutes even for simple configurations. For complex geometries of the coils, it can exceed several hours (for instance, for a 58-turns coil, about 5 hours run time on a recent PC).

3 HARDWARE IMPLEMENTATION

3.1 FPLibrary

A Field-Programmable Gate Array (FPGA) is a semiconductor device containing programmable

logic components ("logic blocks"), and interconnect. Logic blocks can be programmed to perform simple or more complex functions. In most FPGAs, the logic blocks also include memory elements, from flip-flops to more complete blocks of memories.

The hierarchy of programmable interconnects allows logic blocks to be interconnected as needed by the system designer, somewhat like a one-chip programmable breadboard. Logic blocks and interconnects can be programmed by the customer/designer, after the FPGA is manufactured, to implement any logical function (Guell et. al., 2007).

Several libraries of floating-point operators for FPGAs have been published. In this work, we use FPLibrary, developed at Ecole Normale Supérieure de Lyon (Detrey and De Dinechin, 2005) and freely downloadable (Detrey and De Dinechin, 2007). Mantissa size and exponent size parameterize each operator in FPLibrary, allowing one to choose the precision and the dynamic range of the numbers. It provides operators for addition, subtraction, multiplication, division and square root, some useful conversions and some elementary functions (currently exponential, logarithm and sine/cosine). It is written in portable VHDL (Collange et al., 2006).

3.2 System Architecture

The hardware implementation implies the same two phases as the software one, but Phase 1 is not computation-intensive and its implementation is kept in software.

In the Figure 3 below a block diagram of the system is displayed. Three main blocks can be distinguished. The most important block is the pipeline stage, which receives values, computes them, and in a final stage accumulates them.

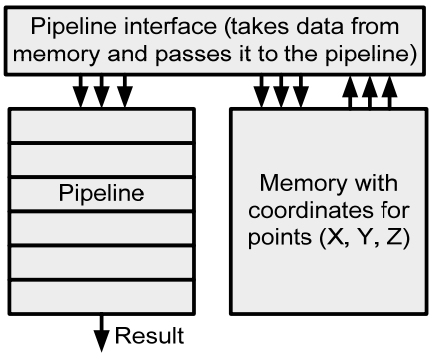

Figure 3: Architecture of the hardware system.

The coordinates are stored in a Block RAM memory. There are 3 memories, one for each coordinate, X, Y, and Z. The synchronization logic, which gives the data to the pipeline, is implemented in a special interface. This interface consists of counters and latches. The counters are orchestrated to generate the proper addresses, while the latches are needed to implement a caching logic, which saves some of the memory used.

The design of the Accumulator is the most important part of the pipeline's architecture, since it computes intermediary values and at the end provides the final result. As mentioned above, special considerations need to be made with regard to the accumulator because of the latencies introduced by the adders in the FPlibrary (3 cycles).

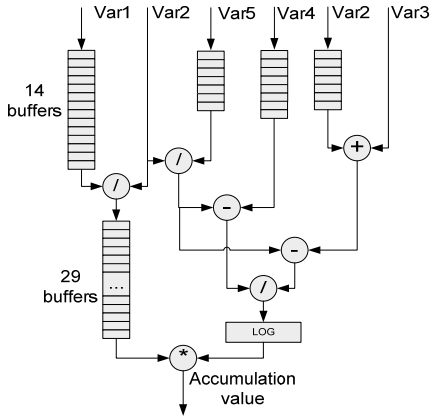

Figure 4: Second stage. Computing accumulation value.

The values that will be accumulated come and enter the final stage, which is an accumulator having a classical structure, using a feedback input.

3.3 Hardware Implementation Issues

The performance and feasibility of the hardware implementation largely depends on its physical support. Our hardware platform was a Digilent Inc. board populated with a Xilinx Virtex2PRO30 FPGA device. The problem with this implementation was that it is quite large: it depleted the space of the FPGA device we had available at this moment. To estimate the total space needed, we synthesized the design for a larger FPGA device (a Virtex4 160LX). A report of the device utilization is shown below:

Selected Device:	4vlx160ff1148-12	
Number of Slices:	23656 out of 67584	35%
Number of Slice Flip Flops:	20834 out of 135168	15%
Number of 4 input LUTs:	44515 out of 135168	32%
Maximum frequency:	137.552 MHz.	

The implementation fits without problems on this Virtex4 board. Regarding an implementation on our Virtex2Pro board two options were available.

The first option was to reduce the precision at which the pipeline operated. This ensured a reduction of both the buffer stages that provided the synchronization between the stages and a reduction in size of the operators.

This option was first implemented. We reduced the mantissa of the operands by 10 bits. Instead of a large mantissa having 23 bits, the mantissa now had only 13 bits. Although the design fitted on a Virtex-II Pro board at about 98% of its capacity, the results obtained with this method were discouraging. They were more then 30% off from the actual result provided by Matlab. Therefore another method needed to be found.

The next option was to reduce the frequency at which the pipeline stage operates and time-multiplex some of the resources (square root – three occurrences in design, some of the adders). This has the advantage of preserving the pipeline's precision, the cost being a reduction in speed: the operating frequency was 85.714, MHz related to the weaker characteristics of the FPGA device and the more precise timing requirements.

4 EXPERIMENTAL RESULTS

The main achievement of the hardware implementation over the software one is the reduction in computation time. By performing one accumulation per clock cycle the hardware solution is indeed efficient and can be used even for the most complex magnetic stimulation systems.

In terms of complexity, both implementations, in software and in hardware, have the same complexity, $O(n^2)$ with n being the number of distinct segments. As mentioned in Section 4, the specific hardware structure performs one accumulation per clock cycle. That means that each clock cycle, a mutual inductivity between two segments is evaluated. The software implementation performs the same computations in a longer time.

We have analyzed our software and hardware implementations using the Slinky_1, Slinky_2 and Slinky_3 configurations (Figure 2). The values are given in Table 1, where a comparison is shown between the results provided by the software and the hardware solutions.

First we analyze simpler cases, 1 to 4 turns. The outer turns are the widest turns on the coil, while the inner ones are the neighbors of the outer turns located closer to the center. Then, the results for these configurations are presented. The analyzed quantity was the inductivity. The number of segments represents an indicator of the complexity.

The results of the two methods analyzed for the three configurations mentioned always stayed in the range of 3-4% of each other, with the Matlab results being slightly bigger than the results given by the hardware implementation. This can be attributed to the fact that Matlab uses by default double precision while in our system we have used only single precision operations. Indeed, a rough worst-case error analysis tells us that the accumulation, in the largest coil test, of 10.1920^2 floating-point numbers introduces a cumulative rounding error that may invalidate up to $\log_2(10.1920^2) = 25$ bits of the result, when the mantissa of a single-precision number holds 24 bits only.

This is a worst-case situation: in an actual simulation, the rounding errors compensate each other – this is why our results are still accurate. However, it shows that we will require increasing the precision of the floating-point format to use this architecture on larger coils. Fortunately, this extra precision is mostly useful in the final accumulator.

Table 1: Comparison of results.

Configuration	Inductivity (Hardware) [μH]	Inductivity (Software) [μH]	Number of segments
1 outer turn	0.097	0.097	64
2 outer turns	0.30	0.30	128
4 turns (2 out. 2 in.)	0.92	0.93	256
Slinky_1 coil	3.81	3.9	640
Slinky_2 coil	8.4	8.6	1,280
Slinky_3 coil	13.32	13.6	1,920

The flexibility of FPGAs allows us to use different precisions in different parts of the architecture. Besides, a format intermediate between single and double precision may be used. For us, a 32- or 36-bit mantissa would already be overkill (double-precision has a 53-bits mantissa). We will test this as soon as we get hold of a board with a larger FPGA than the Virtex-II used here. It should be noted that this more accurate pipeline will require more hardware, but the same execution time: it will still compute one accumulation per cycle.

One can see from Table 2 that the software running time is very large, so software computation becomes prohibitive for large systems.

Table 2: Comparison of performance.

Configuration	Duration (hardware) [no. of clock cycles]	Running speed* (hardware) [seconds]	Running speed (software) [seconds]
1 outer turn	40,960	0.00047	4.2
2 outer turns	163,840	0.00194	18
4 turns (2 out. 2 in.)	655,360	0.00764	72
Slinky_1 coil	4,096,000	0.04705	420
Slinky_2 coil	16,384,000	0.19411	1,680
Slinky_3 coil	36,864,000	0.42941	3,600

* at 85.714 MHz, clock period 11.66 ns

As a global comparison, the hardware solution runs approximately four orders of magnitude faster then the software one. The frequency is related to the physical board we had available, but for a more recent FPGA chip (i.e. Virtex4LX160, for which we did some simulations, or Virtex5), the device's capacity as well as the working frequency will increase, thus leading to an improved performance.

5 CONCLUSIONS AND FUTURE WORK

An adequate geometry of the stimulation coil can lead to a better focality of the stimulus (the ability of a coil to stimulate a small area of the tissue) and it can also improve the efficiency of the energy transfer from the coil to the target tissue. The form and size of the turns, their position inside the coil, the insulation gap between turns are all important parameters that should be considered when designing a magnetic coil. Therefore, in order to establish the most suitable coil geometry for a specific medical application, a large number of structures have to be tested, making of coil design a trial-and-error process, even if the risk involved is only computation time.

In (Creţ et. al., 2007), we analyzed the influence that space distribution of the magnetic coils' turns has on the efficiency of energy transfer from the stimulator to the target tissue. The analysis was performed for a Slinky_3 coil configuration, with applications on transcranial magnetic stimulation (TMS). It turned out that the electrical energy dissipated in the circuit of the stimulator – required in order to achieve the activation threshold – is 25% lower for the most efficient configuration than for the less efficient one, and the coil heating per pulse is also 35% smaller!

This estimation was based on the inductivity calculus described in this paper, and the large number of analyzed structures required a less time-consuming computation technique, the hardware implementation described above.

Since every medical application requires its own optimal structure of the magnetic coil, the results emphasized in this paper can play an important role for future work on coil design.

Because of the large amount of operations involved (several tens of millions just for one coil) it is very hard to debug such a hardware system at least at an acceptable level, but the obtained results show an excellent concordance with those obtained in software. Our implementation has the advantage of greatly speeding up the computation time and hence shortening the design process. On larger FPGA devices the process can achieve a greater speed by accommodating more computational structures in parallel. These structures would evaluate multiple pairs of segments in parallel and accumulate them to the final value.

REFERENCES

Collange, S., Detrey, J., & De Dinechin, F. (2006). Floating Point or LNS: Choosing the Right Arithmetic on an Application Basis. In *Proceedings of the 9th EUROMICRO Conference on Digital System Design*, Dubrovnik, Croatia, 197-203.

Creţ, L., Pleşa, M, Micu, D.D., & Ciupa, R. (2007). Magnetic Coils Design for Focal Stimulation of the Nervous System. In *Proceedings of EUROCON 2007, IEEE International Conference on Computer as a Tool*, Warsaw, Poland, 1998-2003.

Detrey, J, & De Dinechin, F. (2005). A Parameterizable Floating-Point Logarithm Operator for FPGAs. In *Proceedings of the 39th Asilomar Conference on Signals, Systems & Computers*, 1186 – 1190.

Detrey, J, & De Dinechin, F. (2007). FPLibrary. https://lipforge.ens-lyon.fr/projects/fplibrary/.

Griškova1, I., & Höppner, J. (2006). Transcranial magnetic stimulation: the method and application. *Medicina (Kaunas), 42(10)*, 792-804.

Guell, D., El-Ghazawi, T., Gaj, K., & Kindratenko, V. (2007). High-Performance Reconfigurable Computing, *IEEE Computer, 40 (3)*, 23-27.

Mozeg, D., & Flak, E. (1999). An Introduction to Transcranial Magnetic Stimulation and Its Use in the Investigation and Treatment of Depression. *University of Toronto Medical Journal, 76 (3)*, 158-162.

VISION OF THE VIRTUAL PROGRAMMER
Steps Towards Change in Instrument Systems for Implantable Medical Devices

Touby Drew and Steve Goetz
Neuromodulation, Medtronic, Inc., 800 53rd Avenue NE; MS N210, Minneapolis, USA
touby.drew@medtronic.com, steven.goetz@medtronic.com

Keywords: Implant, IMD, Instrument, Software, Trends, Architecture, Mainstream, Programmer.

Abstract: Active implantable medical devices increasingly depend on and interact with external systems of instrument hardware and software. Based on our work in defining and refining the direction of next generation instruments, we submit that there are and will increasingly be a trend towards complex, mainstream instrument systems, which are distributed, decoupled and part of rich modular information ecologies. As this shift occurs, important challenges arise and must be met with domain-specific solutions including those in the areas of security, repartitioning, and changes to instrument architecture and development.

1 INTRODUCTION

Traditionally instruments used to interrogate and configure implantable medical devices (IMDs) have tended to be isolated and proprietary. This paper discusses: (i) the trend for these instruments in the direction of mainstream computing as well as increasing complexity, connectivity, and loose coupling. (ii) security, obsolescence, and development issues becoming critical to the future of the IMD industry as a result; and (iii) means to address these challenges with system architecture, shared infrastructure, and changes in development.

2 BACKGROUND

Currently there is a range of active implantable medical devices (IMDs) and instruments which interact with them. This includes implantable pacemakers, cardioverter defibrillators (ICDs), neurostimulators (INSs), pumps, and other devices which are created by companies such as Medtronic, St. Jude Medical, and Boston Scientific. The scope and prevalence of use of IMDs is significant and growing as "the market for electronically driven implantable devices is set to expand significantly… and will reach $33.8 billion by 2009" (Groen, 2007).

"Instruments" or "programmers" are the systems which accomplish "non-invasive reversible alteration of the electronic performance of an implanted device" (Harthorne, 1983). "Programming" has come to mean any interaction with the data or settings of an IMD. Configuration of IMDs was first accomplished percutaneously, but by the 1980's sophisticated, wireless communication "allowed for the possibility of speedier transmission, bidirectional telemetry, and greater proprietary/security access coding" (Schoenfeld, 1993). As programming evolved, instruments became complex, special purpose computing platforms incorporating communications technology for interfacing with the IMDs.

The term "telemetry" describes the parts and protocols of "programming" directly involved in communication between an IMD and an instrument. Telemetry is proprietary, varied, and optimized for domain constraints (e.g. ECG streaming). At Medtronic, for example, telemetry in use today varies in physical layer encoding, data layer manipulation, and in application messaging to the extent that no single instrument supports all of them.

Recently, telemetry tends towards longer range (e.g. Conexus™), standardization (e.g. MICS-band), and decoupling from other aspects of programming. This decoupling is seen in the proprietary-cable-connected 8840T telemetry head which has its own processor and software but is actually part of the handheld 8840 N'Vision™ Clinician's Programmer used with Medtronic Neuromodulation products.

In addition to telemetry interfaces, programmers often have other specialized functionality. For example, many cardiac instruments include a pacing

system analyzer and a strip chart printer for ECG waveform. These have historically been tightly integrated with telemetry and IMD configuration software on special purpose computing platforms to define traditional programmers.

3 INSTRUMENT TRENDS

Instruments have begun to incorporate modern, mainstream computing platforms, driven by the market and increasingly capable IMDs. Key aspects of this trend include growing complexity as well as more connectivity and looser coupling between instruments and their component technologies.

3.1 Complex and Polymorphic

IMDs have grown beyond their pacemaker roots – INSs alone are being applied by a number of companies in therapies ranging from gastroparesis to epilepsy. As the therapy, diagnostic, and other capabilities of IMDs become increasingly complex and varied so does their programming, instruments, and information management. In one division of Medtronic alone it was estimated that more than 150 applications accounting for several tens of millions of lines of software code are being used and maintained. Though some of this is due to the long support life of IMDs (and corresponding legacy in instruments), some is a result of change in technology and user desire. For example, telemedicine has driven the development of distributed instrument systems like the CareLink™. To this extent, a single instrument system is difficult to achieve and instrument solutions are tailored to user and business needs (e.g. of particular therapies).

3.2 Connected and Loosely Coupled

As new instrument capabilities are introduced, there is increasing pressure to modularize, distribute, and connect instrument functionality (across instruments as well as other external systems). One example is the integration of remote monitoring systems (such as CareLink™, Housecall Plus™, and LATITUDE™) and traditional instruments. A second driver is the increasing prevalence of personal therapy manager (PTM) instruments, which a patient can use to journal or adjust therapy in a manner different from, but complimentary to, clinicians' programming.

There are also internal business motivations for modularizing and connecting instrument functionality. As noted, it is essential that telemetry remain connected, but it is a common target for decoupling from the rest of an instrument. This is partly because of its unique constraints and proprietary nature, but also to facilitate the abstraction and reuse of hardware and software which are required by multiple instruments.

In addition to the growth of connectivity and reuse across programmers, there is increasing connection between programmers and existing clinical and general purpose infrastructure. For example, though proprietary printing capability is built into programmers such as the Medtronic 2090, the 8840 prints via IR and may support other standard interfaces in the future. Similarly, clinicians are increasingly demanding that instruments allow them to export information to and view data from electronic medical record (EMR) systems and their mainstream PCs, where increasingly standardized, networked systems are changing the face of care.

3.3 Instruments and Modern, Mainstream Computing

As previously described trends continue there is crosspollination to the extent that once-entrenched boundaries are now blurring. Companies like Mednet and Raytel allow clinicians to outsource IMD follow-ups. Patients can review and control their own therapy and physiology with patient oriented instruments, reports, and data systems. Clinicians are increasingly able to interact with patients, data, and IMDs, from their home to their patients', using mainstream tools and infrastructure.

In this way, instruments are using and becoming a small part of the rich, modern, general purpose computing technology pool. Starting with cautious steps into carefully controlled and customized commercial components and then connecting electronically for telemedicine and software distribution, programmers like the Medtronic 2090 have evolved and continue to grow in this direction. For example, Advanced Neuromodulation Systems (ANS) released a PDA-based instrument which prominently displays the HP logo on the front and a Microsoft Windows™ logo on the back (Rapid Programmer 3.0, 2007). Though there is some proprietary aspect of programmers like this, they are largely customizations built on general purpose computing platforms. This is apparent in the fact that the ANS Rapid Programmer™ was seen only three years earlier sporting a Compaq rather than HP logo (Pain Medicine Network, 2004).

Instrument manufacturers are realizing that in the near future isolation from the mainstream will be

untenable as the race to meet growing needs reliant on complexity and connectivity progresses. We submit there is a double-edged 'Red Queen's race' in that near continual evolution of not only proprietary instrument capability, but also its integration with mainstream technology will be important to remain competitive.

3.4 The Virtual Programmer Future

Design of next generation instruments should follow a direction consistent with the industry trends described previously. Some distance down this road we submit there may be a `virtual programmer' that, unlike IMD instruments today, relies almost entirely on shared, general-purpose, existing infrastructure such as clinician's PCs and a more virtual, distributed network of functionality. The programmer, in the form of hardware, operating systems, and other components provided by IMD manufacturers disappears – to be replaced by a changing, mainstream, connected pool of resources largely owned and maintained by others.

Commenting on this idea one of Medtronic's regulatory experts noted that this would be a "revolutionary change rather than an evolutionary one" and could not be achieved overnight (Peterson, 2007). To this end, a first step might be to transition to the mainstream, buy and operate on a commercial off the shelf (COTS) platform, and separate from that any domain specific components which must remain proprietary. The IMD manufacturer would still control (in a regulatory and legal sense) the programmer, as has traditionally been the case. The second step would then be to transition to the use of general purpose, clinician owned and maintained PCs, operating systems and technologies in place of all but the essential proprietary components. To our knowledge no such clinician PC based instrument system exists today despite the potential hardware and support cost savings.

4 SHIFTING CONCERNS

As a result of our work towards a virtual programmer, we have begun to see what we believe are key challenges in security, obsolescence, and development which are and will be echoed across the industry. With simple, isolated instruments there is a low attack surface or room for misuse to motivate complicated security concerns. As trends continue toward complex, connected, mainstream components outside the control of the instrument manufacturer, associated migration and development costs beget significant additional concern.

4.1 Security

With instruments, there is the potential for some severe types of harm including discomfort, death, and exposure of protected health information (PHI). Complex, mainstream, connected, general purpose computing is notorious for having a high rate of breach due to a number of different vectors which are not of significant concern for traditional instruments. Windows operating systems (e.g. in the PainDoc™ programmer) are infamous for having their "survival time" measured in minutes when exposed to the Internet (SANS™, 2007). This combination begets a potential for high severity and high frequency security challenges. Also, in a connected, virtual programming environment, one can imagine new and frightening scenarios. One might no longer have to get within a few feet of each implant to program it or interrupt service to it and anyone with internet access could potentially access or affect a tremendous volume of PHI, patients, IMDs and instruments in patients' homes and clinics. Instruments could become a risk to their host clinical environments and they could be severed from their increasingly important information ecology or inadvertently open a backdoor for hospital infrastructure to be compromised.

Though scenarios involving malicious attack against patients (e.g. Vice President Cheney via his ICD), addictive self medication, or even attempts to manipulate the stock of a public instrument manufacturer are regularly raised, perhaps the greatest risk lies in less specifically targeted security scenarios in which needed therapy is unavailable or delayed. In many cases instruments are essential to the therapy of patients to the extent that if programming is unavailable when changes are required or an IMD state is unknown there may be significant patient harm. The ability to program could be lost or interrupted by something as minor as the instrument software not having sufficient resources to operate (e.g. because malcode or user software has used up RAM).

4.2 Obsolescence and Development

Recently companies like St. Jude, and Medtronic (e.g. 2010 programmer) have begun basing their instruments on COTS platforms available from companies like Microsoft, Intel, HP and others from the broader computing market. With these mainstream components come mainstream

capabilities, but also mainstream development cycles and obsolescence concerns.

Medtronic's 8832, for example, was based on the coupling of telemetry hardware with a Handspring™ Visor through the proprietary Springboard slot which is no longer be available. With the hardware platform effectively dead, this is an additional source of replacement cost and lost synergy relative to a more maintainable common PTM platform.

In the case of a virtual programmer the user and third parties would be rapidly altering their software environment creating numerous configurations and interactions which might cause issues. It would be unacceptable to allow users to keep their operating systems unpatched or to require IMD manufacturers to anticipate, support and test every permutation.

5 MEETING NEW CHALLENGES

Despite the magnitude of effort applied to topics related to IMD and instrument futures, we are unaware of any published work exposing these challenges or exploring paths to confront them within the domain and focus laid out earlier in this paper. This section attempts to summarize key approaches and examples related to architecture, infrastructure, and development changes which we submit are valuable to consider in this light.

Careful definition of the recently evolved concept of an independent, proprietary telemetry module (TM) exemplifies how careful repartitioning and organization of instrument functionality can be a valuable approach to consider. Separating critical and proprietary functionality into a decoupled component allows it to evolve and operate independently so long as a standard interface is maintained. Furthermore, an entire class of safety and security concerns related to the failure or unavailability of a COTS clinician's programmer could be addressed for example if the TM it used was developed to include independent "safe mode" and authentication capability.

As instruments become increasingly complex and mainstream, the infrastructure through which they are manufactured, operated, and deployed must fundamentally change from their expensive, isolated, monolithic, IMD manufacturer-proprietary past to leverage the benefits of the technical and business community they are joining. In the virtual programmer scenario, significant development, support and integration costs might be reduced or offloaded by leveraging networks, PCs, IT people, and other key resources from customers and groups which distribute costs. Companies like Intel and Motion Computing are already positioning for such roles in the vertical healthcare market with initiatives like Intel Health and the Motion C5.

Definition and use of standard, domain specific languages and tools may further allow for better (clear, constrained, abstract, etc) development path for programmers. These could include HL7, DICOM, those which may emerge from the IMD domain, and others (McDonald, 1997).

To this end, those who develop instruments may have to be increasingly open to two major changes: 1) extensive partnership, cohesive integration, and cross pollination blurring traditional product, business, and even industry/academic boundaries and 2) a phased approach with multiple steps to achieving long term goals through focussed evolutionary changes.

6 CONCLUSIONS

Instruments for programming IMDs form an interesting domain with trends towards decoupled architectures, connectivity, complexity, and the mainstream which are emerging as part of a poorly defined path towards solving evolving challenges in security, obsolescence, and development.

REFERENCES

Groen, P. Implantable Medical Devices and EHR Systems. Last viewed June 25, 2007. http://www.hoise.com/vmw/07/articles/vmw/LV-VM-06-07-5.html

Harthorne JW. Programmable pacemakers; Technical features and clinical applications. In L Dreifus (ed.); *Pacemaker Therapy*. Philadelphia, PA, F.A. Davis, 1983. pp. 135-147.

McDonald C. The barriers to electronic medical record systems and how to overcome them. *J Am Med Inform Assoc.* 1997;4:213–21.

Pain Medicine Network. page10. *American Academy of Pain Medicine*: Vol. 19, No. 3, Summer 2004.

Peterson, C., K. Ruth-Jarmon, et al. The Programmerless Programmer. May 2007.

Rapid Programmer 3.0. http://www.ans-medical.com/smallwonder/ Last viewed June 24, 2007

SANS™. "Survivial Time." Last viewed June 24, 2007. http://isc.sans.org/survivaltime.htm

Schoenfeld, Mark H. 1993. *A Primer on Pacemaker Programmers Pacing and Clinical Electrophysiology* 16 (10), 2044–2052. doi:10.1111/j.1540-8159.1993.tb00998.x

AUTOMATIC DEACTIVATION DESIGN FOR PHASED ARRAY SURFACE PROBE IN 1.5T MRI

Fotios N. Vlachos, Anastasios D. Garetsos and Nikolaos K. Uzunoglu
School of Electrical and Computer Engineering, Narional Technical University of Athens
9 Iroon Polytechniou, 15773, Zografou, fvlachos@esd.ece.ntua.gr

Keywords: Automatic tuning, phased array, MR imaging, spectroscopy.

Abstract: We have designed and developed an automatic switching mechanism that deactivates and activates a reception coil during the MR experiment according to the phase it is at. The mechanism uses a feedback loop in which a comparator defines whether the current reception signal derives from the RF excitation pulses or the MR signal and then triggers an analog switch at the back-end of the coil accordingly. We applied the mechanism on a custom-made four channel phased array probe and tested its functionality by transmitting RF pulses to the probe of similar length and power to those used in actual MRI systems. The results presented in this paper demonstrate the robustness of the design and its switching accuracy.

1 INTRODUCTION

In the last ten years there has been much progress in the development of fully autonomic probes for MR Imaging and Spectroscopy. In most of the experimental attempts, emphasis is given on the automatic tuning and matching (Hwang and Hoult, 1998; Pérez de Alejo et. al., 2004) of the coils in order to improve the signal-to-noise ratio (SNR) values and accelerate the initialization procedures that keep the patient for an extensive period of time in the MRI bore.

All automatically tuned and matched coils require being compatible with the pulse sequences used in the MR experiment, which implies detuning of the coils during the RF pulse transmission and re-tuning for the MR signal reception. A series of complex automatic deactivation techniques have been developed and tested in the past (Venook et. al., 2005), which function in parallel with the tuning and detuning procedures but suffer robustness and poor results.

The most common deactivation technique that has been applied in both conventional and experimental non-automatic configurations is the use of PIN diodes at the back-end of the probe (Yung et. al., 2003; Barberi et. al. 2000). These configurations, however, are totally dependable on the external signals that the MR scanner supplies in order to turn on or off the PIN diode.

In this study, we present a simple and robust automatic design that undertakes the responsibility of deactivating and activating the probe during the RF pulse transmission and the MR signal reception phase respectively. The design does not require the presence of any external signals and is fully functionable with a large variety of RF pulse lengths and powers.

2 MATERIALS AND METHODS

The automatic deactivation circuitry that was constructed was applied on a prototype human prostate phased array probe, which we designed and developed after simulation modelling and laboratorial measurements.

2.1 Probe Design

The probe is consisted of four rectangular coils of dimensions 8 × 16 cm and the material that was used for their construction was copper tape 1 cm wide and 1 mm thick. The coils are distributed into two pairs of adjacent elements and each pair is positioned inside an orthogonal shaped conductor frame made of acetal (Fig. 1A). When a patient is examined the two frames are locked at a fixed distance so the elements are placed at the center posterior and

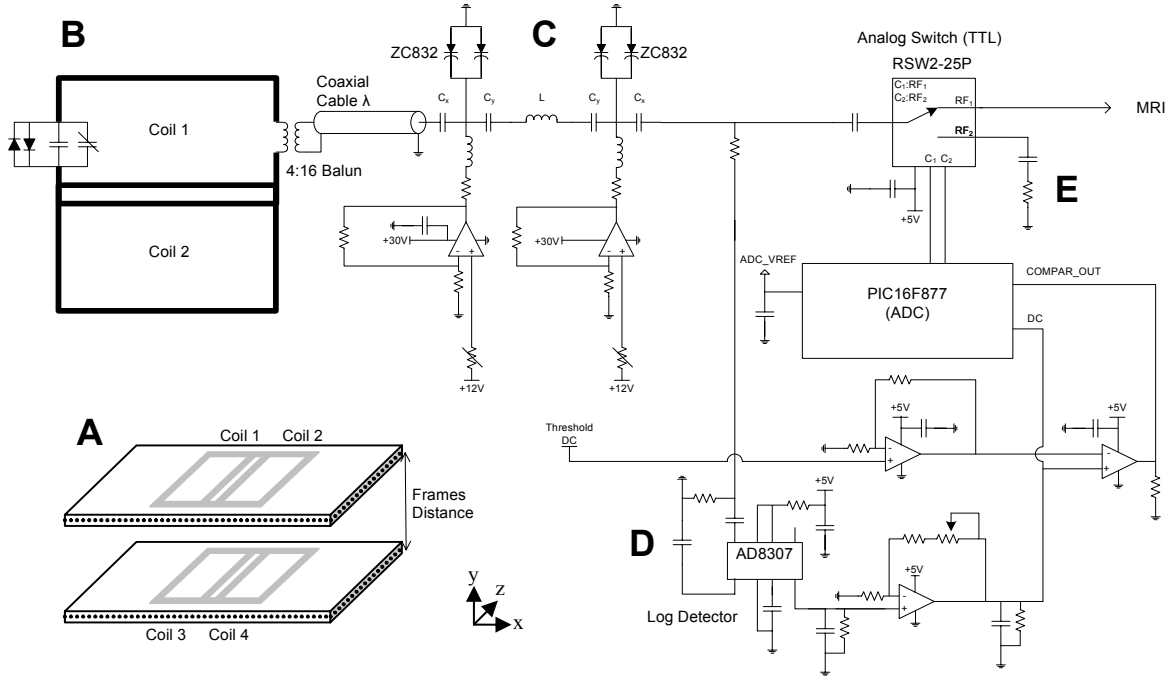

Figure 1: Phased Array probe's design and circuit diagram. Two pairs of coils are positioned inside two acetal frames (A). Each coil carries two antiparallel crossed diodes for passive blocking and a variable capacitor for tuning (B). The fine-tuning/matching circuitries are positioned on four PCBs at λ distance away from the elements. Each PCB includes the automatic deactivation circuitry that interacts with the probe through a feedback loop. The tuning section (C) uses two pairs of ZC832 varactor diodes in a pi-network to match the output impedance. The feedback section (D) rectifies the RF pulses into DC signals, which are then compared to a threshold DC value. The comparator's output is processed in the microcontroller (E), which determines when the probe is in the activation and the deactivation phase and controls an analog switch that connects the probe to the MRI scanner.

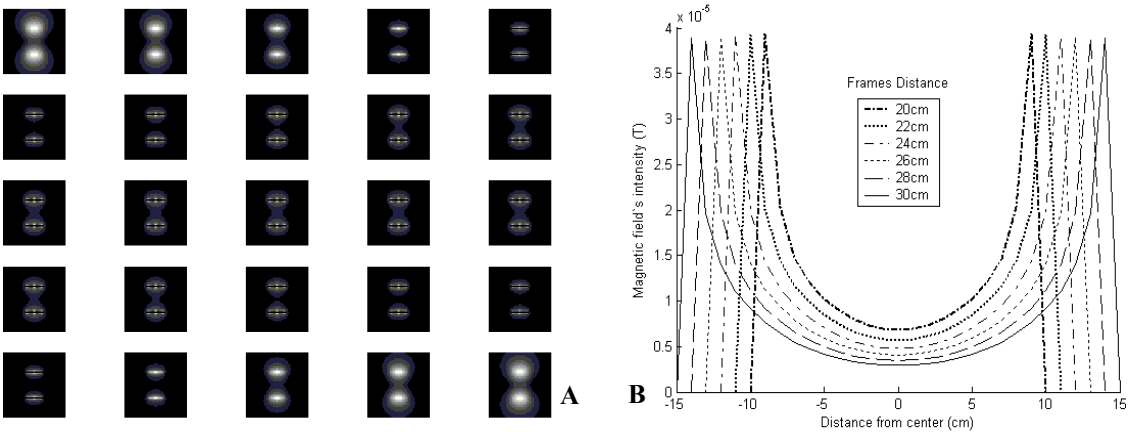

Figure 2: Probe's theoretical simulation results. (A) Computed magnetic field's intensity distribution on various xy planes for frames distance 24 cm. (B) Magnetic field's intensity at the line that connects the centers of the parallel frames for various frames distances.

anterior surface of the pelvic area in order to achieve optimum phased array performance.

Magnetic field and inductance calculations were carried out using the Biot-Savart integral expression (Wright and Wald, 1997). The configuration of the probe was modelled with simulation programming in order to measure the magnetic field's intensity in all three dimensions (Fig. 2A) and calculate the intensity's drop percentage at the center of the pelvic region in comparison to the intensity 1 cm away from the coils at the surface of the test object. The theoretical measurements were done for various distances between the frames of the probe and the

results showed that the drop percentage does not fall under 7.66% in the worst case scenario of frames distance 30 cm (Fig. 2B).

The method that was used for the adjacent elements decoupling was overlapping (Roemer et. al., 1990). Theoretical calculations with simulation programming indicated that the distance the adjacent coils should have in order to minimize the mutual inductance is 6.7 cm. That translates in 8-6.7=1.3 cm coils overlap.

The probe is enhanced with a passive blocking network of two anti-parallel high speed diodes (Fig. 1B) that behave as a short circuit when they are forward-biased and serve as a safety precaution for the rest of the system's electronics (Noeske et. al. 2000; Zhang and Webb, 2005). 4:16 balun elements at the back-end of the rectangular loops convert the balanced output signal of the coils to 50 Ohm unbalanced. The tuning and the matching of the probe is manually controlled from a variable non-magnetic capacitor and 2 pairs of varactors in a pi-network (Fig. 1C), which lies one wavelength (λ) away from the coils.

2.2 Automatic Deactivation Design

The function of the MR probe is divided into two phases: the RF pulse transmission phase, during which the probe should be deactivated and disconnected from the MR scanner and the MR signal reception phase, during which the MR probe should be activated. The transition of the probe from the deactivation to the activation phase is controlled by the automatic deactivation circuitry, which connects between the probe and the scanner's preamplifier. The design of the circuitry is based on a feedback loop, which uses the probe's reception signals to define the phase that it is at.

An analog switch (RSW2-25P) is used to block the output of the probe from connecting to the MR scanner, when the RF pulses are transmitted. The switch is triggered by two signals (C1, C2) that a microprocessor sends (Fig. 1E). When the C1 signal is on (activation phase), the RF1 position of the switch is short-circuited and the scanner receives the MR signal. Contrarily, when the C2 signal is on (deactivation phase), the RF2 position is short-circuited and the high-power transmitted RF pulses are grounded, protecting the scanner's preamplifier. The decision between triggering signal C1 or C2 is taken from a comparator (LM393AD), which compares a pre-defined threshold DC voltage with the output DC signal that is rectified from the transmitting RF pulses, using a log detector (AD8307) and two RC low-pass filters (Fig. 1D). Consequently, when the high power RF pulses are transmitted, then the output DC signal's amplitude is higher than the threshold voltage, the analog switch is turned off and the probe enters the deactivation phase (C2 signal triggering). Contrariwise, when the output DC signal's amplitude is lower than the amplitude of the threshold, the analog switch is turned on and the probe is re-activated (C1 signal triggering), receiving low power MR signal from the hydrogen molecules' resonance.

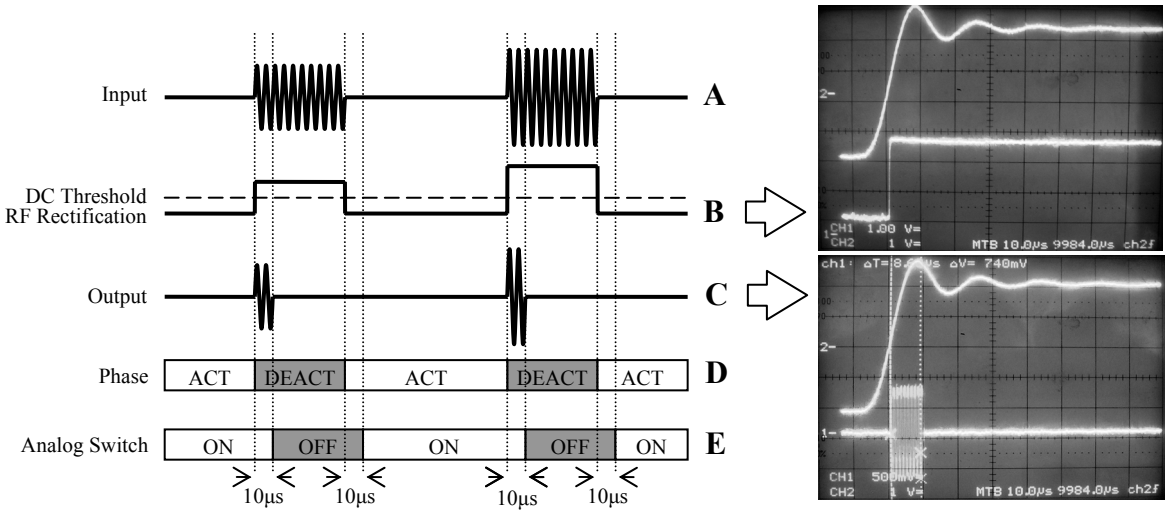

Figure 3: Switching mechanism's experimental results. (A) Transmitted RF pulses that are used as input to define the experiment's phase. (B) DC pulses produced from log detector's RF rectification (lower line in first combiscope figure). (C) Analog Switch's output (lower line in second combiscope figure). 10μs delay was calculated during the switching of the phase. (D) Optimum analog switch's behaviour following the experiment's phases. (E) Actual analog switch's behaviour with the undesired latency. Upper line in both combiscope figures depicts the trigger that generates the RF pulse.

3 RESULTS

Before the testing of the automatic deactivation circuitry we tuned and matched the coils of the probe in the Larmor frequency (63.87 MHz) by applying an average human pelvic region load on the frames and adjusting the values of tuning components. Using the network analyzer (HP8719D) to measure the reflection coefficient we managed to drop the S_{22} parameter at -55 dB, keeping the resonance frequency range below 250 KHz, which led to very accurate tuning. The decoupling between the adjacent elements was also successful, since the transmission coefficient S_{12} drops below -30 dB.

The functionality of the analog switch was tested in the laboratory using a Signal Generator (HP ESG-4000A) and a Combiscope (FLUKE PM3380B). RF pulses of the same power and length with those transmitted from the MRI system were created in the Signal Generator and were sent to the probe as input. The RF pulses varied in length from 2-5 ms and in power from 5-20 dBm.

The first set of measurements examined the log detector's functionality. Specifically, we measured the DC signal produced from the RF pulse rectification (Fig. 3B). The resulting DC pulse is initiated and terminated almost immediately after the beginning and the end of the signal generator's RF trigger respectively. Also, the correspondent DC pulse's amplitude is equal to the RF pulse's amplitude as expected, allowing accurate comparison with the DC threshold.

The second set of measurements showed the output of the probe and verified the turning off and on of the analog switch during the activation and the deactivation phase respectively (Fig. 3C). A potential disadvantage of the method is that there is an undesired latency of 10 μs in the switching process that is capable of producing artifacts in the imaging data (Fig. 3E). The latency is caused mainly from the processing delays of the microcontroller that triggers the analog switch and remains constant without regard to the RF pulse length and power that is triggered.

4 DISCUSSION

Certain improvements could be applied on the automatic switching mechanism of the circuitry in order to overcome the presence of latency in the function of the analog switch. A way to reduce the latency is to control the switch directly from the DC signal that derives from the comparator's output, bypassing the time-consuming processing of the microcontroller.

Also, a practical problem could potentially appear in the clinical application of the automatic deactivation circuitry. The probe detunes itself automatically during the RF pulse transmission and does not require a decoupling signal from the scanner. However, many MRI scanners' protocols run primary tests on the connected probes by sending pulse signals in the opposite direction for software initialization. In that case, the switch would cause compatibility issues and the probe would not be recognized by the MR system.

Our prototype automatic deactivation design is a robust and simplified mechanism that can be applied on self-tunable MR coils. It was tested in various conditions and found to be fully functional and able to switch off or on the probe at all times.

REFERENCES

Hwang, F., Hoult D.I. 1998, Automatic Probe Tuning and Matching, *Magnetic Resonance in Medicine*, 39, pp. 214-222.

Pérez de Alejo, R., Garrido, C., Villa, P., Rodriguez, I., Vaquero, J.J., Ruiz-Cabello, J., Cortijo, M., 2004, Automatic Tuning and Matching of a Small Multifrequency Saddle Coil at 4.7T, *Magnetic Resonance in Medicine*, 51, pp. 869-873.

Venook, R.D., Hargreaves, B.A., Gold, G.E., Conolly, S.M., Scott, G.C., 2005. Automatic Tuning of Flexible Interventional RF Receiver Coils, *Magnetic Resonance in Medicine*, 54, pp. 983-993.

Yung, A.C., Oner, A.Y., Serfaty, J.M., Feneley, M., Yang, X., Atalar, E., 2003. Phased-Array MRI of Canine Prostate Using Endorectal and Endourethral Coils, *Magnetic Resonance in Medicine*, 49, pp. 710-715.

Barberi E.A., Gati J.S., Rutt B.K., Menon R.S., 2000. A Transmit-Only/Receive-Only (TORO) RF System for High-Field MRI/MRS Applications, *Magnetic Resonance in Medicine*, 43, pp. 284-289.

Wright S.M., Wald L.L., 1997. Theory and Application of Array Coils in MR Spectroscopy, *NMR in Biomedicine*, 10, pp. 394-410.

Noeske R., Seifert F., Rhein K-H., Rinneberg H., 2000. Human Cardiac Imaging at 3 T Using Phased Array Coils, *Magnetic Resonance in Medicine*, 44, pp. 978-982.

Zhang, X., Webb, A., 2005. Design of a Four-Coil Surface Array for in Vivo Magnetic Resonance Microscopy at 600 MHz, *Concepts in Magnetic Resonance Part B*, 24B(1), pp. 6-14.

Roemer P.B., Edelstein W.A., Hayes C.E., Souza S.P., Mueller O.M., 1990. The NMR Phased Array, *Magnetic Resonance in Medicine*, 16, pp. 192-225.

STUDY OF A 4DOF UPPER-LIMB POWER-ASSIST EXOSKELETON WITH PERCEPTION-ASSIST

Second Stage of Power-Assist

Kazuo Kiguchi and Manoj Liyanage
Graduate School of Science and Engineering, Saga University, 1 Honjomachi, Saga, Japan
kiguchi@me.saga-u.ac.jp, 06549002@edu.cc.saga-u.ac.jp

Keywords: Power-Assist, Perception-Assist, Exoskeletons, Robots, EMG.

Abstract: As a second stage of the research on power-assist exoskeleton systems, this paper presents a new concept of an upper-limb power-assist exoskeleton that can assist physically weak persons in performing their daily activities. The proposed exoskeleton assists not only the motion of the user but also the perception of the user by using sensors. In the proposed power-assist method, the assisted user's motion can be modified based on the environmental information obtained by the sensors if problems are found in the user's motion. The effectiveness of the proposed concept is evaluated by performing experiments.

1 INTRODUCTION

Decrease in birthrate and increase of percentage of aged people are progressing in several countries. In these societies, the shortage of nursing people has become a serious problem. Many robotic systems such as power-assist robots (Kiguchi, *et al.*, 2001-2007; Rosen, *et al.*, 2001; Kawamoto and Sankai, 2005; Naruse, *et al.*, 2004; Sasaki, *et al.*, 2004; Guizzo and Goldstein, 2005; Vukobratovic, 1975) have been proposed to cope with this problem. We have proposed power-assist exoskeletons to assist the upper-limb motion of physically weak persons such as disabled, injured, and/or elderly persons since the upper-limb motion is important for daily activities. The conventional exoskeletons only assist the motion of the user (Kiguchi, *et al.*, 2001-2007). As a second stage of the research on power-assist exoskeleton robot systems, this paper proposes a new concept of an upper-limb power-assist exoskeleton in order to assist physically weak persons in performing their daily activities.

In the conventional power-assist exoskeletons, the motion of the user is supposed to be assisted in accordance with the user's motion intention. The skin surface electromyogram (EMG) is often used to detect the user's motion intention (Fukuda, *et al.*, 2003) since it directly reflects the user's muscle activity. Therefore, information of the EMG signals and/or force sensors is often used to predict the user's motion intention in the conventional power-assist exoskeletons (Kiguchi, *et al.*, 2001-2007). However, in the case of physically weak persons, the perception ability is also poor sometimes. For example, such persons sometimes unknowingly trip over small obstacles because of their poor perception ability. Therefore, it is important to assist the sensing ability of physically weak persons by using sensors on robotic exoskeletons. Any sensor such as ultrasonic sensors, infrared sensors, and/or CCD sensors can be a candidate for the sensors for the perception-assist.

In the proposed power-assist method, the assisted user's motion can be modified based on the environment information obtained by the sensors if the exoskeleton detects some problems in the user's motion. For example, if the exoskeleton notices that the user's hand is going to collide with an obstacle, an additional assist force including the power-assist force is provided to the user's motion in order to avoid the collision between the user and the obstacle. On the other hand, the exoskeleton attempts to guide the user's hand to an object when the exoskeleton notices that the user is going to grasp that object, but his hand is not moving along the correct trajectory. If the modified motion by the exoskeleton is different from the user's intended motion, the exoskeleton changes its strategy in accordance with the user's motion intention. When motion modification is not required (i.e., when there is no

problem in the user's motion), the control method is the same as the conventional EMG-based power-assist method (Kiguchi, *et al.*, 2007).

In this study, the proposed power-assist method is applied to a 4DOF upper-limb power-assist exoskeleton. The exoskeleton assists shoulder flexion/ extension, shoulder horizontal flexion/ extension, elbow flexion/ extension, and forearm supination/pronation motion.

2 UPPER-LIMB POWER-ASSIST EXOSKELETON

In order to assist 4DOF upper-limb motion, a power-assist exoskeleton (Fig. 1) was developed (Kiguchi, *et al.*, 2007). It mainly consists of a shoulder motion support part, an elbow motion support part, and a forearm motion support part. The exoskeleton system can be installed on a mobile wheel chair.

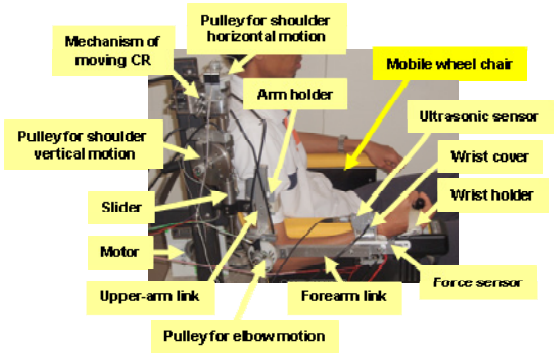

Figure 1: 4DOF upper-limb power-assist exoskeleton.

Usually, the movable range for the human shoulder is 180º in flexion, 60º in extension, 180º in abduction, 75º in adduction, 100-110º in internal rotation, and 80-90º in external rotation. The limit on the range of forearm pronation-supination motion is 50-80º in pronation and 80-90º in supination, and that on the elbow flexion-extension motion is 145º in flexion and -5º in extension. Considering the minimally required motion in everyday life and the safety of the user, the shoulder motion of the 4DOF exoskeleton is limited to 0º in extension and adduction, 90º in flexion, and 90º in abduction. The limit on its forearm motion is decided as 50º in pronation and 80º in supination, and that on the elbow motion is decided as 120º in flexion and 0º in extension.

3 POWER-ASSIST WITH PERCEPTION-ASSIST

In the conventional power-assist robot systems, the user's motion intention is estimated in real-time; subsequently, the estimated motion is assisted by the power-assist robot systems (Kiguchi, *et al.*, 2001-2007). However, the perception ability is also deteriorated sometimes in the case of physically weak persons. Therefore, there is a possibility of colliding with an obstacle, tripping over a small obstacle, or failing to grasp an object even though the motion is assisted according to the user's intention. In this study, the perception of the environment is also assisted by the exoskeleton.

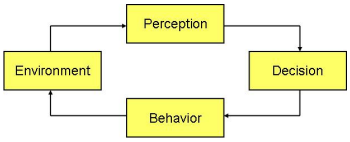

(a) Human behavior cycle.

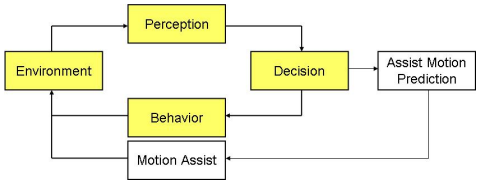

(b) Conventional power-assist cycle.

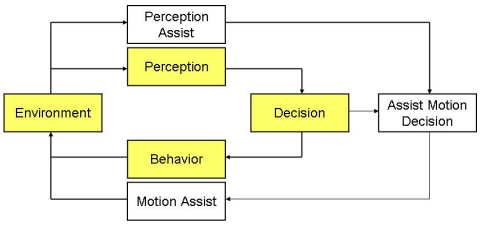

(c) Proposed power-assist cycle.

Figure 2: Power-assist cycles.

The concepts of the human behavior cycle, the conventional power-assist cycle, and the proposed power-assist cycle are depicted in Fig. 2 in order to show the difference among them.

In the proposed power-assist process, when the user's motion is not interacting with the environment, the power assist is the same as the conventional power assist. Moreover, when the user interacts with the environment properly, the power-assist method continues to be the same as the conventional power-assist method (Fig. 3(a)). However, if the exoskeleton infers that the user is attempting to grab an object and the user has miscalculated the position of the object, motion modification is carried out to ensure the correct hand trajectory to the object, as

shown in Fig. 3(b). If the modified motion is correct (i.e., the decision of the exoskeleton is correct), then the ordinal power assist is performed after the motion modification, as shown in Fig. 3(a). However, if the modified motion is wrong (i.e., the decision of the exoskeleton is wrong), the user attempts to reject it (sometimes unconsciously) as shown in Fig. 3(c). This rejection can automatically be detected by the exoskeleton by monitoring the user's EMG signals. Sub sequently, the exoskeleton changes its strategy, and another motion modification is carried out in order to avoid a collision with the object.

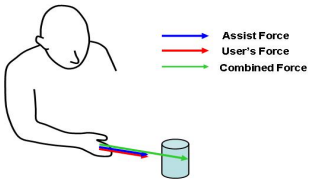

(a) Ordinal power-assist.

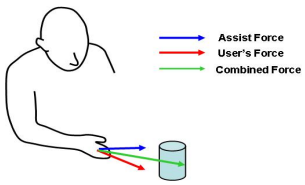

(b) Motion modification.

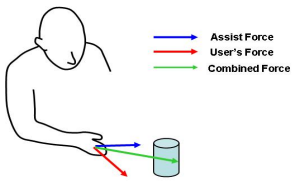

(c) Wrong motion modification.

Figure 3: Motion modification.

4 CONTROL METHOD

4.1 EMG

The EMG signals are used as the main input signals in order to control the exoskeleton in accordance with the user's motion intention. Since it is difficult to use the raw EMG signal as input information for the controller, the root mean square (RMS) value of the signal is calculated to extract the feature from the signal. The equation for the RMS value is written as:

$$RMS = \sqrt{\frac{1}{N}\sum_{i=1}^{N} v_i^2} \qquad (1)$$

where v_i is the voltage value for the i^{th} sampling and N is the number of samples in a segment. In this study, the number of the sample is set to be 100 and the sampling time is 500 μsec.

When a certain motion is performed, the EMG signals of the related muscles show a unique pattern. Therefore, since the magnitude of the RMS of the EMG signal indicates the activity level of the muscles, the upper-limb motion of the user can be predicted by monitoring the EMG signals of certain muscles of the user.

In order to predict the 4DOF motion, the EMG signals from the related muscles of 12 locations are measured in this study (Kiguchi, *et al.*, 2001-2007).

4.2 EMG-Based Control

The basic architecture of the controller is depicted in Fig. 4. The controller basically consists of a power-assist part and a perception-assist part. The power-assist part consists of three stages (first stage: input signal selection stage; second stage: posture region selection stage; and third stage: neuro-fuzzy control stage). This power-assist part is basically the same as the conventional EMG-based controller (Kiguchi, *et al.*, 2007). In the first stage of the power-assist part, the EMG-based control or the wrist-sensor-based control is applied in accordance to the muscle activity levels of the user. In the second stage of the power-assist part, proper neuro-fuzzy controllers are selected according to the shoulder and elbow angle regions. In the third stage of the power-assist part, the torque required for each joint motion assist is calculated by using the selected neuro-fuzzy controllers.

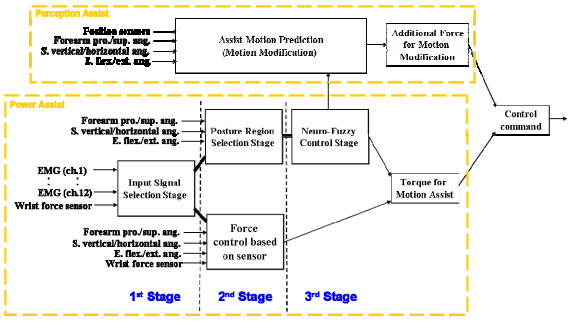

Figure 4: Controller architecture.

In the perception-assist part, the sensor information and the estimated user's motion intention (the output of the neuro-fuzzy controllers) are used to decide the motion to be modified in this part. Sensors such as ultrasonic sensors, infrared sensors, and/or CCD sensors can be used to detect the objects in the environment. In this study, an

ultrasonic sensor [FW-H10R, Keyence] is applied to detect the objects.

The force vector of the assisting motion at the user's hand can be calculated on the basis of the estimated torque (the output of the neuro-fuzzy controllers) from the EMG signals in the third stage of the power-assist part. Since the estimated force vector contains noise and an estimated error, it is averaged with the estimated force vector data in the past. The relationship between the force vector at the user's hand and the joint torque vector of the user's upper-limb is written as:

$$F = J^{-T}\tau \quad (2)$$

where F is the force vector at the user's hand (averaged by using the past data), τ is the joint torque vector of the user's upper-limb, and J is the Jacobian matrix. The estimated force vector of the user directly indicates the user's motion intention.

4.3 Perception-Assist with Ultrasonic Sensor

When a user is moving his/her arm toward an object in order to grab it, the trajectory of the hand (tip of the arm) is the almost a straight line toward the object (Flash and Hogan, 1985). Therefore, the change in the distance of the tip of arm and the reduction in the distance between the tip of arm and the object are supposed to be the same. The change in the distance of the tip of arm is calculated by using the kinematics of the exoskeleton. The reduction in the distance between the hand and the object is calculated by using the ultrasonic sensor. When the arm is moving toward the object, these two values come close to each other but vary in a particular range. This range is determined based on the experimental results. It is important to select this range to be as narrow as possible in order to identify the trajectory of the arm more accurately.

If the exoskeleton identifies that the trajectory required for the user is different from the current user's trajectory, then the exoskeleton attempts to modify the trajectory by applying an additional force at the tip of the arm. If the estimated force vector at the user's hand is changing to the modified trajectory, the exoskeleton assumes that the motion modification strategy as correct. If the user's hand is moving along the correct trajectory to grab the object, no motion modification is provided to the user's motion. However, if the estimation force vector at the user's hand is changing to a direction opposite to the motion modification direction, the exoskeleton assumes that the motion modification strategy is not correct and attempts to determine another possibility. If the exoskeleton can not determine another possibility, then it simply performs the conventional power-assist.

5 EXPERIMENT

The experimental set-up is shown in Fig. 5. As shown, a plastic bottle was used as the object. In the experiment, upper-limb motion was performed toward the object. Two interface boards (RIF–171–1 and JIF–171–1) are used to process the A/D operations of potentiometer signals, force sensor signals, EMG signals, and ultrasonic sensor signals and also to process the D/A operations required to send the calculated torque commands back to the motor drivers to control the motors. The measured EMG signals are amplified by the EMG amplifier before sending them to the interface board. The motor torque commands are calculated in the PC and then sent to the four motor drivers to operate four motors. The output of the ultrasonic sensor is sent to the RIF–171–1 interface board and then processed with the same frequency as the other signals (i.e., 2,000 Hz frequency).

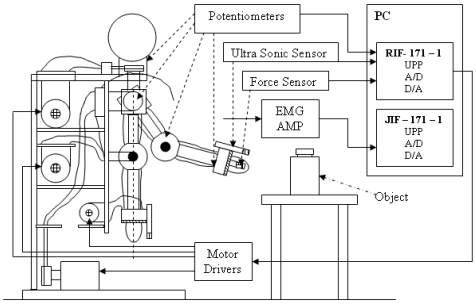

Figure 5: Experimental setup.

Three kinds of experiments were performed on the same subject in order to evaluate the effectiveness of the perception-assist. In the first experiment, the subject attempted to move the hand toward the object to grab it along the correct hand trajectory. In the second experiment, the subject also attempted to move the hand toward the object to grab it, but deliberately along a wrong trajectory. In the third experiment, the subject attempted to move the hand forward to avoid colliding with the object. In this experiment, a wrong trajectory (i.e., the trajectory for which the hand collides with the object) is generated deliberately.

Figure 6 shows the results of the first experiment. The hand trajectory determined by the exoskeleton, the distance to the object measured by the ultrasonic

sensor, the change in the position of the sensor, the raw EMG signal of the deltoid – anterior part, and the RMS value are shown in Fig. 6 (a). The estimated force vector at the user's hand (calculated from the output of the neuro-fuzzy controllers), the combined force vector (modified force vector), the assisted force vector (additional force for the motion modification), and the distance to the object measured by the ultrasonic sensor are shown in Fig. 6 (b). These experimental results show that the exoskeleton effectively performs the power-assist (conventional power-assist) on the basis of the user's motion intention, when there are no problems in the user's motion.

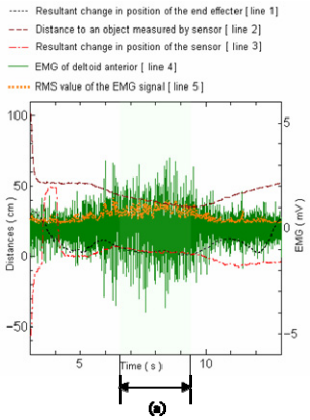

(a) EMG signal.

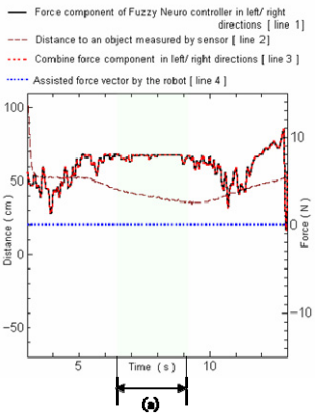

(b) Motion modification.

Figure 6: Experimental results of the first experiment.

Figure 7 shows the results of the second experiment. During the interval (a) in Fig. 7, the motion modification was performed to change the trajectory of the user's hand to the correct trajectory to proceed toward the object since the exoskeleton determined that the hand trajectory of the user is different from the estimated one. Since the decision of the exoskeleton was correct, the ordinal power-assist (power-assist without any motion modification) was performed until the user grasped the object (the interval (b)) after that.

Figure 8 shows the results of the third experiment. During the interval (a) in Fig. 8, the motion modification was performed to change the trajectory of the user's hand to a trajectory leading to the object since the exoskeleton determined that the trajectory of the user's hand was different from the estimated one. During the interval (b) in Fig. 8, the exoskeleton determined that its strategy was wrong and changed it to modify the trajectory of the user's hand to avoid a collision with the object. Since the second decision of the exoskeleton was correct, the ordinal power assist (power assist without any motion modification) was performed.

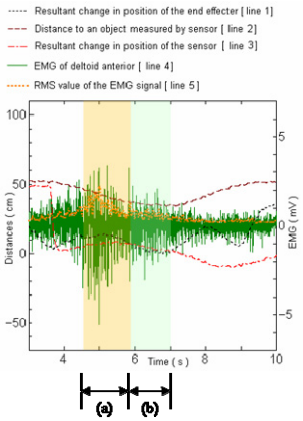

(a) EMG signal.

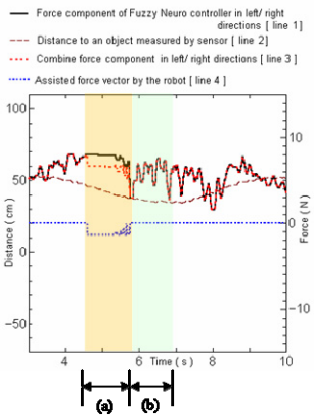

(b) Motion modification.

Figure 7: Experimental results of the second experiment.

These experimental results show the effectiveness of the proposed power-assist method with perception-assist.

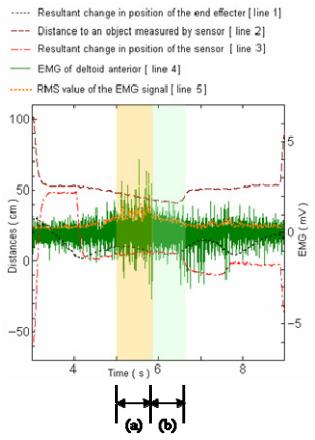

(a) EMG signal.

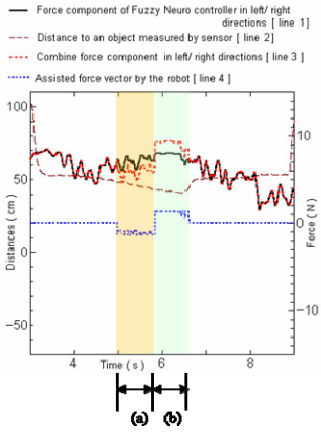

(b) Motion modification.

Figure 8: EMG of elbow biceps (short head) with power and perception assist.

6 CONCLUSIONS

A new concept of a power-assist exoskeleton that assists not only the motion but also the perception of the user by using sensors is proposed. In the proposed power-assist method, the user motion is modified by the exoskeleton if it is necessary, although the conventional power-assist robot never modifies the user motion. The effectiveness of the proposed power-assist exoskeleton was verified by performing experiments.

ACKNOWLEDGEMENTS

The authors gratefully acknowledge the support provided for this research by Japan Society of Promotion of Science (JSPS) Grant-in-Aid for Scientific Research (C) 19560258.

REFERENCES

Flash, T., Hogan, N., 1985. The coordination of Arm Movements: An Experimental Confirmed Mathematical Model, *Journal of Neuroscience*, vol.5, pp.1688-1703.

Fukuda, O., Tsuji, T., Kaneko, M., Otsuka , A., 2003. A Human-Assisting Manipulator Teleoperated by EMG Signals and Arm Motions, *IEEE Trans. on Robotics and Automation*, vol. 19, no. 2, pp.210-222.

Guizzo, E., Goldstein, H., 2005. The Rise of the Body Bots", *IEEE Spectrum*, vol.42, no.10, pp.42-48.

Kawamoto, H., Sankai, Y., 2005. Power Assist Method Based on Phase Sequence and Muscle Force Condition for HAL, *Advanced Robotics*, vol.19, no.7, pp.717-734.

Kiguchi, K., Esaki, R., Fukuda, T., 2005. Development of a Wearable Exoskeleton for Daily Forearm Motion Assist, *Advanced Robotics*, vol.19, no.7, pp.751-771.

Kiguchi, K., Imada, Y., Liyanage, M., 2007. EMG-Based Neuro-Fuzzy Control of a 4DOF Upper-Limb Power-Assist Exoskeleton, *Proc. of 29th Annual International Conf. of the IEEE Engineering in Medicine and Biology Society*.

Kiguchi, K., Iwami, K., Yasuda, M., Watanabe, K., Fukuda, T., 2003. An Exoskeletal Robot for Human Shoulder Joint Motion Assist, *IEEE/ASME Trans. on Mechatronics*, vol.8, no.1, pp.125-135.

Kiguchi, K., Kariya, S., Watanabe, K., Izumi, K., Fukuda, T., 2001. An Exoskeletal Robot for Human Elbow Motion Support – Sensor Fusion, Adaptation, and Control, *IEEE Trans. on Systems, Man, and Cybernetics, Part B*, vol.31, no.3, pp.353-361.

Kiguchi, K., Tanaka, T., Fukuda, T., 2004. Neuro-Fuzzy Control of a Robotic Exoskeleton with EMG Signals, *IEEE Trans. on Fuzzy Systems*, vol.12, no.4, pp.481-490.

Kiguchi, K., Yamaguchi, T., Sasaki, M., 2006. Development of a 4DOF Exoskeleton Robot for Upper-limb Motion Assist, *Proc. of 2006 ASME/JSME Joint Conf. on Micromechatronics for Information and Precision Equipment*, S10_03.

Naruse, K., Kawai, S., Yokoi, H., Kakazu, Y., 2004. Design of Wearable Power-Assist Device for Lower Back Support, *Journal of Robotics and Mechatronics*, vol.16, no.5, pp.489-496.

Rosen, J., Brand, M., Fuchs, M., Arcan, M., 2001. A Myosignal-Based Powered Exoskeleton System, *IEEE Trans. on System Man and Cybernetics*, part A, vol. 31, no. 3, pp. 210 - 222.

Sasaki, D., Noritsugu, T., Takaiwa, M., 2004. Development of Wearable Power-Assist Device for Lower Back Support, *Journal of Robotics and Mechatronics*, vol.16, no.5, pp.497-503.

Vukobratovic, M., 1975. *Legged Locomotion Robots and Anthropomorphic Mechanisms*, Mihailo Pupin Institute, Belgrade.

PERSONAL TELEMETRIC SYSTEM – GUARDIAN

Dalibor Janckulík, Ondřej Krejcar and Jan Martinovič
VŠB – Technical University of Ostrava, FEI, 17. listopadu 15, 708 33 Ostrava, Czech Repulic
dalibor.janckulik.st1@vsb.cz, ondrej,krejcar@vsb.cz, jan.martinovic@vsb.cz

Keywords: PDA, embedded device, biotelemetry, wireless, ECG.

Abstract: This project deals with the problems of utilization of mobile equipment working in the biomedicine field, particularly telemedicine. This field is relatively new; it focuses on the observation of life functions from a distance. Practically developing system works with an ECG sensor connected to mobile equipment, such as PDA/Embedded, based on Microsoft Windows operating system. The whole system is based on the architecture of .NET Compact Framework, and other products, such as SQL Server by Microsoft too. This work also deals with the communication of mobile equipment with sensors and with the server via Bluetooth, WiFi, and GPRS/EDGE. The mobile equipment used serves primarily for measuring and processing of data from the sensors and their visualization as a graph. The data is also given to the server for further processing and the analysis of current health of the patients, due to small efficiency of the mobile equipment (Janckulík, 2007). The main task we deal with in the server part of application is receiving of the data via web services and further processing, management and analysis of this data. For the analysis of received data and further evaluation of the electrocardiogram, there is a self-organizing neural network (Vašíček, 2007).

1 MOTIVATION

Many middle-aged people like businessmen, CEOs, managers and other have very hectic lives with much stress and without good ways of living. Sometimes these people have a collapse, breakdown or heart attack and must be in hospitals or health resorts for a long time to regenerate their bodies. The time that they spend in these institutions, is nonutilisable and very long for them. Possibilities of today physics are restricted by many of prescripts so patients cannot use some of the newest techniques (like hyperbaric or arctic chambers), which make it possible to reduce the regeneration time by weeks or months. For example, these chambers are restricted to patients in the first six months after heart attack due to no information about patients' conditions during the procedure.

Here is the main area of utilization of our telemetric system. Of course the use of our system is not limited only to businessmen, but it is targeted to middle-aged people with some knowledge about new technology like mobile phones. The price of client devices of our system is not low, so we suppose people who can invest to these sorts of assistants.

The basic idea is to create a system that controls important information about the state of a wheelchair-bound person (monitoring of ECG and pulse in early phases, then other optional values like temperature or oxidation of blood ...), his situation in time and place (GPS) and an axis tilt of his body or wheelchair (2axis accelerometer).

Values are measured with the existing equipment, which communicates with the module for processing via Bluetooth wireless communication technology. Most of the data (according to heftiness) is processed directly in PDA or Embedded equipment to a form that is acceptable for simple visualization. Two variants are possible in case of embedded equipment – with visualization and without visualization (entity with/without LCD display). Data is continually sent by means of GPRS or WiFi to a server, where it is being processed and evaluated in detail. Processing and evaluating on the server consists of - receiving data, saving data to data storage, visualization in an advanced form (possibility to recur to the older graph, zoom on a histogram (graph with historical trend), copying from the graphs, printing graphs), automatic evaluation of the critical states with the help of advanced technologies (algorithms) that use

Artificial intelligence to notify the operator about the critical state and its archiving.

Application in PDA, Embedded equipment is comfortable, with minimum time - the first configuration, but also configuration after downfall of application. The level of visualization will be lower. The described system can be used with small modifications for monitoring of patients in hospitals or people working in extremely hard conditions. The biggest limitation is the availability of measuring devices in acceptable and adaptable sizes or comfortable enough to have one around.

The measuring device (ECG, plethysmograph) was tested in extreme conditions in a cryogen room in Teplice (-136°C), where the final system will be installed. Implementation of the data transmission security was not solved. The whole system is classified as „work in progress“ system and it is in a testing phase where we found mistakes and repaired them.

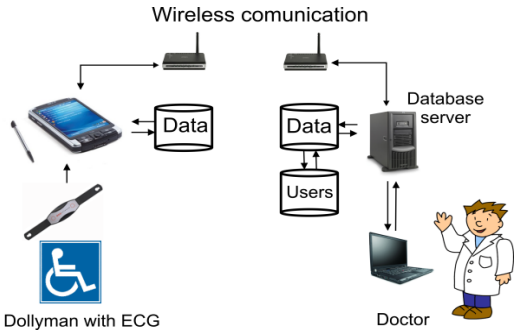

Figure 1: Measurement schema.

2 SYSTEM ARCHITECTURE

This system consists of several interconnected parts that can communicate among themselves, so they can approach their function. These parts are: measuring sensor, PDA or embedded device, and server for data processing and evaluation. Beside these, the most important parts that are worth mentioning are various kinds of accessories, such as GPRS, WiFi, GSM, Bluetooth or GPS modules. By means of them we can communicate. We mostly use the fastest technology in signal coverage.

Data acquisition and data transmission are the most important parts of this system. The Responsible for correct working are: correct sensor configuration, sensor calibration, data transfer synchronization, and mutual communication between sensors and data receiver.

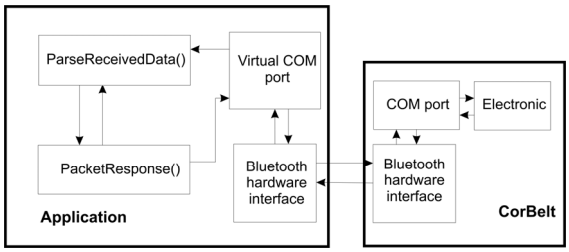

Figure 2: Bluetooth communication.

The system can display saved data from a database file. The doctor can configure or set a neurone network. A change of that is shown in the XML file enshrining, where the neurone network setting of the patient is kept.

The doctor receives information about worsening of patient's status. In case of doctor's reaction, he sends for an expert assistance, such as a helicopter or an ambulance. In case of false alarm, he can configure a neurone network or leave it unchanged if that was a sporadic incorrect interpretation.

The patient can browse data concerning his health status. Measured data is sent to server by WEB service.

Client's data are not only received but also preprocessed (data checking, risk elimination etc.). Measured data is saved. And now, it is possible to analyze the data using a neurone network. If the analysis shows that the measured data from ECG is critical, a warning is sent. That notifies a doctor of incoming data.

2.1 Mobile Part

The main part of the whole system is an Embedded or PDA device. The difference in applications for measurement units is the possibility to visualize the measured data in both Real-time Graph and Historical Trend Graph, which can be omitted on an embedded device.

PDA is a much better choice for Personal Healthcare, where the patient is already healthy and needs to review his condition, or for multiple person usage. Embedded devices can be designed for one user, with the option to use an external display used for settings or with the possibility of usage in extreme conditions.

The application is communicating with an ECG Measurement Unit (Corbelt or Blue Keg) through a virtual serial port using wireless Bluetooth technology. Then, after pushing a button, all necessary parameters are set and the communication may begin. Measured data is stored on a SD

Memory Card in a database in MS SQL Server 2005 Mobile Edition.

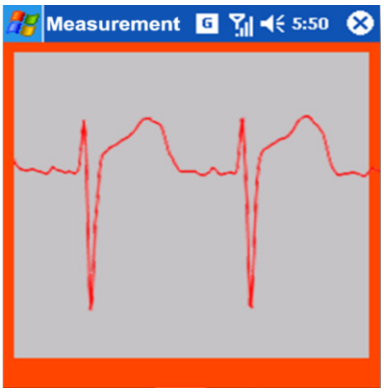

Figure 3: PDA/MDA/SmartPhone visualization.

The performance of available devices seems insufficient for sequential access; parsing of incoming packets is heavily time-consuming. Pseudo paralleling is required. If Windows Mobile OS versions 2003 to 5.0 are used, the processing of data from a professional EKG is not realizable due to thread count limitations. A newer operating system (Windows Mobile 6) can be used to solve this.

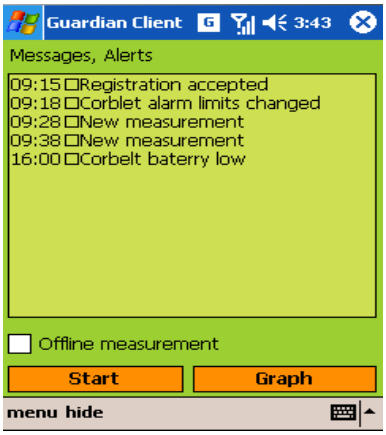

Figure 4: PDA/MDA/SmartPhone application.

Current application is highly specialized and written to accommodate specific hardware. Usage of any other hardware is not possible. This is due to different methods of packet folding, which are unique on each device (Corbelt, BlueEKG datasheet, 2007). This is partly caused by the length of the Telemedicine branch. Operating of the device is simplified as much as possible with the least possible number of steps regarding user registration, measurement device connection and the measurement itself. The informations about user, as ID, name, surname, address and application properties are stored in the system registry (HKEY_CURRENT_USER / Software / Guardian). Working (saving, reading, finding) with registry is easier and faster as saving this informations in file. User registry values are crypted with simple algorithm (shifting char ASCII value).

2.2 Server Part

In order to run a server, an operating system supporting IIS is needed. IIS is an Internet Information Server application allowing users to connect to the web server by the well-known HTTP protocol. The web service transfers data between the server and PDA/Embedded devices. It reads the data, sends acknowledgments, stores the data in the database and reads it from there. The service is built upon ASP.NET 2.0 technology. The SOAP protocol is used for the transport of data, which is in XML format. That is an advantage since it allows communication of multiple different technologies and platforms.

The Wireless ECG approaches a real professional ECG with data rate as high as 800 records per second (Corbelt, BlueEKG datasheet, 2007). That makes 48,000 records per minute and 2,880,000 per hour. Considering 100 patients, the value gets to 288,000,000 records per hour. Even if the server accepted only 50 records per second, the sum of records for 100 patients per hour would be 18 million. That is an extreme load for both the server and the database system; hence a better way of storing data is needed.

Methods that devices communicating with the web service can use include:

- receiving measured data.
- receiving patient data.
- deleting a patient.
- patient data sending.

To observe measured data effectively, visualization is needed. A type of graph as used in professional solutions is an ideal solution. To achieve this in a server application, a freeware Zed Graph library can be used. For data analysis, neural nets are a convenient solution. However, there are problems in the automatic detection of critical states. Every person has a specific ECG pattern. What is completely normal for one person can indicate crisis for another. The Neural net has to learn to distinguish critical states of each patient separately.

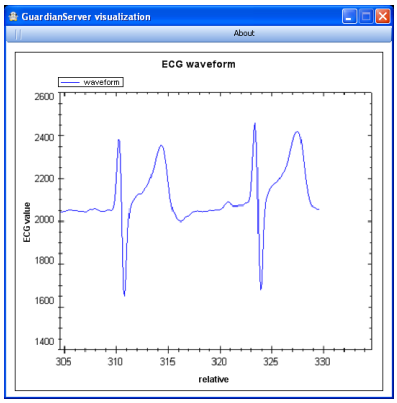

Figure 5: Server visualization.

Basic characteristics of a neuron network:

- 10 x 10 neurons.
- learning is based on 3-4 minutes of recording, which is approximately 36,000-45,000 recorded values.
- incorrect values are filtered out.
- filtering decreases the amount of values to about 10%, which is still good enough for learning.
- the learning cycle with 4,200 values takes approximately 30 seconds (CPU PIII 1.2 GHz) with C# implementation.

To make the specialist's or operator's intervention possible, the system must be provided with a user-friendly interface, possibly imitating those on medical appliances. This area is still in an early phase of development.

3 DATA ANALYSIS

Data acquired from the measuring device is incomprehensible for a man, because it is represented by a HEX format packet. The data needs to be stripped of redundant information like packet numbering and transformed to a recognizable state – a graph. This is done during the packet parsing in PDA/Embedded device, where HEX information 2 bytes in length are transformed to a binary state, where the data is carried on the first 12 bits. It is transformed to a decimal state and sent for further processing – sending the data to the server, storing it in a local database or visualizing it.

The visualization using PDA/Embedded is just a simple visualization of a curve in real-time or historical graph. In the server application, the visualization is far more complex, with the possibility of storing the current curve as an image, printing, or zooming.

Neural net of the SOM type on the server is 10x10 in size. The initial weight of each neuron is random. The weights are assigned progressively by learning. Finally, the whole structure is ready to accept data to analyze. Each patient has his own neural net stored on a server in XML format.

4 CONCLUSIONS

The evolution of Telemedicine is unstoppable and apparent; therefore ways need to be found to improve the quality of hospital services, spa services or hazardous environment workplaces. The area of software products working in embedded devices in hazardous environments or PDAs in personal healthcare is still open and unoccupied. Personal healthcare products are freely available (http://www.omron.com, http://www.weinmann.de) and with minor hardware modifications they can be used for data acquisition using wireless Bluetooth, WiFi or ZigBee technologies. By means of data transfers, the acquired data can be gathered in database systems providing access to your personal doctor, who can be:

- alerted in case of trouble.
- send information and system message to our application.
- remotely change properties of devices (change alarm of critical limits in ECG, e.g.).

Why are there systems available to protect our property and not our health? Is it not the most valuable property of ours?

REFERENCES

Janckulík, D., 2007, bachelor thesis, Personal telemetric system – Personal mobile assistant.

Vašíček, P., 2007, diploma thesis, Personal biotelemetric system.

Corbelt, BlueEKG datasheet, 2007 http://www.corscience.de; http://www.microsoft.com http://www.omron.com; http://www.weinmann.de.

Neuron networks prognosis -http://neuron.felk.cvut.cz/courseware/data/chapter/36nan060/s23.html - (16.4. 2007).

Selforganizing neuron network - SOM, Kohonen maps - http://automatizace.hw.cz/rservice.php?akce=tisk&cisloclanku=2006051401 - (13.3.2007).

NEWBORN HEARING SCREENER BASED ON AUTOMATIC AUDITORY BRAINSTEM RESPONSE DETECTION

Julio Aldonate, Carlos Mercuri, José Biurrun, Juan Manuel Reta, Claudia Bonell
Gerardo G. Gentiletti, Sergio Escobar and Rubén Acevedo
Laboratorio de Ingeniería de Rehabilitación e Investigaciones Neurológicas y Sensoriales, Facultad de Ingeniería
Universidad Nacional de Entre Ríos, Ruta 11 - Km10, Oro Verde, Entre Ríos, Argentina
jaldonate@bioingenieria.edu.ar, cmercuri@bioingenieria.edu.ar

Keywords: Auditory brainstem response, hearing loss, automatic detection, newborn hearing screening.

Abstract: Hearing loss is one of the pathologies with the highest prevalence in newborns. If it is not detected in time, it can affect the nervous system and cause problems in speech, language and cognitive development. The recommended methods for early detection are based on otoacoustic emissions (OAE) and/or auditory brainstem response (ABR). In this work, the design and implementation of an automated system based on ABR to detect hearing loss in newborns is presented. Preliminary evaluation in adults was satisfactory.

1 INTRODUCTION

According to the Health World Organization, 5 per 1,000 neonates are born with significant hearing loss. This pathology has a negative incidence on the nervous system, causing a delay in the development of speech and language, and consequently affecting cognitive and behavioral skills (Priesler, 1999; Jacobson, 1985).

Early detection of hearing impairment is therefore essential, in order to allow a more successful intervention and rehabilitation. Recommended practice begins with universal newborn hearing screening (UNHS) using objective physiological methods, preferably either before being discharged from the hospital or no later than at 2 or 3 months of age (Gracey, 2003).

All over the world, strategies used in UNHS are based on otoacoustic emissions (OAE) and auditory brainstem response (ABR). Particularly, methods based on ABR are well-considered due to their high specificity and sensitivity rates and their high correlation between impairment and alteration in the ABR pattern (American Academy of Pediatric, 1999; European Consensus Statement on Neonatal Hearing Screening, 1998).

However, traditional analysis is complex and time consuming, limiting its use to selective screening of a small percentage of newborns. With the development of Automatic ABR (AABR) analysis, results are obtained faster, facilitating its application on a larger population (Suppiej & Rizzardi, 2007).

In this context, the Facultad de Ingeniería de la Universidad Nacional de Entre Ríos (Argentina), in cooperation with the Hospital Materno Infantil San Roque (HMISR), Paraná, Argentina, and the Centro de Especialidades Médicas Ambulatorias (CEMA), Rosario, Argentina, have begun a technological development project, aiming at designing and building a universal hearing screening system based on AABR. This work presents the design and preliminary results obtained with an implemented prototype, named *AudioScreen*.

2 SYSTEM REQUIREMENTS

A universal hearing screener based on AABR should be able to evoke, record, store and process electroencephalographic (EEG) signals coming out from the brain (McAllister & McCullagh, 2000).
Therefore, suitable hardware and/or software for these purposes must be able to perform the following tasks:

- Stimulate the auditory system according with specific parameters (Mercuri et al., 2006).
- Record the EEG signals from the scalp, synchronizing the acquisition with the stimulation (Acevedo et al., 2006).

- Perform a digital processing on the EEG signals, in order to detect whether the ABR is present or not (Acevedo et al. 2006).

The system has to be flexible enough to allow a range of stimulation and recording options. Tables 1 and 2 summarize specific requirements for this system.

Table 1: Stimulation parameters.

Parameter	Description
Stimulus type	Condensation click
Stimulus width	100 μs
Stimulus intensity	20 to 70 dB peSPL in 10 dB steps
Stimulation frequency	11 and 31 clicks/s
Audio output	Mono
Masking	None

Table 2: Recording parameters.

Parameter	Description
Gains	500 a 100.000 in 10 steps
Bandwidth	100 Hz – 2500 Hz
Input impedance	$> 10^6\ \Omega$
CMRR	> 80 dB
Isolation	$> 3.000\ V_{RMS}$
Sampling frequency	200 Hz to 20 kHz
Sampling period	Up to 15 ms
Resolution	> 10 bits

3 SYSTEM DESIGN

The design of the hearing screener is based on four modules: auditory stimulation (AS), signal conditioning (SC), signal acquisition and digitalization (SAD) and signal processing and visualization (SPV). Figure 1 shows a block diagram of these modules.

As this is the first research prototype, it is planned to be used both in research and clinical environments. The former requires this system to be flexible at the digital processing stage, in order to allow testing and evaluation of different algorithms for automatic ABR detection. For this reason, the SPV module is implemented in software, and a personal computer is required in order to use the screener. Future versions of *AudioScreen* will implement this module in specific hardware, making the system independent from the computer.

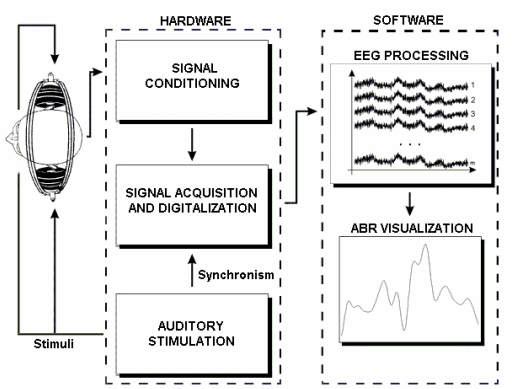

Figure 1: Block diagram of the *AudioScreen* hearing screener modules.

A brief description of the system operation would be as follows: initially, the computer sends a number of configuration parameters for the AS and the SAD modules. When a start signal is received, the stimulator generates acoustic stimuli, which are applied to the patient through headphones. At the same time, a synchronism signal is generated and sent to the SAD module to establish the beginning of the EEG recording which is amplified and filtered in the SC module. Finally, the EEG is digitalized and transmitted to the computer via USB 1.0, where the SPV module stores it for further processing and visualization.

4 SYSTEM IMPLEMENTATION

4.1 Auditory Stimulation Module (AS)

The auditory stimulator produces digital clicks (electrical stimuli) whose amplitude is set by a gain-controlled amplifier (PGA2310 Texas Instruments Inc). Then, the clicks are transduced to auditory stimuli by headphones (Telephonics® TDH39). Two stimulation parameters can be set: intensity, ranging from 20 to 70 dB peSPL in 10 dB steps, and frequency in two possible values, 11 or 33 clicks/s. The selected values are indicated by LEDs on the front panel. In this way, different configurations may be used for auditory stimulation.

The electronic circuit is implemented with an 8-bit RISC microcontroller. The microcontroller configures the gain-controlled amplifier through a serial port interface and it is linked up with the SAD module using two ports: one is used to generate the synchronism signal and the other is used to receive a start signal to begin the stimulation.

4.2 Signal Conditioning Module (SC)

Appropriate integrated circuits (IC) for medical instrumentation are used. This module consists of four parts:

- Instrumentation amplifier: INA128 (Burr-Brown Corp.). This IC has high input impedance (10^{10} Ω) and common-mode rejection (120dB at G ≥ 100), very low offset voltage (50μV) and drift (0.5μV/°C).
- Programmable gain amplifier: OP07 (Analog Devices Inc.). Gain can be set in the range of 500 and 100000 in 10 steps.
- Isolating amplifier: ISO121 (Burr-Brown Corp.). This IC has unitary gain and it is based on a 2 pF differential capacitive barrier, which results in a 3500 V_{RMS} isolation.
- Filter: a band pass filter is implemented using a cascade design of Sallen-Key cells with cutoff frequencies in 2500 Hz for low pass and 100 Hz for high pass. In order to reduce the electromagnetic induction produced by the power line, a Sallen-Key notch filter centered in 50 Hz is implemented. This notch filter can be enabled or disabled using onboard jumpers.

4.3 Signal Acquisition and Digitalization Module (SAD)

This module is based on another 8-bit RISC microcontroller which controls the AD module as well as the communication with the computer. The AD module includes a 12-bits, bipolar input range, analogical to digital converter and a low-noise, temperature-stabilized, precision reference. The sampling frequency can be set to a maximum of 20 kHz and the acquisition window is set to 15 ms.

4.4 Power Supply

The power supply has two stages: one of them is not isolated and the other is isolated according to the IEC 60610 standard. Isolation is achieved using PWR1303A (C&D Technologies Inc.). Table 3 summarizes its specifications.

Table 3: Power supply specifications.

Parameter	Description
Isolated stage	± 5 V, 150 mA, 4 kV DC
Non-isolated stage	± 5 V, ± 12 V, 1 A

Hardware-implemented modules are shown in Figure 2.

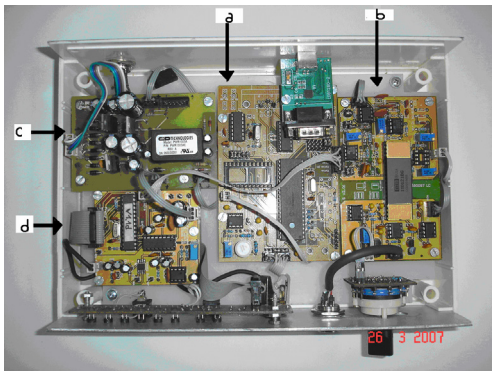

Figure 2: Inside view of the screener; (a) SAD module board, (b) SC module board, (c) power supply board, and (d) AS module board.

4.5 Signal Processing and Visualization Module (SPV)

SPV module block diagram is shown in Figure 3. This module was programmed using Borland® C++ Builder®, and the database was generated with Microsoft® Access® 2003. The user interface was designed taking into account pieces of advice from several professionals of the health centers mentioned above.

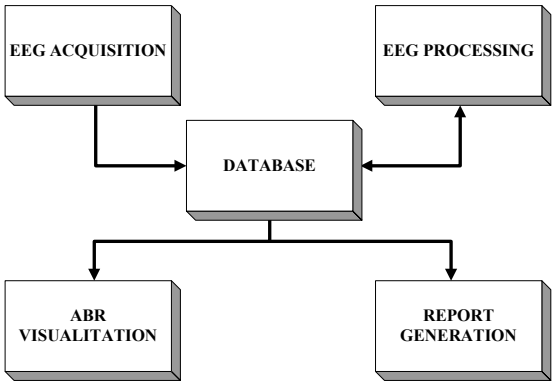

Figure 3: Block diagram of the SPV module.

The database stores all the information about the screening, which basically consists of newborn's and mother's personal information, along with the signals recorded with the EEG acquisition block and the parameters used in the study, e.g. stimulation frequency and intensity.

The EEG processing block performs two main tasks: signal averaging to enhance signal-to-noise ratio, and automatic ABR detection using the FSP algorithm (Gentiletti et al., 2003). The results of the study are visualized in the computer monitor (Figure

4), and can be printed along with a full report of the study.

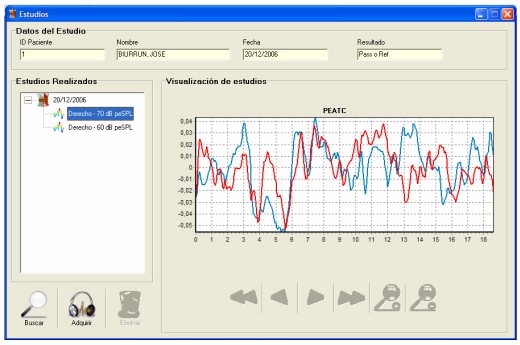

Figure 4: ABR visualization window.

5 EXPERIMENTS AND RESULTS

Figure 5 shows the complete system, which complies with the IEC 60610 standard for medical equipment.

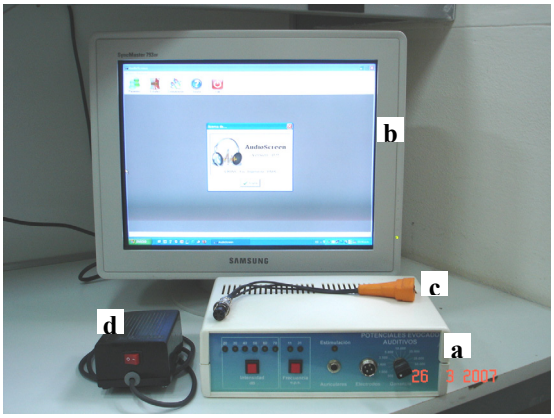

Figure 5: *AudioScreen* system with the software running on the computer; (a) screener; (b) software interface; (c) electrode cable; (d) power supply.

The user interface was assessed by HMISR and CEMA personnel, and the resulting evaluation was satisfactory. Finally, a full set of tests were carried out with healthy patients, which verified the correct performance of the system.

6 CONCLUSIONS

A first prototype of the *AudioScreen* system was designed, built and it's has been tested. It was done using adequate off the shelf electronic components, which met the standard for medical equipment and were fully operational. The following step is to perform system validation at the HMISR as well as the CEMA. In addition, an algorithm of ABR signal detection based on support vector machines is being developed, which will be validated and contrasted against the *Fsp* method.

ACKNOWLEDGEMENTS

This work was supported by the Secretary of Science, Technology and Productive Innovation (SeCTIP) and by the Council of Investigations of the National University of Entre Ríos (CIUNER).

REFERENCES

Priesler G., 1999. *The Development of Communication and Language in Deaf and Severely Hard of Hearing Children: Implications For The Future.* Int J Pediatr Otorhinolaryngol; 49(Suppl 1):S39-43.

T. Jacobson. 1985**.** *The Auditory Brainstem Response, Boston, Editorial Collage-Hill Press.*

Gracey K. 2003.*Current Concepts in Universal Newborn Hearing Screening and Early Hearing Detection And Intervention Programs*. Advances in Neonatal Care, Vol. 3, No. 6 (December): pp 308-317

American Academy of Pediatric, 1999. *Newborn and Infant Hearing Loss: Detection and Intervention.* Pediatrics; 103: 527-30.

European Consensus Statement on Neonatal Hearing Screening. Milan. May 1998.

Suppiej A, Rizzardi E, Zanardo V, Franzoi M, Ermani M, Orzan E, 2007**.** *Reliability of Hearing Screening in High-Risk Neonates: Comparative study of automated OEA, and conventional ABR. Clin Neurophysiol. 2007 Apr; 118(4):869-76. Epub Feb 20.*

McAllister H. and McCullagh P, 2000. *Objective methods of hearing assessment.* Computing and Control Enginnerging Journal. April, 53-64

Mercuri C., Escobar S., Cadirola F., Astiasaran P., Gerardo G., Aldonate J., Bonell C., Acevedo R., 2006. *Estimulador auditivo para audiometría tonal y potenciales evocados auditivos*, Revista Argentina de Bioingeniería, vol 12, nro 2, pp. 13-19.

Acevedo R., Bonell C., Gentiletti G., Aldonate J., Mercuri C., Escobar S., Biurrun J., 2006. *Potenciales Evocados Auditivos De Tronco Cerebral: Aspectos tecnológicos del Registro,* Revista Argentina de Bioingeniería, vol. 12 No. 1, pp. 10-17.

Gentiletti G., Yañez O., Cornejo J, 2003. *Evaluation of Automatic Identification Algorithms for Auditory Brainstem Response used in Universal Hearing Loss Screening.* Proceedings of 25 th Annual International Conference of the IEEE EMBS.

THERMORESPONSIVE POLYMER-BASED MICRODEVICE FOR NANO-LIQUID CHROMATOGRAPHY

Guillaume Paumier, Sovann Siv, Aurélien Bancaud, Jan Sudor and Anne-Marie Gué
LAAS-CNRS, University of Toulouse, 7 avenue du Colonel Roche, Toulouse, France
gpaumier@laas.fr

Keywords: PNIPAM, thermoresponsive polymer, nanoliquid chromatography, sample preparation.

Abstract: We report here on the development of an integrated device for sample desalting and pre-concentration for nanoLC / ESI-MS analysis combining poly-(*N*-isopropyl acrylamide) (PNIPAM) grafted microbeads and the means to dynamically control their temperature. Thermoresponsive properties of PNIPAM induce switchable hydrophobic/hydrophilic surfaces on which peptides can reversibly adsorb and desorb. The device is fabricated on a glass or pyrex substrate with deposited Ti/Au electrodes serving as built-in resistive heating sources. Premolded microfluidic channels and reservoirs made in PDMS are eventually assembled. Electrical and thermal characterization together with multiphysics modeling have been performed. The SiO_2 surfaces of the channels and silica beads used as carriers of the stationary phases have been end-grafted with PNIPAM and employed to study the reversible adsorption and release kinetics of albumin-fluorescein conjugates by fluorescence video microscopy. It is clearly shown albumin-fluorescein complexes adsorb on beads surfaces above the transition temperature of PNIPAM (hydrophobic state), and are released when the temperature decreases (hydrophilic state), yet not fully reversibly.

1 INTRODUCTION

The challenge of proteomics is to develop high-throughput and integrated approaches to identify and understand the structure, functions and interactions of proteins. Nano-liquid chromatography (nanoLC) in combination with electrospray ionization mass spectrometry (ESI-MS) detection has become a major experimental method owing to its high separation power and sensitivity (Ishihama, 2005). In general, proteins are fractionated, isolated and digested into peptides to be analysed and identified by nanoLC / ESI-MS. Miniaturization provides a number of advantages such as low limit of detection, small volumes of analyte required and reduced intermediate manipulation steps (Gauthier and Grimm, 2006). Thus, many efforts have been made to integrate on-chip separation devices providing the column, connection capillaries and MS coupling via a nanospray emitter (Hernández-Borges et al., 2007). Though, due to MS high sensitivity to salts, peptides need to be desalted and concentrated on C4 or C8 columns prior to their analysis (Wilm and Mann, 1996). During this step, certain hydrophobic peptides can be lost on the hydrocarbon surfaces because they show a greater affinity to the stationary phase as compared to the mobile one utilized for desorption of the purified peptides (Peterson et al., 2003).

We propose here a novel approach based on stationary phases prepared from poly(*N*-isopropyl acrylamide) (PNIPAM) that can reversibly adsorb and release peptides upon external activation in a purely aqueous environment. We present the development of an integrated device for sample desalting and preconcentration for nanoLC / ESI-MS analysis, combining PNIPAM grafted surfaces and the means to dynamically control their temperature by integrated microheaters.

2 THEORY

PNIPAM is a stimuli-responsive polymer which undergoes a reversible coil-to-globule transition at its

lower-critical solution temperature (LCST) around 32°C. PNIPAM grafted surfaces can be switched from a swollen, hydrophilic and non-fouling state to a collapsed, hydrophobic and protein-adsorbing state using thermal actuation (Kanazawa et al., 1996; Huber et al., 2002). Such surfaces have been previously reported for spatio-temporal control of flows in fluidic microsystems by our group (Sudor et al., 2006).

The idea presented here is to use PNIPAM-decorated beads as stationary phases to trap peptides during desalting and pre-concentration steps prior to the nano-LC / ESI-MS analysis. The reversible transition of PNIPAM surfaces upon temperature allows controlled adsorption and release of peptides without the change of quality of a solvent. To increase specific surface of interaction between PNIPAM and peptides, PNIPAM is grafted on micrometric silica beads injected into the channel. The channel height is reduced at its center to block the beads, while its width is widened to preserve the constant surface area.

A resistive heating device is directly integrated on the pyrex subtrate to control the temperature inside the channel. Microfluidic pre-molded PDMS channels and reservoirs are eventually assembled to the substrate to form the final fluidic microsystems (Fig. 1).

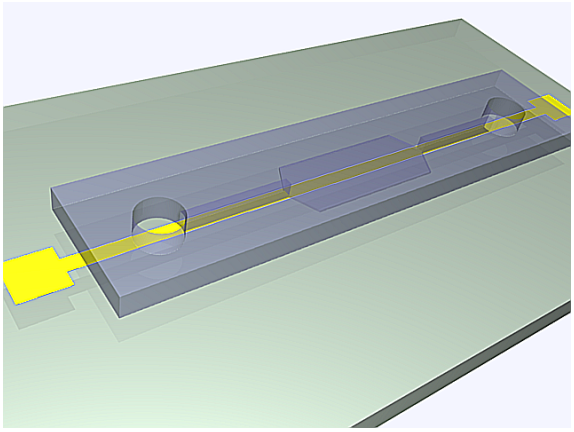

Figure 1: 3D view of the assembled prototype: pyrex substrate, heating line and PDMS channel.

3 EXPERIMENTAL

3.1 Heating Device

Our heating device was made with lines fabricated on a silicon, glass or pyrex substrate with deposited Ti/Au (1000 / 8000 Å) electrodes serving as built-in resistive heating sources. Lines of 100 μm and 500 μm width (respectively 32.5 Ω and 6.75 Ω on pyrex) were realized and characterized. Infrared imaging showed the heated zone was localized around the heater (Fig. 2). Suitable temperatures were obtained for acceptable voltages: 51°C for 4 V (500 μm wide) and 7 V (100 μm wide), given that LCST of PNIPAM is around 32°C. For 500 μm-wide lines around 4 V, we obtained a homogeneous heated zone more than 1.5 mm wide (microfluidic colons are 50 μm wide). Response time in heating is very short (< 1s); cooling happens in seconds.

Multiphysics modeling using Comsol was also performed. First modeling results fit relatively well with experimental data (Fig. 3), however, a slight refinement of the model is still necessary. Work is also underway to develop more complex heating devices allowing more precise control of heated zones (Paumier et al., 2007).

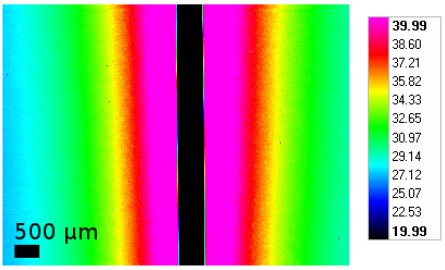

Figure 2: Infrared thermal imaging of the Ti/Au electrode (°C). The resistor appears black because of the infrared reflection on gold.

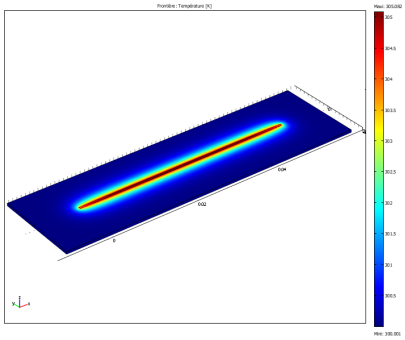

Figure 3: Multiphysics modeling of the heating process using Comsol.

3.2 Surface Chemistry

A 500 nm SiO_2 layer was deposited by plasma-enhanced chemical vapor deposition (PECVD) on the substrate and the electrodes to provide an electric insulator, and to allow homogeneous PNIPAM grafting. The SiO_2 surfaces of the channels and silica beads (used as carriers of the stationary phases)

were end-grafted with PNIPAM according to literature (Hjertén, 1985), through an intermediate silane layer (3-trimethoxysilyl propylmethacrylate). Surfaces were characterized with dynamic contact angle measurements and multireflection infra-red spectroscopy. The latter showed specific peaks identifying chemical groups from PNIPAM (Fig. 4).

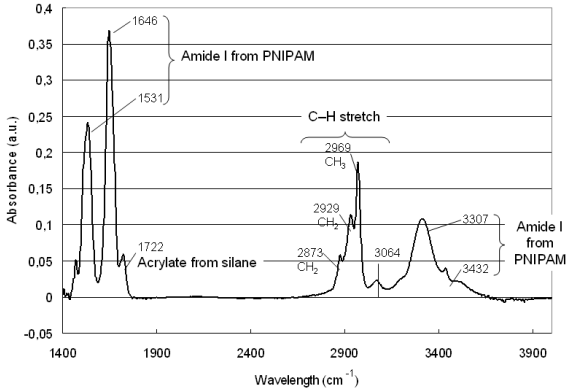

Figure 4: Multiple internal reflection infrared spectrum of surfaces grafted with PNIPAM.

4 RESULTS AND DISCUSSIONS

4.1 Controlled Adsorption/Release of Proteins

To prove feasibility of using beads decorated with PNIPAM to adsorb/desorb proteins, we made our first experiments in capillaries. We used silica beads (5 μm in diameter) end-tethered with PNIPAM chains in fused silica capillaries (100/385 μm inner/outer diameter). The inner surface of the capillary was end-grafted with polyacrylamide (PAM), which is not sensitive to temperature changes in the studied range. Bovine serum albumine (BSA) - fluoresceine conjugate (1 mg/ml) dissolved in sodium phosphate buffer (pH 7) was injected into the capillary. When temperature was increased to about 40°C (above LCST), PNIPAM chains on beads became hydrophobic; they trapped and concentrated BSA-fluorescein conjugates on beads, making them fluorescent, as shown in Fig. 5. By decreasing the temperature below the LCST, BSA-fluorescein conjugates were released into the solution.

The kinetics of reversible adsorption and release was also studied. The graph on Fig. 6 shows the adsorption and release of albumin-fluorescein conjugates on beads. We observed the release of proteins was not fully reversible. A proposed explanation is the low grafting density of PNIPAM chains and consequent protein adsorption on the non-modified surfaces of silica beads.

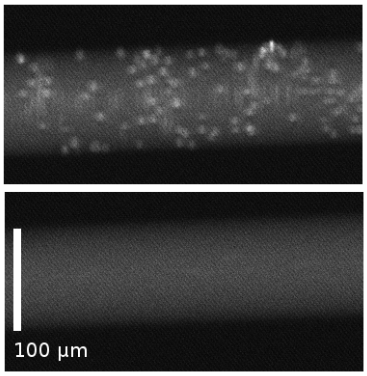

Figure 5: Albumine-fluorescein conjugates adsorbed on 5-μm beads (top, $T > LCST$) and then released (bottom, $T < LCST$). Background fluorescence is due to complexes in solution.

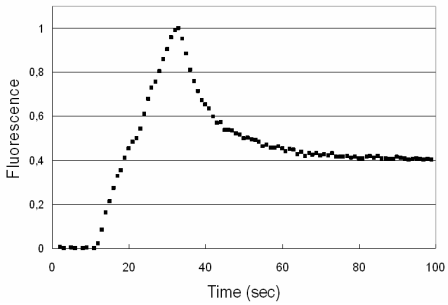

Figure 6: Adsorption/release kinetics of albumin-fluorescein conjugates from glass beads functionalized with PNIPAM (normalized units).

4.2 Beads in Microchannels

Then, we went a step further and injected silica beads inside our PDMS microchannel. Silica beads were not functionalized with PNIPAM at this point. The microchannel was made of three parts. At the center, the channel was 1250 μm wide, 1500 μm long and 4 μm high. Side channels were 50 μm wide, 3000 μm long and 100 μm high each. This geometry allows to trap beads where section changes.

Several sizes of beads and central height of the middle section of the channel were tested and characterized through fluorescence microscopy. When these sizes were too close, beads managed to slip inside the central part, due to PDMS ductility: Young's modulus of PDMS depends on the mixing ratio of elastomer and curing agent but it remains about 10^5 Pa (Armani et al., 1999). We observed this phenomenon with

5 μm beads and 4 μm central height. To prevent this, we injected a limited amount of 10 μm beads prior to the 5 μm beads, that were prevented from entering the central part because of the bigger beads. Experiments with PDMS devices and beads modified with PNIPAM are currently underway.

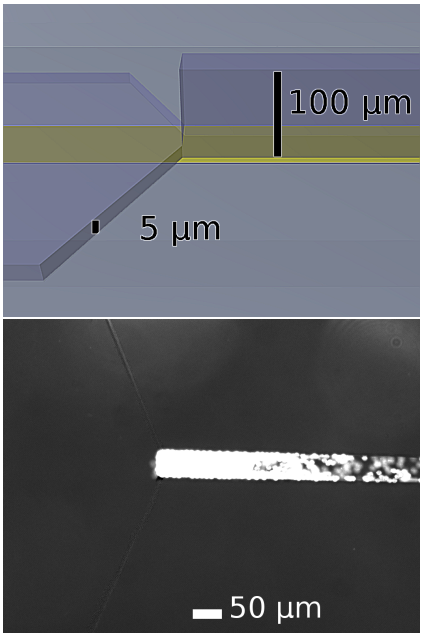

Figure 7: Top: 3D close-up on the channel zone where beads are blocked. Bottom: Top-view of fluorescent 10 μm and 5 μm beads blocked at the entry of the central part.

5 CONCLUSIONS

Thermoresponsive properties of PNIPAM upon temperature are well known and have been demonstrated as switchable surfaces for protein adsorption. We demonstrated in this work the possibility to integrate such switchable surfaces into fluidic microsystems dedicated to sample preparation for nanoLC / ESI-MS. We have developed essential components and know-how about heating sources, reversible protein adsorption and release, and injection of beads in PDMS microchannels. We are now demonstrating the feasibility of the microsystems for desalting and preconcentration of various peptide samples.

REFERENCES

Armani, D., Liu, C., and Aluru, N. (1999). Re-configurable fluid circuits by PDMS elastomer micromachining. In *Proc. IEEE MEMS '99*.

Gauthier, G. and Grimm, R. (2006). Miniaturization: Chip-based liquid chromatography and proteomics. *Drug Discov. Today Techn.*, 3(1):59–66.

Hernández-Borges, J., Aturki, Z., Rocco, A., and Fanali, S. (2007). Recent applications in nanoliquid chromatography. *J. Sep. Sci.*, 30(11):1589–1610.

Hjertén, S. (1985). High-performance electrophoresis: Elimination of electroendosmosis and solute adsorption. *J. Chromatogr. A*, 347:191–198.

Huber, D., Manginell, R., Samara, M., Kim, B.-I., and Bunker, B. (2002). Programmed adsorption and release of proteins in a microfluidic device. *Science*, 301:352–354.

Ishihama, Y. (2005). Proteomic LC–MS systems using nanoscale liquid chromatography with tandem mass spectrometry. *J. Chromatogr. A*, 1067(1-2):73–83.

Kanazawa, H., Yamamoto, K., Matsushima, Y., Takai, N., Kikuchi, A., Sakurai, Y., and Okano, T. (1996). Temperature-responsive chromatography using poly(*n*-isopropylacrylamide)-modified silica. *Anal. Chem.*, 68(1):100–105.

Paumier, G., Sudor, J., Collé, E., Marty, B., Bancaud, A., Camps, T., and Gué, A.-M. (2007). Electrokinetic mixers based on stimuli-responding surfaces. In *Proc. 11th Int. Conf. on Miniaturized Systems for Chemistry and Life Sciences (µTAS'2007)*.

Peterson, D., Rohr, T., Svec, F., and Fréchet, J. (2003). Dual-function microanalytical device by in situ photolithographic grafting of porous polymer monolith: integrating solid-phase extraction and enzymatic digestion for peptide mass mapping. *Anal. Chem.*, 75(20):5328–5335.

Sudor, J., Paumier, G., Gué, A.-M., Vinet, F., Estève, A., and Djafari-Rouhani, M. (2006). Spatio-temporal tuning of stimuli-responding surfaces for dynamic control of electroosmotic flows. In *Proc. 10th Int. Conf. on Miniaturized Systems for Chemistry and Life Sciences (µTAS'2006)*.

Wilm, M. and Mann, M. (1996). Analytical properties of the nanoelectrospray ion source. *Anal. Chem.*, 68(1):1–8.

WIRELESS CONTEXTUAL INFORMATION ELECTRONIC SYSTEM FOR PEOPLE WITH DISABILITIES

S. Borromeo, C. Rodriguez-Sánchez, J. A. Hernández-Tamames and N. Malpica
Electronics Engineering Department, Medical Imaging Group, Rey Juan Carlos University
C/Tulipán S/n Móstoles, Madrid, Spain
susana.borromeo@urjc.es, juan.tamames@urjc.es

Keywords: Wireless Electronics, ICT for people with disabilities, Disability Discrimination, Bioengineering, Pervasive Computing, Bluetooth.

Abstract In this work we present a prototype of two electronic devices for providing relevant information to people with disabilities, such as the blind, deaf or elderly, in public environments (railway stations, airports, etc). Usually, this kind of collectivities is discriminated in terms of information access. Most of the public information is in text panels, monitors or traffic signals. The rights of these people are easily forgotten. With this work we try to make an effort in this direction facilitating the information access to these groups. In order to avoid them feeling different we try to adapt the transmission to standard portable devices. We based the work on bluetooth technology. Concerned by costs, in order to popularize this technology, our designs use off-the-shelf components. We also propose a new device to avoid the proximity marketing spam so that these people don't suffer its consequences.

1 INTRODUCTION

Lately, there is an increasing interest in ICT for People with disabilities. (Busby, G. Whitehouse, D. 1997), (Busby, G. 1997) (Blanchard, S.M. Rohrbach, R.P. 2000).

Blind, deaf and elderly people are usually discriminated in public environments, such as railway stations or commercial centres, when real time information about transport timetables, commercial advices or security warnings is being emitted (Karim, N.A. Nwagboso, C., 2004). Something similar occurs in signalling for urban purposes. This collectivity can not be informed instantaneously and they are unaware about eventual dangerous situations for them such as holes or wet pavements. Signaletics is a discipline susceptible to be completed with new developments based on wireless beacons. In this work we present a general purpose prototype of sender and receiver to be used as wireless beacons based on an off-the-shelf Bluetooth chipset. In fact, the receiver can be substituted by Bluetooth-equipped commercial mobile phones or *PDA*s.

In this sense, some airports and railway stations have arranged systems based on *sms* mobile technology. People with disabilities have to reach a special information desk to borrow a mobile phone explaining her destination and the rest of the travel information. When the transport is close to departure, one *sms* is sent to the mobile. However, people can read signals, can watch *tv* monitors or, in some cases but less now, can listen to advices and messages.

We propose to incorporate wireless beacons to the information system of monitors or panels for sending relevant information to the portable devices.

In this paper we only present the electronic devices needed for a basic communication. One of our major objectives is the development of low-cost, low-consumption and small devices using off-the-shelf electronic modules.

2 SYSTEM ARCHITECTURE

The system consists of a sender device and a receiver device. Both can exchange information through the Bluetooth protocol. Moreover, the receiver can send the information to the mobile or to the PDA of the disabled user.

Figure 1 shows the basic modules of the architecture. A receiver beacon could suffice, and is

cheaper than standard portable devices such as mobile phones or PDA's.

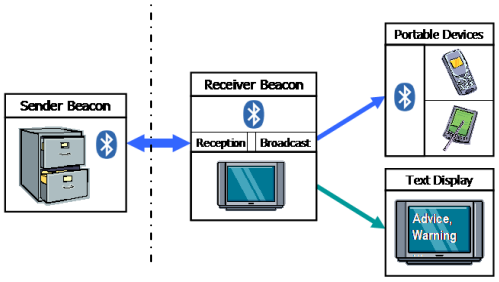

Figure 1: Basic components in the system.

The *sender Beacon* is equivalent to the monitor or panel information system in airports o railway stations. It is also equivalent to a warning advertisement or traffic signal for people in any street or in any commercial centre.

It stores relevant information messages in different data formats (audio, text or image) and transmits them to the receiver beacon.

Receiver beacon consists of a PIC microcontroller, a Bluetooth module and a LCD for showing text messages.

The *receiver beacon* communicates with the sender beacon via the Bluetooth protocol and, optionally, sends complex messages, in audio or image data format, to the portable device when it is present.

Actually, the receiver beacon could be optional whenever a portable device is available. The messages can be sent by the sender beacon to the portable devices directly, but, we have found several advantages to incorporating this small device.

Firstly, as mentioned above, it is cheaper than a mobile phone or PDA. In the case of deaf or elderly users, the receiver beacon is enough for receiving and viewing information. These users don't need to afford an expensive portable device for taking advantage of this technology, something especially interesting in developing countries. In the case of blind users, audio reproduction is currently being added to the beacon.

Secondly, the *receiver beacon,* when used together with a standard portable device, can filter the messages reaching the device. It is particularly interesting for avoiding proximity marketing spam.

3 RESULTS

3.1 Hardware Implementation

Simplicity criteria have been applied in the design of the sender and receiver beacons. Next figure summarizes the hardware subsystems of the sender.

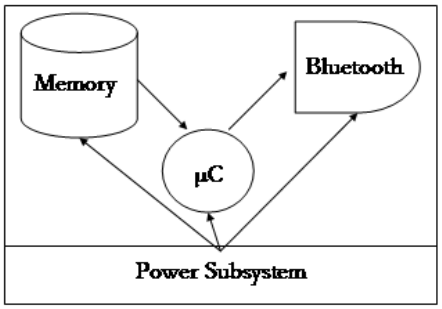

Figure 2: Internal beacon design.

A PIC16F88 (Microchip Inc., Arizona.) is the microcontroller of choice. It responds to a RISC internal architecture and contains a UART (Universal Asynchronous Receiver Transmitter) which is used to connect with the Bluetooth chipset. We highlight the low power consumption, only 0,8 mA at 4MHz and 3,7V. This voltage is the same for the Bluetooth chip so we can simplify the power subsystem.

The EZURIO Bluetooth Chipset (EZURIO Ltd.) is used because it allows a feasible configuration with AT commands, supplied through the UART. Next figure shows the basic connections for this purpose.

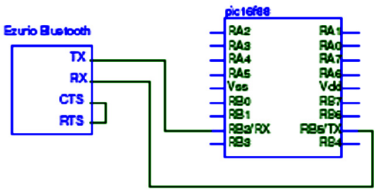

Figure 3: µC – Bluetooth connections through UART pins.

The Memory is a Flash model with a capacity of 512KB divided in 8 sectors and has an access time of 90ns. Its capacity is enough for storing 2 minute messages in mp3 audio format. The addressing mechanism was implemented with three 8-bit cascaded counters using only 19 outputs (the least significant outputs).

The flux control was implemented with an XON/Xoff protocol.

Once the development of the sender was finalized, we redesigned the receiver with a memory subsystem based on EEPROM 24LC512 (64KB and I2C protocol) and adding a LCD Display (Hitachi 44780).

The prototype of the receiver is shown in the next figure.

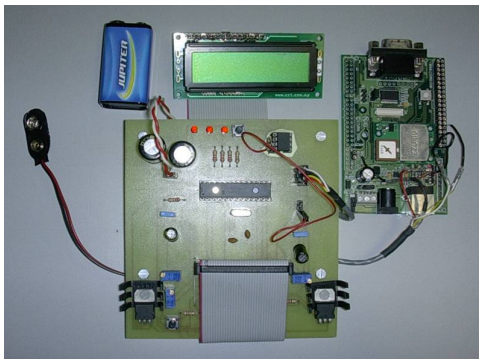

Figure 4: The receiver beacon prototype.

To facilitate the wire connection to the Bluetooth chip, and to test the system, we use the Ezurio Bluetooth development chip. We can see it on Figure 6, on the right. The final prototype has only the Bluetooth chip.

The final result allows the reception of chain characters in the receiver beacon or files in different formats (audio or image) in a PDA or in a mobile phone as shown in the next figure:

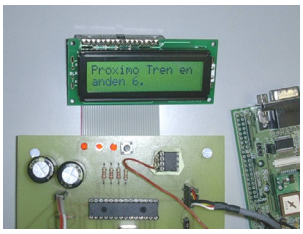

Figure 5: Receiving text and files in the LCD and in the PDA, respectively.

3.2 Software Implementation

The *sender beacon* has to run two main tasks in its PIC microcontroller. Firstly, the PIC must configure a serial communication through its UART. Once the UART is fully operative, the PIC must configure the Bluetooth module by sending AT commands.

In this prototype, the memory was previously loaded using a PC and a Xon/Xoff protocol, as mentioned above. Further developments will allow to load the memory through GSM/GPRS messages.

The files stored are sent to the portable device or the receiver beacon following a simple protocol described below:

- The receiver beacon waits for an external enquiry.
- A Bluetooth connection is established.
- The PIC reads the files from memory and sends them to the receiver beacon.
- When it finishes the connection is released.

The receiver beacon software behaviour is very similar and it is described below:

- The UART and the Bluetooth module are configured in a similar way as in the sender beacon. The receiver beacon is always discoverable. Moreover, the LCD must be configured for files in text data format.
- When the connection between beacons is established, the receiver beacon downloads the file.
- If it is a text file, it is displayed in the LCD. However, if the file data format is for audio or image, the receiver beacon tries to send it to its corresponding PDA or mobile phone.

As can be observed, this second beacon can easily filter spam messages from other devices, in particular, those used in proximity marketing.

All the code was developed with a minimum number of instructions to be stored in the 64KB memory of the PIC.

4 CONCLUSIONS

We have shown the feasibility of a low-cost wireless system for assisting people with disabilities such as blind, deaf or elderly people. A more acute design would allow mass production.

The low cost of the receiver/sender is summarized in the next table:

Table 1: Material Costs.

EZURIO BISMII	22€
Flash Memory/EEPROM Memory	3,45€
8-bit Counters	3,00€
µC PIC16F88	3,13€
LM7805 (Voltage Regulator)	0,60€
Resistors, capacitors, etc	2,50
LCD Display	6€
	≈40€

Further work is in course in order to upload contents to the sender beacon through GPRS. This would allow the contents to be broadcast through a central web-based server.

REFERENCES

Busby, G. Whitehouse, D. 1997. Technology and society: how information and communication technologies can enhance the lives of persons with a disability. *Technology and Society, 1997. 'Technology and society at a Time of Sweeping Change'. Proceedings., 1997 International Symposium on*

Busby, G. 1997. Technology for the disabled and why it matters to you. *Computers in the Service of Mankind: Helping the Disabled (Digest No: 1997/117), IEE Colloquium on*

Blanchard, S.M. Rohrbach, R.P. 2000. Capstone engineering design projects to aid disabled persons. *Engineering in Medicine and Biology Society,. Proceedings of the 22nd Annual International Conference of the IEEE*

Karim, N.A. Nwagboso, C. 2004. Assistive technologies in public transport: meeting the needs of elderly and disabled passengers. *Information and Communication Technologies: From Theory to Applications*, Proceedings. 2004 International Conference on

ULTRASONIC MOTION TRACKING OF INSTRUMENTS IN OPERATING THEATRE

Alejandro Ibarz, Roberto Casas, Álvaro Marco, Héctor Gracia, Rubén Blasco and Jorge Falcó
Instituto de Investigación en Ingeniería de Aragón,(Tecnodiscap Group)
Universidad de Zaragoza. María de Luna 1, Zaragoza, Spain
aibarz@unizar.e, rcasas@unizar.es, amarco@unizar.es, hgracia@unizar.es, rblasco@unizar.es, jfalco@unizar.es

Keywords: Indoor positioning, motion tracking, ultrasound ranging, accurate localization.

Abstract: The purpose of this paper is to address the design of a system to track surgical instrument's movement during an operation. Motion tracking of surgical instruments is one of the most interesting methods to survey the data needed for medical robotics, computer-aided surgery, skills assessment and training progress applications. Over the wide range of tracking technologies, low frequency ultrasound was selected to meet the system's requirements. Factors that bring about measurement inaccuracies are analysed and taken into account when developing the system. Furthermore, a localization algorithm that calculates three-dimensional position using one-dimensional distances and overriding signal blockage is presented. Moreover, experimental results of a resectoscope mock up motion tracking are shown.

1 INTRODUCTION

With the spread of minimally invasive surgery and training in this field, development of metrics for medical robotics, computer-aided surgery, skills assessment and training progress has become increasingly important.

There is a wide range of technologies for motion tracking: computerized tomography, nuclear magnetic resonance imaging, video-based imaging, ultrasound imaging, optical tracking systems, electromagnetic tracking systems, inertial, ultrasound positioning, etc. They can be characterized according its price, complexity, accuracy and drawbacks. Most of these technologies are not suitable for designing a indoor positioning system meant for operating theatres (Tatar, 2006; Bianchi 2007). However, low frequency ultrasound positioning offers promising perspective measuring one-dimensional distances. Moreover, a more thorough analysis will be done to use low frequency ultrasound for motion tracking purposes.

The purpose of this paper is to design an ultrasound indoor positioning system. It has to be able to track the motion of a surgical instrument during the operation. Furthermore, system's requirements are low-cost, low-complexity and accuracy enough to track instrument's position properly. The final and most important requirement is that devices placed on the instrument can not restrict surgeon's movements or put the patient in risk.

Concerning the exactitude of the system, the design of the electronics will be analysed, as well as the method of time of flight measurement to obtain an accuracy of millimetres. In order to obtain this accuracy, it will be necessary to analyse the influence of environmental factors and correct its effects. The ultimate goal is to objectively assess instrument localization in a realistic environment; i.e., the operating room.

2 ULTRASONIC TRACKING

Generally speaking, ultrasonic positioning systems are based on different subsystems: transducers on the mobile that needs to be located, transducers places on known positions and one or several computing units (PC, microprocessor or DSP). In order to obtain mobile's unknown position; one-dimensional distances from fixed transducers to mobile transducers have to be surveyed. After obtaining the one-dimensional data, mobile's coordinates can be calculated by a computing unit using a location algorithm.

A generic ultrasound positioning system has been described. Afterwards, the system has to be adapted to the operating theater characteristics.

The system's architecture is as follows:

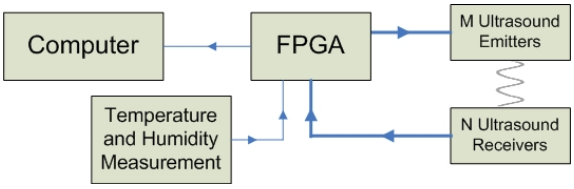

Figure 1: System's architecture.

Emitting transducers (at least 3 to determine mobile's position) need to be placed on the surgical instrument on known position (in order to compute the instrument's position).

Receiving transducers have to be placed on the ceiling to avoid non-line of sight issues. To ensure good performance of the system, the coordinates of receiving transducer should be known as much accurate as possible.

The FPGA assigns a temporal interval to each emitter module. It commands the emitter to generate ultrasound chirps; simultaneously the ultrasonic time of flight (TOF) to the receiving transducers will be computed and stored (as well as ambient temperature and humidity). After the FPGA sends all surveyed data, the computer will obtain the coordinates of all emitting transducers and the instrument's position.

2.1 Ambient Influence in Operating Rooms

In this sub chapter, several factors that may affect system's performance will be analysed. This analysis will take into account operating room (OR) ambient characteristics and several others considerations that may bring about measurement inaccuracies.

Update rate: The frequency of the measurements reported by the tracking system. The higher this parameter the better tracking results are obtained. The TOF system has a low update rate caused by the low speed of sound and the sequential triple emission of pulses.

Misalignment between transducer pairs: Due to the quantity of receiving transducers and the wide range of mobile's movements, we cannot expect to have perfect alignment between transducers pair (emitter-receiver). It has been stated (Lamancusa, 1990) that misalignment between transducer pairs will bring about a distance measurement error.

Ultrasound wave reflection on surfaces: Reflections on surfaces has been used in ultrasound distance measurement systems, using echoes to determine distances to surfaces. Nevertheless, considering the number of medical instruments in OR (lamps, monitors, tables), echoes might bring about measurement errors to our system and affect system's robustness. Therefore, reflection on surfaces should be analyzed and taken into account in system's design.

Airflows: Most of these systems are based on calculating the ultrasound TOF and multiplying it by the sonic air speed to obtain the distance. Therefore, airflow will modify the speed which the ultrasound moves in the air.

Temperature: The temperature is an environmental factor to consider when designing an accurate ultrasound positioning system, as it affects the speed of sound (Liao et al, 2004).

Relative Humidity: The relative humidity modifies the speed of sound, affecting distance measurement (Liao et al, 2004).

Table 1: Inaccuracies due to ambient factors.

Parameter	Accuracy	Max. Error
Temperature	0.3 º C	1.77 mm
Humidity	1.8 % RH	0.4 mm
Misalignment	---	1 mm
Airflows	---	1.3 mm
Total	---	4.4 mm

2.2 Distance Measurement

Once analysed the environmental factors (table 1) that influence distance measurements, we will analyse the measurement process. This part includes: generation of ultrasonic chirps, reception and treatment of the signals; and determination of TOFs.

TOF is the time elapsed between the transmission of a pulse and its reception, from which the target distance can be calculated multiplying speed of sound in air by TOF. Using TOF to measure the distance, the system errors are primarily due to amplitude degradation of the received signal, and uncertainty in the speed of sound.

There is a close relation between generation of ultrasonic chirps and the method to determine TOFs and distances (Tatar, 2006; Huang et al, 2002). Moreover, the chirp generation method can affect system's performance. For example, some methods require longer chirps, lowering system's update rate

and making them less robust to reflections on surfaces.

The chosen method of emission was based on self-interference (Cai, 1993), using short chirps and giving the signal in reception a specific form that will take be used to determine TOF and afterwards the one-dimensional distance. Allocating an event on the signal close to its start will make the method more robust to reflections on surfaces.

The method implemented in the FPGA consists on storing several time stamps of the moments when the signal exceeds a predefined threshold. These data are processed through an algorithm in the FPGA to determine where the event is located, and afterwards this time is corrected to obtain the TOF.

Experimental tests were done to assess the precision of determining the TOF using this method. Placed both emitter and receiver at a fixed distance, the distances obtained had a standard deviation of 300 μm and a resolution of 7 μm. The system was also able to measure distance between transducers with a high degree of misalignment.

2.3 Location Calculation

2.3.1 Problem formulation

We have to solve the classic multilateration problem. Calculate the position of the transmitter (x_P,y_P,z_P) from the estimation of several distances (d_i) to emitters having known coordinates (x_{bi},y_{bi},z_{bi}). Distances have been estimated as indicated in previous subsection.

At least three distances are required to solve the aforementioned trilateration problem. Unfortunately, this is not typically the case in real operations where one or more of the distances may contain large errors produced by multipath effects and the blockage of the ultrasonic signal.

2.3.2 Location Algorithm

Our aim is to solve the proposed problem when it is not possible to use any prior information to solve the multilateration. It is not possible to identify the measurements affected by error, or whether there are any. In the end, there is redundant data within unidentified, erroneous information, which must be filtered out to compute the best solution.

Robust estimators provide methods for detecting outliers, and they obtain trustworthy results even when a certain amount of data is contaminated. The LMedS method used (Casas, 2006) searches in the space of solutions obtained from subsets of the minimum number of data. As we require a minimum of three distances to compute the location and there are a total of n, we make m subsets of three distances:

$$m = \frac{n!}{3!\,(n-3)!} \tag{1}$$

For each subset Si of distances (du, dv, dw), we compute a location Pi (xi, yi, zi) by solving the system of equations of using any traditional technique such as least squares:

$$\left.\begin{aligned} d_u &= \sqrt{(x_i - x_{BSu})^2 + (y_i - y_{BSu})^2 + (z_i - z_{BSu})^2} \\ d_v &= \sqrt{(x_i - x_{BSv})^2 + (y_i - y_{BSv})^2 + (z_i - z_{BSv})^2} \\ d_w &= \sqrt{(x_i - x_{BSw})^2 + (y_i - y_{BSw})^2 + (z_i - z_{BSw})^2} \end{aligned}\right\} \tag{2}$$

where i = 1,…,m and (xBSj, yBSj, zBSj) are the coordinates of BSj being j = u, v, w.

For each location Pi, we obtain the residues Ri as:

$$\begin{aligned} \mathbf{R_i} &= \left((d_1 - \hat{d}_{i1})^2, (d_2 - \hat{d}_{i2})^2, \ldots, (d_n - \hat{d}_{in})^2 \right) \\ \hat{d}_{ik} &= \sqrt{(x_i - x_{BSk})^2 + (y_i - y_{BSk})^2 + (z_i - z_{BSk})^2} \\ k &= 1, \ldots, n \end{aligned} \tag{3}$$

And compute the median Mi of the residues Ri.
The final solution P (x, y, z) is that with the minimum median Mi.

2.4 Instrument's Localization

As an experimental implementation (figure 2), a motorized resectoscope mock up have been used. The distances between emitters and receivers were processed by the computer through the localization algorithm in order to obtain the instrument's unknown position.

According the results (figure 3), can be stated that the system has a good dynamic behavior. Moreover, can be stated the good performance of localization algorithms and solution filtering.

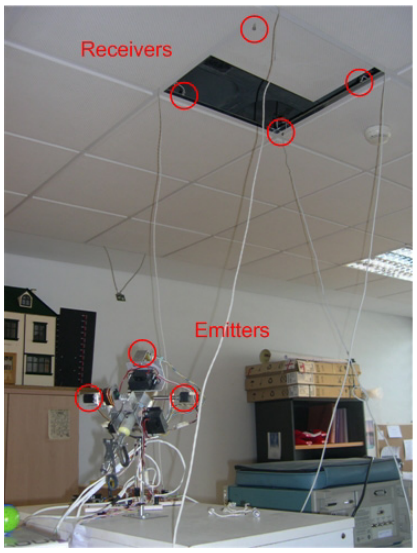

Figure 2: Mock up implementation.

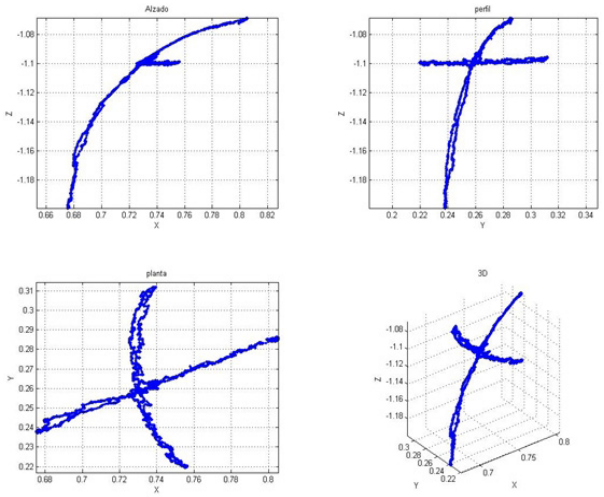

Figure 3: Motion tracking.

3 CONCLUSIONS

As result of this research, a low-cost and low-complexity indoor positioning system has been designed. It meets the requirements stated previously, to fit in a motion tracking application.
The method of determining TOF has a good precision for fixed distances (300 µm) and good performance with high misalignment between transducer pairs. Adding all sources of one-dimensional distances' inaccuracies (worst case scenario), the error might reach 5 mm. This error translated to three-dimensional positioning would mean 8 mm.

Regarding the reliability of the system, with the inclusion of the controlled emission, the system has been able to create signals in reception with a characteristic form. This effect brings about advantages when dealing with reflection on surfaces, important factor in an operating room. In addition, the system will be more robust to external noises in the work frequency. In terms of scalability, the developed system is able to capture the data from up to 20 receiving modules. Observing the obtained results, we can conclude that the system performs in a satisfactory way the motion tracking of the instrument's position and movement.

ACKNOWLEDGEMENTS

This work has been partially supported by the Spanish Ministry of Science and Technology under CICYT project numbers TIC2003-07766 and TIN2006-15617-C03-02. Also by the EU under project MonAmi (IST-5-0535147).

REFERENCES

Bianchi, G., 2007. *Exploration of augmented reality technology for surgical training simulators*, Diss., Eidgenössische Technische Hochschule ETH Zürich, Nr. 16876

Cai, C., Regtien, Paul P. L. , 1993. *Accurate Digital Time of flight Measurement Using Self-Interference*, IEEE Transactions on Instrumentation and Measurement .Vol. 42, No.6, December 1993, Pag. 990-994

Casas, R., et al, 2006. *Robust Estimator for Non-Line-of-Sight Error Mitigation in Indoor Localization*, EURASIP Journal of Applied Signal Processing, 2006, Article ID 43429, pp. 1-8.

Casas, R., et al, 2007. *Hidden Issues in Deploying an Indoor Location System* ,Pervasive Computing, IEEE, Vol.6, Iss.2, April-June 2007 Pages:62-69

Huang. S.S et al, 2002. *A high accuracy ultrasonic distance measurement system using binary frequency shift-keyed signal and phase detection*. American Institute of Physics, Review of Scientific Instruments, Volume 73, Issue 10, pp. 3671-3677.

Lamancusa, John S., Figueroa, J.Fernando, 1990. *Ranging errors caused by angular misalignment between ultrasonic transducer pairs*, The Journal of the Acoustical Society of America, Volume 87, Issue 3, March 1990, pp.1327-1335

Liao et al, 2004. *A new ultrasonic temperature measurement system for air conditioners in automobiles*. Insttitute of Physics, *Meas. Sci. Technol.* 15 413-419

Tatar, F., 2006. *Ultrasound 3D positioning system for surgical instruments*, Doctoral Dissertation, Technische Universiteit Delf.

AUTOMATED CELL CHARACTERIZATION PLATFORM: APPLICATION TO YEAST PROTOPLAST STUDY BY ELECTROROTATION

J. Laforêt[1], M. Frénéa-Robin[2], H. Cérémonie[1], F. Buret[1] and L. Nicolas[1]
[1]*AMPERE, UMR CNRS 5005, Ecole Centrale de Lyon, Ecully, France*
julie.laforet@ec-lyon.fr, helene.ceremonie@ec-lyon.fr, francois.buret@ec-lyon.fr, laurent.nicolas@ec-lyon.fr
[2]*Université de Lyon, Lyon, F-69622, France ; AMPERE Villeurbanne, France*
marie.frenea-robin@univ-lyon1.fr

Keywords: Dielectrophoresis, electrorotation, yeast cells, yeast protoplasts.

Abstract: This paper is about the development of a new automated platform dedicated to cell manipulation and characterization by dielectrophoretic methods. We illustrate its possibilities by studying yeast protoplasts and yeast cells electrorotation spectra, obtained using polynomial microelectrode structures powered by computer-controlled generators. Measurements were made over the frequency range 100 kHz to 80MHz, mostly in a suspending medium of conductivity 50 mS/m inside the rotation chamber. The rotation rate of yeast protoplasts was inferior to that of whole yeast cells. To understand such behavioral differences, yeast protoplasts were modelled as single-shell spheres in a first approach.

1 INTRODUCTION

The term dielectrophoresis (DEP) is used to describe the motion and orientation induced by a non-uniform electric field on polarizable particles, such as cells. In conventional-DEP (c-DEP), stationary fields of inhomogeneous strength are used to translate cells toward field minima or maxima. Electrorotation (ROT) relies on non-uniformities in the phase distribution of the applied field to induce cell rotation at constant velocities.

The effects of chemicals and environmental factors on the cell electric properties are more and more adressed. ROT technique enables the study of various organisms individually without physiological damage and cell characterization by angular velocity measurement. This type of microelectrodes system allows cell handling (separation, selection, electrofusion…) and transport and may be basic components to be integrated into lab-on-a-chips.

Yeasts are eukaryotic cells widely used as model organism in cell biology, mainly because they are quick and easy to grow. Preparation and regeneration of yeast protoplasts are important in fusion, transformation and cloning studies (Kofod and al., 1998). Protoplast fusion can be used to improve anti-bacterial and anti-fungi characteristics of bakery yeast. In this study, spectra are analysed according to a two-shell spherical model for whole yeast cells and single-shell for protoplasts in a first approach.

2 THEORY

2.1 Yeast Cell Model

In this paper, whole yeast cells are modelled by a two-shell spherical model. Cytoplasm, membrane and cell wall are considered as concentric spheres, according to the individual yeast cell model developed by Falokun (Falokun and al., 2006). The complex permittivity of cell interior and membrane are denoted ε_0^*, and ε_1^*.To replace the "smeared out" sphere, we used:

$$\varepsilon_{1eff}^* = \varepsilon_1^* \frac{\left(\frac{R_1}{R_0}\right)^3 + 2\left(\frac{\varepsilon_0^* - \varepsilon_1^*}{\varepsilon_0^* + 2\varepsilon_1^*}\right)}{\left(\frac{R_1}{R_0}\right)^3 - \left(\frac{\varepsilon_0^* - \varepsilon_1^*}{\varepsilon_0^* + 2\varepsilon_1^*}\right)} \quad (1)$$

where R_i is the radius of the shell index i.

Then, the complex permittivity of the equivalent homogeneous cell can be expressed as:

$$\varepsilon_p^* = \varepsilon_2^* \frac{\left(\frac{R_2}{R_1}\right)^3 + 2\left(\frac{\varepsilon_{leff}^* - \varepsilon_2^*}{\varepsilon_{leff}^* + 2\varepsilon_2^*}\right)}{\left(\frac{R_2}{R_1}\right)^3 - \left(\frac{\varepsilon_{leff}^* - \varepsilon_2^*}{\varepsilon_{leff}^* + 2\varepsilon_2^*}\right)} \quad (2)$$

Relative permittivity and conductivity of the suspension medium used in the experiments are 78 and 50 $mS.m^{-1}$. Yeast cells average electrical and geometrical parameters are stored below (Table 1).

Table 1: Properties of different cellular compartments of yeast cells (Falokun and al, 2006 & Zhou and al, 1996).

	Radius or thickness	Conductivity	Permittivity
0: cytoplasm	5 µm	2 $S.m^{-1}$	50
1: membrane	8 nm	9.10^{-6} $S.m^{-1}$	6
2: wall	150 nm	6.10^{-2} $S.m^{-1}$	60

2.2 Electrorotation Theory

The structure and properties of biological cells can be investigated by observing their ROT spectra (Gascoyne and al., 2004). Indeed, the rotation velocity of a spherical particle submitted to a constant rotating electric field can be expressed as:

$$R(\omega) = -\frac{\varepsilon_m \mathrm{Im}[K(\omega)]E^2}{2\eta} \quad (3)$$

where η is the solution viscosity, E and ω are the magnitude and angular frequency of the applied field.

$K(\omega)$ is the Clausius-Mossoti factor (CMF), depending on the particle and its immersion medium complex permittivities ε_p^* and ε_m^*:

$$K(\omega) = \frac{\varepsilon_p^* - \varepsilon_m^*}{\varepsilon_p^* + 2\varepsilon_m^*} \quad (4)$$

The value of ε_p^* varies according to cell type. Therefore, each cell type is characterized by a particular ROT spectrum (as Figures 3 and 4). When $\mathrm{Im}[K(\omega)] > 0$ (angle of the induced dipolar moment with respect to the electric field vector comprised between 0 and 180°), cells exhibit anti-field rotation ($R(\omega) < 0$). On the contrary case, cells share the same rotation sense as the field ($R(\omega) > 0$).

3 MATERIALS AND METHODS

3.1 Experimental Setup

The microelectrode structure used in the DEP and ROT experiments is composed of 4 polynomial electrodes (Au-Ti deposited on glass) disposed in a circular arrangement. Those electrodes are powered by 4 generators delivering sine-wave voltages up to 80 MHz. We simply switch from c-DEP to ROT according to the phase configuration of the 4 signals (Figure 1). An advantage is that cells may be concentrated at the centre of the s by negative DEP before a ROT experiment. Indeed, all the cells situated in this area will experiment the same constant rotating field when undergoing ROT. Only these cells must be taken into account in rotation measurements. In this constant field area (Hughes, 1998), cell translation is reduced during the course of a measurement.

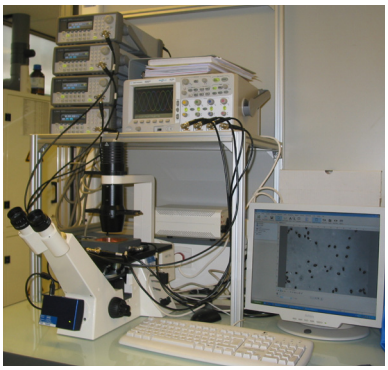

Figure 1: Experimental setup.

Visualization of the applied voltage and impedance matching are achieved thanks to a wide band oscilloscope, whose input impedance can be set to 50 Ohms. All these equipments are controlled by PC through GPIB interface using a software developed under LabView® which enables synchronized signal generation. Voltages are kept constants over the whole frequency range thanks to automatic gain control.

Cell motion is observed under an inverted microscope. Image sequences are captured by a high speed camera. Velocity depends on the electric field frequency and on the dielectric properties of the cell and its surrounding medium. Frequency-dependent rotation rates were first measured with a stopwatch

and then confirmed with a software under development. After an image processing in order to detect and label each isolated cell, the angular velocity is calculated with Matlab® by determining the orientation (angle between its main axis and horizontal axis) in each sequence of images.

3.2 Cell Preparation

Before experiments, the system was rinsed with distilled water, washed with ethanol and dried with an air jet. The samples were centrifuged and the cells were washed 2 times with a solution whose conductivity was adjusted to 50 mS.m^{-1} by addition of KCl and directly measured with a conductivity meter. For protoplasts only, glucose was added to the solution (at a concentration of 30mM) to adjust the osmolarity.

Prior to experiments, a drop of cell suspension (60µL) was deposited onto the electrode system (gap: 400 µm), in a chamber fabricated with a self-adhesive silicone bond. Then, a lid was used to close it and prevent fluid circulation caused by evaporation.

3.3 Protoplast Forming

Yeast cells (*Saccharomyces Cerevisiae*) were suspended and incubated at 35°C during ten minutes in a pre-treatment solution. After centrifugation, they were resuspended two times in a buffer solution which contained 4.7 g.l^{-1} sodium citrate, 10.8 g.l^{-1} potassium dihydrogenophosphate and 21.8 g.l^{-1} sorbitol.

In a second time, they were centrifuged and resuspended in a 500 U.ml^{-1} solution of lyticase enzymes with the buffer solution. Enzymes digested the yeast cell wall during an one hour incubation at room temperature to generate protoplasts.

4 RESULTS AND DISCUSSION

4.1 Simulated ROT Spectra

To obtain the general appearance of the whole yeast cell spectrum, we use the two-shell model with the Table 1. The rotation rate is proportional to the imaginary part of the CMF (3), plotted on Figure 2:

$$R(\omega) = -\chi \, \mathrm{Im}\left[K(\omega)\right] \; where \; \chi = \frac{\varepsilon_m E^2}{2\eta} \qquad (5)$$

In the case of protoplasts, we used the single-shell model, only taking into account the cytoplasm and membrane properties (Table 1), in a first approach.

4.2 Experimental ROT Spectra

First, we have collected typical ROT spectra exhibited by single viable yeast cells by measuring the induced rotational velocities at a medium conductivity of 50 mS.m^{-1} under a constant voltage of 3 V_{pp} (Figure 3). The average ROT spectrum is in agreement with previously reported data (Hölzel, 1997).

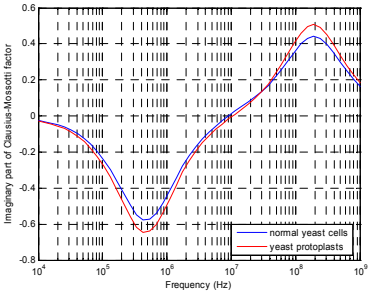

Figure 2: $-\mathrm{Im}\left[K(\omega)\right]$ at 50 mS.m^{-1}.

There are two ROT peaks of nearly the same amplitude. The rotation rate was calculated from about ten cells per point. Positive and negative values respectively indicate co-field and anti-field cell rotation. The results plotted Figures 3 and 4 were averaged across 4 experiments, vertical lines indicated amplitude between the minimal and maximal values.

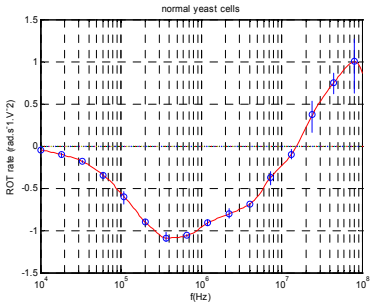

Figure 3: Experimental ROT spectra at 50 mS.m^{-1}.

Then, we have collected ROT spectra exhibited by yeast protoplasts for a conductivity of 50 mS.m^{-1} under a 6 V_{pp} constant voltage (Figure 4). The zero crossing frequency was situated around 15 MHz and 11 MHz for normal yeast cells and protoplasts respectively.

The cells exhibited anti-field rotation at frequencies below the zero crossing and co-field rotation above.

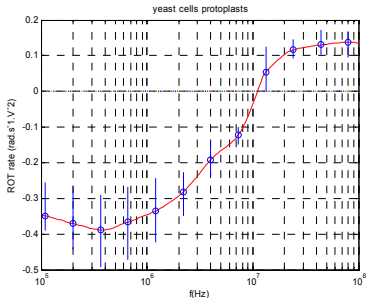

Figure 4: Experimental ROT spectra at 50 mS.m^{-1}.

4.3 Discussion

For whole yeast cells, the overall spectrum (Figure 3) is consistent with that obtained from simulation (Figure 2), up to a multiplicative scalar factor, which could be explained by the fact that the simulated data did not take into account the factor χ (5).

On both experimental spectra, the negative ROT peak happens near 500 kHz despite rotation rate attenuation for yeast protoplasts. The viscosity of the medium suspension, in the case of protoplasts, was almost 5% higher than water viscosity because of glucose (Easteal, 1989), which affects the value of χ. Nevertheless, more precise investigation is necessary to understand this rotation slowdown.

As can be seen from Table 1, the dielectric properties of cell wall are close to medium properties. This may explains the resemblance between yeast cells and yeast protoplast simulated spectra (Figure 2) obtained with our approach, consisting in switching from a model to another by suppressing the shell representing the cell wall.

The approach consisting in modelling protoplasts by the two most inside shells presents its limitations. Indeed, simulated result does not fit the experimental data well in the co-field rotation part of the spectra. For 1.1 mS.m^{-1}, simulation points out more differences between the two spectra (Figure 5).

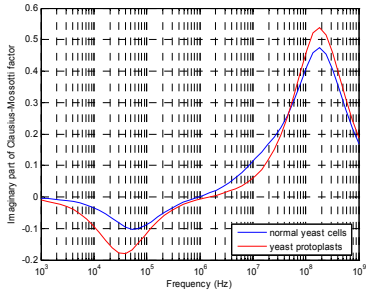

Figure 5: $-\mathrm{Im}\lceil K(\omega)\rceil$ at 1.1 mS.m^{-1}.

5 CONCLUSION

As further developments, we need to improve our experimental setup to cover a wider frequency range and obtain thereby a complete ROT spectrum, including the second peak. Future experiments performed in lower conductivity immersion media (1.1 mS.m^{-1}, for example) may bring more information about the cell wall influence (Figure 5).

Yeast protoplast and whole cell electric properties can be extracted from experimental ROT spectra by parameter identification thanks to a identification process under Matlab®. During this step, more sophisticated models could be used to describe cells, as for instance a N-shell ellipsoidal model. The measurement of cell properties is a step toward the modelling of electromagnetic field-tissue interaction using a bottom-up approach.

LabView® interface allows to realize several series of different experiments. Cell motion was successfully observed over a wide frequency range for yeast cells. Fabrication of microelectrodes enabling travelling-wave dielectrophoresis is the last part of our platform to be developed. Further, these cell manipulation techniques permit to study the effects of various treatments on cells such as response to toxicants for magnetic field exposure and to detect cell pathologies.

REFERENCES

Kofod, L.V., Andersen, L.N., Kauppinen, M.S., Christgau, N.S., Dalboge, H., 1998. Enzyme with P-1,6 endoglucanase activity, *United States Patent. Patent Number 5770406*.

Falokun, C.D., Markx, G.H., 2006. Electrorotation of beads of immobilized cells, *J. of Electrostatics*.

Zhou, X-F., Markx, G.H., Pethig, R., 1996. Effect of biocide concentration on electrorotation spectra of yeast cells, *Bioch. and Biophys. Acta*.

Gascoyne, P. R. C., Vykoukal, J. V., 2004. Dielectrophoresis-based sample handling in general-purpose programmable diagnostic instruments, *Proceedings of the IEEE*.

Hughes, M.P., 1998. Computer-aided analysis of conditions for optimizing pratical electrorotation, *Physics in Medecine and Biology*.

Hölzel, R., 1997. Electrorotation of Single Yeast Cells at Frequencies Between 100Hz and 1.6GHz, *Biophysical J.*

Easteal, A.J., 1989. Can. Tracer diffusion in aqueous sucrose and urea solutions, *J. Chem.*.

COMPACT PULSE OXIMETER USING PIC18F4550 MICROCONTROLLER

Leonardo Zane Vilhegas, Adir José Moreira and Ronaldo Domingues Mansano
Departamento de Engenharia de Sistemas Eletrônicos
Escola Politécnica da Universidade de São Paulo
Av. Prof. Luciano Gualberto, 380 – Bloco A – Sala 46 – CEP: 05508-900, Brazil
Tel:+55 +11 +3091-9719
leozanne@lsi.usp.br, adir@lsi.usp.br, mansano@lsi.usp.br

Keywords: Oxygen Saturation, microcontroller, PIC18F4550, heart rate, USB.

Abstract: In this paper is propose one compact pulse oximeter system using a PIC18F4550 micrcontroller, which use of USB (*Universal Serial Bus*) communication technology. The device has one LCD (*Liquid Crystal Display*) 20x4 to continuous check and has the possibility to get one parallel communication with a PC (*Personal Computer*) to analysis more detailed. The system is compound for oxygen saturation measures (SpO_2) and heart rate. The equipment is compact and show easy to handle and simple use.

1 INTRODUCTION

In the 80 decade beginning, already had emphasized the necessity of the improvement and of scientific development in the biomedic instrumentation area in Brazil, in order to reach the excellency of the medical services (Moraes & Vita, 1981).

With this mind and due to great integration capacity increase of the eletronics devices, as well as the fast technological advance of the microcontrollers, a wide development of applications in the diverse areas of biomedical engineering was allowed (Moron, 2005).

The oxygen is fundamental and vital for the correct functioning of each cell of the human body and its absence, for a drawn out time, it can cause the deaths of these cells (Webster, 1997). The pulse oximetry (Moyle, 1994 - Wukitsch, 1987) is a non-invasive method to measure the arterial oxygen saturation (SpO_2) using two diferents wavelenghts to determine the relative oxyhemoglobin concentration (HbO_2) and deoxyhemoglobin (Hb) in the blood. Already, the pulse oximeter is a device that uses an empirical measurement method and actually is an important SpO_2 continuous monitor device where it offers oxygen saturation results trustworthy similar the convencional methods.

In this article is propose a development of the compact pulse oximeter system. The system is compound for one prototype sensor, one software interface and one pulse oximeter device with a LCD 20x4, where the device contained one PIC18F4550 microcontroller that produce all control of the circuit. The PIC contained the USB technology integrated where the implementation and compacting was easily.

The primary interface has been the ubiquitous serial port. Intel developed the USB in the early 90s, and while many personal computers peripherals now support this interface. Each USB port can support up to 127 devices (Lichtel, 2004).

2 MATERIALS AND METHODS

2.1 Overview of the System

The aim of this study is to design and implement one compact system and with handle facilities and use to SpO_2 monitoring and heart rate. The figure 1 shows the architecture of the considered and developed system.

The major design requirements of project was the following: a) It should be portable and easy mobility; b) it should be easiness to get na supply source; c) it should have a userfriendly interface; d) Compacting of the circuit using the PIC18F4550; e) Possibility to record the data received in a PC; f) it should collect physiological data of arterial oxygen saturation and the heart rate (BPM).

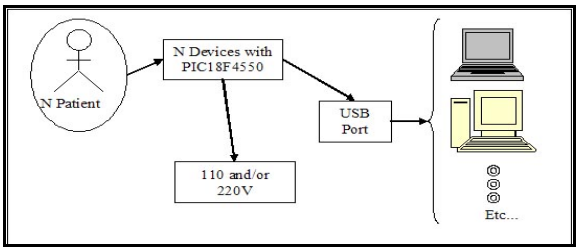

Figure 1: Overview of the development system. Device can be supply by PC or directly by AC 110/220V, using a converter to 5V.

2.2 Prototype Sensor

In the prototype device of the article hadn`t been use neither comercial sensor, it was developed one prototype sensor using comercials LEDs from CROMATEK and one photodiode TSL251R, from TAOSINC ,with transimpedance amplifier integrated. The LEDs has wavelengths of 660nm (red) and 940nm (infrared). The photodiode choice was done by yours caracteristics and someone are about transimpedance amplifier integrated, rise time about 70us, linear voltage response in respect to intensity light, spectral response and good angular displacement, becoming the alignment between emitter and receptor less critical.

2.3 Physiological Acquisition Signals Device

The compact pulse oximeter device using the microcontroller PIC18F4550 has the circuit supply directly by USB port. Using the USB cable, the device can be conect directly in PC and/or using the adaptor, where can be connected directly to electricity network and visualize the data directly on the LCD.

The USB port has 5V and 500mA, this is enough to supply the circuit. The circuit is compound for first condicionning step signal, that proceeding from the sensor, that have a filter pass-band and a signal gain. After the signal treatment the PIC is responsible for diverse other necessary functions of the pulse oximeter device. The sampling frequency that the microcontroller works is 1kHz and takes care of to the necessities of the Nyquist theorem and prevents the aliasing problem. The prototype also has a LCD 20x4 to visualize the data received for the optic sensor. The implementation of the LCD in the system becomes interesting therefore is not necessary no complex computational system to get the value of SpO2 and the cardiac beating. In figure 2 the diagram of blocks of the physiological signals acquisition system can more be seen detailed.

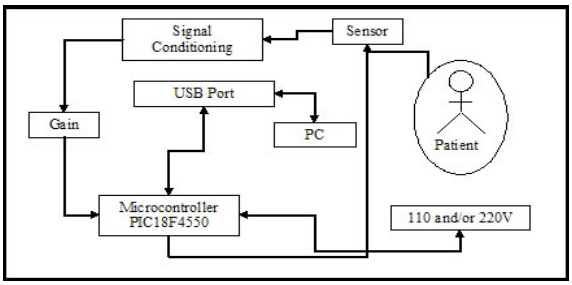

Figure 2: Diagram of blocks of the compact pulse oximeter device.

3 RESULTS

All the prototype system had been developed and implemented. The device (already with protection circuit), which includes the physiological signals is compound (120x80x30mm) and light (<300g). In figure 3 the image prototype device circuit can be seen. The photo of the pulse oximeter with LCD connected together with the USB cable and the eletricity network found in the figure 4. For the sensor development was done one photospectroscopy of the LEDs that had been used in the prototype, to verify if they are in the specific band wavelenght fo the aplication. In figure 5, the graphs of the tests realized through with the emitters can be seen.

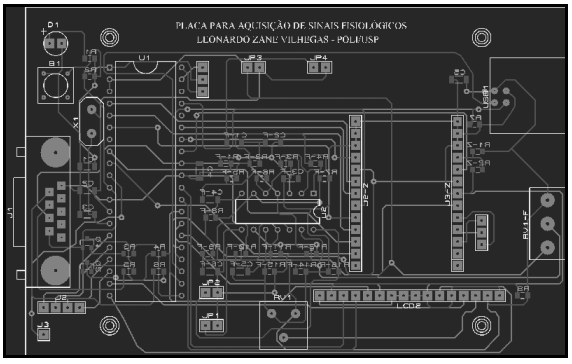

Figure 3: Image of the prototype pulse oximeter device circuit using the PIC18F4550.

The prototype sensor was development with the concern to keep total isolated of the invironment. In figure 6 it can be seen the sensor images, the armored cable and used connector DB9 to realize the connection with device.

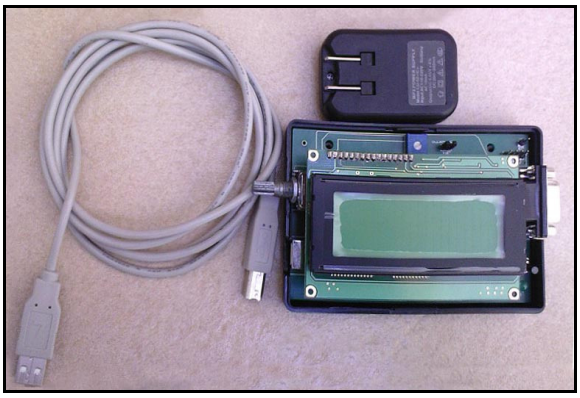

Figure 4: Photograph of the device with the connected LCD, USB cable and adapter for electricity network.

a)

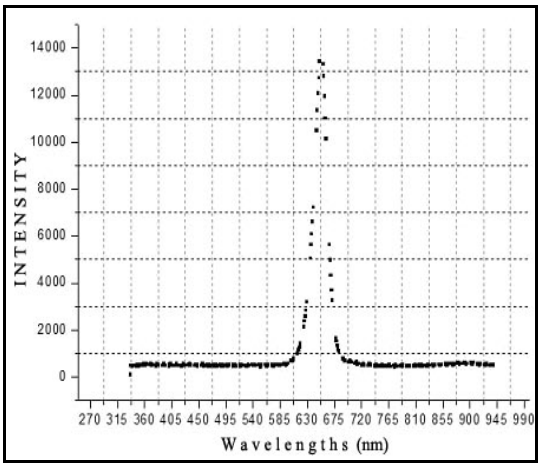

b)

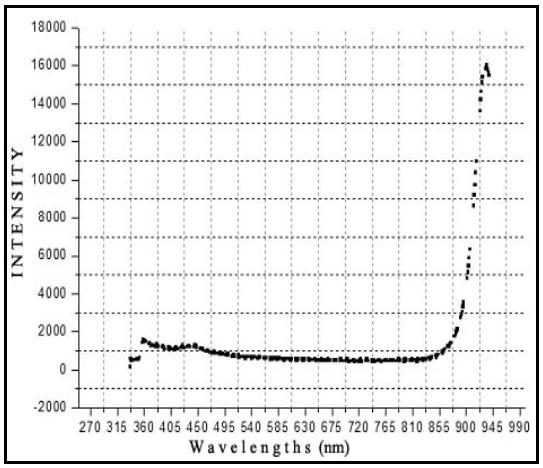

Figure 5: Photospectroscopy: a) LED 660nm (red); b) LED 940nm (infrared).

The program of use for interface the pulse oximeter device with the PC was developed through the utilization of LabVIEW software. The program has the information about amount of oxygen arterial blood (SpO_2), of the photopletysmography signal

a)

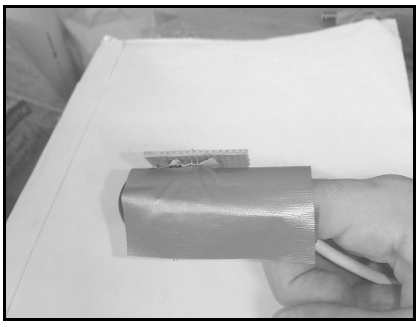

b)

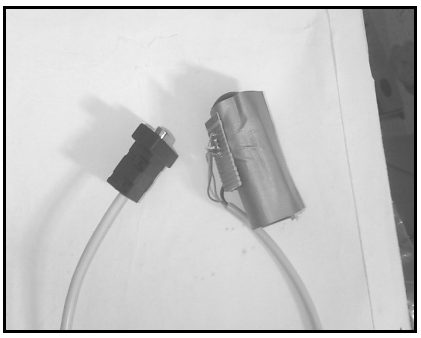

Figure 6: Pototype sensor: a) Sensor to hardwired to the indicating finger; b) Sensor with covering against surrounding light connected with one armored cable and connector DB9.

and heart rate. The software also diverse other funtions as for example, to record the data of the signals received by device, acknowledgment of emergency, etc. In figure 7 the display of the software main control developed for interface of the system can been seen.

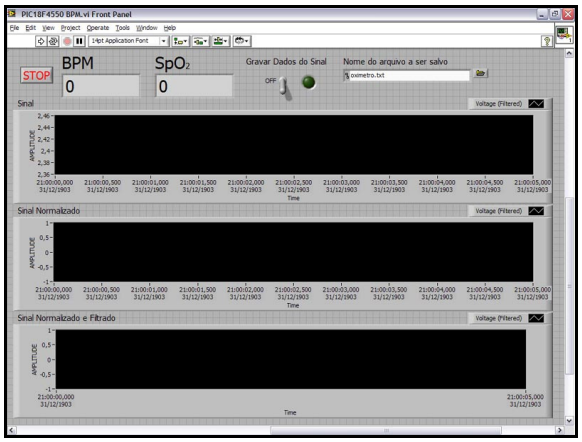

Figure 7: Main display of the responsible interface fo the communication with the device.

4 CONCLUSIONS

The pulse oximeter device using the microcontroller PIC18F4550 was developed. In the module are measured physiological samples of oxygen saturation in the arterial pulse, of photopletysmography and heart rate. The software developed to interface with the computer revealed very friendly however. With resources limited fo not being the focus of the article. The data presented in the LCD are oxygen saturation and cardiac frequency. The supply device for the USB port using a PC or the adapter presented great easiness and fastest in its aplication. The photopletysmography are not presented in the LCD for the display not to be graphical.

REFERENCES

Costill, D. L., Wilmore, J. H., *Fisiologia do Esporte e do Exercício*, São Paulo, Segunda edição, Ed. Manole, 2001.

Lichtel, D.: *Implementing a USB Equipment Interface Using the Microchip PIC16C745,* QEX, June, 2004.

Moraes, J.C.T.B.; VITA, G.M.; *Desafios de problemas da saúde no Brasil à Engenharia Biomédica*, Rio de Janeiro, Anais do VII Congresso Brasileiro de Engenharia Biomédica, p.137-7, 1981.

Moron, M.J.; Casilari, E.; Luque, R.; Gazquez, J.A**.;** *A wireless monitoring system for pulse-oximetry sensors*, Systems Communications, 79 – 84, 2005.

Webster, J.G.; *Design of pulse oximeters*. 1.ed. U.K., Bristol, 1997.

Moyle J., *Pulse Oximitery*. 1994: BMJ Publishing Group.

Wukitsch M., *Pulse oximitery: Historical review of Ohmeda functional analysis*, Journal of Clinical Monitoring and Computing, 4, 161–166, 1987.

DEVELOPMENT OF AN AMPEROMETRIC SENSOR FOR POTASSIUM IONS

Marcos F. S. Teixeira, Alex S. Lima, Patricia Monteiro Seraphim
Dep. of Physical, Chemistry and Biology , Faculty of Science and Technology, University of State of Sao Paulo (UNESP)
Rua Roberto Simonsen, 305 - Presidente Prudente – SP - Brazil
funcao@fct.unesp.br

Nerilso Bocchi
Department of Chemistry, Federal University of São Carlos
Via Washington Luiz, Km 235 - São Carlos – SP - Brazil
bocchi@dq.ufscar.br

Keywords: Sensor for potassium ions, hollandite, voltammetry.

Abstract: Hollandite-type manganese oxides are nanofibrous crystals with sub-nanometer open tunnels that provide a unique property for sensing applications. Sensor based on hollandite-type manganese oxide was investigated for amperometric detection of potassium. With an operating potential of +0.63 V *versus* SCE, potassium ions produce oxidation currents at the sensor, which can be exploited for quantitative determinations. The amperometric signals are linearly proportional to potassium ions concentration in the range 2.7×10^{-4} to 9.1×10^{-4} mol l^{-1} with a correlation coefficient of 0.9990. The construction and renewal are simple and inexpensive.

1 INTRODUCTION

Determination of potassium contents of serum, urine, and foods is very important in clinical and medical fields, since the potassium contents are related to renal diseases. These diseases restrict patients to a diet containing a large amount of potassium. From the potassium determination, medical information concerning physical conditions of the patient can be obtained. In the case of hypopotassemia, alkalosis, cirrhosis of liver, diuretic drugs, etc. are suspected. On the other hand, when potassium concentration in human serum becomes higher than 9 mmol L^{-1}, heart often stops (Harrison *et al*., 1966). Hence, accurate, easy and rapid sensing of potassium ions is very important.

The development of chemical sensors for non-electroactive ions based with modified electrodes has been based in the participation of non-electroactive cations in redox reactions of metal hexacyanoferrates (Karyakin, 2001). Other compound with ability of accommodate non-electroactive cations and promote the electroactivity in function of the insertion cation is the manganese oxide. Manganese oxides represent a large class of materials that have layered and tunneled structures consisting of edge-shared MnO_6 octahedral units. They have attracted considerable interest due to broad potential applications in heterogeneous catalysis, chemical sensing, toxic wastewater treatment, and rechargeable battery technology. In our laboratories, we are also interested in developing highly sensitive and selective methods for the determination of non-electroactive using electrodes modified with different allotropic forms of manganese oxide (Teixeira *et al*., 2004 and Teixeira *et al*., 2004).

In this paper, we propose a new sensor to determine potassium ions.

2 EXPERIMENTAL

2.1 Apparatus

All voltammetric measurements were carried out in a 30ml thermostated glass cell at 25◦ C, containing three electrodes: carbon-paste electrode as a working electrode, saturated calomel as reference electrode (SCE), and platinum wire as an auxiliary electrode. During the measurements, the aqueous solution (TRIS buffer solutions) in the cell was not stirred

and deaerated. Voltammetric measurements were performed with a micro-Autolab Type III controlled by an appropriated software.

2.2 Reagents and Solutions

All solutions were prepared using a Millipore Milli-Q water. All chemicals were analytical reagent grade and were used without further purification. The supporting electrolyte used for most of the experiments was a 0.1 mol l^{-1} Tris buffer solution (pH = 8.30). A 0.01 mol l^{-1} potassium ions solution was prepared daily by dissolving potassium chloride (Merck) in 100 ml of such Tris buffer solution.
Graphite powder (1–2 μm particle size from Aldrich) and mineral oil (Aldrich) of high purity were used for the preparation of the sensor.

2.3 Preparation of Hollandite-Type MnO_2

Hollandite-type manganese(IV) oxide was prepared using a reflux method according to literature (Ching *et al*. 1997). For conversion to hollandite-type manganese oxide, a KMn_2O_4 sample was treated in an aqueous diluted sulfuric acid solution kept under constant stirring during 120 min. When the pH of this mixture was stabilized at a particular value, the solution was decanted and the remaining solid material washed by decantation with deionized water, filtered and dried in air at 90°C.

2.4 Sensor Construction

Sensors with hollandite-type MnO_2 were prepared by carefully mixing the dispersed graphite powder with manganese oxide at varying ratio. Exactly 1 g of this mixture was subsequently added to 0.200 g of mineral oil (20% m/m) and mixed in a 50 ml beaker containing 20 ml of hexane. The final paste was obtained with the solvent evaporation. The carbon-paste electrode was finally obtained packing the paste into a plastic tube (1 ml insulin plastic syringe) and arranged with a copper wire serving as an external electric contact.

3 RESULTS AND DISCUSSION

3.1 Electrochemical Behavior

First, the voltammetric behavior of the CPEM with hollandite-type manganese oxide in Tris buffer solution (pH 8.3) containing 5.0 x 10^{-4} mol L^{-1} potassium ions was investigated. The cyclic voltammograms obtained with the sensor (see Fig. 1) presented one anodic peak (peak I = 0.63 V *vs*. SCE) and another cathodic peak (peak II = 0.08 *vs*. SCE). This electrochemical activity is due to the extraction topotactic process of the potassium ions from the hollandite structure, which occurs in two steps to the electrochemical insertion/extraction processes of the potassium ions (Feng et al., 1995):

$$K_x Mn_x^{3+} Mn_{2-x}^{4+} O_{4\ (s)} \rightarrow 2\square.MnO_{2(s)} + x\ K^+_{(aq)} + x\ e^- \quad (1)$$

$$2\square.MnO_{2(s)} + x\ K^+_{(aq)} + x\ e^- \rightarrow K_x Mn_x^{3+} Mn_{2-x}^{4+} O_{4\ (s)} \quad (2)$$

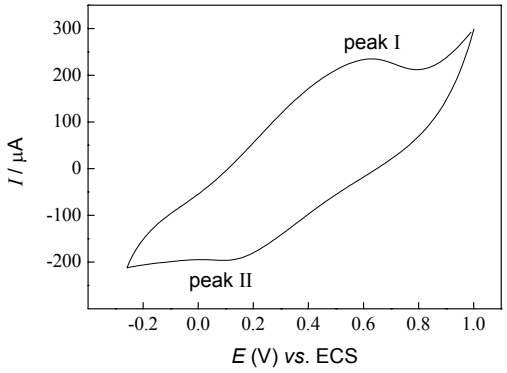

Figure 1: Cyclic voltammogram of the sensor in 5.0 x 10^{-4} mol L^{-1} of potassium ions, at a scan rate of 50 mV s^{-1} between − 0.15 and 1.00 V *versus* SCE.

The enhanced response to potassium ions occurs because the cathodic polarization of the sensor with hollanditel-type manganese oxide is quite enough to reduction the manganese in the solid. Consequently, the potassium ions from the adjacent solution are able to diffuse though the hollandite structure to maintain the electroneutrality principle.
In the absence of potassium ions, no voltammetric response was observed for the sensor, confirming that the response of the sensor is a function of the insertion reaction of potassium ions in the hollandite structure as mentioned previously (see Eq. 3):

$$2\square.MnO_{2(s)} + x\ K^+_{(aq)} + (x/2)\ H_2O_{(l)} \rightarrow K_x Mn_x^{3+} Mn_{2-x}^{4+} O_{4\ (s)} + x\ H^+_{(aq)} + (x/4)\ O_{2(g)}\ (0 < x < 1) \quad (3)$$

where □ is vacant site (tunnel) of the manganese oxide.
The apparent electrochemical rate constant k_e and the electron-transfer coefficient α_{anodic} were calculated for the sensor according to the method described by Larivon (Larivon, 1979). It has been shown by Laviron that for a surface redox couple, α_{anodic} and k_e can be determined from the variation of E_{pa} with scan rate. Figure 2 presents the plot of E_{pa} (V)

versus log v (V s^{-1}) of the sensor in Tris buffer solution (pH 8.3) containing 5.0 x 10^{-4} mol L^{-1} potassium ions. For large enough values of scan rate the E_p – log v plots gave one straight line with slopes of $2.303RT/(1-\alpha_{anodic})nF$ for the anodic branch, where R is the gas constant, T the absolute temperature, F the Faraday constant and n number of electrons involved in the redox couple. Considering that the number of electrons involved in the redox process is 1, the calculated value for the coefficient α_{anodic} was 0.83. These results suggest the redox process tends towards an irreversible system. The apparent electrochemical rate constant can then be determined applying the equation $k_e = 2.303\alpha_{anodic}nFv_o/RT$, in which the value of scan rate (v_o) is determined by extrapolation of the linear branch at higher scan rates and its intersection with the constant peak potential, represented by the peak of the voltammogram at the lower scan rate. The observed value was $k_e = 32.2\ s^{-1}$.

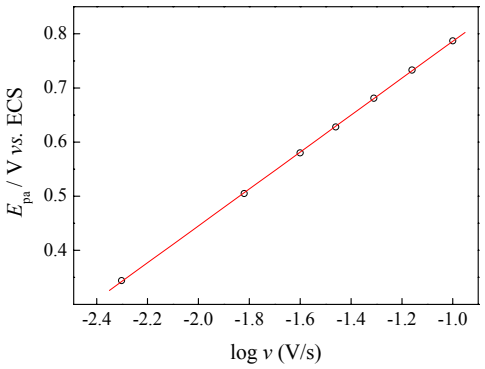

Figure 2: Dependence of E_{pa} with log(v) for the sensor in Tris buffer solution (pH 8.3) containing 5.0 x 10^{-4} mol L^{-1} potassium ions.

The effect of the carbon paste composition in the amperometric response of the sensor was evaluated in Tris buffer solution (pH 8.3) containing 5.0 x 10^{-4} mol L^{-1} potassium ions. The anodic peak current increased with the amount of manganese oxide in the paste up to 25% ($^m/_m$). The anodic peak current decreased significantly when more than 25% is used in the electrode preparation. This probably occurs due to a decrease in the conductive area at the sensor surface. According to these results a sensor composition of 25% ($^m/_m$) modified hollandite-type manganese oxide, 55% ($^m/_m$) graphite and 20% ($^m/_m$) mineral oil was used in further studies.

3.2 Analytical Curve and Repeatability

After optimizing the best operating conditions for the sensor (scan rate of 20 mV s^{-1}), cyclic voltammetries were carried out in Tris buffer solution containing different potassium ion concentrations in order to obtain the analytical curve for such electrode. This curve, illustrated in the Figure 3, was constructed using the anodic peak currents resulting a linear relationship with the potassium ion concentrations from 2.7×10^{-4} to 9.1×10^{-4} mol l^{-1} (I_{pa} (μA) = 2.07 + 200.8 [K^+] (mol L^{-1}); r = 0.9990) with a detection limit of 1.5×10^{-4} mol L^{-1} potassium ions. The precision of the method was also tested by analyzing five replicates containing 5.0 x 10^{-4} mol L^{-1} potassium ions. For each voltammogram, the surface of the sensor was renewed. The variation coefficient was 2.0 %.

4 CONCLUSIONS

As shown above, a sensor based on the hollandite-type manganese oxide exhibits an obvious response to potassium ions. It is necessary to investigate the interaction mechanism between potassium ion and the hollandite-type manganese oxide. The presence of Mn^{3+} in hollandite may increase its activity for the reaction. During the amperometric detection, potassium ions diffuse through the hollandite structure to produce Mn^{+3}, which can be electrochemically reoxidized to Mn^{+4}. The oxidative current is directly related to the concentration of potassium ions. In view of its sensitivity, stability, low working potential and simplicity and low cost of construction, the sensor based on the hollandite-type manganese oxides exhibits prospects for future biosensor work.

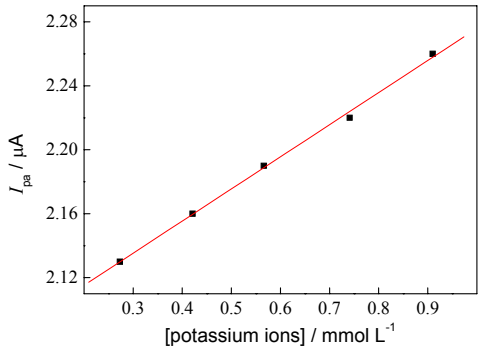

Figure 3: The curve analytical obtained from the anodic currents using sensor based hollandite-type manganese oxide.

ACKNOWLEDGEMENTS

The research support from FAPESP under contract no. 05/01296-4 and also grant by CNPq (no. 372010/2006-7) to A.S.L. are gratefully acknowledged (SJT).

REFERENCES

Ching, S., Roark, J.L., Duan, N., Suib, S.L., 1997. *Chem. Mater*. 9, 750.

Feng, Q., Kanoh, H., Miyai, Y., Ooi, K., 1995. *Chem. Mater.* 7, 148.

Harrison, T.R., Adams, R.D., Bennett, I.L., Resnik, W.H., Thorn, G.W., Wintrobe M.M., (Eds.), 1966. *Principles of Internal Medicine*, 5th edn., McGraw-Hill, New York.

Larivon, E., 1979. *J. Electroanal. Chem.* 101, 19.

Karyakin, A.A., 2001. *Electroanalysis* 13, 813.

Teixeira, M.F.S., Cavalheiro, E.T.G., Bergamini, M.F., Moraes, F.C., Bocchi, N., 2004. *Electroanalysis* 16, 633.

Teixeira, M.F.S., Bergamini, M.F., Bocchi, N., 2004. *Talanta* 62, 603.

WIDEBAND WIRELESS LINK FOR BCI CONTROL
100 kHz – 8/16 Channel for High Resolution EEG

C. P. Figueiredo, N. Dias, J. H. Correia and P. M. Mendes
DEI, University of Minho, Campus de Azurém, 4800-058 Guimarães, Portugal
{celso.figueiredo, ndias, higino.correia, paulo.mendes} @dei.uminho.pt

Keywords: Wireless, Wideband, Biotelemetry, BCI.

Abstract: This work presents a solution to obtain a wireless biopotential acquisition system with high data rate. Wireless systems are currently emerging with the possibility of being used for monitorization of several physiological parameters. However, most of the solutions are based on standard wireless systems. Besides the wireless throughput limitation, those systems are also limited in their software solutions and data acquisition capabilities. A trade-off solution between commercial of-the-shelf and custom design was explored by interfacing a MICAz with external instrumentation, while maximizing the rate of communication. The wireless system is being used for BCI control, operates at 2.4 GHz (Zigbee compliant), with a data rate of 250 Kbps for wireless link, and up to 1 Mbps for serial communication. Signals down to about 23 μV can be detected, and 8/16 single-ended channels are provided with 100 kHz sampling rate.

1 INTRODUCTION

The use of wireless sensor networks to assist in biomedical applications is being pursued by many researchers and will become available as soon as the required sensors and network solutions are made available (Schwiebert *et al.* 2001). However, before turning it into reality there are a few challenges to overcome.

The system must have low power consumption and the network nodes must operate under limited computation. Also, since these systems must operate in the human body, they do have some material constraints. Moreover, continuous operation is required, with high robustness and fault tolerance capability (Schwiebert *et al.*). Recently, the widespread availability of low power sensor devices with physiological monitoring ability is pushing researchers to include them in smart suits that can be used to monitor biological signals in different situations. Their application ranges from monitorization embedded in space suits (Simons *et al.* 2004), to monitorization during jogging activity (Marculescu *et al.* 2003).

However, the requirements of sending only cardiac or respiratory rhythm data are not enough anymore for modern monitorizing systems. Today, in many monitorization devices, it is necessary to route all the acquired data for storage and further processing. The development trend on physiological data acquisition is demanding more and more available bandwidth. As an example, the Brain-Computer Interface (BCI) operation, demands several electroencephalogram (EEG) channels with large bandwidth, which leads to large information amounts handling for feature and artefact extraction.

BCI is trusted to be a very useful tool for impaired people, both in invasive and non-invasive way. Although subjects using invasive approaches usually show evidence of better device control than non-invasive method users, it is barely preferred due to the high risk involved in its research and practical implementation. BCI has the potential to enable people to control a device with their brain signals. In several studies, different BCI approaches have been tested that enable impaired people to communicate and control specific devices (Wolpaw et al. 2000).

This paper will start with the presentation of the hardware platform that was used in this work. Afterwards, the requirements for physiological data acquisition for BCI are introduced, as well as the required hardware modifications. After highlighting the limitations of the available platform, a solution is proposed to overcome them and the obtained results are presented.

2 WIRELESS BCI

The BCI system is mainly made by four software/hardware modules: (1) EEG signal acquisition, (2) features extraction, (3) translation algorithm, and (4) actuator and feedback system.

The system that is being used for BCI records EEG data using a Labview platform, which receives data from a BrainProducts® Quickamp through a socket connection. The Data are digitized at 250 Hz and passed through a 6th order (48 dB per octave) band-pass Butterworth filter of 1-50Hz. This platform extracts the subject specific features, provides feedback and graphical interface to subject.

There are many challenges to be solved before BCI systems can show their full potential. A wideband low-power wireless acquisition platform is of most relevance for BCI operation. Fig. 1 shows a possible solution for a wireless BCI system. The presented solution uses a ZigBee link to transmit the EEG signals.

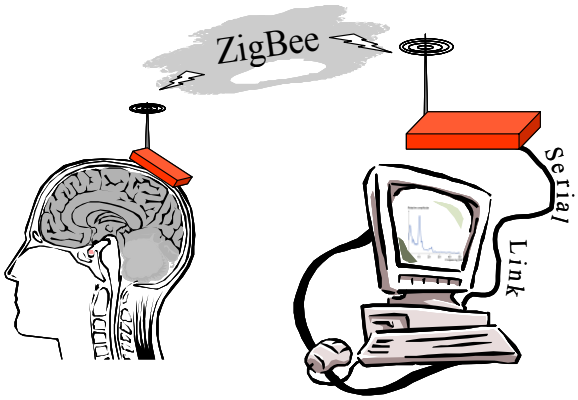

Figure 1: Wireless BCI system under development, (red modules are the target of this work).

2.1 Wideband BCI

A BCI is usually based on the ongoing rhythms of EEG signals. Those rhythms are the so called delta (0.5-4 Hz), theta (4-7.5 Hz), alpha (7.5-13 Hz), beta (15-20 Hz) and gamma waves (20-42 Hz). A bandwidth of 100 Hz would suffice for the acquisition of these potentials. However, during BCI operation, the reactivity of a rhythm to a mental task is usually identified in power spectra that are calculated using the FFT algorithm.

A good BCI control, from the user point of view, is a system with real time feedback. Any action will happen as soon as the user thinks about it. To obtain this, the system should collect as much data as possible in the shortest period of time, limited by the spectral resolution required. In this way, for a specific time window, the higher the number of sampled points, the higher is the spectral content in the calculated spectra. Once 1000 samples per second are recorded, the FFT of a 1 s time window achieves 1 Hz resolution in the frequency domain, together with a spectral content up to 1000 Hz. This sampling rate able the acquisition system to track surface EMG (2-500 Hz bandwidth) signals in order to detect task related muscle activity (Prutchi and Norris, 2004), since a BCI system is supposed to operate in the absence of muscle activity.

BCI systems can be greatly improved if more complex and faster algorithms can be used but this would require routing all the available data to a powerful computing system. The acquisition systems are, due to power saving requirements, very limited to perform this task.

2.2 Wireless Platform

One key element required to implement a wireless BCI system is the wireless platform. There are many solutions to implement it but the MICAz is a very popular one. This platform allows easy implementation of a wireless sensor network formed by individual wireless nodes. Fig. 2 a) shows the node core available for system development. This core includes the microcontroller, the ADC with 10 bits resolution, the ZigBee wireless interface, and the serial interface.

The microcontroller is the ATMEL Atmega128, running the TinyOS operating system. The micro provides access to the ADC, allowing data acquisition at 76.9K samples/s, with a resolution of 10 bits, from a maximum of 7 differential or 8 single-ended channels. The acquired data can then be routed trough the wireless ZigBee link, which allows a throughput of 250 kbps. The other option is to route the data through the serial interface. It uses a RS-232 link with the maximum data rate of 115.2 kbps.

2.3 Data Acquisition

The system can use three different node types, as shown in Fig. 2. The first is the standard wireless platform (Fig. 2-a)), which has a microprocessor with a built in analogue-to-digital converter (ADC). This device allows a maximum data transfer rate of 115.2 kbps. This limitation comes from the serial port connection (RS232), where the PC USART is limited to this speed.

When more resolution is required, it is necessary to use an external ADC. This is required for high resolution EEG and ECG, e.g., to enable the

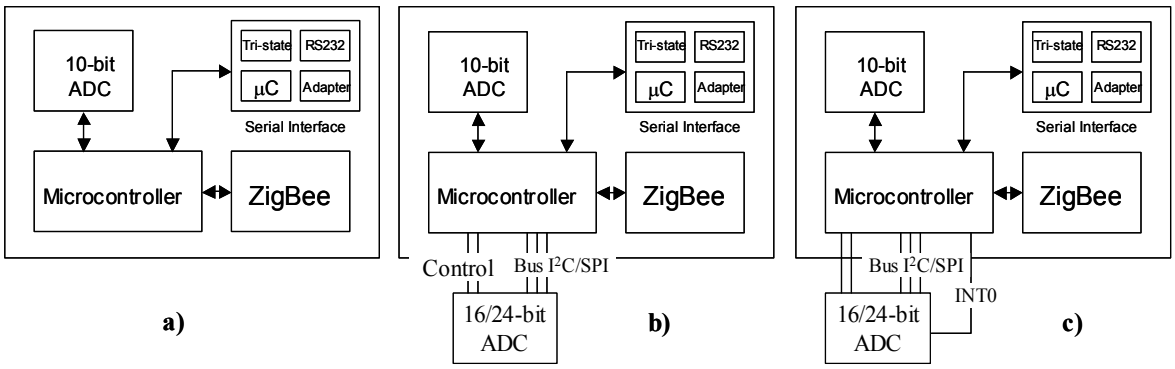

Figure 2: Wireless nodes involved in the physiological data acquisition. a) with internal ADC; b) with external ADC driven by software interrupt; c) with external ADC drive by hardware interrupt.

recording of EEG signals for BCI. For the second node type it the AD7714 ADC was selected for external operation, connected to the Mote I2C bus using a serial link with the SPI port available in the ADC. This solution allows 16 or 24 bits of resolution, with a maximum sampling frequency of 1028 samples/s. However, the data acquisition from the external ADC requires the use of commands from the operating system, the TinyOS. Due to operating system timings, the maximum sampling speed is 4000 samples/s. In this way, it was necessary to implement the third solution, which is a modified version of solution two. Instead of implementing all the external ADC control by software, the time critical tasks were implemented using hardware interruptions. With the third node type it is possible to sample the analogue channels at 8K samples/s, with 16 or 24 bits of resolution. The system limitation is on channel switching, made by software, which takes 3 ADC conversion periods to change between channels, due to resettling of the sigma delta modulator and digital filter.
To overcome this switching limitation, the use of the ADS8345 is proposed. It is an 8-channel, 16-bit, sampling Analog-to-Digital (A/D) converter with a synchronous serial interface. This ADC allows data acquisition from 8 channels at 100 kHz. The channel switching time is only 500 ns, and typical power dissipation is 8mW at a 100kHz throughput rate.

2.4 Data Routing

After solving the problem of data acquisition, it is required to send the EEG data to the host station. This requires a wireless link and a RS-232 link. The first hop will be the wireless link, a ZigBee link with a data rate of 250 kbps. If we consider sampling at 1 kHz, 8 channels, and 16 bits per sample, we have an overall data rate requirement of 128 kbps. This means that the wireless link will be enough to support it.

After receiving the data, the base station needs to route it to the processing unit, a PC. This is done using the RS-232 interface. This means we have a bottleneck in the system since the RS-232 will allow a maximum data transfer rate of 115.2 kbps. However, the microcontroller Atmega128 allows the configuration of his RS-232 port to operate at 921.6 kbps, and it is also possible to use a RS-232 to USB interface, having the possibility to achieve a maximum data rate of 1 Mbps. Considering this, the bottleneck will be on the ZigBee link, but we have then a bandwidth of 250 kbps.

3 PLATFORM PERFORMANCE

3.1 Data Acquisition

In the second solution (fig. 3 b)), the bottleneck is the software driven interruption. To test the maximum sampling frequency, a timer was implemented and each sample was sent together with its time stamp. We have found that the smallest sampling time, Ts, is about 1s (with a 2.5 MHz crystal). Thus, it is not a timer problem, since when the Ts was reduced below 1ms, the system started to fail on the delivering of some data points. In this way, the system does not allow to obtain all the signals at maximum sample rate. The third solution (fig. 2-c)), with the hardware driven interruption, was able to read 16 bit samples at a maximum data rate of 1028 samples/s. This makes an overall bit rate of 131584 bps, which is not a problem for the ZigBee link. However, the data was not reaching the host station, despite the serial configuration of almost 1 Mbps.

3.2 Serial Link

To test the maximum speed possible with this link, it was used the solution of Fig. 2-c) and the INT0 line was used to trigger the data transmission. Instead of sending data from the ADC, the data was generated and transmitted through the system. To detect the wrong samples, each sample was generated from the previous, by adding a fixed amount. In this way, each time a sample was missed, the difference between two consecutive samples allowed the detection of a missing sample. The results are shown in Fig. 3 and Fig. 4. It shows the effect of increasing the sample rate, with the nonzero values representing instants where data packets (of 10 samples) were lost.

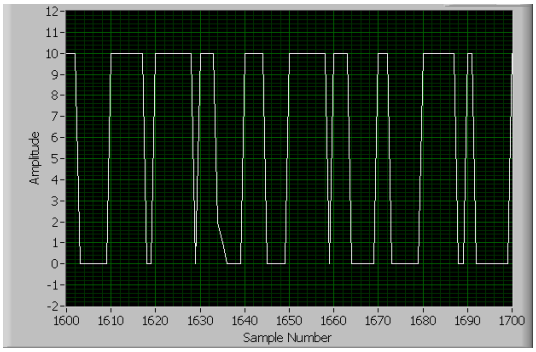

Figure 3: Error plot when data is sampled at 3.95 kHz.

The previous figure shows the received samples when the interrupt signal was set to 3.95 kHz. This corresponds to a total bit rate of 113.76 bps. From the plot, we can see that some data values are corrupted but the system is able to proceed with the transmission of correct values.

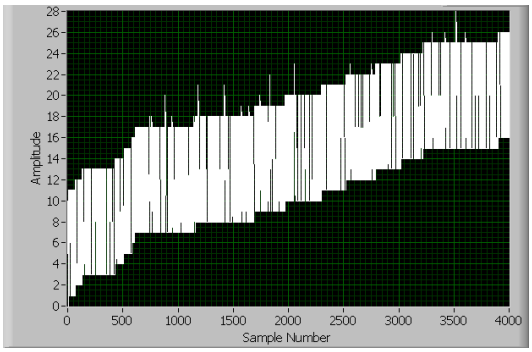

Figure 4: Error plot when data is sampled at 4.3 kHz.

In the previous plot, the overall data rate is 123.84 kHz and we can see that the system is not able anymore to recover and transmit correct values.

The microcontroller associated with this block, which controls the programming steps of the main microcontroller, also allows 1 Mbps and was not the problem. The bottleneck resides on the voltage adapter, responsible for the conversion between PC voltage levels to the micro voltage levels.
This is the MAX3223, which guarantees only 120 kbps of throughput. Our proposal is to use the MAX3223E, fully compatible with the available board, which guarantees a 250 kbps throughput. If required, another adapter for achieving higher data rate can be used. However, the ZigBee link will limit data rate to 250 kbps.

4 CONCLUSIONS

A solution to obtain a high date rate wireless link for physiological data acquisition was presented, operating at 2.4 GHz, with a minimum detectable signal of about 23 μV, and power consumption of 15 mW. The solution is based on a MICAz mote and is used for external ADC management as well as transmitting the acquired data via wireless link to another mote connected to a computer's serial port. The written TinyOS components detect the end of conversion by the ADC via external interrupt, avoiding sampling jitter, and perform read and write operations on its registers through the SPI interface.

This solution was tested for BCI control applications. With the proposed solution it is possible to acquire data from 8/16 channels at 100 kHz sampling frequency, with a data rate limit of 250 kbps.

REFERENCES

Marculescu, D., *et al.*, 2003, "E-textiles: ready to ware," IEEE Spectrum, Volume 40, Issue 10, pp. 28 – 32.

Prutchi, D., Norris, M., 2004, *Design and Development of Medical Electronic Instrumentation*, Wiley, ISBN: 978-0-471-67623-2.

Schwiebert, L., *et al.*, 2001, "Research Challenges in Wireless Networks of Biomedical Sensors," International Conference on Mobile Computing and Networking, Rome, Italy, pp. 151 – 165.

Simons, R. N., *at al.*, 2004, "Spiral Chip Implantable Radiator and Printed Loop External Receptor for RF Telemetry in Bio-Sensor Systems," IEEE Radio and Wireless Conference, 19-22 Sept., pp. 203 – 206.

Wolpaw, J. R., *et al.*, 2000, "Brain–Computer Interface Research at the Wadsworth Center," IEEE Transactions On *Rehabilitation Engineering*, vol. 8, no. 2, pp. 222-226.

OPTIMIZATION OF A FES CYCLING NEUROPROSTHESIS ON STROKE PATIENTS BY MEANS OF THE LEFT AND RIGHT CRANK MEASUREMENTS

Ferrante Simona[1], Comolli Lorenzo[2], Pedrocchi Alessandra[1], Bocciolone Marco[2], Ferrigno Giancarlo[1] and Molteni Franco[3]

[1]*Bioengineering Department, NITLab - TBMLab, Politecnico di Milano, Via Garofalo 39, Milano, Italy*
simona.ferrante@polimi.it, alessandra.pedrocchi@polimi.it, giancarlo.ferrigno@polimi.it
[2]*Department of Mechanical Engineering, Politecnico di Milano, Via La Masa 34, Milano, Italy*
lorenzo.comolli@polimi.it, marco.bocciolone@polimi.it
[3]*Valduce Hospital, Villa Beretta Rehabilitation Center, Via N.Sauro 17, Costamasnaga (LC), Italy*
francomolteni@libero.it

Keywords: FES cycling, rehabilitation, hemiplegia.

Abstract: The use of functional electrical stimulation (FES) is a well established method in the rehabilitation of stroke patients. In particular, a bilateral movement such as cycling induced by FES would be crucial for these patients who had an unilateral motor impairment and had to recover an equivalent use of the limbs. To improve the rehabilitative effects of the FES cycling, a metrologically qualified cycle-ergometer was used, so that the left and right crank torque values are measured in real-time. Three protocols were evaluated. First, healthy subjects performed voluntary pedaling. Second, healthy subjects were stimulated one muscle individually to study the contribution of each single muscle to the cycling. Third, stroke patients executed a complete FES cycling trials. Results demonstrated that the proposed sensors could be successfully used to monitor online the unbalance of the cycling. Single muscle tests showed that only the quadriceps and the hamstrings provided a significant contribution to the crank torque. Patient trials confirmed the difficulty for stroke subjects to carry out symmetrical cycling. The use of the proposed sensors, hence, could offer a good signal for biofeedback neuroprostheses and for closed loop controllers.

1 INTRODUCTION

A neuroprosthesis is defined as a functional electrical stimulation (FES) device used as a substitute for lost neurological function. The use of a neuroprosthesis is a well established method in the rehabilitation of individuals with spinal cord injuries and stroke (Kralj, Acimović & Stanic, 1993, Petrofsky, 2004). Among all the existent neuroprostheses, the cycling movement induced by the stimulation of the major muscles of the lower limbs is now becoming a spread application (Hunt et al., 2004, Trumbower, & Faghri 2005, Szecsi et al., 2007). In the following this artificial movement will be named FES cycling.

One of the most difficult and appealing improvements in FES research is the integration of hardware and software and the development of control systems for the neuroprosthesis in order to enhance the clinical benefits for the patients. Some of the rehabilitation objectives for spinal cord injured patients are an increase in muscular tone, an improvement in the peripheral and cardiac circulation avoiding the occurrence of decubitus ulcera and the prevention of joint rigidity (Hunt et al. 2004). In stroke patients, the neuroprosthesis also becomes therapeutic and in fact, it permits one to learn new motor strategies for Central Nervous System (CNS), exploiting residual capacity (Lee & van Donkelaar, 1995, Sheffler & Chae, 2007). Indeed, FES cycling providing the complete afference of the task to the stroke patients could re-educate the synaptic controls needed to produce a well organized movement. Because of the laterality of the pathology, one of the rehabilitation aims is the recovery of walking and particularly the recovery of the symmetry of the movement. Therefore, the use of FES cycling was investigated as a method to re-learn the bilateral and symmetrical use of the legs.

The feasibility of applying FES cycling to stroke patients was analyzed in a previous study and encouraging results were reached (Ferrante et al., 2006). The stimulation strategy delivered to the quadriceps, hamstrings, gluteus maximus and tibialis anterior of the two legs was exactly the same for both the legs, but shifted of 180° in respect to the crank angle. The patient was asked not to voluntary contribute to the motor task. In this study the total motor torque produced at the crank was measured. Therefore, it was possible to quantify the performance obtained in terms of power output but not in terms of unbalance at the pedals which is a crucial aspect in the rehabilitation of individuals with stroke.

The aim of this study is to develop and test sensors able to measure the torque at the right and left crank in order to provide a step forward in the application of FES cycling on individuals with stroke. In fact, monitoring these signals during the movement would be a crucial starting point in the design of an automatic time variant controller for symmetry.

2 METHODS

2.1 Experimental Setup

A current–controlled 8-channel stimulator and a motorized cycle-ergometer were used for the experiments. It was possible to control the cycle-ergometer by changing the resistant torque and the angular velocity or by directly setting the motor voltage.

As shown in Figure 1, the cycle-ergometer was equipped with instruments able to measure the bending moments and the radial forces at the right and left cranks, so that the torque can be computed (Gföhler et al., 2001). Four Wheatstone full bridge made up of electrical resistance strain gauges were used to measure the strain on the right and left crank during the cycling task. The strain gauge bridges are conditioned through a four-channel wireless device, which allows to transmit the signal from the rotating shaft to the acquisition system. The angular crank position was measured through optical encoders mounted on the main wheel of the ergometer. More details on the instrumentation, the acquisition chain and the metrological characterization of the cycle-ergometer can be found in Comolli et al., 2005 and Bocciolone, Comolli and Molteni, 2008. The cycle-ergometer was equipped with two ankle foot orthoses fixed to the pedals and used to stabilize the legs and to constrain the movement to the sagittal plane.

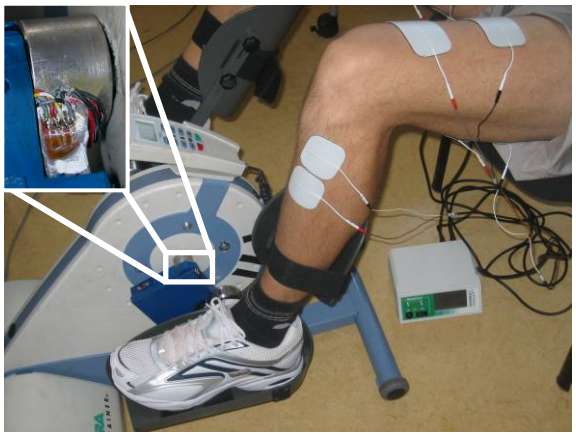

Figure 1: The instrumented cycle-ergometer, the wireless device is in the box on the crank.

All the transducers were connected to a PC for data acquisition and stimulation device control. The real-time acquisition and control system is shown in Figure 2. The stimulation controller set the stimulator parameters according to the crank angle measured in real time. Therefore, each muscle used is activated in a particular angular phase of the cycling movement as explained in the following.

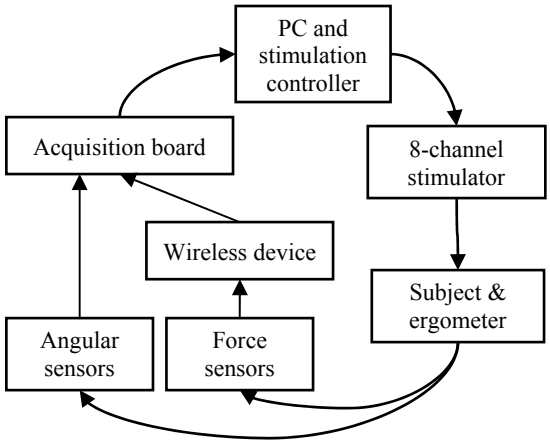

Figure 2: The experimental setup.

2.2 Experimental Protocol

Written informed consent was obtained from all the subjects who took part in the experiments. Three different experimental sessions were performed and are explained in the following paragraphs.

2.2.1 Tests During Voluntary Pedaling

First, the developed sensors were tested during voluntary pedaling of healthy subjects. The protocol required the subject to perform one trial lasting 8 min. The first 2 min the motor of the cycle-ergometer was used and the subject was cycling only passively at 30 rpm. Then, the subject carried out a normal cycling for 2 min, trying to keep the former velocity. After that, 2 min in which the subject was asked to pedal using only the right leg and 2 min using only the left one were performed.

2.2.2 Stimulation of the Muscles Individually

Once tested the sensors, a specific FES cycling experimental protocol was carried out on a healthy subject. Once the subject was sat on the ergometer and the electrodes were placed, an initial trial to choose the stimulation current of each muscle was carried out. The chosen stimulation currents were set at a value that produced a tetanic contraction using a pulse width of 400 µs. The crank angle was set at 0° in correspondence to the point of maximum flexion of the left hip. During the trials 8 muscles, 4 per each lower limbs (quadriceps, hamstrings, gluteus maximus and tibialis anterior) were stimulated. The stimulation strategy, i.e. the choice of the cycling phases in which each muscle was stimulated in respect to the crank angle, were selected following Ferrante et al., 2005. An ON-OFF pulse width profile was used: for all the muscles the pulse width value was fixed at 400 µs during the ON phase and at 0 µs during the OFF phase. The stimulation frequency was set at 20 Hz and all the torque signals were gathered at 500 Hz.

The subject performed a trial with a resistant torque value of 3 Nm. The angular velocity was maintained by the motor at a minimum value of 30 rpm during all the trials.

The trial lasted 10 min: during the initial and final 60 s, the subject was pedaling passively. In the intermediate part of the test, each muscle group was individually stimulated for 60 s within its stimulation range.

2.2.3 First Tests on Stroke Patients

Finally, a feasibility test was carried out on 2 post-acute stroke patients at the beginning of their rehabilitation. Both the patients performed a complete FES cycling trial according to Ferrante et al., 2006.

2.3 Data Analysis

The measured bending moments and radial forces were used to compute the torque at the right and left crank. The torque was expressed as a function of the crank angle. The median and the 5th-95th percentiles of the right and left active torque were computed in each test condition of the trials. Then the left and right active torque at the crank were computed as the difference between the torque produced during the active phases and the one generated during passive pedaling. The total torque was obtained adding together the right and left torque.

3 RESULTS

3.1 Tests During Voluntary Pedaling

Figure 3 shows the results obtained by an healthy subject during the voluntary pedaling protocol in terms of the right and left active torque measured at the crank.

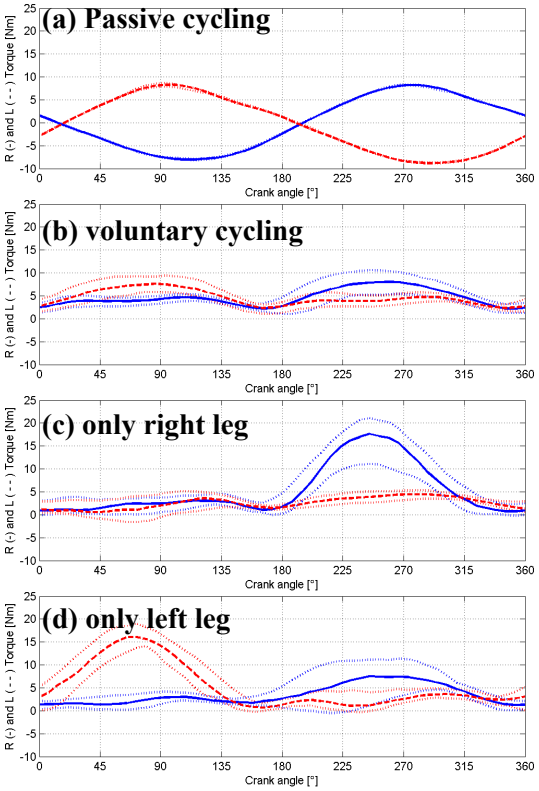

Figure 3: Measurement of the right (solid line) and left (dashed line) passive (a) and active (b,c,d) torque; the median on 15 revolutions are shown. In dotted lines the 5th and 95th percentiles are reported.

In panel (a) the repeatability of the signals during passive cycling is noticeable. In panel (b), the subject was performing a normal pedaling. The effect of the two legs on the right and left active torque was quite similar in amplitude but it showed a shift of 180° in phase. The asymmetrical cycling presented in panels (c) and (d) highlighted a dual behaviour. When only the left leg was cycling actively (c), only the left active torque had a positive peak and the right torque was quite zero during the whole revolution. The peaks of the active torque in panels (b), (c) and (d) were produced when the right quadriceps was pushing. This behaviour agrees with the fact that during a voluntary pedaling the quadriceps muscle gives the greatest contribution to the movement.

The results obtained in the same trials in terms of total torque are reported in Figure 4. The panels are referred to the same working conditions of Figure 3. The total torque seems to be a good signal to distinguish an asymmetry in the cycling movement.

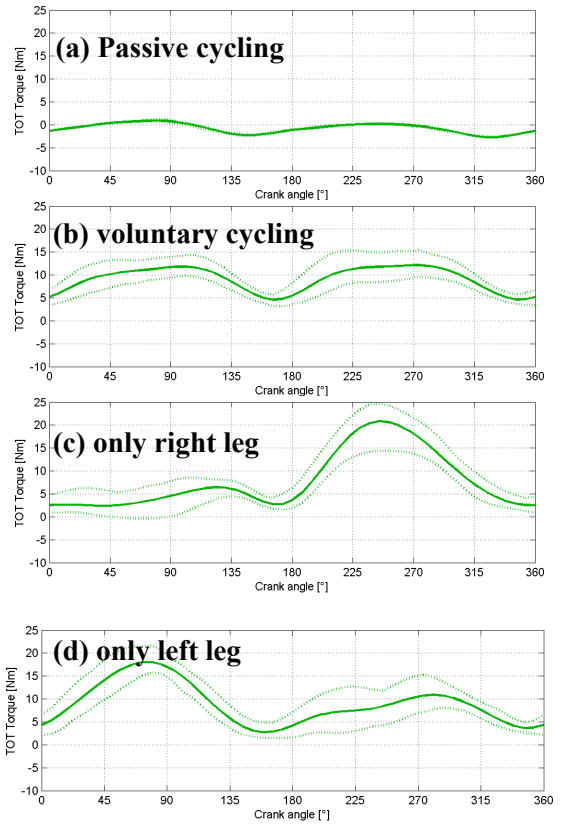

Figure 4: Measurement of the total passive (a) and active (b,c,d) torque; the median on 15 revolutions are shown in solid line. The 5th and 95th percentiles are reported in dotted lines.

3.2 Stimulation of the Muscles Individually

Figure 5 shows the results obtained by the healthy subjects during the FES protocol when only the right quadriceps (a), hamstrings (b), gluteus maximus (c) and tibialis anterior (d) were selectively stimulated. In all the panels of Figure 5 the grey area represent the angular range in which the muscle was stimulated.

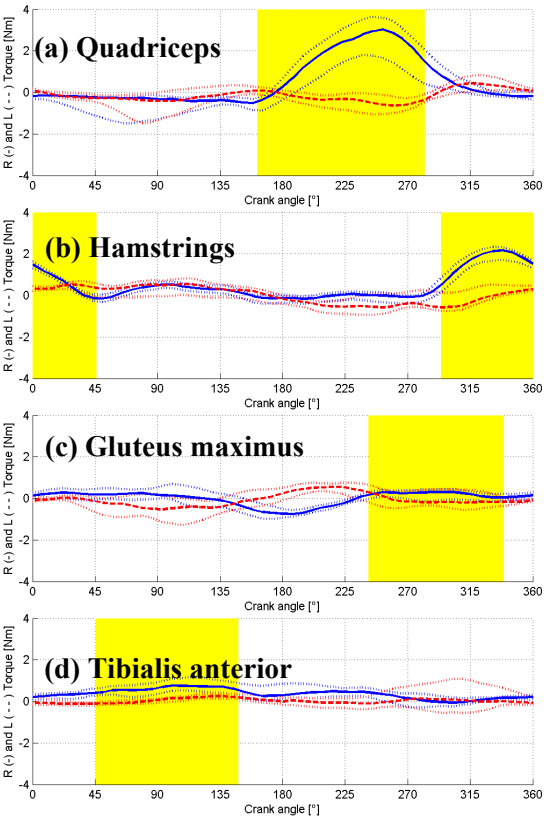

Figure 5: Measurement of the right (solid line) and left (dashed line) active torque; the median on 15 revolutions are shown. The 5th and 95th percentiles are reported in dotted lines.

In panels (a) and (b), a positive peak of the right active torque can be noticed exactly in correspondence to the muscular stimulation range.

This confirms that the muscles were stimulated in their functional range, i.e., when they were assisting the cycling motion.

The active left torque was nearly zero during the whole revolution because the left leg was pedaling passively. The gluteus and the tibialis anterior instead did not produce an effective right active torque at the crank, thus their contributions to the drive torque were negligible. Such a result was

expected because the gluteus, as a proximal muscle acting only on the hip, can transfer a low contribution to the crank, while the effect of the tibialis anterior is limited by the use of the ankle foot orthosis.

These results are confirmed by the total torque shown in Figure 6.

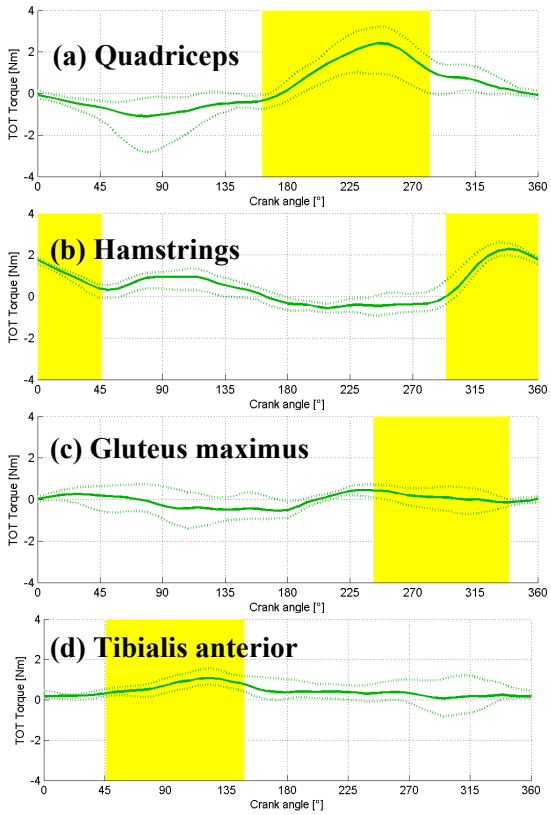

Figure 6: Measurement of the total torque; the median on 15 revolutions is shown in solid line. The 5th and 95th percentiles are reported in dotted lines.

3.3 First Tests on Stroke Patients

Figure 7 reports the results obtained by a post-acute stroke patient during a FES cycling trial performed, stimulating 8 muscles following the stimulation strategy described in Ferrante et al., 2006. As it is shown in panel (a) the positive peak of the left torque is the 40% greater then the one of the right torque, which was correspondent to the pushing of the impaired leg.

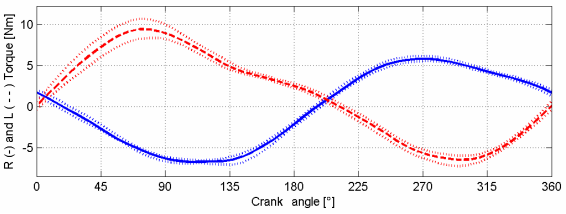

Figure 7: The right (solid line) and left torque (dashed line) are reported. Results are shown in terms of the median torque of 50 revolutions obtained by a stroke patient during an FES cycling trial. This result suggests the idea to use these signals as control signals for a real-time automatic controller to minimize the asymmetry of the movement in stroke patients.

4 CONCLUSIONS

The possibility of using a rhythmic and bilateral movement such as cycling induced by a stimulation pattern delivered in both legs seems to be a good rehabilitative method for post acute stroke patients. These patients, having an unilateral motor impairment, need to be re-educated to the correct use of both the lower limbs together in order to recover the motor control symmetry in more complex and demanding task, such as walking.

The aim of this study was to develop and test sensors designed for a FES cycling neuroprosthesis specific for stroke patients. Custom designed sensors able to measure independently the torque produced by the right and the left leg during cycling were tested both on healthy subjects and stroke patients.

To understand the effect of the stimulation of each muscle on the signals, a proper protocol was defined. Each muscle was stimulated individually in the phase of the revolution in which his action was functional to the movement (Ferrante et al., 2005, Ferrante et al., 2006). The results obtained suggested that the developed sensors allowed to distinguish the effect of the stimulation of the quadriceps and hamstrings during the movement. Instead, the active torque produced by the gluteus maximus and by the tibialis anterior were quite negligible. Other experimental trials using this second protocol presented are now ongoing in our laboratory on more subjects.

This study was crucial to verify that the signal to noise ratio of the torque measurement is sufficient to discern the torque induced by the stimulation of the single muscle, which are an order of magnitude lower than the ones induced by the voluntary active pedaling.

The possibility to monitor the torque at the right and left crank represents an important step forward in the application of FES cycling on stroke patients. It would be possible to use the acquired torques to monitor the unbalance of the movement on line. The unbalance could be used as a biofeedback signal to the patient. Thus, looking at a display where the asymmetry is shown, he could correct the exercise on line giving a voluntary contribution. Alternatively, starting from this unbalance signal it would be possible to develop a closed loop controller aiming at the maximization of the symmetry during the movement. The achieved results also suggest that a simplified first version of the controller could act only on the stimulation of the hamstrings and quadriceps and not on the gluteus maximus and tibialis anterior, which shown a quite negligible effect on the right and left torque.

ACKNOWLEDGEMENTS

This work was supported by the Italian Institute of Technology (IIT), and the Fondazione Cariplo in the framework of the research program HINT@Lecco. This project was realized thanks to the grant INGENIO funded by the European Social Found, the Welfare Ministry and by the Lombardia region.

Authors would like to acknowledge Mauro Rossini (Villa Beretta Rehabilitation Center) for his helpful discussion.

REFERENCES

Kralj, A., Acimović, R., Stanic, U., 1993. Enhancement of hemiplegic patient rehabilitation by means of functional electrical stimulation. *Prosthetics and Orthotics International*, vol. 17, no. 2, pp. 107-114.

Petrofsky, J.S., 2004. Electrical stimulation: neurophysiological basis and application. *Basic and Applied Myology*, vol. 14, no. 4, pp. 205-213

Hunt, K., Stone, B., Negard, N., et al., 2004. "Control strategies for integration of electric motor assist and functional electrical stimulation in paraplegic cycling: utility for exercise testing and mobile cycling. *IEEE Transactions on Neural Systems and Rehabilitation Engineering.*, vol. 12, no. 1, pp. 88–101.

Lee, R.G., van Donkelaar, P., 1995. Mechanisms underlying functional recovery following stroke. *The Canadian Journal of Neurological Sciences*, vol. 22, pp. 257-263.

Sheffler, L.R., Chae J., 2007. Neuromuscular electrical stimulation in neurorehabilitation. *Muscle Nerve*, vol. 35, pp. 562-590.

Ferrante, S., Pedrocchi, A., Ferrigno, G., et al., 2006. FES cycling treatment on hemiplegic patients: preliminary results. In *IFESS 06, 11th Annual Conference of the FES Society*, pp. 77-79.

Ferrante, S., Saunders, B., Duffell, L., et al., 2005. Quantitative evaluation of stimulation strategies for FES cycling. In *IFESS 05, 10th International FES Society Conference*, pp. 94-96.

Gföhler, M., Angeli, T., Eberharter, T., et al., 2001. Test bed with force-measuring crank for static and dynamic investigations on cycling by means of functional electrical stimulation. *IEEE Transactions on Neural Systems and Rehabilitation Engineering*, vol. 9, no. 2, pp. 169-180.

Comolli, L., Cantatore, A., Zappa, E., et al., 2005. HINT@LECCO project: metrological characterization of a cycle-ergometer. In *SIAMOC 05*, *6th Congress of the Italian Society of Movement Analysis in Clinic.*

Bocciolone M., Comolli L., Molteni F., 2008. Metrological characterization of a cycle-ergometer. In *Biodevices 08, International Conference on Biomedical Electronics and Devices.*

Trumbower, R.D., Faghri, P.D., 2005. Kinematic analyses of semireclined leg cycling in able-bodied and spinal cord injured individuals. *Spinal Cord*, vol 43, no 9, pp. 543-549.

Szecsi, J., Krause, P., Krafczyk, S., Brandt, T., Straube, A., 2007. Functional output improvement in FES cycling by means of forced smooth pedaling. M*edicine and science in sports and exercise*, vol 39, no. 5, pp. 764-80.

THRESHOLD LOGIC GENE REGULATORY MODEL
Prediction of Dorsal-ventral Patterning and Hardware-based Simulation of Drosophila

Tejaswi Gowda, Samuel Leshner, Sarma Vrudhula
School of Computing and Informatics, Arizona State University, Tempe, AZ.
{tejaswi, samuel.leshner, vrudhula}@asu.edu

Seungchan Kim
Division of Computational Biology, Translational Genomics Research Institute, Phoenix, AZ.
skim@tgen.org

Keywords: Gene Regulation, Threshold Logic, Drosophila embryo patterning, Modeling and Simulation of Gene Systems.

Abstract: Precise characterization of gene regulatory mechanisms is a fundamental problem in developmental biology. In this paper we present a new gene regulatory network (GRN) model which is based on threshold logic (TL). Two different set of genes are responsible for the cell patterning of the *Drosophila* embryo. By using the proposed threshold logic gene regulatory model (TLGRM), we derive the different gene regulatory rules for the gene products involved. We use these rules to model and explain the interaction between the genes. Very large or complex gene regulatory networks are difficult to simulate using a general purpose CPU. Specialized programmable hardware provides additional concurrency and is an alternative to a large and expensive cluster of machines. The steady state gene expression predicted by the model clearly mimics the actual wild-type gene expression along the dorsal-ventral axis in the *Drosophila* embryo. We thus demonstrate that for a well characterized gene regulatory system, the nature and topology of interaction is enough to model gene regulation. We also demonstrate through proof of concept that using hardware-based simulation, it is possible to achieve orders of magnitude of performance improvement over conventional CPU-based simulation.

1 INTRODUCTION

Understanding how different genes interact with each other to give rise to the different cell types in an organism is an active area of research in development biology (Albert and Othmer, 2003). The human genome project was the first step in this direction (Collins et al., 2003). Now that the methods for gene sequencing have greatly improved (Heller, 2002) it is possible to obtain huge amounts of gene expression data. This data can be analyzed and interpreted to obtain the different regulatory interactions (activation and inhibition) between different gene products (mRNA, protein and protein complexes). Models from mathematics and computer science have are been used to model the interaction of genes (Dougherty et al., 2007) There are two types of gene regulatory models. One assumes the expression of the gene products to be continuous functions which interact with each other in continuous time (*e.g:* (Gursky et al., 2001), (Reinitz and Sharp, 1995)). Another group of models assume that gene expression takes place in discrete levels and gene interaction takes place in discrete time (*e.g:* (Shmulevich et al., 2002), (Albert and Othmer, 2003), (Kauffman, 1993)). The challenge is to come up with a model that captures the temporal and spatial characteristics of gene regulation, and which is easy to construct and simulate. It is generally agreed that merely specifying the type of interaction between genes is not enough to characterize gene regulation (Albert and Othmer, 2003). In this work we try to show that for at least two gene regulatory systems knowing the kind of interaction between genes will suffice to construct an expressive model which can mimic the actual biological process. For the embryo patterning problem that is considered in this paper, we assume a fixed number of discrete levels of expression for gene products. This approach is well suited for this purpose as once the gene is either expressed or not expressed in a cell, it remains that way to enable the cell to develop towards its determined *fate*.

Although the *Drosophila* embryo patterning problem presented in this work uses only a general purpose

CPU for simulation, simulation of large GRNs cannot be done without a large cluster of CPUs. We propose an inexpensive hardware-based simulation technique for GRNs using specialized field-programmable gate arrays.

In (Albert and Othmer, 2003) it is shown that by using two discrete states of gene expression and Boolean logic for gene regulation rules it is possible to explain the action of segment polarity genes in the creation of segments along the anterior-posterior axis of a *Drosophila* embryo. While it has been demonstrated that Boolean logic rules are enough to describe gene interaction, there is little understanding on how to construct Boolean rules for a generic gene regulatory system. We propose that the Boolean rules used in gene regulation belong to a special class of functions called threshold functions. These functions are a subset of Boolean functions. Using this small subset of functions we derive regulatory relationships from the gene interaction graph. We then demonstrate that it is possible to model the interaction of two different sets of genes with these rules. These genes are responsible for the dorsal-ventral patterning and segment formation along the anterior posterior axis of the *Drosophila* embryo.

A *threshold element* (TE) has n binary inputs, x_1, ..., x_n, and a single binary output, y. Its internal parameters are a *threshold* T and *weights* w_1, ..., w_n, where each weight w_i is associated with x_i. The values of T and w_i $(i = 1,...,n)$ may be any real numbers (Dertouzos, 1965; Winder, 1965). The input-output relation of a TE is defined as follows:

$$y = \begin{cases} 1 & \text{if} \sum_{i=0}^{n} w_i x_i \geq T \\ 0 & \text{otherwise} \end{cases} \quad (1)$$

The *weighted sum* in Equation (1), denotes arithmetic summation. *Example:* Figure 1 shows a threshold element that implements the Boolean function $y = a'(b+c)$. Input a,b,c are assigned the weights $-2,1$ and 1 respectively and the threshold (T) is assigned the value of 1. It can be seen that the logic function realized by this threshold element is $y = a'(b+c)$.

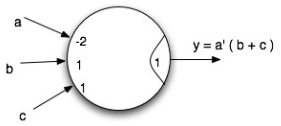

Figure 1: A threshold element.

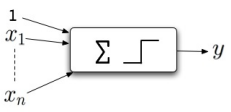

Figure 2: A perceptron.

Boolean *AND* and *OR* functions are threshold (Dertouzos, 1965). Threshold elements are also capable of implementing complex Boolean functions. *e.g:* $ab(c+d)+cd(a+b)$. However, it should be noted that a *single* TE cannot represent all Boolean functions, as not all Boolean functions are threshold (Muroga, 1971; Kohavi, 1970). The TE is similar to a single ***perceptron*** (commonly encountered in neural network literature) with the *step function* as the activating function (Russell and Norvig, 2003), as shown in Figure 2.

Simulation on a large gene regulatory network can be a slow, computation-intensive process, largely due to the fact that a general purpose CPU can only perform so many operations at one time (DeHon, 1996). Consider the sequence of events the CPU must perform to compute the next state for each gene product in the network. The CPU must first obtain a copy of the current state of every gene product in the simulation. Next the updating rules are applied to each gene product in the simulation sequentially, using the current states of the gene products as inputs. Each next state computation requires one or more instructions, depending on the rule being applied. Each next state that is computed must also be saved. Once all next state computations are complete, the current states are replaced with the next states and the process repeats. The total time t required by the CPU for each time step in the simulation is given in Equation (2), where $t_{instruction}$ is the time per instruction, $n_{instruction}$ is the average number of instructions per next state computation, and n_{gene} is the number of gene products in the simulation.

$$t = (t_{instruction})(n_{instruction})(n_{gene}) \quad (2)$$

This is a highly inefficient method of simulation. Since the next state computation of each gene product depends only on the current states of the other gene products in the simulation, it should be possible, given the proper resources, to update all gene products in parallel. This can be achieved using a specialized field-programmable gate array.

The field-programmable gate array, or FPGA, is composed of a matrix-like arrangement of configurable logic blocks, or CLBs, which are joined together by interconnect resources (Brown, 1992). The CLBs and interconnect can be programmed via on-chip memory to realize any design that it possesses the resources to implement. Figure 3 shows the conceptual FPGA architecture.

If the number of input parameters in the next state computation of a single gene product is reasonably low, the next state computation for a single gene product can be implemented and synchronized using a single CLB. Configurable logic blocks synchronized using the same clock signal operate in parallel, thus using a specialized FPGA the next states of all gene

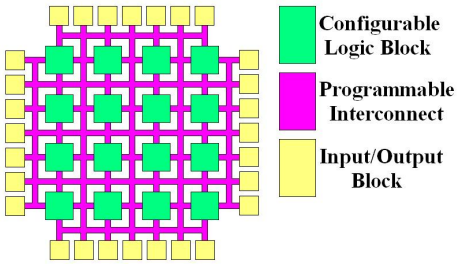

Figure 3: Conceptual FPGA architecture.

products can be computed simultaneously and then synchronized for use in the next time step.

The total time required by the FPGA for each time step is thus given solely by the inverse of the maximum operating frequency, given by the worst-case next state computation delay for the slowest gene product in the simulation. The dependence on the number of gene products in the simulation is no longer a factor in the delay per time step. Despite the fact that FPGAs typically operate at frequencies several times lower than that of a general purpose CPU, the elimination of this dependence can improve the speed of the simulation by orders of magnitude for large gene regulatory networks.

FPGAs are thus capable of reducing the amount of real time required to complete a single simulation by computing the next state of all gene products concurrently, however the FPGA's advantage of parallel computation does not stop at the system level. Given enough resources, multiple copies of a complete system model can be mapped to the FPGA and simulated concurrently, increasing performance yet again by a factor equivalent to the number of simulations running in parallel.

2 APPROACH

The motivation for using threshold logic comes form the *"French flag"* model of cell pattern formation (Wolpert et al., 2002). A chemical whose concentration varies over a region, and is responsible for cell patterning is called a morphogen (Wolpert et al., 2002). A morphogen can create different cells because its concentration varies from cell to cell. The morphogen diffuses from the source (region of high concentration) to the sink (region of lower concentration). The concentration of the source and sink is constant and hence the gradient is maintained.

The cells derive positional information from one or more morphogens before differentiating into a particular type of cell. Threshold logic naturally supports this kind of multiple logic levels. The weighted sum $\sum_{i=0}^{n} w_i x_i$ in Equation 1 can be compared against $(n-1)$ thresholds to generate an output of n levels. *e.g:* If the weighted sum is compared against one threshold we get binary output and if it's compared against two thresholds we get ternary output, and so on. Threshold logic works in the same way irrespective of the number of levels. This is not true for Boolean logic.

Another reason to use threshold rules is because there are only two types of actions that one gene product can have on another – activation or inhibition. Activation can be thought of as a positive influence and inhibition as a negative influence. In a threshold function, these two kinds of influences can be modeled by the polarity of the input weight. We use a positive weight for activators and a negative weight for inhibitors. It is also known that for some genes the action of inhibitors is stronger than that of the activator. This can be easily represented in the model by assigning different magnitudes of positive and negative weights.

The *impact* of different activators and inhibitors can be incorporated into the model by using different weights. *Example:* If g_a has greater impact on on g_z than g_b, then in the TE for g_z, $w_{g_a} > w_{g_b}$.

As shown later, these observations lead us to formulate simple guidelines that can be used to derive the TL rules for gene regulation. This rule generation is simpler than generating Boolean rules. In the rest of the paper we introduce the new model and demonstrate its usefulness by using it to model pattern formation in the *Drosophila* embryo.

The configurable logic block is a programmable cell designed to implement all or part of the next state computation for a single gene product, and then synchronize the output for use in the next time step.

A standard CMOS implementation of the configurable logic block is shown in Figure 4. This is a simple modified version of the CLB used in most general purpose FPGAs, tailored specifically for performing and synchronizing next state computations for individual gene products. The unnecessary flexibility added by more general purpose designs has been removed, yielding a faster, more area efficient functional unit. Inputs in the figure represent the current states of the gene products that promote or inhibit the expression of the gene product the CLB represents. The next state of the gene product the CLB represents is observed at the output.

The CLB is composed of two primary components: the lookup table, which provides the next state computation, and the flip-flop, which provides synchronization. The lookup table observes the unique combination of logic states on all of its inputs (1 = expressed, 0 = unexpressed) and accesses a single bit

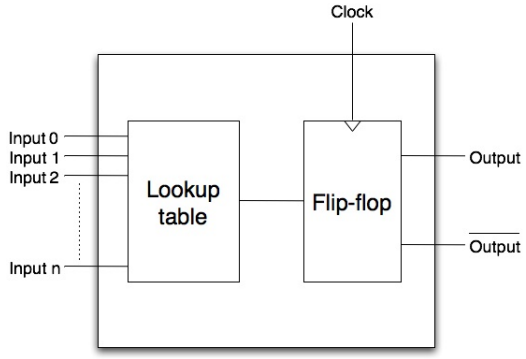

Figure 4: Component-level CMOS implementation of n-input configurable logic block.

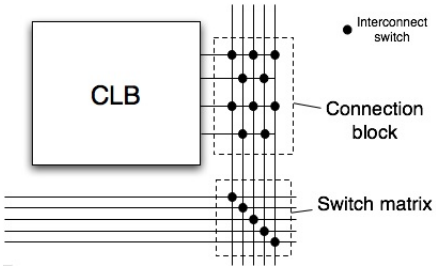

Figure 5: Connection block and switch matrix interconnect components.

entry in an array stored in memory, containing the desired output (Francis, 1992). This value is passed as input to the flip-flop which updates its output with the same value and maintains it until the next time step.

Interconnect is used to join configurable logic blocks together into one cohesive, functionally correct system. There are two types of interconnect components that are of major importance, the connection block and the switch matrix (Brown, 1992). Both of these components are featured in Figure 5.

A connection block is a collection of switches that directly connect the CLBs to the segments of the interconnect. As the figure indicates, connection blocks are located adjacent to CLBs on the FPGA.

A switch matrix is a collection of switches that connect segments of the interconnect to each other. As the figure indicates, switch matrices are located where groups of perpendicular wire segments intersect on the FPGA. Each wiring segment that enters a switch matrix can connect to up to three others.

Preparing a field-programmable gate array for simulation consists of three separate steps. First, each of the gene products in the model is assigned to one or more of the available CLBs. Second, the components of the interconnect are configured to determine the interaction between the CLBs. Finally, the complete placement and routing scheme is replicated to maximize the usage of the FPGA's available resources.

Gene products are assigned to configurable logic blocks with the modular structure of the system in mind. This is especially important when the GRN models multicellular interactions. The following routing assumptions are made when assigning gene products to CLBs:

- The majority of interactions take place between gene products within the same cell.
- Some interactions are expected to take place between gene products of adjacent cells.
- Few (if any) interactions occur between gene products of distant cells.

Using these assumptions, a system can be decomposed in modules of cells, and modules of cells into individual gene products. Cells are organized into a uniform arrangement of CLBs so that they will be able to fit together easily with adjacent cells. Likewise, complete systems are organized into a uniform arrangement of cells so as to maximize the number of simulations that will be able to run concurrently on the FPGA.

Since nearly all interactions take place within a single cell or between adjacent cells, interconnect programming relies on direct connections and short wire segments to assemble disconnected CLBs into a fully functioning system.

3 METHODS

Drosophila is one of the best understood of all developmental systems at the genetic level (Wolpert et al., 2002). *Drosophila*, like many other insects starts its life as an egg, develops into a larva and then undergoes metamorphosis to become an adult. We are mostly interested in the embryonic gene regulation that determines the biological fate of the different regions of the embryo. Like all animals with bilateral symmetry, *Drosophila* is patterned along two distinct, independent axes: the anterior-posterior axis and the dorsal-ventral axis (Wolpert et al., 2002).

Early *Drosophila* embryo patterning occurs within a multi-nucleate syncytial blastoderm. This is formed because of repeated rounds of nuclear division without any cytoplasmic division (Wolpert et al., 2002). The absence of cells in the early embryo is really important, because the mRNA and proteins can now diffuse easily throughout the embryo. This diffusion creates a concentration gradient of different transcription factors and morphogens. The interaction between different gene products creates a sharp and stable concentration gradient of proteins. The presence or absence of certain proteins determine the fate

of the cell (when cellularization occurs). The concentration gradient of maternal mRNA and proteins is known (Wolpert et al., 2002; Roth et al., 1989). The interaction between the different gene products that determine the dorsal-ventral patterning is also known (Wolpert et al., 2002). We make use of this data to build a threshold logic model of gene interaction. We simulate the rules we generate making use of the concentration gradient of the maternal proteins as the initial state. The maternal proteins are the proteins generated by maternal genes. Maternal genes are the genes expressed in the mother fruit fly and not the fertilized egg (Wolpert et al., 2002).

Patterning along the axes is similar to the French flag patterning problem described earlier. The expression of zygotic genes in localized regions differentiate the cells in the embryo. These different cells determine the germ layers that will eventually develop out of them. This patterning starts when the embryo is still a syncytial blastoderm. So the concentration of the proteins we specify corresponds to the internuclear concentration. There is a high concentration of maternal dorsal protein in the nuclei found in the ventral region (Roth et al., 1989). This concentration falls rapidly in the dorsal region.

3.1 TLGRM for D-V Patterning

Since early embryonic patterning is essentially two dimensional, we abstract the dorsal-ventral axis of the embryo into twelve regions. This patterning takes place in the blastoderm, which is syncytial before cellularization takes place. The blastoderm has the cells concentrated in the periphery leaving a hollow in the center. This abstraction of the dorsal-ventral embryonic tissue is shown in Figure 6 (B).

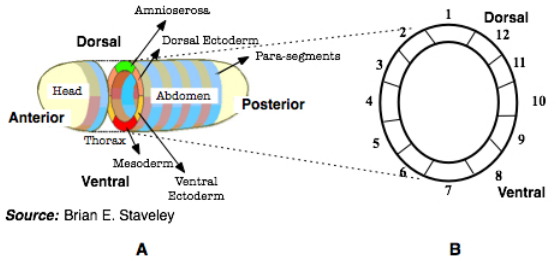

Figure 6: **(A)**: The two axes of a *Drosophila.* embryo. **(B)**: For modeling purposes the D-V section of the embryo is assumed to be made of twelve regions.

Genes which participate in the determination of the dorsal ventral patterning influence the expression of each other via the proteins they synthesize. The *dorsal (dl)* protein initiates a complex gene interaction process that culminates in the formation of well defined regions in the dorsal-ventral axis. Going from ventral to dorsal, the major regions are mesoderm, ventral ectoderm, dorsal ectoderm, and amnioserosa (Figure 6 (A)). The nuclear gradient of the dorsal protein in the blastoderm decreases exponentially from the ventral to the dorsal end of the embryo. The concentration of the dorsal protein is divided into 3 discrete levels $(-1, 0, 1)$.

We now describe the genes that are involved in the dorsal-ventral (D-V) patterning and how they interact with each other. The dorsal protein as mentioned earlier is probably the most important protein involved in the D-V patterning. The other genes involved are *twist(twi), snail(sna), rhomboid(rho), tolloid(tld), decapentaplegic(dpp) and zerknüllt(zen)*. These genes respond to the concentration of dorsal protein in a threshold like manner because of the presence of high- and low-affinity binding sites for the dorsal protein in their regulatory regions (Wolpert et al., 2002).

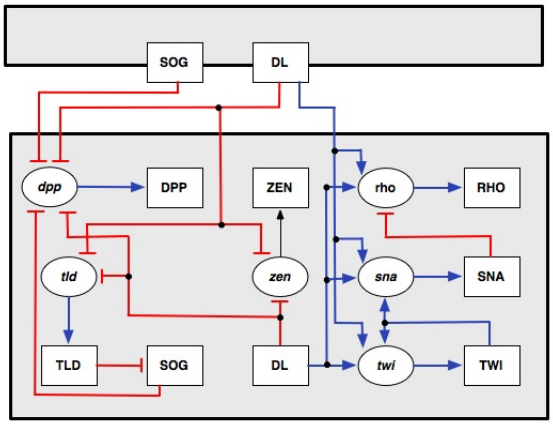

Figure 7: The gene interaction graph representing the regulatory interaction between the gene products that are responsible for the D-V patterning in *Drosophila.*

The interaction between these genes can be represented by a gene interaction graph (Figure 7). The nodes of this graph represent mRNA and proteins. The mRNA nodes are elliptical in shape and the protein nodes are rectangular. Protein nodes are labeled in capital letters and the mRNA nodes are labels in small letters. An arrow $(\rightarrow)$ is used to represent activation and a t-connector $(\dashv)$ represents inhibition. The gray box which contains all the protein and mRNA nodes represents the boundary of the region (one of twelve regions in the blastoderm tissue shown in Figure 6 (B)). Since the gene products usually diffuse to neighboring regions, the gene products in one region can interact with the gene products of the neighboring regions (*e.g:* Gene products in region 1 can interact with the gene products in regions

2 and 12 and vice versa). This is represented by the regulatory interactions (arrows and t-connectors) that span in between the boundaries of two neighboring regions. The complete gene interaction graph for the D-V patterning is shown in Figure 7. This graph was constructed by using the information about the regulatory interactions between mRNA and proteins explained previously.

Using this gene interaction graph we formulate the **threshold logic rules**, using the following guidelines:

1. The weights and threshold are restricted to integers to simplify rule generation. However, this does not limit the expressiveness of threshold logic (Muroga, 1971).
2. Genes and gene products that act as promoters are assigned positive weights. Inhibitors are assigned negative weights.
3. Dependent gene products are selected from the gene interaction graph (Figure 7). *e.g:* Expression of *sna* is dependent on *DL* and *TWI*.
4. Since in general inhibition is stronger than activation, inhibitors have a higher absolute weight than activators.
5. Weight assignments are modified so that the results match with biological observation.

Rule generation example:
The rule generation procedure is explained in detail for the *rho* mRNA. *rho* is activated by *DL* protein in the same region, and the *DL* protein in the two neighboring regions (Figure 7). It is inhibited by the *SNA* protein. We assign weight of $+1$ for each of the three activators (*DL* protein in the region, and *DL* protein in the neighboring regions). We set the threshold to 1 as *rho* is activated when any one of the activators is present. We assign a weight of -3 to *SNA* (inhibitor). This weight is enough to negate the effect of all the three activators. We denote this rule as follows:

$$rho_i^{t+1} = [DL_{i-1}{}^t = +1, DL_i{}^t = +1, DL_{i+1}{}^t = +1, SNA_i{}^t = -3; T = 1].$$

In this notation, the subscript refers to the cell number and the superscript refers to the time step in the model simulation. Each region has a discrete expression value for every gene product. The cell numbers are in the range 1 to 12. After 12, we start over with 1, as we have modeled the dorsal-ventral embryonic section as twelve regions that are arranged in a cycle. These regions are numbered in the counter clockwise direction from 1 to 12. Therefore we can now specify the cells that are adjacent to cell number 1 as $(1+1) = 2$ and $(1-1) = 12$.
Rules are generated for each gene product. These rules are then simulated in discrete time. This is discussed in the results section.

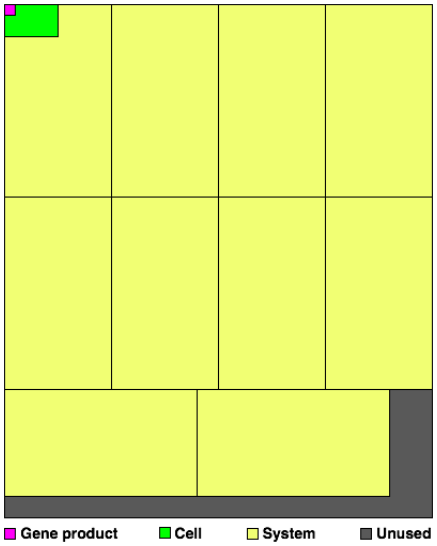

Figure 8: Map of allocated resources for simulation of expression pattern of the dorsal-ventral patterning genes of *Drosophila melanogaster.* on a 48x40 CLB FPGA.

3.2 Hardware Based Simulation

As we can observe from the topology of the interaction graph, each cell in the system is represented by 14 different gene products. Most interactions take place between products within an individual cell, with some intercellular interactions taking place between adjacent cells involving the SOG and DL proteins.

To map an individual cell to the FPGA, at least 14 configurable logic blocks are required. An area of 3x5 CLBs is chosen in which to allocate the gene products. A rectangular cell mapping is desirable since it allows multiple cells to fit together easily on the board without creating large "holes" of unused blocks. Minimization of the cell perimeter is also desirable, as it often reduces routing distances between both blocks within the cell and blocks of adjacent cells.

The complete system for the dorsal-ventral patterning genes is modeled by 12 cells in a cyclical structure. This system is mapped to the FPGA as block of cells two cells wide and six cells deep. A cyclical model is fairly easy to place and route, as each cell in the model has only two adjacent cells.

Depending on size and complexity of both the gene regulatory network and the FPGA being utilized, there may be unused resources remaining on the FPGA after mapping of the complete system. If enough unused resources are available, one or more copies of the system may be placed on the board and simulated concurrently, decreasing the effective real time required to simulate each time step by a factor equivalent to the number of systems on the FPGA.

Figure 8 shows the results of mapping to the FPGA at the gene product, cell, and system levels. As the figure indicates, each cell contains 14 gene products, each system contains 12 cells, and the 48x40 CLB board is large enough to accommodate 10 independent simulations. Complete systems are simulated independently and do not interact with each other, therefore it makes no difference where they are placed on the FPGA relative to each other as long as they do not overlap.

4 RESULTS

Using the "guidelines" proposed earlier, the threshold logic rules for each gene product are derived. The rules for all the gene products involved with dorsal-ventral patterning are as follows :

- *rho:* $rho_i^{t+1} = [DL_{i-1}{}^t = +1, DL_i{}^t = +1, DL_{i+1}{}^t = +1, SNA_i{}^t = -3; T = 1]$.
- *twi:* $twi_i^{t+1} = [TWI_i^t = +2, DL_{i-1}{}^t = +1, DL_i{}^t = +1, DL_{i+1}{}^t = +1; T = 3]$.
- *sna:* $sna_i^{t+1} = [TWI_i^t = +2, DL_{i-1}{}^t = +1, DL_i{}^t = +1, DL_{i+1}{}^t = +1; T = 3]$.
- *dpp:* $dpp_i{}^{t+1} = [SOG_{i-1}{}^t = -1, SOG_i{}^t = -1, SOG_{i+1}{}^t = -1, DL_{i-1}{}^t = -1, DL_i{}^t = -1, DL_{i+1}{}^t = -1; T = -1]$.
- *tld:* $tld_i^{t+1} = [DL_{i-1}{}^t = -1, DL_i{}^t = -1, DL_{i+1}{}^t = -1; T = 0]$.
- *zen:* $zen_i^{t+1} = [DL_{i-1}{}^t = -1, DL_i{}^t = -2, DL_{i+1}{}^t = -1; T = 2]$.
- $RHO : RHO^{t+1} = [rho = +1; T = 1]$
- $TWI : TWI^{t+1} = [twi = +1; T = 1]$
- $SNA : SNA^{t+1} = [sna = +1; T = 1]$
- $ZEN : ZEN^{t+1} = [zen = +1; T = 1]$
- $DPP : DPP^{t+1} = [dpp = +1; T = 1]$
- $TLD : TLD^{t+1} = [tld = +1; T = 1]$

We know the original concentration gradient of *DL* (expressed ventrally and concentration decreases dorsally). We also know that the *SOG* protein is found in the middle regions (Wolpert et al., 2002). The expression of these proteins is assumed to be constant throughout the process of pattern formation, since these proteins are not affected by the other gene products that we consider. The other gene products are assumed to be uniformly unexpressed at $t = 0$.

Starting from the initial state we simulate the threshold logic rules in discrete time steps. The steady state is attained in the dorsal-ventral simulation after about five time steps. This steady state gene expression is shown in Figure 9. We now interpret this steady state expression and predict if this indicates prospective germ layer formation. The position of the different germ layers along the dorsal-ventral axis is shown in Figure 6.

The ventral-most stripe of cells form the mesoderm (Wolpert et al., 2002). Twist and snail genes are activated in this region. Both these proteins are necessary for the formation of mesoderm (Wolpert et al., 2002). Our model also predicts that both *twi* and *sna* are expressed in the ventral regions (Figure 9 (B)). Rhomboid is activated in the cells that form the future neurectoderm (ventral ectoderm) (Wolpert et al., 2002). The region in which the model predicts the expression of *rho* is exactly where the ventral ectoderm develops (Figure 9 (D)).

The *dpp* gene is expressed in the dorsal-most region; the gradient of this protein is crucial for the creation of dorsal-ventral patterning (Wolpert et al., 2002). The expression of *dpp* predicted by the model matches with the biologically observed wild-type expression. The expression of different genes observed in the *Drosophila* embryo that are necessary for dorsal-ventral patterning is shown in Figure 9 (A). Observe that the gene expression predicted by the model matches very well with the actual wild-type expression. Correct spatial expression of these genes is responsible for the creation of the four different germ layers. This simulation takes under *one second* to complete.

Hardware simulation is expected to improve simulation performance significantly. Functionally, the simulation performed on the FPGA is no different from the simulation performed on the CPU. Given the same set of initial states and rules for the next state computation of the gene products, the steady states reached are precisely the same.

A 2-GHz CPU utilizing three address code instructions with register operands requires an average of roughly 8.6 instructions to compute the next state for a single gene product of the genes simulated in this system. If the processor utilizes 4 integer arithmetic logic units, all of which operate on independent instructions, the effective step time of the CPU simulation is approximately 180 ns. A 400-MHz FPGA using the mapping described is able to perform 10 simulations concurrently, resulting in an effective step time of approximately 250 ps, 720 times faster than the general purpose CPU.

5 CONCLUSIONS

In this paper we propose a novel methodology to model gene regulation based on threshold logic. We demonstrate the effectiveness of this method to model the dorsal-ventral and anterior-posterior pattern for-

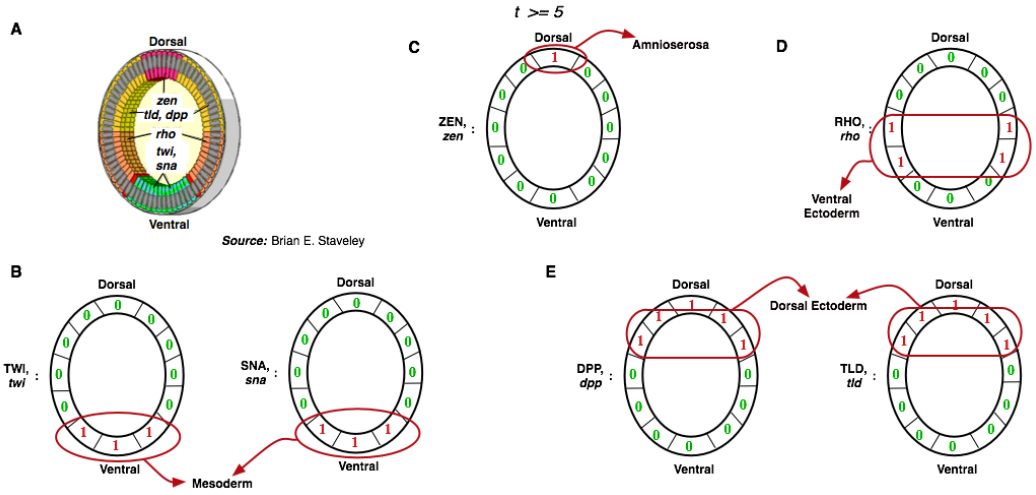

Figure 9: **A**: Biologically observed gene expression in *Drosophila.* blastoderm. **B-E** Steady state expression obtained from simulation of the model. This matches well with the gene expression observed in actual embryos.

mation in *Drosophila*. The model was able to predict the role of different genes and their interaction in determining the pattern formation in the *Drosophila* embryo. The advantage of this model is that it is very simple and makes use of only the nature of interaction (activation and inhibition) between genes. In simulation, field-programmable gate arrays provide a great deal of power in a relatively small package. Through modular decomposition of gene interaction models and highly parallel computation, FPGAs are capable of high speed simulation that greatly surpass the computational ability of a single CPU. Compared with a large computer cluster capable of the same tasks, GRN-application oriented FPGAs are clearly an economical choice in terms of size, cost, and power consumption.

REFERENCES

Albert, R. and Othmer, H. G. (2003). The topology of the regulatory interactions predicts the expression pattern of the segment polarity genes in Drosophila melangogaster. In *J. Theor. Biol.*

Brown, S. (1992). *Field-programmable gate arrays*. Kluwer Academic Publishers, Norwell, MA.

Collins, F. S., Morgan, M., and Patrinos, A. (2003). The human genome project: Lessons from large-scale biology. *Science*, 300(5617):286–290.

DeHon, A. (1996). *Reconfigurable Architectures for General-Purpose Computing*. Ph.D. dissertation, MIT.

Dertouzos, M. (1965). *Threshold Logic : A Synthesis Approach*. The MIT Press.

Dougherty, E. R., Hua, J., and Bittner, M. L. (March 2007). Validation of computational methods in genomics. *Current Genomics*, 8:1–19(19).

Francis, R. (1992). A tutorial on logic synthesis for lookup-table based fpgas. *Proceedings of the NAS*, pages 40–47.

Gursky, V. V., Reinitz, J., and Samsonov, A. M. (2001). How gap genes make their domains: An analytical study based on data driven approximations. *Chaos*, 11:132–141.

Heller, M. J. (2002). Dna microarray technology: Devices, systems, and applications. *Annual Review of Biomedical Engineering*, 4(1).

Kauffman, S. A. (1993). *The Origins of Order: Self–Organization and Selection in Evolution*. Oxford University Press, New York; Oxford.

Kohavi, Z. (1970). *Switching and Finite Automata Theory*. New York: McGraw-Hill Book Company.

Muroga, S. (1971). *Threshold Logic and Its Applications*. New York: WILEY-INTERSCIENCE.

Reinitz, J. and Sharp, D. H. (1995). Mechanism of eve stripe formation. In *Mechanisms of Development*, number 49, pages 133–158.

Roth, S., Stein, D., and Nusslein-Volhard, C. (1989). A gradient of nuclear localization of the dorsal protein determines dorsoventral pattern in the drosophila embryo;. *Cell*, 59(6):1189–1202.

Russell, S. and Norvig, P. (2003). *Artificial Intelligence: A Modern Approach*. Prentice-Hall, Englewood Cliffs, NJ.

Shmulevich, I., Dougherty, E. R., Kim, S., and Zhang, W. (2002). Probabilistic boolean networks: a rule-based uncertainty model for gene regulatory networks. In *Bioinformatics*.

Winder, R. O. (1965). *Threshold Logic*. PhD thesis, Princeton Univiversity.

Wolpert, L., Beddington, R., Jessell, T., Lawrence, P., Meyerowitz, E., and Smith, J. (2002). *Principles of Development*. Oxford University Press.

APPLICATION OF WEIGHTED LEAST SQUARES TO CALIBRATE A DIGITAL SYSTEM FOR MEASURING THE RESPIRATORY PRESSURES

José Leonardo Ferreira, Nadja Carvalho Pereira, Marconi de Oliveria Júnior, João Lucas da Silva
Flávio Henrique Vasconcelos, Carlos Julio Tierra-Criollo
Department of Electrical Engineering, UFMG, Av. Antônio Carlos 6627, Belo Horizonte, Brazil
joseleo@cpdee.ufmg.br , carjulio@cpdee.ufmg.br

Raquel Britto, Verônica Franco Parreira
Department of Physiotherapy,UFMG, Av. Antônio Carlos 6627, Belo Horizonte, Brazil

Keywords: Calibration, measurement uncertainty, respiratory pressures measuring, weighted least squares.

Abstract: This article presents the results associated to calibration and evaluation of the measurement uncertainty of a digital respiratory pressures measuring system developed at the Biomedical Engineering Research & Development Laboratory (NEPEB) of the Department of Electrical Engineering – UFMG. The proposed method uses the least squares weighted regression to establish the measurement model and to evaluate the uncertainty. The standard expanded uncertainty estimated by the model was 1.4 kPa.

1 INTRODUCTION

The qualitative and quantitative characterization of the result of a measurement is a demand of metrology organisms, providing knowledge about the reliability, important to quality control of products and services. In Brazil, the National Institute of Metrology, Standardization and Industrial Quality (INMETRO) is the local NMI (national measurement institute) and as such is organism responsible for metrology politics and for establishing criterions and general normalization relative to expression of uncertainty (INMETRO, 2007).

Brazilian Ministry of Health (MS) established the compulsory certification for medical and hospital equipment (MHE), not only attributing conditions for a major credibility of use, but, also causing a huge demand for calibration services in the country. A non-calibrated medical equipment can lead clinic diagnostic errors, wrong therapies and iatrogeny in patients.

Today, regulation of certification process of MHE quality in Brazil is defined by two normative documents: MS and ANVISA (1999) and MIDIC and INMETRO (2006). The former defines the strategies, while the latter describes the technical details for certification.

A digital system was developed at NEPEB (Silva, 2006) in order to measure the maximum pressures exerted by the muscles of the human respiratory system. It was designed as equipment to be used in diagnostic and therapy and, therefore, must be submitted to metrological evaluation according to the standards of the MS. Thus, the measuring system must be certificated, and this process requires *instrument calibration and the evaluation of the measurement uncertainty*.

The measuring system includes a signal acquisition module for pressure and an analogical to digital signal conversion module that allows the digital data to be acquired using a personal computer (PC) through an USB interface.

2 OBJECTIVES

The signal acquisition module of pressure, denominated manovacuometer, uses two sensors of differential pressure, model MPX5050 by Freescale Semicondutor Inc. (Austin, Texas). The sensor possesses two pressure sides (figure 1) and the measured value corresponds to the differential

pressure taken between the two sides. Nevertheless, it is important to emphasize that pressure in one side (P1) must be always higher than that in the other side (P2).

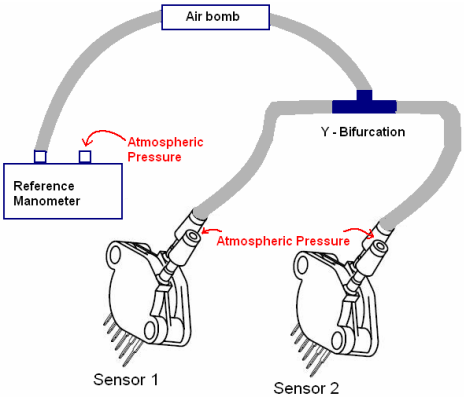

Figure 1: Schematic implementation for prototype calibration.

The purpose of this work is to carry out the calibration of digital manovacuometer developed by NEPEB. The proposed metrological model was built using the weighted least squares method, and, in that way, the measurement uncertainties was evaluated.

3 METHODOLOGY

3.1 Calibration Measurement System Protocol

In order to carry out the calibration of the digital manovacuometer, the protocol describe in (INMETRO, 1997) was used. Two were the motivation for the use of that procedure: (i) the sphygmomanometers with aneroid manometer was one of few clinic equipments that have normalization, regulation and control by INMETRO; (ii) although the normalization is specific for sphygmomanometers with aneroid manometer, this refers to the same type of physical quantity measured by the manovacuometer.

Tests were implemented to get the calibration curves for the two sensors of the developed equipment: i) the maximum indication error test and ii) the hysteresis test.

According to that procedure, the pressure applied to the sensors has to be increased and thereafter decreased. The pressure values (table 1) were applied during approximately five seconds, and an average voltage was evaluated at the output of the manovacuometer. The tests were performed four times, and a curve of the output voltage *versus* applied pressure, for each sensor, was plotted.

Table 1: Reference pressure values applied to prototype.

Pressure (kPa)		
4.0	9.3	12.0
13.3	20.0	26.7
33.3	40.0	46.7
53.3	60.0	–

Curve fitting was implemented using the method of weighted least squares (ABNT and INMETRO, 2003; Lira, 2002; Mathioulakis and Belessiotis, 2000; Press *et al.*, 1992). It was chosen to make the fitting for the average rising and fall curves of each sensor. Hence, two curves (rising and fall) were obtained for each sensor.

The instrument which measure the pressure applied to the prototype was a digital commercial manovacuometer (reference manometer) by Ecil (model BB480003) with reported maximum uncertainty of 0.03% (k=2), traceable to the SI standard. In figure 1, it is illustrated the schematic for calibration of the prototype, built in our laboratory.

3.2 Evaluating Measuring Uncertainty Protocol

The proposed model to calculate the measuring uncertainty, u_{Pc}, which is associated to the pressure corrected value, was built using the regression fitting obtained with the weighted least squares method. The u_{Pc} and the uncertainty of the reference mano-vacuometer lead to the evaluating of the standard combined uncertainty $u_c(P)$ and, consequently, to the expanded uncertainty U_p of the measured pressure with the prototype for a test pressure of 26.7 kPa.

4 RESULTS

Figure 2 shows the average calibration curves (rising and fall) for sensor 1 of the manovacuometer under calibration (similar calibration curves to sensor 2).
For fitting implementation, the linear region (up to 53.3kPa) was used. For each calibration curve, the fitting was approximated by the equation:

$$P_{rc} = b + aV_m \qquad (1)$$

where P_{rc} corresponds to pressure given a voltage on the output of the manuovacuometer (V_m) under calibration.

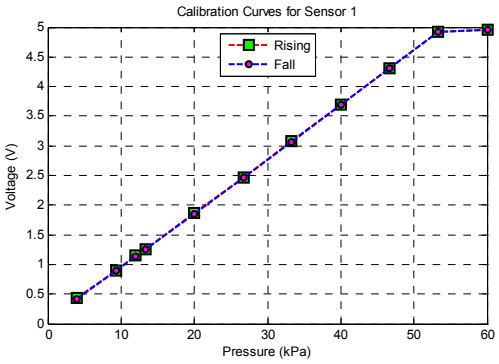

Figure 2: Calibration average curves for sensor 1.

In table 2, are given the reference pressure values associated to measured output voltage values (calibration points) and the respective standard combined uncertainty to rising curve of sensor 2.

Table 2: Reference pressure and output voltage values and associated uncertainties – sensor 2 (rising curve).

P_r (kPa)	u_{Pr} (kPa)	V_m (V)	u_{Vm} (V)
4.0	0.0006	0.4578	0.0024
9.3	0.0014	0.9257	0.0066
12.0	0.0018	1.1753	0.0022
13.3	0.0020	1.2909	0.0036
20.0	0.0030	1.8904	0.0035
26.7	0.0040	2.4955	0.0050
33.3	0.0050	3.0974	0.0047
40.0	0.0060	3.7094	0.0045
46.7	0.0070	4.3333	0.0034
53.3	0.0080	4.9410	0.0050

The uncertainty u_{Pr} associated to reference manovacuometer, was evaluated using the value of the related standard expanded uncertainty, as long as the uncertainty u_{Vm} was estimated based on fluctuation of the repeated readings in each calibration point (Mathioulakis and Belessiotis, 2000), correspondent to type A uncertainty.

The mathematics of linear regression fitting using weighted least squares is described with more details in Lira (2002), Mathioulakis and Belessiotis (2000) and Press *et al.* (1992). The slope a and the intercept b as well as the associated uncertainties u_a e u_b can be obtained from:

$$\left(K^T \cdot K\right) \cdot C = K^T \cdot L \qquad (2)$$

where, C is a vector whose elements are the fitted coefficients a and b; and $W=(K^T.L)^{-1}$ is a matrix whose diagonal elements are the variances of a ($w_{2,2}$) and b ($w_{1,1}$). The off-diagonal elements $w_{1,2}$=$w_{2,1}$ are the covariances between these parameters. K and L are a matrix and a vector, respectively, whose elements are weighted by pounds that depend on the uncertainties u_{Pr} and u_{Vm}. Solving (2), one obtains the parameters and their uncertainties for each average curve. The results are shown in table 3.

Table 3: Values for the parameters a and b and its uncertainties u_a and u_b.

	Sensor 1 - Rising	Sensor 1 - Fall	Sensor 2 - Rising	Sensor 2 - Fall
a (kPa/V)	10.9747	10.9797	11.0159	10.9747
u_a (kPa/V)	0.0050	0.0034	0.0086	0.0026
b (kPa)	-0.5845	-0.5280	-0.9506	-0.7989
u_b (kPa)	0.0169	0.0079	0.0206	0.0077
Cov(b,a) (kPa/V)	-7.44×10^{-5}	-2.13×10^{-5}	-1.43×10^{-4}	-1.71×10^{-5}

Calculation of the uncertainty u_{Pc} associated to calibration points is derived from *the law of propagation of uncertainties* (ABNT and INMETRO, 2003) and equation (1):

$$u_{Pc} = \left(a^2 u_{V_m}^2 + u_b^2 + V_m^2 u_a^2 + 2V_m Cov(b,a)\right)^{1/2} \qquad (3)$$

The standard combined uncertainty, in turn, was obtained by:

$$u_c(P) = u_{Pc}^2 + u_M^2 \qquad (4)$$

where u_M is the uncertainty associated to reference manovacuometer.

The measuring uncertainty was calculated in relation to a calibration point (26.7 kPa) arbitrarily chosen of the average rising curve of the sensor 2. To this point, the average output voltage is V_m= 2.4955 V. The uncertainty u_{Vm} is estimated considering the type A uncertainty, u_V, the sensor accuracy, u_E, and the resolution of manovacuometer under calibration, u_R:

$$u_V = \frac{0.0100}{\sqrt{4}} = 0.0050V \qquad u_E = \frac{0.1125}{\sqrt{3}} = 0.0650V$$

$$u_R = \frac{0.0001}{\sqrt{3}} = 0.00006V \qquad u_{Vm}^2 = u_V^2 + u_E^2 + u_R^2 \Rightarrow u_{Vm} = 0.0652V$$

Taking account these values, those of third column of table 3 and (3) result u_{Pc}=0.7183 kPa. For the reference pressure of 26.7 kPa, the value of u_M is equal to 0.0040 kPa. Hence, the standard combined uncertainty is estimated as 0.7 kPa. Finally, the value for the standard expanded uncertainty is

evaluated using the expression of Welch-Satterthwaite (ABNT and INMETRO, 2003).
For the confidence interval of 95.45%, the obtained value for the effective number of degrees is $v_{eff} \rightarrow \infty$, which indicates a coverage factor of k=2. Therefore, the estimated value for the standard expanded uncertainty is equal to U_p=1.4 kPa.

5 DISCUSSIONS

The repeatability of measurement of calibration curves, as discussed in other works of NEPEB, was confirmed here. The maximum value obtained for the type A uncertainty associated to the values of V_m is equal to 0.0066 V.

Calculations of hysteresis were performed considering the fitting curves. The maximum absolute value obtained for hysteresis was equal to 0.1467 kPa for sensor 1 and 0.2957 kPa for sensor 2. These values are much lower than the value established by INMETRO for sphygmomanometers with aneroid manometer. In the same way, when is considered the linear region, it is noticed that the results obtained in maximum indication error test are also inside the tolerance range determined by INMETRO for this equipment (0.4 kPa).

The standard combined and expanded uncertainties estimated for the prototype (for reference pressure of 26.7 kPa) were 0.7 kPa and 1.4 kPa, respectively. The last value is lower than that suggested in INMETRO (2006) for analogical pressures measuring systems, that is, 12 kPa.

6 CONCLUSIONS

The proposed model to calibrate the digital manovacuometer developed at NEPEB uses the weighted least squares. This model indicates that the hysteresis, maximum indication error and uncertainty of the prototype were inside the tolerance range established by INMETRO.

In future works it must be investigated and inserted to the proposed metrological model other possible factors that can be influencing the result prototype uncertainty, as those associated to A/D converter, temperature variation and correlation between the curves parameters and input pressure.

ACKNOWLEDGEMENTS

To FAPEMIG and CNPq for financial support. To CETEL/SENAI/FIEMG represented for Luiz Henrique, Marcus Vinicius and Reiner that lent the laboratory and reference manovacuometer for the measurements. To Rômulo Martini of FHEMIG.

REFERENCES

ABNT; INMETRO, 2003. *Measurement uncertainty guide* (free translation). ABNT, INMETRO, Rio de Janeiro.

Brazilian Ministry of Development, Industry and Foreign Commerce (MIDIC); INMETRO, 2006. Establishes the evaluation of conformity for MHE. Portaria N^o 86 de 3 de abril de 2006.

Brazilian Ministry of Health (MS); Brazilian National Health Vigilance Agency (ANVISA), 1999. Establishes the certification for MHE. Resolução N^o 444 de 31 de agosto de 1999.

INMETRO, 2007. Homepage: http://www.inmetro.gov.br

INMETRO, 1997. *Procedure for verification of the sphygmomanometers with aneroid manometer* (free translation). INMETRO, Rio de Janeiro.

INMETRO, 2006. *Guidelines to carry out the calibration of analogical system measuring pressure* (free translation). INMETRO, Rio de Janeiro.

Lira, I., 2002. *Evaluating the measurement uncertainty:* fundamentals and practical guidance. Bristol and Philadelphia: IoP.

Mathioulakis, E.; Belessiotis, V. 2000. *Uncertainty and traceability in calibration by comparision*. Meas. Sci. Technol., 11: 771-775

Press, W.; Teukolsky, S.; Vetterling, W; Flannery, B. 1992. *Numerical recipes in C*: the art of scientific computing. 2nd ed. Cambridge University Press, Cambridge, 2nd edition.

Silva, J, 2006. *Development of a digital system for measuring maximum respiratory pressures* (free translation). Monografia (Bacharelado em Engenharia de Controle e Automação) – Escola de Engenharia, Universidade Federal de Minas Gerais, Belo Horizonte.

SOFTWARE FOR EMBEDDED CONTROLLER DESIGN
Application in Air and Water Caloric Electronystagmographic Stimulators

C. Richter, P. Mendes, M. Tavares
Biomedical Engineering Laboratory, Catholic University of Pelotas, Rua Felix da Cunha 412, Pelotas, Brazil
richter@ucpel.tche.br, paulorcm@hotmail.com, mtavares@ucpel.tche.br

V. Alves
PDI, Contronic Sistemas Automaticos Ltda., Rua Rudi Bonow, 275, Pelotas, Brazil
vinicius.alves@contronic.com.br

Keywords: Controller design, digital control, control systems modelling, water caloric stimulator, air caloric stimulator, electronystagmography.

Abstract: This paper describes the development and tests of a software which was projected to support the work of designing and testing dedicated embedded controllers. It was developed to accomplish two main features: helping to model the physical system to be controlled; and helping to easily implement and test a proposed controller to be applied to the physical system. Two practical applications are presented. The first one is the design of a temperature controller for a new version of a water caloric stimulator named E96, which has as main requirement fast and accurate temperature response with no overshoot. The second one is also a caloric stimulator, but the transfer media is air instead of water. Those equipments help otorhinolaryngologists in electronystagmography exam. Details on the caloric stimulators hardware and software, the proposed controllers and the results, are presented. The software was considered functional for the proposed applications.

1 INTRODUCTION

Digital control of a physical system, or plant, can be accomplished using a computer with internal software containing the algorithm that controls, through D/A conversion, the plant input variable. Closed-loop digital control requires the measurement and A/D conversion of the plant output variable. Many different kinds of digital controllers can be used for controlling different physical plants with the most variable range of requirements. Examples of requirements are the percent overshoot and the settling time for the step response of the plant (Dorf, 2001). Prior to the controller design is the modeling of the plant, which requires a modeling technique using, for example, the graphical analysis of the open-loop step response of the plant (Coelho, 2004).

The main motivation for the developed software PACD (*Plataforma para Aplicação de Controladores Digitais*, Digital Controllers Application Platform) was to create a software that, with the aid of an already existent hardware, would help modelling a physical system to be controlled, and additionally help designing a suitable controller for it, which would be validated through real tests. Such an ensemble of software and hardware would be helpful for designing and testing dedicated controllers, which later can be executed from microcontrollers or general purpose low cost DSPs, attempting to develop embedded dedicated controllers. The first practical application of the software PACD was to design temperature controllers in two electro-medical equipments.

Human corporal equilibrium comes from the interaction of three main systems: vision, proprioceptive system and vestibular system. Vestibular-Ocular Reflex (VOR) is responsible for vision focus during head movements (Castagno, 1994). Otorhinolaryngologists use several stimuli to diagnose diseases in the equilibrium systems. Caloric stimulus caused by the irrigation of heated water or air in the auditory conduit cause in healthy patient reflex ocular movements named nystagmus. The electric register of the ocular movements is called electronystagmography (ENG). The first Brazilian computerized system for ENG resulted from the joint work of Catholic University of Pelotas, Dr. Castagno Clinic and Contronic Sistemas Automáticos (Castagno, 1993; Costa, 1995). A

caloric water stimulator named E96, shown in Figure 1 was developed for use during ENG exam, maintaining two water containers at different temperatures. A caloric air stimulator named E107, shown in Figure 2, was recently developed. Two main advantages of the air stimulator are causing less discomfort and allowing the exam in patients with tympanic perforation (Brookler, 2002).

Figure 1: Water caloric stimulator model E96.

Figure 2: Air caloric stimulator model E107.

2 MATHERIALS AND METHODS

2.1 PACD Software

The PACD software was created in C language, under Borland IDE C++ Builder 6. Its initial form presents two operating conditions: modeling or control. Each one includes its own graphical interface. In modeling operating condition, the plant is modeled using a step excitation signal and verifying its time response. Figure 3 presents the modeling interface, which is divided in 3 regions, enumerated in the figure as "1", "2" and "3". In the first region, it is possible to choose the step response modeling method while the second one is used to set the amplitude of the step heating power input, and to set the desired air flow. The third region shows the step temperature response. The horizontal axis shows essay time in seconds. As far as last the essay, this axis keep adjusting to show all essay time range. Vertical axis shows water/air temperature in Celsius degrees (ºC). The available step response modeling methods in PACD allow first order or second order models with or without time delay. Modeling method can be chosen between Ziegler-Nichols, Hägglund and Mollenkamp methods, as presented in Coelho (2004).

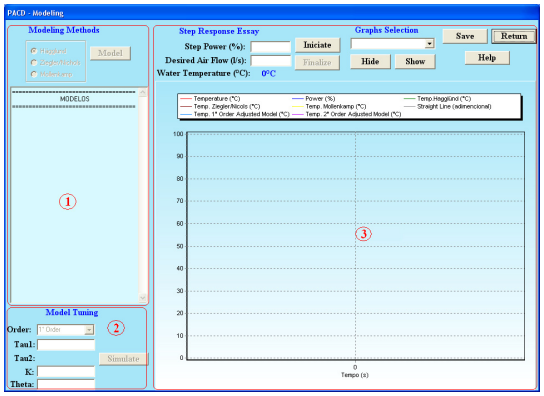

Figure 3: PACD modelling interface.

The control interface, shown in Figure 4, is also divided in three regions. In the first one it is possible to choose the controller type, to insert controller parameters and to command the compilation of the program with the chosen controller or controllers. The second region shows all chosen controllers and their parameters. In the third region it is possible to set the desired water/air temperature, the desired air flow and to start and stop controlling the plant. During the control operation, real water/air temperature in ºC is graphically shown against time in seconds. Horizontal axis is auto-adjustable. Real-time water/air temperature is shown numerically, as well as the difference between the desired temperature and the real one, named error. The control signal is also showed in the same graphic display, from 0% to 100% of the maximum possible power, or -100% to +100% in air equipment.

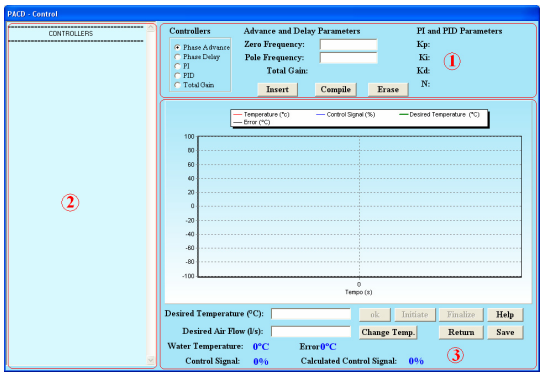

Figure 4: PACD control interface.

The main feature of this interface is the possibility of implementing and monitoring digital controllers in a fast and easy way. As a new essay will be done,

different tuning parameters can be chosen and different cascade controllers can be appended. PACD current available controllers include lead, lag, lead-lag, double-lead, double-lag, PI and PID. The internal structure of PACD uses negative unitary feedback, and it allows to cascade up to 10 controllers of each type. This feature makes it possible to accomplish many different configurations to analyze in different operation essays, so that the controller designer can choose the configuration that gives the best results in terms of the desired plant operation requirements.

2.2 Water Test Setup

A testing setup was assembled, whose main parts are shown in the block diagram shown in Figure 5. The setup is composed by a printed circuit board from E96 equipment, a water container with a heater resistance inside and an additional serial communication interface. The used microcontroller is the Intel's N87C196KB running at 12 MHz. The temperature sensor is LM35DZ (National), accompanied by an amplifier and adjustment trimmer, allowing an adjusted error of 0.2 ºC in the whole temperature range, from 0 ºC to 50 ºC. A special version of the E96 embedded software was created (C language, IAR compiler), so the equipment is commanded through serial communication by PACD software in the external PC. The power control variable is delivered to a heater resistance of 700 W (220 V), and variable percent power is determined by PWM (Pulse Width Modulation) using integral cycle technique, in order to avoid harmonic frequencies in the mains. The PWM period corresponds to 50 cycles of the 60 Hz electric network, so the power driver has 2% resolution.

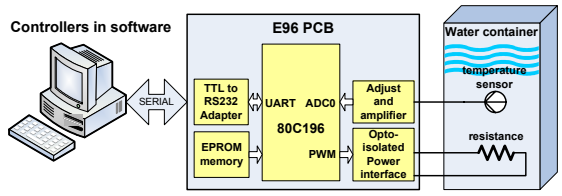

Figure 5: Water caloric setup block diagram.

2.3 Air Test Hardware and Software

Air stimulator E107AR was used with a modified protocol to facilitate the tests, and its basic block diagram is shown in Figure 6. The main parts of the system are composed by: an ADuC841 microcontroller (Analog Devices) running at 20 MHz; a precision resistive NTC sensor used to measure the temperature of the heated or cooled air flow, that after being adjusted by software, provides 0.2 ºC error in the whole temperature range (12 ºC to 50 ºC); an air pump that provides air flow from 4 to 12 liters/minute; and an air heater/cooler module formed by refrigeration sink, a Peltier effect device and a heater/cooler sink.

The internal E107AR software was modified to inhibit the original temperature controller and the periodic temperature sampling. It makes possible to PC software setting the sampling frequency as desired, and also, letting the PC software to control the output air flow and the amount of power to heat or to cool the air. The air pump power interface uses an AC current control technique that delivers AC voltage to the pump according to the microcontroller's D/A converter. The Peltier effect device is driven by an H-Bridge DC power interface, which is controlled by the ADuC841 pulse width modulation (PWM) output. The E107AR also has a built-in RS232 level converter to translate the microcontroller's TTL serial signals to ± 12 V levels on the PC serial port.

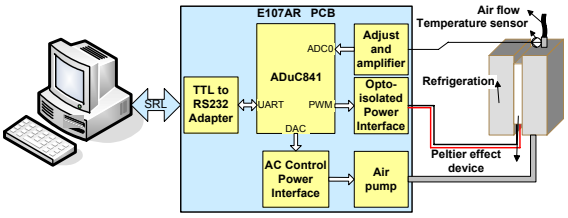

Figure 6: Air caloric setup block diagram.

3 RESULTS

Several tests were accomplished for PACD software validation and to find the best controller for each setup.

3.1 Results from Water Test Setup

For modeling the water temperature system to be controlled, a 25 % power step response was applied and three PACD available model methods where used. Figure 7 shows setup real step response pointed as "A". The letters B, C and D indicate respectively the responses from Hägglund, Ziegler-Nichols and Mollenkamp models. Carrying out a manual adjustment in Ziegler-Nichols obtained model, it was possible to arrive to the time response indicated by "E", which is even closer to the real plant time response. Equation 1 shows this model.

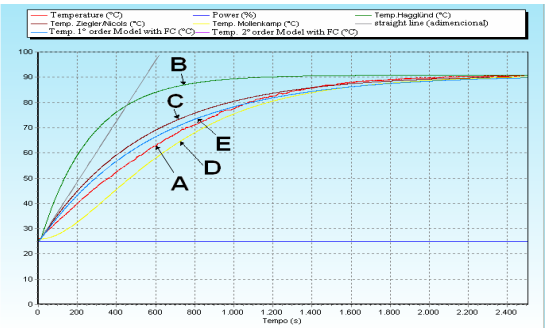

Figure 7: Water plant and models step response.

$$G(s) = \frac{2.592}{600\,s + 1} e^{-14s} \qquad (1)$$

Based on the selected model, several controllers were projected and tested according to classical control techniques (Dorf, 2001). The desired temperature was 44 °C and the initial temperature was 25 °C. An excellent step response of a controller using a cascade of phase-lead and PI compensators is shown in Figure 8, achieving 0% percent overshoot, 100 seconds settling time and ± 0.1 ºC stationary error.

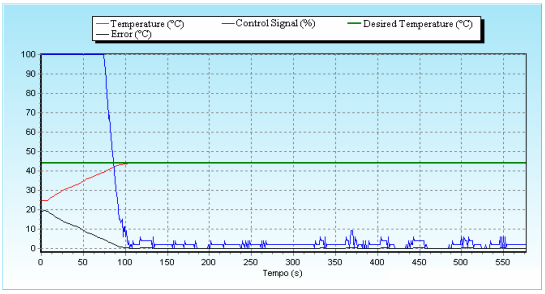

Figure 8: Water phase-lead + PI controller.

3.2 Results from Air Test Setup

Modeling the system from a 25 % power step input, it was obtained the model shown in Equation 2.

$$G(s) = \frac{0.1528}{250s + 1} e^{-3s} \qquad (2)$$

In all tests the desired temperature was 44 °C and the initial temperature was 25 °C, with 12 l/min air flow. After testing several developed controllers, the best step response was obtained from a cascade of phase-lead and PI compensators. Figure 9 shows this result, which achieved 1.80 % overshoot (0.34ºC), 45 seconds settling time and ± 0.31 ºC stationary error.

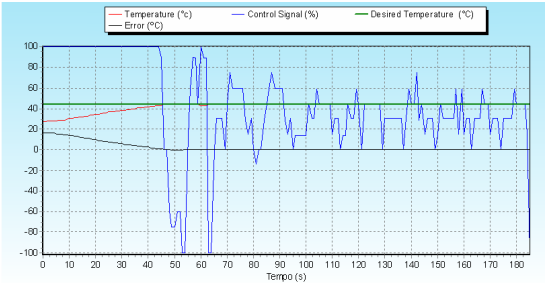

Figure 9: Air phase-lead + PI controller.

4 CONCLUSIONS

Analysing both water and air step responses achieved from cascade phase-lead and PI compensators, the responses where much better than the required results, which where set to 0.5 ºC maximum overshoot, 180 seconds of settling time and ± 0.5 ºC stationary error. This way, the PACD software was considered effective for the proposed applications, allowing the model construction and testing of several controllers, so helping to determine a better choice for the final controller. In the future, PACD will be improved to support other modelling methods and control strategies, such as adaptive control.

ACKNOWLEDGEMENTS

The authors thank Brazilian Agency CNPq for scholarship and financial support through grant 481638/2004-0.

REFERENCES

Dorf, R.C., Bishop, R.H., 2001. *Sistemas de Controle Modernos*. LTC. Rio de Janeiro.

Coelho, A.A.R.; Coelho, L.S., 2004. Identificação de Sistemas Dinâmicos Lineares. Ed. da UFSC. Florianópolis.

Castagno, L.A., Tavares, M.C., Richter, C.M. et al., 1994. Sistema Computadorizado de Eletronistagmografia e Vectonistagmografia "UCPel/Castagno" (Versão 3.0). *Anais do IV CBIS*, pp. 26-31.

Castagno, L.A, Tavares, M.C., Cava, R.A. et al., 1993. Eletronistagmografia computadorizada: o novo sistema de aquisicao de dados ENGc UCPel/Castagno. *Rev. Bras. Otorrinol.*, v. 594, pp. 263-265.

Costa, M.H., Tavares, M.C., Richter, C.M., Castagno, L.A., 1995. Automatic analysis of electronystagmographic signals. *38th Midwest Symposium on Circuits and Systems,* v.2, pp. 1349-1352.

Brookler, K.H., 2002. A case of normal ENG findings on air caloric stimulus that were not substantiated by water stimulus. *Ear, Nose & Throat Journal*, v. 81, n.8.

AN OBJECTIVE METHOD TO EVALUATE FORCE AND KNEE JOINT MOMENTS DURING ISOMETRIC EXTENSION

F. Paez [a,b], C. Frigo [a,b], E. Pavan [a,b], E. Guanziroli [a,b] and S. Frasca [a,b]
[a] *Laboratory of Movement Biomechanics and Motor Control (TBM lab)*
[b] *Department of Bioengineering, Polytechnic of Milan, Milan, Italy*
Address: Via Garofalo, 39 Milan Italy. E-mail: francesco.paez@polimi.it

Keywords: Knee extension, moment of knee joint, isometric knee extensor torque.

Abstract: A simple method to evaluate force and moments of knee joint during isometric extension has been developed and provides to the physicians a fast and objective tool for the evaluation of patients before and after a surgery or rehabilitative program. The experiment was made on normal young patients. Graphs of angle-moment were obtained. The patients started from 90° of knee flexion and extended step-by-step the knee joint until the maximum knee extension was achieved. Force, angle and moment were measured at each step. In comparison with literature, even if significant differences of technical instrumentation, age and activity of the patients are present, the maximum moment-angle behaviour during extension is the same but different magnitude. Future development of this device is to make it easy to use directly in clinical applications.

1 INTRODUCTION

When a patient with a neuromuscular disease is subject to an intervention or physical rehabilitation, it is always necessary to make a physical evaluation to check the functional state of the muscles and joints. In the specific case of spastic patients, several methods exist to see the deficit of active extension angle (DAE) and the maximum extension force (MEF) (Rabaiotti, 2004). Also, most mathematical models describe the forces in the knee under isometric quadriceps contractions (Huss et al.,2000). The most common methods of measure used are: A manual force test, manual dynamometers and isokinetic dynamometers. It is usually assumed that the moment measured by the dynamometer is equivalent to the resultant joint moment (Adamantios et al.,2004). Some of those methods, as the manual force test, are subjective and not precise because it depends on the magnitude of the manual force the evaluator can exert on the patient. Other methods require a big instrumentation or are relatively expensive because of the technology of the machine, such as the Isokinetic Dynamometer.

The aim of the present work is to create a simple, portable and economic device for the measure of forces and moments of knee joint during extension, and to provide to physicians a fast and objective tool for the evaluation of their patients before and after a surgery or rehabilitative programs.

2 MATERIALS

A mechanical device that is attached to the base of the bed where the patients are lying supine (See Fig. 1).This device includes a force cell connected with a string to the leg of the patient in order to calculate the tension force made by the leg of the patient during the knee extension.

An electrogoniometer made by a precision linear potentiometer in order to measure the flexion angle of the knee. A conventional video camera synchronized with the electrogoniometer and the force cell in order to acquire the different positions of the knee during the extension. A Software (*MB Ruler*) for bidimensional analysis of images (distance and angles) in order to calculate the angle of the force cell with respect to the ground and the angle of the string with respect to the leg of the patient during the knee extension. A Software environment in *MATLAB* to acquire and synchronize the data of the angles of the electrogoniometer and the forces of the cell.

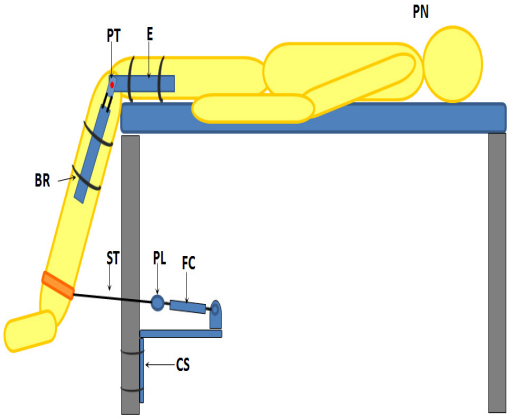

Figure 1: Instrumentation of the patient.

PN: Patient
PT: Precision Linear Potenciometer
E : Elettrogoniometer
ST: String
PL: Pulley
CS: Cell Support and system for attach to bed
BR: Braces for fix the electrogoniometer and the Cell Support
FC: Force cell

3 METHODS

The mechanical device is attached to the bed and supports the force cell that is connected by a string to the ankle of the patient. 26 normal patients participated in the experiment. (9 boys age $10^{+/-}$2.24 years and 17 girls age $10.12^{+/-}$ 1.87years). The patient is in supine position with both legs outside the bed and flexed to 90° (See fig. 1). Considering that there is a decline of $48^{+/-}$11% in the mean dynamic flexion torque by fatigue (Beltman et al., 2003) and that some differences are caused by the time-of-day of the exam (Onambele-Pearson et al.,2007) we recorded only the maximum moment on the first trial for each angle and made the exam to each patient at morning. The patient is instrumented with the electrogoniometer aligned with the axis of rotation of the knee joint, which is defined as the midpoint of the segment connecting the lateral and medial condyles. The knee is flexed initially at 90° and the patient is ordered to extend his knee and as a consequence pulling the string, the force is then recorded by the cell. In a next step the length of the string is manually increased by an operator which controls the pulley and consequently the angle of knee flexion is changed while the force measurement continues until it arrives to the maximum extension of the knee which is at 0°. The conventional video system, synchronized with the electrogoniometer and the force cell is made in order to acquire the different positions of the knee during the extension and be analyzed by the software for bidimensional images in order to calculate the angle of the force cell relative to the ground and the angle of the string with respect to the leg of the patient during the knee extension.

Anthropometric measurements of the patients allowed us to calculate mass properties of the leg and to compensate for gravitational force. A *MATLAB* algorithm takes all the data (electrogoniometer, force cell, inertia properties, anthropometrical data, force cell-ground angles and string-leg angles) to calculate the perpendicular force to the leg during each measure and consequently the resultant knee torque with planar analysis. (See Fig. 2).

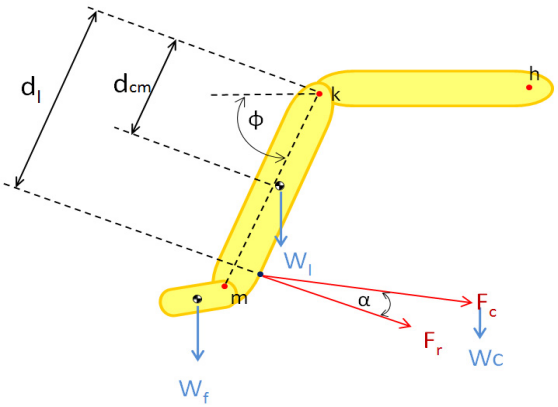

Figure 2: Free body diagram of the patient shank and force cell.

dl : Lever arm of force Fr to the knee joint
dcm: Lever arm of Wl to the knee joint
φ: Angle of knee flexion
α: Angle of resultant force Fr
m: Malleolus joint
k : Knee joint
h: Hip joint
W_f: Weight of foot
W_l: Weight of Leg
W_c: Weight of force cell
F_c: Force in extension and measured by the cell
F_r: Reaction Force of the cell, perpendicular to *mk* segment.

The reaction force Fr was to be assumed perpendicular to the patient shank *mk.*

4 RESULTS

4.1 Construction of the Device

A simple method to evaluate force and moments of knee joint during isometric extension has been developed. It provides to the physicians a fast and objective tool for the evaluation of their patients before and after an orthopaedic surgery or rehabilitative program.

4.2 Extensor Torque in Normal Patients

The obtained information is useful to understand the isometric extensor torque on normal and pathological patients. Normalized moment [N*m/kg] vs. angle [deg] of the normal patients of this study are reported in figure 3. Graphs are separated in male (thin line) and female (thick line) subjects.

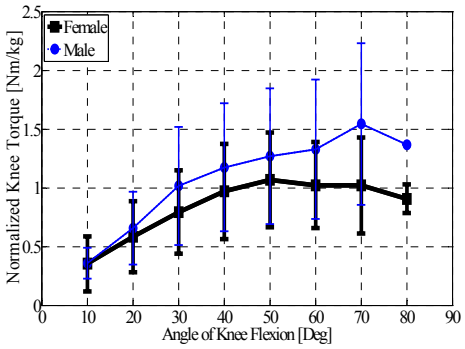

Figure 3: Normalized Moment torque vs. flexion angle.

The results demonstrated significant differences between gender according to Pincivero et al. (2004). The highest torque was generated at 70° for men and 50° for women. Both curves have a continuous growing behavior until his maximum value to decrease until maximum knee flexion as reported in literature (Beltman et al., 2003; Pincivero et al., 2004; Welsch et al., 1998; West et al., 2005).

5 DISCUSSION

5.1 Construction of the Device

Future development of this device is to make it usable in clinical applications. To make the process faster and more precise, it's specifically necessary to eliminate the measures made by the video system and instead install potentiometers to measure the shank-string angle and force cell-ground angle.

5.2 Extensor Torque in Normal Patients

If we make a comparison with literature, even if significant differences of technical instrumentation, age and activity of the patients are present, the results have the same behavior but are different in magnitude: We made the experiment with a self constructed device on 9 occasionally active boys age 10 $^{+/-}$2.24 years and 17 occasionally active girls age 10.12 $^{+/-}$1.87 years, while Pincivero et al. (2004) experimented with a Biodex Isokinetic Dynamometer on 14 men age 25$^{+/-}$4years and 14 women 23$^{+/-}$4 years all physically active, as they reported performing various types of routine exercises. Beltman et al. (2003) doesn't report the data normalized, (only the torque in Nm) but the behaviour of the curve is similar and he used an Isokinetic dynamometer (Lido Active, Loredon Biomedical, Davis) on 7 recreationally active male subjects age 27$^{+/-}$8 years. Welsh et al. (1998) experimented with 39 active men age 29.7 $^{+/-}$12.6 years and 38 active women age 27.2 $^{+/-}$ 11.3 years with an isometric knee flexion extension strength testing device; so we can conclude that differences in age, activity and instrumentation explains the higher values of torque of those experiments with respect to our study.

ACKNOWLEDGEMENTS

The Authors of this study would like to thank the team of the Istituto Clinico Humanitas, Rozzano Italy, Prof. Nicola Portinaro MD., Francesco Pelillo MD. and Federica Spreafico MD. for the collaboration in the study.

REFERENCES

Adamantios Arampatzis, Kiros Karamanidis, G. De Monte, Savvas Stafilidis. Gaspar Morey-Klapsing, Gert-Peter Bruggemann. Differences between measured and resultant joint moments during voluntary and artificially elicited isometric knee extension contractions. Clin. Biomech 19 (2004) 277-283

Beltman J , Sargeant A., Ball D, Maganaris C. Haan A. Effect of antagonist muscle fatigue on knee extension torque. Eur. J. Physiol (2003) 446:735–741

Huss R. A. , Holstein H. , O'Connor J. A mathematical model of forces in the knee under isometric quadriceps contractions. Clin. Biomech. 15 (2000) 112-122

Kaufman, K. R. An, K. Chao. A comparison of intersegmental joint dynamics to isokinetic dynamometer measurements.J. Biomech. 28, 1243-1256. (1995)

Onambele-Pearson N.L. Gladys, Pearson Stephen J. Time-of-day effect on patella tendon stiffness alters vastus lateralis fascicle length but not the quadriceps force–angle relationship. Journal of Biomechanics 40 (2007) 1031–1037

Pincivero Danny M., Salfetnikov Yuliya, Campy Robert M., Coelho Alan J. Angle- and gender-specific quadriceps femoris muscle recruitment and knee extensor torque. Journal of Biomechanics 37 (2004) 1689–1697

Rabaiotti G. Rassegna dei principali metodi di misura della forza muscolare. TdR Servizio di Recupero e Rieducazione Funzionale - Fondazione Salvatore Maugeri - Clinica del Lavoro e della Riabilitazione-IRCCS-Centro M. di Pavia Scienza Riabilitativa. 7-1998

Welsch M. A., Williams P. A., Pollock M.L., Graves J. E., Foster D.N., Futon M.N. Quantification of full range of Motion Unilateral and Bilateral Knee Flexion and Extension Torque Ratios. Arch Phys Med Rehabil. Vol. 79, August 1998

West Sacha J, Smith E Lynne E, Estelle V. Timothy D L. Noakes E, St Clair Gibson Alan. Submaximal force production during perceptually guided isometric Exercise Eur J Appl. Physiol. (2005) 95: 537–542

STUDY OF DENTAL GYPSUM USING FIBRE SENSORS
Analysis of Different Water/Powder Ratios of High Strength Dental Stone

Nélia Alberto[1], Rogério Nogueira[2], Lídia Carvalho[3], Ilda Abe[1]
Hypolito Kalinowski[4] and João L. Pinto[1,2]
[1]*Physics Department, University of Aveiro, Campus Universitário de Santiago, Aveiro, Portugal*
[2]*Institute of Telecommunications, Campus Universitário de Santiago, Aveiro, Portugal*
[3]*Dental Prosthesis IPSN, Paredes, Portugal*
[4]*Federal University of Paraná, Curitiba, Brazil*
nelia@ua.pt, rnogueira@av.it.pt, lcarvalho@mec.ua.pt, ilda.abe@ua.pt, hjkalin@av.it.pt, jlp@ua.pt

Keywords: Fibre optic sensors, Bragg grating, dental gypsum, water/powder ratio.

Abstract: In this work, we present a device to measure strain and temperature, based on fibre Bragg grating (FBG) sensors. The performance of these sensors was assessed in the study of a type of dental gypsum, namely high strength dental stone. It was intended to know the influence of the water/powder (W/P) ratios in the setting time and expansion. The results show that, a change in the W/P ratio influences the setting time as well as maximum strain values. The data was compared with the values foreseen in ANSI/ADA specification nº 25. The information that can be obtained with these sensors is quite important to dental prosthesis technicians, in order to achieve more accurate dental prosthesis and these sensors can be a good substitute to the actually device that is used to evaluate the setting expansion: extensometer.

1 INTRODUCTION

Optic sensors based on fibre Bragg grating (FBG) have attracted much attention in the past few years due to many advantages such as high sensitivity, immunity to electromagnetic interference, wavelength multiplexing, lightweight, low cost and easiness handling, which allows to be embedded into different materials. These characteristics have opened wide fields of applications, from optical communications to biomedicine. Thus, we can find FBGs in civil structures monitoring (Lima, 2007); sensing systems in vehicles, airplanes and ships (Castelli, 2002), in the detection of virus/antibodies (Petrosova, 2007) or even, in linear polymerization shrinkage monitoring of dental materials (Arenas, 2007).

In its simplest form, an FBG consists of a periodic modulation of the refractive index along the fibre length, which is formed by exposure of the core to an intense optical interference pattern of ultraviolet light. The sensing principle of a FBG-sensor is based on the monitoring of the wavelength shift of the reflected Bragg wavelength when it is subjected to strain and/or temperature changes. The Bragg wavelength is given by the following expression:

$$\lambda_B = 2\, n_{eff}\, \Lambda \qquad (1)$$

where n_{eff} is the effective index of the core and Λ is the refractive index modulation period (Kersey, 1997).

Among the dental materials, gypsum is one of most used in dental prosthesis because of its ability to change properties by the addition of different chemical components. When powder particles of the gypsum are mixed with water, a chemical reaction occurs, according with the following equation (Phillips, 1991):

$$(CaSO_4)_2.H_2O + 3H_2O \longrightarrow CaSO_4.2H_2O + \text{heat} \qquad (2)$$

All manufacturers of gypsum products have its own recommendations, concerning proper water/powder (W/P) ratio to be used, to obtain the best performance. However, if the W/P ratio is not correctly followed, accordingly to the manufacturer's recommendations, the gypsum might have different properties, namely the setting expansion.

In this work the influence of the W/P ratios of a high strength dental gypsum stone (type IV) was experimentally studied, namely the setting time and expansion, using devices based on FBG. The setting expansion values obtained were compared with values foreseen in ANSI/ADA specification nº 25, which were measured using an extensometer.

2 EXPERIMENTAL SETUP

The FBGs were written into photosensitive optical fibre (Fibercore PS1250/1500), by illuminating it with ultraviolet light, using an automated phase-mask interferometer system (Nogueira, 2002).

Two sensors were used in this work. One of them was protected mechanically, in order to be only sensitive to temperature variations. For that, the sensor was placed inside a double needle (figure 1).

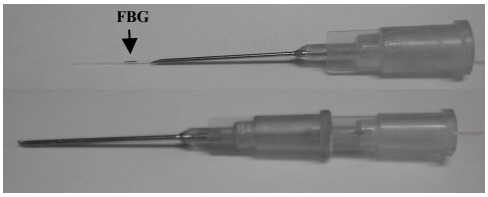

Figure 1: Temperature sensor.

The other sensor consisted in a free FBG, which was in close contact with gypsum, and is sensitive to strain and temperature variations. In the first analysis it was verified that there was sliding of the gypsum along the free FBG. In order to overcome this situation, two plastic spheres were glued to the fibre, down and above the sensor (figure 2), allowing a better response of the fibre to the gypsum expansion/contraction.

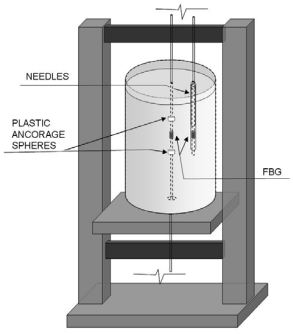

Figure 2: Schematic representation of the experimental setup.

The free sensor was put inside a hard metallic container (diameter = 3.5 cm and height = 7 cm) with a hole in the bottom, through which the fibre is pulled through. The fibre is then bonded to a support and slightly tensioned (about 700 με) allowing measuring both expansion and shrinkage.

Relatively to the W/P ratio, three different values were considered. One corresponds to the value recommended by the manufacturer, which is 0.22, one corresponding to a 15% decrease of the water quantity (W/P = 0.19) and another corresponding to a 15% increase of the water quantity (W/P = 0.26). These values were chosen, according with the reaction' stoichimetry and the W/P ratio recommended by manufacturer. Through reaction' stoichimetry we verified that a 15% decrease of water quantity relatively to W/P ratio recommended by manufacturer is the minimum value requested to occur reaction thus. With a decrease of water below 15% it is impossible to have a full reaction of gypsum. The choice of the other W/P ratio is related to the fact that we consider that usually there is a tendency to add a larger amount of water than the one recommended, facilitating the handling of gypsum.

For each case, the water was added to powder and spatulated, during 45 seconds. Then, the mixture was flowed into the metallic container and finally, the temperature sensor was inserted into the mixture. The Bragg wavelength measurement was made every 5 seconds, during 3 hours, simultaneously for the two sensors. The resolution of the system (sensor+interrogation system) allows measurements of displacement and temperature with a precision of about 1 με and 0.1 ºC respectively.

The measurements were repeated several times for each W/P ratio, being the results presented in this work a result of an average.

3 RESULTS AND DISCUSSION

The evolution of strain and temperature with time, for the two sensors used in the experiments are showed in the graphs of figures 3 and 4, respectively.

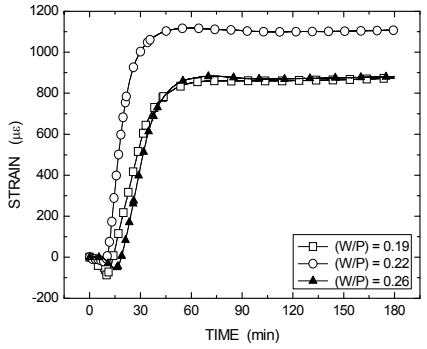

Figure 3: Evolution of strain during setting reaction, for gypsum type IV, for three different (W/P) ratios.

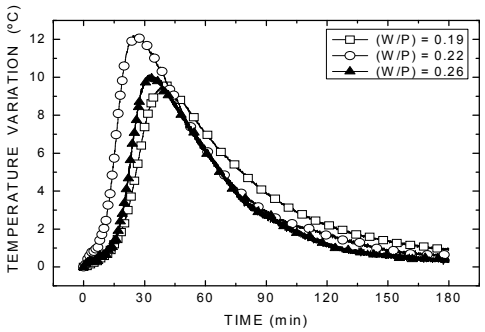

Figure 4: Evolution of temperature during setting reaction, for gypsum type IV, for three different (W/P) ratios.

The strain curve was obtained by subtracting the effect of temperature, obtained with the temperature sensor, in the measurements accomplished by the free FBG. The sensitivity coefficients of the FBG to temperature and strain was 10.6 pm/ºC and 1.1 pm/με, respectively. These values were previously measured.

According with the results obtained, we can observe that when we change the W/P ratio recommended by manufacturer, the maximum strain value and maximum thermal amplitude, reached during the setting reaction of dental gypsum are different (table 1), although the behaviour is similar.

Table 1: Values of maximum strain and maximum thermal amplitude for the W/P ratios analysed.

(W/P) ratios	Maximum strain (με)	Maximum thermal amplitude (ºC)
0.19	874	9.5
0.22	1120	12.3
0.26	884	10.1

Initially, we observe a shrinkage of dental gypsum, being more accentuated in the case of the W/P = 0.19, where it reaches about -90 με. Following, there is an increase of strain, along with an increased of temperature. After 55 min, for W/P = 0.22 and after 65 min, for W/P of 0.19 and 0.26, the setting expansion stabilized and temperature returned slowly to its initial value (room temperature).

Although there is a modification on the setting expansions values when the W/P ratio change, the results obtained experimentally are within the range established by ANSI/ADA specification nº 25, that, in this case, is between 0% and 0.15 %. This range was determined using an extensometer that allows the measurement of length changes within 0.01 mm resolution in a specimen with a length of 100 mm, (100 με of resolution). The proposed device, based on FBG, allows a real time measurement of the evolution of the strain and temperature in the material. Moreover, the resolution is around 1 με. Thus, the use of this device can be an incentive to the revision of actual ANSI/ADA specification nº 25, where we suggest the measurement of the setting expansion, using optic fibre sensors to the detriment of the extensometer because this technique present more resolution, with more reliable results.

When the gypsum is dry, it is also possible to measure the linear thermal expansion coefficient. This thermal property is other information quite important to dental prosthesis technicians, which is defined as the change in length per unit of length of gypsum, when its temperature is raised or lowered 1ºC.

4 CONCLUSIONS

In this work we presented a device for strain and temperature measurements, based on FBGs.

These sensors were applied in the study of the influence of the W/P ratios of dental gypsum, in the setting time and expansion. Also the sensor shows applicability in the determination of thermal expansion coefficient.

The sensors' response showed that, a modification of the amount of water influences the value of maximum strain and, this difference might interfere in the outcome of the technicians work. So, it is advisable following the manufacturer's recommendations.

The present devices can also be a useful tool for gypsum' manufacturers, allowing a real time monitoring of strain and temperature along the production process, what can be very important in

the control and improvement of the gypsum's properties.

ACKNOWLEDGEMENTS

The authors acknowledge support received from FCT SFRH/BD/30551 and SFRH/BPD/14513/2003 and project THRONE PTDC/EEA-TEL/66840/2006 (Portugal).

REFERENCES

Lima, H., Vicente, R., Nogueira, R., Abe, I., André, P., Fernandes, C., Rodrigues, H., Varum, H., Kalinowski, H., Costa, A., Pinto, J. (2007), "Structural health monitoring of the church of Santa Casa da Misericórdia of Aveiro using FBG sensors", *Proc. SPIE – Third European Workshop on Optical Fibre Sensors*, 6619, 661941.

Castelli, P., Falciai, R., Galli, R., Mattiucci, N., Pallaro, N., Trono, C., (2002), "Aplications of FBG sensors for the monitoring of critical components of vehicles", European Workshop on Smart Structures in Enginnering and Technology, 4763, 252 - 258.

Petrosova, A., Konry, T., Cosnier, S., Trakht, I., Lutwama, J., Rwaguma, E., Chepurnov, A., Mühlberger, Lobel, L., Marks, R., (2007), "Development of a highly sensitive, field operable biosensor for serological studies of Ebola virus in central Africa", *Sens and Actuators B*, 122, 578 - 586.

Arenas, G., Noriega, S., Vallo, C., Duchowicz, R., (2007), "Polymerization shrinkage of a dental resin composite determined by a fiber optic Fizeau interferometer", *Opt. Commun.*, 271, 581-586

Kersey, A., Davis, M., Patrick, H., LeBlanc, M., Koo, K., Askins, C., Putnam, M., Friebele, E., (1997), "Fiber Bragg sensors", *J. Lightw. Technol.*, 15, 1442 - 1463.

Phillips, R., (1991), *"Skinner's Science of Dental Materials"*, W. B. Saunders Company, Philadelphia, 9th edition.

Nogueira, R., Abe, I., Kalinowski, H., Pinto, J., Rocha, J., (2002), "Sistema interferométrico autorizado para gravação de redes de Bragg", 13ª Conferência Nacional de Física – Livros de Resumos, Évora, Portugal, 592 - 594.

A MICRO ULTRA LOW POWER RF RADIO FOR NEURAL SIGNAL RECORDING

Rui Zhong, Richard Liu
Cullen College of Engineering,University of Houston, 4800 Calhoun Road, Houston, Texas, United States
rzhong2@uh.edu, cliu@uh.edu

Haleh Fotowat, Fabrizio Gabbiani
Department of Neuroscience, Balor College of Medicine, Houston,Tx, United States
hfotowat@cns.bcm.edu, gabbiani@bcm.edu

Keywords: Micro Radio, Neural Signal Recording, RF Radio, Ultra Low Power.

Abstract: This paper reports the development of a small, light-weight and mini-battery operated low power radio transmitter for neural signal recording. This system allows recording of neural signal down to the level of 50 μV. A micromachined electrode is used to obtain these signals. The neural signal is then amplified 10,000 times and transmitted to the receiver at 433 MHz. The manufactured radio system is 7 mm by 6 mm in size and 0.5 gram in weight, with a power consumption of 750 μW. Radio functionality is tested and verified on locusts.

1 INTRODUCTION

Wireless recording of neural activity from the central and peripheral nervous systems has long been pursued by physiologists as a way to understand the operation of individual neurons, to decipher the relationship between the environment stimuli, nerve system response and the activities generated by the nerve signal (Akin, 1998). One of such research area is visually guided escape behaviors, which are critical to the survival of many animals.

In this design, we are required to detect the neural signals from main nerves of a locust. Therefore a small size, light weight and low power, cell battery based RF wireless telemetry system is needed. Unfortunately, the power consumption of available commercial radio chips is too large to be sustained by a small cell battery. In this design, we simplified the radio structure as much as possible to reduce power consumption. Firstly, a RF BJT oscillator is used to generate the carrier, instead of a Frequency Synthesizer. Secondly, AM modulation scheme is used instead of the typical FSK modulation in commercial radio chips. Thirdly, the whole system is analog. At last, a 30 AWG copper wire with the length of 40mm is used as antenna with the radio transmitter working at 420 MHz.

After several experiments, it is verified that this design is small enough to be carried by a locust and light enough to allow the bug to jump as usual. The received signal provides strength and time information of the neural activities.

2 RADIO SYSTEM DESIGN

2.1 System Overview

The radio transmitter is divided into two functional parts: amplifier stage and transmitter stage. Detected neural signals are typically in the range of 50 to 150 micro volts. In order to process this signal, a high gain amplifier stage is used to amplify it 10,000 times. The amplified neural spikes are then sent to the transmitter stage for transmitting. Direct coupling is used between these two stages. The whole system runs on a 3 Volts cell battery and the power consumption is only 750 μW in total. The complete system schematic is shown in Figure 1

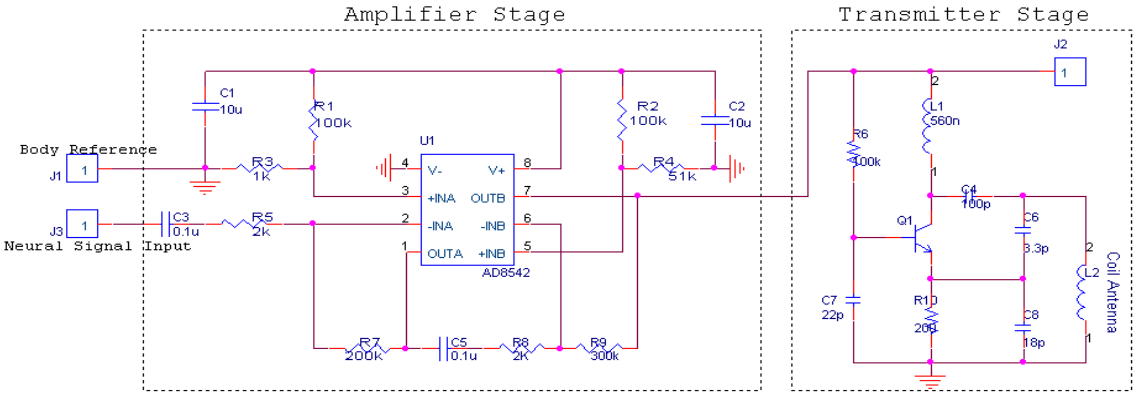

Figure 1: System Overview.

2.2 Transmitter Stage

For most neural experiments, researchers are mainly interested in the when this signal is generated and how many neural spikes are observed, other than their accurate amplitude value. Thus, simplifying the transmitter design has little influence on the research itself, but it can greatly reduce the power consumption, and reduce the size and weight of the system.

In our design, the transmitter is basically a 433 MHz BJT Colpitts oscillator. Colpitts Oscillator is well known for its simplicity and robustness. Figure 2 is the structure of our transmitter stage, which is a common-base (CB) Colpitts oscillator. In Figure 2 we can see that C1, C2 and L1 forms the positive feed back loop, and R1, L2 and R_F provide the DC bias for oscillation. C3 is the capacitor for common base structure.

Because of its wide application area, Colpitts oscillator is well studied. The oscillation frequency of this circuit can be calculated by equation (1).

$$f_0 = \frac{1}{2\pi\sqrt{L_1 \cdot \left(\frac{C_1 \cdot C_2}{C_1 + C_2}\right)}} \tag{1}$$

In this Colpitts oscillator application, the operation frequency is about 433 MHz. Therefore, several issues need to be taken care of. These issues will be discussed in the following subsections.

2.2.1 Selection of Inductor L1

Three issues are important when deciding the L1 inductor value.

First, according to equation (1), the value of L1 is directly related to the oscillation frequency. For 433 MHz band operation, it is usually in the nano-Henry range.

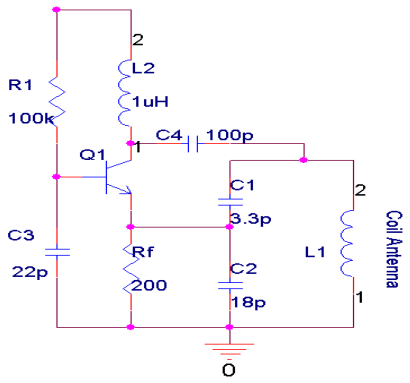

Figure 2: Transmitter Structure.

Second, the value of inductor L1 is also related to the quality factor of Oscillation. The relation is expressed in Equation (2).

$$Q \propto \frac{1}{r}\sqrt{\frac{L_1}{C_\Sigma}} \tag{2}$$

$$\text{Where} \quad C_\Sigma = \frac{C_1 \cdot C_2}{C_1 + C_2} \tag{3}$$

And r is the serial resistance of L1.

In the oscillation loop, larger quality factor Q leads to more stable and accurate oscillation and lower power dissipation. From equation (2), for the same C_Σ, greater L1 and smaller r will contribute to a higher system quality factor. This indicates that we should choose a high Q inductor, whose r is

small. And the L1 to C_Σ ratio should be large enough.

Finally, up limit does exist for the value of L1. Increase L1 too much will decrease its self-resonant frequency and force the corresponding C_Σ decrease to the BJT's parasitic capacitance region, which may cause unstable oscillation (Razavi, 1998).

The selection of L1 value is a compromise between these issues discussed above.

2.2.2 Selection of C1 and C2

According to the analysis in section 2.2.2, to achieve a higher quality factor, C1 and C2 should be as small as possible. On the other hand, however, C1 and C2 can not be too small. Because C1 is in parallel with the junction capacitance C_{CE} and C2 is in parallel with the junction capacitance C_{BE}, Rp is the equivalent resistance. Its relation to the loop is shown in equation (4). The equivalent oscillation loop is shown in Figure 3.

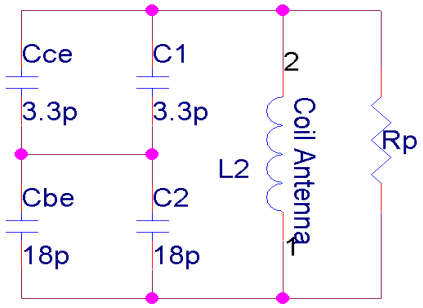

Figure 3: Equivalent Oscillation Loop.

Figure 3 tells us if C1 and C2 are too small, Cce and Cbe will dominate the oscillation frequency. Typically, C1 and C2 should be greater than Cce and Cbe. Therefore, C_Σ should lies inn the range of 1 pf to 4 pf.

Also, known C_Σ, the value of C1 to C2 directly depends on their ratio, C1/C2. Again, compromise exists when selecting this ratio. Smaller C1/C2 ratio means larger loop quality factor but smaller positive feedback gain, while larger C1/C2 ratio gives greater feedback gain but lower quality factor (Razavi, 1998). In practice, experiment shows that 3.3pf and 18pf capacitor pair gives stable oscillation and makes it easy to start the oscillation. Now, we can modify equation (1) to obtain practical equation for oscillation frequency f_0.

$$R_P = (1 + C_1 / C_2)^2 / g_m \quad (4)$$

$$f_0 = \frac{1}{2\pi\sqrt{L_1 \cdot \left(\frac{C'_1 \cdot C'_2}{C'_1 + C'_2}\right)}} \quad (5)$$

Where $C'_1 = \frac{C_1 \cdot C_{CE}}{C_1 + C_{CE}}$ (6)

And $C'_2 = \frac{C_2 \cdot C_{BE}}{C_2 + C_{BE}}$ (7)

2.2.3 Selection of Rf and R1

R_F is a DC negative feedback resistor, which helps stabilize the transistor current gain. R1 is used to set up the collector I_C. However, R_F and R1 are also the main power consumption components in this circuit. The power they consume can be estimated by equation (7) and (8).

$$P_{Rf} = I_C^2 * R_f \quad (7)$$

$$P_{R1} = I_B^2 * R_1 \quad (8)$$

Since I_C is usually large, R_F should be as small as possible. And because I_B is typical in uA range, thus P_{R1} is usual less than 50 uW. In practical design, for the purpose of low power consumption, we simultaneously decrease R_F and increase R1, the final power consumption of the oscillation is only 750 uW, compared to the typical 10 mW power consumption for a commercial transmitter, this is a great advantage.

2.3 Amplifier Stage

Figure 6 is the structure for amplifier stage. It consists of two JFET operational amplifiers. Each stage runs on a single power supply and has a gain of 100. To save power, an OPA with only 40 uA current consumption at 2V is used. Important design rules about amplifier stage are exploded below.

2.3.1 Power Line Decoupling

In practical application, the battery has non-zero internal impedance, which induces AC voltage on the power line.

If not carefully decoupled, the AC voltage on the power becomes an input to amplifier stage. This will cause the amplifier stage self-oscillate. Also, smaller R20 and R19 (as shown in Fig 4) value may be necessary to further ensure no self-oscillation will occur.

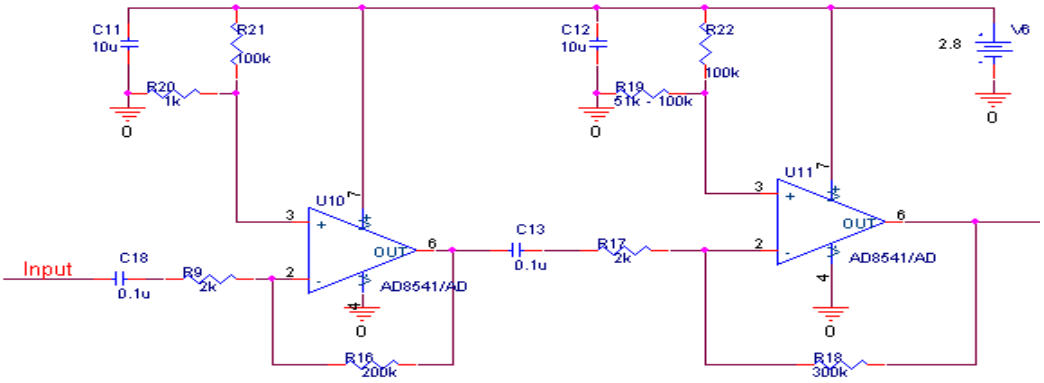

Figure 4: Amplifier Stage Structure.

2.3.2 Direct Coupling

In this design, we can use the DC bias component of the OPA as the power supply voltage V_{CC} for the next transmitter stage. Therefore, a direct coupling is used between amplifier stage and transmitter stage.

When no neural signal input appears, the output voltage of the amplifier should be half of the battery voltage. That is the V_{CC} power supply for the next transmitter stage.

When neural signal is connected to the amplifier input, the amplified signal of interest will directly couples to transmitter, that is add to V_{CC}

3 EXPERIMENT RESULTS

Figure 5 shows the radio installed on a locust. A pair of micromachined electrode is used to collect neural signal from the locust. Figure 6 demonstrates the neural spikes collected and observed at the receiver side oscilloscope.

Figure 5: Locust with micro radio installed.

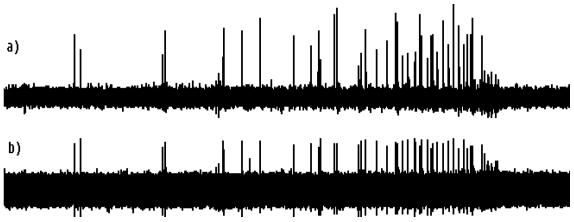

Figure 6: a) neural spikes measured on the transmitter side b) neural spikes observed on the receiver oscilloscope.

4 CONCLUSIONS

This paper discusses a design scheme of a single BJT transistor oscillator based RF Radio for neural signal recording. Comparing to other radio existing, this design has two important advantages. First, it is an ultra low power radio, with a power consumption of only 750 uW, only 7.5% of the available commercial transceiver chips. This feature makes it possible to be powered by a tiny watch battery. Second, this radio is small and light, it is only 7 mm by 6 mm in size and 0.5 gram in weight. These two advantages make this radio especially suitable for wireless recording tasks performed on small animals, insect, such as locusts and pigeons. The communication range of this radio is up to 20 feet.

REFERENCES

Akin, T., 1998. A Wireless Implantable Multichannel Digital Neural Recording System for a Micromachined Sieve Electrode, *Solid-State Circuit, VOL 33, No 1*. IEEE Journal of.

Razavi, B., 1998. *RF Microelectronics*, Prentice-Hall, Inc., New York, 2nd edition.

SOFT GELS WITH HIGH ELECTRIC, ULTRASOUND CONDUCTIVITY AND STABLE THREE-DIMENSIONAL CONFIGURATION AS ENERGY TRANSMISSIBLE MEDIA

Yasuo Shikinami, Kazuhiro Yasukawa
Takiron Co.,Ltd. Medical Institute.7-1-19, Minatojima, Minamimachi, Chuo-ku, Kobe, 650-0047, Japan
sikinami@takiron.co.jp, yasukawa@takiron.co.jp

Kaoru Tsuta
Takiron Co.,Ltd. Medical Institute.7-1-19, Minatojima, Minamimachi, Chuo-ku, Kobe, 650-0047, Japan
k-tuta@takiron.co.jp

Keywords: Soft gel, Energy transmissible media, Electric conductivity, Ultrasound transmission, 3D configuration.

Abstract: We had synthesized single component permanent gels, segmented polyurethane gels (SPUGs), essentially consisting of gelatinizing component-only, of which almost of segments and dangling chains are liquid state at ambient temperatures. SPUGs transmit energy well such as electricity, light and ultrasound. In this article, SPUGs were improved by adding dispersive media into swollen SPUGs (S-SPUGs), which acquired higher electric conductivity (1.2×10^{-3} S/cm) at room temperature and lower ultrasound attenuation (0.13 dB/ MHz cm) than SPUGs and readily responded to very low mechanical stress (Young modulus 3.7×10^{4} Pa) due to its high flexibility like soft tissues of living body. The S-SPUGs, which have three-dimensionally casting moldability and stable configuration, are potentially applicable to soft biomaterials with energy transmissible, transducing faculty.

1 INTRODUCTION

This research relates to potential application of novel soft gels with stable three-dimensional configuration and high electric, ultrasound conductivity as energy transmissible media for biomaterials.

Gels generally consist of the both components of a material to be gelatinized and dispersion media, and are classified from various viewpoints. In a viewpoint, gels usually form a collection of mobile molecular chains including dispersion media, of which reticular structures are three-dimensionally developing through aggregation, intertwining, molecular orientation, and covalent bonds. The swollen gel that a polymer has absorbed the dispersion medium generally shows molecular aggregation of morphology (A) or (B) in Figure 1. Both of them are two-component systems, and non-ionic gels belonging to (A) are the commonest. The morphology (B) shows polyelectrolyte as hydrogels, which repeatedly shrink and swell in response to external stimulations such as pH, salt concentration, composition of the solvent, ionic composition, temperature, electricity, and light, and the applications as mechanochemical actuators, which directly convert chemical energy into mechanical energy, is being evaluated (Tatara, 1989). Hydrogels categorized in (A) that gelatinizing materials absorbed water as the medium are popularly used as various foods and sanitary goods as well as biomaterials regarded as substitutes for biological gels. However, the medium, water evaporates with time in an open system. Therefore hydrogels are unstable and cannot be used excepting in the closed circumstance where water is always existing. Similarly, organic solvents in organogels, lipid solvents in lipogels and alcohol in alcoogels easily release from the gels with time because of poor interaction between gelatinizing materials and voluminous dispersion media. In view of the disadvantages of these swollen gels, more than 20 years ago, we had synthesized stable single component permanent gels, segmented polyurethane gels (SPUGs) (Shikinami, 1991, Shikinami, 1992) essentially consisting of a single gelatinizing component, of which almost all of segments in a

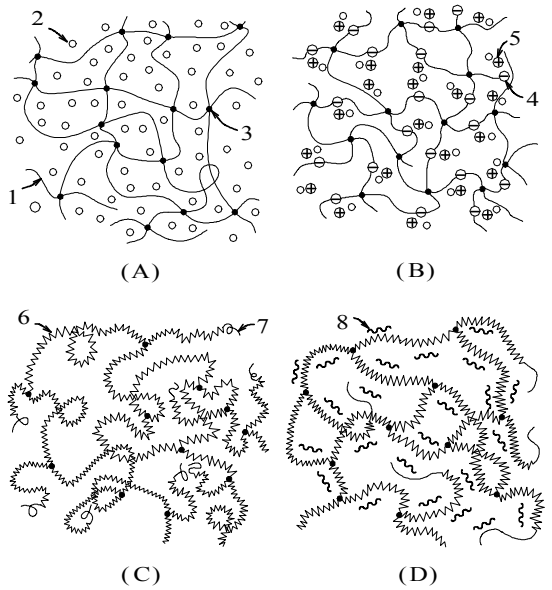

Figure 1: Morphologies of molecular aggregation of swollen gels. SPU consists of PAO (EO/PO) segments (liquid state at ambient temperatures). Swollen SPUG (D) incorporates liquid dispersion media among the PAO network.

1. molecular chain
2. dispersion medium (water, organic solvent, oil)
3. junction 4. ion group 5. pair ion
6. liquid segment 7. dangling chain
8. dispersive media

three-dimensionally cross -linked polymer and its dangling chains are in liquid state at ambient temperatures. Figure 1 (C) shows the molecular aggregation morphology of single component SPUGs, of which segments and dangling chains consist of low weight molecule, oligomers.

2 PURPOSE OF THIS STUDY

In SPUGs, liquid segments three-dimensionally entangles at junctions move fluidly and dangling chains with free terminals are not involved in the rigidity but increase the viscosity by serving as dispersion media. Therefore, SPUGs with much dangling chains are extremely flexible like highly viscous liquids and have an adhesive surface. A SPUG doped by $LiClO_4$ and a SPUG-alone have been respectively used for functional pressure-sensitive adhesives as skin contact media such as bio-electrodes (disposable electrodes, therapeutic electrodes for low-frequency electric stimulation) and acoustic coupler gels for ultrasonographic examination. In this research, we improved SPUGs into swollen SPUGs (S-SPUGs) without releasing excessive dispersive media in order to enhance the electric conductivity and ultrasound acoustic characteristics, which are flexible and remaining stable three-dimensional (3D) configuration as energy transmissible media for soft biomaterials (Figure 2).

Figure2: S-SPUG as an ultrasonographic coupler gel.

3 METHODS AND RESULTS

Methods, apparatuses and conditions used in this study summarized in Table 1 and each result of S-SPUGs with SPUGs was shown in Table 2.

Table 1: Methods.

	Method, Apparatus and Condition
Density	Density determination device with balance (METTLER TOLEDO Co., Ltd) in hexane at 25°C
Elasticity (Young modulus)	Venustron Biosensor (AXIOM Co., Ltd) at 23°C
Transparency Transmission rate at 600nm [%T]	UV-VIS spectrometry (SHIMADZU Co., Ltd) Wavelength; 600nm Sample thickness; 2mm / 10mm
Ultrasound velocity and attenuation	Sing-around method at 20°C and a reference
Attenuation	Sing-around method by means of UVM-2 (Ultrasonic Industry Co.)
Acoustic impedance	Sound velocity x density
Electric conductivity	Impedance analyzer Li/O = 5 / 100 Frequency(υ); 1kHz at 24°C
Fungus resistance	Test for Fungus Resistance (Japanese Industrial Standards Z-2911)

Table 2: Comparison of S-SPUGs with SPUGs.

Sample		Young modulus [Pa]	Transmission rate at 600nm [%T]	Ultrasound velocity [m/s]	Attenuation [dB/MHz cm]	Electric conductivity (Li/O=5/100) [S/cm]
SPUG	OH/NCO=2.10	4.1×10^{4}	t=2mm 90.0 t=10mm 88.8	1506	1.1	—
S-SPUG-I	OH/NCO=2.10 PC 50wt%	3.7×10^{4}	t=2mm 90.7 t=10mm 89.8	1468 (1450-1550)*	0.13	1.2×10^{-3}
S-SPUG-II	OH/NCO=1.45 TG 50wt%	1.18×10^{4}	t=2mm 90.0 t=10mm 89.3	(1477-1563)*	0.09	3.7×10^{-4}
Human body (Soft tissues)	—	Side abdomen 6.7×10^{4} Stomach 1.06×10^{5} Arm (outside) 1.45×10^{5} (inside) 2.01×10^{5}	—	1540	0.5	—

Density; SPUG=1.03, Swollen SPUG-I=1.13, Swollen SPUG-II=1.02
PC; Propylene carbonate, TG; Tetraglyme
PC 25wt%; E.C. = 5.0×10^{-4}S/cm, PC 60wt%; E.C. = 2.1×10^{-3} S/cm, TG 25wt%; E.C. = 1.1×10^{-4} S/cm
Li/O; ratio of Li ion versus ether oxygen in poly alkylene oxide as segments and dangling chains
OH/NCO; end group of PAO, OH versus end group of Isocyanate, NCO
* Depending upon the concentration of poly acrylic powder contained in the gel

3.1 Molecular Design of SPUGs and Swollen SPUGs

One method to obtain single component gels, of which category has never been found until we had developed (Shikinami, 1998), is to extend low-molecular weight polymers, which are liquid at room temperature, and to loosely crosslink them. SPUGs have liquid segments and dangling chains, which chemically compose of polyalkylene oxides (PAOs) (EO/PO; ethylene oxide and propylene oxide copolymer chains, preferably random copolymers) that function as a medium incorporated into cross-linking segmented polyurethane chains. We have practically used them so far in the field of medical engineering (ME) as skin contact media for energy transmission. Polyethylene glycol (PEG) and its mono methyl ether having molecular weights (Mw) of less than 600 and polypropylene glycol (PPG) having Mw of less than tens of thousands are liquid and flow at room temperature. Also copolymers of ethylene

oxide and propylene oxide (EO/PO) are viscous, fluid liquids at room temperature depending on the ratio of EO in EO/PO and the molecular weight. The aggregation energy of components of these PAOs (Bunn, 1955) and surface tension of the terminal groups and units of repetition are relatively low (0.8~1.77 Kcal/mol). The aggregation energy of the urethane bond (-NHOCO-) obtained as the OH group at the terminal of PAO reacts with the NCO group of poly isocyanate including liquid PAO (these groups are used as multi-functional groups for chain extension or formation of reticulation) is high at 8.74, and makes a highly restrained junction. Therefore, if a segmented polyether urethane (SPEU) consisting of almost all of liquid segments and having many dangling segments of M-PEG can be synthesized, it is expected to be a single component gel-state molecular aggregation. Figure 3

shows the structure of the basic molecule of SPUG. This selection was adequate, and many kinds of SPUGs could be obtained.

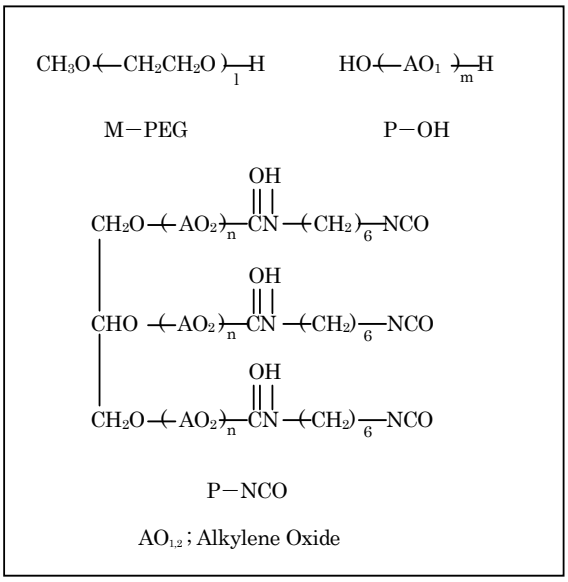

Figure 3: Structures of liquid molecular chains.

3.2 Electric Characteristics of SPUGs (Shikinami, 1991)

The mechanism by which complexes of PAOs, PEG or EO / PO copolymers and $LiClO_4$ enhance electric conductivity due to ionic conduction has already been clarified (Ccallum, 1987). Solid solution of $LiClO_4$ with PAO as a medium is produced by interaction between dipoles (ligands) in PAO and ions. Ionic conduction is originated when Li^+ moves to the other ether oxygen in the physical space with surfboard riding-like motion resulting from molecular movement of PAO (Wright, 1975) segments. As the glass transition temperature (Tg) of the PAO segments is lower, molecular movement becomes greater, and ionic conduction becomes higher, hence a greater specific electric conductivity. From this fact, SPUGs and $LiClO_4$ are also considered to form complexes with large specific electric conductivity because of their low Tg. This specific electric conductivity is obviously dependent on the molecular configuration of segments of PAO. In the ion-conductive SPUGs that we synthesized as skin contact pressure sensitive adhesives, the ionic conduction rate σ (S/cm) becomes highest when the segments of P-OH and P-NCO components are random copolymers of EO/PO (molar ratio: 50/50) was 10^{-4}~10^{-5} at RT~100°C, and 10^{-6} at 0°C when the salt concentration [Li] / [-0-] was 1/100 ~10/100. These values of ionic conductivity are considered to be one of the highest among various ion conductive PAO materials studied to date. This SPUG is presently used as the contact medium of disposable leads for electrocardiography and of stimulation electrodes of various low frequency therapeutic instruments. The SPUG conducts accurately various low-frequency waveforms through the electrode to the skin. However, SPUGs would be utilized in furthermore various ways if electric resistance were lower than these values by one figure, 10^{-3} (S/cm). S-SPUGs were developed for the purpose.

3.3 Ultrasound Acoustic Characteristics of SPUGs

Ultrasound characteristics, conduction velocity, acoustic impedance and absorption coefficient of body tissues have already been examined. Despite slight variations according to the water contents at different sites of the body, i.e. blood, brain, adipose tissue, kidney, liver, muscle, excepting bone, the velocity of ultrasound conduction is around 1,500m/s, and the ultrasound impedance (ρC), which is the product of the density and the sound conduction velocity, is about 1.4 to 1.7(10^6kg/m^2 s), approximately equal with water and the body fluid. Attenuation (α; dB/MHz cm) is about 0.2 to 3.3, while that of water is very low at 0.0022. These values of SPUGs are insufficient for use in the phantom gels for ultrasonograph and improved by S-SPUGs (α; 0.13) as shown in Table 2.

4 CONCLUSIONS

S-SPUGs increased electric conductivity and decreased ultrasound attenuation (impedance) of SPUGs remaining moldability with 3D stable configuration, so that these soft gels serve the potentialities of electroactive polymers for artificial muscles as the electric conductive media and of the stable phantom gel for ultrasound transmission according to the international quality standards that examine ultrasonographic faculty with good fungus resistance unlike unstable hydrogels. The casting moldability into stable 3D configuration and high flexibility give the artificial soft body and muscle for androids with the energy transmissible, transducing faculty (Minato, 2005), in addition to applications as skin contact media of existing SPUGs for disposable electrodes, therapeutic electrodes and ultrasonographic coupler gels.

REFERENCES

Bunn, C.W., 1955. *J. Polym. Sci*., 16, pp323-343.
Ccallum, J.R.M., 1987 and 1989. *Polymer Electrolyte Rev. 1 and 2. Elsevier Applied Science, London and New York*.
Minato, T., Shimada, M., Itakura, S., Lee, K., and Ishiguro, H., 2005. *Proc. of the 4th IEEE International Conference on Development and Learning*, pp.106-111.
Shikinami, Y., 1991. *Jpn. J. Adh. Soc.*, 27, pp526-533.
Shikinami, Y., Hata, K., Morita, S., and Kawarada, Y., 1991. *Jpn. J. Adh. Soc*., 27, pp266-274.
Shikinami, Y., Hata, K., Morita, S., and Kawarada, Y., 1991. *Jpn. J. Adh. Soc*. 27, pp313-319.
Shikinami, Y., Morita, S., Tsuta, K., and Taniguchi, M., 1992. *Jpn. J. Polym. Sci. and Tech*., 49, pp19-28.
Shikinami, Y., Morita, S., Tsuta, K., and Taniguchi, M., 1992. *Jpn. J. Adh. Soc*. 49, pp29-36.
Shikinami, Y., Tsuta, K., and Taniguchi, M., 1998. *Jpn. Soc. Polym. Sci.* 47, pp356.
Tatara, Y., 1989. *Functional & Materials*. 9, pp53-57.
Wright, P.V., 1975. *Br. Polym. J*., 7, 319.

PATIENT-ADAPTABLE BIOMEDICAL DEVICES
Benefits and Barriers for Granting Patients More Control

James Andrew Smith and André Seyfarth
Locomotion Laboratory (Lauflabor), Institute for Sports Science, University of Jena, Jena, Germany
jasmith@cim.mcgill.ca, oas@uni-jena.de

Keywords: Orthosis, prothesis, implanted medical device, insurance, risk, control, adaptability.

Abstract: End-users of biomedical devices, like many patients undergoing treatment in healthcare systems, often demonstrate an active interest in their therapy. Patient-specific customization of medical devices, such as orthoses, prostheses and implants, is an expensive, time-consuming process. Given how many of these patients are pro-active and self-motivated it seems appropriate to the authors that these characteristics be harnessed to make the adaptation of the device to the patient more cost effective. In short, it is proposed that the device end-user – the patient – play an active role in the tuning and adaptation of the device, especially in the out-patient context. However, the perceived risk associated with a more pro-active and independent role for the patient is a barrier to this possibility. These factors are examined and a proposal for a practical approach to a patient-controlled device optimization process is put forward.

1 INTRODUCTION

The customization of medical devices, such as orthoses, prostheses and implants, to the patient is an expensive, time-consuming process. By reducing factors which lead to patient noncompliance and by harnessing the pro-active and self-motivated nature of many patients it is likely that the patient-device adaptation process can be made more cost effective. The barriers towards granting greater control to patients in the updating process will also be examined. Finally, general strategies that are conducive to the development and use of adaptable devices are put forward.

2 WHY PATIENT-ADAPTABLE DEVICES?

Here, we examine general issues related to treatment procedures which involve biomedical devices, as well as reasons why adaptable devices can prove beneficial to such situations.

In traditional medical practice, physical proximity between medical personnel and patients is desirable and often necessary. Often, patients travel to clinical settings to obtain medical services such as check-ups and monitoring. In other cases, emergency or not, medical personnel undertake the travelling to visit patients. In both cases, the associated costs with travelling and visitation, in terms of both time and money, can be important. In fact, these costs can quickly rise when the patient normally resides in a remote community which has insufficient medical resources. Additionally, delays associated with transport can have adverse effects on the treatment of both diagnosed and undiagnosed conditions.

In addition to distance playing a role on transportation costs, frequency of visits can also have a significant effect on costs and effectiveness of treatment. The customization of medical devices, whether they be implantable medical devices (IMD) or external protheses or orthoses, often requires frequent visits by the patient to a clinical setting. Delays are often encountered due to complications in both patient and medical personnel schedules. This can lead to missed appointments or a reduction in the optimal number of scheduled visits. Both situations can have adverse effects on patient treatment regimes. Therefore, solutions which reduce the requirement for physical transportation of either patients or medical personnel, to or

from clinical settings are desirable.
Treatment associated with the prosthetic devices almost always requires multiple meetings between clinician and patient. When available, telemetry gathered by the device (either under in- or out-patient conditions) can be provided during these sessions to the clinician, complementing the traditional discussions between patient and clinician. To ensure optimal effect of the device on the patient such information will be monitored over the course of many sessions. In the process, changes to the device, or complete replacement of the device can occur. The reasons for this vary from suboptimal tuning of the device to a breakdown of the device, as well as to changes in the patients condition or environment conditions that the patient encounters.
Changes in the aforementioned conditions can happen outside the clinical setting. In the event of such changes it is advisable that appropriate actions be taken as quickly as possible. This is especially important where the change in condition has an adverse effect that could endanger the patient. Even in cases where the change does not endanger the patient, but leads to discomfort or diminished confidence in the device, it is advisable that the problem be addressed relatively quickly. Therefore, solutions that ensure a high frequency of monitoring and updating are desirable. However, updating or adaptation of the device does not necessarily need to be done by a clinician or therapist. In cases of misadjustment of a prosthetic leg, the resulting skin ulcers can dramatically reduce a patient's ability to use the prosthetic device, with a consequent reduction or total loss of mobility (Brandt, 2004). The ability of a patient to actively modify the device without the need for clinical supervision can be beneficial when such services are unavailable or impractical. This is apparent in the treatment of pain through the use of patient-adjustable bracing (Draganich et al., 2006) or in cosmetic and comfort adjustments with respect to heel height in foot prosthetics. In these cases, it is far more practical to allow the patient to make adaptations without direct clinical supervision. This is especially relevant since, as will be discussed in the next section, treatments that reduce ambulation ability can also become more vulnerable to patient non-compliance (Aldridge et al., 2002).
The goal of the clinical visitations is often related to monitoring a patients general health and the status of any diagnosed condition. In the cases that the patient has been previously prescribed a medical device related to a diagnosed condition the health service provider often uses the clinical visitation time to also monitor the condition of the medical device. Updates to the device may also be performed during this time, as the health care provider is often an expert in the adjustment of such devices. Outside of the clinical setting, prior-art (Bardy, 2003) demonstrates that such device monitoring and update work can also be done in an autonomous and remote fashion. While these devices are not necessarily directly adaptable by the patient, they do contain the functionality for adaptability outside the clinical setting. A number of patents (Duffin et al., 1995) (Linberg, 1999) have been assigned for such remote expert system updatability , including at least one which permits the patient to input activity and environmental conditions for optimal implant performance (Boies et al., 2000).

Although customizable and updatable systems (remotely or locally) can have both therapeutic and cost benefits, there are barriers to their implementation. The next section explores some of these issues.

3 BARRIERS TO PATIENT-ADAPTABLE DEVICES

The development and use of patient-adaptable biomedical devices shares many of the same barriers encountered in by any biomedical device.

First, regardless of the intention of the clinician or manufacturer, without patient compliance the device will be ineffective. A patient's existing living conditions or environment may not be compatible with the proposed device and treatment strategy (Pinzur et al., 1992). Likewise, psychological or physiological factors may preclude usage of the device. Without proper counselling and education, cognitive, motivational and emotional barriers can also be barriers to effective use of a given medical device (Pinzur et al., 1992).

The possibility of critical failure of a device, especially in cases where such failures can place people in danger, must be weighed by manufacturers, end-users and prescribers of such devices. This applies to many fields, not just the biomedical field.

In the case of lower extremity prosthetic or orthotic devices the possibility of falling is of particular concern, as such falls can lead to serious injury or death. With some justification, the fear that such an event can occur is "pervasive" (Miller et al., 2001) within the amputee community. This leads to particular lines of action by both device manufacturers and patients to reduce the possibility of fall.

Actual falls, as well as the fear of falling can have repercussions on mobility and social activities. The psychological effects related to the fear can lead to

self-imposed restrictions which, in turn, lead to deterioration in physiological conditions (Miller et al., 2001). Given that this downward spiral runs counter to the original intentions when equipping an amputee with a prosthetic leg, it is important that the possibility of fall and the related fear be addressed as seriously and openly as possible.

The evaluation of risk, either by a patient or a device manufacturer can have serious ramifications, both positive and negative. During the risk evaluation process it is important to remember that risk determination should not only be founded on the device itself but also on the proposed use of the device. This requires weighing the risk against the beneficial uses of the device. If the addition of a feature promotes the use of the device, either through increased user convenience or confidence, the short-term possibility of increased user risk for falling may be offset by lessened possibility of longer-term psychological consequences, as outlined above.

4 THE WAY FORWARD

Devices which maximize user comfort, convenience and confidence are most likely to be successful in patient treatment. In cases such as treatment of Charcot's Foot, total contact casting is the "gold standard" for treatment, patient non-compliance plays a roll in its relatively high failure rate. The reduced mobility that results from such treatment can be so deleterious, and thereby resulting in patient non-compliance, that alternative forms of treatment have been developed that allow the patient some form of ambulation (Aldridge et al., 2002). The device should, if at all possible, usable within the patient's existing lifestyle, which in many cases requires a significant degree of mobility.

The development of patient-adaptable devices is an effective avenue for many forms of treatment. These are especially effective when the patient feels an immediate and persistent self-motivation with respect to the device. One such example, that of patient-adjustable valgus-producing knee braces, can have immediate, short-term pain- and stiffness-relief benefits for patients (Draganich et al., 2006). Devices such as the Ossur Elation and Proprio feet allow the amputee to adjust heel height, thus permitting the use of high-heel shoes, for instance. While the use of these types of shoes may place the amputee at greater risk for fall, the long-term psychological consequences of this convenience would seem to outweigh the short-term physical risk. Of course, to maximize the potential of these adjustable devices, the adjustment mechanisms must be as convenient as possible.

Making the device convenient to use is not sufficient, however. While its use and its adjustment mechanisms (if any) may seem intuitive to an expert, this cannot be assumed to be the case with the patient. Given that non-compliance can, in many cases, be traced to misunderstanding by the patient (Smith and Smith, 1994), it is important that special attention be paid to patient education. The practitioner should be especially aware of the fact that relevant documentation often given to the patient is written in a manner which leads to misunderstandings (Smith and Smith, 1994). Therefore, patient education – which is intimately tied to the notion of informed patient consent – should be tailored to the comprehension level of each patient in order to reduce the possibility of patient non-compliance based on misunderstanding.

Simply allowing the patient to make active changes to the device, as outlined above, is not the only strategy for involving the patient in the therapy "feedback loop". Within the clinical context (i.e. under the direction of a trained therapist or clinician), a device that adapts to the patient in a semi-autonomous fashion has enormous potential. The device can take a co-operative approach to the patient interface and does not necessarily require direct or conscious adaptation strategies by the patient. In fact, "human-centred robotic" gait trainers are currently being developed which combine robotic mechanisms that adapt their movement to the muscular efforts of the patient, as well as the patient's passive mechanical properties (Riener et al., 2006). These patient-adaptable devices still require the expertise of therapists to develop strategies for therapy, but promise to increase patient comfort and therapy effectiveness.

From a manufacturer's point of view, the calculation of acceptable risk for device feature sets must be conducted. This begins with setting a threshold for tolerance of risk, followed by the determination of a device's intended use and required feature set. Next, the feature-by-feature risk is estimated by examining the probability of a given event and the consequent level of operator or patient harm. Features which approach the tolerance threshold will require special justification with respect to physiological or psychological benefits, while those which exceed it must be discarded. Next, testing is conducted to verify the assumptions on which the risk levels are based, alarm and compensatory devices are implemented. Finally, the cycle is repeated until verifications produce results which match the declared risk tolerance threshold. This process is a straight-forward one that results from an attempt to adhere to risk management strategies that conform to international standards such as

ISO 14971 and IEC 60601-1; these standards are, in turn, a result of regulatory requirements by national and international agencies.

Finally, the device must be made affordable to the patient in absolute terms, as well as relative to possible alternatives which may or may not include adjustable functionality. Where alternatives include immobilization and long-term hospitalization, it is critical that comparisons be made with respect to the additional costs related to diminished mobility. Given the role of third-party payees such as government agencies or private insurance companies, the cost of such devices must also be justifiable to them. This is especially important in cases where utilization management and technology assessment studies result in limited outcomes due to small sample size or absence or randomized controlled trials in peer-reviewed journals (Fish, 2006). Therefore, rigourous and independent case-by-case studies need to be made to verify the potential short-term (e.g. adjustable valgus-producing knee unloader braces) and longer-term (e.g. the adjustable heel height feet) benefits of patient-adjustable biomedical devices.

5 CONCLUSIONS

The benefits for adaptable prosthetic devices has been examined, as have the barriers for both these and biomedical devices in general. General strategies for implementation have been examined, as well. In the end it is important for trained personnel to make a holistic evaluation of the patient, taking into account patient lifestyle issues, physiological and psychological factors, costs, requirements by third-party payees, etc. Engaging the patient through education and good design practice are key to the development and use of these types of devices.

ACKNOWLEDGEMENTS

The authors would like to thank Donald Smith, Cathy Huth and Michelle Huth for their feedback. As well, the authors would like to thank the following people for their valuable input: Dr. Robert Farley at the Scottish Executive Health Directorate, Drs. Stefan Bircher and Burkhard Zimmerman at Hocoma AG Medical Engineering, Roland Auberger at Otto Bock Health Care, and Knut Lechler at Ossur R&D.

REFERENCES

Aldridge, R., Jamali, M., Guffey, J. S., Yates, D. A., and Ward, M. (2002). Patient compliance: its relevance to the management of a patient with charcot's foot. *Int J Low Extrem Wounds*, 1(3):179–183.

Bardy, G. H. (2003). System and method for collection and analysis of patient information for automated remote patient care. US Patent 7,134,996, Cardiac Intelligence Corporation, Seattle, WA, USA.

Boies, S. J., Dinkin, S., Greene, D. P., Grey, W., Moskowitz, P. A., and Yu, P. S. (2000). Apparatus, system, method and computer program product for controlling bio. US Patent 6,539,947, International Business Machines, Armonk, NY, USA.

Brandt, R. (2004). The right fit. *View*, pages 22 – 25.

Draganich, L., Reider, B., Rimington, T., Piotrowski, G., Mallik, K., and Nasson, S. (2006). The effectiveness of self-adjustable custom and off-the-shelf bracing in the treatment of varus gonarthrosis. *J Bone Joint Surg Am*, 88(12):2645–2652.

Duffin, E. G., Thompson, D. L., Goedeke, S. D., and Haubrich, G. J. (1995). World wide patient location and data telemetry system for implantable medical devices. US Patent 5,752,976, Medtronic, Inc., Minneapolis, MN, USA.

Fish, D. (2006). The development of coverage policy for lower extremity prosthetics: The influence of the payer on prosthetic prescription. *Journal of Prosthetics and Orthotics*, 18(1S):125 – 129.

Linberg, K. R. (1999). Apparatus and method for automated invoicing of medical device systems. US Patent 6,385,593, Medtronic Inc., Minneapolis, MN, USA.

Miller, W. C., Speechley, M., and Deathe, B. (2001). The prevalence and risk factors of falling and fear of falling among lower extremity amputees. *Arch Phys Med Rehabil*, 82(8):1031–1037.

Pinzur, M. S., Littooy, F., Daniels, J., Arney, C., Reddy, N. K., Graham, G., and Osterman, H. (1992). Multidisciplinary preoperative assessment and late function in dysvascular amputees. *Clin Orthop Relat Res*, 281:239–243.

Riener, R., Lunenburger, L., and Colombo, G. (2006). Human-centered robotics applied to gait training and assessment. *J Rehabil Res Dev*, 43(5):679–694.

Smith, C. R. and Smith, C. A. (1994). Patient education information: Readability of prosthetic publications. *Journal of Prosthetics and Orthotics*, 6(4):113 – 118.

AN RFID TRANSPONDER LOCATION SYSTEM

Mou Tang, Graeme Chester and Jeffrey Neasham
School of Electrical, Electronic and Computer Engineering, Newcastle University, Newcastle upon Tyne, UK
mou.tang@ncl.ac.uk, graeme.chester@ncl.ac.uk, j.a.neasham@ncl.ac.uk

Keywords: CDMA, Location, RFID Transponder.

Abstract: This paper describes a location system based on RFID technology. This system can be used to map the image of an endoscope. Compared with other endoscope location systems, this is a wireless system. The transponder mounted along the shaft of an endoscope does not increase the size of the endoscope or affect the flexibility of endoscope. We build the mathematical model of this location system and verify this model by experiments. Although experiments are for a transponder moving along one dimension, we can develop a three-dimensional system based on our results.

1 INTRODUCTION

The magnetic endoscope imager (MEI) system was developed independently by (Bladen, 1993) and (Williams, 1993). The physical principles of the three-dimensional location system are straightforward. The image of the endoscope is mapped in three dimensions using a set of coils that are installed in the instrument along the shaft. Coils measure the rate of change of the magnetic field flux according to Faraday's law of induction: the change in magnetic flux through the coil produces a voltage in the coil circuit. Since the voltage depends uniquely on the location (x-y-z) and orientation ($\theta - \varphi$) of coil, it is possible to get the location and orientation information of each coil. This information is collected several times each second, and is used to map the image of the endoscope.

The dimensions of the coil are critical to sensitivity (and to some extent to location accuracy). The larger is the coil, the greater is the sensitivity. However to fit the physical size of an endoscope, a typical size of coil is 1 cm long along the axis of instrument. Low frequency fields render the body transparent and low field strengths ensure safety (Bladen, 1993).

One advantage of a magnetic imager system is the elimination of the need to pass a separate imaging catheter during procedures, thereby freeing the accessory channel for suctioning, lavage, and therapeutic manoeuvres (Friedland, 2002). The other advantage is that the loops in the path of endoscope become clear in the MEI system (Bladen, 1993) compared with a conventional radiological imager system.

Research work by (Bladen, 1993), (Wehrmann, 2002), (Shah, 2002) and (Geng, 2004) proves that MEI is a reliable and accurate method. The systems studied in their work are cabled systems. Voltage signal are communicated by leads connected to coils. The more coils that are used, the more leads are mounted along the shaft of instrument. The leads increase the diameter and affect the flexibility of the instrument. In this paper, we describe a wireless location system which can be a replacement of the previous cabled system. In our system, we replace the coils with RFID (Radio Frequency Identification) transponders which load the read circuit in a changing pattern over time and identify each transponder by ID information stored in it.

2 RFID & CDMA BACKGROUND

We identify each transponder by ID information stored in it. Here, we use spread-spectrum codes to program transponders. The following parts describe the characteristics of RFID and CDMA technology and explain the reasons why we use spread-spectrum codes to program RFID transponders in our system.

2.1 RFID Technology

RFID technology has existed for many decades. An RFID system consists of two components: RFID transponder and reader (Finkenzeller, 2003).

Normally the reader is connected to a computer and used to read and write data. The RFID transponder is programmed with a unique code and located on object to be identified. The RFID transponder can be active or passive (Weinstein, 2005). The built-in battery of the active transponder increases its size and limits its applications. In this paper, when we say RFID transponder, it is a passive transponder.

Passive transponders operate at different frequencies. As mentioned before, we chose a low frequency transponder in our system. The size of the passive transponder can be as small as several millimetres, such as TK5552 (Atmel, 2003) which is only 12 mm long with plastic housing. The length of TK5552 is almost the coil's length used in (Bladen, 1993). The power in the electromagnetic field received from the reader is the only power used for the data transmission between reader and transponder (Finkenzeller, 2003).

The operating principle of the RFID transponder is transformer-type coupling between transponder and reader. When the transponder is in a magnetic field, the alternating current in the reader coil induces a current in the transponder's antenna coil and this current is used to power the transponder electronics. ID infromation stored in the transponder is sent back to the reader by loading the transponder's coil in a changing pattern over time, which affects the induced e.m.f. in the reader (Want, 2004). This process is called load modulation.

2.2 CDMA Technology

As described in Part 1, we find the image of the endoscope by locating transponders installed along the shaft of the endoscope. Our system is a wireless system, and all transponders share the same frequency resource, so the received signal is a combination signal from all transponders. To separate each transponder's signal at the receiver, we program each transponder with a different spread-spectrum code. When the received signal goes through a corresponding correlator, each signal is separated individually. But this does not mean we can use an unlimited number of transponders in our system. MAI (Multiple Access Interference) is a factor which limits our system performance.

The other reason that we use spread-spectrum code is to increase SNR. We know the modulation method for RFID system is load modulation. Since the RFID transponder we used is very small (diameter of TK5552 is less than 3 mm) (Atmel, 2003), and it works at a long distance (up to 35 cm), the coupling of transponder coil and reader coil is very weak. This results in the voltage variation on the reader coil being very small. The location and orientation of each transponder are calculated by this voltage. To get accurate location information, we need to increase SNR. The definition of processing gain of a spread spectrum system tells us if the spread-spectrum code is N bits long, the processing gain is N (Proakis, 2001) and SNR in dB increases by

$$SNR_{improved} = 20\log_{10} N \tag{1}$$

Now we can see, by combinating RFID and CDMA techonology, it is possible to replace wired coils in previous systems with RFID transponders.

3 LOCATION THEORY

To estimate each transponder's location (x-y-z), three pairs of circular coils are used in this system. Each axis has a pair of parallel co-axial reader coils like Figure (3). We use two parallel reader coils instead of one reader coil on each axis for two reasons. One reason is to get powerful enough fields to activate the RFID transponder, and the other is to cancel the effects due to modulation index. Part 4.1.2 gives the explanations in details.

We start from a simple case: the transponder moves along the x direction. If we can locate a transponder which moves along the x-axis or moves along a trail parallel to the x-axis, it is possible for us to extend it to three dimensions by replication.

The detected voltage signal at the reader coil is an induced voltage which depends on the mutual inductance of the reader coil and transponder coil. To locate a transponder is to find out the mathematical relation of this induced voltage and distance between reader coils and transponder coil. This part aims to find out this relation.

3.1 Mutual Inductance of Coils

The Biot-Savart law tells us that the magnetic field flux density B at any point P of a circular coil can be calculated by (Stratton, 1941):

$$B_{axis} = \frac{\mu_0 I}{2\pi}\eta[K(k) + \frac{(a^2 - r^2 - x^2)}{(a-r)^2 + x^2}E(k)] \tag{2}$$

$$B_{radius} = \frac{\mu_0 I}{2\pi}\frac{x\eta}{r}[-K(k) + \frac{(a^2 + r^2 + x^2)}{(a-r)^2 + x^2}E(k)] \tag{3}$$

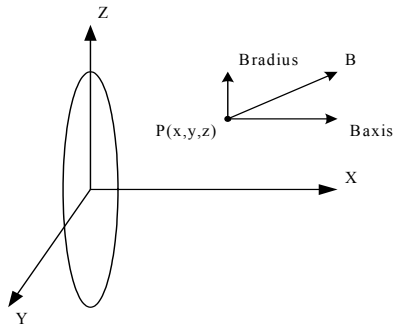

Figure 1: B-field of a circular coil.

μ_0 is the permeability constant of free space;

I is the current in the coil;

$\eta = \dfrac{1}{\left[(a+r)^2 + x^2\right]^{\frac{1}{2}}}$;

a is the radius of the reader coil;

x is the distance to the reader coil;

$r = \left[y^2 + z^2\right]^{\frac{1}{2}}$ is the distance to axis of reader coil;

$k = \sqrt{\dfrac{4ar}{(a+r)^2 + x^2}}$;

K(k) and E(k) are complete elliptical integrals of the first and second kinds.

When a small single loop coil is in the field of this circular coil, we assume that small coil is situated in a uniform flux density B. The mutual inductance of two coils is

$$M = \frac{B_{axis} S \cos\alpha + B_{radius} S \sin\alpha}{I} \qquad (4)$$

S is the plane area bounded by the small coil;

α is the angle between $\vec{S}$ and the x-axis.

Equation (4) gives the relationship between mutual inductance and distance of two coils.

3.2 Induced Voltage

Assuming a transponder moving in the x direction, we only need the pair of parallel coaxial reader coils on the x-axis to determine the transponder's x-location. Our RFID location system's topology for a pair of reader coils is shown in Figure 2. It is a 3-coil coupling system. This means that the received signal at any reader coil is a combination of signal from transponder coil and signal from the other reader coil.

In the system, AC power source is used to drive two reader coils and generate magnetic fields to activate RFID transponder. It does not contribute to the received signal.

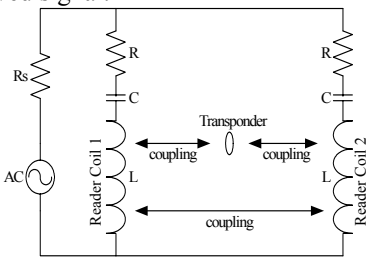

Figure 2: Topology of RFID transponder location system.

A real system's arrangement looks like Figure 3.

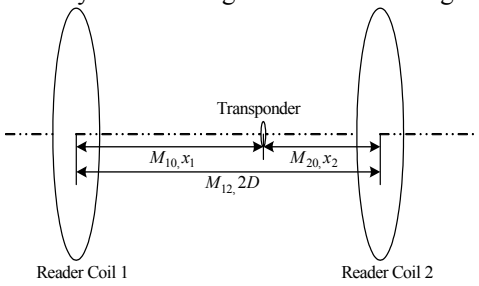

Figure 3: Three coils coupling system.

M_{10} is the mutual inductance of reader coil-1 and transponder;

M_{20} is the mutual inductance of reader coil-2 and transponder;

M_{12} is the mutual inductance between reader coils;

x_1 is the distance of transponder to reader coil-1;

x_2 is the distance of transponder to reader coil-2;

2D is the distance between two reader coils.

Assume the complex current in the transponder is $\mathbf{I_0}$, and $\mathbf{I_0} = I_0 e^{j\omega t}$. The induced complex voltages on reader coil-1 $\mathbf{V_{10}}$ and on reader coil-2 $\mathbf{V_{20}}$ are

$$\mathbf{V_{10}} = j\omega M_{10} \mathbf{I_0} \qquad (5)$$

and

$$\mathbf{V_{20}} = j\omega M_{20} \mathbf{I_0} \qquad (6)$$

Complex current $\mathbf{I_{20}}$ in reader coil-2 due to $\mathbf{V_{20}}$ is,

$$\mathbf{I_{20}} = \frac{\mathbf{V_{20}}}{\mathbf{Z_2}} = j\omega M_{20} \frac{\mathbf{I_0}}{\mathbf{Z_2}} \qquad (7)$$

where $\mathbf{Z_2}$ is the total impedance of terminals 2a and 2b in Figure 4.

The induced voltage on reader coil-1 $\mathbf{V_{12}}$ due to $\mathbf{I_{20}}$ is

$$\mathbf{V_{12}} = -\omega^2 M_{12} M_{20} \frac{\mathbf{I_0}}{\mathbf{Z_2}} \tag{8}$$

So the received complex voltage on reader coil-1 is

$$\mathbf{V_1} = j\omega M_{10}\mathbf{I_0} - \omega^2 M_{12} M_{20} \frac{\mathbf{I_0}}{\mathbf{Z_2}} \tag{9}$$

In the same way, we can find the received complex voltage on reader coil-2 is

$$\mathbf{V_2} = j\omega M_{20}\mathbf{I_0} - \omega^2 M_{12} M_{10} \frac{\mathbf{I_0}}{\mathbf{Z_1}} \tag{10}$$

where $\mathbf{Z_1}$ is the total impedance of terminals 1a and 1b in Figure 4.

Two reader channels are symmetric, so we have

$$\mathbf{Z} = \mathbf{Z_1} = \mathbf{Z_2} \tag{11}$$

When the distance of two reader coils is fixed, the mutual inductance of two reader coils M_{12} is a constant. We define

$$\lambda = \frac{\omega M_{12}}{\mathbf{Z}} \tag{12}$$

Equation (9) and (10) are

$$\mathbf{V_1} = \omega \mathbf{I_0}(jM_{10} - \lambda M_{20}) \tag{13}$$

and

$$\mathbf{V_2} = \omega \mathbf{I_0}(jM_{20} - \lambda M_{10}) \tag{14}$$

When we only take the coupling data signal into account, the system in Figure 2 can be converted into Figure 4. There are two signal sources in system $\mathbf{V_1}$ and $\mathbf{V_2}$. Both of them contribute to the received signal at reader coils.

When the resonant frequency of two read channels is equal to the frequency of AC power source, the impedance of the read channel is resistive and λ in Equation (12) is real. The received complex signal at reader coil-1 $\mathbf{V_{r1}}$ is

$$\mathbf{V_{r1}} = \omega^2 L \mathbf{I_0}\left[\left(\frac{M_{20}}{\rho_2} - \frac{M_{10}}{\rho_1}\right) + j\lambda\left(\frac{M_{10}}{\rho_2} - \frac{M_{20}}{\rho_1}\right)\right] \tag{15}$$

where $\rho_1 = \dfrac{R^2 + 2RR_s}{R + R_s}$ and $\rho_2 = \dfrac{R^2 + 2RR_s}{R_s}$.

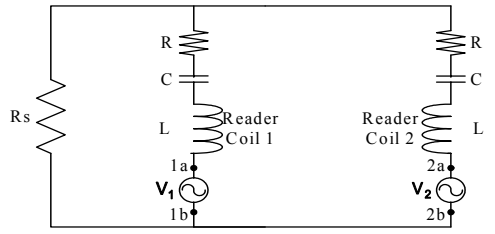

Figure 4: Simplified system topology.

The amplitude of received signal on reader coil-1 V_{r1} is

$$V_{r1} = \omega^2 L I_0 \sqrt{\left(\frac{M_{20}}{\rho_2} - \frac{M_{10}}{\rho_1}\right)^2 + \lambda^2\left(\frac{M_{10}}{\rho_2} - \frac{M_{20}}{\rho_1}\right)^2} \tag{16}$$

The amplitude of received signal at reader coil-2 V_{r2} is similar to reader coil-1

$$V_{r2} = \omega^2 L I_0 \sqrt{\left(\frac{M_{10}}{\rho_2} - \frac{M_{20}}{\rho_1}\right)^2 + \lambda^2\left(\frac{M_{20}}{\rho_2} - \frac{M_{10}}{\rho_1}\right)^2} \tag{17}$$

The ratio of two received signal is

$$\frac{V_{r1}}{V_{r2}} = \frac{\sqrt{(\rho - M_{ratio})^2 + \lambda^2(\rho M_{ratio} - 1)^2}}{\sqrt{(\rho M_{ratio} - 1)^2 + \lambda^2(\rho - M_{ratio})^2}} \tag{18}$$

where $\rho = \dfrac{\rho_1}{\rho_2}$ and $M_{ratio} = \dfrac{M_{10}}{M_{20}}$.

3.3 Induced Voltage and Distance

Equation (2), (3) and (4) tell us when the transponder only moves in the x direction, M is a function of x and α. Equation (4) is:

$$\frac{B_{axis} S \cos\alpha + B_{radius} S \sin\alpha}{I} = F(x, \alpha) \tag{19}$$

$$M_{ratio} = \frac{F(x_1,\alpha)}{F(x_2,\alpha)} \tag{20}$$

$x_1 = D + x$ and $x_2 = D - x$

$$M_{ratio} = \frac{F(D+x,\alpha)}{F(D-x,\alpha)} = M(x,\alpha) \tag{21}$$

We define

$$V_{ratio} = \frac{V_{r1} - V_{r2}}{V_{r1} + V_{r2}} = \frac{\sqrt{\left[\rho - M(x,\alpha)\right]^2 + \lambda^2\left[\rho M(x,\alpha) - 1\right]^2}}{\sqrt{\left[\rho M(x,\alpha) - 1\right]^2 + \lambda^2\left[\rho - M(x,\alpha)\right]^2}} - 1 \Big/ \sqrt{\frac{\left[\rho - M(x,\alpha)\right]^2 + \lambda^2\left[\rho M(x,\alpha) - 1\right]^2}{\left[\rho M(x,\alpha) - 1\right]^2 + \lambda^2\left[\rho - M(x,\alpha)\right]^2}} + 1 \tag{22}$$

The left of Equation (22) is V_{ratio}, which is determined by the received signal at two reader coils. The right of Equation (22) is a function of transponder's location x. Equation (22) gives out the relation of received signal at two reader coils and the location of the transponder. We will explain why we use voltage ratio $\frac{V_{r1} - V_{r2}}{V_{r1} + V_{r2}}$ to describe our system in Part 4.1.2.

4 EXPERIMENTS

In Part 3 we gave the mathematical description of the location system. The theory is validated by experimental measurements in this section and it will be shown that the system performs as predicted, even though some difficulties arise in implementation.

4.1 Problems in Implementation

4.1.1 Physical Size Effects and Calibration

In Part 2, we assume the RFID transponder is an ideal small point and the reader coils are filamentary. This means that the physical sizes of transponder and reader coils are not taken into account. But for a real system, this is not true. The physical centres of the read coils and the transponder are not the magnetic centres of the read coils and the transponder any more. To make sure the theory in Part 2 works, we should choose a transponder as small as possible. And we need to determine the effective magnetic centres of the transponder and two reader coils.

The magnetic centre can be determined by experiments. First, we estimate any point of a transponder as magnetic centre and put the transponder at any point of the axis in two opposite directions like Figure 5. If this point is the real magnetic centre of transponder, the voltage ratios for these two directions should be the same. Otherwise we need to adjust the estimated centre position until the two ratios are equal.

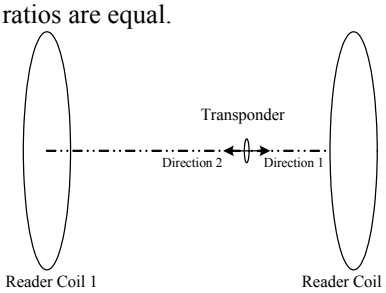

Figure 5: Determination of the magnetic centre of reader coils and transponder coil.

After we find the magnetic centre of the transponder, we can use the transponder to determine the original point of our location system. Moving the transponder along the axis of the reader coils, the point which satisfies the voltage ratio in Equation (22) equal to zero is the centre of the reader coils and is the original point of the location system as well.

4.1.2 Modulation Index

The transponder is powered by the magnetic fields, so the strength of the magnetic fields also affects the received signal. Figure 6 is our measured modulation index of the RFID transponder TK5552 used in our experiments. And Figure 6 agrees with TK5552's data sheet.

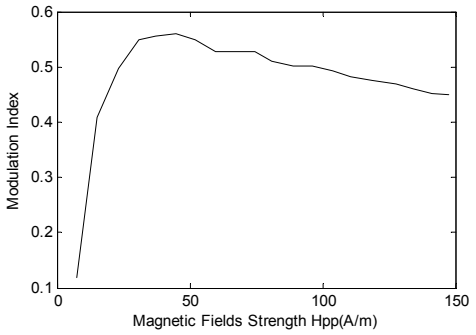

Figure 6: Modulation index versus field strength.

It is clear that the modulation index is not a constant. This means that the received signal is not only dependent on the distance but also affected by the modulated index. This is why we use voltage ratio (between two parallel reader coils) instead of voltage itself to describe our location system in Part 3.

The non-constant modulation index means there is no determinate relation between voltage of received signal and transponder's location. If we use a voltage ratio based system, modulation index effects are cancelled. In fact, when we use voltage ratio, the numbers of turns in the reader coils and transponder coil are cancelled as well.

In Part 3, we use voltage ratio $\frac{V_{r1}-V_{r2}}{V_{r1}+V_{r2}}$ instead of $\frac{V_{r1}}{V_{r2}}$ to describe our system. Figure 7 and Figure 8 are voltage ratio curves of $\frac{V_{r1}}{V_{r2}}$ and $\frac{V_{r1}-V_{r2}}{V_{r1}+V_{r2}}$ when the transponder moves along the x-axis. The signal received on one reader coil becomes small when the transponder is close to the other one. Due to the limited precision of the ADC used to capture data, there is an error in the received signal. From Figure 7, we can see that an error in a small received signal will result in a large error in $\frac{V_{r1}}{V_{r2}}$. To reduce this quantisation error, we use $\frac{V_{r1}-V_{r2}}{V_{r1}+V_{r2}}$ to derive position as shown in Figure 8.

4.1.3 Constant λ and ρ

In Equation (22), we define two constants λ and ρ, once the system is built, the values of these are also determined. However it is difficult to determine their exact values by the definition in Part 3 for a real system. Fortunately Equation (22) tells us that λ and ρ can be estimated by voltage ratio and distance.

$$[\lambda,\rho] = X(V_{ratio},x,\alpha) \tag{23}$$

In Part 4.1 we have determined the original centre of the location system, so it is possible to measure a transponder's location and angle. By putting a transponder at any point on the axis, we can get a set of voltage ratio and location data. Using two sets of voltage ratios and locations (V_{ratio1}, x_1) and (V_{ratio2}, x_2), we can estimate the values of λ and ρ. To get a much more accurate calculation of λ and ρ, we can use several sets of (V_{ratio}, x) at different points to estimate their values.

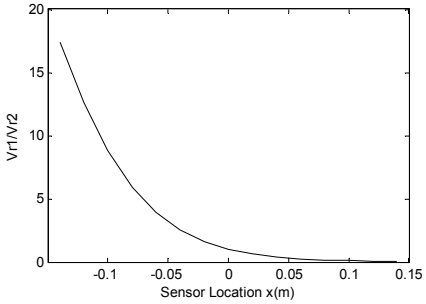

Figure 7: Voltage ratio curve of Vr1/Vr2.

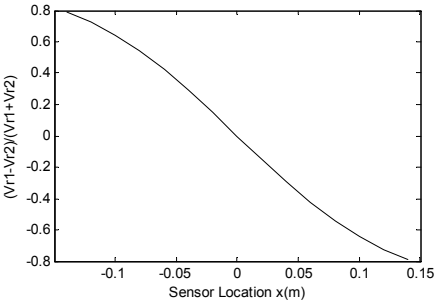

Figure 8: Voltage ratio curve of (Vr1-Vr2)/(Vr1+Vr2).

4.2 Experiment Results

After solving the problems faced in a real system, we have constructed a system to verify our theory in Part 3. The parameters of the system are as follows:

- The number of reader coil turns N=20;
- The radius of reader coil a=24.5 cm;
- The separation of two reader coils= 35.6 cm;
- RFID transponder is TK5552;
- The constant $\lambda = 0.046$ and $\rho = 0.13$.

Our experiments measure a transponder moving along the x direction. To extend a one dimension system to three dimensions, we need to test the transponder moving not only along the x-axis, but also along trails parallel to the x-axis. We also need to take angle into account. Since three axes are orthogonal each other, we only measure the worst case: angle is 45 degrees. When the angle is beyond 45 degrees with one axis, it means the angle with another axis is smaller than 45 degrees.

Figures 9 to 11 are experimental results. Figure 9 shows voltage ratio curves for a transponder moving along the axis. Figure 10 and 11 are voltage ratio

curves for a transponder moving along a trail parallel to the x-axis (y=-15cm, z=0cm). Each figure has two curves. One is the voltage ratio from experiments, and the other one is calculated by Equation (22).

The results show that our mathematical equation in Part 3 can correctly describe our system. Figure 10 tells us that Equation (22) still works when the transponder is off axis. Figure 11 shows that the transponder still works when the angle is 45 degrees. Experimental results show that it is possible to develop a three-dimensional system based on our experiments, and this is the subject of ongoing research.

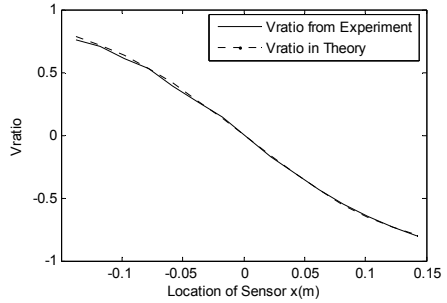

Figure 9: Vratio when transponder moves along x-axis ($\alpha = 0$).

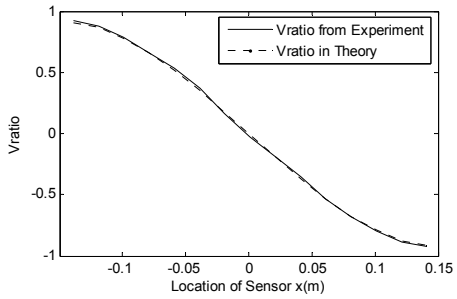

Figure 10: Vratio when transponder moves along a trail parallel to x-axis (y=-15cm, $\alpha = 0$).

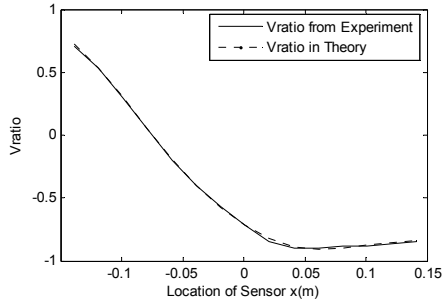

Figure 11: Vratio when transponder moves along a trail parallel to x-axis (y=-15cm, $\alpha = 45^\circ$).

5 CONCLUSIONS

In this paper, we describe a location system based on RFID technology. Although our experiments are for a one-dimensional system, the results and analysis show it is possible to develop a three-dimensional system. Also spread-spectrum coding, which is used to program transponders, lets us track multiple transponders. Using this location system with multiple RFID transponders, we expect to be able to map the images of endoscopes without attaching extraneous wires.

REFERENCES

Bladen, J.S., Anderson, A.P., Bell, G.D., Rameh, B., Evans, B., Heatley, D.J., 1993. Non-radiological technique for three-dimensional imaging of endoscopes. *Lancet,* **341**, pp.719-22.

Williams, C., Guy, C., Gillies, D., Saunders, B., 1993, Electronic three-dimensional imaging of intestinal endoscope. *Lancet,* **341**, pp.724-725.

Friedland S., Van Dam J., 2002. A global positioning system for the colon. *Endoscopy*, **34**(11), pp.900-4.

Wehrmann, K., Fruhmorgen, P., 2002. Evaluation of a New Three-dimensional Magnetic Imaging system for Use During Colonoscopy. *Endoscopy*, **34**(11), pp.905-8.

Geng, D., 2004. *High Refresh Rate Three Dimension Positioning System Using Frequency-Multiplexed Electromagnetic Fields.* Ph.D. Newcastle University.

Finkenzeller, K., 2003. *RFID Handbook,* Carl Hanser Verlag. Munich, Germany, 2nd edition.

Weinstein, R., 2005, RFID: A Technical Overview and Its Application to the Enterprise. *IT Professional*, **7**(3), pp.27-33.

Atmel, 2003. Read/Write Transponder TK5552.[online]. Available from: http://www.atmel.com/dyn/resources/prod_documents/doc4698.pdf, [cited 8 July 2007].

Want, R., 2004. The Magic of RFID. *ACM Queue*, October, pp.41-8.

Landt, J., 2005. The History of RFID. *Potentials, IEEE,* **24**(4), pp.8-11.

Proakis, J.G., 2001. *Digital Communications,* McGraw -Hill Company. Boston, 4th edition.

Stratton, J.A., 1941. *Electromagnetic Theory,* McGraw -Hill Book Company, Inc. New York, 1st edition.

DESIGN OF ANALOG SIGNAL PROCESSING INTEGRATED CIRCUIT FOR MULTI-CHANNEL BIOMEDICAL STRAIN MEASUREMENT INSTRUMENT

Wenchao Qu, Syed K. Islam
Department of Electrical Engineering, The University of Tennessee, 1508 Middle Dr., Knoxville, TN 37996, USA
wqu1@utk.edu, sislam@utk.edu

Gary To, Mohamed R. Mahfouz
Center for Musculoskeletal Research,The University of Tennessee, 1414 Circle Dr., Knoxville, TN 37996, USA
gto@utk.edu, mmahfouz@utk.edu

Keywords: Analog digital conversion, SAR ADC, instrumentation amplifier, strain measurement, biomedical instrumentation.

Abstract: An analog signal processing integrated circuit for micro-cantilever array is designed for strain measurement in biomedical applications. The chip includes an analog multiplexer, an instrumentation amplifier, a sample and hold circuit, an on-chip voltage and current reference, a successive approximation register analog-to-digital converter and a digital control unit. The 8-bit ADC attains 45.4 dB signal-to-noise-and-distortion ratio and 56.4 dB spurious-free-dynamic-range while operating at 772 KHz. The chip occupies an area of 1.54 mm^2 and consumes 17.8 mW power with a single 3.3 V supply. The chip has been fabricated in a 0.35μm 2-poly 4-metal CMOS process technology.

1 INTRODUCTION

The use of prosthetic joint implants to treat patients with severe osteoarthritis and other joint degenerative diseases began in the early 70s. During the knee joint implant surgery, surgeons need to perform accurate resections depending on various instruments such as spacer block, tensioner and tram adapter. These instruments provide valuable information about the gap shape and size during the bone resection process. However, the feedback of instrument such as the spacer block is qualitative and the degree of tightness of the ligaments is inaccessible.

A new space blocker, shown in figure 1, is designed by fully taking advantage of the sensors, the ASIC and the telemetry technology. The sensors and chips are on the surface with a battery inside the spacer block, and the antenna is also designed to fit in the handle. The surface of the instrument was encapsulated by epoxy with fully FDA compliance.

In this paper, we mainly present the design of an analog signal processing IC for biomedical strain measurement system. In Section 2, we briefly introduce the system design and then present the circuit design in detail in Section 3. The measurement results are given in Section 4, followed by a summary in Section 5.

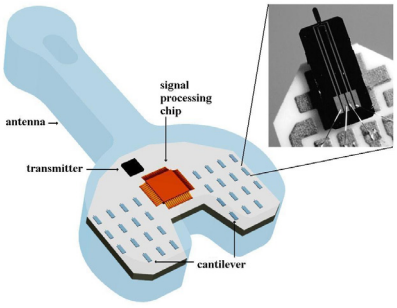

Figure 1: 3-D model of spacer block with embedded chip and sensor array.

2 SYSTEM OVERVIEW

The system block diagram is shown in figure 2. The system can be partitioned into three parts based on

their functions. The first part is the sensor array. There are 30 strain-sensing micro-cantilevers distributed evenly on the two sides of the biomedical instrument top plate. The Wheatstone bridge configured sensors convert the physical strain to a resistance change and then to voltage signal under DC excitation. The middle part shown in figure 2 includes two chips, one chip for signal processing and another one for signal transmitting. The signal-processing chip amplifies the signal coming from the sensors and digitizes the analog signal to digital domain. The transmitter chip sends out the signal using ASK modulation with 335MHz carrier frequency. The receiver part receives and recovers the data remotely. Furthermore, the data will be post-processed by software and shown graphically on the display.

In this paper, the scope mainly focuses on the design and implementation of the signal processing integrated circuit.

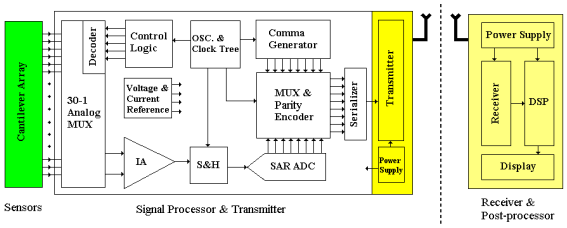

Figure 2: Sensor array signal processing system block diagram.

3 CIRCUIT IMPLEMENTATION

Instrumentation Amplifier. The Instrumentation Amplifier (IA) amplifies the difference signal between the two input terminals and rejects the common mode signals on both inputs (Kitchin and Counts, 2000). Unlike normal opamp, the feedback of IA uses an internal resistance network but the gain is set by an external resistor.

The external gain setting resistor provides maximum design flexibility for the system designer to accommodate the input signal level. The gain can be set using the following equation

$$A_V = 1 + \frac{2R}{R_g} \tag{1}$$

where, R is internal resistor and R_g is off chip gain setting resistor.

A classical 3 opamps configuration is chosen and an additional opamp provides variable output DC level to accommodate the following stage circuit.

Voltage and Current Reference. Both the ADC and the DAC in the system need either the voltage or the current reference. Bandgap voltage reference is selected for its extraordinary performance of process, power supply and temperature variation independence (Meyer and Gray, 1993, Brokaw, 1974). The reference is generated by adding a negative temperature coefficient (TC) voltage and a weighted positive TC voltage. Hence, a zero TC can be achieved by adjusting the value of R2 and R1 based on the following equation

$$V_{BG} = V_{be} + \frac{R_2}{R_1} V_T \ln k \tag{2}$$

where, V_{be} is the base-emitter junction voltage, V_T is thermal voltage and k is the geometry ratio of Q1 and Q2. The bandgap reference circuit shown in figure 3 has two operation points. To guarantee the circuit always works at the right point, a startup circuit is also included.

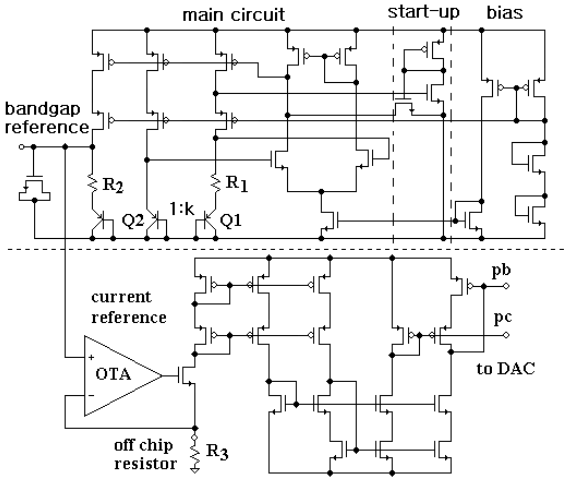

Figure 3: Voltage and Current Reference Schematic.

The current reference for the current-steering DAC cannot be fully generated on-chip due to the lack of a high precision absolute value resistor. With the aid of a low TC and high precision external resistor, and the bandgap voltage reference, an accurate current reference can be obtained. The current reference circuit is shown in the lower part of figure 3.

Sample and Hold. In order to relax the dynamic requirements for the ADC, a sample and hold circuit is inserted between the amplifier and the ADC (Waltari and Halonen, 2002). The sample and hold grabs the fast changing signal and stores it in the sampling capacitor Cs. In the meantime, the thermal noise is also trapped into the capacitor during the turning off of the switch. For an 8-bit ADC, the minimum required sampling capacitor Cs can be calculated by the following equation

$$C_S = n_f \frac{k_B T}{V_n^2} \tag{3}$$

where, k_B is Boltzmann constant, T is absolute temperature, V_n^2 is quantization noise power, and the coefficient n_f models the noise from the amplifier and has a value between 0~1. In (3), we assume that the quantization noise power is equal to the thermal noise power.

The settling error for linear one pole settling is expressed as

$$\varepsilon_r = e^{-\frac{\omega_{-3dB}}{2f_S}} = e^{\frac{-1}{2f_S R_S C_S}} \tag{4}$$

where, f_S is sampling frequency and R_S is the equivalent on-resistance of sampling switch. The maximum allowed settling error for 8-bit ADC is 0.39%. Then the equivalent resistance for the switch can be calculated by

$$R_S = \frac{1}{2} \frac{1}{f_S C_S \ln \frac{1}{\varepsilon_r}} \tag{5}$$

where, ε_r is settling error. Once we know the minimum equivalent on-resistance of the switch, the switch size can be determined by the transistor parameters.

SAR ADC. The Successive Approximation Register (SAR) ADC (Scott et al., 2003) is selected as the data conversion unit for several reasons. First, the SAR ADC is suitable for moderate speed and moderate resolution data conversion. Also, the SAR ADC is extremely power and area efficient. The SAR ADC shown in figure 4 has three parts: comparator, SAR logic (Anderson, 1972) and DAC. The conversion mechanism behind the SAR ADC is similar to binary search algorithm. First, the DAC MSB is set to 1 while all other bits are set to 0, then converted to analog domain and compared with the stored input signal. Then the SAR logic will keep or reset the MSB signal based the comparison result. The procedure is iterated until the LSB is resolved. Apparently, the conversion time is 8 periods for an 8-bit ADC plus 1 period for sampling. The timing and conversion procedure is shown in figure 4b.

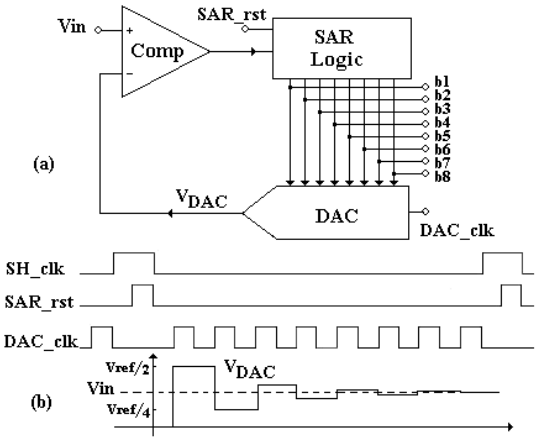

Figure 4: SAR ADC block and timing diagram.

4 EXPERIMENTAL RESULTS

Figure 5 shows the signal process chip micrograph. The core die area (excluding the pad and ESD circuit) is about 1.54 mm^2.

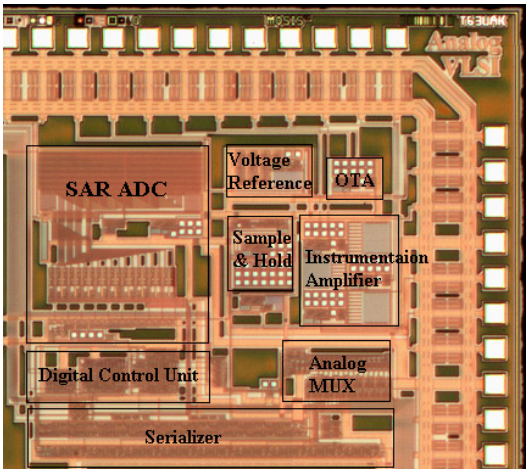

Figure 5: Chip prototype micrograph.

The voltage gain frequency response of the IA is shown in figure 6 for three different external gain setting resistors. The unity gain bandwidth for different voltage gain is almost fixed and has a value about 2.5 MHz.

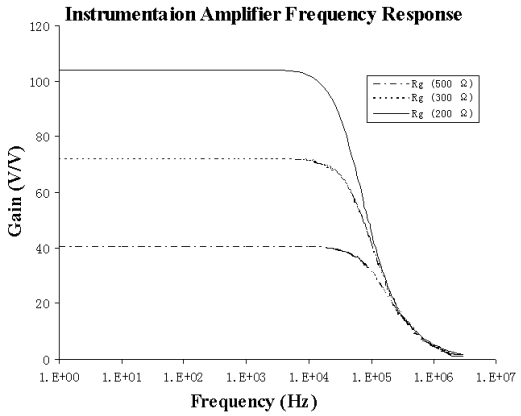

Figure 6: Voltage gain frequency response of instrumentation amplifier.

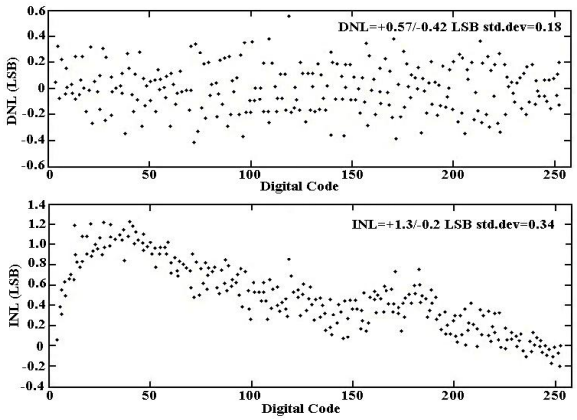

Figure 7: Integral and differential nonlinearity of ADC.

Table 1: Prototype chip performance summary.

	Parameter	Value
ADC	Resolution	8 bit
	ENOB	7.24 bit
	SNDR	45.4 dB
	SFDR	56.4 dB
	Conversion Rate	772 KHz
	DNL	+0.57/-0.42 LSB
	INL	+1.3/-0.2 LSB
	Area	0.43 mm^2
	Power	17.8 mW
Instrumentation Amplifier	Voltage Gain	20~200 V/V
	Unity Gain Bandwidth	2.5 MHz
Total	Area	1.54 mm2
	Power	17.8 mW

The DNL and INL of the SAR ADC are obtained by histogram testing (Plassche, 2003) and are shown in figure 7. The DNL is 0.57/-0.42 LSB and INL is 1.3/-0.2 LSB with zero missing code. Parts of the test results are summarized in table 1.

5 CONCLUSIONS

The prototype chip presented here was fabricated in a 0.35 μm 2-poly 4-metal CMOS process. The operating voltage is 3.3 V and the chip can also work for the voltage range of 2.6 V ~ 4 V. The area of the chip (core area) is 1.54 mm2, and consumes 5.4 mA current. The measurement results of the signal processing chip verify the design concept and meet the specifications for the biomedical instrument system. A wireless strain measurement instrument is being developed based on this chip design.

REFERENCES

Anderson, T. O. (1972) Optimum Control Logic for Successive Approximation AD Converters. *Computer Design,* 11**,** 81-86.

Bienstman, L. A. & De Man, H. J. (1980) An eight-channel 8 bit microprocessor compatible NMOS D/A converter with programmable scaling. *Solid-State Circuits, IEEE Journal of,* 15**,** 1051-1059.

Brokaw, A. P. (1974) A simple three-terminal IC bandgap reference. *Solid-State Circuits, IEEE Journal of,* 9**,** 388-393.

Kitchin, C. & Counts, L. (2000) A Designer's Guide to Instrumentation Amplifiers. *Analog Devices*.

Meyer, R. G. & Gray, P. (1993) *Analysis and design of analog integrated circuits*, Wiley.

Plassche, R. J. V. D. (2003) *CMOS integrated analog-to-digital and digital-to-analog converters,* Boston, Kluwer Academic Publishers.

Scott, M. D., Boser, B. E. & Pister, K. S. J. (2003) An ultralow-energy ADC for Smart Dust. *Solid-State Circuits, IEEE Journal of,* 38**,** 1123-1129.

Waltari, M. E. & Halonen, K. A. I. (2002) *Circuit techniques for low-voltage and high-speed A/D converters,* Boston, Kluwer Academic Publishers.

DEVELOPMENT OF AN ALTERNATIVE SYSTEM FOR SUSPENDED GAIT ANALYSIS

Gustavo Freitas de Lima and Alberto Cliquet Jr.
Electrical Engineering Department, University of São Paulo, Av. Trabalhador São-carlense, 400, São Carlos-SP, Brazil
Department of Orthopedics, State University of Campinas, R. Tessalia Vieira de Camargo, 126, Campinas-SP, Brazil
gflima@hotmail.com, cliquet@fcm.unicamp.br

Keywords: Functional Electrical Stimulation, suspended gait, ground reaction forces, knee joint angles, paraplegic, rehabilitation, Spinal Cord Injury.

Abstract: Spinal Cord Injury (SCI) may impair an individual's gait. For these cases, a rehabilitation technique that has become more popular is Functional Electrical Stimulation (FES). Gait analysis is an important technique to evaluate rehabilitation of patients undergoing FES-assisted therapy. This work proposes a system that monitors gait variables – knee joint angles, and ground reaction forces (heel and metatarsal) – and uses them as inputs for gait analysis of paraplegic patients. The methods for building the data acquisition hardware (transducers and interface) and software are described, along with the transducer calibration methods. The results show the final prototype for the gait analysis system, which allows comparison between different individuals' gaits, as well as different rehabilitation stages for the same individual. The software has a recording feature, as well as digital control outputs, which may be used in the future for training an Artificial Neural Network (ANN) and controlling the individual's FES stimulator. In the near future, the system may be of great applicability for suspended FES-assisted gait analysis and control.

1 INTRODUCTION

1.1 Human Gait

Gait may be defined as a form of biped progression in which lower limb repetitive movements include periods of double support – in which both feet are in contact with the ground – followed by periods in which only one foot supports the body (stance) and the other is being moved above the ground (swing) (Wall, 1999).

On a normal gait, the stance phase constitutes 60% of the gait cycle, and is defined as the interval in which the reference foot is in contact with the ground. The swing phase begins with heel contact and ends when the foot leaves the ground (toe off surface).

1.2 Gait Analysis

For individuals that suffer Spinal Cord Injury (SCI), a technique that has contributed for rehabilitation is Functional Electrical Stimulation (FES) (Castro and Cliquet Jr., 2000). FES treatment may be associated with dynamic suspension (Field-Fote, 2001). This suspension allows a weight reduction, maintaining the load on the lower limbs at a level they are able to stand. It also stabilizes the trunk, resulting in better balance for the patient, and lowers upper-limb overload, frequently observed on walker-aided training for paraplegic patients.

Gait analysis is an important tool for biomechanical studies of the rehabilitation process. Veltink, Liedtke, Droog, and van der Kooij (2005) developed a gait analysis system using two commercial six-degrees-of-freedom force and moment sensors under a sandal. Giacomozzi and Macellari (1997) constructed a compound instrument by superimposing a dedicated pressure platform on a commercial force platform.

The objective of this work is the development of an alternative system for gait analysis, to be used on the evaluation of patients' rehabilitation for suspended FES-assisted gait.

2 METHODS

2.1 Determination of Variables

The first task was to determine which variables would serve as inputs for the system. Various works have been done proposing different models (Tong and Granat, 1999; Pappas et al., 2004; Popovic et al., 1998), each one showing advantages and disadvantages. For this work, the idea was to be able to measure the actual values for ground reaction forces, and use them for comparison on gait analysis, not as triggers for detection of foot contact.

Popovic et al. (1998) stated that ground reaction forces alone could not be used for satisfactory gait phase characterizing. In order to avoid this problem, an extra variable was chosen to serve as system input. The data posted on the CGA Normative Gait Database (Kirtley, 2006) show kinematic and kinetic analysis for healthy adults and children. Taking in consideration the movement amplitude, easiness to mount sensors, sensor stability during movement and amount of signal noise, the variable selected was knee flexion/extension.

2.2 Transducer Selection

Based on the studies conducted by Cunha (1999), the chosen transducers for knee flexion/extension angle determination were shape sensors. These sensors use 0.25 mm diameter fiber optics, specially treated to lose light by refraction proportionally to the deflection suffered by the fibers. They present some important characteristics, such as light weight and a simple electronic signal processing package, incorporated to the fiber optics.

For the ground reaction forces, the analysis was based on the studies conducted by Leite (2003). The author developed an instrumented crutch to measure vertical reaction forces applied by patients during gait, using strain gages.

Strain gages are resistors composed of a very thin conductive layer over an isolating compound. The sensor is glued on a structure, and when there is some deformation caused by applied forces on the structure, it is possible to determine the value of the force, since it depends only on the type of material and the geometry of the structure.

The fact that strain gages require a rigid structure to operate represents a disadvantage for this kind of sensors. The solution found for the problem was to construct cylindrical aluminum rings to work as load cells for the strain gages. For each load cell, a metal base and a semi-spherical top were constructed, so that the top's radius helps bring the applied loads as close as possible to vertical. Figure 1 shows one of the load cells with the strain gages attached (left) and with the protective covering, metal base and top (right).

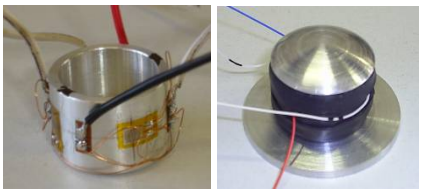

Figure 1: Ground reaction force sensors (load cells).

Three load cells were made for each foot, and they were attached to a sandal, mounted on cylindrical metal plates. One load cell was positioned in the heel area, and the other two were positioned in the metatarsal area, connected in parallel – in order to compensate different styles of stepping patterns.

2.3 Hardware Interface

The hardware interface circuit consists of anti-alias filters (cutoff frequency of 18 Hz), voltage regulators (± 5VDC), and amplifiers with adjustable gains for the strain gages. The information was acquired using a data acquisition board.

The circuit is enclosed in a box, connected to the data acquisition board, and also to a smaller interface box, which is positioned around the patient's waist, and has connection hubs for the instrumented sandals and shape sensors. The transducers connected to the patient's interface box are shown in Figure 2.

Figure 2: Transducers and patient's interface.

2.4 Transducer Calibration

To calibrate the shape sensors, they were attached to two articulated flat metal bars, and a protractor. The voltage values corresponding to each 5º angle interval, from -140º to 140º, were collected.

For the load cells, the calibration was performed using a dynamometer, and the voltage values for each 50 N interval, from 0 to 1000 N were collected. For both cases, the results showed a linear behavior.

2.5 Software Interface

The software used to program the system was LabVIEW 6.1. It has some advantages, including user-friendly graphic interface, and compatibility with the data acquisition board.

The interface software has a monitoring module, which allows visually following the behavior of knee flexion/extension angles, and ground reaction forces – heel and metatarsal. It is also possible to record them in a spreadsheet file for data analysis.

The visual interface shows three screens (selectable using tabs): the "Main" screen, which has all the controls and configuration options; the "Angles" screen, which shows the graphics for the knee flexion/extension angles, and the "Forces" screen, which shows the graphics for the ground reaction forces. Figure 3 illustrates the "Forces" screen.

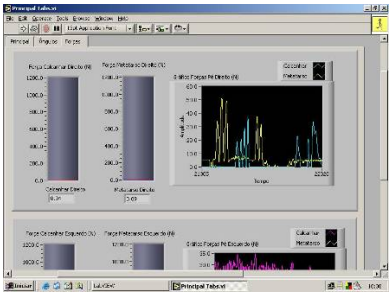

Figure 3: Graphical interface for force measurements.

On the main screen, there is a calibration function. This function should be used when the patient already has the sandals on, but has not stood up yet. The function performs 200 force acquisitions for each load cell, and then calculates the average of these forces. The result is then used as linear coefficients for the calibration curves of the force transducers. This way, the value shown with the patient sitting is zero, despite the applied force for tightening the sandals.

3 RESULTS

The final prototype was mounted on a healthy individual and tested, to check its functionality. The individual's characteristics are: male, 25 years old, height of 1.81m, weight of 69.0kg. Figure 4 shows the subject wearing the instrumented sandals and the shape sensors.

Figure 4: (A) System mounted on healthy individual; (B) Detail of sensor positioning in the sandal; (C) Instrumented sandal.

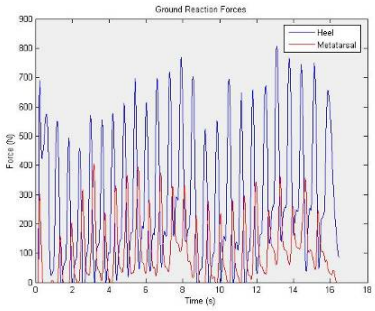

Figure 5: Ground reaction forces on right foot for healthy individual.

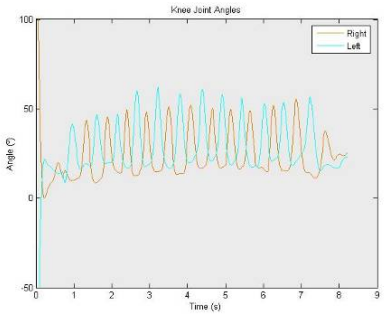

Figure 6: Knee joint angles for healthy individual.

The individual was asked to walk normally in a straight line for about 15m while the values of ground reaction forces and knee joint angles were recorded. Figures 5 and 6 show the resulting values for the ground reaction forces on the left foot, and the knee joint angles, respectively.

For the angle values, the convention adopted was zero for straight vertical position, positive angles for knee flexion and negative angles for knee extension.

4 DISCUSSION

The ground reaction forces observed in Figure 5 show peaks of about 780N on the heel, which correspond to 113% of the individual's weight. On the metatarsal area, the peak force values are around 380N (55% of the individual's weight). This may be due to the softness of the sandal sole, which may still absorb part of the applied forces. It's possible to distinguish the gait phases of initial contact (heel force peak), mid stance (heel and metatarsal force intersection), and terminal stance (metatarsal force peak).

The knee joint angles observed in Figure 5 follow the pattern presented on the CGA Normative Gait Database (Kirtley, 2006). The waveforms present a repetitive pattern, confirming that the shape sensors did not move during the acquisitions.

5 CONCLUSIONS

The values of ground reaction forces and knee joint angles may be observed during the gait, and the recorded values may be used for further analysis, comparing different styles of gait, or different rehabilitation stages for the same individual.

This system may be used as an alternative to the force platforms. The disadvantages are that it requires some time for donning, and it can only measure vertical forces. But it presents some advantages, such as: the subject may walk freely (within the limitation of the cables), and does not have to step exactly on the load cell, resulting in a more natural gait; also, the system allows monitoring two critical force points for each foot, and not just the resulting force.

Considering the aforementioned advantages, an important possible application for this alternative system is suspended FES-assisted gait. In this case, therapists may follow the recovery of patients undergoing this kind of treatment by analyzing the gait on different stages of the rehabilitation process.
In the future, the recordings of gait sessions may be used as inputs for a closed-loop FES control. The system already has two digital inputs and two outputs, which may be used to trigger an electrical stimulator. Since the software is open, an Artificial Neural Network (ANN) may be programmed to control the FES during gait, using the patient's own recorded data for training. With this implementation, the patient will not need to trigger the stimulation manually, and may direct all the attention to the walking activity.

ACKNOWLEDGEMENTS

The authors would like to acknowledge the support of the State of São Paulo Foundation for Research – FAPESP and the Coordination for the Improvement of High Education Personnel – CAPES – Ministry of Education, Brazil.

REFERENCES

Castro, M, C. F.; Cliquet Jr., A. An artificial grasping system for the paralysed hand. *Artificial Organs*. 2000;24:185-188.

CGA Normative Gait Database. Produced by Chris Kirtley. [cited 2007 Jul 10]. Available from: <http://www.univie.ac.at/cga/data/index.html>.

Cunha, F. L. *Obtenção e uso dos acoplamentos cinemáticos interfalangianos e interdigitais no projeto de próteses antropomórficas para membros superiores*. Vitória: UFES; 1999.

Field-Fote, E. C. Combined use of body weight support, functional eletric stimulation, and treadmill training to improve walking ability in individuals with chronic incomplete spinal cord injury. *Arch Phys Med Rehabil.* 2001;82: 818-824.

Giacomozzi, C.; Macellari, V. Piezo-Dynamometric Platform for a More Complete Analysis of Foot-to-Floor Interaction. *IEEE Transactions on Rehabilitation Engineering*. 1997;5: 322-330.

Leite, F. I. L. Desenvolvimento de uma muleta instrumentalizada para fins de acompanhamento clínico. São Carlos: EESC-USP; 2003.

Pappas, I.; Keller, T.; Mangold, S.; Popovic, M. R.; Dietz, V.; Morani, M. A reliable gyroscope-based gait-phase detection sensor embedded in a shoe insole. *IEEE Sensors*. 2004;4:268-274.

Popovic, M. R.; Keller, T.; Ibrahim, S.; Von Büren, G.; Morani, M. Gait identification and recognition sensor. *International Workshop on Functional Electrical Stimulation*; 1998; Vienna, Austria; 1998. p. 153-156.

Tong, H.; Granat, M. H. A practical gait analysis system using gyroscopes. *Medical Engineering & Physics*. 1999;21:87-94.

Veltink, P. H.; Liedtke, C.; Droog, E.; van der Kooij, H. Ambulatory Measurement of Ground Reaction Forces. *IEEE Transactions on Neural Systems and Rehabilitation Engineering*. 2005;13:423-427.

Wall, J. C. The Gait. In: Durward, B. R.; Baer, G. D.; Rowe, P.J., editors. *Functional human movement: measurement and analysis*. Oxford: Butterworth Heinemann; 1999. p. 93-105.

PULSE-TYPE NEURO DEVICES WITH SPIKE TIMING DEPENDENT SYNAPTIC PLASTICITY

Katsutoshi Saeki,Yugo Hayashi
College of Science and Technology, Nihon University, Funabashi-shi, Chiba, Japan
ksaeki@ecs.cst.nihon-u.ac.jp, hayashi@hippo.ecs.cst.nihon-u.ac.jp

Yoshifumi Sekine
College of Science and Technology, Nihon University, Funabashi-shi, Chiba, Japan
ysekine@ecs.cst.nihon-u.ac.jp

Keywords: Neural Network, Pulse-Type, STDP, Synaptic Weight, Neuro Device, Noise Tolerance.

Abstract: Even though the neurons in the human brain are sensitive to noises, human central nervous systems can operate correctly under a noisy environment. Since neural networks have superior information processing functions, many investigators have attemptted to model biological neurons and neural networks. A number of recent studies of neural networks have been conducted with the purpose of applying engineering to the brain. Especially, neuro devices have been created that focus on how to have a learning function. Here, we focus on spike timing dependent synaptic plasticity (STDP) and construct pulse-type neuro devices with STDP using analog VLSI technology. We show that it is possible to extract phase differences representing the reinforcement part of the synaptic weight by using pulse-type neuro devices with STDP. Moreover, we investigate noise tolerance for thermal noise and fluctuation of time.

1 INTRODUCTION

An artificial neural network that performs similarly to the human brain would be required to construct a brain-type information processing system. Our human central nervous systems can operate correctly in noisy environments even though the neurons in the brain are sensitive to noise. On the other hand, it would be necessary to use neuro devices as components in an environment without noise. To focus on this superior function, investigators are studying the noise tolerance of artificial neural networks. Because it is not possible to learn correctly when influenced by noise, an information processing system cannot be constructed. The classical Hebbian learning rule is proposed as the learning rule. (Hebb, 1949). This rule is thought to play an important role in the synaptic plasticity of neural networks in the brain. This rule uses mean spike firing correlations between pre- and postsynaptic neurons to drive learning. Recently, the form of synaptic plasticity was seen to be dependent on the order and time intervals of pre- and postsynaptic spikes (STDP: spike timing dependent synaptic plasticity (Bi and Poo, 1998, Nishiyama, Hong, Mikoshiba, Poo, and Kato, 2000)), as was observed in the hippocampus and cerebral cortex. (Patrick and Curtis, 2002, Sakai and Yoshizawa, 2003, Tsukada, Aihara, Kobayashi and Shimazaki, 2005). STDP manifests itself as the potentiation of a synapse if the presynaptic spike precedes the postsynaptic spike, and as depression if the presynaptic spike follows the postsynaptic spike. Potentiation and depression were determined from the results of experiments on rat hippocampal neurons (Patrick and Curtis, 2002) and frog tectal neurons. (Zhang, Tao, Holt, Harris and Poo, 1998). The timing based learning rule enhances the excitatory postsynaptic potentials induced by coincident input spikes, since the synaptic connections already contributing to postsynaptic firing are further strengthened. (Gerstner, Kempter, van Hemmen and Wagner, 1996). It is reported these characteristics are useful and effective for the extraction of synchronous firing so that STDP is buried in the noise. (Fukai and Kanemura, 2001, Saeki, Hayashi and Sekine, 2006). In addition, the hardware model with STDP (Bofill-i-Petit and Murray, 2004) has been proposed based on the physiological experiment results. However these

models are complex circuits and don't study the noise tolerance.

On the other hand, we proposed a pulse-type neuro device that approximately simulates pulse signals as an information transmission means in the brain. (Sekine 1999, Saeki, Sekine, and Aihara, 1999, Sekine, Sumiyama, Saeki and Aihara, 2001).

In this paper, we discuss the construction of neural networks from pulse-type neuro devices with STDP. We show that it is possible to extract the phase difference representing the reinforcement part of synaptic weight. Moreover, we investigate the noise tolerance of thermal noise and the fluctuation of time.

2 CIRCUIT OF NEURO DEVICES WITH STDP

An STDP block diagram is shown in Fig. 1. This block diagram has cell body blocks and an STDP block. When pulses are inputted to each temporal summation block, output pulses from each temporal summation block have first-order delays and are transmitted to the subsequent blocks. When the post-synaptic cell generates the pulses, the synaptic weight W_p between pre- and post-synaptic cells is reinforced based on the output amplitude of the temporal summation block with the pre-synaptic cell. On the other hand, when the pre-synaptic cell generates the pulses, W_p is suppressed based on the output amplitude of the temporal summation block with the post-synaptic cell.

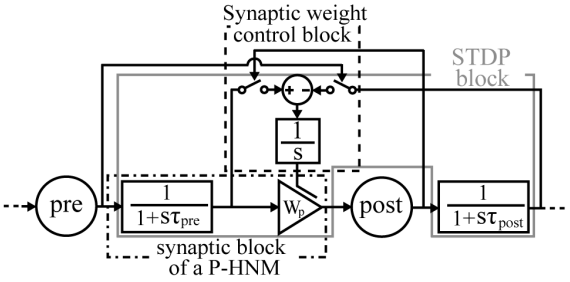

Figure 1: STDP block diagram.

A pulse-type neuro device is shown in Fig. 2. The pulse-type neuro device consists of a cell body circuit and a synaptic circuit. Figure (a) shows the cell body circuit. When I_{out} is inputted to the cell body circuit, output pulses are generated. This circuit has a threshold and a refractory period characteristic. Figure (b) shows the synaptic circuit. When pulses are inputted to the input terminal V_{pre} of the synaptic circuit from the pre-synaptic cell, I_{out} is generated. The current I_{out} changes according to V_w. Therefore, the synaptic weight between the pre- and post-synaptic cells can be controlled by V_w. Spatial summation circuits can also be constructed when a series circuit of M_{sy1} and M_{sy2} is connected in parallel.

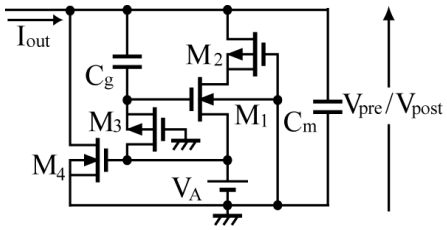

(a) Cell body circuit.

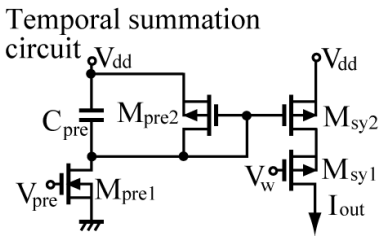

(b) Synaptic circuit.

Figure 2: Pulse-type neuro device.

The synaptic weight generation circuit is shown in Fig. 3. This circuit consists in part of three blocks; two temporal summation circuits and a synaptic weight control circuit. The voltage V_w is the output voltage of this circuit and is the parameter that controls the synaptic weight between the pre- and post-synaptic cells.

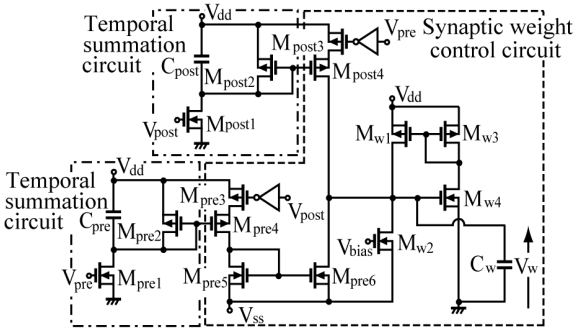

Figure 3: Synaptic weight generation circuit.

A function of V_w in the synaptic weight generation circuit is shown in Fig. 4. The horizontal axis is the time interval $\Delta t'$, which is the time of the pre-synaptic pulse minus the time of the post-synaptic

pulse, and the vertical axis is the amount of voltage change ΔV_w of V_w after generating pulses in pre- and post-synaptic cells. This figure shows that V_w increases when a pulse generated in the post-synaptic cell after a pulse is generated in the pre-synaptic cell, but decreases when the pulse generated in the pre-synaptic cell follows the pulse generated in the post-synaptic cell. Furthermore, as $\Delta t'$ becomes shorter, ΔV_w increases exponentially.

From these results, we clarify principles of the operation of the proposed circuits when the circuit in

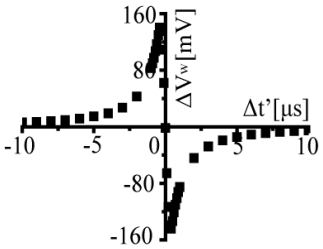

Figure 4: Characteristic of V_w in the synaptic weight.

Fig. 2 is controlled with V_w in Fig. 3. Therefore, controlling the circuit depicted in Fig. 2 with V_w, as depicted in Fig. 3, generates the STDP function.

3 EXTRACTION OF PHASE DIFFERENCE INFORMATION

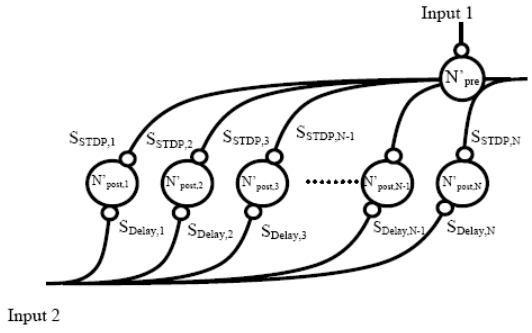

Figure 5 : A neural network that extracts phase.

Figure 5 shows an example of a neural network composed of $S_{Delay,(1\sim k\sim L)}$ that represents the synaptic circuits of each difference in the propagation delay time, $S_{STDP,(1\sim k\sim L)}$ that represents the synaptic circuits, with synaptic weight control circuits, N'_{pre} and parallel $N'_{post,(1\sim k\sim L)}$. Moreover, inputs 1 and 2 are made in the same cycle. The synaptic weight control voltage of $S_{STDP,(1\sim k\sim L)}$ is $V_{W,STDP(1\sim k\sim L)}$, and the synaptic weight control voltage of $S_{Delay,(1\sim k\sim L)}$ is a constant value $V_{W,STDP(1\sim k\sim L)}$ = 0.0 V. The propagation delay time of $S_{Delay,k}$ is assumed to be the next equation. $\tau_k = \Delta\tau \cdot (k-1)$ (1)

In equation, τ_k is the propagation delay time. $\Delta\tau$ is the sampling time of the propagation delay time.

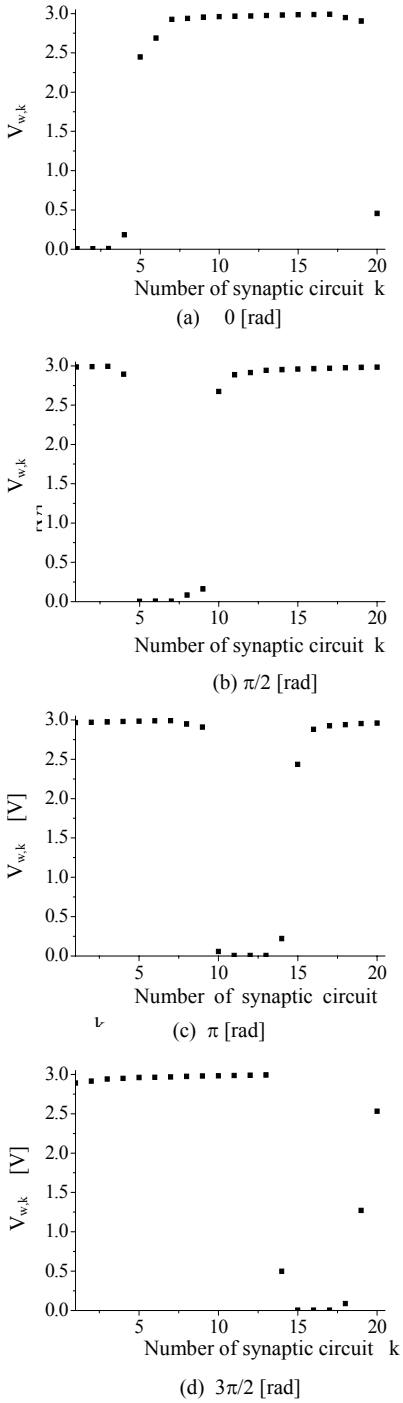

Figure 6: Synaptic weight control voltage.

Input 2 is transmitted $N'_{post,(1\sim k\sim L)}$ through the $S_{STDP,(1\sim k\sim L)}$, and $N'_{post,(1\sim k\sim L)}$ outputs pulses at each different time. The synaptic weigh control voltage of the synaptic circuit, which connects the cell body circuit and input 1 corresponds to the phase difference between inputs 1 and 2, decreases because the cycles of inputs 1 and 2 are the same. As a result, the phase difference can be learned as the number of the synaptic circuit which it reinforces. Moreover, the cell body circuit connected with the reinforced synaptic circuit can output a pulse when input 1 is inputted again after the learning finished, and the phase difference between inputs 1 and 2 can be extracted.

Figure 6 shows the characteristics of each synaptic weight control voltage $V_{w,k}$ to the phase difference of input 2 based on input 1. In this case, we use the parameters, T=10μs, L=20 and Δτ=0.5μs. The horizontal axis is the number of the synaptic circuits, and the vertical axis is $V_{W,STDP(1\sim k\sim L)}$. This figure shows that $V_{w,k}$ with the minimum value neighbourhood appear to be 1~4, 5~9, 12~16 and 17~20 for phase differences between inputs 1 and 2 of 0, π/2, π and 3π/2, respectively. That is to say, the minimum neighbourhood depends on the phase difference between inputs 1 and 2. Therefore, it is possible to extract the phase difference from pulse-type neuro devices with STDP.

4 NOISE TOLERANCE

4.1 Thermal Noise

In this section, thermal noise is assumed, and tolerance to white noise is investigated.

The signal of the next equations is used as a train of pulses that adds white noise to a periodic train of pulses of the cell body circuit.

$$S'_{pre} = \sum_{i=1}^{m} v_{pre,i}(T \cdot i) + v_{white}(\sigma') \quad (2)$$

$$S'_{post} = \sum_{j=1}^{n} v_{post,j}(T \cdot j + dt) + v_{white}(\sigma') \quad (3)$$

In these equations, v_{white} shows white noise that generates random numbers. σ' is the standard deviation of distribution, shows noise tolerance. In this case, we use these parameters, T=10μs and dt=1μs.

Figure 7 shows a characteristic of the synaptic weight control voltage to the strength of the white noise. The horizontal axis is the strength of the white noise and the vertical axes are the average of V_w (■) and the ratio that becomes V_w less than 1V (○), respectively. We assume that it is transmitted to the pulses from N_{pre} to N_{post}, when V_w less than 1V. This figure shows that not more than σ' =1.0V is displayed below V_w=1.5V, and σ' =1.05V is displayed above V_w=1.5V. Noise strength shows that if the influence of the reinforcement displays below σ' =1.0V, the influence of the suppression appears as σ' =1.05V. As well, the rate that V_w becomes not more than 1V is 100% within the range of σ' =0.8V or less. This suggests a neural network with STDP that has a learning function with tolerance for white noise of 0.8V or less.

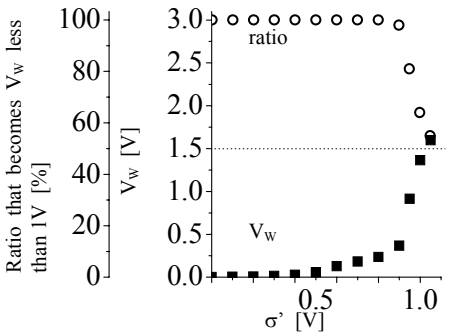

Figure 7: Synaptic weight control voltage to the strength of white noise.

4.2 Fluctuation of Time

Next, the difference of the pulse timing caused by the wiring capacity etc. is investigated. The signal of the next equations is used as a train of pulses that adds the fluctuation of the timing of the cell body circuit.

$$S''_{pre} = \sum_{i=1}^{m} v_{pre,i}\left(T \cdot i + t_{Nrand,i}(\sigma'')\right) \quad (4)$$

$$S''_{post} = \sum_{j=1}^{n} v_{post,j}\left(T \cdot j + dt + t_{Nrand,j}(\sigma'')\right) \quad (5)$$

In these equations, $t_{Nrand,i}$ $t_{Nrand,j}$ show the fluctuation of time. σ'' is the standard deviation of the distribution, showing the noise tolerance. In this case, we use the parameter, T=10μs.

Figure 8 shows a characteristic of the synaptic weight control voltage to the fluctuation of the time. The horizontal axis is σ'' and the vertical axes are the average of V_w (■) and the ratio that becomes V_w

less than 1V (○), respectively. This figure shows that not more than σ'' =1.8μs is displayed below V_w=1.5V, and σ'' =2.0μs is displayed above V_w=1.5V. The fluctuation of time shows that the influence of reinforcement is displayed below σ'' =1.8μs, and the influence of suppression appears at σ'' =2.0μs. As well, the rate at which V_w becomes not more than 1V is 100% within the range of σ'' =0.6μs or less. This suggests a neural network with STDP that has a learning function with tolerance for the fluctuation of time of 0.6μs or less.

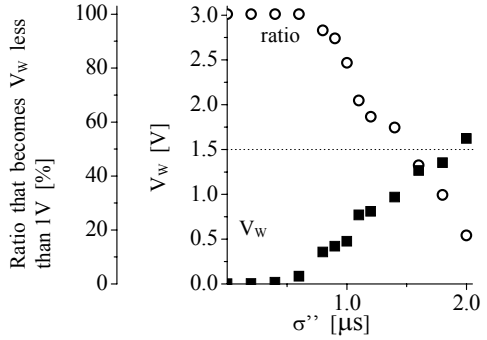

Figure 8: Synaptic weight control voltage to fluctuation of the time.

5 CONCLUSIONS

In this paper, we focus on STDP and we construct neuro devices with STDP to study the effect of STDP on the ability to extract phase differences. Using these devices, we construct a neural network that extracts phase difference information. As a result, it is possible to extract the phase differences of pulse-type neuro devices with STDP, representing the reinforcement component of synaptic weight. Moreover, we investigated the noise tolerance of the proposed model. As a result, we demonstrated pulse-type neuro devices with STDP that have a learning function with tolerance for white noise of 0.8V or less, and for fluctuation of time of 0.6μs or less. That is to say, we showed that pulse-type neuro devices with STDP had a learning function with noise tolerance for the thermal noise and the fluctuation of the time.

In our future work, we will construct an integrated circuit with pulse-type neuro devices with STDP.

ACKNOWLEDGEMENTS

This work was supported in part by Amano Institute of Technology.

REFERENCES

Hebb, D. O, 1949. "The organization of behavior, A Neuropsychological Theory", *New York*.

Bi G-q., Poo M-m., 1998. "Synaptic modifications in cultured hippocampal neurons, Dependent on spike timing, synaptic strength, and postsynaptic Cell Type", *J. Neurosci*.

Nishiyama M., Hong K., Mikoshiba K., Poo M-m., & Kato K., 2000. "Calcium stores regulate the polarity and input specificity of synaptic modification", *Nature*.

Patrick D. R., Curtis C. B., 2002. "Spike Timingdependent synaptic plasticity in biological systems", *Bio.Cybern*.

Sakai Y., and Yoshizawa S., 2003. "Mechanisms of synaptic competition and regulation in spike-time-dependent synaptic plasticity rules", *IEICE Technical Report*.

Tsukada M., Aihara T., Kobayashi Y., Shimazaki H., 2005. "Spatial analysis of spike-timing-dependent LTP and LTD in the CA1 area of hippocampal slices using optional imaging", *Hippocampus*.

Zhang li I., Tao HW., Holt CE., Harris WA., Poo M-m., 1998. "A critical window for cooperation and competition among developing retinotectal synapses", *Nature*.

Gerstner W, K, R., van Hemmen JL., Wagner H., 1996. "A neuronal learning rule for sub-millisecond temporal coding, *Nature*.

Fukai T. and Kanemura S., 2001. "Noise-tolerant stimulus discrimination by synchronization with depressing synapses", *Biological Cybernetics*.

Saeki K., Hayashi Y.,, Sekine Y., 2006. " Extraction of Phase Information Buried in Fluctuation of a Pulse-type Hardware Neuron Model Using STDP", *2006 International Joint Conference on Neural Networks (IJCNN2006)*.

B-i-P Adria and Murray A, F., 2004, "Synchrony Detection and Amplification by Silicon Neurons With STDP Synapses", *IEEE Trans. on Neural Networks*.

Sekine Y., 1999. "Pulse-Type Hardware Neuron Model", *Computer Today*.

Saeki K., Sekine Y., and Aihara K., 1999, "A Study on a Pulse-type Hardware Neuron Model using CMOS," *International Symposium on Nonlinear Theory and Its Applications (NOLTA99).*

Sekine Y., Sumiyama M., Saeki, K. and Aihara K., 2001. " A Λ-Type Neuron Model using Enhancement-Mode MOSFETs", *IEICE Trans*.

HIGH RESOLUTION ECG AND DEPTH DATA LOGGER

A Novel Device to Study Breath Hold Diving Induced Variations of the PQ Interval

A. Sieber [1, 2] , R. Bedini [3], X. Yong [4], A. Navarri [3], M. Dalle Luche [3], A. L'Abbate [2] and P. Dario [2]

[1] *Profactor Research and Solutions GmbH, Seibersdorf, Austria*

arne.sieber@profactor.at

[2] *Scuola Superiore Sant' Anna, Pisa, Italy*

[3] *CNR, Istituto di Fisiologia Clinica, Pisa, Italy*

[4] *MEMS Center of Chongqing University, China*

Keywords: ECG, breath-hold, apnoe, diving, PQ interval.

Abstract: Breath hold diving induces several physiological effects. The authors speculate that next to bradycardia, vasoconstriction, splenic contraction and blood shift, the form of the ECG and especially the PQ interval are also affected. Investigations of this effect requires a high resolution ECG monitor which is also capable of recording depth. This paper describes our data logger prototype. It samples ECG data at 1200 Hz, is equipped with three temperature and a pressure sensor that allows depth measurement up to 140 m and stores all the data in an ASCII text file on a SD flash card in FAT 16 or FAT32 file format. The prototype is then encapsulated in a Lexan tube with an outer diameter of 42 mm and an overall length of 18cm that should withstand 20 bar pressure equal to 200 m depth.

1 INTRODUCTION

Freediving or breath hold diving history dates back at least 4500 years ago to pearl divers of the south pacific. In 1911, one of the first freediving competitions was held when a Greek fisherman, Yorgos Haggi Statti, sometimes called "the father of freediving", successfully reached more than 60m depth with a total apnoe close to seven minutes. Today breath hold diving enjoys a wide popularity, both recreationally and competitively. Actual depth record in the breath hold diving discipline No-Limits is already beyond 200m (Nitsch, H., 11.07.2007, 214m No-Limit, Greece). A big stimulus for this sport was and still is Luc Besson's cult film "Le Grand Bleu" or "The Big Blue", which depicts the life of the elite apnoe divers Jacques Mayol and Enzo Maiorca and their life-long competition in freediving. However research on breath hold diving is also shown, where experiments in a mountain lake in gorgeous scenery in Peru are carried out (Mayol, J., 2000) to demonstrate bradycardia during breath hold diving. Other adaptations made by the human body while underwater and at high pressure include (Gooden, B.A., 1994), (Andersson, J.P.A., Line, M.H., Ruenow, E., Schagatay, E.K.A.,2002):

- Vasoconstriction: Blood vessels shrink. Blood stream is directed away from limbs for the benefit of heart, lungs and brain.
- Splenic contraction: Releasing red blood cells carrying oxygen.
- Blood shift: Blood plasma fills up blood vessels in the lungs and reduces residual volume. Without this adaptation, the human lung would shrink and wrap into its walls, causing permanent damage at depths greater than 30 meters.

Recent experiments with a novel underwater Doppler-Echography system also demonstrate cardiovascular changes during breath hold dives at 3 and 10m (Marabotti, C., Scalzini, A., Chiesa, F. Bedini, R., Reale, L., Passera, M. Belardinelli, A. Pingitore, A., Cialoni, D., Data P.G,2005). We speculate that these cardiovascular changes also affect the timing of the ECG. To investigate possible variances of the PQ or the PR interval dependent on the depth, a novel data logger was developed that combines a high resolution ECG (16 bit, 1200 Hz sampling rate) and depth recorder in a small, watertight housing.

2 METHODS

2.1 Introduction to ECG

The typical ECG signal (Figure 1) is characterized by six peaks and valleys labelled with successive letters of the alphabet P, Q, R, S, T and U (Malmivuo, J., Plonsey, R., 1995).

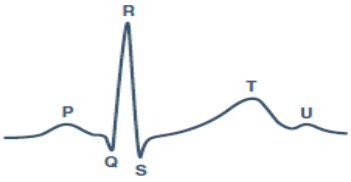

Figure 1: Typical form of a ECG signal.

A typical electrocardiogram (ECG) shows peaks of up to 5 mV. For the proper design of a ECG amplifier DC components up to +-300 mV, resulting from the electrode-skin contact, and a common-mode component of up to 1,5 V, resulting from the potential between the electrodes and ground, have to be taken into account. The bandwidth of an ECG monitoring system, depends on its application. It ranges from 0,5 Hz to 50 Hz in intensive care units up to 1kHz for late-potential measurements (pacemaker detection). A standard clinical ECG application has a bandwidth of 0.05 Hz to 100 Hz.

A typical PQ interval is about 160ms. A correlation is given between heart rate and PQ interval (Atterhög, J., Loogna, E., 1977). Recent studies have shown that this is not always the case, for example directly after a heavy workload (Busse, M., Nißing, A., Tegtbur, U., Miltzow, S., Thomas, M., Fikenzer, S., 2004). To study variances in the PQ interval a high spatial time resolution is required (Ward, S., Shouldice, R.B., Flanagan, M., Heneghan, C.,2004).

2.2 Principle Design of the Module

The prototype consists of two boards: the ECG signal acquisition board including amplifiers and a high resolution AD converter and the data logger board, comprising mainly an 8 bit RISC microcontroller, a display, a Secure Digital memory card slot and a 10 bar pressure sensor to monitor the depth.

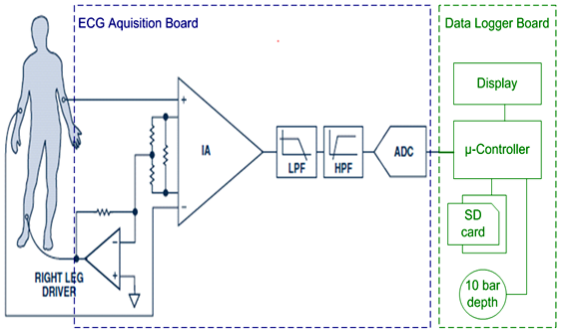

Figure 2: schematics of the developed module.

2.3 ECG Acquisition Board

For the analogue front ECG amplification stage we use the typical approach (Company-Bosch E., Hartmann, E., 2003) with an instrumentation amplifier (IA) and a right leg common-mode feedback op amp. For the IA we have chosen the AD620 [Analog Devices], a low cost, high accuracy instrumentation amplifier, with excellent DC performance: CMRR>>100 dB to nearly 1kHz, 50µVmax offset voltages, low input bias current (1nA max), and low input voltage noise (0.28µVfrom 0.1Hz to 10Hz).

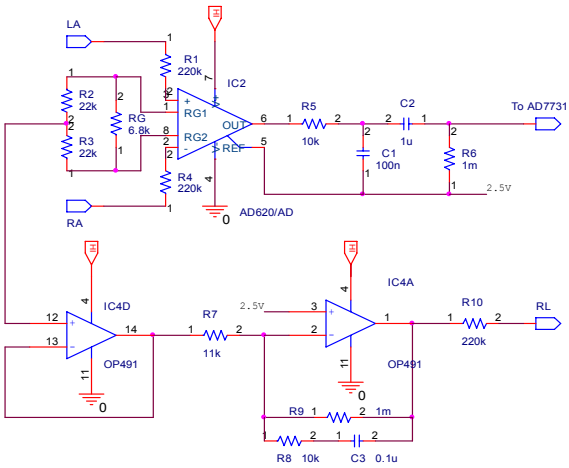

Figure 3: Schematic of the ECG amplifier.

The AD620 requires only a single external gain-setting resistor R_G (figure 3). Resistors R_2 and R_3 change the normal gain equation to:

$$Gain = 1 + 49.4k\Omega / R_G + (49.4k\Omega / 2) / 22k\Omega$$

To avoid output saturation, the usable gain is limited by the output swing and the maximum input voltage to the IA. Here, Gain is conservatively set to 9 by choosing RG=6,8 kΩ.

The OP491 form Analog Devices is used in the right-leg common-mode feedback circuit. It is a high precision operation amplifier with a low power consumption and high common-mode rejection (70 dB minimum). This circuit applies an inverted version of the common-mode interference to the subjects right leg, with the aim of cancelling interferences. The op amp has a voltage gain for the common-mode voltage of 91 (R_9/R_7=1MΩ/11kΩ) with a low-pass cut off at about 160Hz for stability. (f_{-3dB}=1/2π x 10kΩx0,1μF)). For simplicity, a passive low-pass filter and a passive high-pass filter are adopted to accomplish both gain and frequency selectivity. The filter will allow all signals to pass through unaffected as long as their frequency is between the low-pass corner frequency at 160Hz and the high-pass corner frequency at 0.1Hz (f_{-3dB}=1/2π x 1MΩx1μF)).
The required power for the module is supplied with a battery. The +5V supply required for the AD620 and OP491 is handled through the voltage power regulator TPS76950 [Texas Instruments] which offers the benefits of low dropout voltage, ultra-low power operation and miniaturized packaging (5-pin SOT-23 package). The +2,5 V reference for the AD620 is accomplished with one of the four operational amplifiers integrated in the OP491 (figure 4).

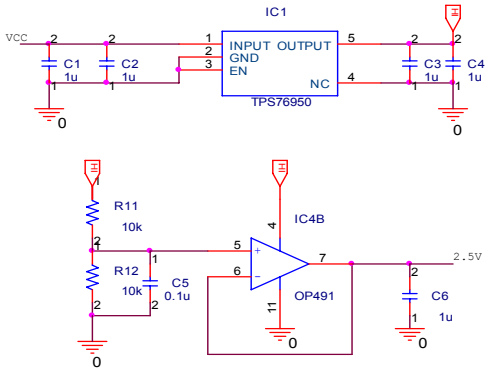

Figure 4: Power supply of the ECG board.

A AD7731 AD converter from Analog Devices follows the analog section. It is a low noise, high throughput 24 bit Sigma-Delta ADC with buffered differential inputs and programmable low pass digital filtering allowing adjustment of filter cut-off, output rate and settling time. The device has a proprietary programmable gain front end that allows it to accept a range of input signal ranges, including low level signals. Figure 5 shows the peripheral setup of AD7731.

JAD is the interface aimed for the communication between AD7731 and Atmega32 which is located on the data logger board.

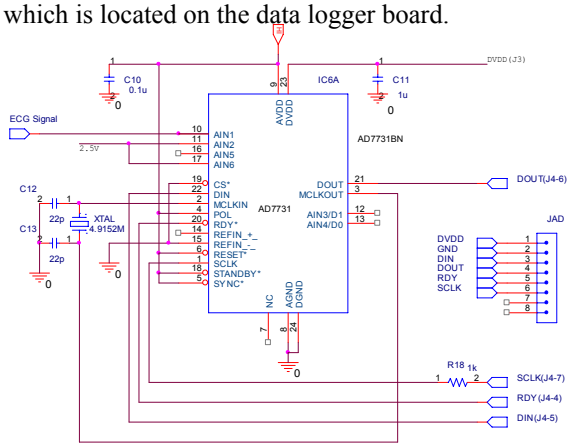

Figure 5: Schematics of AD7731.

2.4 Data Logger Module

The core component of the data logger board is an ATMEL Atmega32 microprocessor with the following specifications:

- 32 kbyte Flash Program Memory
- 2 kbyte SRAM
- 1 kbyte EEPROM
- programmable 8 channel 10 bit ADC
- 16 MIPS @ 16MHz
- TQFP44 housing

The board can be programmed via J1. A Secure Digital memory card connector is connected to the SPI interface of the μ-processor (PB4-PB7). As the SD card is powered with 3,3V, three voltage dividers (R16 – R21) are deployed to decrease the 5V digital output signals to 3,3V. As the Atmega32 interprets digital signals above 2,7V as high, the digital output can be directly connected to the input of the SPI interface (MISO, PB6).

Two low drop low power consumption voltage regulators are used to provide 3,3 V for the SD card and 5V for the rest of the components. Additionally the 3,3 V regulator can be switched in standby mode via dropping the enable pin to ground (via PB2). The EA-DP204 4x20 characters display can be controlled in 4 bit parallel, 8 bit parallel or SPI mode. To simplify the circuit by minimizing the necessary connections we have chosen SPI mode. Therefore the displays clock SCLK and serial input SDI are connected to PB0 and PB1. The ADC's ready pin is interfaced to the external interrupt pin INT1 of the μ-processor (PB3).

To dedicate the μ-processor's inbuilt SPI bus solely to the SD card, the routines for interfacing the

AD converter and the Display are software implemented.

The device mainly addresses ECG recordings in hyperbaric environments like in diving. Therefore a digital pressure sensor needs to be integrated. For this reason the MS5521B 14 bar absolute pressure sensor was chosen [Intersema, Switzerland]. Even if it is not mentioned in the datasheet, the sensor is suitable for pressure measurement up to 33bar. Moreover a digital temperature sensor is integrated in the part.

This sensor requires a 3.3V supply, therefore again voltage dividers (R5-R10) are used to reduce the pins output voltage. The output of the pressure sensor can be directly connected to the microprocessor. For correct operation of the sensor a clock signal is needed (MCLK). This clock signal is generated with the internal Timer 2 from the Atmel ATMEGA32.

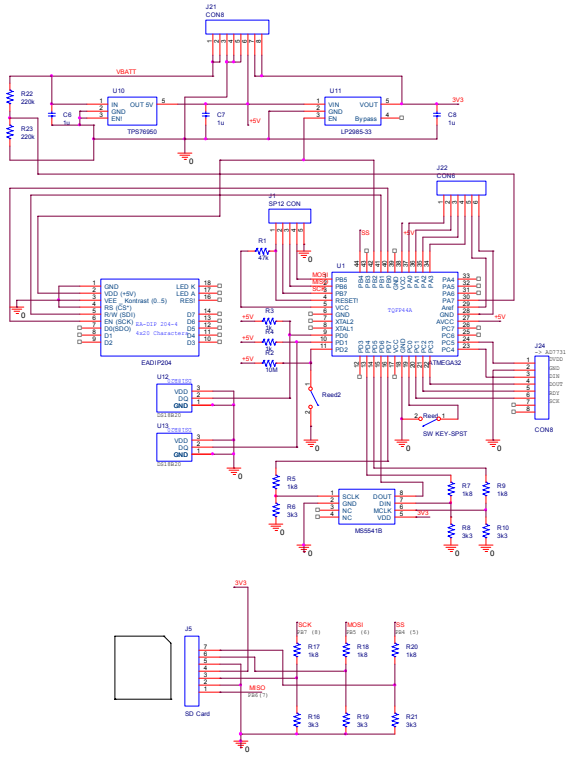

Figure 6: Schematics of the datalogger board.

Body skin temperature and water temperature are parameters that influence the physiological diving response. Therefore two temperature sensors are integrated in the design. These sensors can be for example placed under the diving suit to measure the skin temperature.

As temperature sensors two “one wire” DS18B20 [Maxim] were selected. The “one-wire” feature allows to use just two lines for power supply, communication and ground. In principle the two sensors could be connected to the same port pin, but to increase communication speed by parallel read out, each of the sensors was connected to one separate pin.

2.5 Software

The firmware of the module detailed in figure 7I is developed in C under the Atmel AVR Studio 4 [Atmel] and the GNU C compiler WinAVR (http://winavr.sourceforge.net/).

The implementation of a DOS compatible FAT 16 of FAT 32 filesystem on the SD card requires in total 1,6 kbyte of ROM to mirror the boot sector, the file allocation table (FAT) and to provide a buffer for data storage.

Data storage on SD card in FAT 16 of FAT 32 file system is performed in blocks of 512 bytes each. To enable a high sampling rate of 1200 Hz, it is necessary to treat data storage and read out of the ADC separately, as the data storage of a 512 byte block may last up to 7µs.

Every time an AD conversion is complete, an interrupt is generated via the external interrupt pin INT1.

In the interrupt routine the result is stored in a FIFO buffer. As soon as there are 10 entries in the FIFO buffer, the data is converted in an ASCII string and stored together with the actual depth on SD card.

The “one-wire” protocol [Maxim] is software implemented. Every two seconds the two temperature sensors are read out.

The MS5541B is interfaced via SPI bus. Every two seconds values for pressure and temperature are read out and stored on SD card. Together with 6 calibration parameters stored on the sensor and usually read out at the beginning of the program, pressure and temperature can be calculated. To reduce overall processing time depth and temperature are not calculated on the microprocessor but later under LabView.

A reed contact is used to switch the system on and off via a magnet (in underwater applications magnet switches are preferred as they require no mechanic connection to a switch that needs to be sealed). Once the magnet is removed, the system switches in standby mode. Placing the magnet over the reed contact creates an interrupt on INT0, waking up the module.

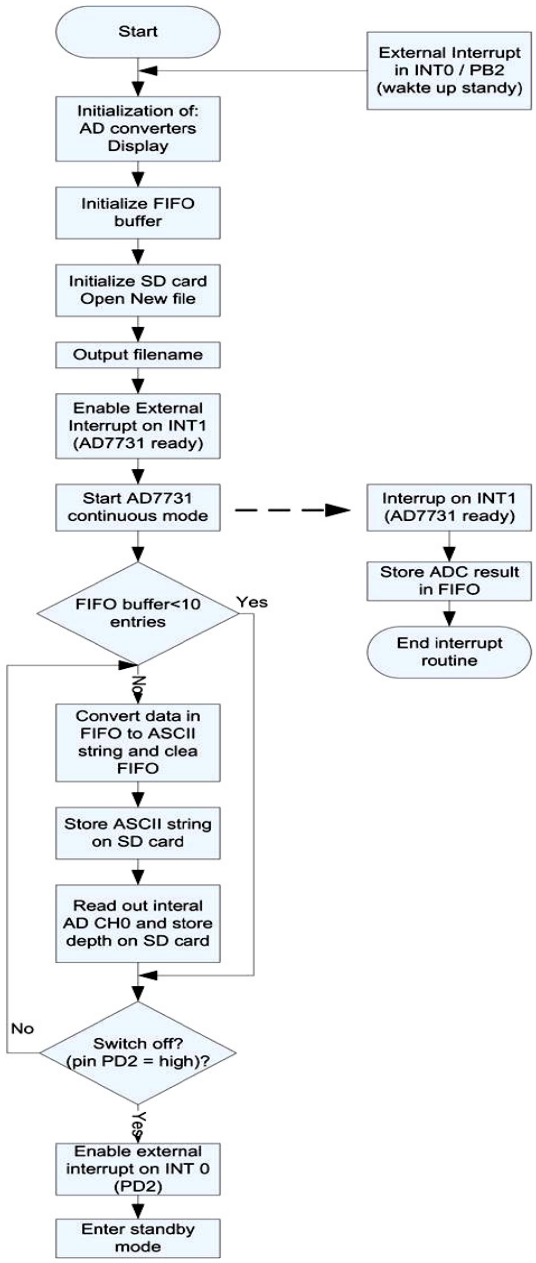

Figure 7: Software flow diagram.

2.6 ECG Data Processing

A software to preview and analyze the collected data software was developed under Labview 7.1 [National Instruments]. To suppress the 50 Hz noise, a optimized Notch filter is implemented (2nd order IIR filter, 45-55 Hz). (Josh, Y.V., Dutta Roy, S.C.,1997), (Chivapreecha,, S., Dejhan, K., Yimman, S., 2005) (see also figure 9A and 9B).

3 RESULTS

A first prototype with the following specifications was build up:

Power consumption[1)]	34 mA
Module size	80x30x25mm³
Battery supply	5,5 … 10 V
Sampling rate ECG	1200 Hz
Resolution ECG	16 bit
Resolution depth sensor	10 bit / 10cm
Sampling rate depth	120 Hz
Bytes / sec	6,4 kbyte/s
File format	FAT16/FAT32
Depth sensor	14 bar (33 bar)
Housing, lexan:	250 m rated

[1)] The power consumption depends also on the SD card (Kingston 256 MB: 34 mA; Lbd, 32MB: 130 mA). In Standby Mode the power consumption drops to 0,3 mA.

Moreover the board is equipped with a second ECG channel with a second AD converter. To enable sampling of low frequency signals a AD8730 AD converter from Analog Devices was additionally integrated in the first prototype. It offers 10 programmable channels with a resolution of 16 bit (application: measurement of skin conductance, breathing sensor, temperature, etc.).

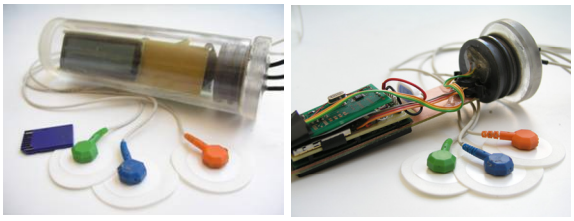

Figure 8A and 8B: First prototype in the double o-ring sealed housing.

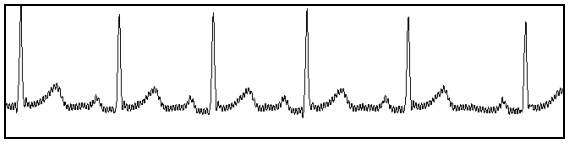

Figure 9A: ECG raw data.

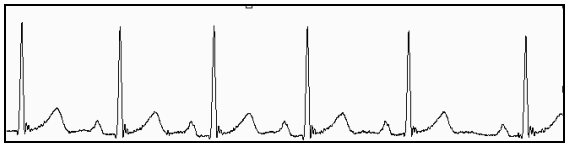

Figure 9B: ECG raw data after filtering with the 50Hz Notch filter.

Figure 8A shows the first prototype encapsulated in the lexan housing. The electronics consist of two boards, one (yellow-brown) with the µ-processor, SD card slot and the display and a second (green) board with the ECG circuit (Figure 8B).

Figure 9A shows a sample ECG recoding. The Notch filter allows an effective suppression of the 50Hz noise signal (figure 9B). This noise suppression is especially necessary when recording the ECG signal on the surface when the diver is preparing for the apnoe immersion. Once under water 50Hz noise signals are usually not seen due to the electrical conductivity of salt water.

Previous experiments have shown that during the first meters of the immersion electrodes with a sponge give bad signals. We speculate that this is due to the small amounts of air next to the sponge that is getting compressed by increasing deph causing electrode movement thus causing also artefacts in the ECG signal. To avoid this problem Kendall Arbo H34SG [Tyco Healthcare] electrodes were selected, as there electrode gel is placed over the electrode without a sponge.

As described earlier (Bedini, R., Reale, L., 2003) recording of an ECG underwater requires a proper sealing of the electrodes. Therefore we use two components impression material (Elite H-D+, Zhermack Hydrphilic Vinyl Polysiloxane)] (Figure 10A). This works well for short dives like breath hold dives. If the electrodes are exposed for longer times like several hours to sea water, we connect the electrode cables directly to the electrode and seal the connection with Epoxy (5 min Epoxy, 155105-1, R&G GmbH, Waldenbuch, Germany).

3.1 Pool Tests

Several tests on apnoe divers were carried out in a 10.5 m deep research pool (Divesystem, Massa Marittima, Italy).

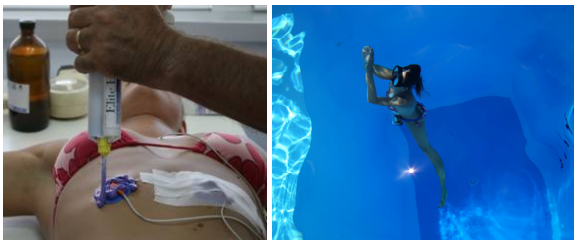

Figure 10A and 10B: 10A: sealing of the electrodes, 10B: test dive in the research pool.

For visualisation and analysis of the recorded data a software was developed under National Instruments Lab View 7.1 which is also offering several data processing utilities.

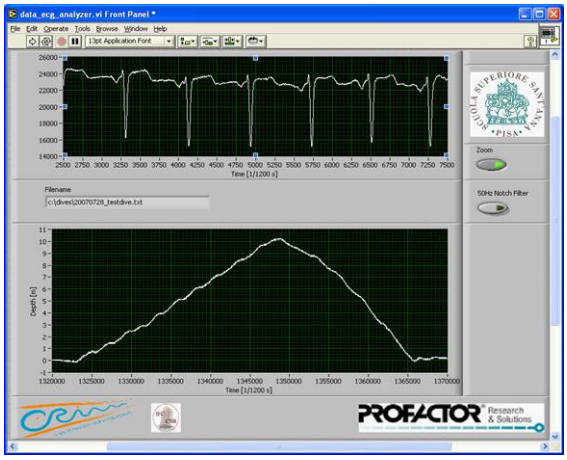

Figure 11: Lab View data visualisation software, in the upper graph the ECG is visualized, down you can see the depth profile.

3.2 Long Term ECG Recordings

An adapted version of the system with a to 250 Hz decreased sampling rate was used to record the ECG of Francesco Colletta during his world record dive in Siracusa, Sicily, Italy on September 8th to 9th. The total dive time was 32h.

Figure 12 A,B: Francesco Colletta after 32h underwater and our especially for this dive adapted ECG measurement device (at the end of each of the two black cables one temperature sensor is encapsulated in epoxy resin).

4 CONCLUSIONS

Research of breath-hold diving induced effects on the ECG requires a high resolution ECG and depth storage device. A novel prototype was developed that is able to store one or two channel ECG with 16 bit resolution at a sample frequency of 1200 Hz on secure digital memory card. This high sampling rate is the basis for a precise estimation of the PQ-interval. The authors are convinced that data gained from elite apnoe divers during the world championship in October 2007 in Egypt will lead to

a better understanding of the physiological effects of breath hold diving.

Other applications of this device are ECG, depth and temperature recording during SCUBA dives.

5 FUTURE WORK

4 more prototypes will be fabricated to be then deployed during the AIDA freediving world championship in October 2007 in Sharm el Sheikh.

An enhanced second version of this prototype is planned to address SCUBA diving applications. It will be expanded with the following sensors: breathing frequency, water temperature, skin temperature and skin conductivity.

Software will be developed to allow an automatic measurement of the PQ-interval. This will be based on triggering on the QRS complex and then calculating the time to the beginning of the P wave.

REFERENCES

Mayol, J., 2000, *Homo Delphinus The Dolphin Within Man*, ISBN 1928649033.

Gooden, B.A., 1994, *Mechanism of the human diving response*. Integr Physiol Behav Sci 29: 6–16, 1994

Andersson, J.P.A., Line, M.H., Ruenow, E., Schagatay, E.K.A.,2002, *Diving response and arterial oxygen saturation during apnea and exercise in breath-hold divers*, J Appl Physiol 93: 882–886.

Marabotti, C., Scalzini, A., Chiesa, F. Bedini, R., Reale, L., Passera, M. Belardinelli, A. Pingitore, A., Cialoni, D., Data P.G,2005, *Echocardiographic changes during breath-hold diving*, Proceedings of Blue 2005, Pisa Dec 1-4, 2005, Ed. Star CNR Pisa.

Malmivuo, J., Plonsey, R., 1995, *Bioelectromagnetism - Principles and Applications of Bioelectric and Biomagnetic Fields*, Oxford University Press, New York.

Atterhög, J., Loogna, E., 1977, *P-R interval in relation to heart rate during exercise and the influence of posture and autonomic tone*, Journal of Electrocardiology 10 (4): 331 – 336.

Busse, M., Nißing, A., Tegtbur, U., Miltzow, S., Thomas, M., Fikenzer, S., 2004, *EKG-Parameter und Herzfrequenz bei Belastung II. PQ-Zeit und Herzfrequenz bei Belastung*, Klinische Sportmedizin, KCS 2004, 5(2): 45-49.

Ward, S., Shouldice, R.B., Flanagan, M., Heneghan, C., 2004, *Electrocardiogram Sampling Frequency Errors in PR Interval Spectral. Analysis*, Proc. IEEE PGBIOMED'04, Southampton, U.K.

Company-Bosch E., Hartmann, E., 2003, *ECG Front-End Design is Simplified with MicroConverter*, Analog Dialogue 37-11.

Josh, Y.V., Dutta Roy, S.C., 1997, *Design of IIR Digital Notch Filters*, Circuits Systems Signal Processing, Vol. 16, NO. 4, 1997, PP. 415-427.

Chivapreecha, S., Dejhan, K., Yimman, S., 2005, *Design of IIR Notch Filter for Removal of Baseline wander and Power Line Interference from ECG Signal*, ICCAS2005.

Bedini, R., Reale, L., 2003, *Rassegna per immagine sulla Ativita di Biotelemetria nel Diving.*

AUTHOR INDEX

AUTHOR INDEX (CONT.)

AUTHOR INDEX (CONT.)

Proceedings of BIODEVICES 2008
International Conference on Biomedical Electronics and Devices
ISBN: 978-989-8111-17-3